2013

PREDICTING THE DYNAMIC BEHAVIOR OF COAL MINE TAILINGS USING STATE-OF-PRACTICE GEOTECHNICAL FIELD METHODS

Ali Salehian
University of Kentucky, asale2@uky.edu

STUDENT AGREEMENT:

I represent that my thesis or dissertation and abstract are my original work. Proper attribution has been given to all outside sources. I understand that I am solely responsible for obtaining any needed copyright permissions. I have obtained and attached hereto needed written permission statements(s) from the owner(s) of each third-party copyrighted matter to be included in my work, allowing electronic distribution (if such use is not permitted by the fair use doctrine).

I hereby grant to The University of Kentucky and its agents the non-exclusive license to archive and make accessible my work in whole or in part in all forms of media, now or hereafter known. I agree that the document mentioned above may be made available immediately for worldwide access unless a preapproved embargo applies.

I retain all other ownership rights to the copyright of my work. I also retain the right to use in future works (such as articles or books) all or part of my work. I understand that I am free to register the copyright to my work.

REVIEW, APPROVAL AND ACCEPTANCE

The document mentioned above has been reviewed and accepted by the student's advisor, on behalf of the advisory committee, and by the Director of Graduate Studies (DGS), on behalf of the program; we verify that this is the final, approved version of the student's dissertation including all changes required by the advisory committee. The undersigned agree to abide by the statements above.

Ali Salehian, Student

Dr. Michael E. Kalinski, Major Professor

Dr. Kamyar C. Mahboub, Director of Graduate Studies

PREDICTING THE DYNAMIC BEHAVIOR OF COAL MINE TAILINGS USING STATE-OF-PRACTICE GEOTECHNICAL FIELD METHODS

DISSERTATION

A dissertation submitted in partial fulfillment of the
requirements for the degree of Doctor of Philosophy in the
College of Engineering at the University of Kentucky

By

Ali Salehian
Lexington, Kentucky

Director: Dr. Michael E. Kalinski, Ph.D., P.E., Professor of Civil Engineering

Lexington, Kentucky

2013

ABSTRACT OF DISSERTATION

PREDICTING THE DYNAMIC BEHAVIOR OF COAL MINE TAILINGS USING STATE-OF-PRACTICE GEOTECHNICAL FIELD METHODS

This study is focused on developing a method to predict the dynamic behavior of mine tailings dams under earthquake loading. Tailings dams are a by-product of coal mining and processing activities. Mine tailings impoundments are prone to instability and failure under seismic loading as a result of the mechanical behavior of the tailings. Due to the existence of potential seismic sources in close proximity to the coal mining regions in the United States, it is necessary to assess the post-earthquake stability of these tailings dams.

To develop the aforementioned methodology, 34 cyclic triaxial tests along with vane shear tests were performed on undisturbed mine tailings specimens from two impoundments in Kentucky. Therefore, the liquefaction resistance and the residual shear strength of the specimens were measured. The laboratory cyclic strength curves for the coal mine specimens were produced, and the relationship between plasticity, density, cyclic stress ratio, and number of cycles to liquefaction were identified.

The samples from the Big Branch impoundment were generally loose samples, while the Abner Fork specimens were dense samples, older and slightly cemented. The data suggest that the number of loading cycles required to initiate liquefaction in mine tailings, N_L, decreases with increasing CSR and with decreasing density. This trend is similar to what is typically observed in soil. For a number of selected specimens, using the results of a series of small-strain cyclic triaxial tests, the shear modulus reduction curves and damping ratio plots were created.

The data obtained from laboratory experiments were correlated to the previously recorded geotechnical field data from the two impoundments. The field parameters including the SPT blow counts $(N_1)_{60}$, corrected CPT cone tip resistance (q_t), and shear wave velocity (v_s), were correlated to the laboratory measured cyclic resistance ratio (CRR). The results indicate that in general, the higher the $(N_1)_{60}$ and the tip resistance (q_t),

the higher the CSR was.

Ultimately, practitioners will be able to use these correlations along with common state-of-practice geotechnical field methods to predict cyclic resistance in fine tailings to assess the liquefaction potential and post-earthquake stability of the impoundment structures.

KEYWORDS: mine tailings, liquefaction, cyclic stress ratio, modulus reduction curves, cyclic triaxial test

Ali Salehian

April 15, 2013

PREDICTING THE DYNAMIC BEHAVIOR OF COAL MINE TAILINGS USING STATE-OF-PRACTICE GEOTECHNICAL FIELD METHODS

By

Ali Salehian

Michael E. Kalinski, Ph.D.
Director of Dissertation

Kamyar C. Mahboub, Ph.D.
Director of Graduate Studies

April 15, 2013
Date

To my beloved Parents, Ahmad Salehian and Farideh Shojai,
For their unconditional love and endless support

To my dear brothers, Mehran Salehian and Mehrdad Salehian
For their inspiration and encouragement

To Kristi Briggs,
For her continuous love and motivation

None of this would be possible without them.

ACKNOWLEDGEMENTS

Without a doubt, this is the most difficult part of my dissertation. This dissertation would have not been possible without the help of so many people in so many ways. I would like to express my deepest gratitude to my advisor, Dr. Michael Kalinski, for his excellent guidance and patience. He never doubted my ability to complete my work and encouraged independence. I am grateful for his trust in me. I am indebted to Dr. Sebastian Bryson for believing in me and initiating my journey at the University of Kentucky. He helped to develop my background in geotechnical engineering and was always willing to offer his guidance throughout my Ph.D. research. His support and sincere interest in my studies and engineering career are very much appreciated.

I would like to thank Dr. Edward Woolery for his willingness to help in many situations throughout my Ph.D. studies. His sincere help and support will never be forgotten. Working with him as a student or a researcher, enhanced my understanding of the research topic and diversified my skills as a geotechnical engineer. I would like to appreciate the other members of my dissertation committee, Dr. Braden Lusk and Dr. Jerry Rose, and the outside examiner, Dr. Michael Siegler for contributing in one way or the other to the success of this research. Dr. Kamyar Mahboub, the director of graduate studies at the Civil Engineering department, provided constant guidance and support even before starting my life in Lexington. He facilitated my experience at the University of Kentucky and contributed in many ways to my success. I would like to thank Mr. Barry Thacker at Geo/Environmental Associates who was instrumental in facilitating the

communication and cooperation between the University of Kentucky and the personnel at the Abner Fork and Big Branch impoundments, which allowed this study to be carried on at these sites.

My time at the University of Kentucky was enriched through the interactions with a great group of friends, colleagues, and students. I am indebted to Kristi Briggs whom introduced me to American ways and culture, stood by me through every obstacle, and motivated me to go forward. Gene Yates constantly supported me during my years as the geotechnical laboratory instructor and helped me to provide a high quality service to the students. In the past few years, many individuals with their support and friendship provided an unforgettable experience at the University of Kentucky. Among them: April Barnes Welshans, Tom Lutz , Salman Hakimzadeh, Kyle Guenther, Yongwei Shan, Grace Northcutt, Melanie Anderkin, Josh Phillips, Isabel Gomez Gutierrez, Corrie Walton-Macaulay, Alireza Zeinali, Sourena Sahraeeian, Ebrahim Sadrzadeh, Brock Kidd, Jordan Kirkendoll, Scott Embry, Alfred Susilo, Derrick Dennison, Chris Jones, Alex Krumenacher, Brian Phillips, Ricky Teachey, Le Daisy Cao, Julie Heiser, Christian Wilder, and Nithin Agarwal. I would like to thank the Civil Engineering department chair, Dr. George Blandford, and staff including Shelia Williams, Beth Northcutt, Suzy Wampler, and Bettie Jones which without their patience and help this work would not have been possible.

I would like to thank my colleagues at ENGEO, Leroy Chan, Stefanos Papadopulos, Dan Haynosch, Brian Flaherty, Ben Serna, and Pedro Espinosa who helped me develop my professional skills. During my short experience at S&ME, my understanding of the industry

was significantly improved and I would like to thank my colleagues, Justin Wilson, Johnathan Hale, Chris Pennington, Steve Bennett, Chisa, Jacob Folsom, and Jerry Baber for that.

Lastly but most importantly, I would like to sincerely thank my family for their unparalleled support and sacrifice. Although words cannot express my feelings towards them, I would like to offer my deepest appreciation to my parents, Ahmad Salehian and Farideh Shojai, and my brothers, Mehran and Mehrdad whom from far distance have supported me, inspired me and kept me motivated.

Table of Contents

List of Tables

List of Figures

Chapter 1

Introduction

1.1 Background

Tailings dams are constructed to contain waste materials produced as a result of mining activities associated with coal and metals. Tailings dams consist of a dike of coarse refuse (i.e. well-graded sand and gravel) with fine refuse hydraulically placed behind the dike from a discharge point near the embankment crest. Tailings dams are constructed in three basic methods including upstream, centerline, and downstream construction as schematically illustrated in Figure 1.1. However, construction methods are most commonly a combination of upstream and centerline.

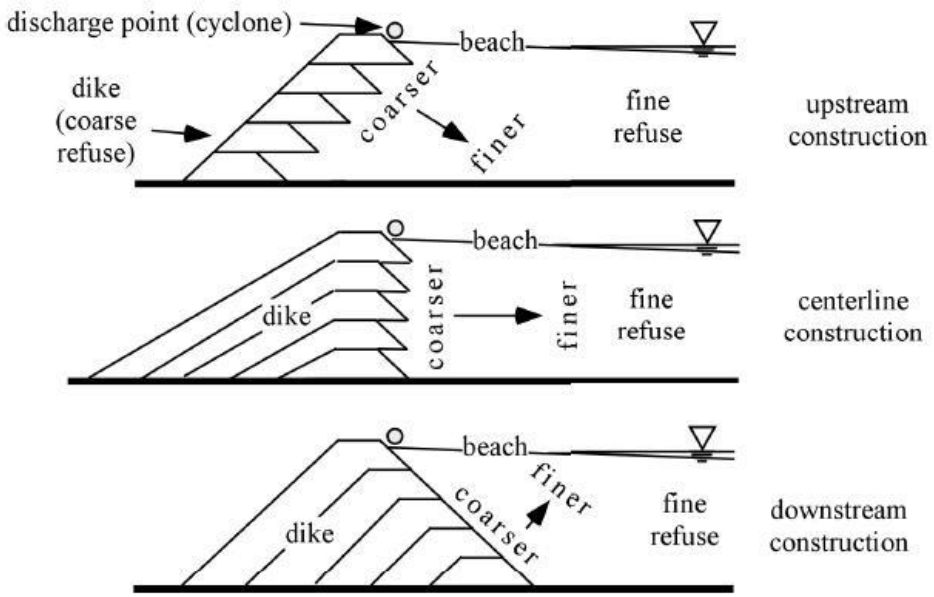

Figure 1.1: Construction methods of coal mine tailings impoundments

As the dam is filled with fine refuse, the dike is expanded upward. Consequently, the tailings dams can reach hundreds of feet in height. Since the material is discharged into the impoundment (Figure 1.2) at the embankment crest, a gradation will appear in grain size within the fine refuse as depicted in Figure 1.1. Coarser particles will settle near the discharge point, and finer particles are carried further away. Also, unless adequate drainage is provided, the sedimented tailings remain under-consolidated for many years (Ishihara et al., 1981). The upstream construction method is the most critical among the three construction types with respect to slope stability, considering that most of the critical failure surface passes through the weaker fine refuse. However, the upstream method is common because it requires the least amount of effort and materials to construct the dike, and the impoundment does not progressively increase in size in the downstream direction to occupy the available mining area and crowd the existing facilities.

Figure 1.2: The discharge point at the crest of Abner Fork tailings impoundment.

Approximately, 1,555 tailings impoundments exist in the United States, with coal tailings dams mainly concentrated in Appalachia as illustrated in Figure 1.3, and metal

tailings dams concentrated in the west (NSF, 2003). Bituminous coal is the most plentiful form of coal and is used primarily to generate electricity and produce coke for steel production. As it appears from Figure 1.3, the majority of medium and high volatile bituminous coal mines in the United States are produced in the Appalachian basin, Illinois basin, and Western Interior basin. According to the National Inventory of Dams, approximately one-third of the 1,555 tailings structures in the United States are determined to be high-hazard potential, where failure would result in loss of human life. Although the majority of tailings dam failures have been contributed to static liquefaction (Davies, 2002), earthquake-induced liquefaction is a concern especially for the dams constructed using the upstream method.

Tailings dams are also a common method in mining throughout the world. In the past 40 years, approximately 94 tailings dams have failed worldwide, which were accompanied with an uncontrolled release of waste material. Fifteen of these failures were the result of liquefaction due to earthquake shaking. An important example is the March 28, 1965 El Cobre dam system failure in Chile, where the release of roughly 2 million tons of material destroyed the town of El Cobre located 7 miles downstream and killed over 200 people (Dobry and Alvarez, 1967). Another example is the January 15, 1978 Mochikoshi tailings dams failures in Japan, where one dam failed during the earthquake, while another failed 24 hours later due to the gradual increase in pore pressures from liquefaction of the material behind the dam (Marcuson et al., 1979; Ishihara et al., 1981; Ishihara, 1993a).

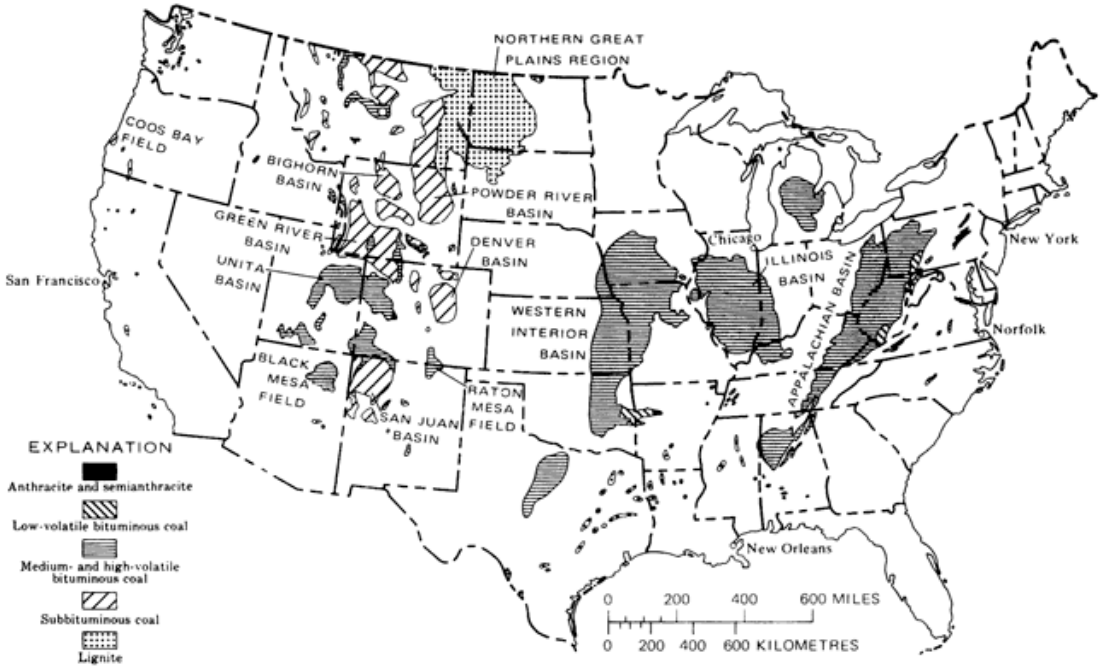

Figure 1.3: Location of various types of coal mines based on the heat value from the highest to the lowest in the United States. (Averitt, 1975).

The consequences of mine tailings impoundments failures are intensified by considering the release of the tailings material mixed with the mined material residue such as coal or metals contaminated with the chemicals utilized for processing the material. These materials could potentially be carried down the stream for a few miles with the liquefied tailings and pollute the environment. For example, as reported by the Mine Safety and Health Administration (MSHA, 2001), the static failure of the coal tailings dam of Martin County Coal Corporation's preparation plant near Inez, Kentucky, resulted in a release of a slurry consisting of an estimated 250 million gallons (950,000 m^3) of water and 155,000 cubic yards (118,500 m^3) of coal waste into local streams. About 75 miles (120 km) of rivers and streams turned an iridescent black, causing a fish kill along the Tug Fork of the Big Sandy River and some of its tributaries. Towns along the Tug were forced

to turn off their drinking water intakes due to measurable amounts of metals, including arsenic, mercury, lead, copper and chromium. The full extent of the environmental damage was not known and estimates of the cleanup costs were as high as $60 million. In Figure 1.4, an aerial view of the 1985 Veta De Agua tailings dam failure in Chile is illustrated. Another example of the downstream devastation as a result of coal mine tailings release at Manalapan Mining, Brookside, Kentucky in 1980 is illustrated in Figure 1.5.

Figure 1.4: An aerial view of the 1985 Veta De Agua tailings dam failure in Chile (Castro and Troncoso, 1989).

Other outstanding static liquefaction of coal mine tailings cases include the failure of Merriespruit mine, South Africa in 1994, Los Frailes mine, Spain in 1997, Omai mine, Guyana in 1994, and Stava mine, Italy in 1985. As a result of the failure of Merriespruit mine in South Africa on February 22nd, 1994, over 600,000 m^3 (~785,000 yd^3) of tailings and 90,000 m^3 (~23.8 million gallons) of water were released. The slurry traveled about 2

km (1.2 mile) covering nearly 500,000 m^2 (123.6 acre) and killed 17 people. The failure of Los Frailes mine in Spain in 1997 resulted in release of more than 3 million m^3 (3.9 million yd^3) of process water and tailings. This publicized event caused a significant financial loss for the owner of the mine in the following year.

Figure 1.5: Devastation of downstream as a result of tailings slurry flow at Manalapan Mining, Brookside, Kentucky in 1980, (courtesy of Josh Phillips, 2012).

The failure of Omai mine in Guyana in 1994 involved a dam breach and the release of cyanide-laden water to the Omai River and then to the much larger Essequibo River. This event caused debatable environmental damage with reports of downstream devastation beyond the extent of decontamination procedures (Haile, 1997 and Vick, 1997). The failure of a fluorite mine, located near Stava in Northern Italy, had both of its tailings dams fail suddenly on July 19th, 1985 and release approximately 240,000 m^3 (314,000 yd^3) of liquefied tailings. The liquefied mass moved up to speeds of 60 km/h (~37

mph) obliterating everything in its path for a stretch of approximately 4 km (2.5 mile). The flow slide destroyed the village of Stava and also caused considerable damage at Tesero, at the junction of Stava Creek and the Avisio River at the 4 km (2.5 mile) point from the mine (Davies and Martin, 2000).

During the processing of the coal by separating it from the rock and soil, the refuse material is mixed with coal particles. Therefore, the density of the refuse material is lower than the average observed densities in soil. Also, the fine refuse contains a considerable amount of fine grained soil including silts and clays and rock powder. As a result, the permeability of the fine refuse is in the lower ranges and it takes a long time to drain the water that was mixed with the tailings during transportation and processing. Therefore, the tailings pond remains undrained and keeps the tailings saturated.

In Appalachia it is common to build the tailings dam in narrow valleys formed in the mountains which in the local culture are known as hollers (hollows). This method of storage provides natural containment and eliminates the need to build embankments in various directions. However, constructing tailings dams on slopes imposes an instability issue due to the natural geometry compared to the tailings dams built on flat lands. Also, the proximity of the area to active seismic sources that are discussed in Section 1.3 is another element that contributes to the need to investigate the stability of tailings dams. Therefore, a combination of factors such as lower densities, saturation of the tailings, the geometry of the construction zone, and the close distance to active seismic sources make the coal mine tailings dam susceptible to liquefaction.

The liquefaction of soil has been studied for decades in depth since the occurrence of the devastating earthquakes in Alaska and Nigita, Japan in 1964. These studies were pioneered by Professor H. B. Seed and I. M. Idriss by publishing an empirical methodology called the “simplified procedure” for assessing the liquefaction resistance of soils (Seed & Idriss, 1971). To date a considerable number of studies have investigated the performance of natural silty soils (Polito and Martin, 2001; Boulanger et al. 1998; Bray et al, 2004; Wijewickreme, 2007; Wijewickreme and Sanin, 2004; Wijewickreme et al., 2005), however the available published information on the cyclic shear response of fine grained mine tailings is limited (Wijewickreme et al., 2005). A compilation of cyclic resistance ratio (CRR) curves from various mine tailings was published by Vick (1983). The studies on silty tailings investigated the results of index tests, cyclic shear tests, and undrained monotonic post-cyclic behavior of remolded and undisturbed samples of tailings. A study on the behavior of tailings from copper mines by Moriwaki (1982) showed that under static undrained shearing the tailings slimes exhibit contractive behavior. In this study, the cyclic response was evaluated by performing triaxial testing.

The influence of consistency characteristics and plasticity of remolded silty tailings of several different minerals were studied by Ishihara et al. (1980). Ishihara et al. (1981) also investigated the behavior of undisturbed tailings samples from several tailings dams in Japan utilizing cyclic triaxial testing. The cyclic strength characteristics of silty tailings are also studied by McKee et al. (1979) and Poulos et al. (1985). In a study by Peters and

Verdugo (2003) on tailings using a cyclic triaxial apparatus, it was shown that at the same void ratio, by increasing fines content the cyclic shear resistance was decreased.

Laboratory tests have been continuously used to investigate the variations in pore water pressure and shear deformations during cyclic loading. To understand the performance of structures during seismic loading, these laboratory shear based criteria are used as an approach to determine liquefaction triggering (NRC, 1985; Wu et al., 2004). From the field observations in Adapazari, Turkey by Bray et al. (2004), the suitability of such laboratory shear strain based criteria to assess liquefaction susceptibility of soils was demonstrated. In this study, Bray et al. found that the structures built on soil layers that display cyclic mobility in the laboratory have settled or tilted excessively. It was also noted that under conditions of cyclic mobility, the occurrence of surface expressions such as sediment ejecta was possible.

The majority of current state-of-practice liquefaction evaluation methods for fine grained soils are based on simple soil parameters and properties (Bray et al. 2004; Andrews and Martin, 2000; Finn et al, 1994; Marcuson et al., 1990). However, these empirical methods have shown some shortcomings in liquefaction evaluation of silty soils and were not proven to be reliable in determining the liquefaction potential of such soils (Boulanger et al., 1998; Atukorala et al., 2000). Reviewing the summary report by the National Center for Earthquake Engineering Research (NCEER) on the empirical methods for liquefaction evaluation indicates a lack of agreement on this matter. It is believed that

this is mainly due to lack of reliable data for such conclusions. Laboratory testing is one of the ways to provide data that could be used to improve these empirical methods.

In order to understand the behavior of tailings during earthquakes, some of the studies are focused on advanced laboratory strength testing. In these laboratory studies including cyclic triaxial tests, and cyclic direct simple shear tests, the in situ stresses and loading during earthquakes are simulated. Although the majority of studies on the cyclic behavior of tailings during earthquake are based on cyclic triaxial testing, this method cannot fully simulate the stress path followed during such manner of loading. During the cyclic loading occurring in earthquakes, the magnitudes of principal stresses change in addition to the simultaneous changes in the direction of principal stresses (Arthur et al., 1980; Wijewickreme and Vaid, 1993; Wijewickreme, 2005). However, the cyclic direct simple shear apparatus allows for such variations to be simulated. Therefore, for the simulation of earthquake loading, the direct simple shear test is considered more appropriate (Vaid and Finn, 1979).

In an effort to provide an insight into the dynamic behavior of coal mine tailings material, this study was performed on tailings from two coal mines in Kentucky. Performing laboratory strength tests on undisturbed coal mine tailings samples is costly and time consuming. Therefore, compared to soils, the dynamic behavior of such material is not studied as much by researchers. In addition to that, it is not practical and cost-effective for consulting firms to achieve undisturbed samples and carry laboratory tests on this material. This study was aimed on providing a method to predict the liquefaction

susceptibility of coal mine tailings by performing in situ tests without the need for undisturbed sampling and laboratory strength testing. To achieve this goal, this study was divided into three phases: in situ testing, laboratory testing, and correlating the in situ results to laboratory results. These phases are discussed in Section 1.4 and the chapters in this dissertation follow the same order.

1.2 Investigated Tailings Impoundments

To meet the objectives of this study, two coal mine tailings impoundments were selected for sampling and assessment. The considered impoundments were identified in cooperation with the Mine Safety and Health Administration (MSHA) to represent:

1) the most critical and common cases of upstream or mixed upstream/centerline construction as depicted in Figure 1.1;
2) Mature, active impoundments possessing old and new tailings materials;
3) High hazard structures since their safety is critical to protecting the public; and
4) Structures located in zones possessing a reasonable amount of seismicity.

Considering the proposed budget and time frame, only two impoundments were selected which were in the Appalachian coal mining region of the eastern United States. This region is in relatively close proximity of active seismic zones such as the Eastern Tennessee Seismic Zone, the Charleston, South Carolina area, and the New Madrid Seismic Zone. The selection of these impoundments was facilitated through the guidance

and information provided by MSHA and Geo/Environmental Associates Inc. of Knoxville, Tennessee.

All volumes (capacities) and permit numbers of the structure were provided by www.coalimpoundment.org, a website designated for location and information pertaining to all permitted structures. Elevations of each structure were obtained from plan sheets provided by Geo/Environmental Associates Inc. All other information was provided through discussions with superintendents on site at each impoundment. Information regarding the location, geometry, dimensions and other details of the two impoundments is provided in the following sections.

1.2.1 Abner Fork Impoundment

The Abner Fork Impoundment (MSHA ID Number: 1211-KY07-07011-10) is located in Harlan County, Kentucky, approximately 5.0 miles northeast of the city of Evarts on Kentucky Highway 38. The latitude and longitude of the property are 36° 53’ 21” and 83° 06’ 37”, respectively. A schematic map of the location of this impoundment is depicted in Figure 1.6. The impoundment remains in operation and has been active since the early 1980’s. Original construction was performed by Eastover Mining Company, a subsidiary of Duke Power. Ownership was passed to Manalapan Mining in the late 1980’s, who purchased all of Eastover’s interests in the area. Currently, the impoundment is operated by Dixie Fuel Company, a subsidiary of locally owned Harlan Cumberland Coal Company.

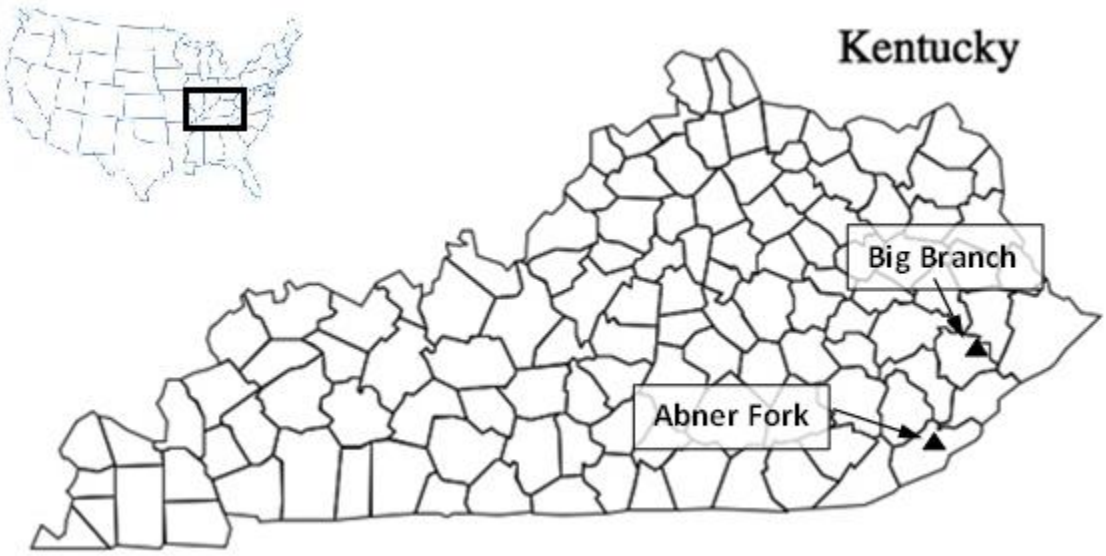

Figure 1.6: Approximate location of the Abner Fork and Big Branch impoundments in Kentucky.

The impoundment is an upstream, cross-valley constructed dike system with a total permitted capacity of 1600 acre-feet (69,696,000 cubic feet or 521,362,291 gallons) as illustrated in Figure 1.7 and Figure 1.8. Total maximum pool elevation is scheduled to be 2340 feet (713.2 m) when the impoundment is filled to capacity, with the toe of the structure being at an elevation of 1580 feet (481.6 m). At the time of original construction, the impoundment serviced one of the higher production preparation plants of its time. The estimated remaining life of the structure is five years based on projections of current mining sections utilizing the facility.

Figure 1.7: Aerial photo of Abner Fork impoundment, (Google Maps, 2013a).

Figure 1.8: Upstream view of the Abner Fork impoundment in Harlan County, Kentucky.

All tailings (fines) are hydraulically placed in the pool, while dikes are built of coarse refuse by means of rear-end dumps, bull dozers and smooth-drum rollers. Upon

completion of testing, final top soil covers were being placed at the toe of the dam and will continually progress upstream.

1.2.2 Big Branch Impoundment

The Big Branch Impoundment (MSHA ID Number: 1211-KY07-07005-08) is located in Knott County Kentucky approximately 1.5 miles (2.4 km) south of Raven on Kentucky Highway 899. The latitude and longitude of Big Branch impoundment are 37° 23’ 01” and 82° 48’ 33”, respectively and the approximate location is shown in Figure 1.6. This impoundment was originally constructed in the early 1980’s and sat dormant for much of the last two decades as mining operations supporting the preparation plant were suspended. Currently, the structure is owned by Penn Virginia Corporation. International Coal Group (ICG) currently operates the impoundment through agreed leases with Penn Virginia. Mining operations on the property resumed in late 2006. The Big Branch Impoundment is also an upstream, cross-valley dike system (Figure 1.9 and Figure 1.10). The maximum permitted pool elevation is 1298 feet (395.6 m), while the toe of the dam is at 940 feet (286.5 m).

Figure 1.9: Aerial photo of Big Branch impoundment, (Google Maps, 2013b).

Currently, five on-site mining sections feed the preparation plant along with other surface mines located within a few miles of the facility. Approximately 10,000 tons (9070 metric tons) of raw coal are washed and crushed at the prep plant annually, with close to 40% being reject material (i.e. fine and coarse refuse requiring disposal). The produced reject is much higher than the estimated design, so the remaining life of the structure is questionable. The total design capacity of the impoundment is 50 acre-feet (2,178,000 cubic feet or 16,292,572 gallons). The tailings materials are placed hydraulically, with the dikes constructed much like those at Abner Fork. Upon completion of testing, the tailings dam was being retrofitted with a haul road, providing access to the toe of the structure,

and the uppermost containment dike was redesigned to impound more of the existing hollow to provide more storage space for refuse.

Figure 1.10: Big Branch impoundment, (a) Downstream, (b) Upstream

1.3 Seismicity of the Region

The failure of tailings impoundments due to earthquakes has been associated with liquefaction of fine-grained materials, although this phenomenon is often related to the coarse grain materials. To date, earthquake-induced tailings dam failures have not occurred in the United States. However, the proximity of these structures to the seismic zones such as the New Madrid and Wabash Valley, East Tennessee, Northeast Kentucky, and Giles County Virginia demands an in depth investigation of the dynamic stability of such structures. Also, the historic earthquake of 1886 Charleston, South Carolina and the recent 2011 Virginia earthquake that was felt in a vast zone on the Eastern part of the United States (A zone that is generally believed to be not affected by earthquakes) intensifies the need for a thorough seismic study of high-hazard structures, including coal mine tailings impoundments. In Figure 1.11, the approximate location of the mentioned earthquakes and seismic sources relative to the investigated tailings in Eastern Kentucky is illustrated.

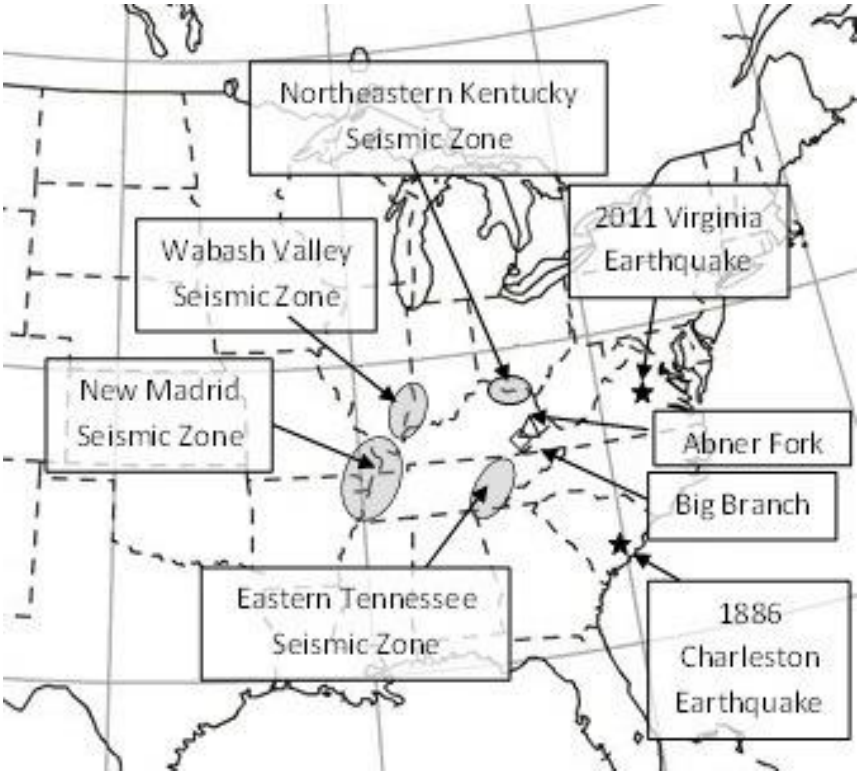

Figure 1.11: Location of the selected tailings impoundments in this study, the nearby seismic sources and historic seismic events.

Earthquakes in the central and eastern United States, although less frequent than in the western United States, are typically felt over a much broader region. East of the Rockies, an earthquake can be felt over an area as much as ten times larger than a similar magnitude earthquake on the west coast. A magnitude 4.0 eastern U.S. earthquake typically can be felt at many places as far as 100 km (60 mi) from where it occurred, and is capable of causing damage near its source. A magnitude 5.5 eastern U.S. earthquake usually can be felt as far as 500 km (300 mi) from where it occurred, and sometimes causes damage as far away as 40 km (25 mi).

1.3.1 New Madrid Seismic Zone (NMSZ)

The New Madrid Seismic Zone is a major seismic zone and a prolific source of intraplate earthquakes (earthquakes within a tectonic plate) in the southern and Midwestern United States as depicted in Figure 1.12, stretching to the southwest from New Madrid, Missouri.

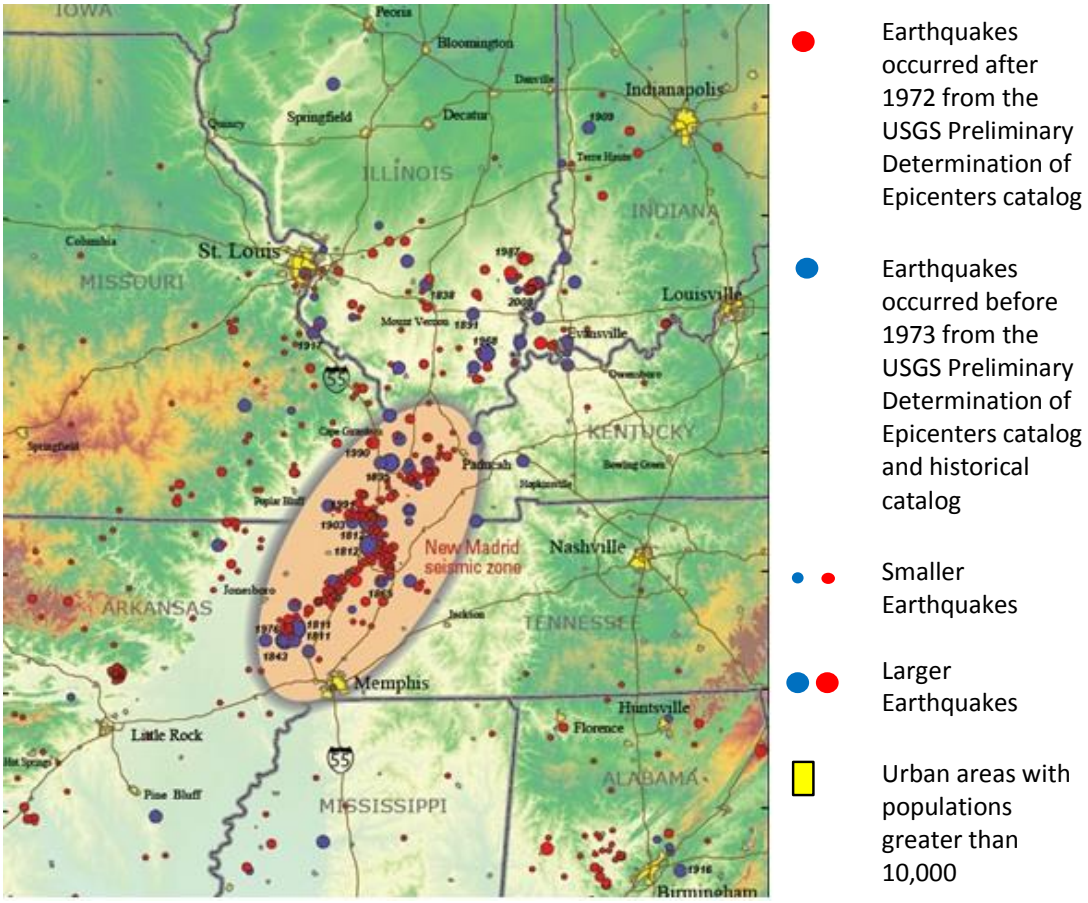

Figure 1.12 : Topographic map showing earthquakes greater than magnitude 2.5, USGS image (Frankel et al., 2009).

The first principal earthquake, M7.7, occurred at about 2:15 am (local time) in northeast Arkansas on December 16, 1811. The second principal shock, M7.5, occurred in Missouri on January 23, 1812, and the third, M7.7, on February 7, 1812, along the

Reelfoot fault in Missouri and Tennessee. The earthquake ground shaking was not limited to these principal main shocks, as there is evidence for a fairly robust aftershock sequence. The first and largest aftershock occurred on December 16, 1811 at about 7:15 am. At least three other large aftershocks are inferred from historical accounts on December 16 and 17. These three events are believed to range between M6.0 and 6.5 in size and to be located in Arkansas and Missouri. This would make a total of seven earthquakes of magnitude M6.0-7.7 occurring in the period December 16, 1811 through February 7, 1812. In total, Otto Nuttli reported more than 200 moderate to large aftershocks in the New Madrid region between December 16, 1811, and March 15, 1812: ten of these were greater than about 6.0; about one hundred were between M5.0 and 5.9; and eighty-nine were in the magnitude 4 range. Nuttli also noted that about eighteen hundred earthquakes of about M3.0 to 4.0 during the same period (Petersen et al., 2008).

There is broad agreement in the scientific community that a continuing concern exists for a major destructive earthquake in the New Madrid Seismic Zone. Many structures in Memphis, Tennessee, St. Louis, Missouri, and other communities in the central Mississippi River Valley region are vulnerable and at risk from severe ground shaking. This assessment is based on decades of research on New Madrid earthquakes and related phenomena by dozens of Federal, university, State, and consulting earth scientists.

In the past few years, considerable interest has developed from media reports that the New Madrid Seismic Zone may be shutting down. These reports are originated

from published research using global positioning system (GPS) instruments with results of geodetic measurements of strain in the Earth's crust. Due to the lack of measurable strain at the surface in some areas of the seismic zone over the past 14 years, these studies have suggested that within the New Madrid Seismic Zone the buildup of stress at depth is stopped and the zone may no longer pose a significant hazard.

As part of the consensus-building process used to develop the national seismic hazard maps, the United States Geological Survey (USGS) convened a workshop of experts in 2006 to evaluate the latest findings in earthquake hazards in the Eastern United States. These experts considered the GPS data from New Madrid available at that time that also showed little to no ground movement at the surface. The experts did not find the GPS data to be a convincing reason to lower the assessment of earthquake hazard in the New Madrid region, especially in light of the many other types of data that are used to construct the hazard assessment (Frankel et al., 2009).

The earthquakes caused the ground to rise and fall - bending the trees until their branches intertwined and opening deep cracks in the ground. Deep seated landslides occurred along the steeper bluffs and hillsides; large areas of land were uplifted permanently; and still larger areas sank and were covered with water that erupted through fissures or craterlets. Huge waves on the Mississippi River overwhelmed many boats and washed others high onto the shore. High banks caved and collapsed into the river; sand bars and points of islands gave way; whole islands disappeared. Surface fault rupturing from these earthquakes has not been detected and was not reported, however.

The region most seriously affected was characterized by raised or sunken lands, fissures, sinks, sand blows, and large landslides that covered an area of 78,000 - 129,000 square kilometers (30,116 – 49,807 mi^2), extending from Cairo, Illinois, to Memphis, Tennessee, and from Crowley's Ridge in northeastern Arkansas to Chickasaw Bluffs, Tennessee. Only one life was lost in falling buildings at New Madrid, but chimneys were toppled and log cabins were thrown down as far distant as Cincinnati, Ohio, St. Louis, Missouri, and in many places in Kentucky, Missouri, and Tennessee (Stover and Coffman, 1993; Johnston and Schweig, 1996; Hough, 2009).

A notable area of subsidence that formed during the February 7th, 1812, earthquake is Reelfoot Lake in Tennessee, just east of Tiptonville dome on the down-dropped side of the Reelfoot scarp. Subsidence there ranged from 1.5 to 6 meters (4.9 to 19.7 ft), although larger amounts were reported. Other areas subsided by as much as 5 meters (16.4 ft), although 1.5 to 2.5 meters (4.9 to 8.2 ft) was more common. Lake St. Francis, in eastern Arkansas, which was formed by subsidence during both prehistoric and the 1811-1812 earthquakes, is 64 kilometers (39.8 mile) long by 1 kilometer (0.62 mile) wide. Coal and sand were ejected from fissures in the swamp land adjacent to the St. Francis River, and the water level is reported to have risen there by 8 to 9 meters (26.2 to 29.5 m). Large waves (seiches) were generated on the Mississippi River by seismically-induced ground motions deforming the riverbed. Local uplifts of the ground and water waves moving upstream gave the illusion that the river was flowing upstream. Ponds of

water also were agitated noticeably (Stover and Coffman, 1993; Johnston and Schweig, 1996; Hough, 2009).

These dramatic accounts clearly show that destructive earthquakes do not happen only in the western United States. In the past 25 years, scientists have learned that strong earthquakes in the central Mississippi Valley are not freak events but have occurred repeatedly in the geologic past. Earthquakes in the central or eastern United States affect much larger areas than earthquakes of similar magnitude in the western United States. For example, the San Francisco, California, earthquake of 1906 (magnitude 7.8) was felt 350 miles (560 km) away in the middle of Nevada, whereas the New Madrid earthquake of December 1811 rang church bells in Boston, Massachusetts, 1,000 miles (1610 km) away. Differences in geology east and west of the Rocky Mountains cause this strong contrast (CUSEC, 2002). In Figure 1.13, the New Madrid seismic zone hazard map for a hypothetical 7.7 magnitude earthquake is illustrated. As it appears, the predicted modified Mercalli intensity for eastern Kentucky is determined to be VII, which is considered very strong.

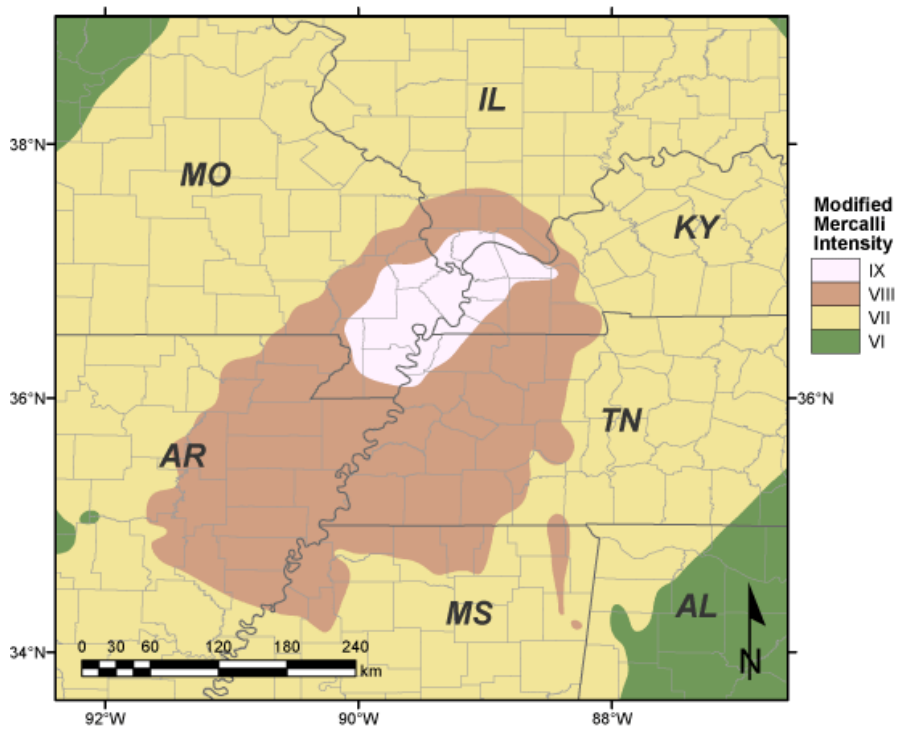

Figure 1.13: New Madrid seismic zone hazard map for a hypothetical 7.7 magnitude earthquake, (USGS, 2013).

For the most active part of the NMSZ, Nuttli and Herrmann (1978) proposed the magnitude-recurrence relation as the following:

$$\log_{10} N_c = 3.90(\pm 0.53) - 0.92 m_b \quad (1.1)$$

where N_c is the number of earthquakes per year and m_b is body wave magnitude.

1.3.2 Wabash Valley Seismic Zone (WVSZ)

The Wabash Valley Seismic Zone (WVSZ; also known as the Wabash Valley Fault System or Zone) is a tectonic region located in the Midwest of the United States, centered on the valley of the Lower Wabash River, along the state line between southeastern Illinois and southwestern Indiana. This seismic zone was suggested by Nuttli and

Herrmann (1978) and since their work, Obermeir et al. (1992), Munson et al. (1997), and Pond and Martin (1997) have found evidence for four or more strong earthquakes (magnitude from 6.8 to 7.8) centered in southern Indiana. The fault system consists of a network of normal faults that trend North-Northeastward from Gallatin and White Counties in southern Illinois and adjacent Posey County in southern Indiana.

The faults in the WVSZ extend at least 97 km (60 miles) and span across an area that is about 48 km (30 miles) wide. The faults dip steeply to both the east and west, and displacements on parallel sets of faults have created sets of horsts and grabens in the subsurface beneath the region. Many of the faults have been penetrated by numerous petroleum test wells, but none of the faults are expressed at the surface.

According to the United States Geological Survey, on April 18, 2008, an earthquake of magnitude 5.4 occurred 35 km (20 miles) southwest of Vincennes, Indiana and 205 km (125 miles) SW of Indianapolis, Indiana. There is evidence that earthquakes stronger than the April 18 earthquake have shaken the region in the geologically recent past (Obermeier et al. 1993). Geological field studies in the past 20 years have identified paleoliquefaction features along the banks of rivers, and creeks indicate that at least eight strong earthquakes have occurred in the lower Wabash Valley region in the past 20,000 years, each having an estimated magnitude between 6.5 and 7.5. The largest of these paleoearthquakes is thought to have occurred about 6,100 years ago and was probably centered about 25 km (15 miles) west of Vincennes, Indiana. The shaking from

earthquakes in the magnitude range of 6.5 to 7.5 would be 20 to 200 times stronger than the April 18 earthquake (Obermeier et al. 1993).

In Figure 1.14, the locations of the New Madrid and Wabash Valley seismic zones are illustrated. In this USGS map, earthquakes are represented by circles and the larger the earthquake was the larger the circles are depicted. Red circles indicate earthquakes that occurred from 1974 to 2002 with magnitudes larger than 2.5 located using modern instruments. Green circles denote earthquakes that occurred prior to 1974.

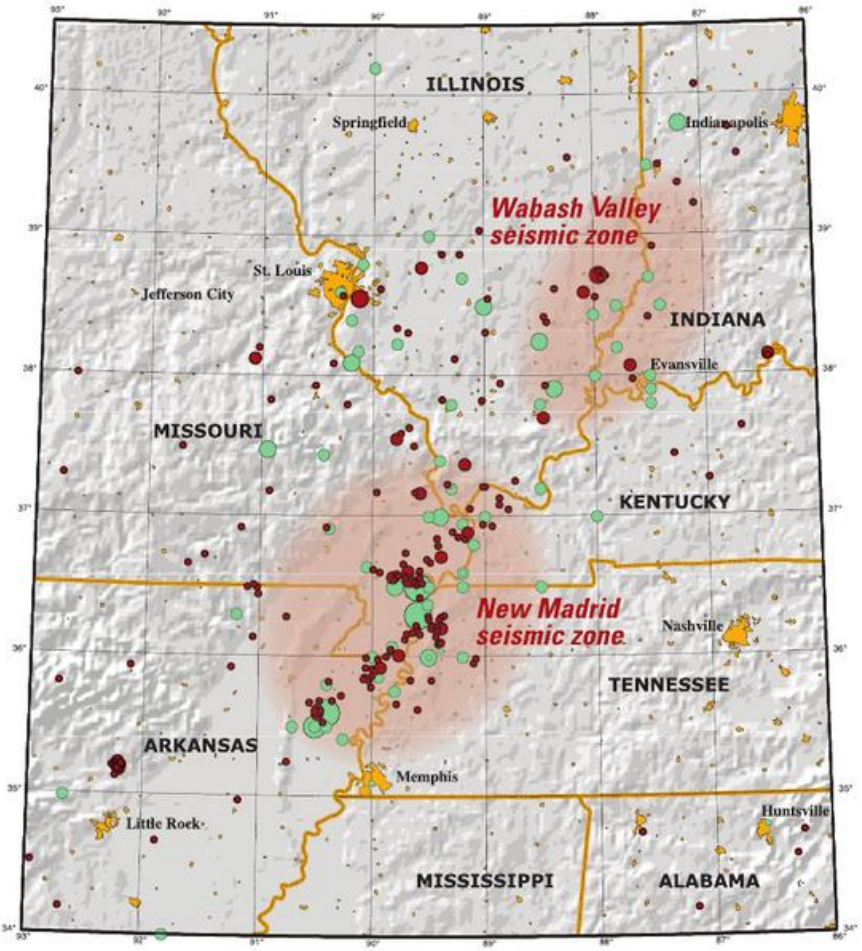

Figure 1.14: Topographic map showing earthquakes greater than magnitude 2.5 (circles) in the New Madrid Seismic Zone, (USGS, 2002).

Moderately damaging earthquakes have historically occurred at irregular intervals in this region, with a significant earthquake typically occurring every decade or so. The largest historical earthquake in the Illinois basin region was a magnitude 5.4 event in November 1968 that caused damage in southern Illinois. In June 1987, a magnitude 5.2 earthquake also struck southern Illinois, and a magnitude 3.9 earthquake occurred in southern Indiana on December 7, 2000. More recently a magnitude 4.6 near Darmstadt, in southwestern Indiana, occurred on June 18, 2002. Typically, smaller-magnitude earthquakes are felt in the area about once or twice a year. Because earthquake waves travel efficiently through the bedrock in the central and eastern United States as was discussed before, it is not surprising that this earthquake was felt hundreds of miles away, and as far south as Florida.

The WVSZ was originally suggested by Nuttli and Hermann (1978) and the proposed maximum-magnitude earthquake was 6.6 m_b and the magnitude recurrence relation was as follows:

$$\log_{10} N_c = 3.10 - 0.92m_b. \quad (1.2)$$

1.3.3 East Tennessee Seismic Zone (ETSZ)

The Eastern Tennessee Seismic Zone (ETSZ), which extends from the west tip of Virginia to northeast Alabama (Figure 1.15), is one of the most active earthquake areas in the southeast. Although the zone has not had a large earthquake in historic times, a few earthquakes have caused slight damage. The largest recorded earthquake in this seismic zone was a magnitude 4.6 that occurred in 1973 near Knoxville, Tennessee. Sensitive

seismographs have recorded hundreds of earthquakes too small to be felt in this seismic zone. Small, non-damaging, felt earthquakes occur about once a year.

On the basis of strain energy release, the Eastern Tennessee Seismic Zone (ETSZ) is the second most active seismic zone in the United States east of the Rocky Mountains (Powell et al. 1994). The largest earthquake to have occurred in the ETSZ is the November 30, 1973, event near Maryville, Tennessee which Stover and Coffman (1993) assigned a magnitude of 4.7 m_b and a maximum Mercalli intensity of VI to the event. Bollinger et al. (1989) suggested the recurrence relationship for the ETSZ as the following:

$$\log_{10} N_c = 2.75(\pm 0.10) - 0.90(\pm 0.04) m_b, \qquad (1.3)$$

where N_c is the cumulative number of earthquakes of m_b or greater occurring in the seismic zone in one year. Using this relationship, it is found that a 4.7 m_b event should occur about every 30 years in the seismic zone. Assuming Nuttli's 1981 recommended 1,000 year recurrence interval (Nuttli, 1981) to estimate the return period between maximum-magnitude earthquakes in eastern and central United States seismic source zones, the recurrence relationship of Bollinger et al. (1989) (using mean values) yields a body wave maximum magnitude of 6.4.

In Figure 1.15, the locations of the New Madrid and Wabash Valley seismic zones are illustrated. In this USGS map, earthquakes are represented by circles and the larger the earthquake was the larger the circles are depicted. Red circles indicate earthquakes

that occurred from 1974 to 2002 with magnitudes larger than 2.5 located using modern instruments. Green circles denote earthquakes that occurred prior to 1974.

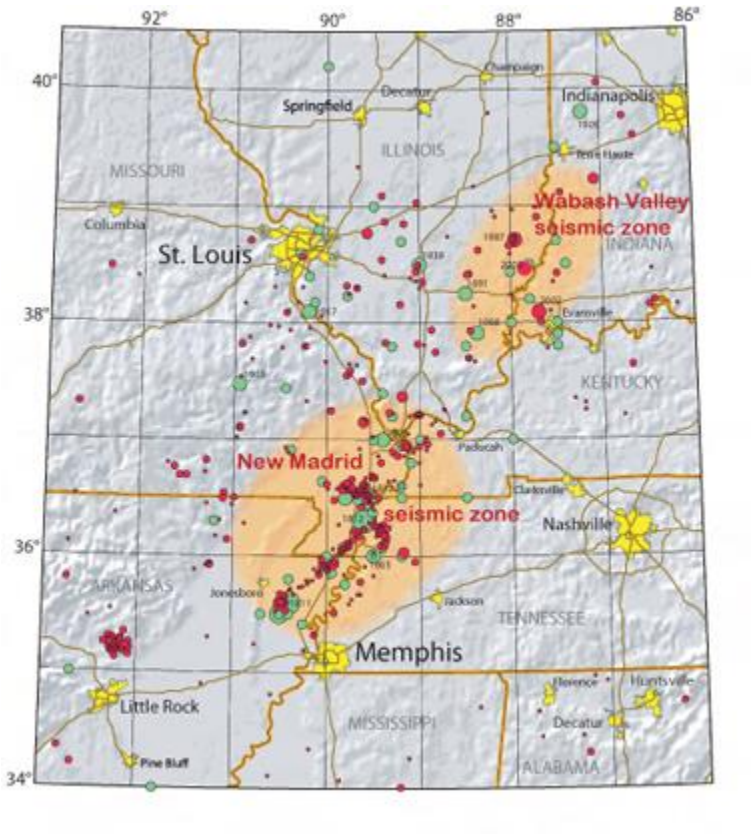

Figure 1.15: Topographic map showing earthquakes greater than magnitude 2.5 (circles) in the Wabash Valley, (USGS, 2002).

1.3.4 Northeast Kentucky and South-central Ohio Seismic Zone (NESZ)

A minor amount of earthquake activity has occurred in northeastern Kentucky south-central Ohio. Therefore, the seismic activity in northeastern Kentucky and south-central Ohio is incorporated into a seismic zone referred to as the Northeastern Seismic Zone (Figure 1.16). Several earthquakes of body wave magnitudes less than 3.5 have been

detected in this area since the installation of the University of Kentucky Seismic Network in the early 1980's.

Four damaging earthquakes with intensities greater than VI have occurred in the NESZ, with the largest one being associated with a body wave magnitude 5.2 event on July 27, 1980 near Sharpsburg, Kentucky. The Sharpsburg earthquake had a maximum Mercalli intensity (MMI) of VII, and caused approximately $4 million in damage over a five-county area in northern Kentucky (Street, 1982). The second largest earthquake in the NESZ is the Judy, Kentucky earthquake of September 7, 1988. It occurred approximately 11 km southeast of Sharpsburg, and was measured at 4.6 m_b. The event produced an MMI of VI (Street et al., 1993). In south-central Ohio, an MMI of VI earthquake occurred near Portsmouth, May 17, 1901, and a MMI of VII earthquake occurred near Pomeroy, on November 5, 1926. Stover and Coffman (1993), based on felt areas, estimated the body wave magnitudes of these earthquakes as 4.2 and 3.8, respectively.

Nuttli showed that for the seismicity in the New Madrid and Charleston, South Carolina, seismic zones, the historical and prehistorical earthquake recurrence data in those zones predicted the maximum magnitude earthquakes when averaged over a 1,000 years interval. Assuming this generality also holds true for the NESZ, Street and Woolery (2000) proposed the recurrence relationship as follows:

$$\log_{10} N_c = 1.95 - 0.9m_b. \quad (1.4)$$

This relationship predicts approximately four to five magnitude 4 events per 200 years, which agrees well with the observations.

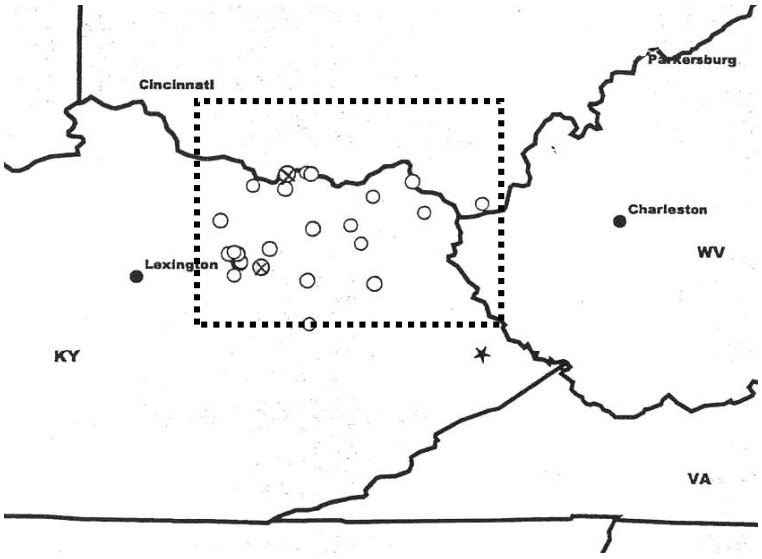

Figure 1.16: Map showing earthquakes with magnitudes between 1.0 to 4.99 which occurred between 1988 and 2000 in the Northeast Kentucky and South-Central Ohio, (After Street and Woolery, 2000).

1.3.5 Giles County seismic Zone (GCSZ)

Since at least 1828, the Giles County Seismic Zone of southwestern Virginia and adjacent West Virginia (Figure 1.17) has produced small earthquakes, as well as some larger damaging earthquakes. The largest damaging earthquake (magnitude 5.9) in the GCSZ occurred in 1897. Nuttli et al. (1979) and Street (1980) estimated the body wave magnitude of the earthquake to be 5.8. Smaller, slightly damaging earthquakes occur at variable intervals, but in the GCSZ they tend to occur a few decades apart. Still smaller earthquakes that cause no damage are felt once or twice a decade.

Bollinger et al. (1989) gave the recurrence relationship for the GCSZ as:

$$\log_{10} N_c = 1.065 - 0.64 m_b. \quad (1.5)$$

For a recurrence rate of 1,000 years, this equation yields a maximum-magnitude earthquake of 6.4.

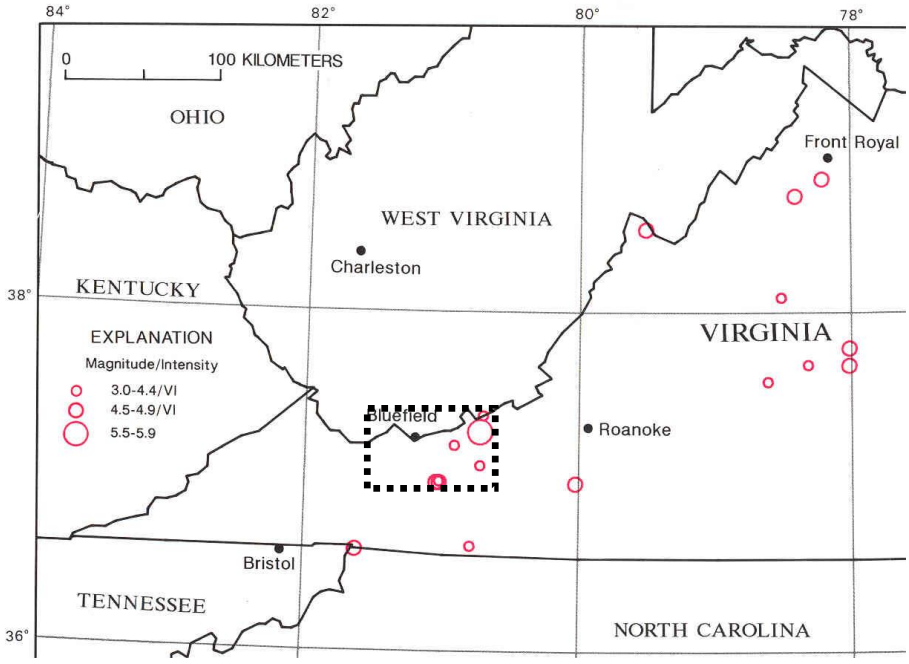

Figure 1.17: Earthquakes in Virginia with magnitudes > 4.5 or intensity > VI (After Stover and Coffman, 1993).

1.3.6 2011 Virginia Earthquake

The 2011 Virginia Earthquake occurred on August 23 within a previously recognized seismic zone, the Central Virginia Seismic Zone (Figure 1.11) as reverse faulting on a north or northeast-striking plane with a magnitude of 5.8. The Central Virginia Seismic Zone has produced small and moderate earthquakes since at least the 18th century. The previous largest historical shock from the Central Virginia Seismic Zone occurred in 1875. The 1875 shock occurred before the invention of effective seismographs, but the felt area of the shock suggests that it had a magnitude of about

4.8. The 1875 earthquake shook bricks from chimneys, broke plaster and windows, and overturned furniture at several locations. A magnitude 4.5 earthquake on December 9, 2003 also produced minor damage.

Previous seismicity in the Central Virginia Seismic Zone has not been causally associated with mapped geologic faults. Previous, smaller, instrumentally recorded earthquakes from the Central Virginia Seismic Zone have had shallow focal depths (average depth about 8 km). They have had diverse focal mechanisms and have occurred over an area with length and width of about 120 km (74.6 mile), rather than being aligned in a pattern that might suggest that they occurred on a single causative fault. Individual earthquakes within the Central Virginia Seismic Zone occur as the result of slip on faults that are much smaller than the overall dimensions of the zone. The dimensions of the individual fault that produced the August 23, 2011 earthquake will not be known until longer-term studies are done, but other earthquakes of similar magnitude typically involve slippage along fault segments that are 5 to 15 km (3.1 to 9.3 mile) long (Tarr and Wheeler, 2006).

1.3.7 Charleston Earthquake (1886)

The Charleston Earthquake of 1886 was a powerful intraplate earthquake that occurred at an epicenter near Charleston, South Carolina (Figure 1.11). The earthquake is estimated to have been between 6.6 and 7.3 on the Richter scale, with an MMI of X near the epicenter. After the 1811 and 1812 earthquakes in New Madrid, Missouri, it is one of the most powerful and damaging earthquakes to hit the southeastern United States. The

earthquake caused severe damage in Charleston, damaging 2,000 buildings and causing $6 million worth in damage (over $141 million in 2009 dollars), while in the whole city the buildings were only valued at approximately $24 million. Between 60 and 110 lives were lost. Some of the damage was still evident as recently as the late 1960s (Coffman and Von Hake, 1970).

Structural damage was reported several hundred kilometers from Charleston (including central Alabama, central Ohio, eastern Kentucky, southern Virginia, and western West Virginia), and long-period effects were observed at distances exceeding 1,000 kilometers (620 miles). Effects in the epicentral region included about 80 kilometers (~50 mile) of severely damaged railroad track and more than 1,300 square kilometers (~500 mi^2) of extensive cratering and fissuring. Damage to railroad tracks, about 6 kilometers (3.7 mile) northwest of Charleston, included lateral and vertical displacement of tracks, formation of S-shaped curves and longitudinal movement.

The formation of sand boils was widespread in the epicentral area, but surface faulting was not observed. Many acres of ground were overflowed with sand, and sand boils as much as 6.4 meters across were formed. In a few locations, water from the sand boils spouted to heights of about 4.5 to 6 meters (14.8 to 19.6 ft). Fissures 1 meter wide (3.3 ft) extended parallel to canal and stream banks. A series of wide cracks opened parallel to the Ashley River, and several large trees were uprooted when the bank slid into the river.

The intraplate epicenter of this major shock is not unique for large earthquakes in the Eastern and Central United States. Other intraplate earthquakes include those at Cape Ann, Massachusetts (1755) and New Madrid, Missouri (1811-1812). Earthquakes occurring along boundaries of plates (e.g., San Francisco, 1906) are well understood in terms of plate tectonics, but those occurring within plates are not similarly understood. This problem still is being studied more than 100 years after the earthquake. This earthquake was reported from distant places such as Boston, Massachusetts, Milwaukee, Wisconsin, Chicago, Illinois, Cuba, and Bermuda (Stover and Coffman, 1993).

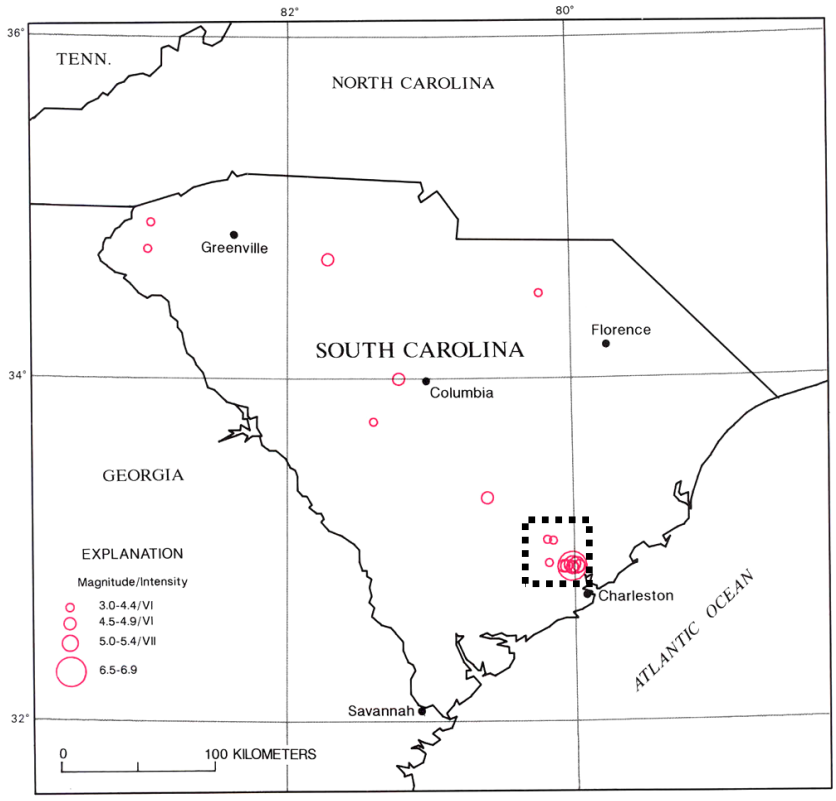

Figure 1.18: Earthquakes in South Carolina with magnitudes > 4.5 or intensity > VI (After Stover and Coffman, 1993).

1.4 Scope of Work and Dissertation Layout

This study was performed in three main phases: In situ testing, laboratory testing, and correlation between in situ tests results and laboratory results. These phases were followed in sequential order to enhance the understanding of the problem and provide information for the next stage. The chapters of this dissertation follow the same sequence and logical order as well.

1.4.1 In Situ Testing and Sampling Program

The University of Kentucky, in collaboration with Horn and Associates, Fugro Consultants, and GeoEnvironmental Associates, executed this phase of the study during the summer months of 2006 and 2007 at the selected sites. The selected sites included the Big Branch and Abner Fork tailings impoundments in eastern Kentucky. An extensive description of the history and dimensions of the sites is presented in Section 1.2. Most of the in situ tests in this study were performed in the fine-grained coal mine tailings, although some tests were carried out in the coarse-grained tailings material.

The in-depth field investigation program consisted of subsurface studies by performing Standard Penetration Tests (SPT), Cone Penetration Tests (CPT), and vane shear tests. In some of the testing locations, the CPT tests were accompanied by pore water pressure and shear wave velocity measurements (sCPTu). Also, in some locations the shear wave velocity profiles were acquired using the Spectral Analysis of Surface Waves (SASW) and downhole seismic methods. An in-depth description of the equipment and methods applied in this study to perform the in situ tests are provided in Chapter 2.

The in situ tests were performed at two points in two locations (toe and crest) of the embankment at each impoundment. One of these points was assigned to CPT testing and the other was used for the SPT tests, vane shear tests, and piston sampling. Therefore, a total of 4 CPT profiles were provided, with two of them being the sCPTu type. The CPT profiles extended to approximately 150 to 230 ft (45.7 to 70.1 m). The SPT tests were performed at approximately 20-ft (6-m) intervals following the ASTM D6066 standard using a truck-mounted automatic hammer.

The main objective of this study was to provide a liquefaction assessment method based on in situ testing techniques common in geotechnical engineering practice. However, to establish this method based on the dynamic geotechnical properties of the coal mine tailings material, an in depth laboratory testing program was required. Therefore, at 20-ft (6-m) intervals between the SPT testing depths, piston sampling was performed to obtain undisturbed fine-grained coal mine tailings. The sample tubes were transported to the geotechnical laboratory of the University of Kentucky for laboratory testing. At a depth of approximately 3 ft (0.9 m) below each of SPT and piston sampling depth, a vane shear test was performed to measure the peak and residual shear strength of the material.

1.4.2 Laboratory Testing Program

The primary objective of the laboratory testing program was to characterize the large strain dynamic and strength properties of the fine grained coal mine tailings stored at the tailings impoundments.

The majority of the laboratory testing program was devoted to performing cyclic triaxial tests at the geotechnical laboratory of the University of Kentucky. Basic geotechnical tests including water content, specific gravity, Atterberg limits, and gradation analysis were part of the geotechnical characterization study. Also, after performing cyclic triaxial tests on undisturbed coal mine tailings samples, they were subjected to Unconsolidated Undrained (UU) compression triaxial tests. Following the triaixial tests, the post cyclic peak and residual shear strength of the material was measured through performing laboratory vane shear tests. Detailed description of the procedures and the equipment used in this phase of the study as well as the methodology followed to obtain "undisturbed" samples are presented in Chapter 3.

The differences in the geotechnical properties of the two selected impoundments provided an opportunity to study the influence of various factors on the geotechnical behavior of fine grained coal mine tailings. The investigated factors included plasticity, void ratio, confining stress, age, and the applied deviator stress. The provided samples had a moderate range of plasticity from 0-16% and a relatively wide range of void ratio from 0.51 to 1.23. These plasticity properties of the material along with the void ratio proved to be significant factors in determining the dynamic behavior of coal mine tailings. Approximately, 140 cyclic triaxial tests were performed during the laboratory studies, which 40 of them were to investigate the liquefaction properties of the material and 100 of them were devoted to measure the shear modulus and damping properties of the material.

The laboratory results of some of the representative samples are discussed in detail in Chapter 4. The results of each individual test are presented in Appendix A. Appendix A1 presents the cyclic triaxial results, Appendix A2 provides the post liquefaction UU triaxial tests, and Appendix A3 presents the results of the cyclic triaxial tests performed to measure the shear modulus and damping properties. In Appendix B, the procedures followed to perform the cyclic laboratory tests with the available equipment is presented.

In Chapter 4 the results of representative samples from various laboratory tests are discussed and the influence of various geotechnical properties on the results are reviewed. Also, the effectiveness of various criteria to assess the liquefaction susceptibility of the fine grained coal mine tailings are investigated.

1.4.3 Correlation between Laboratory and Field Results

The main objective of this study was to provide a method to predict the dynamic behavior of coal mine tailings based on in situ testing results. After completion of the laboratory program and achieving in-depth knowledge of the dynamic properties of the material, the laboratory results were correlated to the field results. Therefore, by performing some common in situ testing techniques and following the proposed correlations, an in depth understanding of the dynamic behavior of coal mine tailings would be achieved without the need to perform such complicated laboratory tests. These correlations are presented in Chapter 5.

An overall review of the study and the conclusions are provided in Chapter 6. These conclusions include an assessment of the quality of the correlations and suggestions for future studies. It was found that some of the results were site dependent and therefore due to the limited number of samples, further studies are required to propose comprehensive guidelines for liquefaction assessment of fine grained coal mine tailings. However, this study provides an overall assessment of the dynamic behavior of the investigated material and therefore the results can be used in dynamic geotechnical analysis of similar investigations with engineering judgment.

Chapter 2

In Situ Testing

2.1 Introduction

The need for a thorough geotechnical assessment of coal mine tailings impoundments was brought to light by the incidence of earthquake-induced failures of such impoundments around the world, the significant number of these structures in the close proximity of active seismicity in the United States, and the shortcomings in the state-of-practice construction techniques. A significant portion of this study was devoted to obtaining the in-situ geotechnical properties of coal mine tailings to ensure that the mechanisms involved in the failure were well understood and that the profession was not ignoring potentially important earthquake hazards. In this chapter, the procedures followed to obtain the in-situ geotechnical properties of the coal mine tailings material are presented.

2.2 In Situ Tests and Locations

The field testing program consisted of undisturbed sampling, disturbed sampling, and in-situ testing. In-situ tests included Standard Penetration Tests (SPT), vane shear, Cone Penetration Test (CPT), and downhole seismic testing. Undisturbed and disturbed sampling was performed by piston sampling and SPT sampling respectively. For each impoundment, two testing locations were chosen which consisted of the crest and the

toe of the most recent embankment as shown schematically in Figure 2.1. These locations were selected such that both coarse and fine tailings material of different ages and consolidation pressures would be tested and sampled.

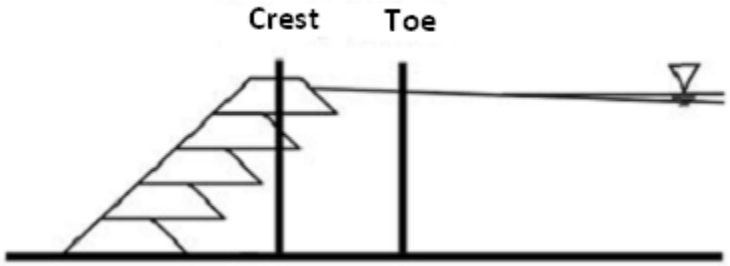

Figure 2.1: Schematic sampling locations at each impoundment.

Since fine refuse is more influential in the overall stability of the structures, particularly in the upstream construction method, most of the testing was performed in the fine refuse material. At each location, two testing spots were selected 20 ft (6 m) apart and used for various tests as shown in Figure 2.2 and Figure 2.3.

Figure 2.2: Performing sCPTu and SPT testing at location A (crest) at Abner Fork.

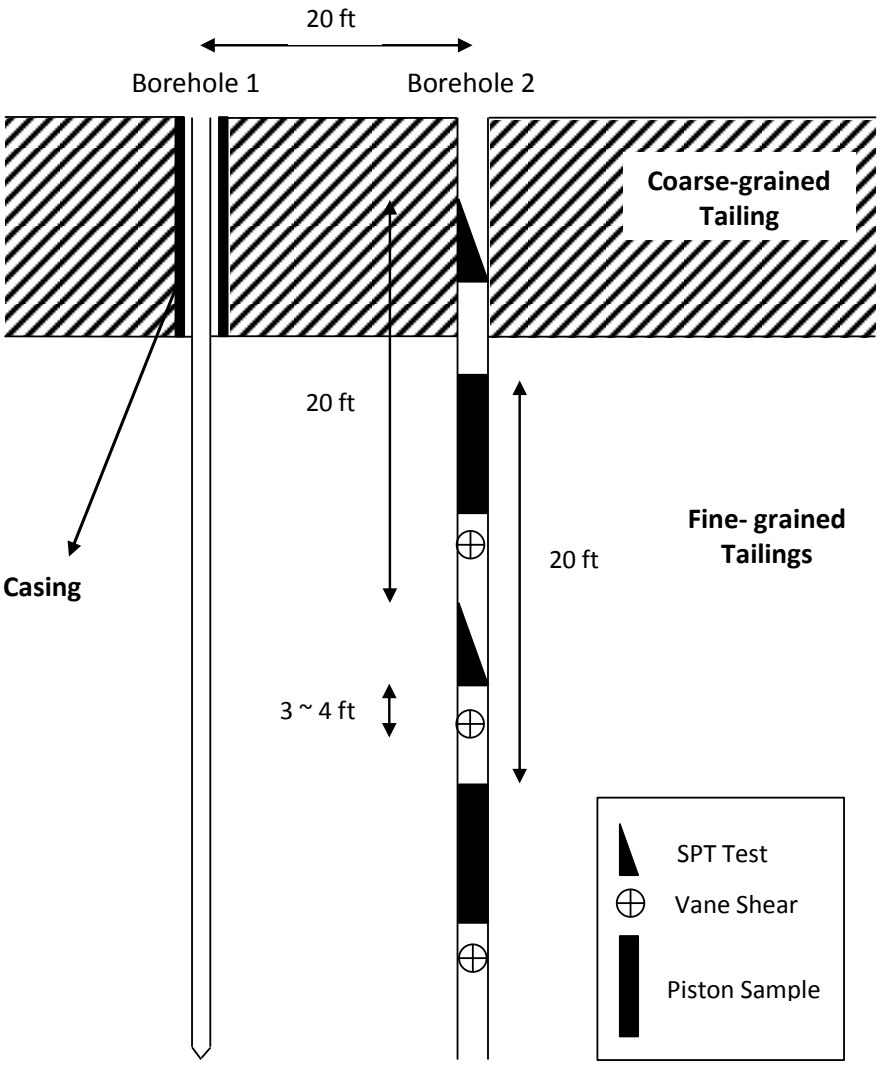

Figure 2.3: Schematic presentation of in-situ tests and testing intervals at each location.

According to Robertson (2013), the minimum spacing between adjacent SPT and CPT bore holes should be 10 times the diameter of the borehole in order to minimize the soil matrix disturbance due to SPT testing. In this study, considering the approximate borehole diameter of 8.0 in, the 20 ft (~ 610 cm) distance between two holes appears to be sufficient compared to the prescribed distance (20 ft > 10 × 8 in) . At each of these locations, the following were performed:

- In borehole 1, the coarse refuse was drilled to the top of the fine refuse layer, casing was installed, and seismic cone penetrometer testing with pore pressure measurement (sCPTu) testing was performed to the bottom of the fine refuse material.
- In borehole 2, standard penetration testing (SPT) was performed in the coarse and fine refuse at a depth interval of 20 ft (6 m).
- In borehole 2, through the fine refuse layer, fixed piston samples were obtained at a depth interval of 20 ft (staggered by 10 ft relative to the SPT testing), and vane shear tests were carried out following the SPT and piston samples at a depth interval of 10 ft (3 m).
- In borehole 2, after performing the fixed piston sampling, SPT and vane shear tests, PVC casing with a cap at the bottom was installed. The casing was filled with water to counter balance the buoyancy forces of grouting while the grout cured. Once the grout cured, the casings were bailed.

At each impoundment, the crest and toe location were denoted by different letter codes as depicted in the aerial photos in Figure 2.4, Figure 2.5, and Figure 2.6.

Figure 2.4: Testing and sampling locations at Abner Fork impoundment, (Google Maps, 2013a).

Figure 2.5: Testing and sampling locations at Big Branch impoundment, (Google Maps, 2013b).

Figure 2.6: (a) Test locations D and A at Big Branch, (b) Test locations A and B at Abner Fork.

At Abner Fork, location A was situated on dry, competent material near the crest of the most recent dike, and was accessible by conventional equipment. Location B was situated within the soft beach portion of the impoundment, which restricted operation of heavy drilling and sampling equipment. Therefore, testing at location B was performed by constructing a pad of coarse refuse out into the impoundment, which served to distribute surface pressures and allow equipment to be operated on a "peninsula" that extended out into the beach area as depicted in Figure 2.7. This approach has been used for other tailings dam investigations (e.g. Vidich et al., 1998), and proved to be a successful method in this study as well. At Big Branch, location D was situated on the crest

and location D was located at the soft beach. The same methodology used at Abner Fork was applied for testing and sampling at Big Branch.

Figure 2.7: Performing sCPTu test at location B (beach, toe) at Abner Fork.

Due to the displacement of fine refuse with coarse refuse in the pool during upstream construction, depth to fine refuse was about 50% greater than expected at both locations (Kalinski and Phillips, 2008). Therefore, the thickness of the fine refuse layer was less than expected and as a result, less in-situ tests and undisturbed sampling were performed than the initial plan. Field sampling yielded a total of 16 piston samples, 27 vane shear tests, and 43 SPT tests at both impoundments combined. The sCPTu produced continues profile of the CPT tip resistance and shear wave velocities. In addition, 14 measurements for shear wave velocity and the dissipation of excess pore water pressure during the sCPTu was carried out at Abner Fork. The number of various in-situ tests performed at each impoundment is provided in Table 2.1.

Table 2.1: Number of in-situ tests at each impoundment

Tailings Dam	Location	Date	SPT	Vane Shear	Piston Sample	CPT Shear Wave
Abner Fork	A	Aug-06	18	3	3	6
	B	Aug-06	7	5	3	8
Big Branch	A	Aug-07	9	11	6	0
	D	Aug-07	9	8	4	0
Total			43	27	16	14

2.3 In Situ Testing Procedures

In this study, a significant part of the information collected regarding the mechanical behavior of the coal tailings material is provided by the in-situ properties of this material. The field geotechnical investigation at each of the selected impoundments included the following:

- CPT and SCPTu testing;
- Downhole seismic testing;
- SPT testing;
- Fixed piston sampling; and
- Vane shear testing.

In the following sections, a detailed description of the equipment and procedures used to perform these tests is presented.

2.3.1 Cone Penetration Test (CPT)

Cone penetration testing (CPT) was performed by Fugro Consultants following the ASTM D3441-98 standard. The Abner Fork testing was performed using a truck-mounted

rig (Figure 2.7) while the Big Branch testing was performed using a track-mounted rig (Figure 2.8). Different rigs were used due to the availability of equipment during testing (summer 2006 for Abner Fork and summer 2007 for Big Branch). The cone angle was 60° with a cone base area of 15 cm^2 (shown in Figure 2.9b) and a cone area ratio of $a = 0.80$. The piezocone was located behind the cone and the length of the friction sleeve, located above the cone, was 30 cm and the rod increments length was 100 cm (Figure 2.9a).

Figure 2.8: CPT equipment used at the Big Branch impoundment.

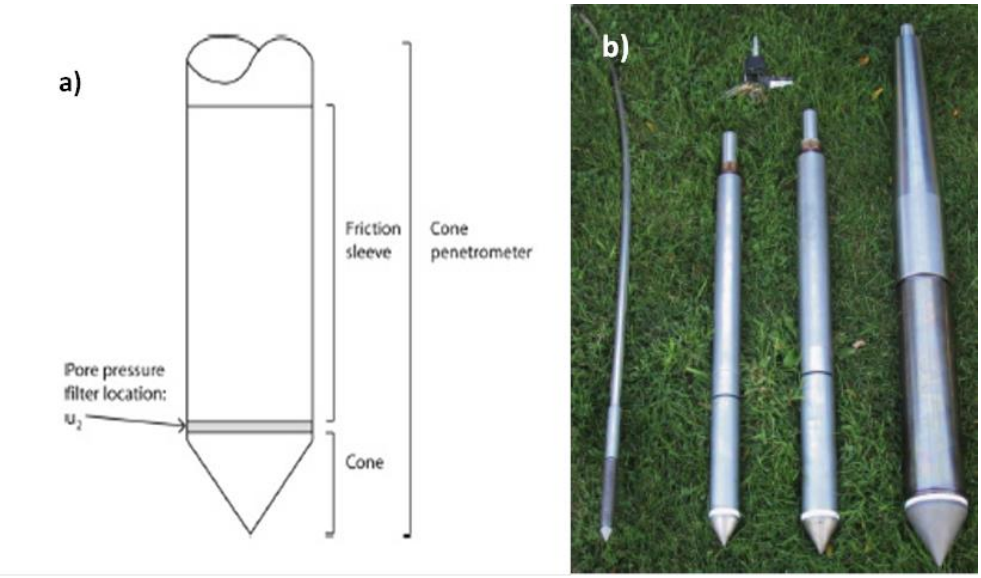

Figure 2.9: a) CPT probe terminology, b) Range of CPT probes, from left, 2cm^2, 10 cm^2, 15 cm^2, and 40 cm^2 (Robertson, 2010).

Tip resistance, sleeve friction, and pore water pressure were measured at 2-cm intervals. The rate of penetration constantly was held at 2 cm/sec (~0.8 in/sec) through fine refuse layers. Pushing the CPT cone directly through the coarse refuse would ruin the cone. Therefore, at the crest of the tailings dam, a pilot hole was drilled through the coarse refuse material to the top of the fine refuse. The casing was installed to prevent caving of the coarse refuse material into the drilled hole and the CPT sounding was started at the bottom of the hole (i.e. top of the fine refuse).

2.3.2 Seismic Cone Penetration Test (sCPTu):

The CPT test described in Section 2.3.1 was accompanied by shear wave velocity measurements at 10-ft (3.0-m) intervals, where shear wave arrival is measured using an accelerometer installed on the probe. At 10-ft (3.0 m) intervals, the CPT cone was

stopped, and the induced excess pore pressures were measured as they dissipated. After the dissipation of the excess pore water pressure, the CPT truck was jacked up slightly by a hydraulic jack placed on a steel beam as illustrated in Figure 2.10.

Figure 2.10: Performing seismic CPT test using a sledge hammer.

A downgoing shear wave was generated by hitting the steel beam with a sledge hammer in the horizontal direction similar to a golf swing. An accelerometer in the hammer was used to mark the start time of the wave, and the accelerometer in the cone was used to detect the downgoing wave (Figure 2.11). The depth of the cone is divided by the difference in arrival times between the hammer and the cone to calculate the average S-wave velocity, and the average S-wave velocity profile is inverted to calculate the variations in S-wave velocity with depth. After a given measurement was performed, the truck was lowered and pushing of the cone was resumed.

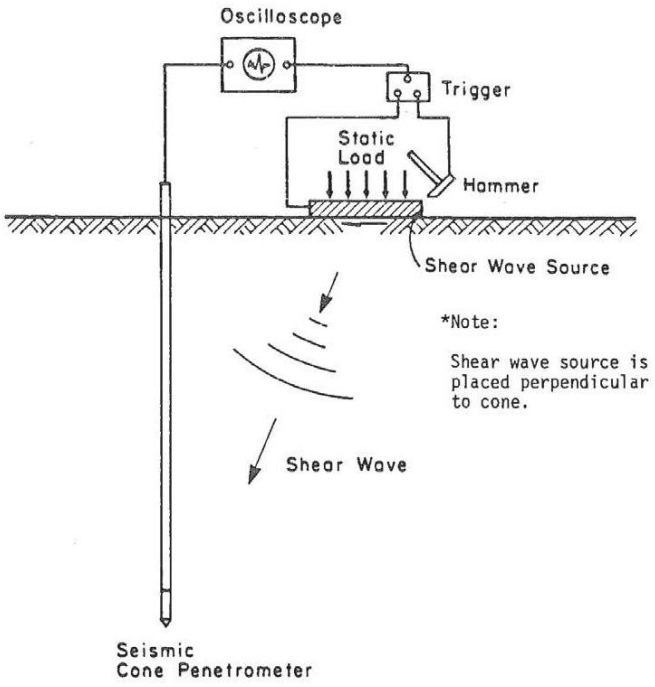

Figure 2.11: Schematic layout of downhole seismic cone penetration test, (Robertson et al., 1986).

2.3.3 Soil Borings

The soil testing was performed by Horn and Associates of Winchester, Kentucky using the drill rig shown in Figure 2.12. Soil tests included fixed piston sampling, SPT testing, and vane shear testing following ASTM standards D1587, D1586, and D2573, respectively. Drilling was performed using the hollow stem auger method. Drilling was stopped every 10 ft (3 m) and either a fixed piston or a SPT test was performed. The testing was alternated between SPT and piston sampling. Also, after each of the SPT testing and fixed piston sampling, (i.e. 10 ft intervals), a vane shear test was performed.

Figure 2.12: Performing drilling, SPT testing, and fixed piston sampling at Big Branch.

2.3.4 Standard Penetration Test (SPT)

The SPT tests were performed by Horn and Associates Inc. using a truck mounted rig model D-120 made by Diedrich Drill with a mast elevation of 26 feet (~8 m). The drilling was performed in the coarse and fine deposits following the ASTM D1586 standard by using hollow stem auger method with 4.25 in (~10.8 cm) internal diameter augers to prevent caving of the coal mine tailings.

Standard Penetration Test (SPT) is a commonly used in-situ testing method to evaluate the liquefaction susceptibility of soil material. In this test, a standard 140-lb (63.5 kg) hammer is lifted 2.5 feet (76 cm) and dropped on a surface and the impact energy is transmitted to the split spoon sampler at the bottom of the borehole via the attached rods. The number of blows to penetrate 1.5 feet (~46 cm) in the soil in three 6 inch (15.2

cm) intervals is recorded and the summation of the number of blows for the last foot is presented as the SPT number of blow counts (N). After performing the penetration, the sampler is pulled out of the borehole and the disturbed sample contained in the split spoon sampler is retrieved. A schematic presentation of the sampler is shown in Figure 2.13. The application of the hammer blows can be performed by the operator or via an automatic system. If the operator is lifting the hammer, the system includes a rope, pulleys, and a cathead.

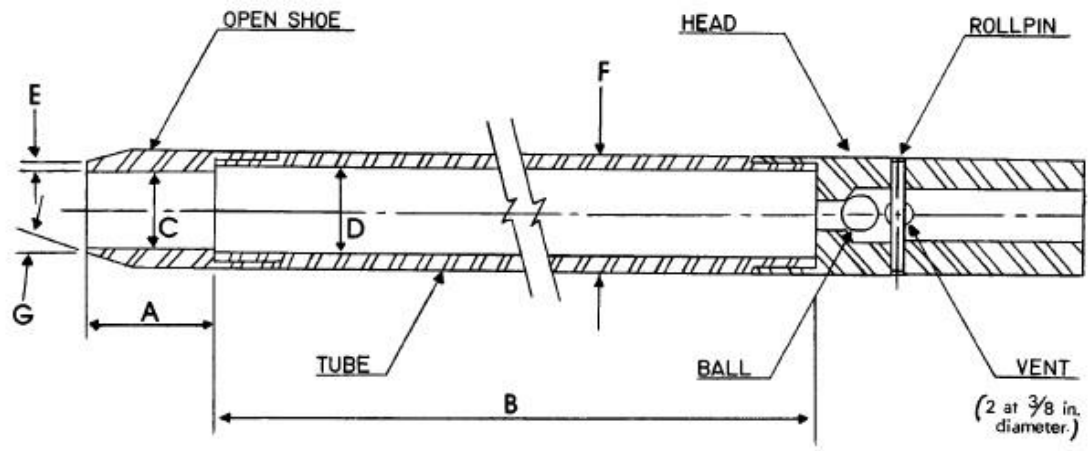

A = 1.0 to 2.0 in. (25 to 50 mm)
B = 18.0 to 30.0 in. (0.457 to 0.762 m)
C = 1.375 ± 0.005 in. (34.93 ± 0.13 mm)
D = 1.50 ± 0.05 − 0.00 in. (38.1 ± 1.3 − 0.0 mm)
E = 0.10 ± 0.02 in. (2.54 ± 0.25 mm)
F = 2.00 ± 0.05 − 0.00 in. (50.8 ± 1.3 − 0.0 mm)
G = 16.0° to 23.0°

Figure 2.13: Schematic presentation of split-barrel sampler, (ASTM D1586).

One of the key pieces of information in performing this test is the percentage of the delivered energy from the hammer to the sampler during penetration. The percentage of the delivered energy to the sampler, energy ratio, depends on many factors including the hammer type, the hammer release mechanism, diameter of the cathead, size of the cathead, size of the rope, number of wraps of the rope around the cathead,

hammer type, rod diameter, tightness of the rod connections, verticality of the rod string, and the experience of the operator. In this study, an automatic trip hammer system was used and therefore many human errors involved with the rope and cathead system were avoided. The human errors usually are in the form of inconsistencies in applying the hammer blows and therefore resulting in less accurate results. However, it should be noted that the number of blows required to penetrate 1 ft (30.5 cm) in the soil is recorded by the operator and therefore, even by using an automatic hammer, the human error factor is not completely obliterated. At the end of the penetration test, the split spoon sampler is pulled out of the borehole and the sample is retrieved as shown in Figure 2.14. The obtained disturbed sample can be further evaluated in the laboratory.

Figure 2.14: An example of the SPT sampler and the obtained disturbed sample.

2.3.5 Downhole Seismic Testing

To measure the shear wave velocity of the tailings material at various depths, a series of downhole seismic tests were performed. At each testing location, at the end of drilling and performing various tests such as the SPT tests, vane shear tests and piston sampling, the borehole was prepared for downhole seismic test. Casing and grouting was performed to support the walls of the boring and prevent caving of the tailings material. To perform high quality shear wave velocity measurements, an accelerometer was installed on an inflatable packer and lowered to the desired depth. The method of using an inflatable packer is patented (Kalinski, 2012). The method for performing the downhole seismic test was the widely used accepted technique in the industry, although at the time of testing, an ASTM procedure did not exist. This method is identical to the standard procedure introduced in ASTM D7400-08.

2.3.6 Spectral Analysis of Surface Waves (SASW)

SASW testing consists of measuring the surface wave dispersion curve [i.e., a plot of Rayleigh wave velocity versus frequency (or wavelength)] at the site and interpreting it to obtain the corresponding shear wave velocity profile. A dynamic source is used to generate surface waves of different wavelengths (or frequencies) which are monitored by two or more receivers at known offsets. Data from forward and reverse profiles are averaged together. An expanding receiver spread is used to avoid near field effects associated with Rayleigh waves and the source-receiver geometry is optimized to

minimize body wave signal. During data analysis, all phase data are manually checked through an interactive masking process to discard low quality data. The measurement and interpretation of dispersion curves obtained in this way, known as Spectral Analysis of Surface Waves (SASW) (Heisey et al., 1982; Nazarian et al., 1983; Stokoe et al., 1994), is one of the most significant recent advances in shallow seismic exploration (Kramer, 1996). In this study a sledge hammer was used as the dynamic source.

2.3.7 Undisturbed Sampling

Undisturbed sampling using the fixed piston sampling technique was performed at 20-ft (6-m) intervals through the fine refuse layer. The samples were obtained using 30-in long (76.2 cm), 3.000-in outer diameter (7.62 cm), 2.875-in (7.32 cm) inner diameter steel Shelby tubes pushed by a hydraulic jack installed on the drill rig. To prevent sample slipping due to gravity during lifting from the bottom of the hole to the surface, a fixed piston sampler was used to provide suction on the tube and hold the sample inside. In Figure 2.15, a schematic illustration of the Osterberg piston sampler used in this study is presented. To prevent the loss of moisture, the top and bottom of the tubes were sealed with wax and sealed with plastic bags, plastic caps, duct tape, and electric tape.

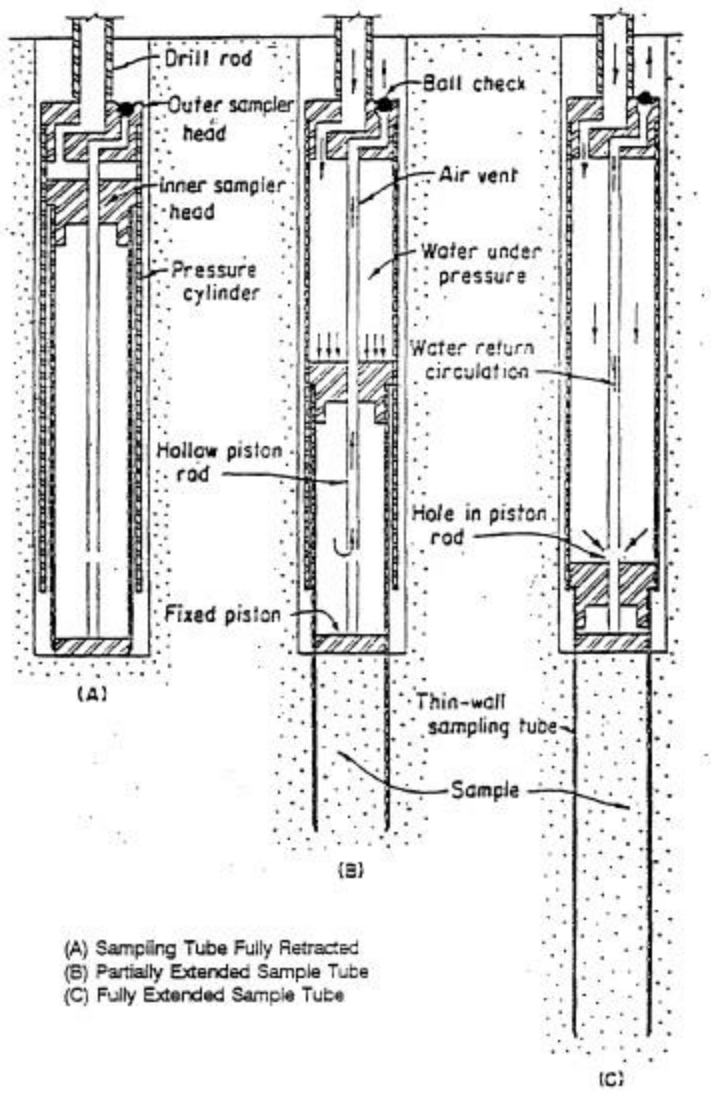

Figure 2.15: Schematic presentation of fixed piston sampler.

2.3.8 Field Vane Shear Test

At 10 ft intervals (3 m), vane shear tests were performed using a shear vane in compliance with ASTM D2573. The tapered vane had a 45° angle and height and diameter of 100 mm (3.94 in) and 50 mm (1.97 cm) respectively following the ASTM recommended 2:1 ratio as shown in Figure 2.16 and Figure 2.17. The vane shear testing was performed 3 ft (~0.9 m) below the SPT or fixed piston sampling point and was performed at a torque

rate of about 6° per minute. These measurements provided peak undrained shear strength, S_p, and residual undrained shear strength, S_r, for the fine refuse coal tailings material at various depths. Shear force was calculated using a torque wrench (Figure 2.18), and was converted to shear strength based on the dimensions of the vane.

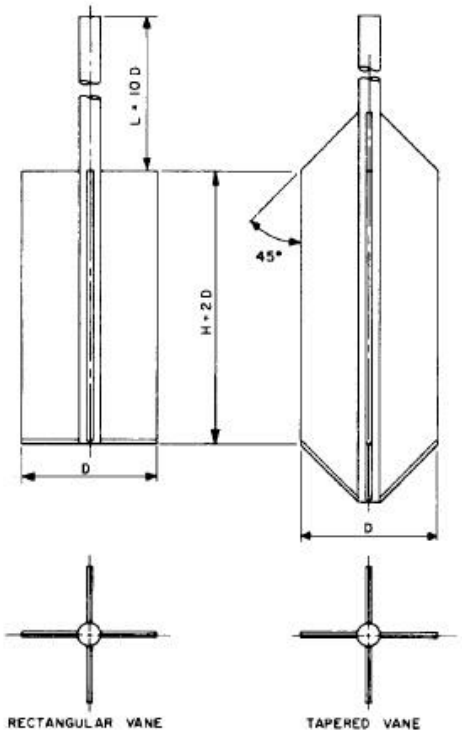

Figure 2.16: Geometry of field vanes, (ASTM D2573).

Figure 2.17: Tapered vane used for in-situ vane shear test.

Figure 2.18: Measuring in-situ undrained shear strength using a torque wrench.

Chapter 3

Sampling and Laboratory Testing

3.1 Introduction

In this chapter, the methodology followed to obtain undisturbed samples in the field is discussed. Also, the procedures and equipment used to perform laboratory cyclic triaxial tests and vane shear tests are explained. Additional laboratory geotechnical tests included moisture content, specific gravity, Atterberg limits, and gradation analysis tests which were performed following the ASTM D2216, D854, D4318, and D422 standards, respectively.

The main objective of this research was to correlate the in-situ geotechnical behavior of the coal mine tailings to the laboratory parameters. Therefore, following the in-situ testing, undisturbed samples were retrieved by fixed piston sampling and were transported to the geotechnical laboratory of the University of Kentucky.

3.2 Field Sampling Locations

As was mentioned in Chapter 2, two impoundments were selected for in-situ geotechnical testing and sampling. At each of these impoundments, field testing locations were determined based on the current construction stages. As seen in the schematic in Figure 3.1, both dams were tested on the crest and the toe of the most recent dike. Sampling at the crest allowed for retrieving samples of varying ages, representative of varying stages of consolidation due to excess overburden pressures. To perform testing

and sampling at the toe, beaches were constructed out in the slurry pool as shown in Figure 3.2. Sampling at the toe provided newly deposited coal mine tailings specimens.

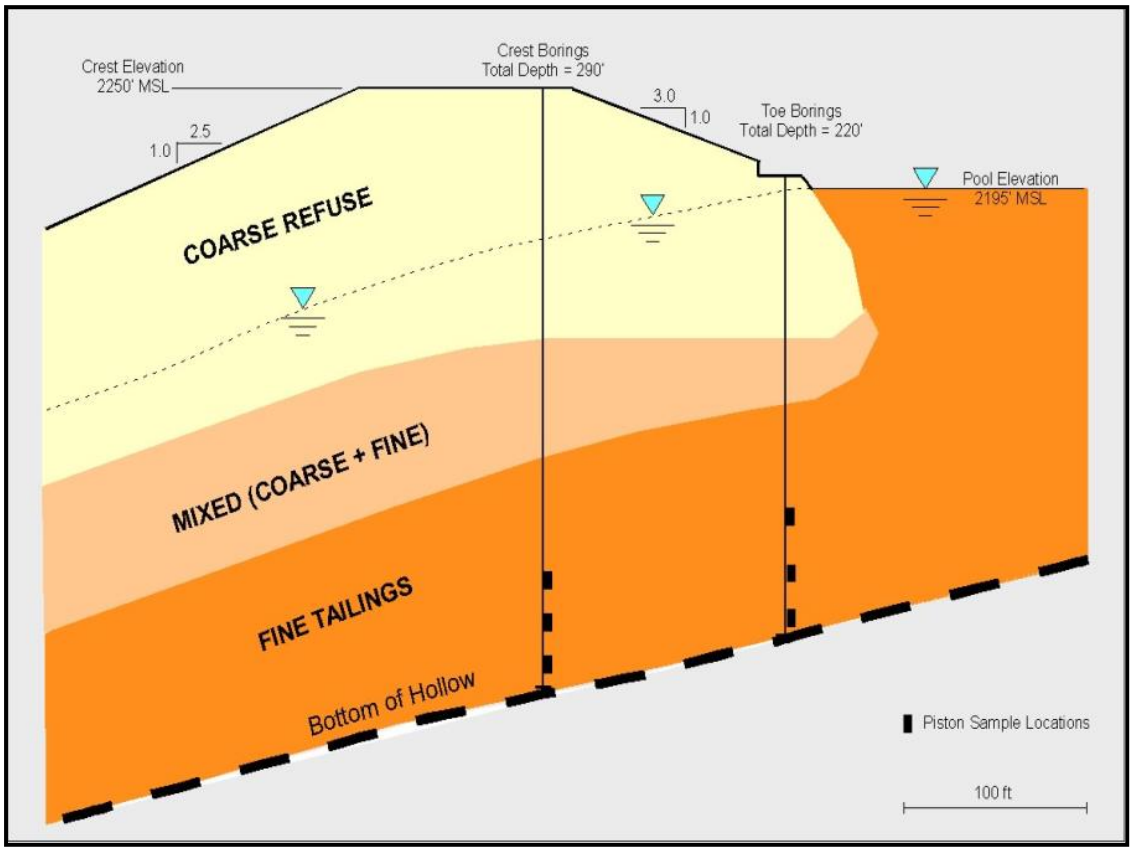

Figure 3.1: Schematic Illustration of the field testing and sampling locations (shown for Abner Fork).

Figure 3.2: Constructed beach in the slurry pool.

3.3 Field Sampling Procedures

Observations in the past studies (Ishihara et al., 1981) indicate that in both silt sized and sand sized tailings, cyclic strength of in-situ material is better evaluated by testing undisturbed samples rather than reconstituted specimens. Therefore, in this study, the dynamic behavior of tailings was studied by obtaining undisturbed samples. Undisturbed samples were obtained by fixed piston sampling method following drilling to the desired sampling depth. Piston sampling was performed by Horn and Associates using stationary piston sampling equipment. As mentioned in Chapter 2, at the borehole used to perform Standard Penetration Testing (SPT), undisturbed sampling was performed as well. The sampler tool was a stationary piston sampler which obtained samples in steel

tubes of constant internal diameter with an inside and outside diameter of 2.875 in (7.62 cm) and 3.000 in (7.32 cm), respectively. An exterior rod string was used to push the tubes into the tailings while the “fixed piston” was attached to an internal rod string that was not allowed to move. Using a hydraulic jack mounted on the drilling equipment, the tubes were pushed a length between 20 in (~51 cm) to 30 in (~76.2 cm). This method is commonly used in soft, sensitive materials to minimize sample disturbance.

Following the removal of the tubes from the borehole, the Shelby tubes were detached from the sampler, cleaned, and sealed with wax, a plastic bag, plastic cap, duct tape, and electrical tape. The tubes were placed in a transportation box in upright position and were transported by a truck from the impoundment to the geotechnical laboratory of the University of Kentucky.

In any soil laboratory testing based on undisturbed samples, the stress-strain response of the specimens are influenced by the stress changes and straining during sampling, handling, transportation, and sample preparation. The effects are summarized under the term sample disturbance.

3.4 Sample Disturbance

During soil sampling, the sampler tube affects the structure of the soil matrix by applying shear deformations and changing the in situ stress. Also, the water content, void ratio, and the soil structure may be influenced further more during handling, transportation, storage, and sample preparation. During storage, prolonged exposure to

untreated containers such as steel tubes may also change the chemical content of the soil structure (Hvorslev, 1949).

During deposition of soil material in a sedimentary environment like a lake or the sea, the overburden stress is gradually built up as additional material is deposited from above. As the overburden increases, the sediments consolidate and decrease in volume. If the area of deposition is relatively large compared to the thickness of the deposit, then the compression can be considered essentially one-dimension. In this case the stress ratio would be constant and equal to the coefficient of earth pressure at rest, K_0 (Holtz et al., 2011). Figure 3.3 presents the stress path during sedimentation and consolidation.

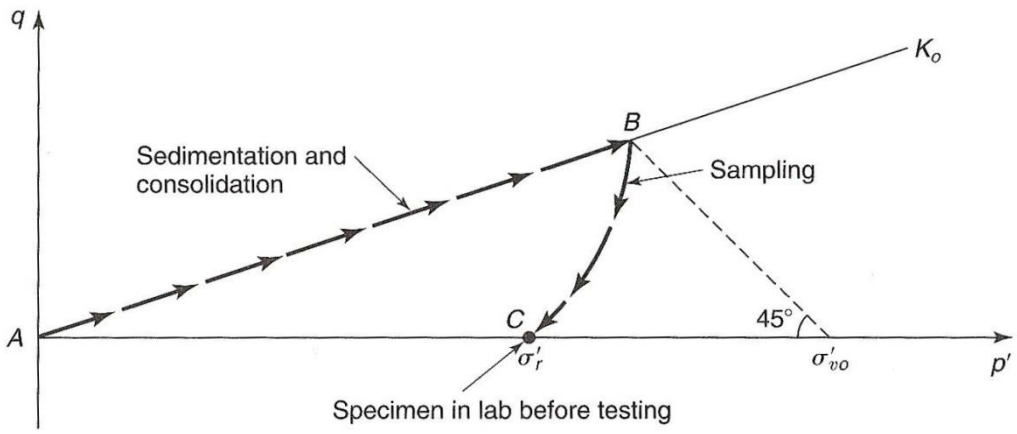

Figure 3.3: Stress path during sedimentation and sampling of normally consolidated clay, K_0<1, (Holtz et al, 2011).

The hypothetical stress path that a soft, nearly normally consolidated clay may experience between the sampling and the laboratory testing is presented in Figure 3.4. In Figure 3.4, point 1 corresponds to point B in Figure 3.3. As can be seen in Figure 3.4, sampling has the greatest effect on changing the stress history of the specimen. The loading of the specimen from in situ stresses to failure is represented by stress path 1-A,

while the stress path 9-B shows the loading of a typical undisturbed sample in the laboratory to failure. As it is illustrated in this figure, the measured undrained shear strength, represented by point B, is often much less than in situ strength, denoted by point A. By following the recommendations provided by various researchers (Hvorlslev, 1949; Hight et al., 1992; Hight and Georgiannou, 1995; and Ladd and DeGroot, 2003), the effects of sample disturbance can be minimized.

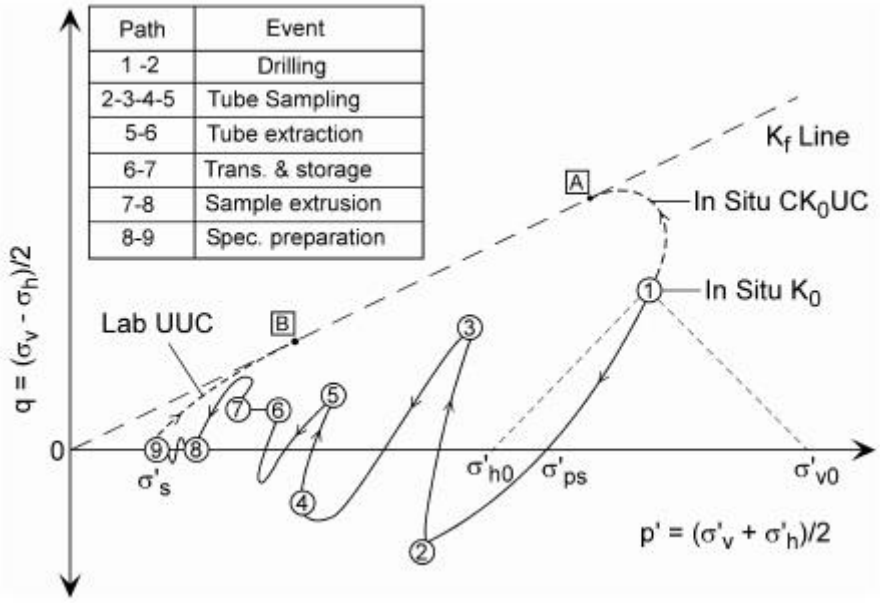

Figure 3.4: Hypothetical stress path during tube sampling and specimen preparation of a soft, nearly normally consolidated clay (Ladd and DeGroot, 2003).

For an ideal laboratory test, it can be assumed that the stress path followed during loading is identical to stress path 1-A. However, even the most meticulous sampling effort can result in a loss of shear strength of up to 10% (Holtz et al, 2011; Skempton and Sowa, 1963; Ladd and Lambe, 1963; and Noorany and Seed, 1965).

3.4.1 Disturbance during Sampling

For a soil element under level ground surface, the in situ mean effective stress is defined as

$$p'_0 = \sigma'_{v0}.\frac{(1+2K_0)}{3} \quad (3.1)$$

Where σ'_{v0} is the vertical effective stress and K_0 is the coefficient of earth pressure at rest. During sampling of a saturated soil the majority of the confining stress of the sample is released and the only confinement is provided by the sampling tube. After extruding the sample, the remaining confining stress is released as well and the sample is subjected to no confinement. However, during the extrusion, negative pore pressures are produced within the sample and the resulting capillary tension temporarily holds the sample together. In performing laboratory tests on the samples in their intact state, the ability of the specimen to remain intact under this capillary tension is fundamental, although cohesion also plays a role in clayey specimens.

Additionally, the amount of required capillary stress to keep the sample intact depends on the in situ effective stress, the in situ degree of saturation, and other factors that may decrease or increase the mean effective stress (Sancio, 2003; and Hight and Georgiannou, 1995). According to the "Perfect Sampling" approach (Ladd and Lambe, 1963; and Skempton and Sowa, 1963), the total stresses acting on the soil are removed when a saturated soil sample is obtained and brought to the surface. If the stress removal occurs under undrained conditions, the state of stress becomes isotropic which is equal

to the capillary tension in the pore water and is denoted by σ'_{ps}. The expression for σ'_{ps} is presented as a function of the in situ vertical effective stress, σ'_{v0} as follows:

$$\sigma'_{ps} = \sigma'_{v0}[K_0 + A_u(1 - K_0)] \quad (3.2)$$

In which, $A_u = (\Delta u - \Delta\sigma_h)/(\Delta\sigma_v - \Delta\sigma_h)$. Considering that for normally consolidated clays (Jamiolkowski et al. 1985) and clayey silts (Ladd and Lambe, 1963) and for overconsolidated clays (Ladd and Lambe, 1963) the A_u parameter is very small, for practical purposes the equation 4.2 can be reduced to

$$\sigma'_{ps} = \sigma'_{v0}.K_0 \quad (3.3)$$

It should be noted that the maximum sustainable suction in the soil limits the magnitude of σ'_{ps}. The maximum sustainable suction in the soil is the limit at which pore water begins to flow out of the extruded sample and is replaced by air (Hight and Georgiannou, 1995). Some soil types cannot provide sufficient suction in the sample after extrusion and therefore the sample experiences excessive disturbance. However, for some soil types some other inter-particle attraction forces such as electrostatic and electromagnetic (Van der Waals) and cementation are capable of providing sufficient integrity for the sample after extrusion which reduces the level of disturbance.

The magnitude of sustainable suction depends on the size of the pore space which is governed by the soil mineralogy, soil particle gradation, stress history, etc. To calculate an estimate of the required capillary tension in the tailings material, it is assumed that the effective pore diameter is approximately 20% of the effective grain size, D_{10} as suggested

by Holtz and Kovacs (1981) and Sowers (1979). By following the empirical equation suggested by Holtz and Kovacs (1981), the maximum capillary tension can be calculated by $u_c = -1.4515/D_{10}$ by using D_{10} in mm and u_c in kPa.

The magnitude of isotropic state of stress after extrusion from the sampling tube for representative samples from the Abner Fork and Big Branch impoundments are calculated using Equation 3.3. In this calculation, an average unit weight of 98 pcf (15.4 kN/m^3) and 95 pcf (14.9 kN/m^3) was assumed for the Abner Fork and Big Branch samples respectively based on measurement of recovered specimens. The water table was measured to be at the surface of the fine grained pond. By assuming that this state of stress after extrusion can be provided by capillary tension, the magnitude of σ'_{ps} is assumed for the required u_c. By using the empirical equation provided by Holtz and Kovacs (1981) the required D_{10} to keep the integrity of the specimen after extrusion is calculated. This value was compared to the measured D_{10} for the representative samples and it was observed that the measured effective grain size, D_{10}, for the coal tailings samples were much smaller than the required D_{10}. Therefore, it is believed that the coal tailings samples were capable of providing the required capillary suction after extrusion in the laboratory. The results of this assessment are presented in Table 3.1.

In the Perfect Sampling approach, the possible changes in water content and the strains applied on the specimen during sampling is not considered. However, the imposed stains by tube sampling were calculated by Baligh et al. (1987) in their Ideal Sampling approach. This method was based on the assumption that sampling subjects saturated,

homogenous, isotropic clays in an initial isotropic state of stress to an undrained process (Baligh, 1985). Although in practical applications, these calculations should be performed cautiously, they provide a reasonable approach to the magnitude of induced strains during sampling.

Table 3.1: Comparison between the required effective grain size, D_{10}, and the measured D_{10} for representative samples from Abner Fork and Big Branch impoundments.

Sample	depth ft	σ'_{v0} psf	p'_{ps} Psf	u_c kPa	Required D_{10} mm	Measured D_{10} mm
TBBLAPST12	55	1793	897	-43.0	0.034	0.001
TBBLDPST1	84	2973.6	1487	-71.4	0.021	0.001
TAFLBPST3	220	7788	3894	-186.9	0.008	0.001
TAFLAPST1	239	8460.6	4230	-203.1	0.007	0.0005

3.4.2 Disturbance Due to Drying

Another factor influencing the disturbance of the samples between sampling and performing the laboratory tests is the loss of moisture. As pointed out by Hight et al. (1992), sample drying can result in an increase in the mean effective stress. The influence of sample drying in addition to other factors is illustrated in Figure 3.5. As the sample begins to lose moisture, the water vapor pressure in the sample is decreased and therefore suction is developed in the sample. An increase in the level of suction in the sample causes an increase in the mean effective stress; i.e. acting as an isotropic confining stress. The maximum value of suction is limited by the size of the pore space as was previously discussed in Section 3.4.1. Excessive drying can affect some of the laboratory measured properties of soil such as pre-consolidation pressure. Therefore, in between

the sampling and laboratory testing of the specimen the loss of moisture should be minimized.

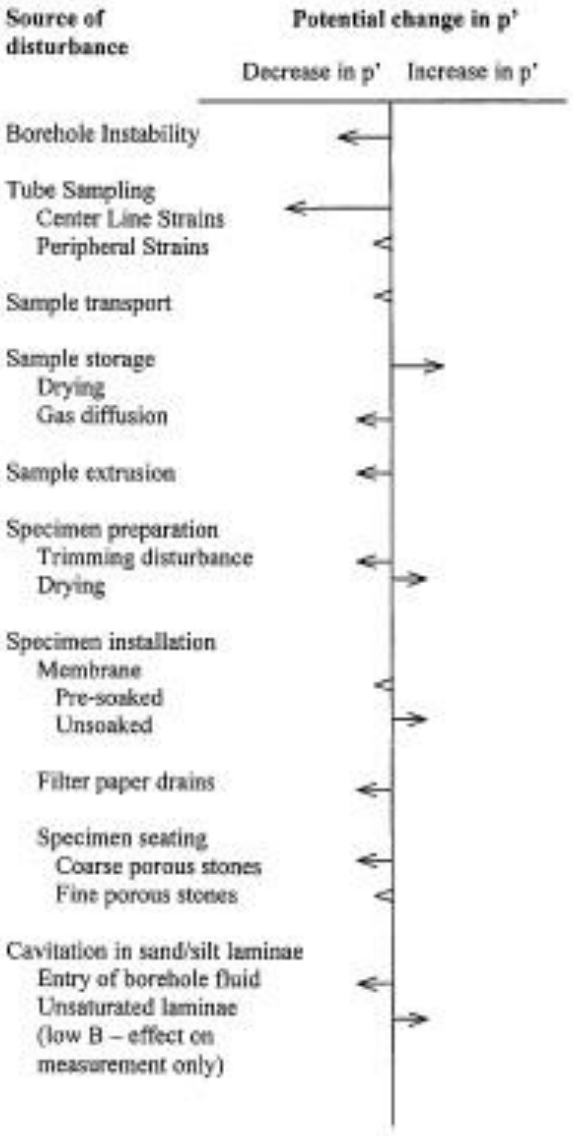

Figure 3.5: Factors influencing the mean effective stress of soft clay (after Hight et al., 1992).

In this study, to prevent sample drying the common methods were applied. Immediately after sampling and pulling the tube from the tailings impoundment, the top and bottom of the tube were sealed with wax, the ends were wrapped with plastic bags, and covered with plastic caps. The caps were sealed airtight by using duct tape and electric tape.

However, due to inevitable delays in performing the laboratory tests, the specimens were contained in the Shelby tubes for an excessive time between three to four years. Therefore, it is expected that the samples were desiccated to some extent and had experienced some level of disturbance due to drying. Also, the extended period of exposure to the stainless steel tube could have influenced the chemical composition of the surface of the specimens. Therefore, the results of this study should be taken into account considering this drawback.

3.4.3 Disturbance during Specimen Preparation

Depending on the property of the soil measured in the lab, the required quality of the specimen can vary (Jamiolkowski et al., 1985; Sancio, 2003). For instance, the peak strength of sensitive soils and small strain shear modulus could be significantly influenced by small changes in soil structure and stress regime. Conversely, large strain strength characteristics, such as residual strength and compressibility, could be measured reliably even by the inevitable disturbance during careful sample preparation.

To illustrate the influence of sample preparation, Atkinson et al. (1992), carried out a series of undrained triaxial compression tests on intact Bothkennar soil recovered

using a Laval sampler. A Laval sampler is a high quality but expensive and time consuming tube sampling method shown schematically in Figure 3.6. The laboratory test samples were cut from the Laval sample using different techniques including pushing a thin-walled tube, trimming with a wire saw and variations of the method described by Landva (1964). The results showed that the method of sample trimming had a significant influence on the strengths and stiffnesses measured. They concluded that for Bothkennar clay, sample preparation using wire saw trimming caused the least disturbance. However, they observed that the difference in measured strength gradually decreased as the samples were strained further.

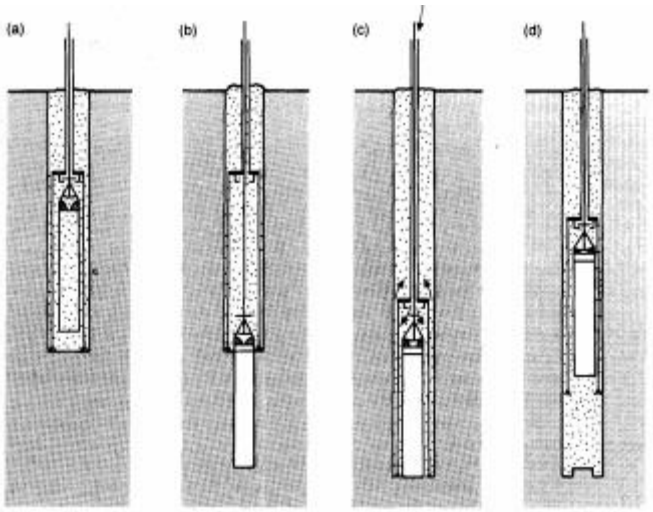

Figure 3.6: General operation of Laval sampler (La Rochelle et al. 1981; Clayton et al. 1995).

3.5 Undrained Triaxial Tests

During earthquakes, the soil matrix experiences various forms of loading. However most of the energy is imparted to the soil elements in the form of vertically propagating shear stress waves. The magnitude of the developed shear stresses is

variable, but can be assumed to be equivalent to a harmonic loading pattern by appropriate weighting of the amplitudes. This pattern of loading is simulated as a series of harmonic cyclic shear stresses applied in the direction of principal directions (i.e. horizontal and vertical) of a soil element (Figure 3.7).

Figure 3.7: Stress and strain conditions applied to an element of soil below level ground surface by vertically propagating shear waves at four different times (Kramer, 1996).

At stage A, the soil element is at rest condition and only horizontal and vertical components of overburden pressure are being applied. At stage B, application of the vertically propagating shear wave and the resulting shear stresses and distortion of the soil element are shown. Due to their cyclic nature, shear stresses reverse their direction; hence resulting in an intermediate at rest condition shown as stage C (identical to stage A). Afterwards, the stresses are applied in the opposite direction shown in stage D. This loading pattern can approximately be reproduced in the laboratory by performing cyclic triaxial tests. Therefore, cyclic triaxial test has been commonly used as the testing technique in geotechnical earthquake engineering studies.

To perform the triaxial test, the sample is covered with a thin membrane and placed between the top and bottom platens. As shown in Figure 3.8, the chamber is filled with liquid or air (oil in this study) and is pressurized. The pressurized chamber provides

radial confinement, and the axial load is applied through a rod attached to the top platen. Therefore, the principal stresses in the specimen are always vertical and horizontal.

Figure 3.8: A typical cyclic triaxial test configuration.

The deviator stress, symbolized as σ_d is the difference between the principal stresses (axial and radial stresses). In cyclic triaxial test, the deviator stress is applied cyclically, either under stress-controlled or strain-controlled conditions. The required deviator stresses are applied by setting the axial loader to a pre-determined maximum and minimum loading stresses. In strain controlled tests, axial displacement is set as the control variable which is measured by Linear Variable Differential Transformer (LVDT) sensors. Cyclic triaxial tests are most commonly performed with the radial stress held constant and the axial stress cycled at a frequency of about 1Hz following the standard

ASTM D5311 procedures. For samples with lower hydraulic conductivity, lower frequencies can be used to allow adequate time for homogenous distribution of generated pore pressure within the specimen (Vaid et al., 1987 and Omarov, 2010).

Figure 3.9 illustrates the simulation of stresses during triaxial testing. By applying an axial stress of σ_d, a shear stress of $\sigma_d/2$ is induced on the 45 degree shear plane. The direction of shear stresses change when the direction of axial stress is reversed. The additional normal stress acting on the shear plane is ignored due to its compressive nature which is mostly transmitted to the pore water without affecting the existing effective confining stress. In cyclic triaxial testing, stress conditions on the shear plane are the same as those produced on the horizontal plane in the ground during earthquakes (Ishihara, 1996). This correspondence serves as the main reason for the cyclic triaxial testing to produce meaningful data in studying the dynamic behavior of soil material.

Cyclic triaxial testing has been used for determining the laboratory stress-strain behavior of soil in numerous geotechnical earthquake engineering studies. Results of studies suggest that the cyclic resistance of soil material to liquefaction in triaxial testing is mainly influenced by factors including initial confining stress, amplitude of cyclic shear stress or strain, number of loading cycles and void ratio (Ishihara, 1996).

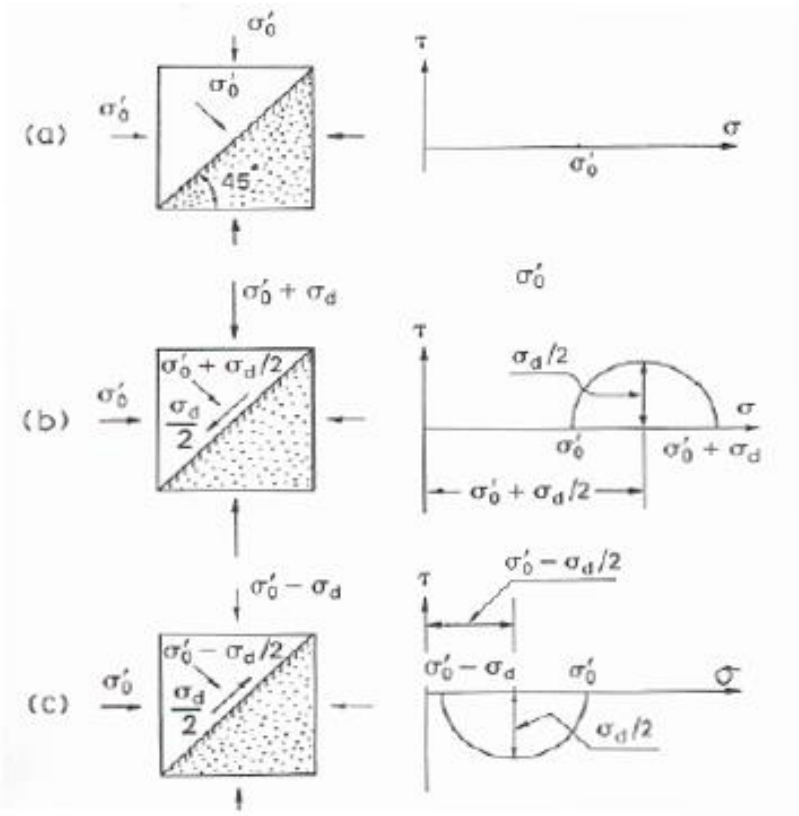

Figure 3.9: Stress conditions during the cyclic triaxial testing (Ishihara, 1996).

Despite the widely accepted use of cyclic triaxial testing in geotechnical research, some drawbacks have been reported in the literature (Seed and Peacock, 1971; Seed, 1976; Casagrande, 1976). These shortcomings are listed herein:

a) In the field, the stress conditions are anisotropic while in the triaxial testing, the stress conditions are applied isotropically unless the K_0-consolidation method is followed.

b) The intermediate principal stress, σ_2, in the field is governed by plane strain conditions (unidirectional shaking; $\sigma_2 = \nu(\sigma_1 + \sigma_3)$). However, in triaxial testing, the intermediate principal stress is equal to the major principal stress

during half of the cycle and equal to the minor principal stress during the other half ($\sigma_2 = \sigma_1$ or $\sigma_2 = \sigma_3$).

c) In cyclic triaxial testing, principal stresses rotate instantaneously from 0° to 90° during each cycle of loading, while in in-situ conditions, the orientation of principal stresses rotate slightly and smoothly (from 0° to 40°).

d) By approaching liquefaction, the specimens can experience necking in extension. This can cause non-uniform application of stresses and thus lead to a premature failure.

e) Specimen preparation is another influencing factor in the limitations of cyclic triaxial testing, especially in stress controlled tests. To evaluate the precise dynamic behavior of in situ samples, high quality undisturbed samples need to be collected.

However, cyclic triaxial testing is relatively inexpensive and easy to perform. In addition, by careful testing some of the abovementioned drawbacks of cyclic triaxial testing can be minimized. By considering these facts and also the availability of the equipment cyclic triaxial testing was chosen as the method of laboratory testing in this study.

3.5.1 Specimen Preparation

To perform high quality laboratory tests and impose minimal disturbance to the specimens, the tubes were handled carefully and were stationary in the laboratory. However, one of the drawbacks in the laboratory phase of this study is that the samples

obtained from the field were not used for about three to four years. The prolonged sitting time warranted additional consideration in preparation of the samples. For cutting the tubes in diameter, a hand pipe cutter was used considering the excessive vibrations produced by using an electric pipe cutter. Following the ASTM D5311 standards, the length to diameter ratio of between 2.0 to 2.5 was considered before cutting the tubes. The pipe cutter was turned slowly while applying gentle pressure on the blade to prevent sample disturbance. No visual evidence of reduction in diameter due to inward folding of the tube edges was observed. To retrieve the samples from the cut portion of the tube, two separate methods were chosen depending on the condition of the sample.

For newer/softer samples, the samples were pushed out using a hydraulic jack. The sample was pushed upward in the same direction of movement during sampling. To reduce the disturbance of the samples due to negative pressures produced during pushing, some small holes were drilled along the perimeter of the sample. The holes provided air passages during pushing and were patched before testing. For these samples, the tubes could not be cut using an electric saw considering excessive vibrations which could result in liquefaction of the sample in the tube.

For older/stiffer samples, the Shelby tubes were cut along the length using an electric saw. These cuts created small grooves along the length which were patched later during the preparation. As a result of the extended sitting time, the older samples had created a relatively strong iron rust bond with the tubes. This bond could cause a

significant disturbance if the sample was pushed out of the tube using the hydraulic jack and therefore the pushing method was not applied.

In both cases, the top and bottom one inch length of the samples were disturbed during the retrieving stage. Therefore these portions were cut by a wire saw and used for water content and plasticity measurements. To ensure cutting the sample at a straight edge, an aluminum cutting mold was used. The grooves and other minor damage on the sample surface were patched by using a frosting knife and the excess material that had been cut from the sample. The sample was weighed for calculating the density. The capillary stresses in these fine-grained mine tailings was sufficient to hold temporary freestanding samples.

The sample was carefully placed over the filter paper on top of the bottom platen. Since hydraulic oil was used to confine the sample in the triaxial chamber, neoprene membranes were used instead of latex. These 0.012-in (~0.31 mm) thick membranes were more resistant to chemical degradation and were placed around the sample using a membrane stretcher. The top platen and filter paper were placed on top of the sample and the membrane was sealed to the platens using four O-rings. The top and bottom drainage lines were connected to the sample and a small vacuum was applied. The vacuum level was consistently lower than the in-situ effective stress of the sample.

After the vacuum had consolidated the sample, the length and diameter were measured using a caliper. Following the ASTM D5311 recommendations, the diameter was measured at the top, middle, and bottom of the sample and in three directions at

each location. The average of the values was used as the diameter of the specimen. Comparison of height measurements performed before and after the application of vacuum show small (< 0.5%) variations in height due to vacuum application. Since these measurements include the seating between the sample and the platens, they are indicative of high precision in sample preparation.

The triaxial cell was assembled and the chamber was filled with oil as depicted in Figure 3.10. The sample and drainage lines were flooded with de-aired water using a differential vacuum method. This stage was followed by backpressure saturation and consolidation as described in Section 3.5.3.

Figure 3.10: Cyclic triaxial chamber filled with oil.

The height of the sample was measured during each stage of specimen preparation and the variation was incorporated in weight-volume calculations before performing the cyclic traixial test. During the abovementioned stages, the machine was set to apply and maintain a zero deviator stress to minimize sample disturbance. Thus the machine could respond automatically to sample height variations during saturation and consolidation and maintain the zero deviator stress.

3.5.2 Testing Equipment

All the triaxial tests in this study were performed using the GCTS cyclic triaxial machine shown in Figure 3.10 at the geotechnical laboratory of the University of Kentucky. This system is a modification of the SBEL resilient modulus device. The instrumentation of this system includes four sensors: an internal load cell, an external LVDT, and two pressure transducers to monitor the axial load, vertical displacement, chamber pressure, and pore-water pressure respectively. The volume change was measured using graded burettes. The system is controlled by a personal computer through the SCON 1500 software (Version 1.0), and allows stress controlled cyclic loading. The triaxial chamber is capable of applying the load through a hydraulic actuator and hence a loading frame is not required. The computer controls the actuator by using high pressure hydraulic oil provided by a hydraulic pump and valves.

3.5.3 Testing Procedure

In the initial stages of the test, before applying the confining pressure the specimen is introduced to negative pore pressure to prevent disturbance. This vacuum

pressure which is always kept lower than the in situ effective stress keeps the sample together while the apparatus is being prepared for applying the confining stress. In most triaxial systems, the chamber is filled with the confining liquid using vacuum. During this stage, the vacuum levels in both the specimen and the chamber were constantly monitored to maintain the appropriate effective stress on the sample.

During an undrained triaxial test, and in particular during a cyclic triaxial test, full saturation of the sample is essential to measure the pore pressure response accurately. The mine tailings samples may lose saturation during sampling, transportation, sample preparation. Also, to achieve full saturation, the entrapped air in the porous stones, drainage lines, and in between the membrane and the sample should be replaced with de-aired water.

The saturation of samples is commonly achieved by back pressure saturation. Back pressure saturation is performed by incrementally increasing the pore pressure and chamber pressure at the same rate. Therefore, the pore pressure is increased while maintaining a constant effective stress. By increasing the pore pressure, two mechanisms result in the reduction of air volume in the sample, hence increasing the saturation level. These two mechanisms are described by Boyle's Law and Henry's Law. According to the Boyle's Law, an increase of the pressure of an ideal gas causes a reduction in the volume of the gas. The product of pressure and volume is constant, so when pressure is doubled, volume is cut in half. Also, according to Henry's Law, an increase in pressure of a system containing and ideal gas and liquid (e.g. air and water) forces the gas to dissolve in the

liquid. Therefore, the required time to reach the full saturation stage depends on the initial volume of air entrapped in the system, the initial degree of the sample saturation, the permeability of the material, the ambient temperature, and the maximum pore pressure provided by the equipment.

To reduce the required time to fully saturate the samples, the system was flooded for approximately 24 hours with de-aired water to push the air bubbles out of the system. After mounting the specimen and filling the chamber with oil, a small confining pressure of approximately 4.0 psi (27.6 kPa) was applied to the chamber. The bottom of the sample was connected to a 2.0 psi (13.8 kPa) pore pressure, while the top was introduced to approximately 8.0 psi (55.2 kPa) of vacuum pressure. The difference between the top and bottom pressure levels created a hydraulic gradient that caused the de-aired water to flow from the bottom of the specimen to the top and bring the air bubbles out of the system. It should be noted that the difference in the effective stresses on top and bottom of the sample would result in a difference in the structure of the specimen. However, since for nearly all of the samples, the in-situ effective stress was higher than 12 psi (82.7 kPa), and also the samples were consolidated to the in-situ stresses, the induced stress history during the flooding stage was eliminated in the consolidation stage. For a few samples retrieved from shallow depths, application of vacuum pressure would exceed the in-situ effective stress. In these instances, the top of the sample was open to the ambient pressure (i.e. a gauge pressure of zero).

After permeating approximately one full burette of de-aired water through the sample or nearly 125 cm^3 (7.63 in^3), the vacuum pressure on top of the sample was disconnected and the top of the sample was introduced to a pore pressure level equal to the bottom pore pressure by a T connection. The pore pressure was allowed to equilibrate throughout the sample.

After pore pressure equalization, the chamber pressure and the pore pressure were increased in simultaneous 5.0-psi (34.5-kPa) increments. As was mentioned in Section 3.3.1 the machine was set to maintain a zero deviator stress during all stages before shearing to compensate for swelling or shrinking of the sample without inducing any stress history. The incremental pore pressure increase provided sufficient time for the machine to adjust the LVDT position for this purpose. The incremental pore pressure increase was continued to at least 70 psi (482.6 kPa) for most of the samples. While maintaining the small 2 psi (13.8 kPa) confining stress on the sample, the saturation stage was allowed to continue for approximately 24 hours.

The required duration of the saturation stage and the pore pressure were primarily dependent on the success of removing air pockets from the system. During the saturation phase, the degree of saturation was estimated using Skempton's B-value, which is defined as the ratio of the increase in pore water pressure to the increase in chamber pressure ($\Delta u/\Delta CP$). To measure this parameter, the top and bottom pore pressure valves were closed and the chamber pressure was increased 10 psi (68.9 kPa). The increase in the pore pressure was monitored until it would reach a constant value

and the B value was measured (i.e. an increase in cell pressure was taken by the pore pressure under undrained conditions). In all cases, a B-value greater than 0.98 was achieved with a relatively high backpressure (i.e. u > 70 psi).

After achieving satisfactory B values, the specimens were isotropically consolidated ($\sigma_3' = \sigma_1' = \sigma_c'$) to match the in-situ stress conditions. In situ stress conditions were estimated based on the estimated unit weight of the tailings, depth of sample recovery, and location of the phreatic surface. The pore volume flowing in or out of the sample was monitored from the beginning of the saturation stage until the end of the consolidation. Following the consolidation phase, the samples were loaded cyclically under undrained conditions.

Cyclic tests were performed by applying stress controlled sinusoidal loading at a frequency of 1 Hz following the ASTM D5311 recommendations. The sampling rate for data acquisition was 10 samples/sec. Following the common geotechnical earthquake engineering practice, the deviator stress was characterized in terms of the Cyclic Stress Ratio (*CSR*). In cyclic triaxial testing, this term is defined as the ratio of the maximum peak shear stress ($\sigma_d/2$) to the initial effective consolidation pressure, σ_c'. The term σ_d is defined as the deviator stress in this research (i.e. the difference between the major and minor principal stresses). The range of applied *CSR* values in this research was between 0.1 and 0.5. The cyclic loading was applied until a pore pressure ratio of 1.0 was achieved or the sample has visually liquefied. The pore pressure ratio is defined as $r_u = \Delta u/\sigma_c'$ in

this research, where Δu is the excess pore pressure observed in the specimen during cyclic loading.

After the completion of each cyclic triaxial test, the specimen was subjected to a strain-controlled undrained monotonic compression test. For performing this test, the drainage valves were remained closed to maintain the increased pore pressure. The post-liquefaction strength of the sample was measured by applying a constant strain rate of 0.5%/min.

3.6 Shear Modulus Measurement Using the Cyclic Triaxial Method

In determination of site response analysis in geotechnical engineering, the shear modulus and damping ratio parameters of the material are commonly used. For coal mine tailings material, such parameters are not readily available, and could be measured by performing cyclic triaxial tests in the elastic deformation range. Therefore, a series of cyclic triaxial tests were performed to obtain such parameters following the ASTM D3999 recommendations. However, it should be noted sample disturbance can influence the strength measurements of the soil in the small strain range (Jamiolkowski et al., 1985). The “undisturbed” samples used in this study were not used immediately after sampling and therefore sample drying and chemical composition variations due to prolonged contact with the stainless steel tubes could result in some level of disturbance.

These tests were identical to the cyclic triaxial tests explained in Section 3.3 in all the steps except for the shearing stage. In the cyclic triaxial tests with the objective of

liquefaction of the material, the applied cyclic deviator stresses were relatively large and resulted in significant deformation and pore pressure build-up. However, to measure the shear modulus and damping ratio of the material, the tests were performed in the elastic range of deformation and hence the applied cyclic deviator stress was relatively small. Therefore, the deformation of the sample was very small and not visible and the increase in the pore pressure was minimal.

By starting at a low stress level, and considering that the deformations remained in the elastic range, the sample could be re-tested at a higher stress level. After each test, the deformation of the sample was assessed to detect plastic deformations following the ASTM D3999 recommendations. By reaching the plastic deformation threshold, the testing was stopped and the sample was retrieved and prepared for additional geotechnical testing. In this study, the applied cyclic deviator stress was between 1 psi peak-to-peak and 40 psi (275.8 kPa) peak-to-peak depending on the strength of the sample and the in-situ effective stress of the specimen.

By carrying out the cyclic triaxial test on the specimen, the axial stresses and strains are measured. However, the intent for these series of cyclic triaxial tests was to measure the shear modulus and the damping ratio of the sample at a certain shear strains level. Therefore, by following the method described in the ASTM D3999 standard, these parameters were calculated as follows. A schematic hysteresis loop produced in a cyclic triaxial test is illustrated in Figure 3.11.

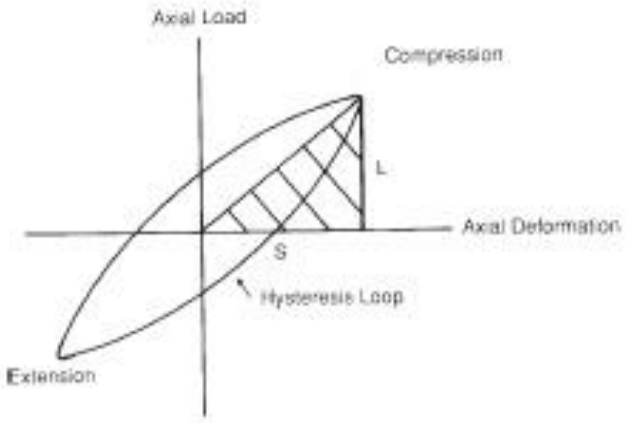

Figure 3.11: Schematic illustration of a hysteresis loop in cyclic triaxial testing (ASTM D3999).

The damping ratio of the material at the specific shear strain level imposed to the sample by harmonic cyclic loading is calculated as:

$$\mathrm{D} = \frac{\mathrm{A_L}}{4\pi \mathrm{A_T}} \tag{3.4}$$

where, $\mathrm{A_L}$ is the area of the loop and $\mathrm{A_T}$ is the area of the hatched triangle.

The shear modulus of the sample at this strain level is calculated by $\mathrm{G} = \mathrm{E}/2(1+\nu)$, in which E is the Young's modulus of the specimen and ν is the Poisson's ratio. Since the samples were saturated before applying the load, the Poisson's ratio was assumed to be 0.5. The Young's modulus is calculated using:

$$\mathrm{E} = \frac{\mathrm{L_{DA}}}{\mathrm{S_{DA}}} \times \frac{\mathrm{L_S}}{\mathrm{A_S}} \tag{3.5}$$

where, L_{DA}, is the double amplitude load, S_{DA}, is the double amplitude deformation, L_S, is the height of the specimen after consolidation, and A_S, is the area of the specimen after consolidation.

The imposed shear strain in this loop is calculated by using:

$$\gamma_{SA} = \varepsilon_{SA}.(1 + \nu) \tag{3.6}$$

where, ε_{SA}, single amplitude axial strain, is found by using $\varepsilon_{SA} = \varepsilon_{DA}/2$, where ε_{DA} is the double amplitude axial strain and is calculated by $\varepsilon_{DA} = S_{DA}/L_S$. Additional considerations were followed per recommendations of the ASTM D3999.

3.7 Laboratory Vane Shear Testing

To measure the peak and residual post liquefaction shear strength of the coal mine tailings, i.e. S_p and S_r, laboratory vane shear testing was performed. The vane shear testing was carried out following the ASTM D4648 by a Wykeham Farrance equipment shown in Figure 3.12.

Figure 3.12: Laboratory vane shear equipment

Following the cyclic and monotonic triaxial testing, the triaxial machine was disassembled and the sample was carefully extracted to avoid contamination with the chamber hydraulic oil. The sample was transported to the vane shear equipment, the blades were pushed in the material following the recommended ASTM depth, and the machine was cranked while monitoring the spring deflection gauge.

The blades were turned at the rate of 60^{o}/minute to 90^{o}/minute while the spring deflection gauge was monitored for the peak and residual values. The recorded deflection values were converted into strength parameters using the calibration factors provided with the equipment.

Chapter 4

Laboratory Test Results

4.1 Introduction

In this chapter, the results of laboratory tests performed at the University of Kentucky geotechnical laboratory are presented. The goal was to measure the required parameters to investigate the liquefaction susceptibility of coal mine tailings.

4.2 Cyclic Triaxial Tests

Following the destructive 1964 earthquakes in Alaska and in Niigata, Japan, Professors H. B. Seed, I.M. Idriss and other researchers began to develop the new research area of geotechnical earthquake engineering. Introducing the cyclic triaxial test (Seed and Lee, 1966) was a part of the effort to study the dynamic behavior of soil material. Due to the origin of the observed failures at that time, their research was mainly focused on the liquefaction of saturated sands under free field conditions. Since then, the cyclic triaxial test has been widely utilized in cyclic loading to measure the variation of pore water pressure and strain potential of saturated soils subjected (Seed et al., 1969, Lee and Roth, 1977, Andersen et al., 1988, Zergoun and Vaid, 1994, Boulanger et al., 1998). A brief review of the theory of this test is provided as follows.

In Figure 4.1, the stress conditions during various stages of a cyclic triaxial test are illustrated. To simulate the in situ stress conditions of an isotropically consolidated soil sample, the specimen is initially loaded to a hydrostatic stress equal to σ_0'. Considering

that the stresses applied in all directions are equal, the initial stress conditions are depicted by one point using the Mohr circle method. This point is located on the coordination of $(\sigma_0', 0)$ in the (σ, τ) space.

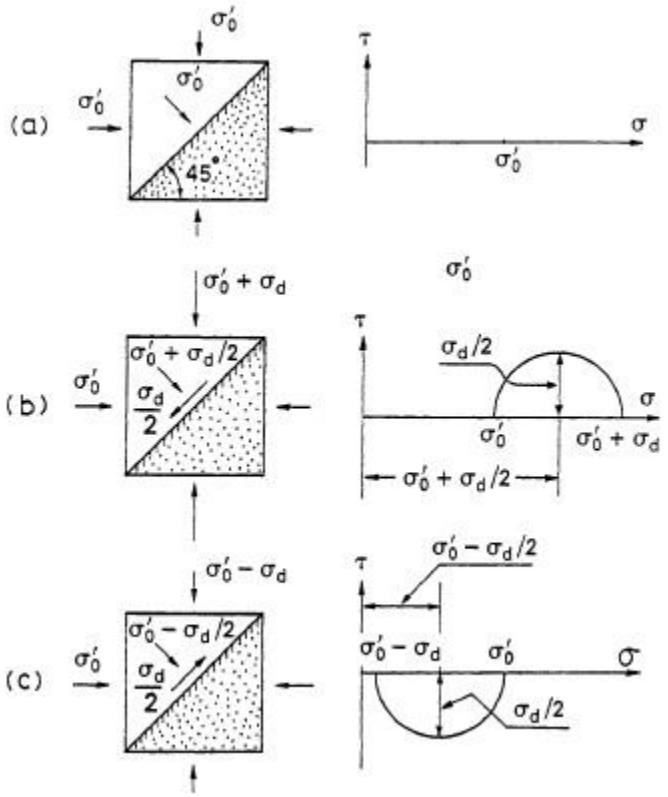

Figure 4.1: Stress conditions during cyclic triaxial testing (After Ishihara, 1996).

The deviator stress is applied at the axis of the sample in a cyclic form, reaching the desired maximum amplitudes in compression and extension. In fact, for the coal mine tailings samples tested in this study, the extension phase is a "reduced compression" phase since the axial stresses did not gain a negative value and were always maintained in the positive range. The cyclic deviator stress is typically applied at a frequency of 1.0 Hz until 1) the excess pore pressure value equals the confining stress, 2) a predetermined axial strain level is reached, or 3) a given number of loading cycles have been applied.

It should be noted that at the point that the loading direction shifts from compression to extension, the orientation of principal stresses change and rotate 90°. During the compression phase of the cycle, the major principal stress coincides with the axis of the sample, while during the extension phase the major principal axis is perpendicular to the axis of the sample. Further discussion on the applied stresses and the assumptions involved is provided by Seed and Lee (1966) and Seed and Peacock (1971).

One of the disadvantages of interpreting the cyclic behavior from the results of a cyclic triaxial test is that the compressional and extensional behaviors of the sample are evaluated in the same test. As a common strength property of soil material, the tensile resistance is much less than the compressional resistance. Therefore, the axial strain in extension is greater than the compressional axial strain.

The interpretation of cyclic triaxial testing generally involves the measurement of the number of cycles required for the specimen to generate excess pore water pressure equal to the initial confining stress. The same material is tested over a range of various deviator stress amplitudes which results in various numbers of cycles to produce excess pore water pressure equal to the confining stress. A cyclic strength curve is built by connecting the data points when plotting the deviator stress and the number of cycles for each sample on the y and x axes, respectively. The amplitude of the deviator stress is commonly used to define the applied Cyclic Stress Ratio (*CSR*). For the cyclic triaxial tests, the *CSR* is denoted by CSR_{TX}, and is defined as the ratio of the half the applied peak

deviator stress to the initial isotropic effective stress ($CSR_{TX} = \sigma_d/2\sigma_c'$). Under undrained conditions (i.e. a Mohr-Coulomb failure envelope with a friction angle of zero), the term $\sigma_d/2$ is equal to the cyclic shear stress, τ_{cyc}.

In some studies such as Silver et al. (1976) and Vessely et al. (1996), "initial liquefaction" is defined as the moment during the test when the excess pore water pressure equals the initial confining pressure. At this point during the test, the specimen commonly experiences significant strain levels. The term "liquefaction" was used by Lee et al. (1975) to describe this moment when the confining stress of the sample reaches zero irrespective of the experienced and subsequent strain levels. To clarify the terminology regarding liquefaction, the use of the term "initial liquefaction" was discontinued and instead, the term "peak cyclic pore pressure ratio of 100%" was introduced by Seed (1979).

For sandy and silty soils, liquefaction resistance is commonly related to the number of cycles required for the sample to reach "initial liquefaction". This is defined by Lee and Seed (1967) as when the specimen shows negligible resistance to deformation over a wide strain range during the cyclic loading. Therefore, this definition is not based on the value of the effective stress, but is related to the strength of the sample. It is mentioned by Lee and Seed (1967), that although unlikely, saturated sand may reach excessive strains without liquefying at all. Also, "complete liquefaction" was defined by Lee and Seed (1967) as when the soil exhibits no resistance to deformation over a wide range of strain.

The meaning of the term “liquefaction” has been introduced in various ways by researchers and geotechnical experts in the past decades. Such discussions on liquefaction terminology can be found in the studies presented by Castro (1975), Seed (1976), Castro and Polous (1977), Marcuson et al. (1978), Pyke (1979), Seed (1979), Poulos et al. (1985), Kramer (1996), and Roebertson and Wride (1998). The objective of this study is to evaluate the dynamic behavior of coal mine tailings which eventually could be utilized in post-earthquake slope stability analysis of coal mine tailings impoundments. Such studies are stability studies and not deformation problems. Therefore, the point of interest in this study, is the onset of peak pore pressure and loss of effective confining stresses. As stated by Poulos et al. (1985), the momentarily 100% pore pressure buildup does not imply zero strength. The minimum undrained strength that remains after 100% pore pressure buildup is the undrained steady-state strength, which is solely a function of void ratio and cannot be lost. In this study, the following terms are borrowed from Seed (1979) and used hereafter:

Liquefaction: denotes a condition where a soil will undergo continued deformation at a constant low residual stress or with residual resistance, due to the pore water pressure buildup and maintenance of high pore water pressure, which reduces the effective confining pressure to a very low value; pore pressure buildup leading to liquefaction may be due either to static or cyclic stress applications and the possibility of its occurrence will depend on the void ratio or relative density of a sand and the confining pressure; it may

also be caused by a critical hydraulic gradient during upward flow of water in a sand deposit.

Peak cyclic pore pressure ratio of 100%: denotes a condition where, during the course of cyclic stress applications, the residual pore water pressure on completion of any full stress cycle becomes equal to the applied confining pressure; the development of a peak cyclic pore pressure ratio of 100% has no implications concerning the magnitude of the deformations that the soil might subsequently undergo; however, it defines a condition that is a useful basis for assessing various possible forms of subsequent soil behavior.

Peak cyclic pore pressure ratio of 100% with limited strain potential, or cyclic mobility or cyclic liquefaction: denotes a condition in which cyclic stress applications develop a peak cyclic pore pressure ratio of 100% and subsequent cyclic stress applications cause limited strains to develop either because of the remaining resistance of the soil to deformation or because the soil dilates, the pore pressure drops, and the soil stabilizes under the applied loads. Cyclic mobility may also be used in a broader sense to describe the cyclic straining that may occur even with pore pressure ratios less than 100% in which cause the actual peak value of pore pressure ratio may simply be stated.

In the cyclic traixial equipment used in this study, the pore water pressure was measured using a pressure transducer connected to the bottom of the specimen. The reliability of the pore water pressure values recorded by the transducer depends on the

hydraulic conductivity of the specimen and the rate at which the pore pressure variations distribute throughout the sample. These tests were performed at the commonly used frequency of 1.0 Hz, recommended by the ASTM 5311 standard which is a suitable rate for samples of coarse grained material and low plasticity silts. Since most of the obtained coal mine tailings specimens were classified as low plasticity silt, ML, the applied rate of 1.0 Hz was slow enough to allow equaliziation of pore water pressure. Some of the samples were classified as low plasticity clay, CL, with moderate hydraulic conductivity. For these samples, the cyclic triaxial tests were performed at the frequency of 1.0 Hz as well. Although the frequency might have been slightly fast for these samples, but since the results were to be compared with the low plasticity silts, and due to the limited number of undisturbed specimens, the rate was chosen to remain unchanged. A summary of a few representative tests are presented in Section 4.2.1 and the results of all cyclic triaxial tests are presented in Appendix A.

In Figure 4.2, the methodology employed to count the number of cycles required to reach a specific strain level is shown. In this study, single amplitude strain (SA) refers to the maximum strain either in compression (positive sign) or extension (negative sign), and double amplitude (DA) refers to the peak-to-peak strain or the addition of the absolute values of the single amplitude strain in compression and extension. The amplitude and the type of the achieved strain at any moment during a test should be stated similar to the following examples: 2.5% single amplitude strain in compression or 5% double amplitude strain.

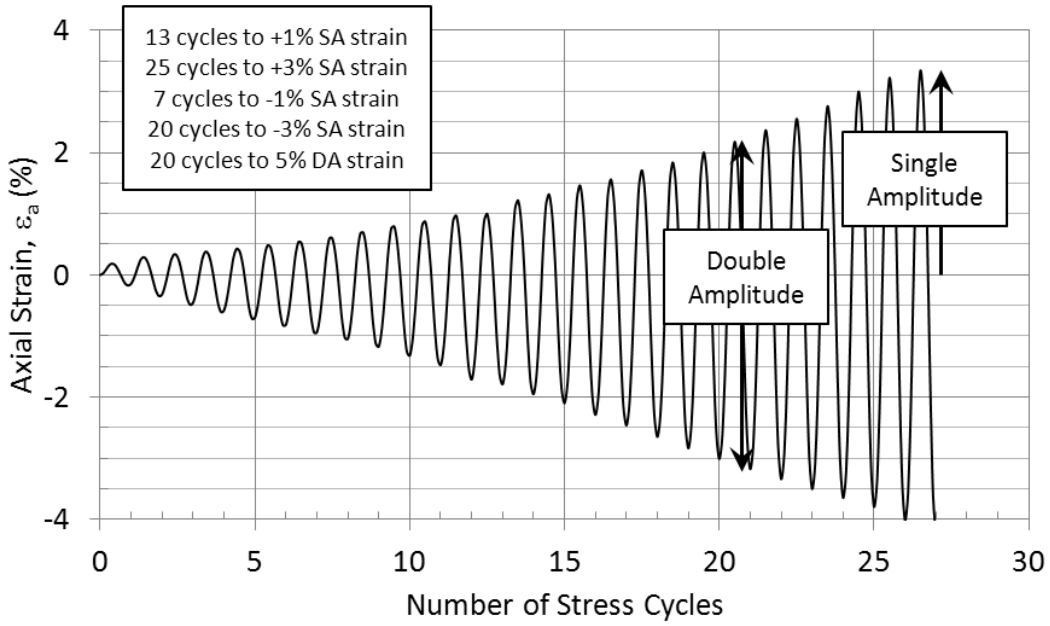

Figure 4.2: Definition of single amplitude (SA) and double amplitude (DA) strains and examples of the methodology used to count the cycles to a specific strain level.

Definition of failure based on a specified strain level in a cyclic triaxial test has been a matter of debate, and the proposed criteria have not been universally accepted (Lee and Focht, 1976). Examples of such criteria are as follow: 3% single amplitude axial strain (e.g. Boulanger et al. 1998), 5% single amplitude axial strain (e.g. Lee and Roth, 1977), 5% double amplitude axial strain (e.g. Campanella and Lim, 1981), 10% double amplitude axial strain (e.g. Lee et al. 1975, Silver et al. 1976), 15% double amplitude strain (e.g. Andersen et al. 1988), and 20% double amplitude strain (e.g. Lee and Seed, 1967).

The definition of failure is significantly related to the specifications of the investigated site and the level of acceptable deformations. As stated by Sancio (2003), selection of a specific pre-established value to define failure has limitations due to the fact that it is difficult to relate the achieved strain in a cyclic test to the experienced deformation by an element of soil in the field conditions. The selection of a particular

strain level for an investigated case should be related to the correlations between the laboratory test and physical models and also to the observation of a related phenomenon at that strain level in the laboratory test. However, it should be noted that the focus of the study performed by Sancio (2003) was on the deformations observed at the foundation of buildings as a result of pore pressure buildup during earthquakes. As was discussed previously, this study is focused on the dynamic behavior of coal mine tailings and the results of this study could be utilized in post-earthquake stability analysis of coal mine impoundments. In the analysis of stability of impoundments, the identification of zones with zero effective pressure as a result of 100% pore pressure buildup is significantly important. Therefore the point of interest in this study, is the point of obtaining cyclic mobility and not a certain level of deformation.

In the following sections, the results of the cyclic triaxial tests on the coal mine tailings specimens are presented. Based on the results of the cyclic triaxial tests the methodology to develop the liquefaction resistance curve is considered and discussed.

4.2.1 Isotropically Cyclic Triaxial Tests

To facilitate the data management and the presentation of the results, a code system including alphabetical characters and digits was employed herein. To refer to each individual sample, the impoundment, location, piston number, and the sequence of the sample in the tube from which the sample was obtained was considered. For example, a specimen obtained from the Abner Fork impoundment, at location B (toe), from piston 3, and by considering that it was the second sample from the top of the tube to be retrieved,

was named TAFLBPST3S2 (T = tube, AF = Abner Fork, LB = Location B, PST3 = piston sample #3, S2 = second sample in piston).

Typical results from a representative cyclic triaxial test are illustrated and discussed in this section. The sample TBBLAPST13S4 was obtained from the Big Branch impoundment, at location A (crest), from piston 13, and was the fourth sample retrieved from that piston. This low plasticity coal tailings sample, which is located barely above the A-line in the Casagrande plasticity chart (CL), was tested at the frequency of 1.0 Hz.

In Figure 4.3, the time history of the cyclic deviator stress $(\sigma_d = \sigma_1 - \sigma_3)$ is illustrated. In Figure 4.4, the accumulated excess pore water pressure (u) is presented. In Figure 4.5 the lateral effective stress $(\sigma_3' = \sigma_3 - u)$ is illustrated. The variation of the pore pressure ratio with number of cycles is shown in Figure 4.6. Also, in Figure 4.7, the variation of pore pressure ratio with normalized number of cycles is illustrated. In this figure, the number of cycles is normalized by dividing the number of cycle to the total number of cycles to reach the pore pressure ratio equal to 100%. In Figure 4.8, the axial strain (ε_a) achieved by the sample is presented. The initial isotropic confining stress of the specimen $(\sigma_c' = \sigma_1' = \sigma_2' = \sigma_3')$ was 21.5 psi (148.2 kPa), and the applied symmetrical sinusoidal deviator stress oscillated about zero with a peak amplitude of 12 psi (82.7 kPa).

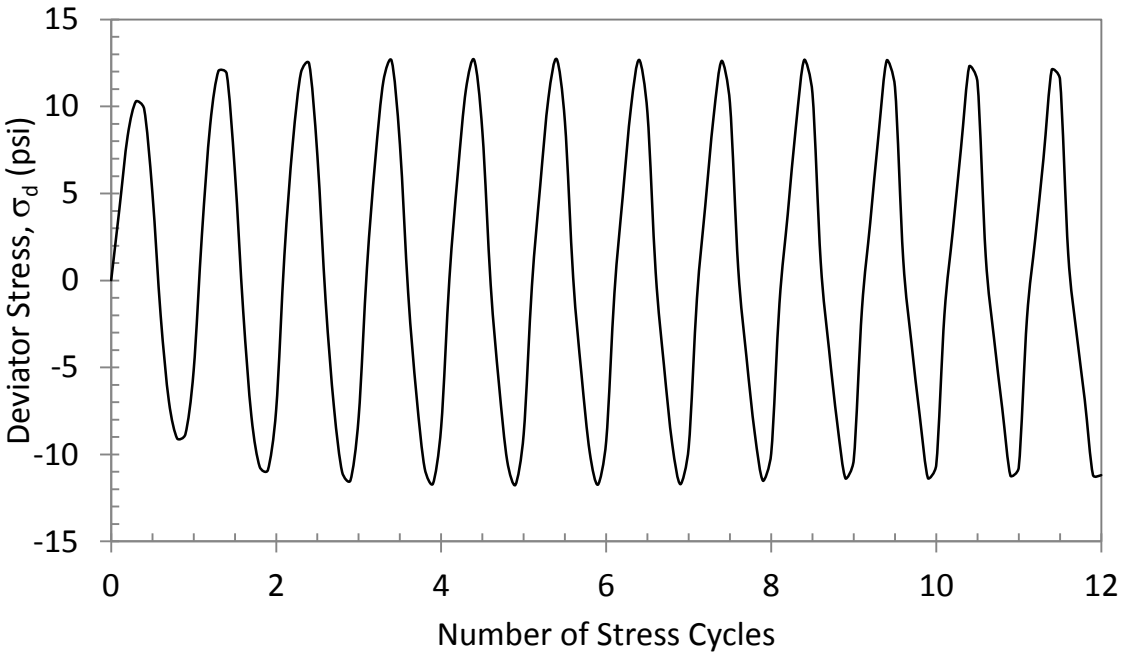

Figure 4.3: Time history of the cyclic deviator stress for sample TBBLAPST13S4.

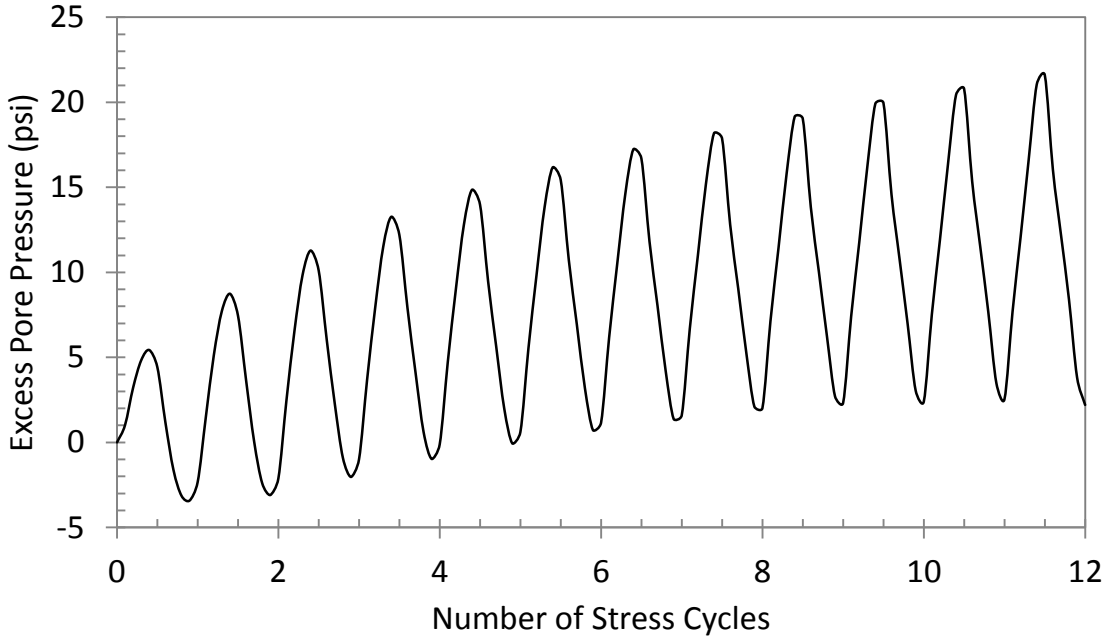

Figure 4.4: Time history of the excess pore water pressure for sample TBBLAPST13S4.

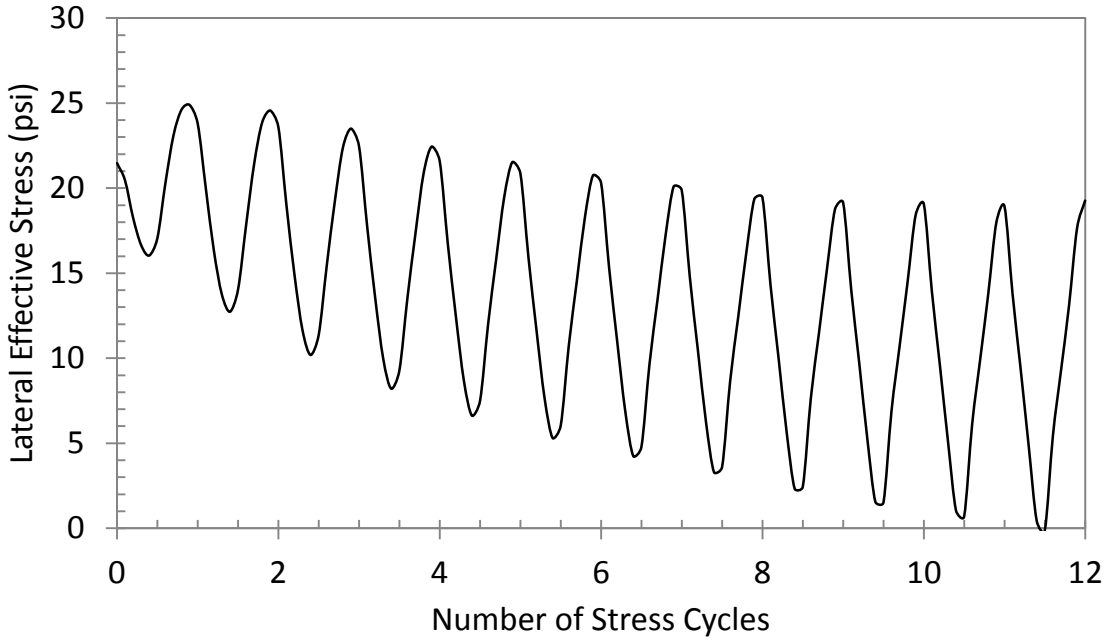

Figure 4.5: Time history of the lateral effective stress for sample TBBLAPST13S4.

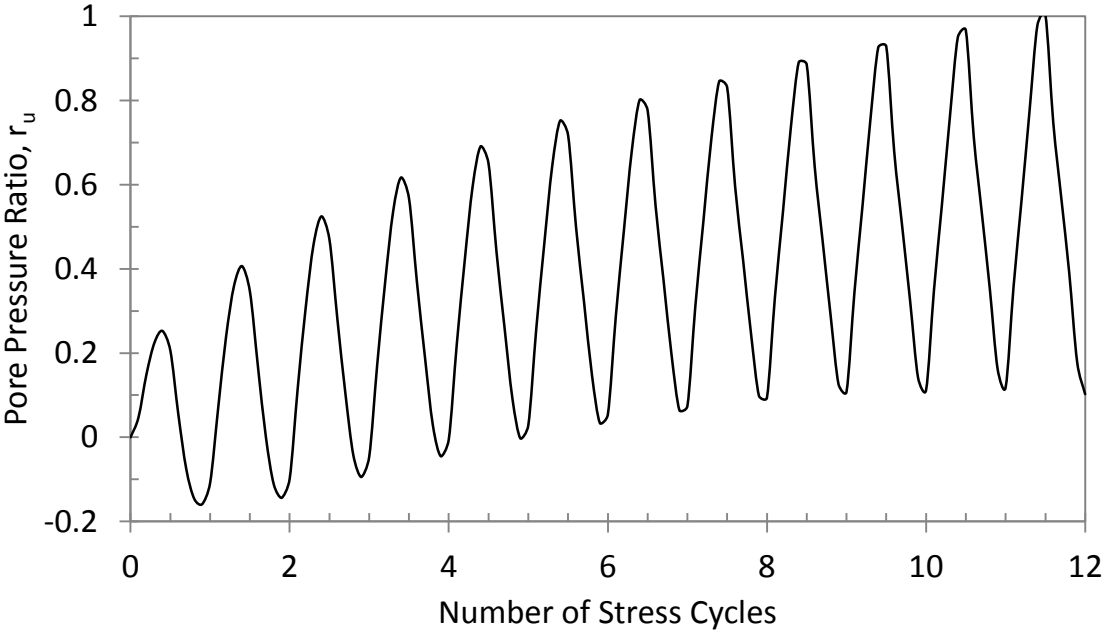

Figure 4.6: Time history of pore pressure ratio for sample TBBLAPST13S4.

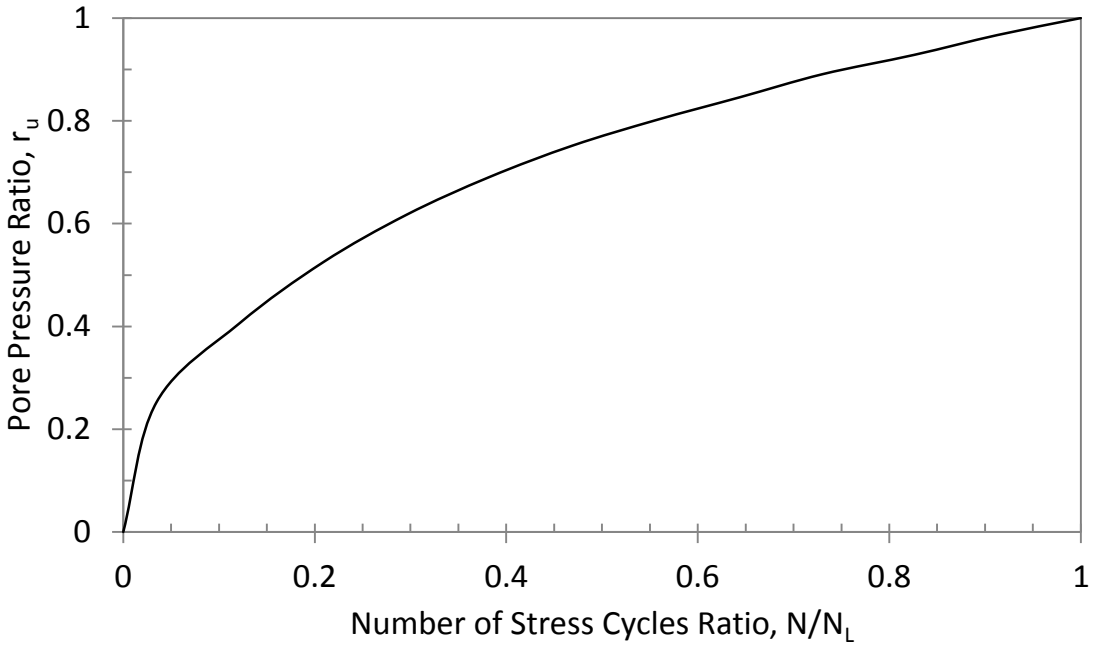

Figure 4.7: Pore pressure ratio versus normalized loading cycles to achieve the peak pore pressure ratio.

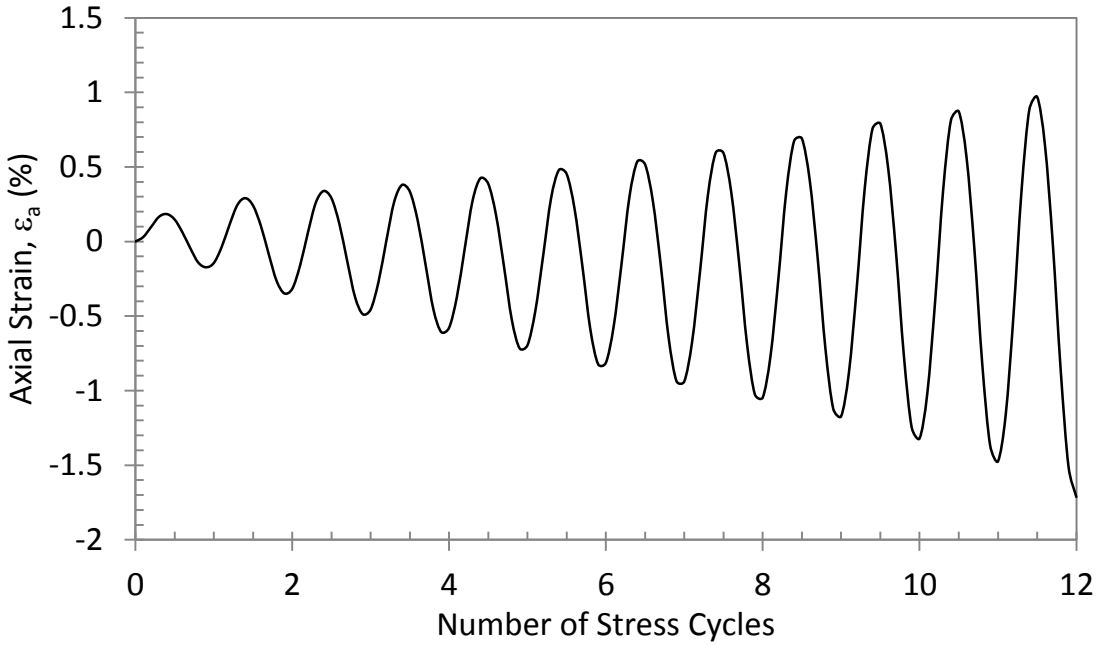

Figure 4.8: Time history of the axial strain for sample TBBLAPST13S4.

By inspecting Figure 4.3 it is understood that the loading began by applying incremental compression to the sample in the first quarter of the first cycle and the

specimen experienced contraction (Figure 4.8). As a result, the pore pressure was increased (Figure 4.4) and the lateral effective stress was reduced (Figure 4.5). At the end of the first quarter of the cycle, the lateral effective stress was reduced to 73% of the initial value and the axial strain reached to 0.2% (Figure 4.8). During the first quarter, the major principal stress, σ_1', was the vertical effective stress and the minor and intermediate principal stresses, σ_3' and σ_2' respectively, were both equal to the confining stress. At the peak compression, the mean effective stress, $p' = (\sigma_1' + \sigma_3')/2$, was equal to 21.8 psi (150.3 kPa).

During the second quarter of the first cycle of loading, the compression load was incrementally reduced to zero psi (Figure 4.3) and the sample went under dilation (Figure 4.8). At this moment, the specimen was under isotropic confining pressure again and the mean effective stress was reduced to 90% of the initial mean effective stress (21.5 psi). While the second quarter of the load was being applied, the orientation of the major, intermediate and minor principal stresses remained the same as the first quarter.

By the beginning of the third quarter of the first cycle of loading, the orientation of the principal stresses changes. The minor principal stress becomes equal to the vertical stress, and the maximum and intermediate principal stress equals the lateral effective stress. During the third quarter of loading, the extension load was applied and the specimen continued to dilate (Figure 4.8). The lateral effective stress continued to increase (Figure 4.5) and reached the maximum value of 24.9 psi (171.7 kPa) at the peak

extension which was approximately 16% higher than the initial value. At this moment, the sample had experienced 0.14% of axial strain.

Over the last quarter of the first loading cycle, the deviator stress was reduced to zero. The lateral effective stress was decreased to 20.1 psi (138.6 kPa) with a corresponding pore water pressure of 1.4 psi (9.6 kPa). The mean effective stress at the end of cycle 1 was equal to 21.3 psi (146.9 kPa) which was almost identical to the initial mean effective stress. The sustained axial strain by the sample at this point was in the extension direction and the amplitude was only 0.03%.

As the equipment continued the loading (cycle 2), similar processes with slightly different values continued to occur. As the compression stage of loading was applied (Figure 4.3), the sample experienced contraction and achieved a peak value of 0.24%; strain greater than the previous cycle (Figure 4.8). As the compressive load was removed, the sample went under dilation and recovered most of the experienced compressive strain. As the loading progressed to the extension stage of the cycle 2, the sample continued to dilate and reached a peak extension strain of 0.26% which was 85% higher than the peak extensional strain in cycle 1. At the end of the cycle 2, when the deviator stress was reduced to zero, the mean effective stress was equal to 16.94 psi (116.8 kPa) which was 80% of the initial value with a corresponding pore water pressure of 2.45 psi (16.9 kPa) which was 1.75 times of the value at the end of cycle 1 (Figure 4.4).

By continuing the application of the cyclic load, the process described above was repeated in each cycle and the mentioned parameters continued the same trend. The

pore water pressure continued to rise, the lateral effective stress became smaller, and the amplitude of the strain in each direction continued to increase. However, the magnitude of the axial strain in extension was continuously greater than the compressive axial strain in each cycle. The lateral effective stress reached the minimum level in each cycle at the point of peak compression deviator stress. In this test, the lateral effective stress reached a temporary zero value or "peak cyclic pore pressure ratio" of 100% $(r_u = 1.0)$ during cycle 12 and the subsequent cycles afterwards. The specimen developed 3% axial strain in extension in 20 cycles, 3% compressive axial strain in 25 cycles, and 5% double amplitude strain in 20 cycles as illustrated in Figure 4.9.

The observed response from specimen TBBLAPST13S4 during the cyclic triaxial loading, presented in Figure 4.3 to Figure 4.8, was consistent with the definition of a sample experiencing "Peak cyclic pore pressure ratio of 100% with limited strain potential" $(r_u = 1.0)$, or "Cyclic mobility". By achieving a state of $(r_u = 1.0)$ in cycle 12 and the subsequent cycles, the effective stress momentarily reached zero during each cycle. However, the experienced axial deformations were not significant at the onset of peak cyclic pore pressure and only by continuing the cyclic loading, the sample experienced greater deformation levels. The majority of the coal mine tailings samples tested in this study demonstrated similar behavior (Cyclic mobility).

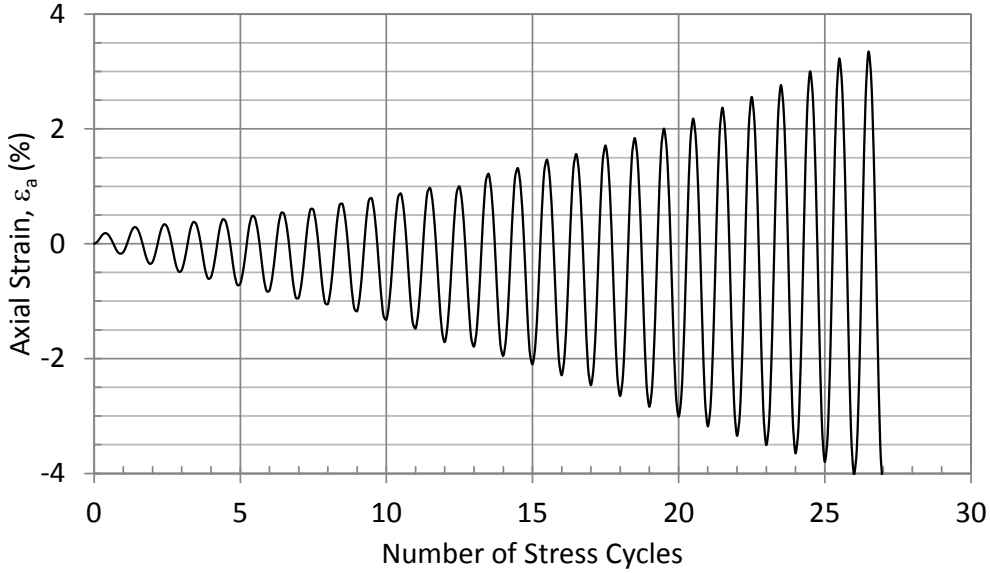

Figure 4.9: A complete time history of the axial strain for sample TBBLAPST13S4.

Some of the specifications of the sample studied in this section were as follows: LL=36, PI=12, $\omega_c/LL = 0.8$, and percentage of particles smaller than 5 μm was 50% as determined from the hydrometer test. By following the procedure known as the "Chinese Criteria", provided in Youd et al. (2001), this specimen would not be classified as susceptible to liquefaction, although it experienced cyclic mobility in 12 cycles, and reached 5% double amplitude strain in 20 cycles.

The stress-strain relationships (Hysteresis loops) of the cyclic triaxial test for sample TBBLAPST13S4 are illustrated in Figure 4.10. In this figure, the sequence of cycles from the beginning of the test to the point of achieving 3.0% single amplitude compression strain is presented. In the beginning of loading, as shown in Figure 4.10, as the sample experiences strains in both compression and extension directions, the hysteresis loops appear to have a shape of a "football". However, by gaining more axial strain in both directions, the loops appear to shift the shape to a "banana loop". It should

be noted that by comparing the shape of the loops in Figure 4.10, the influence of achieving the peak pore pressure ratio ($r_u = 1.0$) during cycle 12 becomes clearer. Before cycle 12, the onset of maximum pore pressure ratio or the "initial liquefaction", the increase in the strain level is not significant and the loops are relatively close to each other. However, after triggering the point of cyclic mobility at cycle 12 and achieving the peak pore pressure ratio, the loops begin to expand at a higher rate and appear to be slightly separated when compared to the initial loops.

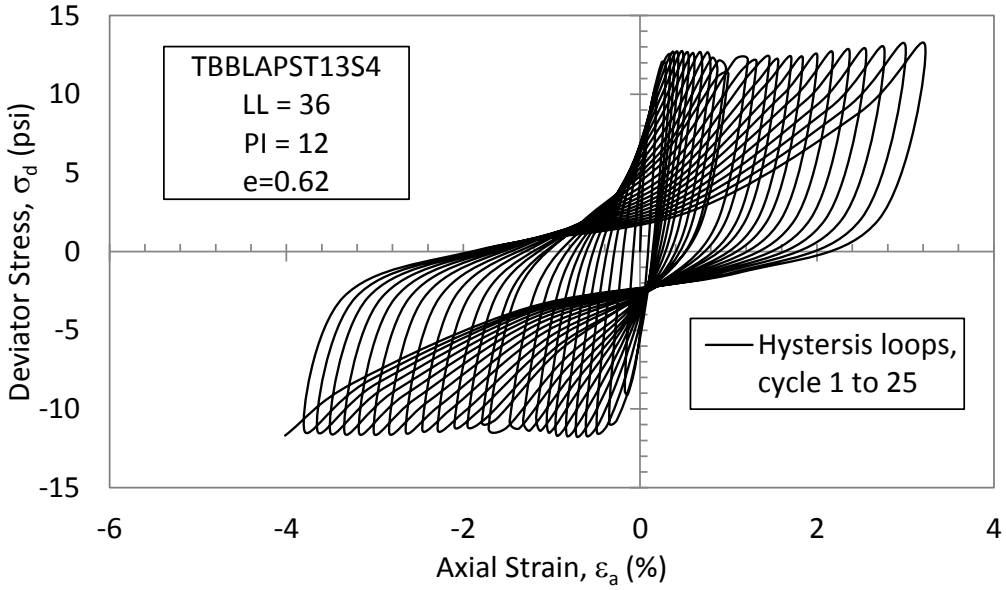

Figure 4.10: Stress-strain relationship for sample TBBLAPST13S4.

Some of the individual hysteresis loops in the cyclic triaxial test for sample TBBLAPST13S4 are illustrated in Figure 4.11 to Figure 4.13. As shown in Figure 4.11, in 6 cycles, the hysteresis loop becomes much broader as the sample experiences higher strain levels. Therefore the hysteresis loop dissipates considerably more energy contrary to the observed narrow loops typical to the sand-like materials. At this stage of the test,

the behavior appears to be similar to the behavior of clay-like materials as stated by Boulanger and Idriss (2004). However, by inspecting the hysteresis loops from cycles 12 and cycle 20, as presented in Figure 4.12 and Figure 4.13, the behavior appears to slightly resemble a sand-like sample behavior. The "banana loops" are developed and the inverted tips appear at the peak strain levels. The plunging inverted corners or the S-shaped loop is indicative of dilation which limits the deformation (strain hardening) of the specimen and causes a temporary increase in the shear stiffness. This typical behavior of sand-like materials under cyclic loading causes the sample to experience cyclic mobility with limited strains. Considering both the shape and the width of the loops, the behavior of the specimen appears to coincide with the behavior of the transitional materials between sand-like and clay-like soil as stated by Boulanger and Idriss (2004).

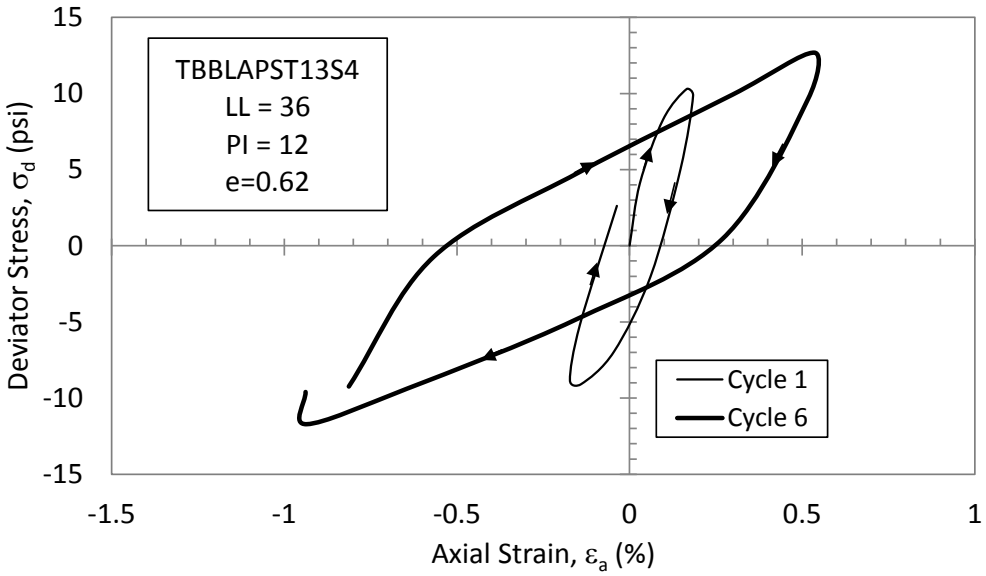

Figure 4.11: Stress-strain relationship in cycle 1 and cycle 6 for sample TBBLAPST13S4.

It should be noted that even after reaching significant deformation levels at cycle 20 which is accompanied by repeated development of a peak excess pore pressure ratio

of 1.0 after cycle 12, the shear modulus never becomes zero. The loops at this stage do not become flat in the middle portion as is normally expected for a sand-like material. On the contrary, they maintain a slight slope which is an indicative of low shear modulus. During each cycle of loading, the middle portion represents the time that the pore pressure increase is at the temporary highest level in that loop which results in the momentarily lowest value of the shear modulus of the sample. However, as the specimen reaches the momentarily peak strains in compression or extension in each loop, a slight dilation occurs which results in a higher shear modulus for the sample. This temporary increase in the shear modulus is seen as the slight "plunge" of the loops at each end which become more evident by the increase in the strain level.

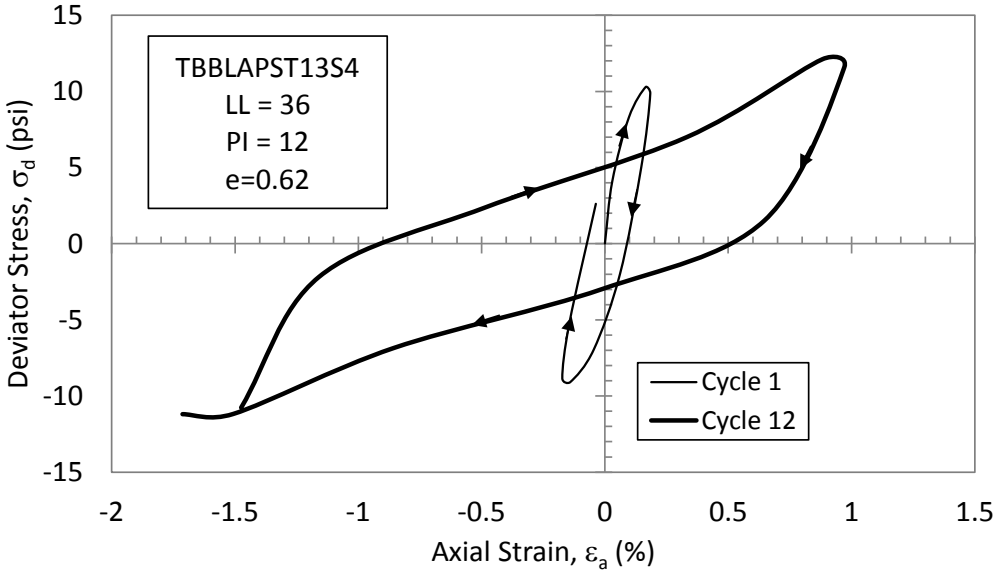

Figure 4.12: Stress-strain relationship in cycle 1 and cycle 12 for sample TBBLAPST13S4.

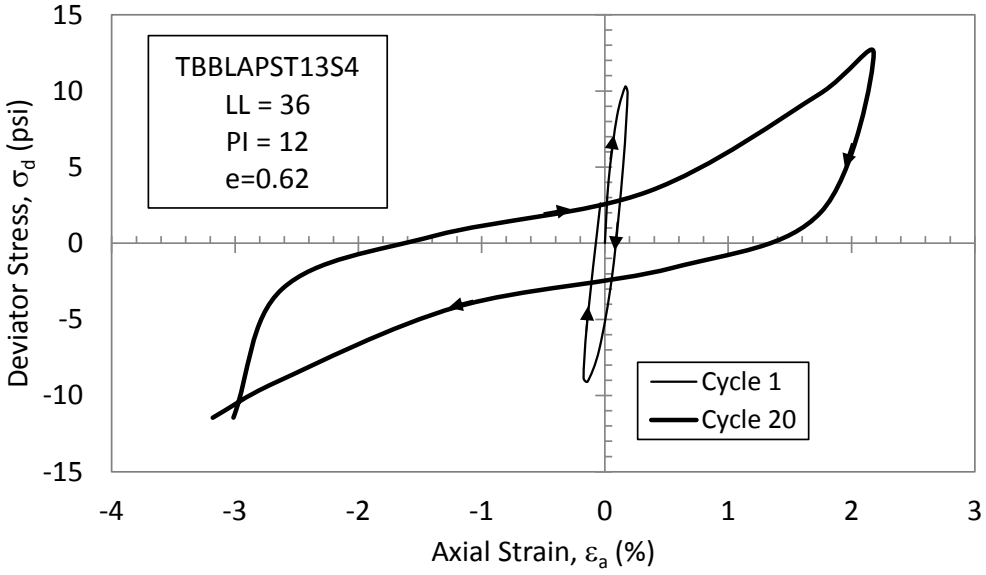

Figure 4.13: Stress-strain relationship in cycle 1 and cycle 20 for sample TBBLAPST13S4.

The stress path for sample TBBLAPST13S4 is shown in Figure 4.14 and Figure 4.15. The parameters p' and q are the mean effective stress and the deviatoric stress for the axisymmetric conditions respectively which are defined as follows:

$$p' = \frac{\sigma_1' + \sigma_2' + \sigma_3'}{3} = \frac{\sigma_1' + 2\sigma_3'}{3} \tag{4.1}$$

$$q = \sigma_1 - \sigma_3 \tag{4.2}$$

Since this test was performed at isotropic stress conditions, the initial p' value for this test was equal to the initial effective radial and axial stresses (σ_1' and σ_3' respectively). By applying the cyclic load, the deviator stress (q) began to increase from 0 psi to 12 psi (82.7 kPa) and the mean effective stress began to decrease from the initial value of 21.5 psi (148.2 kPa). The reduction in the mean effective stress is due to the compression in the sample which resulted in an increase in the pore pressure, which in turn reduced the effective confining stress. However, as the loading continued and the second half of the

loading cycle (i.e. reduced compression stage or lateral compression) was applied, the sample experienced dilation. The dilation behavior is identified by the increase in the mean effective stress (p') during the second half of the first loading cycle. During dilation, the pore pressure was reduced which in turn resulted in limited deformations and a temporary increase in the mean effective stress. However, by continuing the cyclic loading, the pore pressure gradually increased and the mean effective stress was decreased. Therefore, it appears that by applying further cycles of loading, the stress path moved to the left which corresponds to lower p' values. As the stress path migrated to the left (lower p' values), it approached the critical state line or the failure envelope line. Since monotonic compression and reduced-compression triaxial tests were not performed on these samples, the critical state parameters of this material are unknown. However, for clarification purposes, in Figure 4.14 two arbitrary failure envelopes are depicted for compression and reduced-compression. The strength of soil material is different in compression and extension. Therefore, the slopes of the failure envelope lines in these two directions are not necessarily the same. By further application of the loading cycles, the pore pressure became greater and the pore pressure ratio of 1.0 was momentarily achieved. At this point, the stress path encountered the failure envelope and the sample experienced failure during the reduced-compression stages (i.e. lateral compression) of the loading cycles. In Figure 4.15, the mean effective stress (p') and the deviator stress (q) are normalized by dividing both parameters by the initial mean effective stress (p_c'). The mechanical behavior of the sample TBBLAPST13S4 illustrates the

"cyclic mobility" behavior of coal mine tailings which agrees with the behavior observed from the hysteresis loops presented in Figure 4.10.

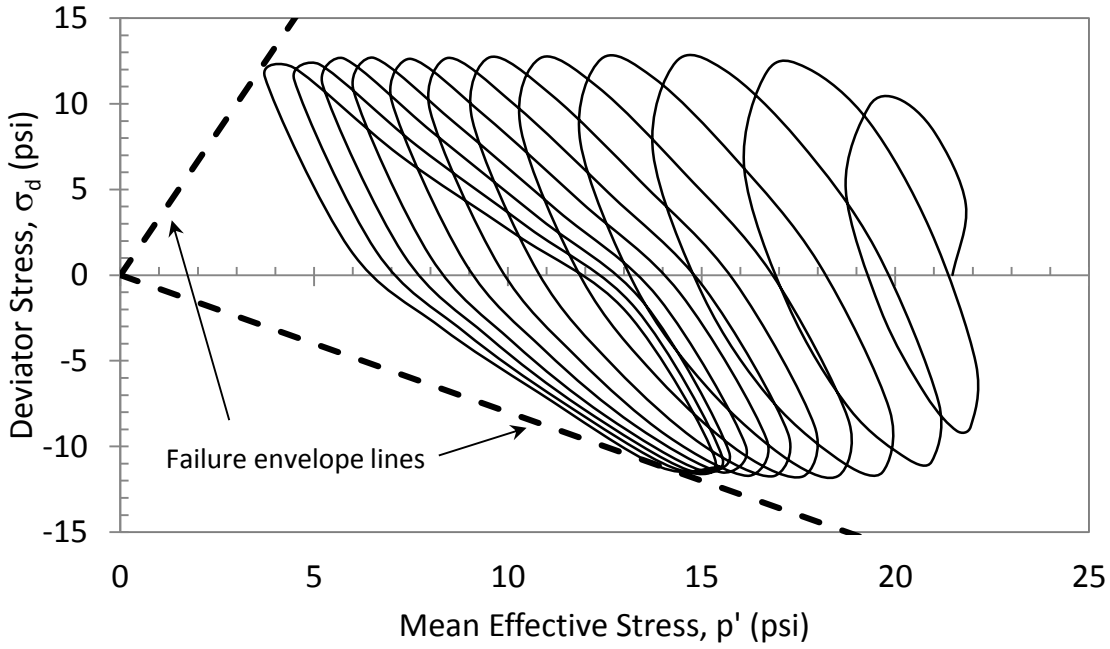

Figure 4.14: Stress path for sample TBBLAPST13S4.

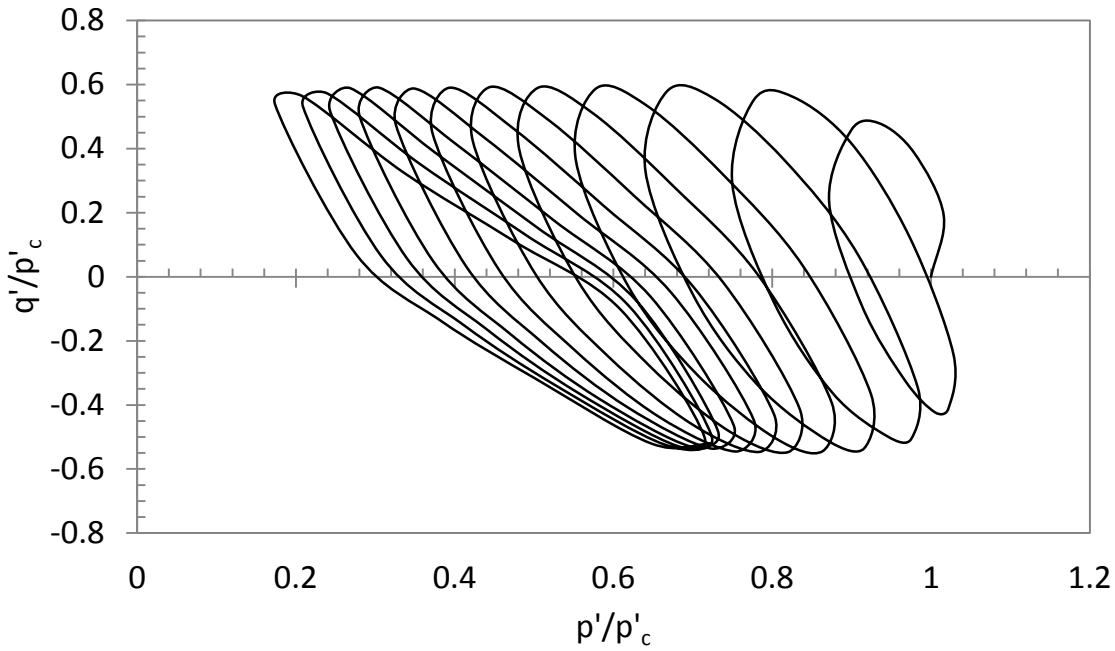

Figure 4.15: Normalized stress path for TBBLAPST13S4.

In Table 4.1, the grain size distribution, index properties, and the cyclic triaxial test results of all the samples are presented. The results of the entire set of geotechnical testing including the hydrometer and the cyclic triaxial tests are presented in Appendix A.

Table 4.1: Summary of the geotechnical properties and results of cyclic triaxial tests performed at a frequency of 1 Hz on isotropically consolidated coal mine tailings samples.

Sample	Classification						e_i	G_s	w_c/LL	σ'_c	σ'_d	# of cycles									
	FC %	5μ %	2μ %	LL %	PI %	USCS				psi	psi	r_u= 1.0	+1% SA	+2% SA	+3% SA	+4% SA	-1% SA	-2% SA	-3% SA	-4% SA	5% DA
TBBLDPST1S2	92	47	27	39	9	ML	0.55	1.95	0.8	23.0	12.0	70	94	131	169	--	106	--	--	--	--
TBBLDPST1S3	92	47	27	39	9	ML	0.58	1.95	0.7	20.6	13.2	6	12	22	36	55	8	17	--	--	46
TBBLDPST2S2	83	44	27	37	10	ML	0.97	2.5	0.5	24.2	17.2	4	3	5	9	16	1	2	3	4	4
TBBLDPST2S3	83	45	27	37	10	ML	0.97	2.5	0.9	31.9	17.0	20	5	11	18	26	5	13	23	--	17
TBBLDPST2S4	83	45	27	37	10	ML	0.89	2.5	0.8	33.4	13.0	140	34	73	100	117	64	--	--	--	114
TBBLDPST3S2	87	43	27	38	11	ML	0.72	2.09	0.9	30.0	18.5	109	35	108	--	--	4	27	--	--	--
TBBLDPST3S3	87	43	27	38	11	ML	0.81	2.09	0.9	30.0	9.5	65	4	13	23	33	--	--	--	--	--
TBBLDPST4S1	89	32	18	38	5	ML	0.72	1.89	0.7	25.7	15.0	12	18	23	26	29	14	--	--	--	29
TBBLDPST4S2	89	32	18	38	5	ML	0.72	1.89	0.9	30.8	13.0	155	115	132	143	149	111	130	--	--	138
TBBLDPST4S3	89	32	18	38	5	ML	0.78	1.89	0.9	27.6	14.0	47	48	59	64	68	47	--	--	--	64
TBBLAPST11S3	88	45	36	30	0	ML	0.62	1.69	1.0	16.0	7.7	26	9	26	42	60	4	11	--	--	--
TBBLAPST11S4	88	45	36	30	0	ML	0.63	1.69	1.3	7.1	6.7	15	26	41	--	--	26	--	--	--	--
TBBLAPST12S1	70	29	18	33	8	ML	0.62	1.76	1.0	11.1	4.4	79	--	--	--	--	131	--	--	--	--
TBBLAPST12S2	70	29	18	33	8	ML	0.55	1.76	1.0	12.3	6.6	84	37	--	--	--	37	--	--	--	--
TBBLAPST13S4	89	49	31	36	12	CL	0.62	2.08	0.8	21.5	12.0	11	11	19	25	31	7	14	20	26	20
TBBLAPST14S3	87	47	29	38	14	CL	0.97	2.47	0.9	28.4	16.2	11	3	7	10	14	1	3	7	--	7
TBBLAPST14S4	87	47	29	38	14	CL	1.07	2.47	0.9	25.7	13.6	20	9	22	33	46	6	18	--	--	27
TBBLAPST15S1	82	41	25	39	10	ML	0.56	1.92	0.8	29.9	14.5	55	36	66	--	--	29	--	--	--	--
TBBLAPST15S2	82	41	25	39	10	ML	0.62	1.92	0.8	30.2	20.8	6	5	11	17	26	2	7	--	--	17
TBBLAPST15S3	82	41	25	39	10	ML	0.62	1.92	0.8	28.0	15.6	24	16	29	--	--	5	--	--	--	--

Table 4.1 (cont.): Summary of the geotechnical properties and results of cyclic triaxial tests performed at a frequency of 1 Hz on isotropically consolidated coal mine tailings samples.

Sample	Classification						e_i	G_s	w_c/LL	σ'_c	σ'_d	# of cycles									
	FC %	5μ %	2μ %	LL %	PI %	USCS				psi	psi	r_u= 1.0	+1% SA	+2% SA	+3% SA	+4% SA	-1% SA	-2% SA	-3% SA	-4% SA	5% DA
TBBLAPST15S3	82	41	25	39	10	ML	0.62	1.92	0.8	28.0	15.6	24	16	29	--	--	5	--	--	--	--
TBBLAPST15S4	82	41	25	39	10	ML	0.61	1.92	0.7	26.5	13.3	281	333	--	--	--	301	--	--	--	--
TBBLAPST16S1	83	31	19	43	7	ML	0.96	2.16	0.8	31.8	27.5	2	2	4	9	18	1	2	4	7	4
TBBLAPST16S2	83	31	19	43	7	ML	1.23	2.16	0.9	32.0	22.0	3	4	6	9	14	1	--	--	--	11
TAFLBPST1S1	79	37	28	39	10	ML	0.53	1.91	0.6	40.3	22.2	35	10	27	38	48	--	--	--	--	51
TAFLBPST1S2	79	37	28	39	10	ML	0.52	1.91	0.6	40.7	33.6	7	110	139	156	168	82	133	168	--	146
TAFLBPST2S1	84	45	33	43	16	ML	0.51	1.90	0.6	51.8	40.8	10	173	--	--	--	116	173	194	207	204
TAFLBPST3S1	80	41	26	42	16	ML	0.61	2.06	0.6	58.0	34.4	125	68	93	112	119	50	84	111	--	104
TAFLBPST3S2	80	41	26	42	16	ML	0.64	2.06	0.6	54.9	44.0	37	46	70	85	95	13	40	57	71	64
TAFLAPST1S1	84	48	33	38	14	CL	0.52	2.02	0.5	58.9	44.1	21	5	16	27	--	3	10	18	26	17

Definitions:

FC: percentage of particles smaller than 75 μm

5 μ: percentage of particles smaller than 5 μm

2 μ: percentage of particles smaller than 2 μm

LL: Liquid Limit

PI: Plasticity Index

USCS: Unified Soil Classification System

e_i: initial void ratio at which the test was performed

G_s: Specific Gravity

ω_c/LL: Ratio of the in-situ water content and the liquid limit

σ_c' : Applied effective consolidation stress

σ_d' : Applied peak deviator stress

$r_u = 1.0$: Number of cycles to reach the peak pore pressure ratio

+1% SA: Number of cycles required to reach 1% axial strain in compression

+1% SA: Number of cycles required to reach 1% single amplitude axial strain in compression

-1% SA: Number of cycles required to reach 1% single amplitude axial strain in extension

5% DA: Number of cycles required to reach 5% double amplitude axial strain

4.2.2 Influence of Initial Confining Stress

The undrained shear strength of a normally consolidated saturated soil is proportional to the applied effective confining stress. This forms the basis of the commonly used Mohr-Coulomb failure criterion. For cyclic strength of soils, similar trend has been observed. Based on tests performed on reconstituted Sacramento River sand, Lee and Seed (1967) state that the peak deviator stress required to cause peak cyclic pore pressure ratio of 100% increased linearly with an increase of the initial effective confining stress. Castro and Poulos (1977) reported the same results for the tests on sand specimens.

To include the overburden stress influence in determining the factor of safety against liquefaction, Seed (1983) introduced the correction factor K_σ to extrapolate the liquefaction susceptibility evaluation to soil layers with overburden pressures greater than 100 kPa (14.5 psi). Seed and Harder (1991), suggested modifications to calculate K_σ for clean sands which assumed a nonlinear decreasing trend for K_σ with a value of one at 1 atm (14.5 psi) and 0.44 at 8 atm (117.5 psi). Based on the studies performed by Hynes and Olsen (1999), Youd et al. (2001) suggested an equation for K_σ in the following form: $K_\sigma = (\sigma'_{v0}/P_a)^{(f-1)}$, where σ'_{v0} is the effective vertical stress, P_a is the atmospheric pressure, and f is an exponent that is a function of the soil's relative density. This equation produces lower values of K_σ for higher confining stresses as well. In Table 4.2, the summary of geotechnical properties of the samples obtained from the Big Branch and Abner Fork impoundments along with their test results are presented.

Table 4.2: Summary of geotechnical properties of the coal mine tailings used to develop the cyclic strength curves.

Sample	depth (ft)	FC (%)	5μ (%)	2μ (%)	USCS	Gs	e_i	LL (%)	PI (%)	σ'_{v0} (psi)	σ'_{vc} (psi)	OCR	σ'_d (Psi)	CSR
TBBLDPST1S2	85	92	47	27	ML	1.95	0.55	39	9	21	23	0.9	12.0	0.26
TBBLDPST1S3	86	92	47	27	ML	1.95	0.58	39	9	21	21	1.0	13.2	0.32
TBBLDPST2S2	106	83	44	27	ML	2.5	0.97	37	10	26	24	1.1	17.2	0.36
TBBLDPST2S3	106	83	45	27	ML	2.5	0.97	37	10	26	32	0.8	17.0	0.27
TBBLDPST2S4	107	83	45	27	ML	2.5	0.89	37	10	26	33	0.8	13.0	0.19
TBBLDPST3S2	125	87	43	27	ML	2.09	0.72	38	11	31	30	1.0	10.0	0.17
TBBLDPST4S1	145	89	32	18	ML	1.89	0.72	38	5	36	26	1.4	15.0	0.29
TBBLDPST4S2	146	89	32	18	ML	1.89	0.72	38	5	36	31	1.2	13.0	0.21
TBBLDPST4S3	146	89	32	18	ML	1.89	0.78	38	5	36	28	1.3	14.0	0.25
TBBLAPST11S3	36	88	45	36	ML	1.69	0.62	30	0	8	13	0.6	7.7	0.30
TBBLAPST12S1	55	70	29	18	ML	1.76	0.62	33	8	12	11	1.1	4.4	0.20
TBBLAPST13S4	77	89	49	31	CL	2.08	0.62	36	12	17	22	0.8	12.0	0.28
TBBLAPST14S3	97	87	47	29	CL	2.47	0.97	38	14	22	28	0.8	16.2	0.29
TBBLAPST14S4	97	87	47	29	CL	2.47	1.07	38	14	22	26	0.8	13.6	0.26
TBBLAPST15S1	115	82	41	25	ML	1.92	0.56	39	10	26	30	0.9	14.5	0.24
TBBLAPST15S2	116	82	41	25	ML	1.92	0.62	39	10	26	30	0.9	20.8	0.34
TBBLAPST15S3	116	82	41	25	ML	1.92	0.62	39	10	26	28	0.9	15.6	0.28
TBBLAPST16S1	135	83	31	19	ML	2.16	0.96	43	7	30	32	1.0	27.5	0.43
TBBLAPST16S2	136	83	31	19	ML	2.16	1.23	43	7	31	32	1.0	22.0	0.34
TAFLBPST1S2	171	79	37	28	ML	1.91	0.52	39	10	41	41	1.0	33.6	0.41
TAFLBPST3S1	220	80	41	26	ML	2.06	0.61	42	16	53	48	1.1	34.4	0.36
TAFLBPST3S2	220	80	41	26	ML	2.06	0.64	42	16	53	55	1.0	44.0	0.40
TAFLAPST1S1	240	84	48	33	CL	2.02	0.52	38	14	59	59	1.0	44.1	0.37

Definitions:

$\sigma_{v0}^{'}$: In-situ effective consolidation stress

$\sigma_{vc}^{'}$: Applied effective consolidation stress

See Table 4.1 for full definitions

The samples presented in Table 4.2 developed a peak pore pressure ratio of 1.0, during the cyclic triaxial test and, therefore, are used in developing cyclic strength curves. The number of uniform stress cycles to reach the peak pore pressure ratio, $r_u = 1.0$, versus the applied peak cyclic deviator stress are illustrated in Figure 4.16. The empty data points depict the data from the Big Branch impoundment while the filled data points are representative of the samples from the Abner Fork tailings dam. By inspection of the Abner Fork data, it appears that the cyclic strength is influenced by the effective confining stress applied in the lab. For example, at 20 cycles, the deviator stress necessary to achieve the $r_u = 1.0$ for the Abner Fork sample with 59 psi (406.8 kPa) initial confining stress is 44 psi (303.4 kPa), while this value for the Abner Fork sample with 56 psi initial confining stress is slightly lower (97%) and equal to 43 psi (296.5 kPa). The Abner Fork sample with the 41 psi (282.7 kPa) initial confining stress is located considerably lower compared to the other samples from Abner Fork. This trend confirms the idea that an increase in the confining stress increases the strength of the sample. However, due to lack of sufficient data points this comparison cannot be quantified.

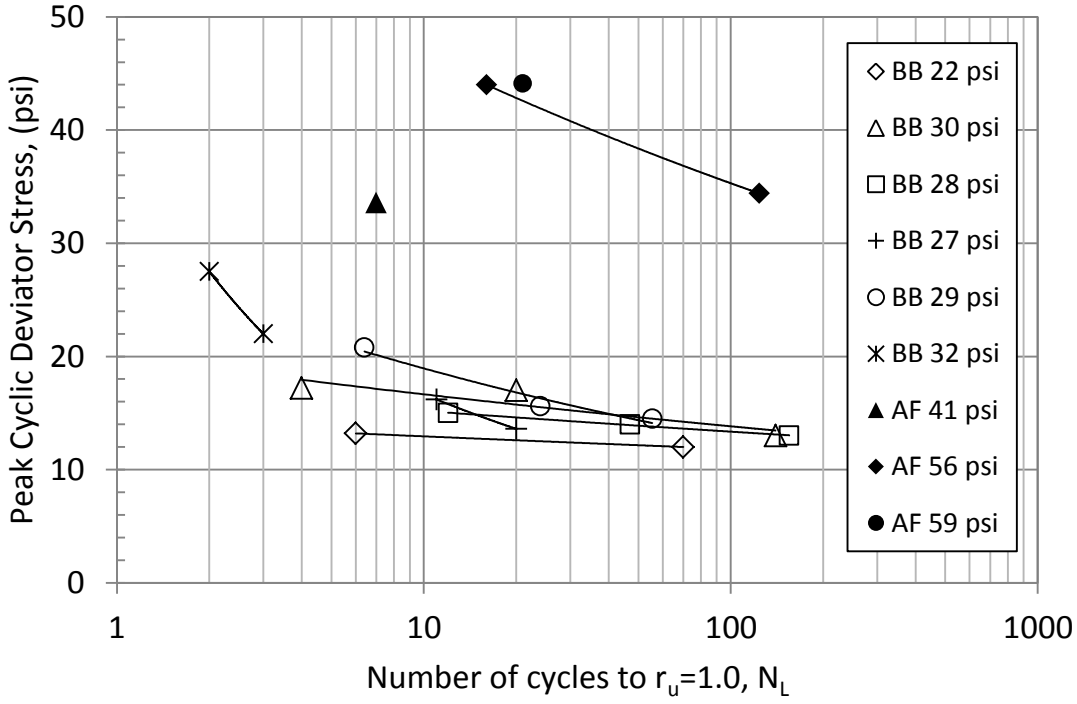

Figure 4.16: Influence of confining stress on number of cycles required to develop r_u=1.0 versus applied peak deviator stress for specimens from Big Branch (BB) and Abner Fork (AF).

Based on close inspection of the results, it appears that the Big Branch samples are also slightly influenced by the laboratory applied confining stresses. The Big Branch sample with the lowest initial confining stress (22 psi or 151.7 kPa) has the lowest strength among all the samples, i.e. 62% of the 29 psi (199.9 kPa) sample. The samples with the higher values of initial confining stresses (29 psi to 32 psi or 199.9 to 220.6 kPa) exhibited the highest strength in this test. Also the samples with the initial confining stress between the maximum and minimum such as 27 psi and 28 psi performed with a medium strength and are located between the lowest and highest strength samples on this plot. In general, it appears that the Abner Fork samples with higher initial confining stresses required higher cyclic deviator stresses to obtain pore pressure ratio of 1.0. Although the influence

of initial confining stress on the strength of the samples from each individual impoundment is not significant.

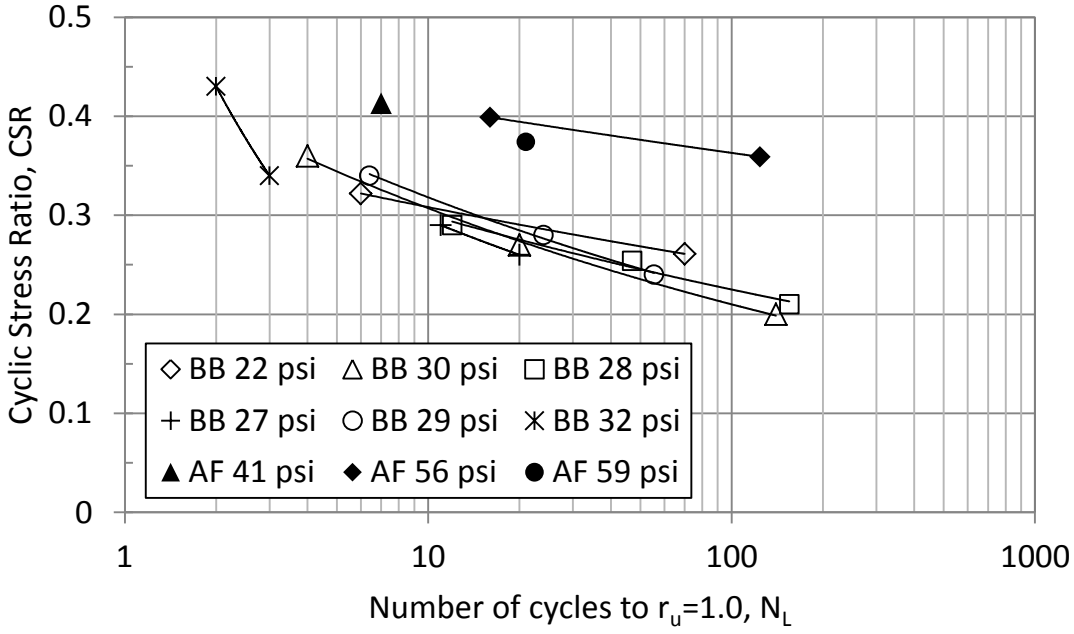

Figure 4.17: Influence of confining stress on the number of cycles required to develop r_u = 1.0 versus applied cyclic stress ratio for specimens from Big Branch (BB) and Abner Fork (AF).

The data presented in Figure 4.16 suggest that it might be possible to ignore the site effect and not differentiate between the sites that the samples were recovered from. By not considering whether the samples were recovered from the Abner Fork or the Big Branch impoundments, it appears that the higher the initial confining stress is the higher the strength of the sample will be. However, due to lack of sufficient data, it is preferred to not generalize this conclusion. Also, it should be considered that these samples are "undisturbed" samples that are obtained from two different locations. The plasticity, the fabric of the sample and the age can be influential although the two latter are not quantified in this study. Therefore, it is believed that the results are site specific and the

generalization of this conclusion by ignoring the site effect will be left pending on future studies with a broader number of samples.

In Figure 4.17, the same results as Figure 4.16 are presented with the exception that the peak deviator stress is converted to cyclic stress ratio, *CSR*, to represent the strength of the sample. It is observed that normalizing the deviator stress by the confining stress, $CSR = \sigma_d'/2\sigma_c'$, eliminates the effect of confining stress for each site. However, the results from the two sites are still distinctively apart and using the CSR parameter did not eliminate the site effect.

In Figure 4.18 the correlation between the CSR values and the number of cycles to reach the pore pressure ratio of 1.0 for the coal mine tailings in this study is compared to the results of similar tests on various mine tailings provided by Wijewickreme et al. (2005). Some of the data points from previous studies included in Figure 4.18 are provided by cyclic triaxial testing and are labeled by CTX and the rest of the data points including the results of Wijewickreme et al. (2005) are measured through Direct Simple Shear testing and are labeled by DSS. The results presented in Figure 4.18 indicate that the cyclic resistance ratio of mine tailings measured by cyclic triaxial testing are significantly higher than those measured by direct simple shear testing for the same mine tailings material. Wijewickreme et al. (2005) state that although this difference could be considered mainly a result of the difference in the mode of loading between DSS and triaxial tests (Roscoe, 1970; Seed and Peacock, 1971; Finn et al., 1978; Donaghe and Gilbert, 1983), it may also be attributable to the manner in which τ_{cy} in DSS tests and $(\sigma_d)_{cy}/2$ in triaxial tests are

normalized (i.e., the use of σ'_{vc} for normalizing both test types). It seems that the correlation provided by this study on the Big Branch coal mine tailings samples is in close agreement with the results of the cyclic triaxial tests performed by Ishihara et al. (1980) on Quartz slime. However, it is noted that Ishihara et al. (1980) considered the state of liquefaction as when the samples experienced a double amplitude strain of 5%, while in this study the liquefaction was defined based on pore pressure ratio of 1.0. The Abner Fork samples appear to exhibit the highest cyclic resistance ratio among all of the various studies. However, the Abner Fork samples experienced the longest storage time in the laboratory testing and the results could be influenced as was discussed in Section 3.4.

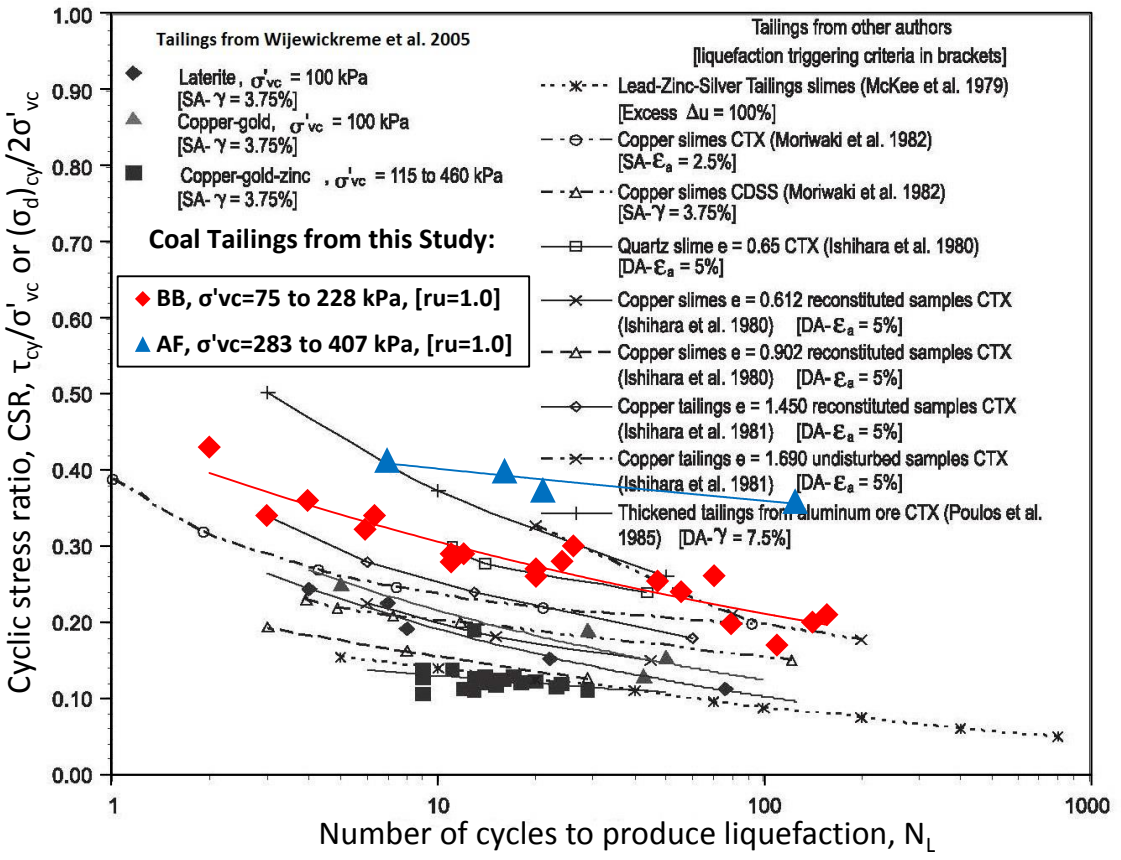

Figure 4.18: Comparison of the correlation between CSR and number of cycles for the coal mine tailings and the correlations presented by Wijewickreme et al. (2005).

4.2.3 Influence of Overconsolidation Ratio

The influence of overconsolidation on the cyclic strength of some soils has been investigated in a number of studies. These studies that were mainly performed on sandy soils, suggest that for a given soil density, the required stress to reach failure after a certain number of cycles increases with an increase in the overconsolidation ratio (e.g. Seed and Peacock, 1971, Lee and Focht, 1975, Ishihara et al., 1978, Ishihara and Takatsu, 1979, Dobry et al., 1981, Campanella and Lim, 1981, Stamatopoulos et al., 1995, Nagase et al., 1996). Herein, overconsolidation ratio (OCR) is defined as the maximum previous effective confining pressure divided by the in situ effective confining pressure.

The effect of overconsolidation on the number of cycles required to achieve a peak cyclic pore pressure ratio of 1.0, $r_u = 1.0$ was first studied by Seed and Peacock (1971). In their study, sand specimens with a relative density (D_r) of 50% were tested in simple shear conditions. Seed and Peacock (1971) observed that the cyclic stress ratio required to reach $r_u = 1.0$ increased by a factor of 1.6 when the OCR was increased from 1 to 4.

The applied peak cyclic deviator stress versus the number of cycles to obtain $r_u = 1.0$ in the coal mine tailings specimens recovered at the Big Branch impoundment with an emphasis on the over-consolidation ratio are demonstrated in Figure 4.19.

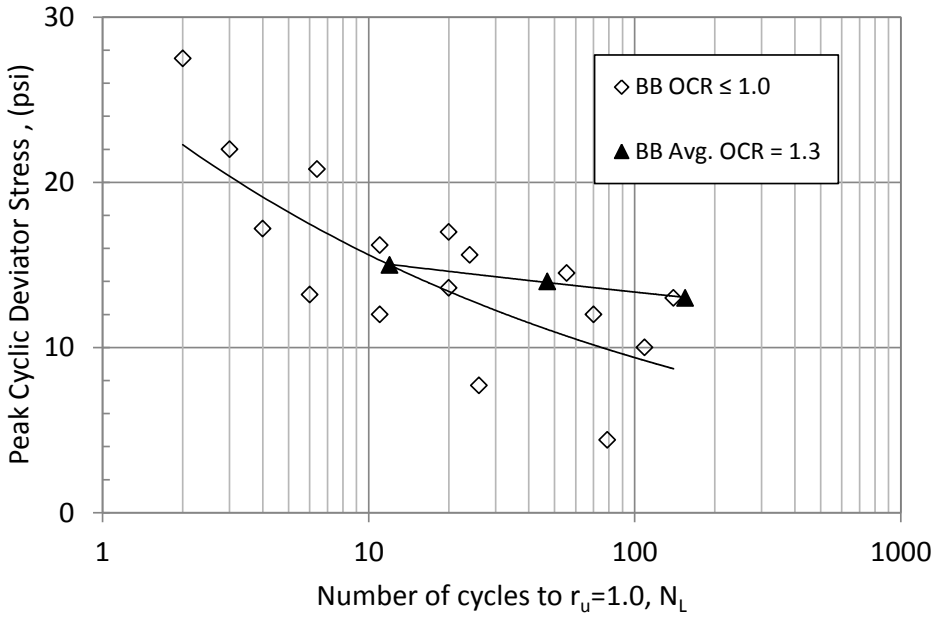

Figure 4.19: Influence of over-consolidation on the number of cycles to develop r_u=1.0 versus applied peak deviator stress for the Big Branch specimens (BB).

In this study, due to a lack of sufficient undisturbed samples, the influence of the overconsolidation could not be investigated in depth. To investigate the effect of overconsolidation, the stress history of the sample should be determined accurately by performing laboratory consolidation tests. Due to the limited number of available undisturbed samples, laboratory consolidation tests were not performed on the coal mine tailings specimens and therefore the in-situ effective stress of the samples was estimated based on the depth, density, void ratio, and elevation of the phreatic surface. Most specimens were tested at their estimated in-situ estimated confining stress and only the samples obtained from one piston were tested at a consolidation stress slightly lower than the estimated initial confining stress. Consequently, the samples obtained from the Big Branch impoundment provided in piston 4, were tested at an overconsolidation ratio of 1.3.

Observation of the results from Figure 4.19 suggests that the slightly overconsolidated coal mine tailings samples did not behave significantly different to reach $r_u = 1.0$. The data points from the slightly overconsolidated samples are clustered within the normally consolidated samples and do not exhibit a significant difference. These results are also presented in Figure 4.20 by converting the cyclic deviator stress to cyclic stress ratio. As it appears, even the slight difference between the trends of the two sets of data is eliminated by normalizing the deviator stress by the confining stress. It is believed that to investigate the influence of overconsolidation on the cyclic behavior of coal mine tailings, a broader study with sufficient number of undisturbed samples and application of higher OCR values is necessary.

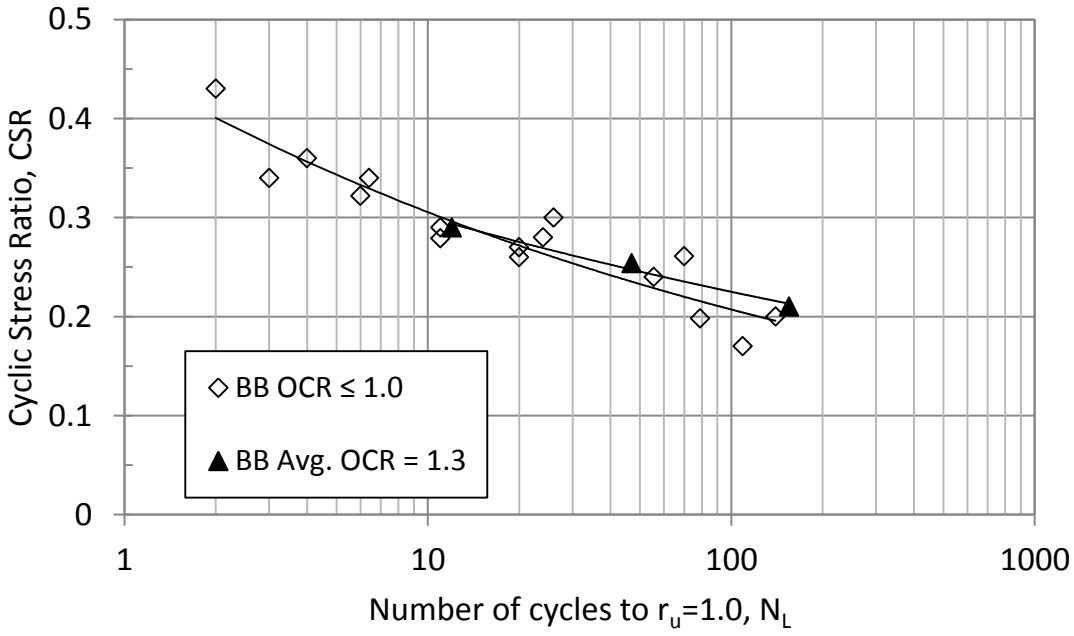

Figure 4.20: Influence of over-consolidation on the number of cycles required to develop r_u = 1.0 versus applied cyclic stress ratio for specimens obtained from the Big Branch impoundment (BB).

4.2.4 Influence of Soil Plasticity

The average value, standard deviation, minimum value, and maximum value of void ratio, liquid limit, plasticity index, fines content, amount of particles smaller than 2 μm, and amount of particles smaller than 5 μm for the coal mine tailings samples used in this study are presented in Table 4.3 and Table 4.4. These tables include the results of the samples obtained from the Big Branch and Abner Fork impoundments. The information regarding these samples was presented in Table 4.2 and used to prepare the plot of the cyclic strength of the material versus the number of cycles to achieve $r_u = 1.0$.

Table 4.3: Average index properties of the Big Branch samples listed in Table 4.2.

	e_i (1)	LL % (2)	PI % (3)	FC % (4)	2μ % (5)	5μ % (6)
Average Value	0.78	38	9	85	25	40
Standard Deviation	0.2	2.9	3.4	4.9	5.1	6.8
Minimum Value	0.55	30	0	70	18	29
Maximum Value	1.23	43	14	89	36	49

Definitions:
e_i: initial void ratio at which the test was performed
LL: Liquid Limit
PI: Plasticity Index
FC: percentage of particles smaller than 75 μm
2 μ: percentage of particles smaller than 2 μm
5 μ: percentage of particles smaller than 5 μm

A comparison between the values of the parameters presented in Table 4.3 and Table 4.4 demonstrates that the amount of fine particles by any of the selected criteria is similar in both of the Big Branch and Abner Fork impoundments. However, it is noticed that generally, the Abner Fork samples compared to the Big Branch samples exhibited lower void ratios (denser samples) and higher plasticity indices. The average liquid limit

values from both dams are similar, but the minimum liquid limit for the Abner Fork samples is higher compared to the Big Branch specimens.

Table 4.4: Average index properties of the Abner Fork samples listed in Table 4.2.

	e_i (1)	LL % (2)	PI % (3)	FC % (4)	2μ % (5)	5μ % (6)
Average Value	0.57	40	14	81	28	42
Standard Deviation	0.1	2.1	2.8	2.0	3.3	4.6
Minimum Value	0.52	38	10	79	26	37
Maximum Value	0.64	42	16	84	33	48

Definitions:
e_i: initial void ratio at which the test was performed
LL: Liquid Limit
PI: Plasticity Index
FC: percentage of particles smaller than 75 μm
2 μ: percentage of particles smaller than 2 μm
5 μ: percentage of particles smaller than 5 μm

Due to the differences in mineralogy, particle size, gradation, and plasticity, direct comparisons cannot be made between the densities of individual samples to investigate the effect of void ratio on their liquefaction resistance. For example, specimen TBBLDPST4S1 with a void ratio of 0.72, and plasticity index of 5.0% required 12 cycles to obtain $r_u = 1.0$ at a cyclic stress ratio of 0.29. On the other hand, sample TBBLAPST15S3 with a void ratio of 0.62, and plasticity index of 10.0% required 24 cycles to obtain $r_u = 1.0$ at a cyclic stress ratio of 0.28. It is observed that by applying approximately equal cyclic stress ratios to these samples, the sample with a higher plasticity index and lower void ratio required more cycles to achieve a peak pore pressure ratio of 1.0. However, this increase in the number of cycles cannot be solely attributed to either the individual effect of void ratio or plasticity. These results suggest that the increase in cyclic stress

ratio between the two specimens is partly due to lower void ratio and partly due to higher plasticity.

On the other hand, by comparing sample TBBLDPST4S1 to sample TBBLAPST11S3, an opposite effect is observed. The specimen TBBLDPST4S1 with a void ratio of 0.72, and plasticity index of 5 required 12 cycles to obtain $r_u = 1.0$ by applying CSR=0.29, while the specimen TBBLAPST11S3 with a void ratio of 0.62, and plasticity index of 0 required 26 cycles to obtain $r_u = 1.0$ by applying CSR=0.30. Therefore, the looser sample with higher plasticity index required less cycles to obtain $r_u = 1.0$ compared to the denser sample with lower plasticity index. Here, it appears that the influence of the plasticity was masked by the effect of void ratio. Therefore, the looser sample with higher plasticity index required less cycles to reach the "cyclic mobility". It should be noted that the individual samples that were chosen to be compared, had experienced similar cyclic stress ratios. The number of samples tested in this study was limited and therefore not many samples with the same CSR could be selected for comparison. Thus, no clear conclusion can be drawn based on individual comparisons to assess the influence of plasticity index and void ratio. However, when the samples are grouped together as representative samples of each tailings dam, some trends were observed which are presented later in this study.

Some researchers have reported some trends on the influence of plasticity index and void ratio on the cyclic behavior of tailings material. By performing laboratory tests, Ishihara et al. (1980) and Ishihara et al. (1981) demonstrated that relative density "does not serve as a useful measure to consistently express the denseness and looseness of the

materials" considering that the grain size of typical tailings materials ranges from that of clay to coarse sand. Ishihara et al. (1980) found that the cyclic resistance of tailings samples correlates well with the void ratio. In their study they found the material to have greater cyclic resistance at lower void ratios. Nonetheless, their study suggested that for specimens at the same void ratio, the cyclic strength of the material increases as the plasticity index decreases for plasticity indices less than 11%. However, Ishihara et al. (1980) also concluded that samples with plasticity indices in the range of 15-20% had significantly higher cyclic strength compared to nonplastic tailings. In this study, plasticity index of 74% of the Big Branch samples was equal to or lower than 11, while plasticity index of 75% of the Abner Fork samples was greater than 11. Therefore, the opposite effect of plasticity index on cyclic behavior of some of Big Branch samples (higher plasticity, same void ratio, required lower number of cycles to achieve $r_u = 1.0$) agrees with the observed behavior by Ishihara et al. (1980). However, due to lack of sufficient evidence in this study, this trend is not concluded for the samples from the same tailings dam. By studying the results of cyclic triaxial tests on various tailings materials including, zinc, lead, gold, silver, and copper, Ishihara et al. (1981) found that the cyclic strength of the tailings specimens was not closely related to variation in void ratio or grain size. However, they found that for the tailings samples exhibiting plasticity index between 10 and 40, the cyclic strength tended to increase as the plasticity index became larger. They suggested that the samples with higher void ratios in their study also contained greater percentage of fines and thus benefitted from the increased resistance to shearing due to increased cohesion.

In Figure 4.21, the results of cyclic triaxial tests performed on four of the Big Branch samples at the frequency of 1.0 Hz and approximately the same *CSR* are presented. In these plots the first cycle and the cycle at which the tailings material experienced the peak pore water pressure ratio, $r_u = 1.0$, are depicted.

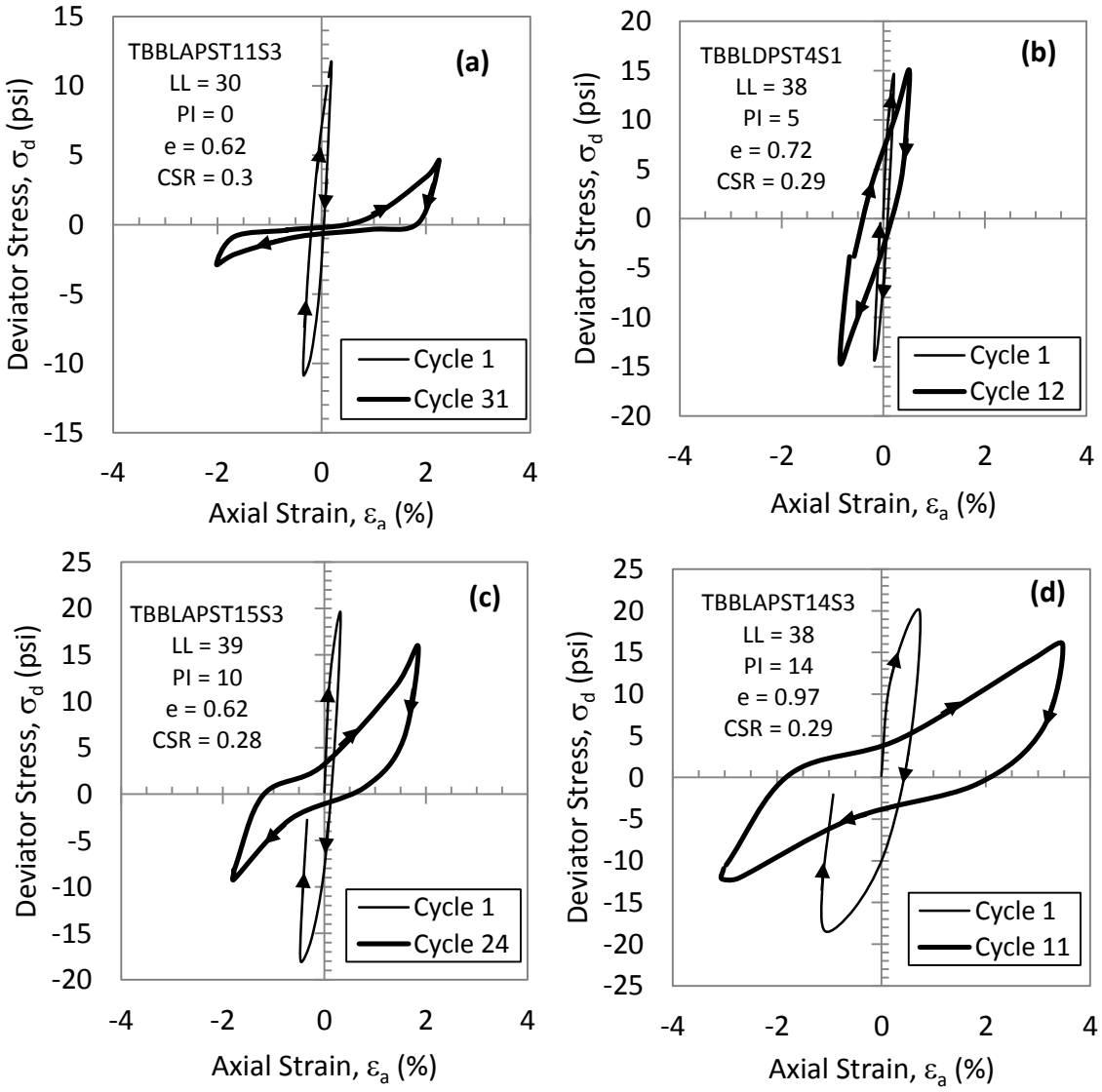

Figure 4.21: Stress-strain relationship for the first cycle of loading and the cycle at which the sample obtained r_u = 1.0 for representative Big Branch specimens.

For these samples, the *PI* and *e* range from 0-14% and 0.62-0.97, respectively. By inspection, some differences between the behaviors of these samples were observed. For example, it appears that during the first cycle, specimens with lower plasticity have developed lower strain levels in extension. Also, it is noticed that generally the looser samples, i.e. higher void ratio, required fewer cycles to obtain $r_u = 1.0$. For example, the sample presented in Figure 4.21b required fewer cycles compared to the sample presented in Figure 4.21b. The same trend is identified between Figure 4.21b and Figure 4.21c in which the denser sample required higher number of cycles. This trend is consistent with observations that have historically been made in soils (Vucetic and Dobry, (1991), Guo and Prakash (1999), Prakash and Puri (2006), El Hosri et al. (1984)).

By comparing any of the sample results presented in Figure 4.21, it is observed that an increase in the plasticity index is not necessarily accompanied by an increase in the void ratio. Also, by an in depth comparison between the plots, it appears that the influence of the plasticity index is dependent on the magnitude of the *PI*. For the samples with lower *PI* values such as the ones presented in Figure 4.21a, Figure 4.21b, and Figure 4.21c, the denser samples required more cycles to experience cyclic mobility irrespective of the *PI* value.. However, by comparing the samples presented in Figure 4.21d and Figure 4.21b, based on the effect of void ratio it is expected that the looser material achieves the peak pore pressure ratio more rapidly. However, this sample required almost the same number of cycles (11 cycles) by having a higher void ratio and a higher plasticity index.

Another aspect that can be perceived from the plots presented in Figure 4.21 is the shape of the stress-strain loops for the coal mine tailings samples. By inspecting these plots, one of the shortcomings of the testing equipment becomes evident. The required cyclic deviator stress was supposed to be uniform and have the same amplitude regardless of the strain level in the specimen. However, except for the sample presented in Figure 4.21b, as the samples exhibited cyclic mobility behavior and experienced larger strain levels, the equipment could not apply the requested load in the given time (i.e. frequency = 1 Hz) and the applied deviator stress became smaller than the requested level. However, regardless of this issue the shape of the loops was studied as was suggested by Boulanger and Idriss (2004). It is noticed that by an increase in the plasticity index, the shape of the loops varied considerably. By an increase in the PI value, it seems that the cyclic behavior changes from sand-like behavior to clay-like behavior. The sample presented in Figure 4.21a, with the PI=0, has almost flat portions in the middle of the loops and the loops have no width which are indicators of complete loss of the strength and exhibition of classic liquefaction behavior. By increasing PI values, the loops become broader and the slope of the loops gain some value which indicates that the sample still has some strength and the shear modulus is greater than zero and thus it can be considered a clay-like behavior with exhibition of “cyclic mobility”. It is interesting to note that eventually all of the samples except for the one presented in Figure 4.21b, experienced dilation during shearing leading to the development of “banana loops”.

In Figure 4.22, the relationship between the number of cycles to achieve the peak pore pressure ratio and the applied cyclic stress ratio for the samples obtained from the

Big Branch and Abner Fork impoundments is depicted. As it is illustrated, the Abner Fork samples with higher plasticity indices and lower void ratios exhibited higher cyclic strength compared to the generally looser Big Branch specimens with lower plasticity. For example, as shown by the best fit lines, to reach the peak pore pressure ratio in 10 cycles, the Big Branch samples would most likely require a cyclic stress ratio of 0.3 while this number is increased to CSR=0.4 for the Abner Fork samples. This shows an approximate 33% increase in the CSR while the average PI is increased by 44% and the void ratio is decreased by 27%. It is believed that a combined effect of void ratio and the plasticity behavior results in the difference between the cyclic strength values observed in the coal mine tailings and a differentiation between the effects of these two geotechnical properties cannot be made.

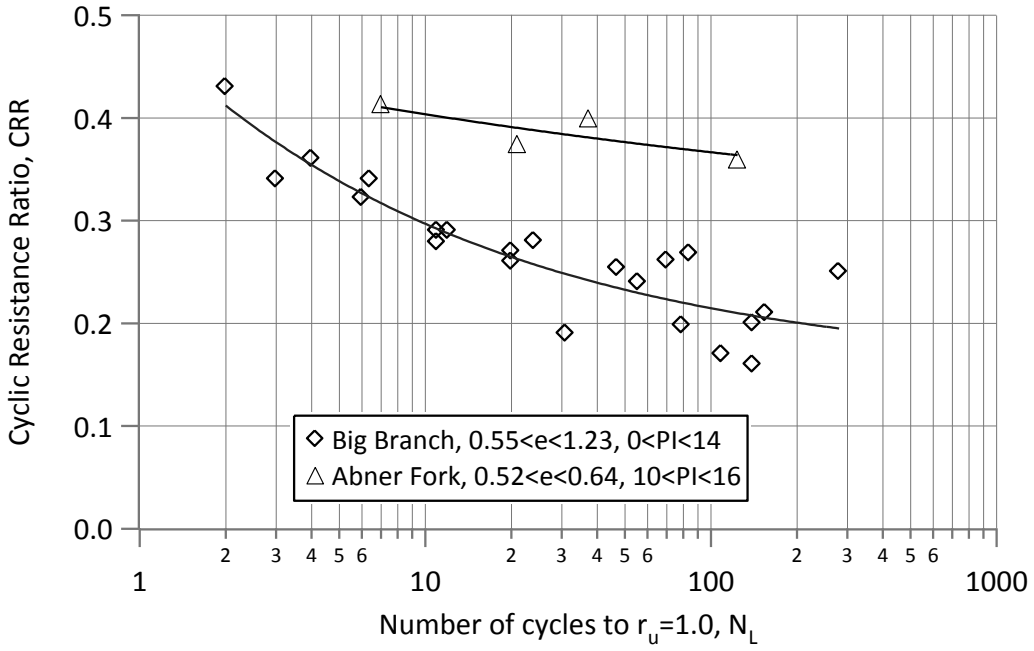

Figure 4.22: Influence of void ratio and plasticity on the number of cycles required to develop r_u = 1.0 versus applied cyclic stress ratio for coal mine tailings specimens from Big Branch (e_{avg}=0.78, PI_{avg}=9) and Abner Fork (e_{avg}=0.57, PI_{avg}=13).

The cyclic stress ratio required to obtain the peak pore pressure ratio, $r_u = 1.0$, in coal mine tailings samples investigated in this study ranged between 0.17 to 0.43. It was observed that by applying lower CSR values, for example closer to 0.10, it became almost impossible to cause a significant increase in the pore pressure. Thus the samples exhibited the ability to go under virtually infinite number of cycles without developing high pore pressure ratios to be considered under the category of "cyclic mobility". By applying CSR values higher than 0.40, the Big Branch samples experienced cyclic mobility in only 2 to 3 cycles while the Abner Fork sample required 7 cycles (3.5 times) to achieve cyclic mobility.

4.3 Post Cyclic Triaxial Tests

After observation of excessive deformation or occurrence of liquefaction or cyclic mobility during the cyclic triaxial test, the loading was terminated and the sample was subjected to a strain controlled monotonic triaxial test following the ASTM D2850 standard. As stated in previous studies (e.g. Seed, 1987; Seed and Harder, 1991; and Stark and Mesri, 1992), the measurement of the undrained shear strength of soil after liquefaction can assist in the stability assessment or estimation of deformation of earth structures.

During an earthquake, some of these low plasticity coal mine tailings might experience liquefaction and begin to flow down the slopes that the tailings impoundment has been built on. However, most of the samples demonstrated cyclic mobility behavior, which is characterized by high pore pressure and small deformation. In this case, when strong ground motion stops, the relatively low plasticity material would have high pore

water pressures and reduced strength. Therefore, post-liquefaction monotonic triaxial tests were performed. Unconsolidated-undrained (UU) triaxial tests were performed in accordance with ASTM D2850 to estimate the short-term peak and residual undrained shear strength, which would be critical immediately after the earthquake.

On most of the cyclic triaxial samples, a post-cyclic UU-type triaxial test was performed. One of the main shortcomings of the equipment in this stage of test inhibited performing this test thoroughly. Considering that the triaxial equipment had a frameless loading mechanism and also acknowledging that the load cell was placed inside the chamber, the triaxial cell did not have sufficient stroke to perform the monotonic test to the maximum level of strain. Therefore, most of these tests were stopped automatically by the equipment by reaching the lowest possible LVDT position, although some of these tests were performed completely.

To perform these tests, the cyclic triaxial machine would be stopped at the point of liquefaction, cyclic mobility, or observation of excessive deformation as discussed earlier. Another issue with the machine was that normally it would not stop at the desired point which was the end of each cycle. At the end of the cycles after the occurrence of peak pore pressure ratio, the pore pressure was equal to the cell pressure and the deviator stress was zero. For the cases that the machine would stop at any point other than the end of the cycle, i.e. zero deviator stress, the LVDT position needed to be adjusted and the sample was allowed to go under additional deformation to reach zero deviator stress while the drainage valves would remain closed. The sample would sit for

a while to allow the distribution of pore water pressure inside the specimen. Considering the additional deformation enforced to the sample after the end of the cyclic loading, the pore pressure could have a different value compared to the point of peak pore pressure ratio. The UU-type triaixal tests were performed at a strain rate of 0.8%/min following ASTM D2850 recommendations.

In Figure 4.23, representative results of three samples from such tests are illustrated. The samples TBBLAPST11S3, TBBLAPST12S2, and TBBLAPST15S4 were obtained from the Big Branch impoundment at the toe location from one boring at depths of 36.5 ft, 56.5 ft, and 117.1 ft (11.1 m, 17.2 m, and 35.7 m), respectively. Considering the sample TBBLAPST15S4, as the sample was loaded, it experienced contraction which is evident from the increase in the pore water pressure. At about 2.2% strain the sample yielded and began to dilate which resulted in a reduction in the pore pressure and exhibition of strain hardening response. At the yield point, the curvature of the stress-strain curve also shifts from upward to downward. The observation of strain hardening response was consistent in all of the post-liquefaction UU tests.

This sample had been under 26.5 psi (182.7 kPa) in-situ vertical effective pressure before sampling based on its depth and the estimated elevation of the phreatic surface at the time of sampling. Thus, to perform a normally consolidated cyclic triaxial test, the sample was re-consolidated to the in-situ vertical effective pressure. However, at the end of the triaxial test, the effective stress reached zero as a result of pore pressure reaching the confining stress magnitude and achieving a peak pore ratio of 1.0. Therefore, it is

expected that this sample behaves as a heavily overconsolidated sample during the UU test considering the stress history of the sample. Inspection of the stress path from the plot of deviatoric stress q' versus mean effective stress p' proves that the sample indeed performed as a heavily overconsolidated sample. The excess pore water pressure reached negative values at larger strains and also the stress path that is begins as an approximate vertical straight line and after yielding it bends to the right to reach the critical state line at failure.

The deviator stress at the point of yielding was 10 psi which, if traced on the stress path plot, indicates the point that the curvature of the path changes significantly. The stress path in the beginning of the test (i.e. in the elastic region) was not a perfect straight line as it is expected in the theory which is an indicator of negligible volumetric strain. As the specimen experienced greater deformations beyond the point of yielding (2.2% strain), it dilated progressively. The pore pressure continued to decrease and the stress path deviated towards the critical stress line (CSL) as the sample went under plastic deformations.

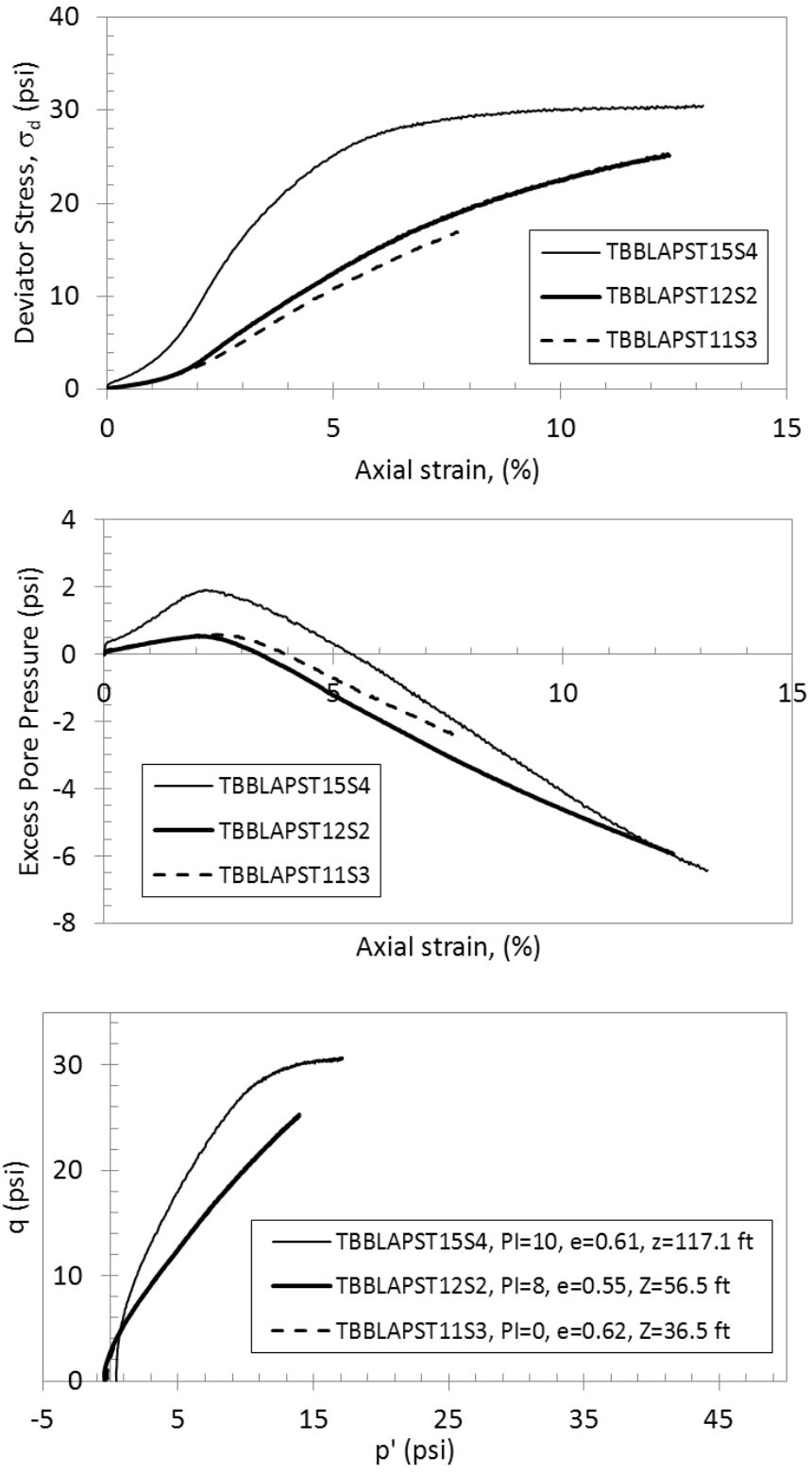

Figure 4.23: Typical results of post-liquefaction loading consisting of unconsolidated undrained monotonic compression triaxial test on samples from different tubes.

The sample gradually approached failure at approximately 13% strain where the equipment was stopped due to lack of sufficient stroke. As demonstrated in Figure 4.23c, the stress path was bent towards the critical state line significantly at this point. It is expected that if the test was continued, the stress path could reach the CSL and the value of parameter $M = q'/p'$, at failure could be determined precisely.

The stress-strain behavior, excess pore water pressure, and stress path of samples TBBLAPST11S3 and TBBLAPST12S2 are presented in Figure 4.23 as well. It is noted that these samples showed similar behavior to the TBBLAPST154 specimen although the tests could not be continued to high levels of strain. Assuming that if the samples would follow the trend that is observed in the plots, it is likely that the specimen with the highest plasticity and in-situ confining stress (TBBLAPST15S4) would have experienced the highest shear strength and the highest drop in the pore pressure.

In Figure 4.24, the stress-strain behavior, excess pore water pressure, and stress path of samples from the same Shelby tube is presented. The behavior of samples TBBLAPST15S1, TBBLAPST15S3, and TBBLAPST15S4 are similar and their observed stress path roughly the same. However, sample TBBLAPST15S2 showed a lower undrained strength compared to the other specimens from the same tube. Also, the pattern of variation of excess pore water pressure is different and it appears that the behavior of the sample changes from compression (increasing pore pressure) to dilation (decreasing pore pressure) at approximately 0.2% axial strain while the other samples experienced this shift in behavior at approximately between 2.0% to 3.5% of axial strain. In addition,

this sample did not follow the same stress path exhibited by the other samples. These differences show the heterogeneity of coal mine tailings which is due to the method of construction. Even the samples obtained in the same 2.5 ft (0.76 m) Shelby tube did not exhibit the same mechanical behavior.

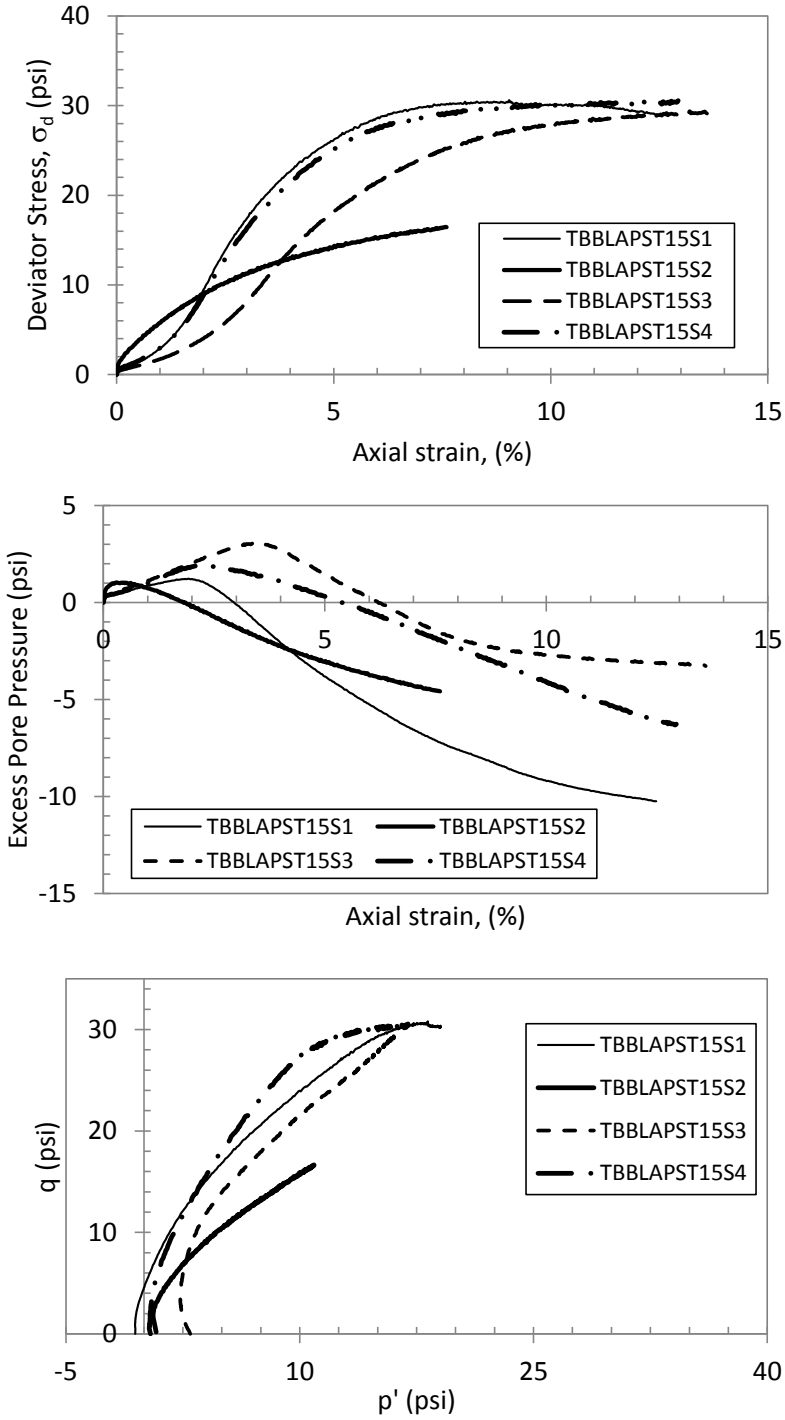

Figure 4.24: Typical results of post-cyclic loading consisting of unconsolidated undrained monotonic compression triaxial test on samples from the same tube

In Table 4.5, the index properties and post cyclic undrained shear strength of the samples at various strain levels are presented.

Table 4.5: Summary of the geotechnical properties of the samples tested in post-cyclic strain-controlled unconsolidated undrained monotonic compression triaxial tests.

Sample	depth ft	LL %	PI %	USCS	e_i	G_s	σ'_c psi	S_u at 4% ε_a psi	S_u at 8% ε_a psi	S_u at 12% ε_a psi	S_u at max ε_a psi
TBBLDPST1S2	84.9	39	9	ML	0.55	1.95	23.0	4.5	8.8	--	9.0
TBBLDPST1S3	85.6	39	9	ML	0.58	1.95	20.6	3.0	9.3	12.0	12.0
TBBLDPST2S2	105.5	37	10	ML	0.97	2.5	24.2	3.0	6.8	--	7.3
TBBLDPST2S3	106.1	37	10	ML	0.97	2.5	31.9	1.8	6.8	9.8	9.8
TBBLDPST2S4	106.7	37	10	ML	0.89	2.5	33.4	1.4	--	--	--
TBBLDPST3S2	125.3	38	11	ML	0.72	2.09	30.0	--	--	--	--
TBBLDPST3S3	125.7	38	11	ML	0.81	2.09	30.0	--	--	--	--
TBBLDPST4S1	144.8	38	5	ML	0.72	1.89	25.7	0.8	2.8	8.0	--
TBBLDPST4S2	145.5	38	5	ML	0.72	1.89	30.8	1.5	8.5	14.0	14.5
TBBLDPST4S3	146.2	38	5	ML	0.78	1.89	27.6	--	--	--	--
TBBLAPST11S3	36.5	30	0	ML	0.62	1.69	16.0	4.0	--	--	8.5
TBBLAPST11S4	36.9	30	0	ML	0.63	1.69	7.1	9.3	--	--	14.0
TBBLAPST12S1	55.3	33	8	ML	0.62	1.76	11.1	8.0	10.5	--	10.5
TBBLAPST12S2	56.5	33	8	ML	0.55	1.76	12.3	4.8	9.8	12.3	12.5
TBBLAPST13S4	76.7	36	12	CL	0.62	2.08	21.5	--	--	--	--
TBBLAPST14S3	96.5	38	14	CL	0.97	2.47	28.4	1.3	3.9	--	4.4
TBBLAPST14S4	97.0	38	14	CL	1.07	2.47	25.7	1.5	5.3	--	6.5
TBBLAPST15S1	115.2	39	10	ML	0.56	1.92	29.9	10.8	14.8	15.0	15.3
TBBLAPST15S2	115.8	39	10	ML	0.62	1.92	30.2	6.5	--	--	8.3

Table 4.5 (Cont.): Summary of the geotechnical properties of the samples tested in post-cyclic strain-controlled unconsolidated undrained monotonic compression triaxial tests.

Sample	depth	LL	PI	USCS	e_i	G_s	σ'_c	S_u			
								at 4% ε_a	at 8% ε_a	at 12% ε_a	at max ε_a
	ft	%	%				psi	psi	psi	psi	psi
TBBLAPST15S3	116.4	39	10	ML	0.62	1.92	28.0	7.0	13.0	14.5	14.8
TBBLAPST15S4	117.1	39	10	ML	0.61	1.92	26.5	10.8	14.5	15.3	15.3
TBBLAPST16S1	135.3	43	7	ML	0.96	2.16	31.8	--	--	--	--
TBBLAPST16S2	136.0	43	7	ML	1.23	2.16	32.0	9.8	--	--	11.0
TAFLBPST1S1	170.4	39	10	ML	0.53	1.91	40.3	--	--	--	10.5
TAFLBPST1S2	171.2	39	10	ML	0.52	1.91	40.7	16.5	--	--	23.0
TAFLBPST2S1	200.0	43	16	ML	0.51	1.90	51.8	29.5	--	--	32.5
TAFLBPST3S1	219.6	42	16	ML	0.61	2.06	58.0	--	--	--	19.0
TAFLBPST3S2	220.1	42	16	ML	0.64	2.06	54.9	8.0	18.0	32.0	34.0
TAFLAPST1S1	239.6	38	14	CL	0.52	2.02	58.9	4.0	10.0	22.5	24.5

Definitions:
LL: Liquid Limit
PI: Plasticity Index
USCS: Unified Soil Classification System
e_i: initial void ratio at which the test was performed
G_s: Specific Gravity
$\sigma_c^{'}$: Effective consolidation stress
S_u at 4% ε_a: Undrained shear strength at axial strain equal to 4%
S_u at max ε_a: Undrained shear strength at maximum measured axial strain

The post-cyclic undrained strength at 4% axial strain of the coal mine tailings has been found to correlate relatively well with the liquid limit and plasticity index as illustrated in Figure 4.25 although variation in the data is observed. It appears that by increasing plasticity indices the undrained shear strength of the samples has increased as well. However, more data would be very beneficial in helping to validate this assertion.

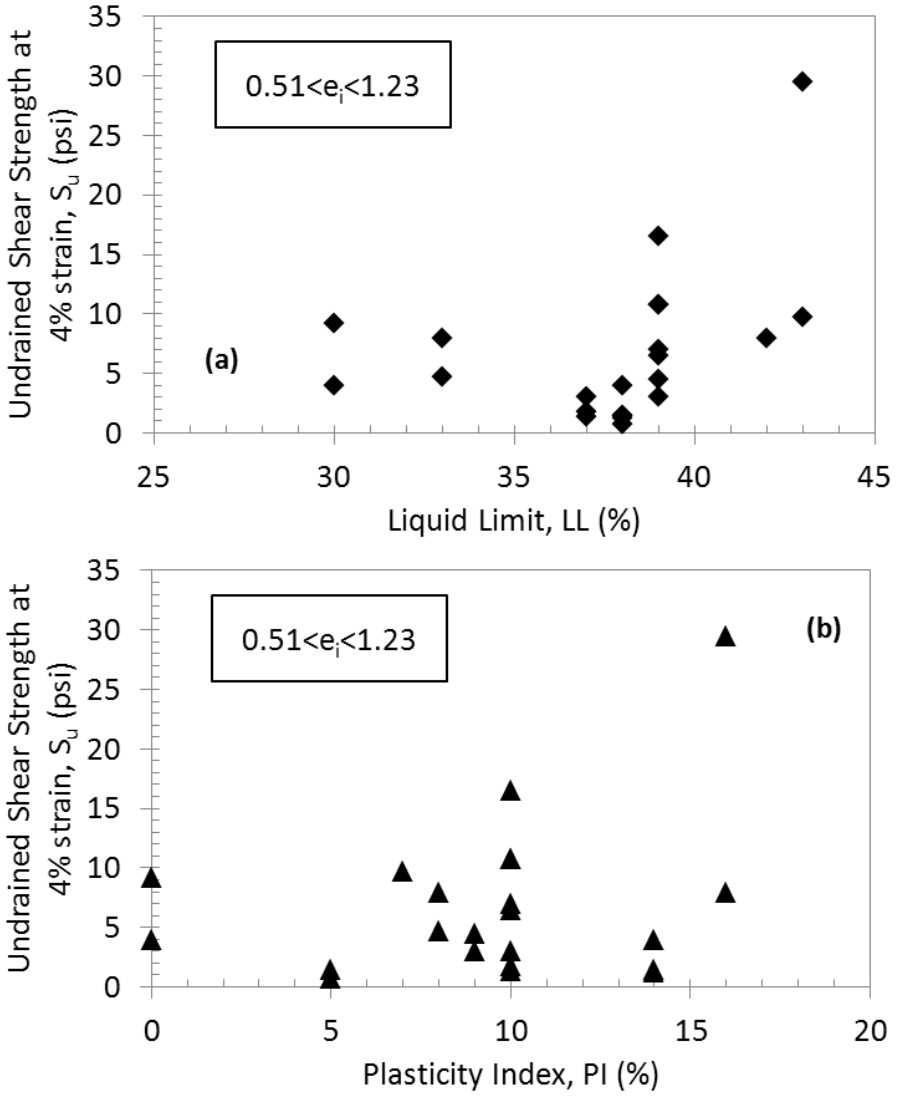

Figure 4.25: Relationships between undrained shear strength at 4% axial strain and (a) Liquid limit, and (b) Plastic limit.

In Figure 4.26, the same results as Figure 4.25 are presented except that the undrained shear strength values are measured at 8% axial strain. Due to the fact that some of the samples did not achieve 8% axial strain the number of data points are less than the data set presented in Figure 4.25.

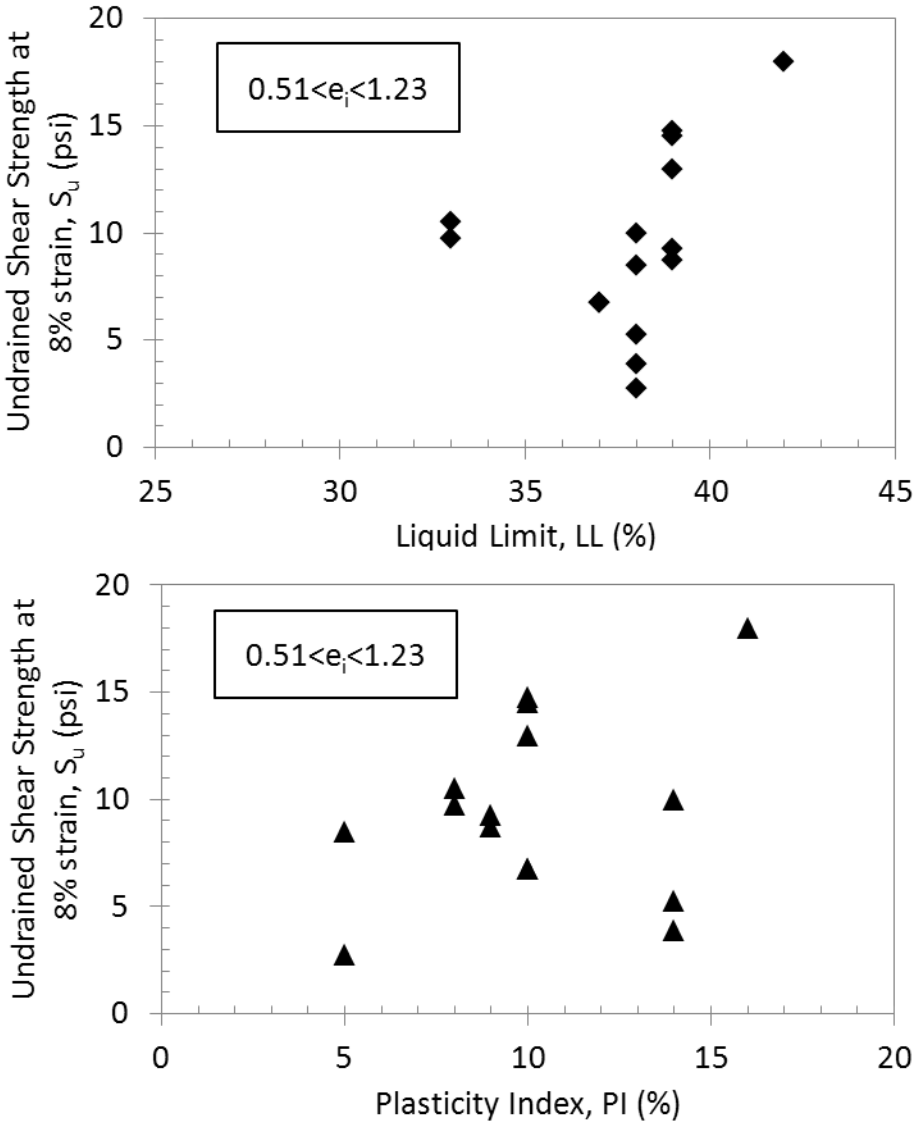

Figure 4.26: Relationships between undrained shear strength at 8% axial strain and (a) Liquid limit, and (b) Plastic limit.

4.4 Dynamic Small-Strain Parameters Measurements

To measure the shear modulus (*G*) and material damping (*D*) of coal mine tailings as a function of shear strain (γ), three cyclic triaxial tests following the ASTM D3999 standard were performed. The relationship between *G*, *D*, and γ is typically used to quantify the response of soil and rock sites to strong ground motion where large strains are generated. As strain increases in soil or rock, shear modulus decreases and material damping increases, so it is necessary to account for this effect to properly predict the dynamic behavior of the site. These curves are typically referred to as modulus reduction curves, and may be obtained experimentally, or estimated using established methods (e.g. Hardin and Drnevich, 1972; Vucetic and Dobry, 1991). Since mine tailings are different than soil, laboratory experiments were performed herein to derive modulus reduction data specific to tailings.

4.4.1 Measurement Procedures

The index properties, gradation, and basic geotechnical specifications of the samples used are presented in Table 4.6. These tests are identical to the cyclic triaxial tests described in Section 4.2 in the sample retrieving, preparation, saturation and consolidation stages. Thus, the same procedures were followed to prepare the sample for the loading stage of the test. However, the amplitude of cyclic load in the shearing stage in this type of cyclic triaxial testing is much smaller than the described method used in liquefaction assessment.

The loading stage of the cyclic triaxial tests with the objective of measuring the shear modulus and damping ratios consists of applying small cyclic deviator stress on the sample and measuring the response of the sample through the load cell, pore pressure transducer and deformation gauge. The amplitude of the cyclic load should be small enough to avoid imparting large plastic deformations to the sample but, at the same time, should be large enough to trigger a measurable response from the sample.

Table 4.6: Summary of geotechnical properties of the coal mine tailings used to develop the shear modulus reduction curves and damping ratio plots.

Sample	Classification						e_i	G_s	σ'_c	depth	σ'_{vc}	OCR
	FC %	5μ %	2μ %	LL %	PI %	USCS			psi	ft		
(1)	(2)	(3)	(4)	(5)	(6)	(7)	(8)	(9)	(10)	(11)	(12)	(13)
TBBLAPST13S2	89	49	31	36	12	CL	0.7	2.1	18.8	75.4	17	0.9
TAFLBPST2S3	84	45	33	43	16	ML	0.58	1.90	44.4	201	44	1.1
TAFLAPST1S2	84	48	33	38	14	CL	0.53	2.02	58.3	240	58	1

Definitions:
FC: percentage of particles smaller than 75 μm
5 μ: percentage of particles smaller than 5 μm
2 μ: percentage of particles smaller than 2 μm
LL: Liquid Limit
PI: Plasticity Index
USCS: Unified Soil Classification System
e_i: initial void ratio at which the test was performed
G_s: Specific Gravity
σ'_c: Effective consolidation stress
σ'_{vc}: Effective consolidation stress at which the test was performed
OCR: Over-consolidation ratio

The test starts by applying relatively small cyclic loads to the sample, and proceeds by gradually increasing the load amplitude. In this study, the loading started by applying a 2 psi (13.8 kPa) peak-to-peak deviator stress and continued to 40 psi (275.8 kPa) peak-to-peak amplitude. The criterion to terminate the test is 0.01% shear strain as stated in ASTM D3999. By terminating the test at a relatively low shear strain, the likelihood of

imparting plastic deformation to the specimen is minimized, so that variations in shear modulus and material damping can be attributed to shear strain rather than plastic deformation. In this section, the results of a trial "n" of a representative sample TBBLAPST13S2n which was obtained from the depth of 75.4 ft (~23 m) at Location A (toe) of the Big Branch impoundment with a void ratio of 0.74, liquid limit of 36%, and plasticity index of 12% are presented.

To perform accurate measurements of the Young's modulus, *E*, and consequently shear modulus, *G*, the cyclic deviator plots need to be precise, smooth, and without any noise induced by the equipment as stated by the ASTM D3999 standard. Some representative examples of acceptable and unacceptable deviator stress curves are presented in Figure 4.27. To assess the quality of the deviator stress plots after each test, the results were inspected. The ability of the equipment to apply small cyclic loads in this type of test is a determining factor. As illustrated in Figure 4.28, the loading started at 8.0 psi (55.2 kPa) peak-to-peak at a rate of 1.0 Hz which, by considering the effective confining stress of the sample at 18.8 psi (129.6 kPa), equates to a cyclic stress ratio of 0.11.

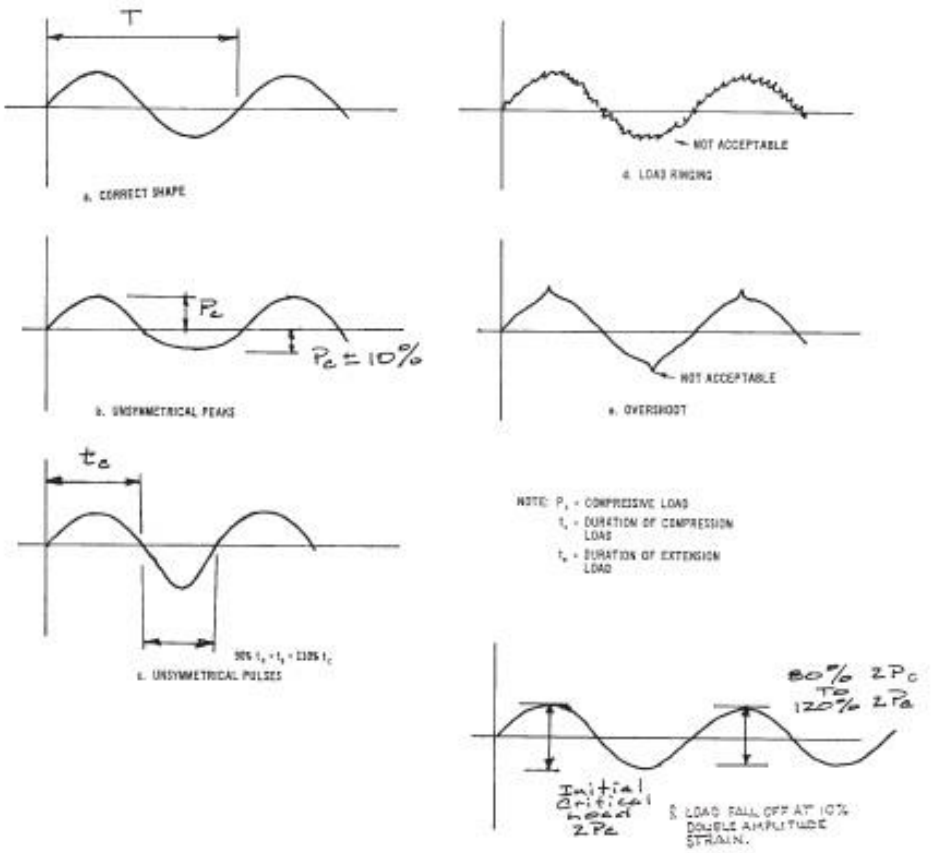

Figure 4.27: Examples of Acceptable and Unacceptable Sinusoidal Loading Wave Forms For Cyclic Triaxial Load Control Tests (ASTM D3999).

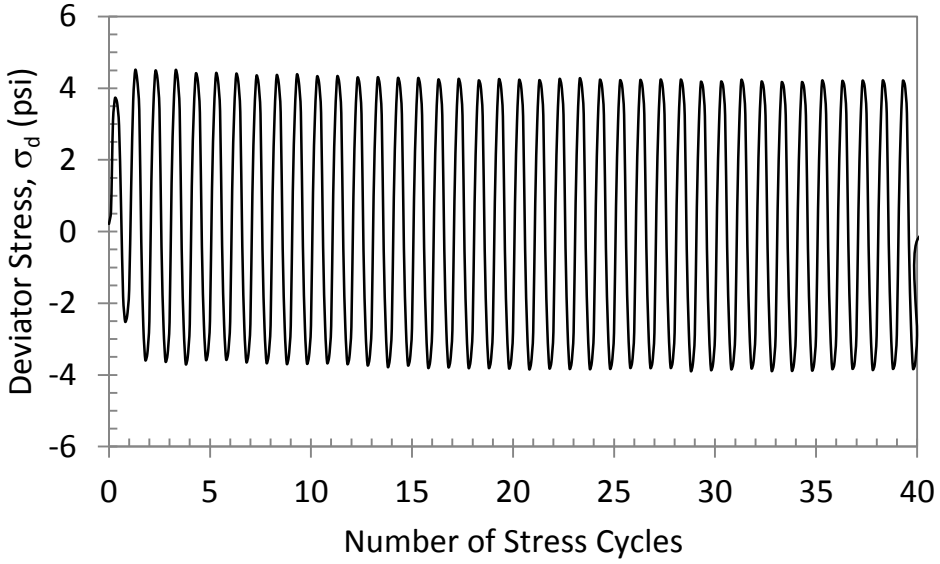

Figure 4.28: Time history of the cyclic deviator stress in trial n for sample TBBLAPST13S2.

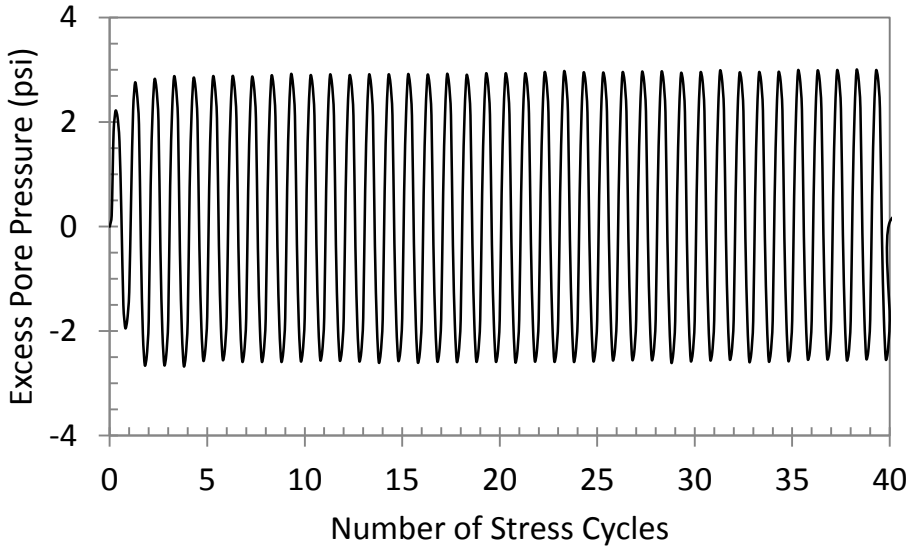

Figure 4.29: Time history of the excess pore pressure in trial n for sample TBBLAPST13S2.

The low deviator stress caused the pore water pressure to increase by 3.0 psi illustrated in Figure 4.29. In Figure 4.30, the variation of pore pressure ratio is illustrated. The maximum achieved r_u in this test was 0.12 which demonstrates that the state of the sample was far from cyclic mobility or liquefaction, i.e. $r_u = 1.0$. According to the small variations in the pore pressure level, the effective confining pressure variations were small as well and therefore small, elastic deformations are expected during this test. However it should be noted that determining whether the samples experienced plastic deformations or not is by checking the applied shear strains against the recommended value of 0.01% by ASTM D3999.

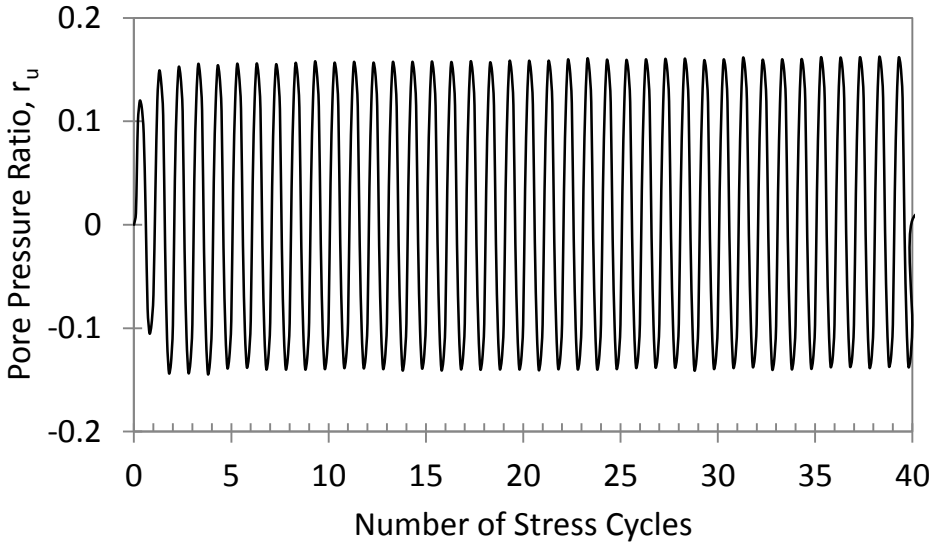

Figure 4.30: Time history of the pore pressure ratio in trial n for sample TBBLAPST13S2.

The experienced deformations during this test are shown in Figure 4.31. As expected, the deformations were small and within the elastic range. As was mentioned, the deformations should be checked for excessive plastic deformations which this measurement is explained in this section. At the end of the cyclic loading stage, the deformations were recovered and no permanent deformations were experienced. Therefore, stains remained within the elastic, recoverable range.

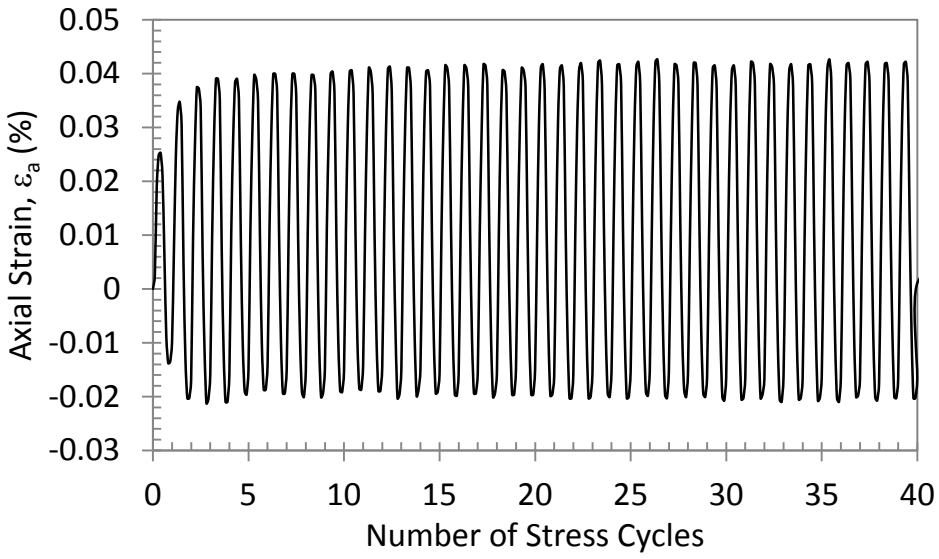

Figure 4.31: Time history of the axial strain in trial n for sample TBBLAPST13S2.

To measure the corresponding shear modulus and damping ratio of sample TBBLAPST13S2n in this test, one of the deviator stress cycles was selected and the equivalent stress-strain loop is presented in Figure 4.32. The Young's modulus is defined as the ratio of the uniaxial stress over the uniaxial strain and the shear modulus is calculated by either measuring or assuming a value for the Poisson's ratio, ν, and using the equation $G = E/\big(2(1+\upsilon)\big)$. Following the ASTM D3999 method, the point of the peak deformation and peak deviator stress was chosen by inspection of the stress-strain curve. The applied stress and the experienced strain level at this moment were used to calculate the slope of the stress-strain curve or the Young's modulus. Due to the lack of lateral deformations gauges, the actual Poisson's ratio of the specimen could not be measured. However, considering that the sample is completely saturated, it is assumed that it is a rigid material and the Poisson's ratio was chosen to be 0.50. For this course of loading, by applying the CSR =0.106, the Young's and shear moduli were measured to be

12.39 ksi and 4.13 ksi (85.4 MPa and 28.5 MPa) respectively. The results of the remaining tests are presented in Appendix A3.

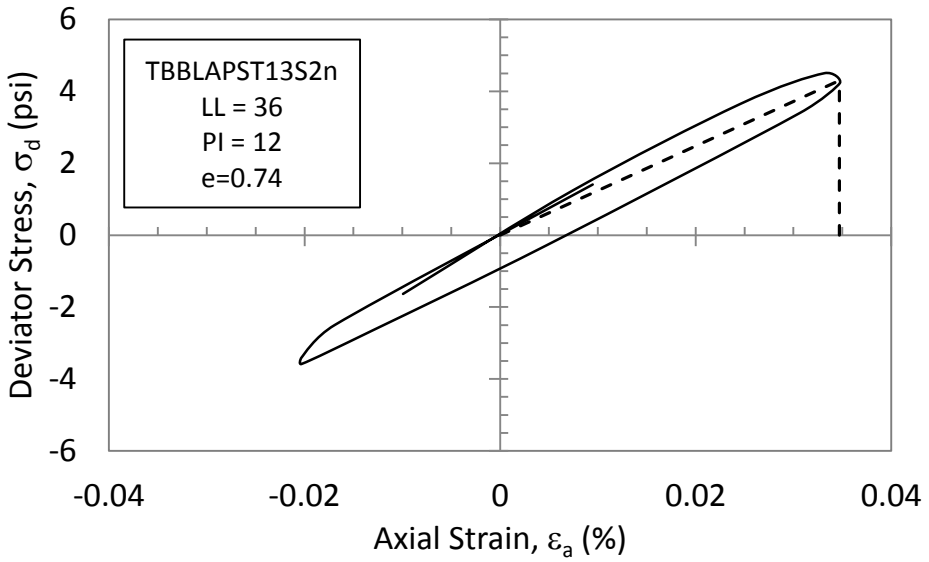

Figure 4.32: A typical stress-strain loop used to calculate the Young's modulus (The point of maximum stress and strain is indicated by the dashed lines).

Since the determination of Young's modulus and damping ratios at any strain level depend on the ability to identify a distinct hysteresis loop, it is necessary to restrict the maximum closure error (Δc) between two successive peaks as shown in Figure 4.34 to 0.2% (ASTM D3999). From Figure 4.34 the closure error for the representative sample TBBLAPST13S2n is measured to be 0.0031% which indicates that the recorded data is valid.

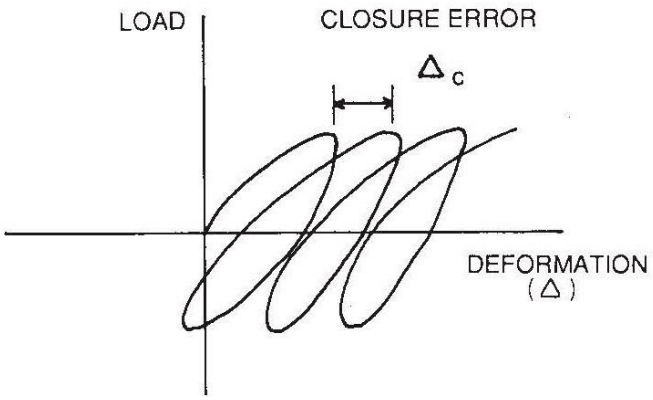

Figure 4.33: Definition of closure error (ASTM D3999).

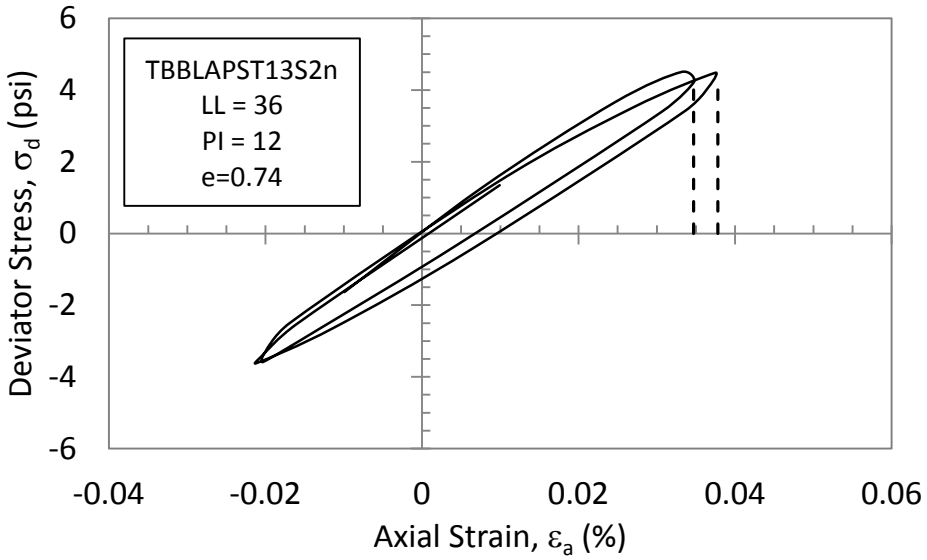

Figure 4.34: Measurement of closure error in performing the cyclic triaxial tests; closure error is defined as the difference in strain between successive cycles as seen by the spacing between the two dashed lines.

4.4.2 Modulus Reduction and Damping Ratio Curves

The results of this series of cyclic triaxial tests were used to find the relationship between the shear modulus, *G*, and the damping ratio, ξ, versus the cyclic shear strain, γ_c. The values of shear modulus, *G*, with respect to cyclic shear strain, for the samples from the Big Branch and Abner Fork impoundments are depicted in Figure 4.35. To illustrate the observed trend, a power function trend line is fitted to each dataset. The

procedure to calculate the shear strain is explained in the ASTM D3999 and is presented in Section 3.6.

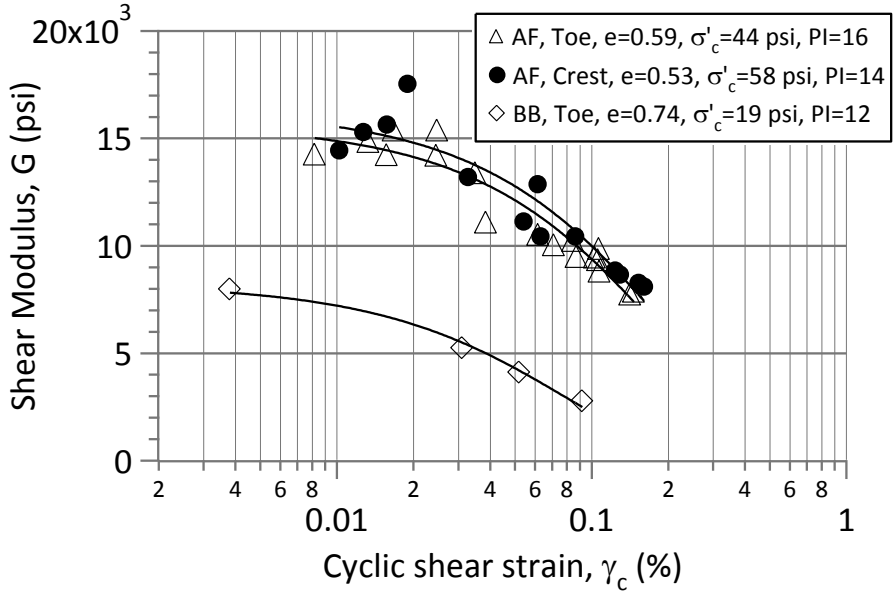

Figure 4.35: Shear modulus reduction curves for representative coal mine tailings specimens from the Big Branch (BB) and Abner Fork (AF) impoundments.

As can be seen in Figure 4.35, the data from the Big Branch impoundment matches very well with this trend line. The distribution of the data is roughly following the power function trend line, although a scatter is observed. As it appears from Figure 4.35, the sample from the Big Branch impoundment responded with the lowest values of shear modulus and demonstrated the softest response among the three samples. The highest and lowest values obtained for the shear modulus of this sample were approximately 8000 psi (55.2 MPa) and 2700 psi (18.6 MPa) respectively. In these tests, the response of the specimens from the Abner Fork impoundment that were obtained from the toe and the crest were considerably similar. For the Abner Fork samples, the highest shear modulus value recorded at the lowest shear strain was 14200 psi (97.9 MPa) and the

lowest value was 8200 psi (56.5 MPa). However, as the trend suggests, at lower shear strains higher values of shear modulus could be expected.

The softer response of the Big Branch specimen compared to the Abner Fork samples can be attributed to the lower in-situ confining stress which also resulted in the higher values of void ratio. Due to the lower confinement and looser structure, the Young's modulus of the sample was lower compared to the Abner Fork specimens and resulted in smaller value of G. It should be noted that the plasticity of the Abner Fork samples were also higher than that of Big Branch samples.

The shear modulus values for the coal mine tailings specimens were normalized to the maximum shear modulus value, G_{max}, obtained from the best fit curve at 0.001% of shear strain. These values can be used in seismic site response analysis of coal mine tailings materials. In Figure 4.36, the proposed shear modulus reduction curves are compared with the curves presented by Vucetic and Dobry (1991) for fine grained soils. It appears that the measured shear modulus curves are not following the same trend as the Vucetic-Dobry curves. At smaller strains (<0.02%), the Abner Fork and Big Branch samples with an average plasticity index of 15 and 12 follow the same pattern as the curves suggested for fine grained soil with plasticity index of 50 and 30 respectively. At strains greater than 0.02% the values of Abner Fork and Big Branch curves decrease sharply compared to Vucetic-Dobry curves and appear to be similar in shape to highly plastic soils curves (PI=200). In other words, at higher shear strains, the shear modulus values decrease at a higher rate for coal mine tailings samples compared to fine grained soils.

Also, it is noted that the Big Branch and Abner Fork curves with average plasticity indices of 12 and 15 are widely separated compared to the curves suggested for soils in the same range of plasticity.

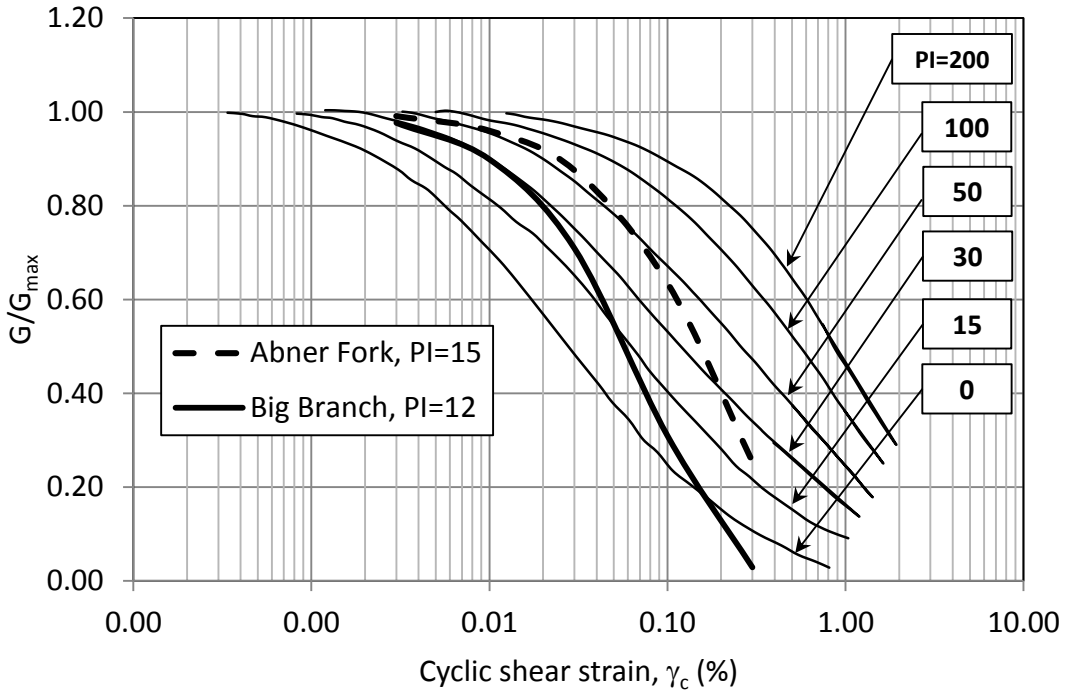

Figure 4.36: Comparison between the normalized shear modulus (G/G_{max}) of Big Branch and Abner Fork samples and the relationships suggested for fine grained soils by Vucetic and Dobry (1991).

One of the influencing parameters that is not quantified in these tests and has possibly affected the results is the age of the specimens. The construction of both of the impoundments began in the early 1980's. However, the Abner Fork impoundment has been an active tailings dam since then, while operations at the Big Branch impoundment were suspended for much of the past two decades. Therefore, the samples in Abner Fork had a longer time to consolidate and create a fabric in the structure of the sample. Also, after piston sampling, the Abner Fork samples were not used for 4 years, while the Big

Branch samples were kept in the tubes for 3 years. The additional time during which the samples were left in the tube provided sufficient time to create a stronger rust bond between the steel tubes and the tailings samples and also for the possibility of sample drying. Although the samples were saturated before testing, the drying and wetting phases could have altered the stress history of the sample and consequently changed the stress history of the specimen. In general, the Abner Fork samples felt much stiffer to the touch and could be handled easily as a rigid material compared to the Big Branch samples, which were softer and needed to be handled with special care.

In Figure 4.37, the damping ratio variations of the coal mine tailings are illustrated. As can be seen from this figure, the data points are scattered, although a trend is observed. The reason for having the scatter in the data can be attributed to the lack of high precision deformation measurements. The axial deformations in these tests were measured through an LVDT with an accuracy of 0.5 mills (0.0127 mm). By using higher precision LVDTs installed on the sample directly, the axial deformation could be measured more precisely and reduce the scatter of the data. The procedure to calculate the damping ratio is explained in detail in Section 3.6.

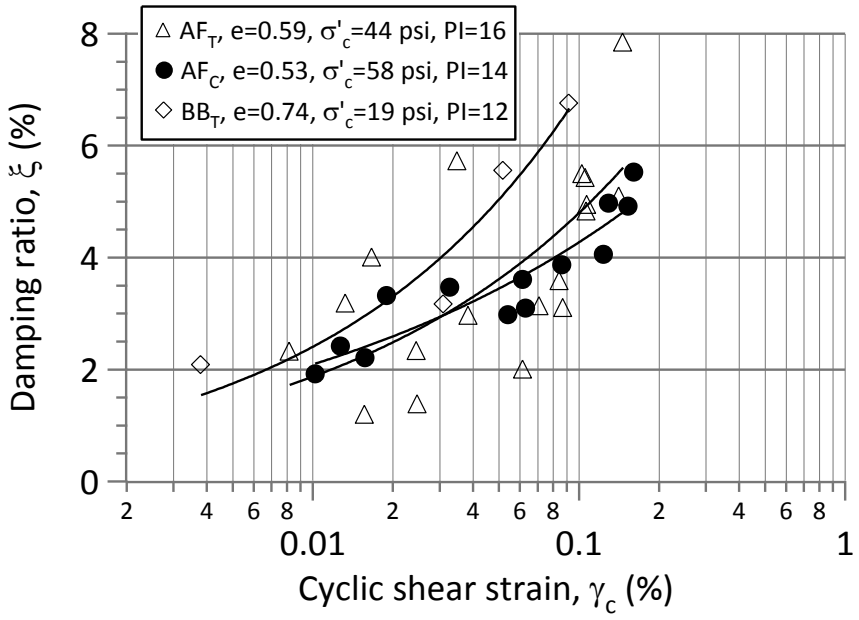

Figure 4.37: Damping ratio variations for the coal mine tailings specimens from Big Branch (BB) and Abner Fork (AF) impoundments.

By a closer inspection of Figure 4.37, it may be asserted that the damping ratios measured for the Big Branch coal mine tailings sample are higher than the values for the Abner Fork samples. Considering the looser state of the Big Branch samples, this trend is reasonable. In Figure 4.38 a comparison is shown between the damping ratio of the Big Branch and Abner Fork coal tailings and the suggested curves for fine grained soils by Vucetic and Dobry (1991). It should be noted that the curves proposed for coal tailings in this study are best fit lines as was shown in Figure 4.37. It seems that the shape of the damping ratio curves for the coal tailings samples has a similar trend to that of fine grained soils, however the values of damping ratios for the coal tailings are lower compared to the fine grained soils with the same plasticity index values. For example the curve for Abner Fork samples with PI=15 roughly coincides with the curve for soils with

PI=100. However, it is emphasized that the number of tests in this study were limited and the measurement of small strains were not highly accurate.

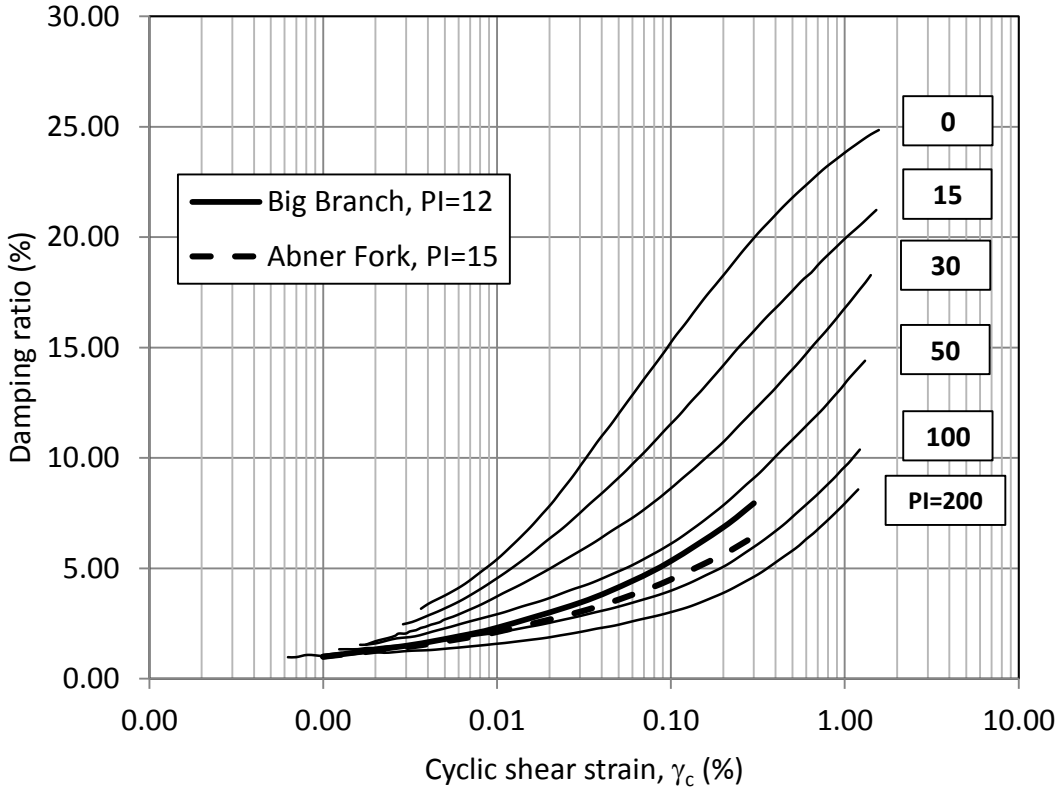

Figure 4.38: Comparison between the damping ratios of Abner Fork and Big Branch samples and relationships suggested for fine grained soils by Vucetic and Dobry (1991).

4.5 Laboratory Vane Shear Tests

The post liquefaction peak and residual undrained shear strength of the samples were measured by using a laboratory vane shear machine after performing the cyclic triaxial and unconsolidated undrained triaxial tests following the procedure explained in Section 3.7. The results of these measurements are presented in Table 4.7.

Table 4.7: Post liquefaction peak and residual undrained shear strength of coal mine tailings samples by performing laboratory vane shear tests.

sample name	depth (ft)	LL %	PI %	e_i	CSR	N_{ru}	τ_p psi	τ_r psi
TBBLAPST11S3	36.5	30	0	0.62	0.15	92	5.2	
TBBLDPST4S1	144.8	38	5	0.72	0.29	12	13.6	
TBBLDPST4S2	145.5	38	5	0.72	0.21	155	5.4	
TBBLDPST4S3	146.2	38	5	0.78	0.25	47	6.7	
TBBLAPST16S1	135.3	43	7	0.96	0.43	2	10.3	
TBBLAPST16S2	136.0	43	7	1.23	0.34	3	7.0	
TBBLAPST12S1	55.3	33	8	0.62	0.20	79	7.7	
TBBLDPST1S2	84.9	39	9	0.55	0.26	70	8.1	
TBBLDPST1S3	85.6	39	9	0.58	0.32	6	7.9	2.9
TBBLDPST2S2	105.5	37	10	0.97	0.36	4	5.5	
TBBLDPST2S3	106.1	37	10	0.97	0.27	20	12.0	
TBBLDPST2S4	106.7	37	10	0.89	0.20	140	20.9	
TBBLAPST15S1	115.2	39	10	0.56	0.24	55	4.5	
TBBLAPST15S2	115.8	39	10	0.62	0.34	6	21.0	
TBBLAPST15S3	116.4	39	10	0.62	0.28	24	14.2	
TAFLBPST1S2	171.2	39	10	0.52	0.41	7	45.6	14.1
TBBLDPST3S2	125.3	38	11	0.72	0.17	109	39.6	
TBBLAPST13S4	76.7	36	12	0.62	0.28	11	4.1	
TBBLAPST14S3	96.5	38	14	0.97	0.29	11	8.6	2.1
TBBLAPST14S4	97.0	38	14	1.07	0.26	20	7.8	
TAFLAPST1S1	239.6	38	14	0.52	0.37	21		
TAFLBPST3S1	219.6	42	16	0.61	0.36	124	48.5	
TAFLBPST3S2	220.1	42	16	0.64	0.40	37	51.0	15.9
TBBLDPST1S1	84.3	39	9	0.64	0.20		14.6	
TAFLBPST2S1	200	43	16	0.51	0.40		37.6	11.7
TAFLBPST2S2	200.6	43	16	0.51	0.32		30.6	7.1

LL: Liquid Limit

PI: Plasticity Index

e_i: initial void ratio at which the test was performed

CSR: Cyclic Stress Ratio

N_{ru}: Number of cycles to obtain the peak pore pressure ratio r_u=1.0

τ_p: peak undrained shear strength by laboratory vane shear test

τ_r: residual undrained shear strength by laboratory vane shear test

These results are presented in Figure 4.39 which illustrates the correlations between the peak undrained shear strength and the cyclic stress ratio (CSR) by considering the plasticity index of the samples.

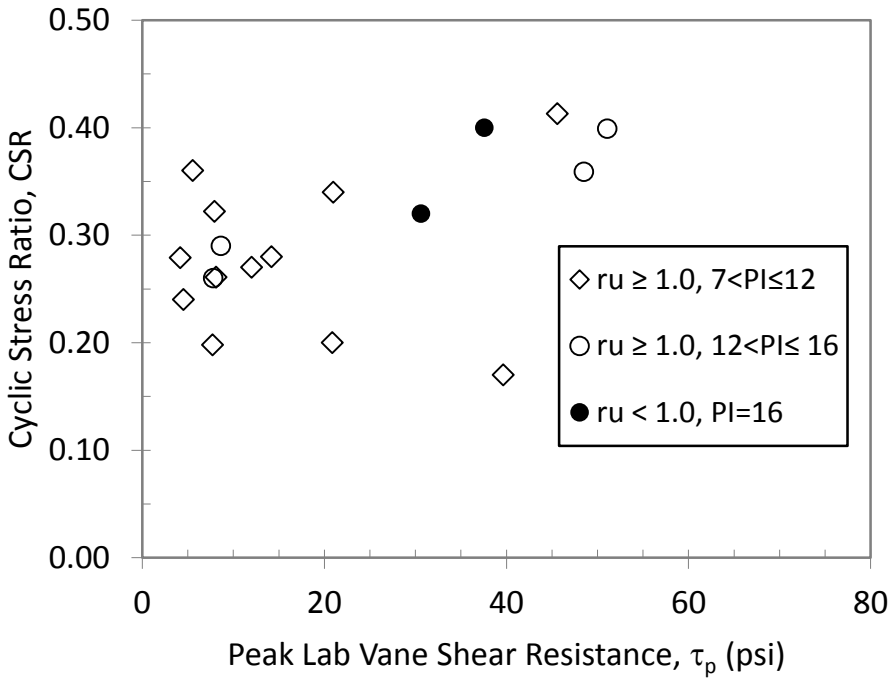

Figure 4.39: Correlations between cyclic stress ratio and peak laboratory vane shear resistance, τ_p.

As shown in Figure 4.39, generally the cyclic strength of the samples increased as the peak laboratory vane shear resistance increased, although some scattered data points are observed. It should be noted that in this figure, only the results of the samples with PI greater than 7 are considered. The samples with PI lower than 7 are non-plastic or low plastic and performing vane shear tests on them produces erroneous results due to the fact that the pore water drains easily out of the pore space during shearing and the measured strength parameter is not undrained shear strength.

Although in Figure 4.39, a categorization is made between the samples with plasticity indices greater or lower than 12, the results are not distinctively apart. However it should be considered that the number of data points were limited. The samples that did not obtain the peak pore pressure ratio r_u=1.0 did not show any significant difference in their peak laboratory vane shear resistance. Due to the limited number of residual laboratory vane shear tests results the results are not correlated to the other parameters of the material.

4.6 Evaluation of Liquefaction Susceptibility Criteria

In this section, the liquefaction susceptibility of coal mine tailings material using the available liquefaction criteria is investigated. These criteria include the Chinese criteria (based on Wang, 1979), Andrews and Martin (2000), Seed et al. (2003), and Bray et al. (2004). It should be noted that the majority of the specimens tested in this study achieved the peak pore pressure ratio of 1.0, i.e. $r_u = 1.0$, and did not necessarily experience excessive deformations. Hence, most of them exhibited cyclic mobility and not necessarily the classic liquefaction accompanied with excessive deformation. The location of the samples on the Casagrande plasticity chart is shown in Figure 4.40. The Unified Soil Classification System (USCS) classification of these samples was limited to low plasticity silt, ML, and low plasticity clay, CL.

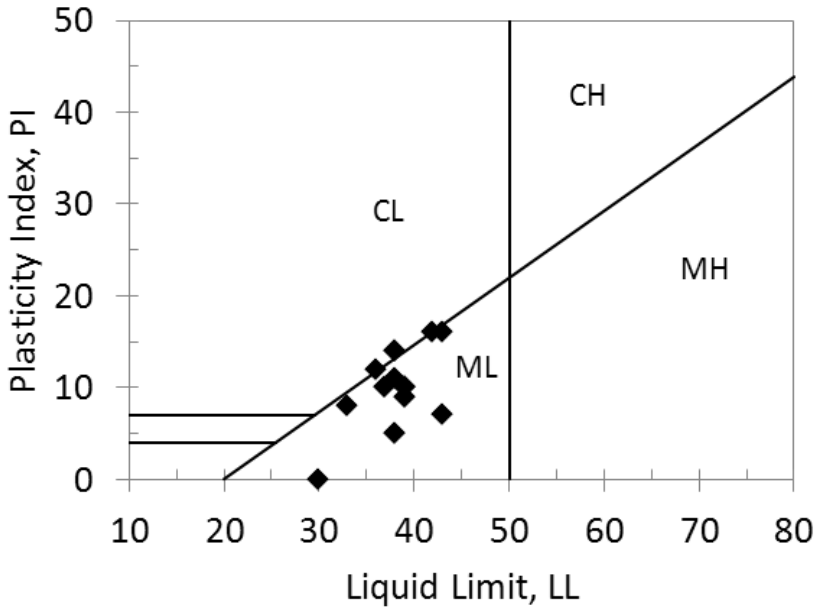

Figure 4.40: Location of the coal mine tailings specimens on the Casagrande plasticity chart.

4.6.1 Chinese Criteria

The effectiveness of the Chinese Criteria in evaluation of liquefaction susceptibility for coal mine tailings is illustrated in Figure 4.41. It should be noted that the study by Wang (1979) which the Chinese Criteria is based on was not specific about the observations that led to the use of the term “liquefaction”. In Figure 4.41, filled diamonds are used to depict the samples that achieved the peak pore pressure ratio of 1.0 regardless of the magnitude of axial deformation. Empty diamonds are used to illustrate the samples that even after numerous cycles of loading did not obtain the peak pore pressure ratio of 1.0.

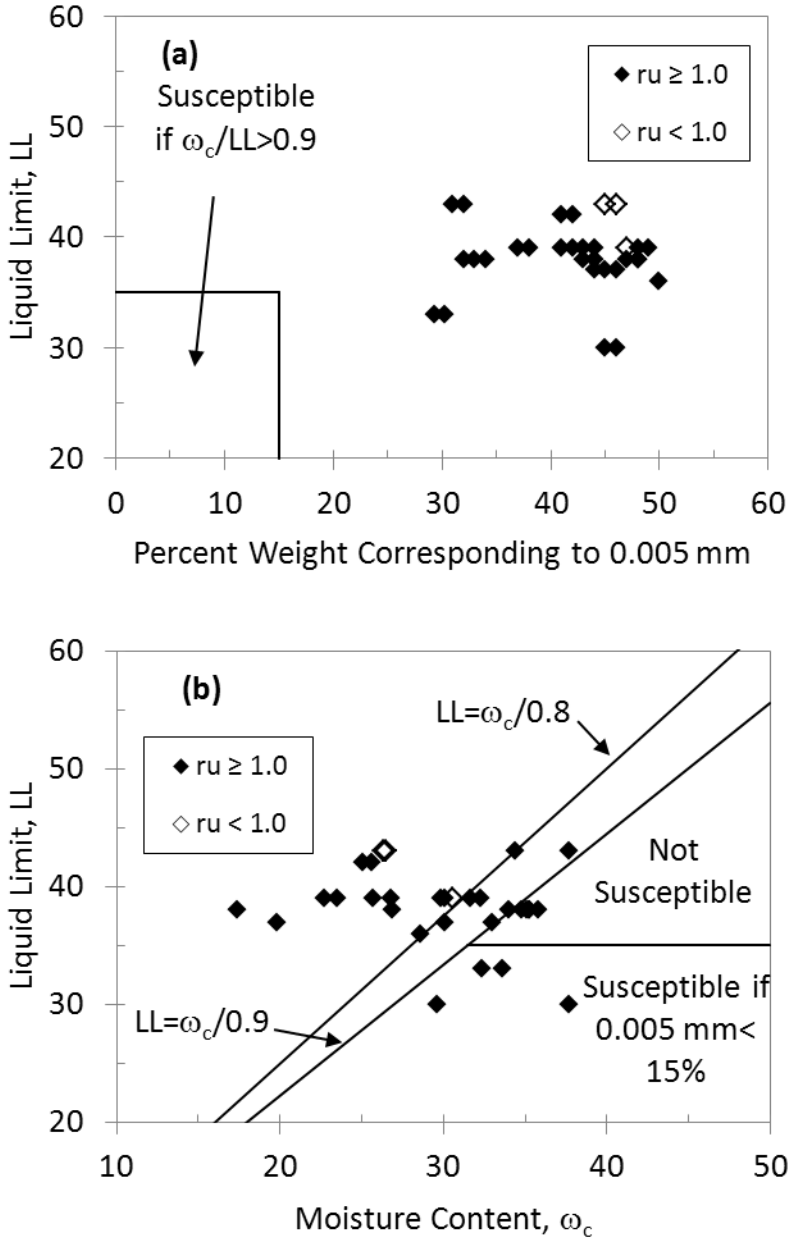

Figure 4.41: Application of the Chinese Criteria to evaluate the liquefaction susceptibility of coal mine tailings material.

Of the 28 samples that were found to be susceptible to "$r_u = 1.0$" in this study and experienced considerable deformation, none of them met all three conditions of the Chinese Criteria and hence would be considered "non-liquefiable". As can be seen in Figure 4.41a, none of these samples fell in the designated area to be considered

susceptible, and therefore the ω_c/LL criterion would not make any difference. Of the 31 investigated samples, only 3 (9.7%) did not experience $r_u = 1.0$ and were considered "non-liquefiable" by the Chinese Criteria as well. However, as can be observed in Figure 4.41b, only 4 of the samples meet both of the liquid limit and water content criteria, i.e. right bottom corner of the plot, but since none of them met the particle size criterion, none were considered susceptible.

4.6.2 Andrews and Martin Criteria

To investigate the effectiveness of the Andrews and Martin (2000) criteria in evaluation of liquefaction susceptibility of coal mine tailings, Figure 4.42 was prepared. This method is relying on the liquid limit and the amount of clay particles based on the AASHTO standards. It should be noted that the hydrometer and Atterberg limits tests in this study were performed on representative samples prepared by mixing samples from the top middle and bottom of each Shelby tube. Therefore, the values of plasticity parameters and the particle size are assigned to each tube and not a specific sample. Hence, the number of data points in this method is reduced to 15 compared to 31 in the Chinese Criteria.

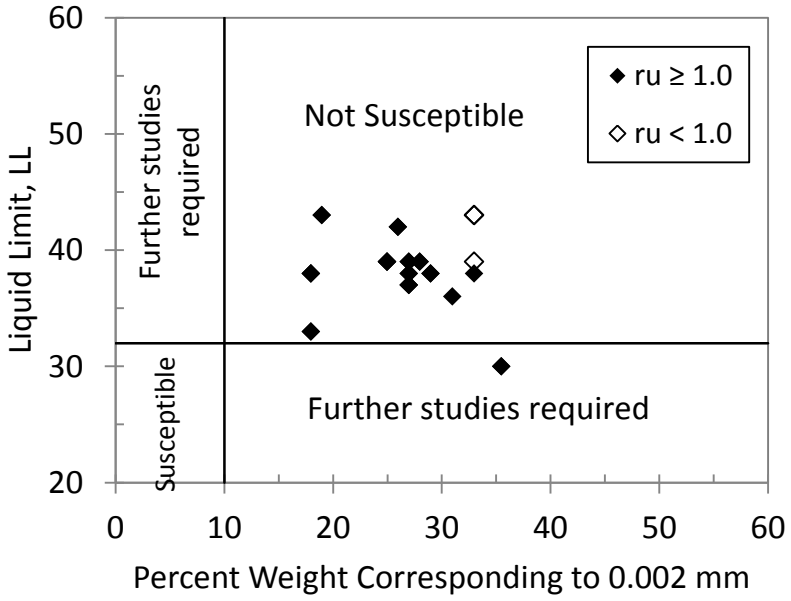

Figure 4.42: Application of the Andrews and Martin (2000) method to evaluate the liquefaction susceptibility of coal mine tailings material.

Of the 13 data points depicted in Figure 4.42, none of them met the two criteria to be considered liquefiable by the Andrews and Martin (2000) method. Only one sample that experienced "cyclic mobility" is located in the zone that "further studies" are recommended. Out of 14 data points that are located in the "not susceptible" zone, only 2 (14%) did not experience "cyclic mobility".

4.6.3 Bray et al. (2004) Method

The effectiveness of the Bray et al. (2004) criteria in evaluation of liquefaction susceptibility of coal mine tailings is presented in Figure 4.43. In this method, the influence of particle size distribution is not considered a determining factor and rather the type of soil minerals present in the structure of the soil are taken into account. The

two parameters considered are the plasticity index, PI, and the water content over the liquid limit ratio, ω_c/LL.

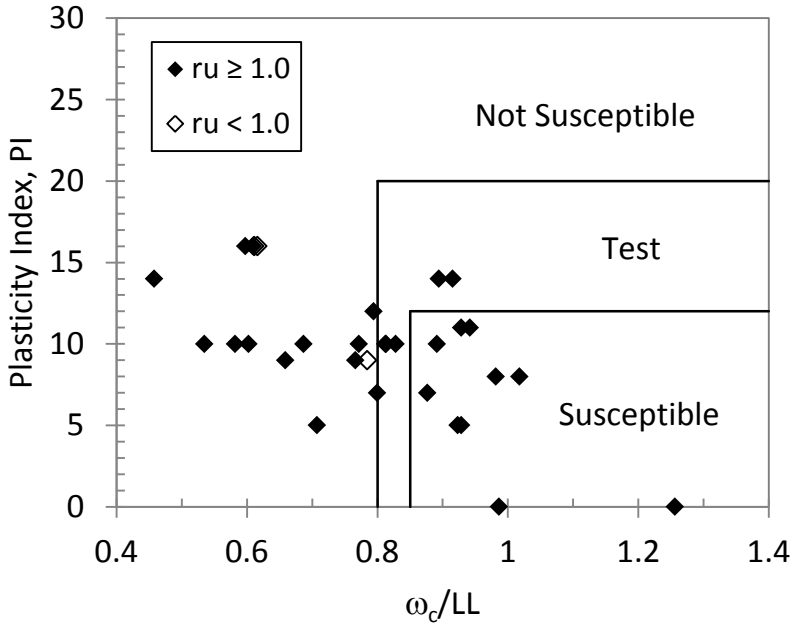

Figure 4.43: Application of the Bray et al. (2004) method to evaluate the liquefaction susceptibility of coal mine tailings material.

Of the 28 coal mine tailings samples that achieved the peak pore pressure ratio of 1.0, 15 (54%) of them are either considered susceptible or recommended to be tested for further information. The three samples that did not achieve the peak pore pressure ratio are considered “non-susceptible” as they were considered the same following the other criteria. It should be noted that the samples obtained for this study were not used for at least 3 years. Leaving the samples in the tubes can cause corrosion of the steel tube and also drying of the samples. Therefore, it is believed that if the samples were tested immediately after obtaining them from the field, the percentage of the susceptibility to

"$r_u = 1.0$", predicted by this method could be considerably higher. However, this assumption cannot be quantified.

4.6.4 Seed et al. (2003) Method

The effectiveness of the Seed et al. (2003) criteria in evaluation of liquefaction susceptibility of coal mine tailings Figure 4.44 is presented. Application of this method is recommended for the soil types with fine contents greater than 20% if the plasticity index is greater than 12, i.e. $FC \geq 20\% \; if \; PI > 12\%$, and for the soil types with fine contents greater than 35% if the plasticity index is smaller than 12, i.e. $FC \geq 35\% \; if \; PI < 12\%$. The fine contents for all of the coal mine tailings samples investigated in this study were at least 70% and therefore this method can be applied.

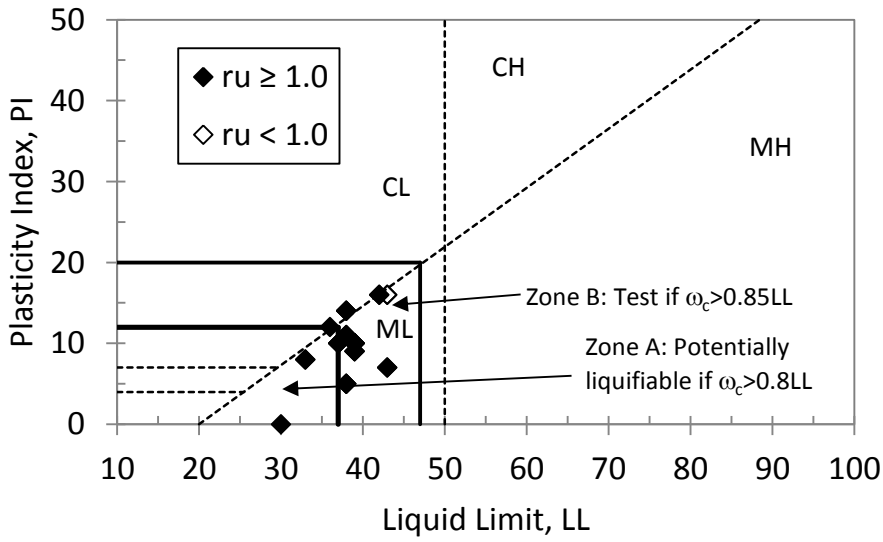

Figure 4.44: Application of the Seed et al. (2003) method to evaluate the liquefaction susceptibility of coal mine tailings material.

It appears that for coal mine tailings samples this method can determine the liquefaction susceptibility very well. Similar to the Andrews and Martin (2000) method,

by using the LL and PI parameters, the number of data points is reduced to 15. All of the 13 tubes of coal mine tailings material that obtained the peak pore pressure ratio, $r_u = 1.0$, are considered either liquefiable or recommended for further studies. Also, the 2 tubes that were considered "no-susceptible" by the other three methods are considered for further geotechnical testing which appears to be a reasonable judgment. The samples from these 2 tubes had similar plasticity parameters to the other samples, but during the test did not achieve the peak pore pressure ratio. However, it should be noted that similar to the Bray et al. (2004) method, some of the specimens investigated in this study, do not satisfy the ω_c/LL condition. As it was mentioned before, the specimens were left in the tubes for 3 to 4 years which could cause corrosion of the steel tubes and the drying of the samples. Therefore, the water content criterion cannot be assessed correctly.

Following the guidelines suggested by Boulanger and Idriss (2004), based on the results of the studies performed by Ishihara (1993), Ishihara et al. (1975), Boulanger and Idriss (2004b), Romero (1995), Moriwaki et al. (1982), and other researchers, the observed cyclic behavior of the coal mine tailings is categorized in Table 4.8. To perform an in-depth investigation of the effectiveness of the Seed et al. (2003) method in conjunction with the cyclic behavior of the samples, Figure 4.45 is presented.

Table 4.8: Summary of the geotechnical properties of the coal mine tailings samples that obtained the peak pore pressure ratio and classification of their cyclic behavior based on Boulanger (2004)

Sample (1)	ω_c % (2)	LL % (3)	PI % (4)	FC % (5)	5μ % (6)	2μ % (7)	ω_c/LL (8)	USCS (9)	r_u = 1.0 (10)	Cyclic Behavior (11)
TBBLDPST1S2	29.9	39	9	92	47	27	0.77	ML	Yes	clay-like
TBBLDPST1S3	25.7	39	9	92	47	27	0.66	ML	Yes	clay-like
TBBLDPST4S1	26.9	38	5	89	32	18	0.71	ML	Yes	clay-like
TBBLAPST12S1	33.6	33	8	70	29	18	1.02	ML	Yes	clay-like
TBBLAPST13S4	28.6	36	12	89	49	31	0.79	CL	Yes	clay-like
TBBLAPST14S4	34.8	38	14	87	47	29	0.92	CL	Yes	clay-like
TBBLAPST15S2	32.3	39	10	82	41	25	0.83	ML	Yes	clay-like
TBBLAPST16S1	34.4	43	7	83	31	19	0.80	ML	Yes	clay-like
TAFLBPST1S2	22.7	39	10	79	37	28	0.58	ML	Yes	clay-like
TAFLBPST3S1	25.6	42	16	80	41	26	0.61	ML	Yes	clay-like
TAFLBPST3S2	25.1	42	16	80	41	26	0.60	ML	Yes	clay-like
TAFLAPST1S1	17.4	38	14	84	48	33	0.46	CL	Yes	clay-like
TBBLDPST2S2	19.8	37	10	83	44	27	0.54	ML	Yes	transition
TBBLDPST2S3	33	37	10	83	45	27	0.89	ML	Yes	transition
TBBLDPST4S3	35.1	38	5	89	32	18	0.92	ML	Yes	transition
TBBLAPST14S3	34	38	14	87	47	29	0.89	CL	Yes	transition
TBBLAPST15S3	31.7	39	10	82	41	25	0.81	ML	Yes	transition
TBBLAPST16S2	37.7	43	7	83	31	19	0.88	ML	Yes	transition
TBBLDPST2S4	30.1	37	10	83	45	27	0.81	ML	Yes	sand-like
TBBLDPST3S2	35.3	38	11	87	43	27	0.93	ML	Yes	sand-like
TBBLDPST4S2	35.3	38	5	89	32	18	0.93	ML	Yes	sand-like
TBBLAPST11S3	29.6	30	0	88	45	36	0.99	ML	Yes	sand-like
TBBLAPST15S1	30.1	39	10	82	41	25	0.77	ML	Yes	sand-like

Definitions:
ω_c: In-situ water content
LL: Liquid Limit
PI: Plasticity Index
FC: percentage of particles smaller than 75 μm
5 μ: percentage of particles smaller than 5 μm
2 μ: percentage of particles smaller than 2 μm
ω_c/LL: Ratio of the in-situ water content and the liquid limit
USCS: Unified Soil Classification System
e_i: initial void ratio at which the test was performed
$r_u = 1.0$: Indicating if the sample achieved the peak pore pressure ratio
Cyclic Behavior: Cyclic behavior classification based on Boulanger (2004)

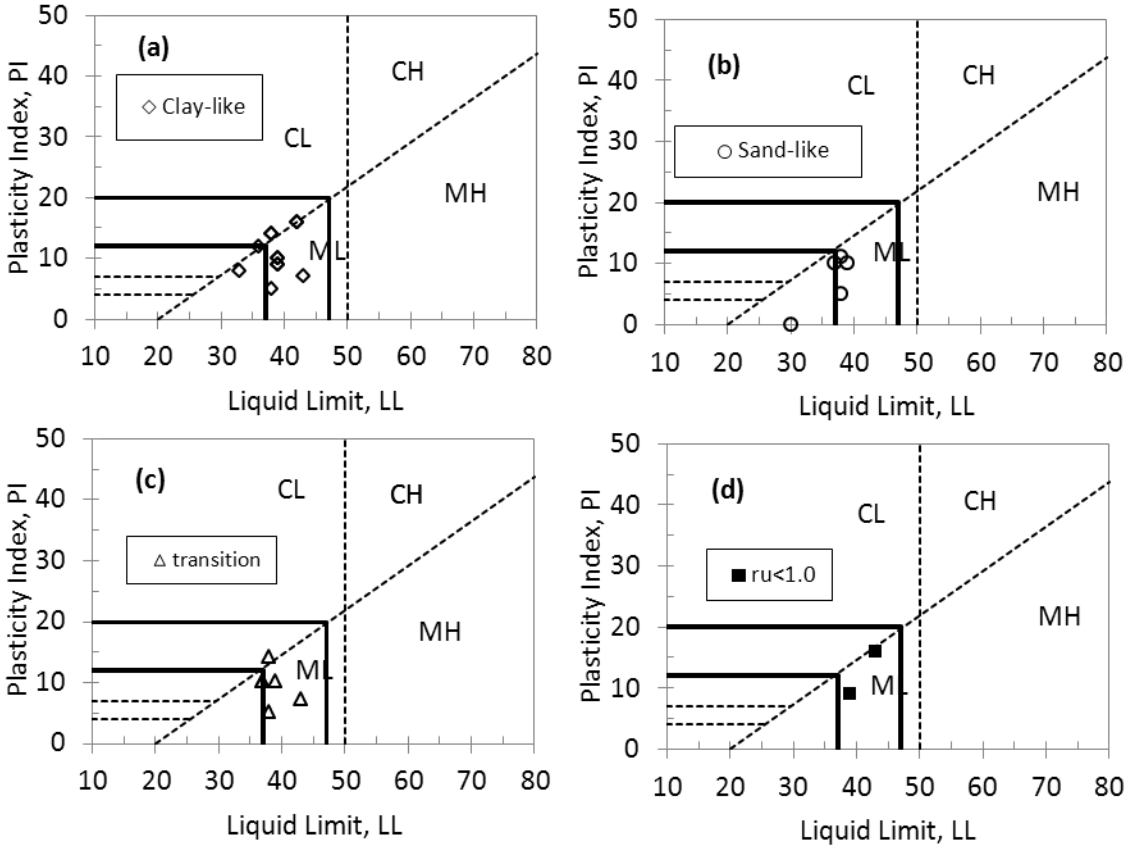

Figure 4.45: classification of cyclic behavior of coal mine tailings based on Boulanger (2004) and the liquefaction susceptibility method after Seed (2003).

In this Figure, based on the cyclic behavior of the samples during the cyclic triaxial tests, the coal mine tailings are categorized into clay-like, sand-like, and transitional types. As it appears from Figure 4.45a, the clay-like samples are mainly scattered in zone B. Therefore, it is acknowledged that these samples are potentially liquefiable and further studies are recommended. In Figure 4.45b, the sand-like samples are either located in zone A or are depicted roughly on the transition line between zone A and zone B. This indicates that this method considers these samples susceptible to classic liquefaction

which is consistent with the observation of peak pore pressure ratio and large deformations.

In Figure 4.45c, the samples that exhibited transitional behavior between sand-like and clay-like soils are depicted. It appears that similar to the clay-like samples, these samples are mainly located in zone B. However, by comparing them to the clay-like samples, it is noted that they are roughly clustered in the lower limits of zone B and are not scattered over the zone B. In Figure 4.45d, the locations of the samples from the two tubes that did not achieve the peak pore pressure ratio, are illustrated. As it was discussed it is reasonable to recommend these samples for further testing considering the similar plasticity indices to the other specimens. During these tests, it was noticed that even after numerous cycles of loading, these samples could not exhibit cyclic mobility behavior.

4.7 Summary and Conclusions

In this chapter, the laboratory test results performed on the coal mine tailings obtained from Big Branch and Abner Fork impoundments were presented. These observations are summarized as follows:

The Abner Fork samples with higher confining stresses (52 psi average or 358.5 kPa) relative to Big Branch samples (25 psi average or 172.4 kPa), required significantly higher cyclic stress ratios to achieve the peak pore pressure ratio $r_u = 1.0$. Due to the limited number of specimens, the influence of confining pressure could not be quantified for the samples of each individual tailings dam.

The comparison of the cyclic strength curves (correlation between the cyclic stress ratio and the number of cycles to obtain peak pore pressure ratio $r_u = 1.0$) between the coal mine tailings and other tailings materials provided by Wijewickreme et al. (2005) indicates that the Big Branch samples behaved similar to the Quartz slimes from Ishihara et al. (1980) study and the general behavior was in agreement with the rest of the tailings material types. It appears that the Abner Fork samples exhibited higher cyclic strength compared to the other tailings material. However, these samples were kept for an extended time in the Shelby tubes and the results could be affected.

The influence of overconsolidation ratio was not studied in depth due to limited number of undisturbed samples from each impoundment. However, the samples from one Shelby tube were tested at an overconsolidation ratio of 1.3. These lightly overconsolidated specimens did not exhibit a significant different behavior than the other samples and the results were in the same range.

The influence of plasticity of the coal tailings samples was investigated. The average plasticity index for Big Branch samples was 9 ranging from 0 to 14, while the Abner Fork specimens had an average PI of 14 ranging from 10 to 16. By comparing the samples obtained from the same impoundment it was observed that samples with higher PI values could require higher or lower number of cycles to achieve the peak pore pressure ratio $r_u = 1.0$, and therefore no clear trend was suggested. Also by studying this influence in conjunction with the influence of void ratio, the trend was not clear. However, by grouping the results of each impoundment together, a clear trend was

observed. Abner Fork specimens with higher plasticity indices and lower void ratios exhibited higher cyclic strength when compared to Big Branch samples. The increase in the CSR value with the increase in PI value is in agreement with the results of the study by Ishihara et al. (1981) on a broad range of tailings samples throughout Japan. Although they did not observe a close correlation between the void ratio and the cyclic strength of the material.

Following the ideas presented by Boulanger and Idriss (2004), it was observed that the coal tailings samples exhibited sand-like, clay-like and transitional type cyclic behavior. Almost all of the samples dilated when reaching the state of peak pore pressure ratio and developed “banana loops” in their stress-strain curves.

Unconsolidated Undrained compression triaxial (UU) tests were performed on the samples after the cyclic traixial test. All of the samples exhibited highly overconsolidated behavior which is in agreement with the laboratory loading history of them. The coal tailings samples are usually normally consolidated due to the method construction. They have been constantly loaded and the overburden stress has never been removed. However, if the construction of the dam and filling of the pond is stopped, the top layer could be desiccated due to extended exposure to elements and therefore becomes overconsolidated. In the lab, the samples were tested in the cyclic triaxial chamber as normally consolidated samples. After achieving the peak pore pressure ratio, the effective confining stress essentially becomes zero. Since the post-cyclic triaxial tests are performed as unconsolidated undrained tests, the samples behave as highly

overconsolidated samples. The pore pressure was increased slightly at smaller strains and was decreased significantly at higher strains which indicates the dilation of the samples. The samples from the same tube could behave slightly different due to the difference in the stratigraphy of the material.

The post-cyclic undrained shear strength of the samples at different levels of strain measured by post-cyclic triaxial testing was studied in correlation with their PI value. It appears that samples with higher PI values exhibited higher undrained shear strength, although some scatter was observed in the results.

Modulus reduction curves and damping ratio curves were provided for the coal tailings samples. It appears that the Abner Fork samples with lower void ratios, higher plasticity indices, and higher in-situ vertical effective pressures had higher modulus and lower damping ratio values. The effect of structure and aging was not measured quantitatively, however based on practical experience with the samples during handling in the lab, the Abner Fork samples appeared to be more rigid and resilient to deformation. The normalized shear modulus curves and the damping ratio curves were compared with the curves presented by Vucetic and Dobry (1991). The modulus reduction curves of coal tailings samples follows those of higher plasticity soils and the values decrease at a faster rate at higher strains compared to fine grained soils. The shape of the damping ratio curves follows the trend of fine grained soil curves, although the values fall in the range of highly plastic soils.

The liquefaction susceptibility of coal mine tailings material was investigated by using the available liquefaction criteria such as Chinese criteria, Andrews and Martin (2000), Seed et al. (2003), and Bray et al. (2004). The performance of Chinese criteria as shown by other researchers, was not satisfactory. Of the 28 samples that were found to be susceptible to $r_u = 1.0$ in this study and experienced considerable deformation, none of them met all three conditions of the Chinese Criteria and hence would be considered "non-liquefiable". None of the samples met the criteria presented by Andrews and Martin (2000) either. By using Bray et al. (2004) criteria, 54% of the samples were considered susceptible to liquefaction or further tests were recommended. By using the Seed et al. (2003) criteria all of the samples were considered susceptible or further testing was recommended. Therefore, the Seed et al. (2003) method was the most effective procedure in determining the liquefaction susceptibility of coal mine tailings.

The cyclic behavior of the coal mine tailings was studied by using the ideas presented by Boulanger and Idriss (2004) and were categorized into sand-like, clay-like, and transition type material. This classification was shown to be effective in distinguishing the determining cyclic behavior type of coal mine tailings and the potential for liquefaction.

Chapter 5

Correlating Field Results to Laboratory Results

5.1 Introduction

In this chapter, the analysis of in situ tests results performed on coal mine tailings materials at the Big Branch and Abner Fork impoundments is addressed. Also, the correlation between the field-testing results and the laboratory measured geotechnical parameters is discussed. Several field tests are commonly used for the evaluation of liquefaction resistance of soils, including the cone penetration test (CPT), the standard penetration test (SPT), and the shear-wave velocity measurement. In this study, the geotechnical field tests included the Standard Penetration Test, SPT, the Cone Penetration Test accompanied with pore water pressure and shear wave velocity (sCPTu) measurements, in situ vane shear testing, and shear wave velocity measurements by the SASW (Spectral Analysis of Surface Waves) and downhole seismic methods.

The SPT and CPT methods are widely used in various studies performed on soil, and extensive databases and experience are available in geotechnical practice (e.g. Youd et al., 2001, Idriss and Boulanger, 2004; Idriss and Boulanger, 2007; Idriss and Boulanger, 2008; Campanella et al., 1983; Ishihara, 1993; Robertson and Wride, 1998; Robertson, 1994; Robertson, 1990; Robertson, 2009; Robertson, 2010; Robertson, 2012; Stark and Olsen, 1995). Recently, the CPT method has become very popular for site characterization and predicting liquefaction potential because of its greater repeatability and the

continuous nature of its profile compared to other field tests (Robertson, 2009; Zhang et al., 2002). Also, the use of shear wave velocity, V_s, as an index of liquefaction resistance is soundly based because both V_s and liquefaction resistance are similarly but not proportionally influenced by many of the same factors (e.g., void ratio, state of stress, stress history, and geologic age), and the advantages of a V_s-based method have been demonstrated by many researchers (e.g. Andrus and Stokoe 2000, 1997; Youd et al. 2001; Zhou and Chen, 2007).

5.2 Field Testing Results

5.2.1 Overview

In this section, the results of geotechnical field testing performed at the Big Branch and Abner Fork impoundments are presented. As was mentioned in Section 2.2, two locations were designated at each impoundment for performing the field tests and piston sampling. At Big Branch, locations A and D refer to the upstream toe and crest, respectively. Two other locations designated as Abner Fork, locations A and B represent the crest and upstream-toe respectively as depicted in Figure 5.1. Also, it was mentioned in Section 2.2 that Cone Penetration Testing in the fine grained coal mine tailings, required installation of a cased pilot hole through the overlying coarse refuse to avoid damaging the tool. Once the casing was installed through the coarse refuse, the cone was lowered through the casing and the fine refuse was tested.

The results of the in-situ geotechnical tests performed at the Big Branch impoundment are presented in Table 5.1 and

Table 5.2. It should be noted that at each location (crest or toe), SPT, field vane shear tests, and piston sampling were performed in the same borehole, while Cone Penetration Testing accompanied by pore water pressure and shear wave velocity measurements (sCPTu) was performed at a point approximately 20 ft (6 m) from the first boring. Piston sampling was performed at 20 ft intervals. The SPT tests were performed at 20-ft (6-m) intervals in between the piston sampling locations. Therefore, the SPT and piston sampling locations were staggered at about 10-ft (3-m) intervals. After performing each of the SPT tests or piston sampling, a vane shear test was performed. The details of performing these in-situ tests are presented in Chapter 2 and Chapter 3.

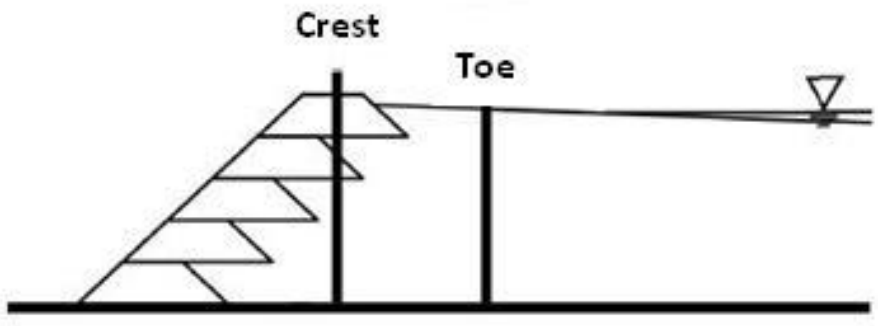

Figure 5.1: Schematic field testing locations at each impoundment.

Table 5.1: In-situ geotechnical parameters measured at Big Branch, Location D (crest).

Depth (ft)	Elevation (ft)	Piston	SPT		CPT			Vane Shear	
			N_m	$(N_1)_{60}$	q_t (tsf)	FR (%)	Q_{tN}	S_{PF} (psf)	S_{RF} (psf)
9	1154.7		47	72.9					
29	1134.7		17	14.7					
49	1114.7		0	0.0					
59	1104.7		11	8.1	10.0	1.4	3.7		
79	1084.7		WOT	0.0	12.5	1.8	3.4		
84	1079.7	Piston 1			11.0	2.8	2.4		
88	1075.7				12.0	1.8	2.6	434	217
94	1069.7		WOT	0.0	10.8	1.7	1.9		
100	1063.7				12.3	3.1	2.2	543	109
105.5	1058.2	Piston 2			12.5	2.1	2.0		
108	1055.7				14.4	2.8	2.5	543	217
114	1049.7		3	1.8	13.4	2.0	2.0		
120	1043.7				13.6	2.8	1.8	652	326
125.25	1038.4	Piston 3			30.4	1.4	6.2		
128	1035.7				15.8	1.9	2.1	543	217
134	1029.7		WOT	0.0	27.0	4.1	4.8		
140	1023.7				49.7	2.1	10.1	760	326
144.8	1018.9	Piston 4			18.7	2.5	2.3		
148	1015.7				22.6	2.5	3.2	652	326
154	1009.7		WOT	0.0	31.8	3.7	5.0		
160	1003.7				52.8	2.2	9.2	760	326

Definitions:
Depth: depth of the location relative to the surface
Elevation: Elevation of the test location relative to the bench mark
Piston: Undisturbed piston sample number
N_m: Uncorrected Standard Penetration Test blow counts (blows/ft)
$(N_1)_{60}$: Overburden corrected Standard Penetration Test blow counts (blows/ft)
WOT: Spoon advanced under the weight of tool itself
q_t: Corrected CPT Test tip resistance
FR: Corrected CPT sleeve friction resistance
Q_{tN}: Normalized cone resistance
S_{pf}: Peak field vane shear resistance
S_{rf}: Residual field vane shear resistance

Table 5.2: In-situ geotechnical parameters measured at Big Branch impoundment, Location A (upstream-toe). See Table 5.1 for definitions of terms.

Depth	Elevation	Piston	SPT		CPT			Vane Shear	
			N_m	$(N_1)_{60}$	q_t	FR	Q_{tN}	S_{pf}	S_{rf}
(ft)	(ft)				(tsf)	(%)		(psf)	(psf)
9	1142.5		5	7.9					
29	1122.5		2	1.8					
34	1117.5	Piston 11			7.0	2.5	5.4		
38	1113.5				9.1	3.3	6.7	652	326
44	1107.5		WOT	0.0	5.9	2.8	8.0		
51	1100.5				7.4	2.4	9.6	326	109
55	1096.5	Piston 12			14.0	3.0	10.5		
58	1093.5				9.1	2.4	8.5	652	217
59	1092.5				8.3	2.0	11.1		
64	1087.5		1	0.7	7.9	1.8	11.1		
71	1080.5				7.5	2.2	11.1	217	109
75	1076.5	Piston 13			8.2	1.9	14.9		
78	1073.5				8.3	1.9	14.9	217	109
84	1067.5		0	0.0	8.6	1.8	14.9		
91	1060.5				9.8	1.9	14.9	434	217
94	1057.5	Piston 14			10.2	2.0	18.7		
98	1053.5				11.1	2.2	18.7	652	217
104	1047.5		0	0.0	11.3	2.3	18.7		
111	1040.5				12.8	2.1	21.2	434	217
114	1037.5	Piston 15			12.7	2.0	21.2		
118	1033.5				14.4	2.3	23.6	652	217
124	1027.5		4	2.4	14.5	1.9	23.6		
131	1020.5				13.6	2.1	23.6	434	217
134	1017.5	Piston 16			13.3	1.9	23.6		
138	1013.5				13.5	1.9	23.6	869	543
144	1007.5		12	6.9	16.6	1.8	23.6		
149	1002.5		33	18.6	57.8	4.5	23.6		

The $(N_1)_{60}$ parameter is the SPT blow counts, N_m, normalized to an overburden pressure of approximately 1 tsf (100 kPa) and a hammer energy ratio of 60%. The normalization of this parameter involves consideration of the effective overburden stress, the type of hammer, the borehole diameter, the rod length, and the usage of liners in the sampler which is presented by Youd et al. (2001). The following relationship was used for normalization of this parameter

$$(\mathrm{N_1})_{60} = \mathrm{N_m C_N C_E C_B C_R C_S} \quad (5.1)$$

in which, C_N is the factor to normalize N_m to a common reference effective overburden stress, C_E is the correction for hammer energy ratio (ER), C_B is the correction factor for borehole diameter, C_R is the correction factor for rod length, and C_S is the correction for samplers with or without liners. The overburden correction factor normalizes the effective overburden pressure, σ'_{v0} , to a reference pressure of $P_a = 1.0\ tsf \cong 100kPa$ and is defined by equation 5.2:

$$C_N = (P_a/\sigma'_{v0})^{0.5} \quad (5.2)$$

For calculation of these factors, the recommendations of Youd et al. (2001), Skempton (1986), and Robertson and Wride (1998) were considered. The hammer used in this study was an automatic trip hammer which for such hammers the correction factor C_E ranges from 0.8 to 1.3. The energy ratio was not measured in this study, but was chosen according to the suggestion given by Seed et al. (2003). They suggested that "*values roughly central to the mid-third of the range are more common than outlying values*". Therefore, the C_E was chosen equal to 1.0. To drill the borehole, a hollow stem auger with an internal diameter of 4.25 in (108 mm) was used. The borehole diameter was approximately 6 in (152 mm) and therefore the C_B equal to 1.05 suggested for a 150 mm borehole from Youd et al (2001) and Seed et al (2003) was used. No samples were taken above 33 feet and therefore the correction factor for the rod length C_R was set equal 1.0. For the SPT split spoon the sampler factor C_S equal to 1.0 was used.

The CPT soundings are recorded almost continuously (every 0.02 m ~ every 0.065 ft) as the cone is pushed in the ground, however at certain depths (corresponding to SPT and field vane shear tests) the CPT parameters are selected and presented in

Table 5.2 and Table 5.1. The full data set of the CPT sounding is presented in Appendix B and the graphical presentation of the full profile is illustrated in Section 5.2.1. The in-situ parameters recorded during CPT sounding were q_c, cone tip resistance, f_s, the sleeve friction resistance, and u_2, the pore pressure measured during cone pushing. The strength parameters q_c and f_s were corrected for the effect of the measured pore water pressure u_2 and the overburden stress following the recommendations of Robertson and Campanella (1983a, 1983b), Robertson and Wride (1998). Robertson (2010), and Youd et al. (2001). The corrected cone tip resistance q_t and friction ratio RF were reported in

Table 5.2 and Table 5.1. The corrected cone tip resistance q_t was calculated by using the equation given by Robertson and Campanella (1983)

$$q_t = q_c + u_2(1 - a) \tag{5.3}$$

in which, u_2 is the total dynamic pore pressure, $u_2 = u_0 + \Delta u$, and "a" is the bearing net area ratio. The parameter u_o is the equilibrium water pressure and Δu is the excess pore pressure generated during cone pushing. According to Robertson and Campanella (1983), the bearing net area ratio, a, ranges from 0.6 to 0.8 for common shapes of the cones.

However, Robertson and Cabal (2012) reported typical values to range between 0.70 and 0.85. In this study a cone with a bearing net area ratio of 0.8 was used.

The pore pressure corrected cone resistance, q_t, can be corrected for the overburden stress and the type of soil (Robertson, 2009) using the following equation:

$$Q_{tN} = [(q_t - \sigma_v)/p_a](p_a/\sigma'_{vo})^n \quad (5.4)$$

in which, σ_v is the total overburden stress, p_a, is the reference atmospheric pressure in the same units of of σ_v and σ'_{v0}, σ'_{v0} is the effective overburden pressure, and n is the stress exponent that varies with the soil behavior type index (SBT) also known as the I_c. The normalized soil behavior type index (SBT_N) is calculated using the following equation:

$$I_C = ((3.47 - logQ_{tn})^2 + (logF_r + 1.22)^2)^{0.5}. \quad (5.5)$$

In equation 5.5, Q_{tn} is calculated using the equation presented above and F_r is the normalized friction ratio (Robertson, 1990; Robertson 2012). Normalized friction ratio is obtained by using the CPT sleeve friction values:

$$F_r = [f_s/(q_t - \sigma_{v0})] \times 100\%. \quad (5.6)$$

As can be seen from the presented equations, the normalization and correction procedure for the tip resistance is an iterative effort. The normalization of the tip resistance to calculate Q_{tN} relies on the value of the exponent n, which is related to the value of Ic, which in turn depends on the value of Q_{tN}. Therefore, usually an initial value of n equal to 1.0 is selected which is suitable for clayey soils. Then the value of the

calculated I_c is checked against the range suggested for clayey soils. If this value is greater than 2.6 then the assumption of clayey soils has been valid and the procedure is complete. If not, the calculation is repeated with the n value equal to 0.5 for granular soils. Other considerations were taken into account following the full procedure provided by Robertson and Wride (1998) and Youd et al. (2001). In Figure 5.2 and Figure 5.3 the results of the in-situ geotechnical tests including CPT sounding, SPT, and field vane shear test performed at the Big Branch impoundment at locations D (crest), and A (toe) are illustrated.

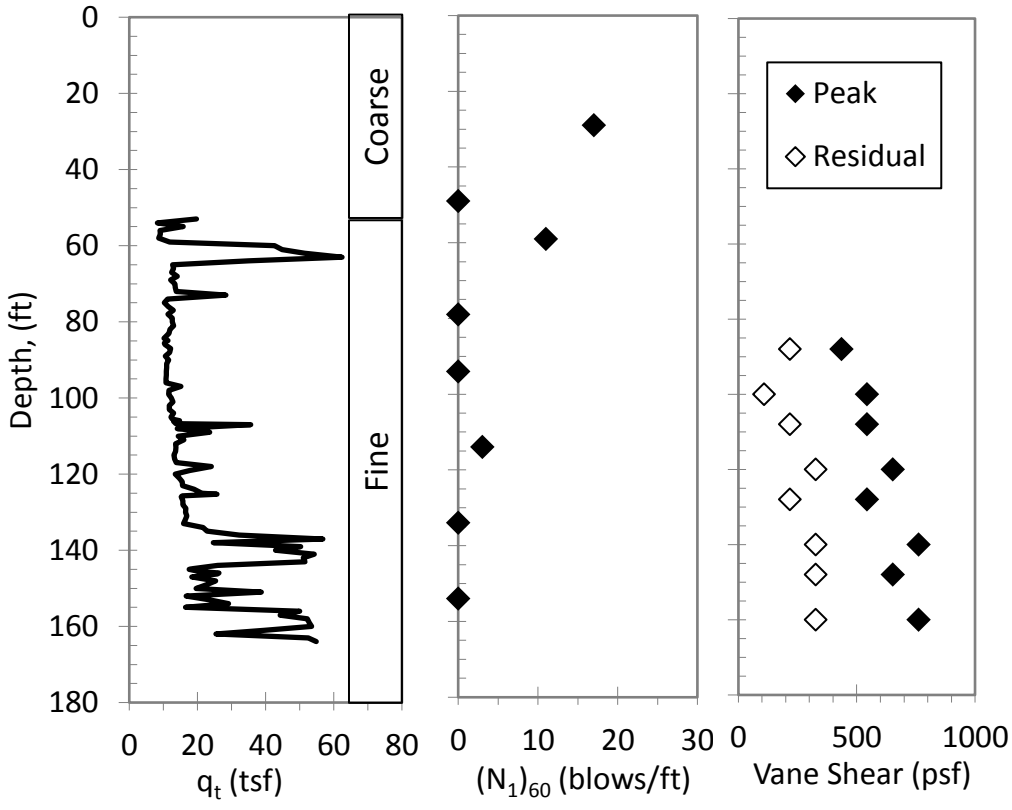

Figure 5.2: In-Situ Strength parameters at Big Branch location D (crest).

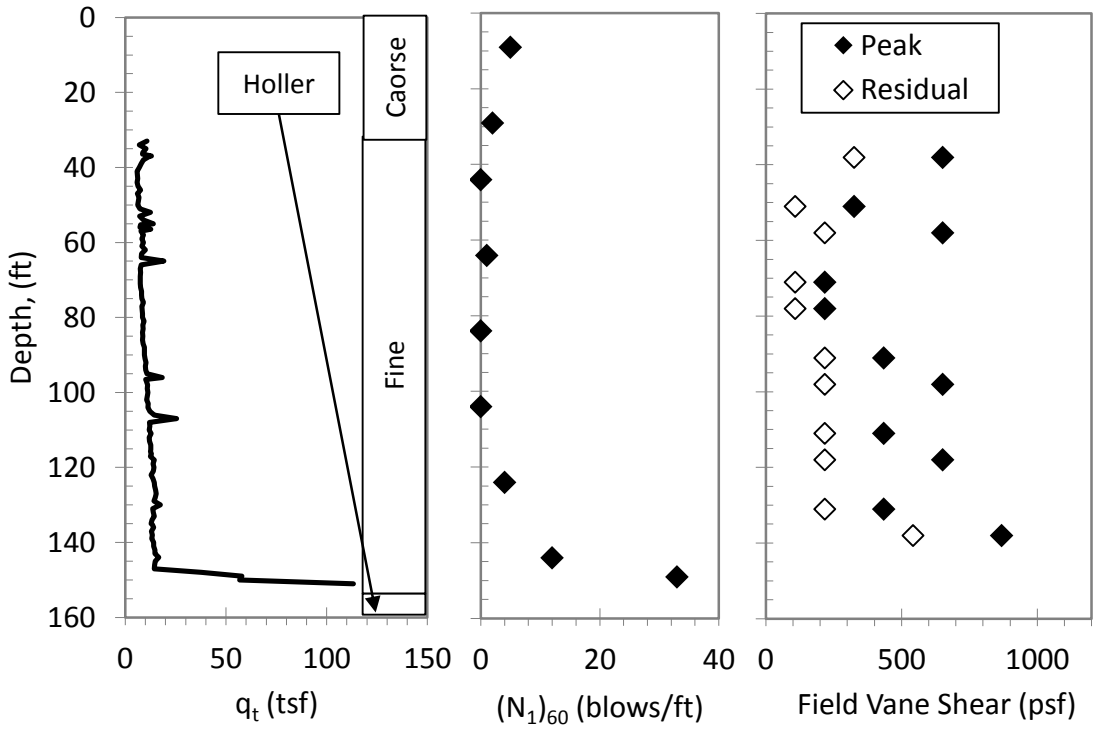

Figure 5.3: In-Situ Strength parameters at Big Branch location A (toe)

The results of the in-situ geotechnical tests performed at the Abner Fork impoundment are presented in Table 5.3 and Table 5.4. The field measured parameters at the Abner Fork impoundment are illustrated in Figure 5.5 and Figure 5.4. These results are discussed in detail in the following sections.

Table 5.3: In-situ geotechnical parameters measured at Abner Fork, Location A (crest).

Depth	Elev.	Piston	SPT		CPT					Vane Shear		SASW	
			N_m	$(N_1)_{60}$	q_t	RF	Q_{tN}	v_s	v_s'	S_{PF}	S_{RF}	v_s	v_s'
(ft)	(ft)				(tsf)	(%)		(m/s)	(m/s)	(psf)	(psf)	(m/s)	(m/s)
19	2230		73	77.9								442	449
39	2210		38	28.3								518	481
59	2190		72	43.6								518	457
79	2170		63	33.5								488	417
99	2150		25	12.7								488	412
119	2130		55	26.8								488	408
139	2110		31	14.6								488	404
159	2090		35	15.9				335	275			335	275
169	2080		42	18.7	51.2	5.1	8.3	358	293			335	274
179	2070		32	14.0	38.7	2.3	5.3	472	384			335	273
189	2060		40	17.3	93.4	4.9	14.8	503	408			488	395
199	2050		47	20.0	84.1	3.5	12.4	518	418			488	394
209	2040		46	19.3	90.7	3.2	12.8	518	417			488	392
230	2019		26	10.6								488	389
235	2014									8686	3722	488	389
239	2010	Piston 1										488	388
242	2007									9306	6204	488	388
250	1999		28	11.1								488	387
252	1997									9306		488	386
259	1990	Piston 2										488	386
270	1979		25	9.6								488	384
272	1977		44	16.9								488	384
279	1970	Piston 3										488	383
290	1959		45	16.9								488	382

Definitions:

Depth: depth of the location relative to the surface

Elev.: Elevation of the test location relative to the bench mark

Piston: Undisturbed piston sample number

N_m: Uncorrected SPT blow counts (blows/ft)

$(N_1)_{60}$: Overburden corrected SPT blow counts (blows/ft)

WOT: Weight of tool

q_t: Corrected CPT Test tip resistance

FR: Corrected CPT sleeve friction resistance

Q_{tN}: Normalized cone resistance

V_s: Shear wave velocity measured by seismic CPT, or SASW

V_s': Corrected V_s measured by seismic CPT, or SASW

S_{pf}: Peak field vane shear resistance

S_{rf}: Residual field vane shear resistance

Table 5.4: In-situ geotechnical parameters measured at Abner Fork, Location B (toe); See Table 5.3 for definitions of terms.

Depth	Elevation	Piston	SPT		CPT					Vane Shear		SASW	
			N_m	$(N_1)_{60}$	q_t	RF	Q_{tN}	CPT v_s	CPT v_s'	S_{PF}	S_{RF}	v_s	$v_{s'}$
(ft)	(ft)				(tsf)	(%)		(m/s)	(m/s)	(psf)	(psf)	(m/s)	(m/s)
29	2184		21	21								396	382
59	2154		33	27								396	350
89	2124		34	24								396	336
119	2094		23	15								396	331
149	2064		5	3	167.2	1.0	41.8					396	326
169	2044	Piston 1			86.6	5.2	15.5	411	336			396	324
173	2040				23.1	2.6	2.5	366	298	4963	1809	396	323
189	2024		8	4	27.7	2.7	2.9	792	642			762	617
192	2021				28.0	2.2	2.9	320	259	6204	2585	762	617
199	2014	Piston 2			26.7	2.5	2.5	335	271			762	615
203	2010				24.4	2.0	2.1	335	270	6204	2482		
209	2004		0	0	25.8	2.3	2.2	335	270				
212	2001				22.5	2.0	1.6	305	245	9306	4963		
219	1994	Piston 3			25.3	2.2	1.9	366	293				
222	1991				27.5	2.1	2.2	366	293	8065	3412		

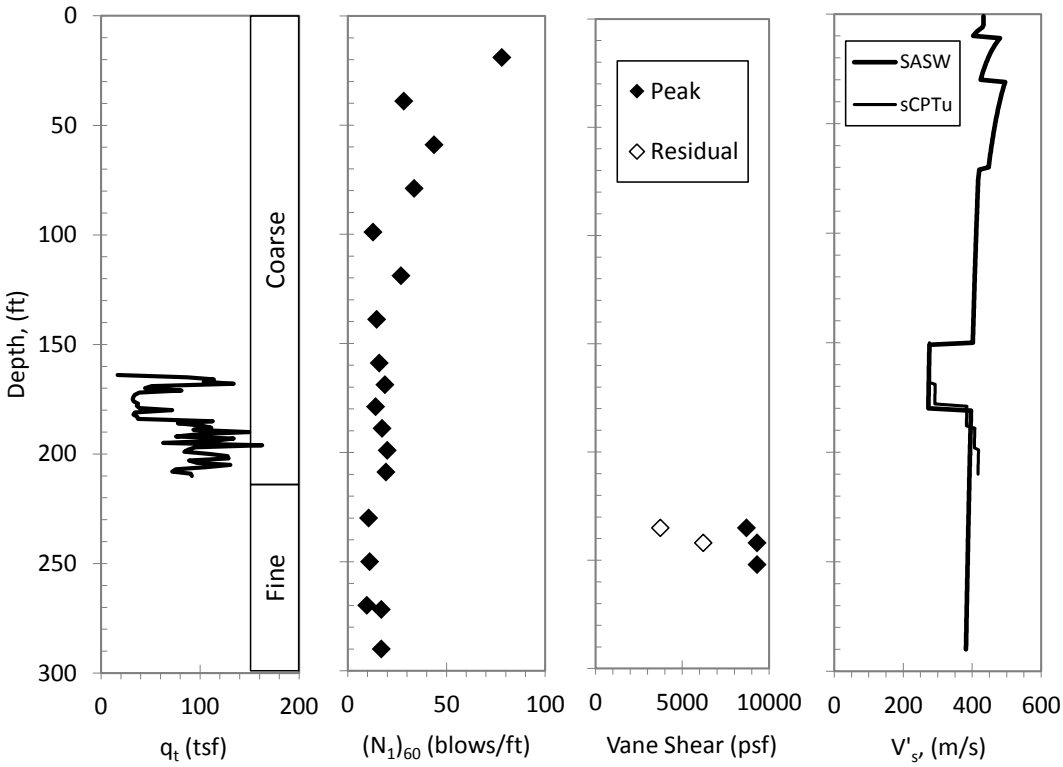

Figure 5.4: In-Situ Strength parameters at Abner Fork Location A (crest).

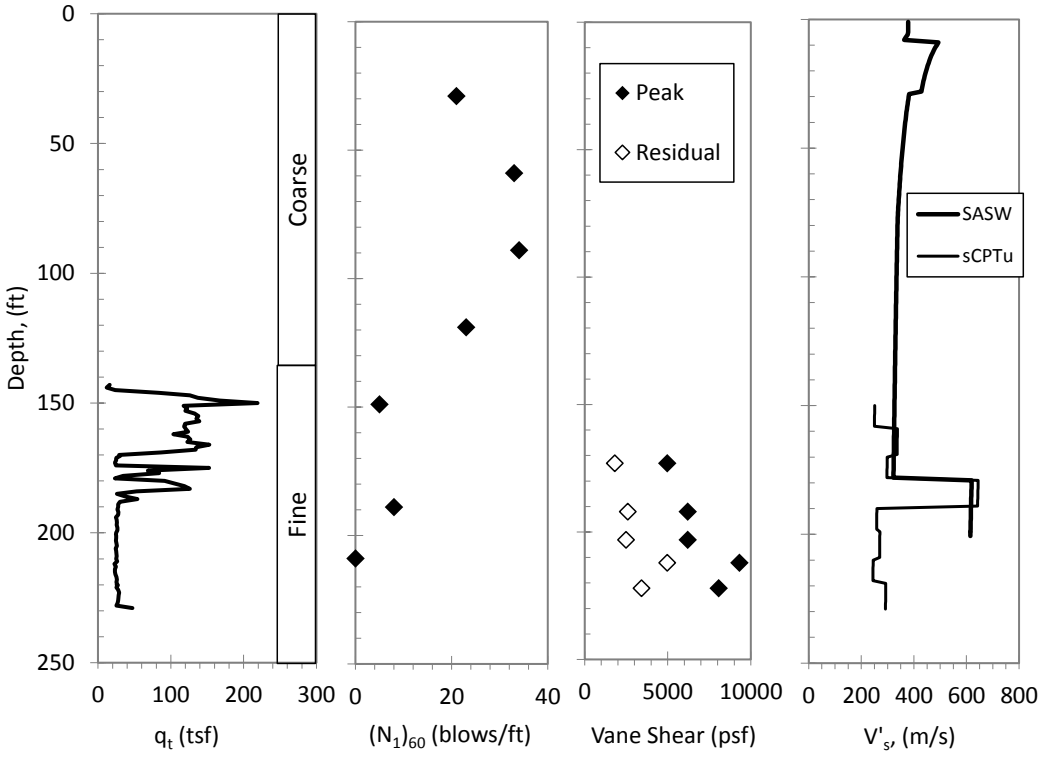

Figure 5.5: In-Situ Strength parameters at Abner Fork Location B (toe).

5.2.2 Cone Penetration Tests Results

In Figure 5.6, the results of the Cone Penetration Testing performed at the crest (Location D) of the Big Branch impoundment are illustrated. By following the procedures discussed in Section 5.2, the CPT tip resistance values, q_c, were corrected for the excess pore water pressure and q_t values, pore pressure corrected tip resistance values, were obtained. Also, q_t values were corrected for the overburden pressure and normalized to produce Q_{tN} parameter for each location.

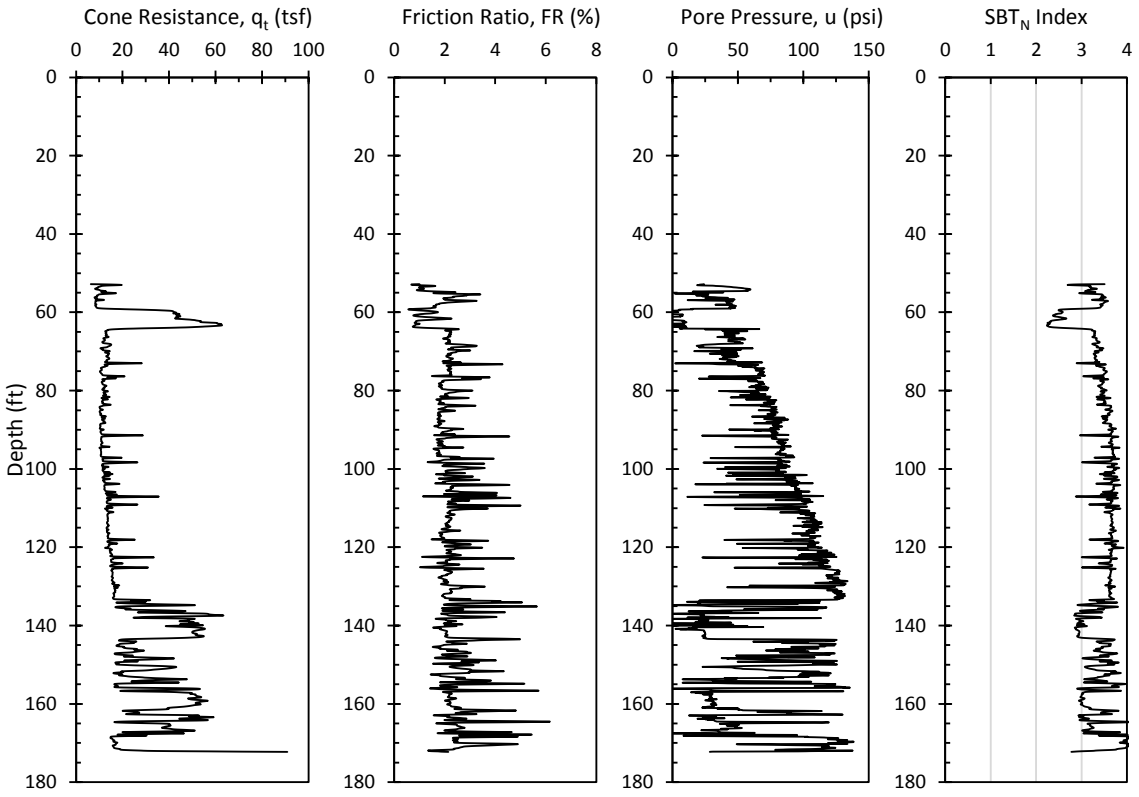

Figure 5.6: CPT sounding results at the Big Branch impoundment, Location D, (crest).

The pore pressure corrected CPT tip resistance values, q_t, at the crest of the Big Branch impoundment approximately ranged between 10 tsf to 60 tsf (958 kPa to 5746 kPa). However, it should be noted that the high values of CPT tip resistance were recorded

relatively close to the top surface and this sharp increase as it is depicted in Figure 5.6, could be the result of measurement in the coarse refuse or a mixture of fine-coarse material. As was illustrated in Figure 5.1, by constructing newer dikes, the older dikes could be mixed with the fine refuse material near the existing pond. Thus, by performing the CPT test from the top of the most recent dike, the tip of the tool could encounter some mixed zones and as a result, the CPT value can be greater than the adjacent layers of fine refuse.

The fine refuse material is transported from the mine to the impoundment by pumping the slurry to the existing pond. Due to high amount of water mixed with the fine refuse, the fine tailings become segregated and therefore, the heavier grains settle closer to the discharge point and the lighter grains are carried further. Thus, the surface of the pond consists of heterogeneous fine grain coal tailings zones and the gradation and the texture of the material changes from one point of the impoundment to the other. As the pond becomes deeper, the heterogeneity propagates in the vertical direction as well and therefore any zone in the fine refuse layer has different physical and geotechnical properties than the other zones. Considering the construction method of the impoundments including the slurry pumping and also the mixing of the coarse and fine refuse explained in the previous paragraph, it is expected that the fine refuse or slimes to be highly stratified. The results of CPT testing illustrated in Figure 5.6 confirm this assumption. Layers with lower tip resistance values which are accompanied with higher measured pore water pressure values indicate the presence of coal tailings comprised of finer grained material while the layers with higher tip resistance and lower measured pore

pressure indicate the layers consisting of coarser grained tailings. During cone pushing, coarser grained soils dissipate the induced pore pressure quickly and therefore the measure pore pressure is lower compared to the fine grained layers. The variation of the Normalized Soil Behavior Type Index (SBT_n) which is also known as the I_c parameter is presented in Figure 5.6. The procedure to calculate this parameter is presented in Section 5.2. This parameter determines the location of the sample in a soil behavior zone chart with the normalized friction ratio F_r on the x-axis and the normalized cone penetration resistance Q_{tn} on the y-axis. Therefore, I_c is the radius of the essentially concentric circles that represent the boundaries between each SBT zone. For the majority of the Big Branch impoundment profile at location D, the values of normalized I_C vary between approximately 3.0 and 4.0. According to Robertson (1990) these values represent clays (silty clay to clay) which agrees with the classification of the samples by USCS method categorizing them and silts (ML) and low plasticity clays (CL). The soil behavior type reference chart and the range of I_C for each zone is presented in Figure 5.7.

Mixed refuse zones consisting of coarse and fine refuse are also indicated by highly variable tip resistance within the interval, whereas the tip resistance of fine refuse is generally more uniformly distributed with the exception of minor stratification in the tailings as it was deposited. At an approximate depth of 170 ft, the CPT tool reached the bottom of the original ground surface contour (i.e. the holler) and testing was stopped.

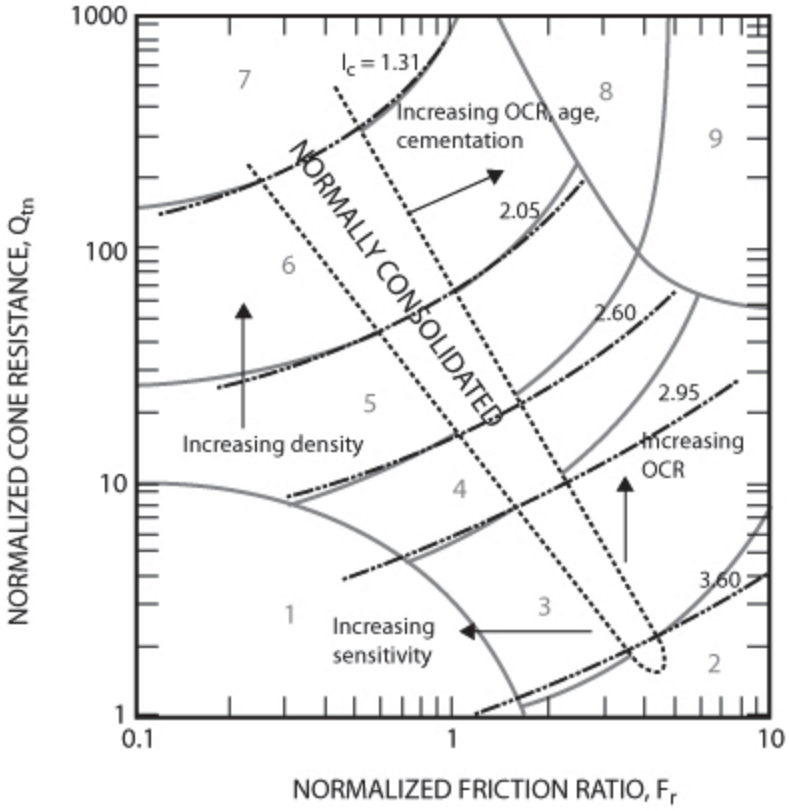

Zone	*Soil Behavior Type*	I_c
1	*Sensitive, fine grained*	N/A
2	*Organic soils – clay*	> 3.6
3	*Clays – silty clay to clay*	2.95 – 3.6
4	*Silt mixtures – clayey silt to silty clay*	2.60 – 2.95
5	*Sand mixtures – silty sand to sandy silt*	2.05 – 2.6
6	*Sands – clean sand to silty sand*	1.31 – 2.05
7	*Gravelly sand to dense sand*	< 1.31
8	*Very stiff sand to clayey sand**	N/A
9	*Very stiff, fine grained**	N/A

** Heavily overconsolidated or cemented*

Figure 5.7: Normalized soil behavior type (SBT_N) chart and the range of Ic for each zone (Robertson, 1990; Robertson, 2010).

To estimate the in situ pore pressure during CPT sounding at each of the locations, a pore water pressure dissipation test was performed. The CPT cone is stopped and sufficient time is allowed for the excess pore pressure to dissipate and as a result the pore pressure reaches a constant value. The obtained value is utilized to calculate the depth of the water above the cone. Typical results of a dissipation test are illustrated in Figure 5.8.

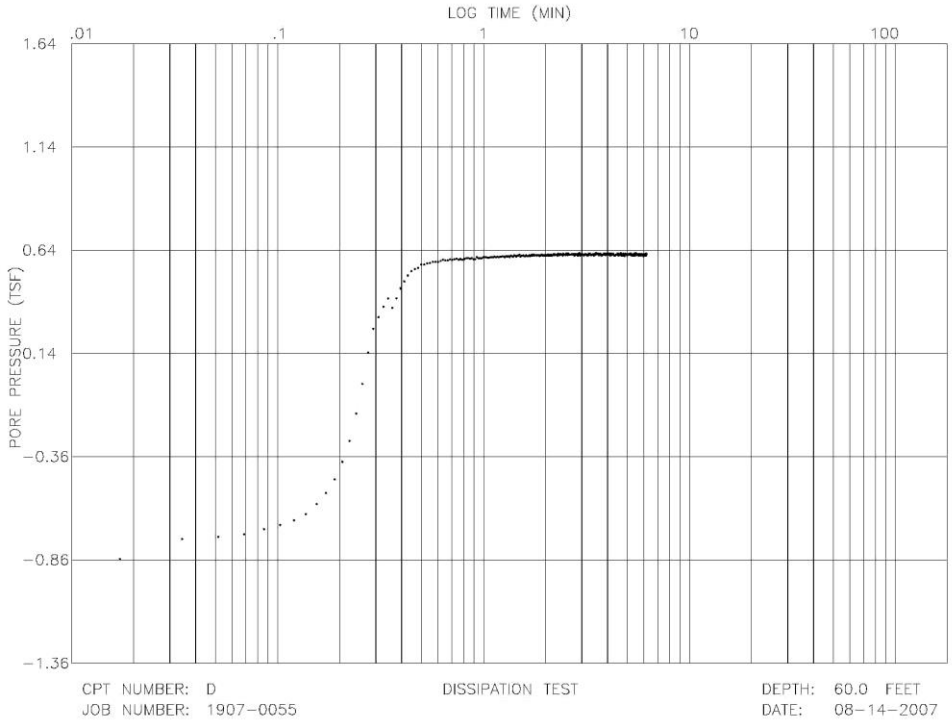

Figure 5.8: Excess pore water pressure dissipation test results at Big Branch impoundment, location D (crest) at the depth of 60 ft.

The procedures proposed for determining the soil behavior and classification are implemented into a commercial software known as CLiq (Version 1.7). This software was used to compare the calculated parameters and produce the SBT chart. In Figure 5.9, the variation of the normalized SBT index is presented. Green data points represent the layers with I_c values greater than 2.6 (higher fine content) and are likely susceptible to cyclic softening rather than liquefaction. The red data points identify the layers with I_c values

smaller than 2.6 which are likely to experience liquefaction rather than cyclic softening. The variation of corrected tip resistance, friction ratio, pore pressure, and SBT index values with depth obtained from CLiq (Version 1.7) are presented in Figure 5.10.

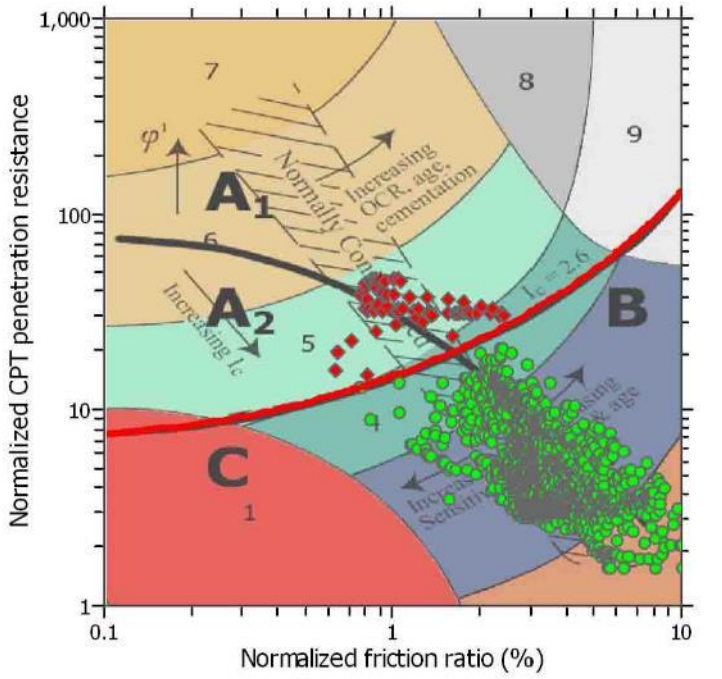

Zone A_1: Cyclic liquefaction likely depending on size and duration of cyclic loading
Zone A_2: Cyclic liquefaction and strength loss likely depending on loading and ground geometry
Zone B: Liquefaction and post-earthquake strength loss unlikely, check cyclic softening
Zone C: Cyclic liquefaction and strength loss possible depending on soil plasticity, brittleness/sensitivity, strain to peak undrained strength and ground geometry

Figure 5.9: Normalized soil behavior type index (SBT_N) chart for the CPT sounding at Big Branch location D (crest), CLiq (Version 1.7).

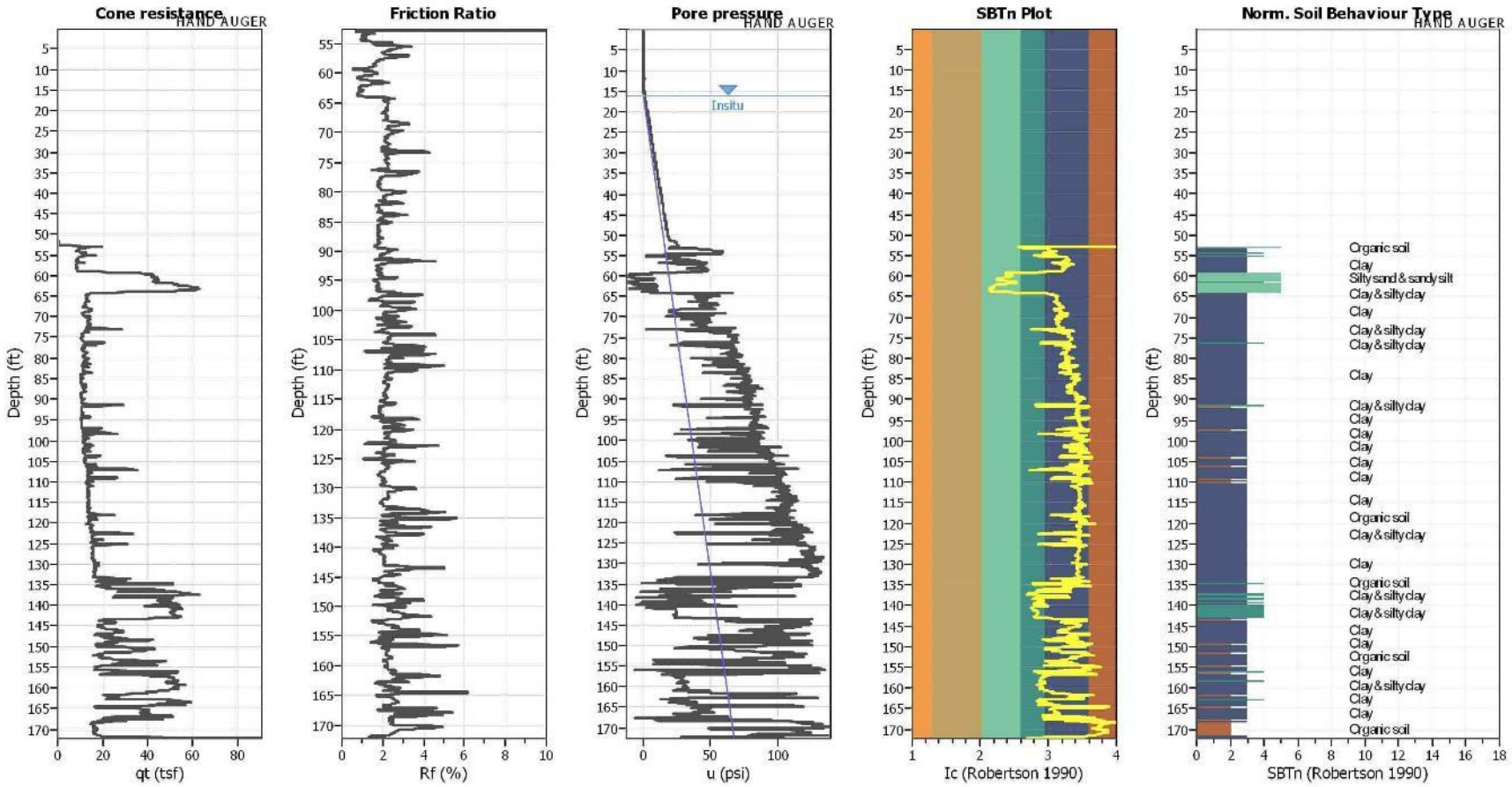

Figure 5.10: Variation of corrected tip resistance, friction ratio, pore pressure, and SBT index values for Big Branch location D (crest) obtained from CLiq (Version 1.7).

It should be noted that approximately the first 50 ft (15.24 m) of the CPT hole at Big Branch location D was drilled by a hollow stem auger. Therefore, no data were recorded and as shown in Figure 5.10, the software uses the term "hand auger" on the results due to lack of data. Also, on the soil profile representing the soil classification based on I_c values, the first 50 ft (15.24 m) are labeled as "sensitive fine grained" which does not apply in this case. The variation of the pore water pressure in this figure shows that at the layers with higher fines content, the measured pore pressure has been higher than the in situ pore pressure. At any layer that the CPT cone reaches the layers with lower fines content the induced pore pressure dissipates quickly and the values are closer to the in situ results.

In Figure 5.11, in addition to the normalized tip resistance Q_{tN} and normalized sleeve friction, F_r, the variation of apparent fines content, FC, coefficient K_c, and clean sand corrected normalized cone tip resistance $(Q_{tN})_{CS}$ with depth for the samples obtained from Big Branch at location D (crest) are presented. The apparent fines content using the CPT data is calculated by the following equations:

If $I_c < 1.26$ then FC (%) = 0

If $1.26 < I_c < 3.5$ then FC (%) = $1.75 I_c^{3.25}$-3.7 (5.7)

If $I_c > 3.5$ then FC (%) = 100

The coefficient K_C is function of grain characteristics (combined influence of fines content, mineralogy and plasticity) and it is estimated as follows:

If $I_c \leq 1.64$, $K_C = 1.0$ (5.8)

If $I_c > 1.64$, $K_C = -0.403I_C^4 + 5.581I_C^3 - 21.63I_C^2 + 33.75I_C - 17.88$

The parameter $(Q_{tN})_{CS}$ is the equivalent clean sand normalized tip resistance for soils with higher fines content and is calculated by utilizing equation 5.8:

$$(Q_{tN})_{CS} = K_C Q_{tN} \quad (5.9)$$

In Figure 5.11, the apparent fines content estimated from the soil behavior type index is compared to the fines content measured in the laboratory. The laboratory data are represented by filled circles and the line represents the estimated fines content from the I_c values. A reasonable agreement is observed between the laboratory measured fines content and the apparent fines content for the coal mine tailings samples in this location.

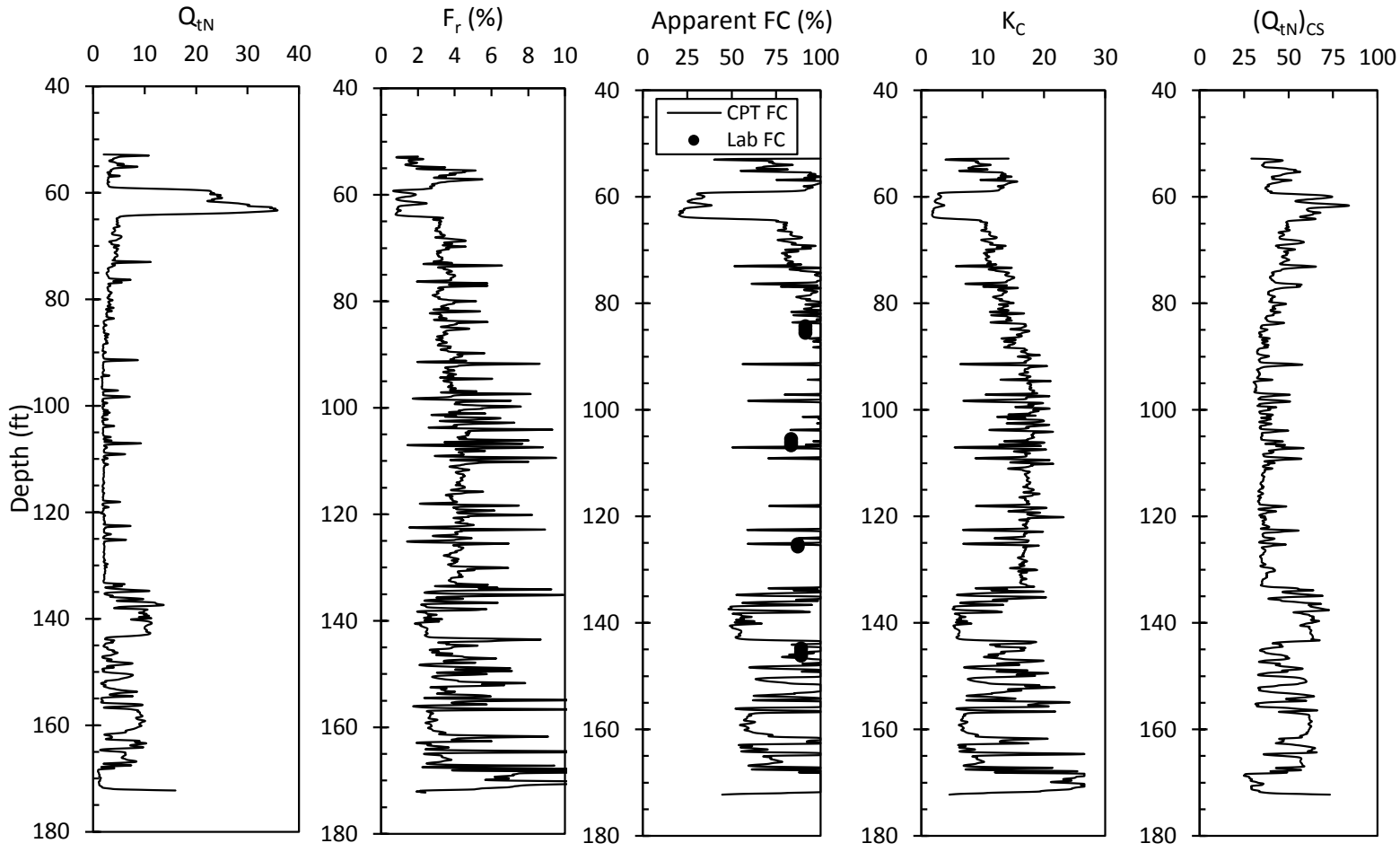

Figure 5.11: Variation of normalized cone tip resistance, normalized sleeve friction, apparent fines content, Kc, and the equivalent clean sand normalized cone tip resistance $(Q_{tN})_{CS}$ with depth for the Big Branch impoundment at location D (crest).

The variation of cone tip resistance, friction ratio, pore pressure, the SBT index recorded at the toe of the Big Branch impoundment (location A) is illustrated in Figure 5.12. It is believed that due to the same reasons that cause the heterogeneity of tailings impoundments (discussed in Chapter 1) and also the geometry of the tailings dam, the likelihood of encountering mixed zones at the toe location is lower. Therefore the corrected CPT profile at location A appears to be more uniform. Also, it is observed that the CPT values relatively become larger with the depth. The pore pressure corrected tip resistance values, q_t, vary between 5 to 25 tsf (479 to 2394 kPa) which is generally a smaller range compared to the values recorded at the crest location. At an approximate depth of 150 ft (45.7 m), the CPT tool reached the bottom of the pond (natural ground surface) and the testing was stopped.

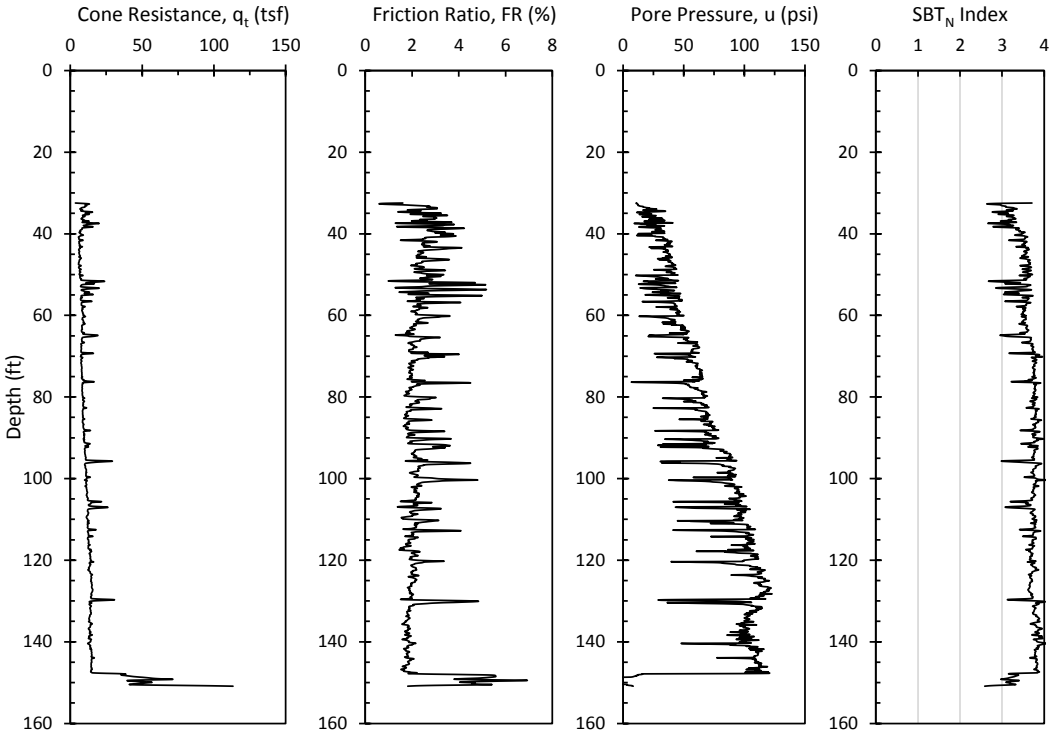

Figure 5.12: CPT sounding results at the Big Branch impoundment, Location A (toe).

The range of values for friction value parameter is roughly in the same range as the values recorded at the crest (location D) of the impoundment. The SBT values in the fine grained material in this location range approximately between 2.5 and 4.0 which as was presented in Figure 5.7, is an indicator of silt mixtures and clays. The variation of the SBT index for this location is illustrated on the SBT chart in Figure 5.13 using CLiq (Version 1.7). In this plot, red diamonds and green circles represent the coarser grained and finer grained tailings layers respectively. The boundary line shown in red represents the soil behavior type index of 2.6 which is the boundary between the coarse grained and the fine-grained soils. It is observed that the number of data points shown with red diamonds is far less than the same ones shown for the crest location presented in Figure 5.9. This indicates that the number of mixed (fine-coarse) layers encountered at this location have been less at the toe location which is in agreement with the location of this CPT and the geometry of the impoundment.

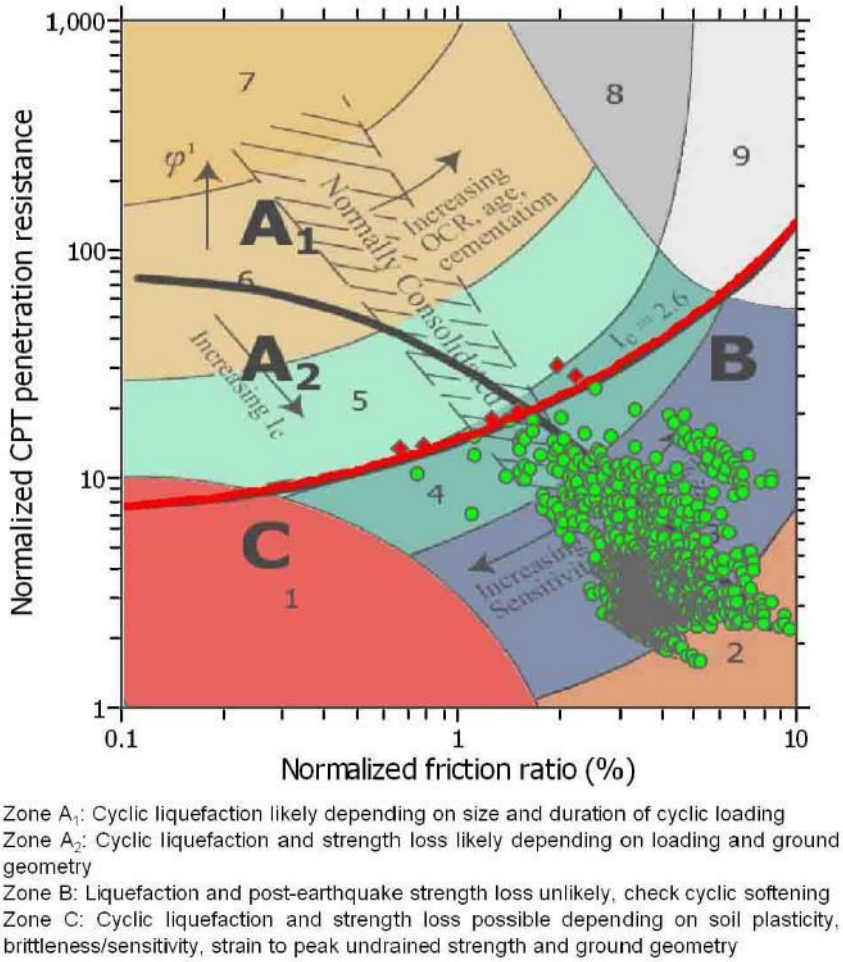

Figure 5.13: Normalized soil behavior type index for the CPT sounding at Big Branch impoundment Location A (toe), CLiq (Version 1.7).

The variation of corrected tip resistance, friction ratio, pore pressure, and SBT index values with depth obtained from CLiq (Version 1.7) for location toe (A) at Big Branch impoundment are presented in Figure 5.14.

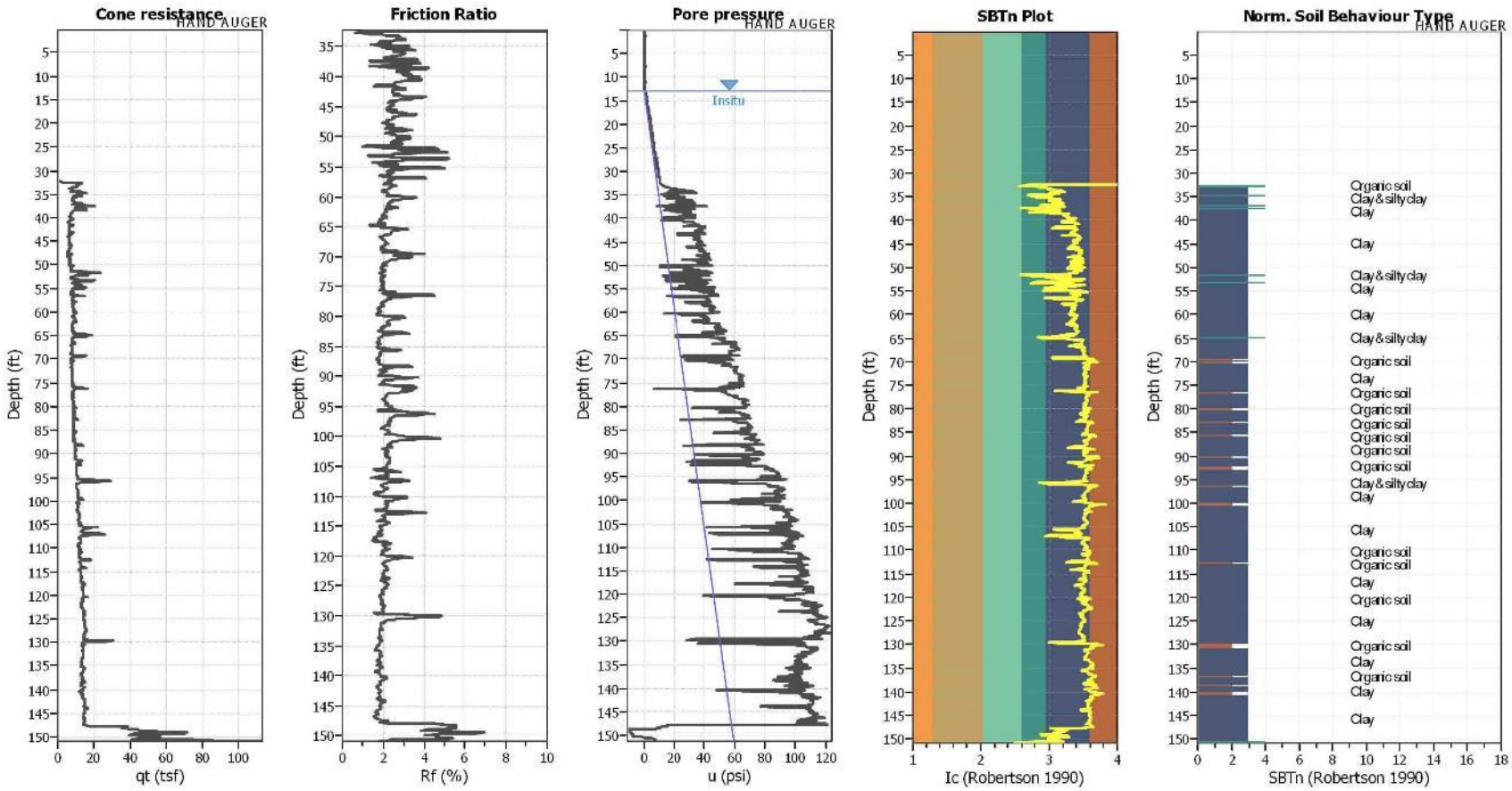

Figure 5.14: Variation of corrected tip resistance, friction ratio, pore pressure, and SBT index values for Big Branch location A (toe) obtained from CLiq (Version 1.7).

Comparison of the SBT index plots in Figure 5.14 and Figure 5.10, shows that the ground profile at Location A (toe), from approximately 35 to 105 ft (10.7 to 32 m) is primarily classified as clay while at Location D (crest) the majority of the full profile is classified as clay/silty clay. This type of classification, i.e. clay/silty clay, is observed for the bottom third of the ground profile at Location toe (A) from approximately 105 to 150 ft (32 to 45.7 m).

In Figure 5.15, the variation of normalized tip resistance, Q_{tN}, normalized sleeve friction, F_r, apparent fines content, FC, coefficient K_c, and clean sand corrected normalized cone tip resistance $(Q_{tN})_{CS}$ with depth for the samples obtained from Big Branch at Location A (toe) are presented. It seems that for the samples with approximately 75% fine content, the apparent fines content is estimated as 100%. Although the fines content estimation is not precise, but for the engineering purposes this difference would not create a significant discrepancy in the results.

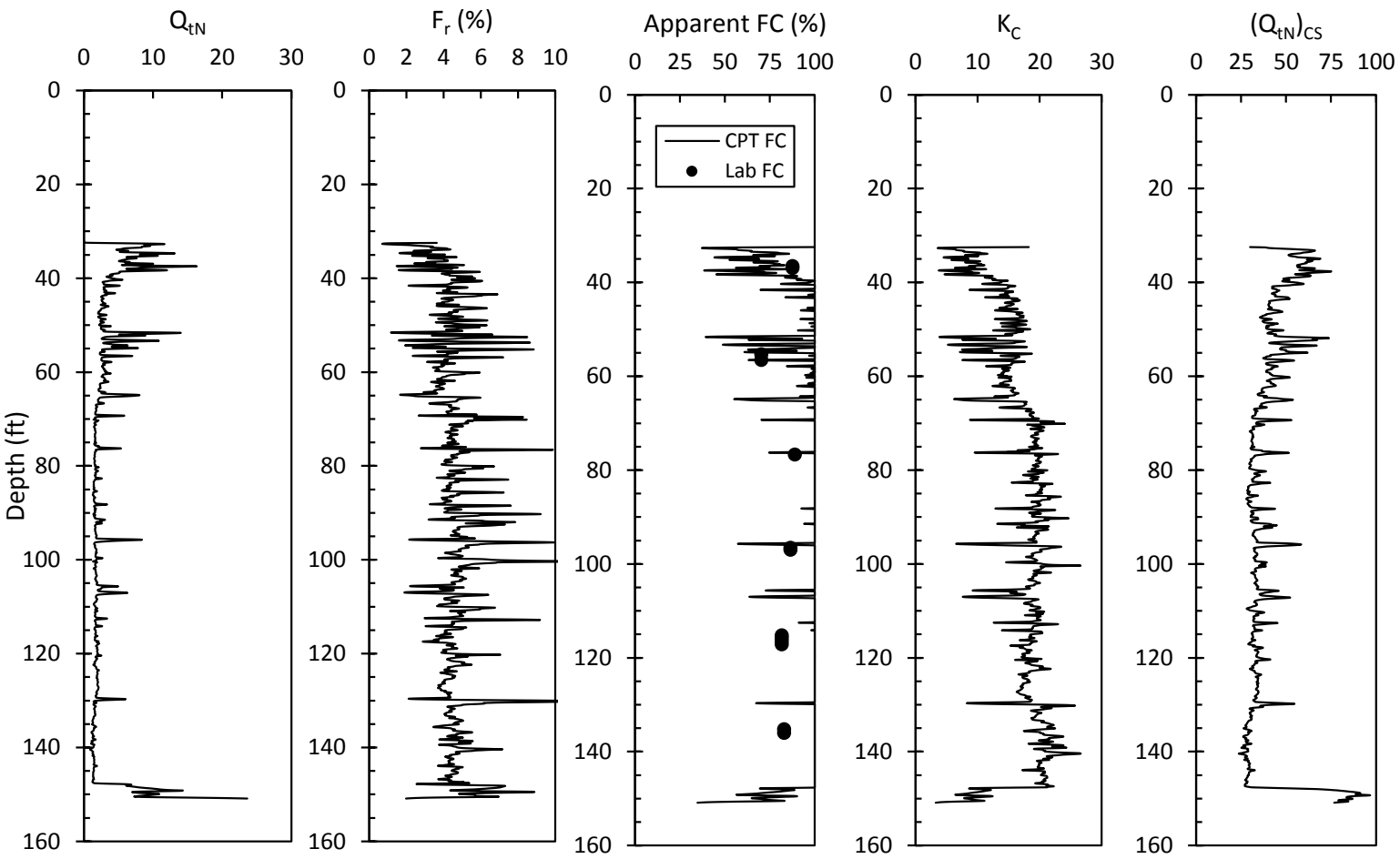

Figure 5.15: Variation of normalized cone tip resistance, normalized sleeve friction, apparent fines content, Kc, and the equivalent clean sand normalized cone tip resistance $(Q_{tN})_{CS}$ with depth for the Big Branch impoundment at location A (toe).

The variation of cone tip resistance, friction ratio, pore pressure, and the SBT index recorded at the crest of the Big Branch impoundment (Location A) is illustrated in Figure 5.16. As it was illustrated in Figure 5.4, the CPT sounding started in the zones consisted of mixed fine and coarse tailings material. However, mixed tailings were encountered all the way to the bottom of the impoundment. The pore pressure corrected tip resistance, q_t, at this location ranged from 40 to 160 tsf (3,830 to 15,321 kPa) and temporarily reached high values of approximately 250 tsf (23,940 kPa). This range of tip resistance at this location is considerably higher compared to the values recorded at Big Branch impoundment which by considering both locations (crest and toe) ranged from 5 to 60 tsf (479 to 5,746 kPa). At an approximate depth of 210 ft (64 m), the original surface of the holler was encountered and the test was stopped.

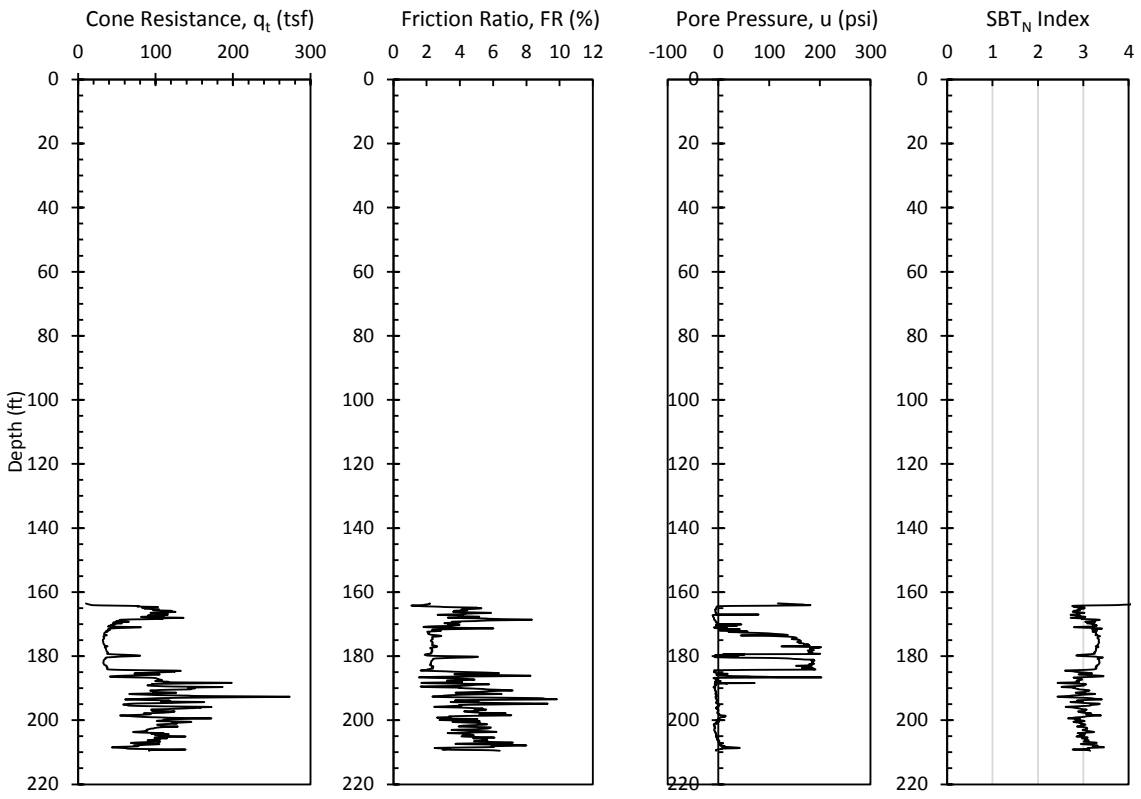

Figure 5.16: CPT sounding results at the Abner Fork impoundment, Location A (crest).

The SBT chart obtained from CLiq (Version 1.7) for this CPT sounding is presented in Figure 5.17. According to this chart, only a few layers had I_c values smaller than 2.6 and therefore only a few red diamonds representing coarse grained soil are shown on this chart. Also, by comparing this chart to the charts presented for Big Branch impoundment in Figure 5.13 and Figure 5.9 and the reference chart by Robertson (1990) shown in Figure 5.7, it is understood that the majority of the ground profile at Abner Fork, Location A (crest) is comprised of stiffer fine grained soils possibly with higher overconsolidation ratios.

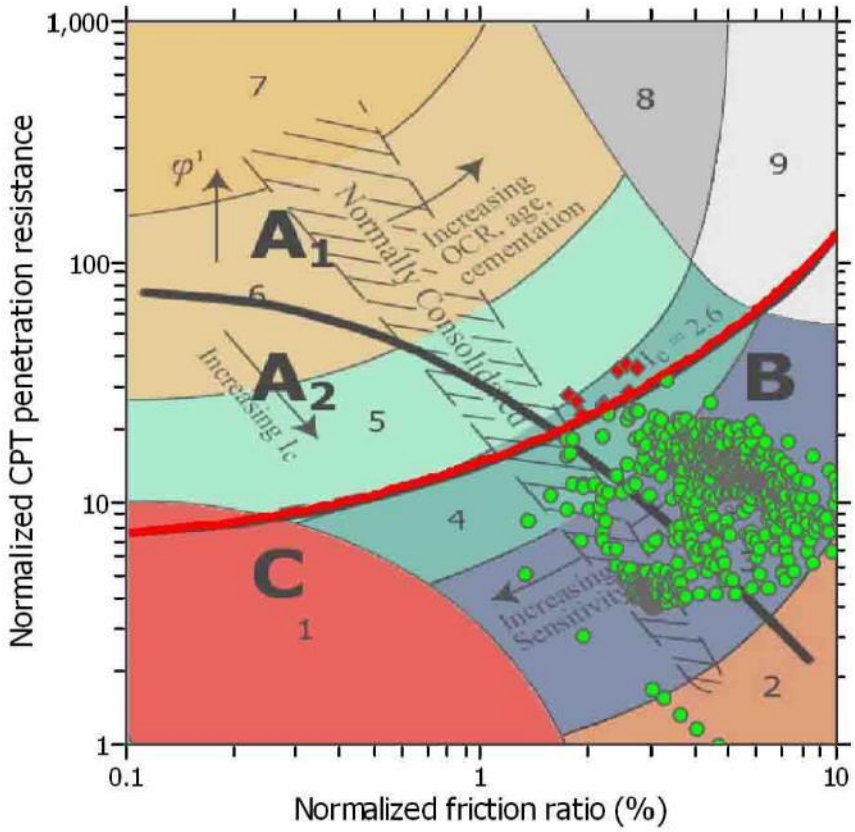

Zone A_1: Cyclic liquefaction likely depending on size and duration of cyclic loading
Zone A_2: Cyclic liquefaction and strength loss likely depending on loading and ground geometry
Zone B: Liquefaction and post-earthquake strength loss unlikely, check cyclic softening
Zone C: Cyclic liquefaction and strength loss possible depending on soil plasticity, brittleness/sensitivity, strain to peak undrained strength and ground geometry

Figure 5.17: Normalized soil behavior type index for the CPT sounding at Abner Fork impoundment Location A (crest), CLiq (Version 1.7).

The variation of corrected tip resistance, friction ratio, pore pressure, and SBT index values with depth obtained from CLiq (Version 1.7) for Location A (crest) at the Abner Fork impoundment are presented in Figure 5.18. By comparing the SBT values calculated for this location to the values from the Big Branch impoundment, it seems that the majority of the I_c values are smaller than 3.6, which suggests that the material behaved less like a clay-like soil and more like a silty soil. Also, it appears that from 170 to 185 ft (52 to 56.4 m) the recorded pore pressure was greater than the in situ pore

pressure. However, from 185 ft (56.4 m) to the bottom of the CPT hole, the pore pressure was in fact smaller than the in situ pore pressure. This behavior suggests dilation and therefore, considering the observed Ic values, it is concluded that the material could be classified as stiff silts or dense fine grained sand. In Figure 5.19, the variation of normalized tip resistance, Q_{tN}, normalized sleeve friction, F_r, apparent fines content, FC, coefficient K_c, and clean sand corrected normalized cone tip resistance $(Q_{tN})_{CS}$ with depth for the samples obtained from Abner Fork at location A (crest) are presented. In this location, the CPT sounding could not be pushed deep enough to the depths that the undisturbed sampling was performed and therefore the comparison between the laboratory measured fines content and the apparent fines content could not be performed.

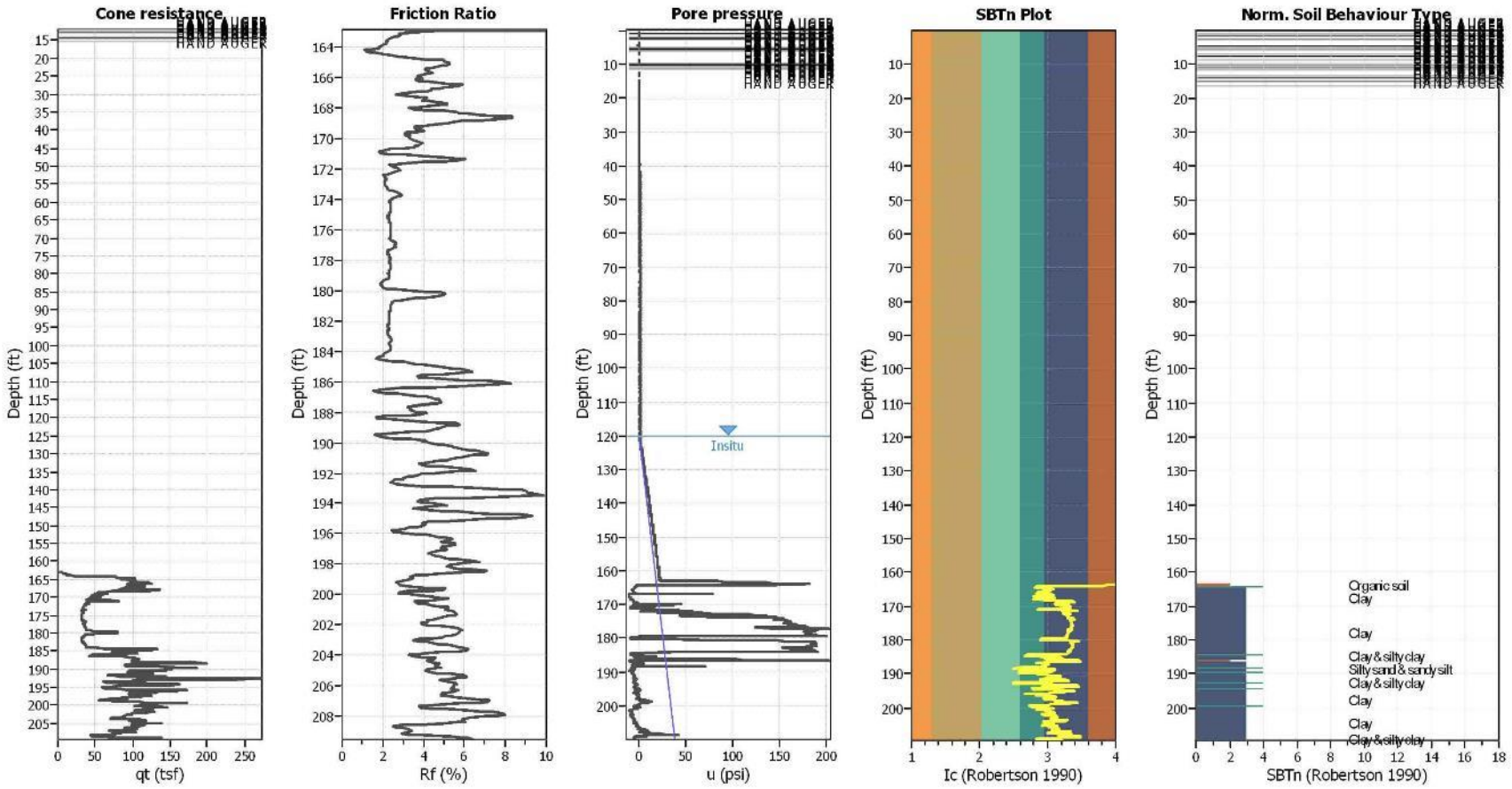

Figure 5.18: Variation of corrected tip resistance, friction ratio, pore pressure, and SBT index values for Abner Fork impoundment location A (crest) obtained from CLiq (Version 1.7).

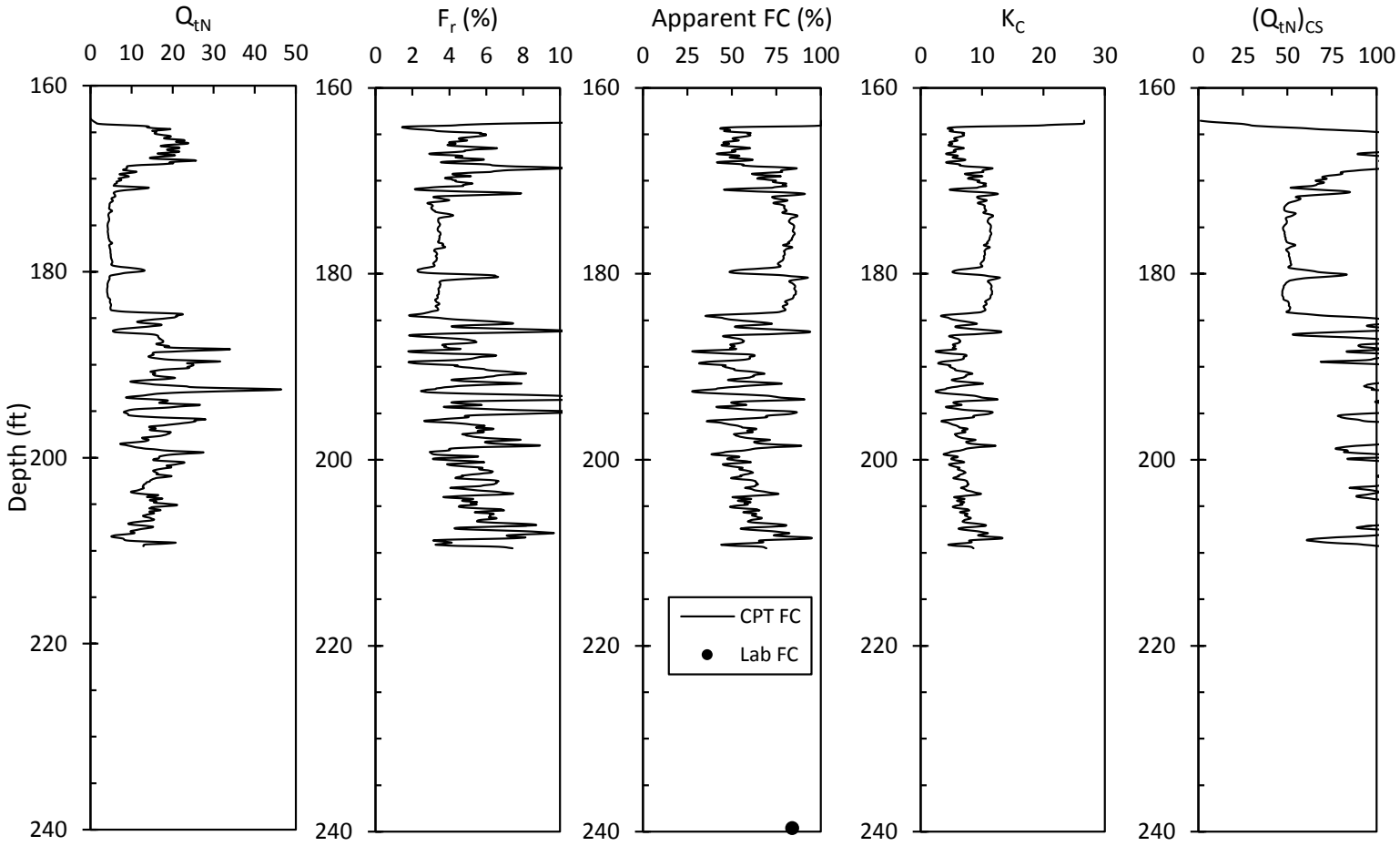

Figure 5.19: Variation of normalized cone tip resistance, normalized sleeve friction, apparent fines content, Kc, and the equivalent clean sand normalized cone tip resistance $(Q_{tN})_{CS}$ with depth for the Abner Fork impoundment at location A (crest).

The variation of cone tip resistance, friction ratio, pore pressure, the SBT index recorded at the toe of the Big Branch impoundment (Location B) is illustrated in Figure 5.20. It appears that between depths of 145 to 170 ft (44.1 to 51.8 m), the cone was pushed through a mixed zone of fine-grained and coarse-grained tailings. The tip resistance values are higher in this range compared to the bottom section of the CPT profile as is expected for coarse-grained soils. In this range of depth, the pore pressure corrected tip resistance generally varies between 5 to 150 tsf (479 to 14,364 kPa) with a temporarily high value of approximately 300 tsf (28,728 kPa). At depths greater than 190 ft (57.9 m), the tip resistance is approximately 25 tsf (2,394 kPa) which is in a similar range observed at Big Branch.

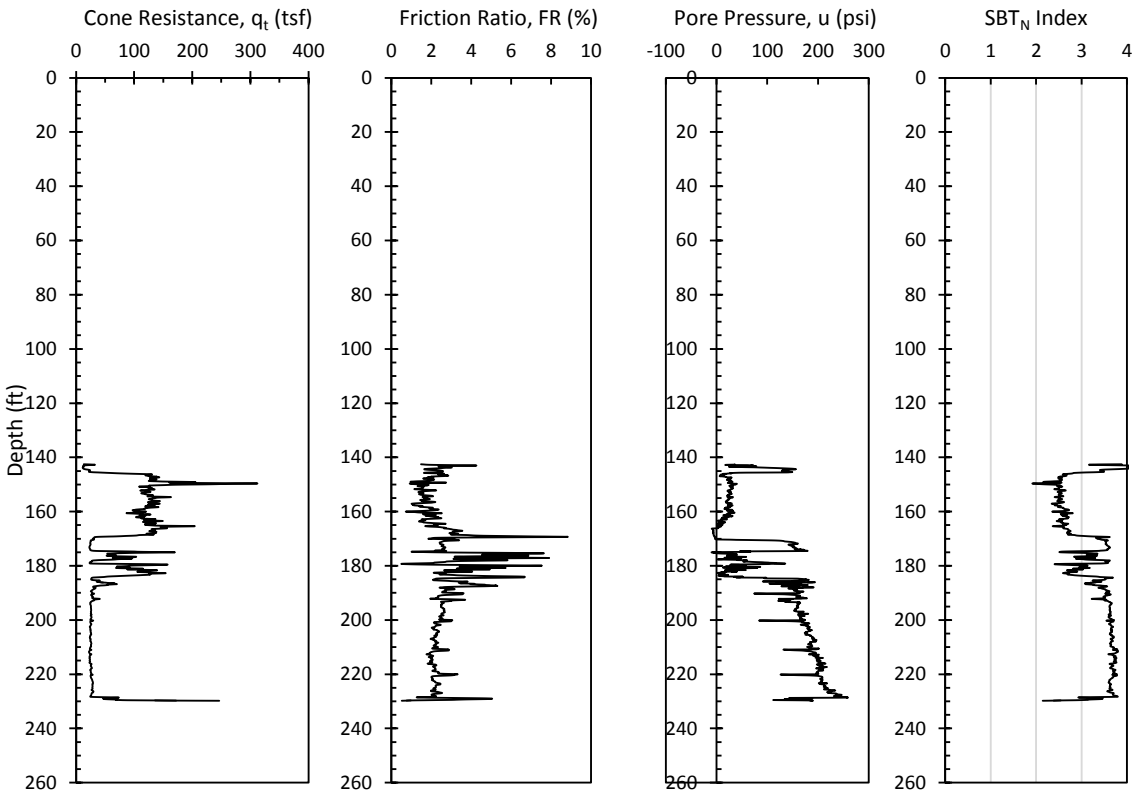

Figure 5.20: CPT sounding results at the Abner Fork impoundment, Location B (toe).

The tip resistance varies between 2.0 to 4.0 with the higher values primarily in depths below 185 ft (56.4 m) which is indicative of clay-type soils. The SBT chart obtained from CLiq (Version 1.7) for this CPT sounding is presented in Figure 5.21.

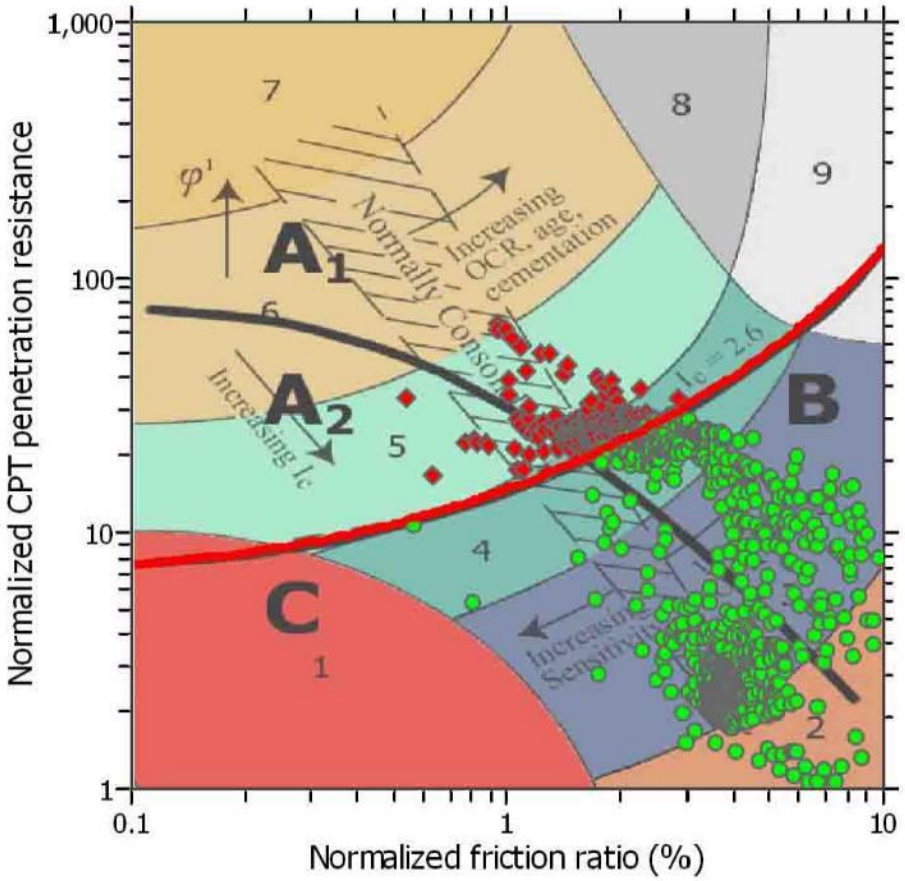

Zone A_1: Cyclic liquefaction likely depending on size and duration of cyclic loading
Zone A_2: Cyclic liquefaction and strength loss likely depending on loading and ground geometry
Zone B: Liquefaction and post-earthquake strength loss unlikely, check cyclic softening
Zone C: Cyclic liquefaction and strength loss possible depending on soil plasticity, brittleness/sensitivity, strain to peak undrained strength and ground geometry

Figure 5.21: Normalized soil behavior type index for the CPT sounding at Abner Fork impoundment, Location B (toe), CLiq (Version 1.7).

It appears that some layers behaved as coarse-grained soils ($I_c < 2.6$) and therefore some red diamonds representing coarse-grained soils are shown in this plot. By comparing the SBT chart presented in Figure 5.21 with the reference chart by Robertson

(1990) shown in Figure 5.7 it appears that the majority of the ground profile behaved as fine grained soils (Silts and clays) with I_c values greater than 2.6. The variation of corrected tip resistance, friction ratio, pore pressure, and SBT index values with depth obtained from CLiq (2012) for Location A (crest) at the Abner Fork impoundment are presented in Figure 5.22. As shown in this figure, at depths above 185 ft (56.4 m), some thin layers of very stiff silt or very dense sandy soils have been encountered which was accompanied with dilation. The measured pore water pressure for these layers fell below the in situ ground water level during cone pushing. The majority of layers encountered below 170 ft are classified as clay and silty clay type soils.

In Figure 5.23, the variation of normalized tip resistance, Q_{tN}, normalized sleeve friction, F_r, apparent fines content, FC, coefficient K_c, and clean sand corrected normalized cone tip resistance $(Q_{tN})_{CS}$ with depth for the samples obtained from Abner Fork at Location B (toe) are presented. It appears that similar to the Big Branch samples, for the samples with approximately 75% fine content, the apparent fines content is estimated as 100%. Although the fines content estimation is not precise, but for the engineering purposes this difference would not create a significant discrepancy in the results.

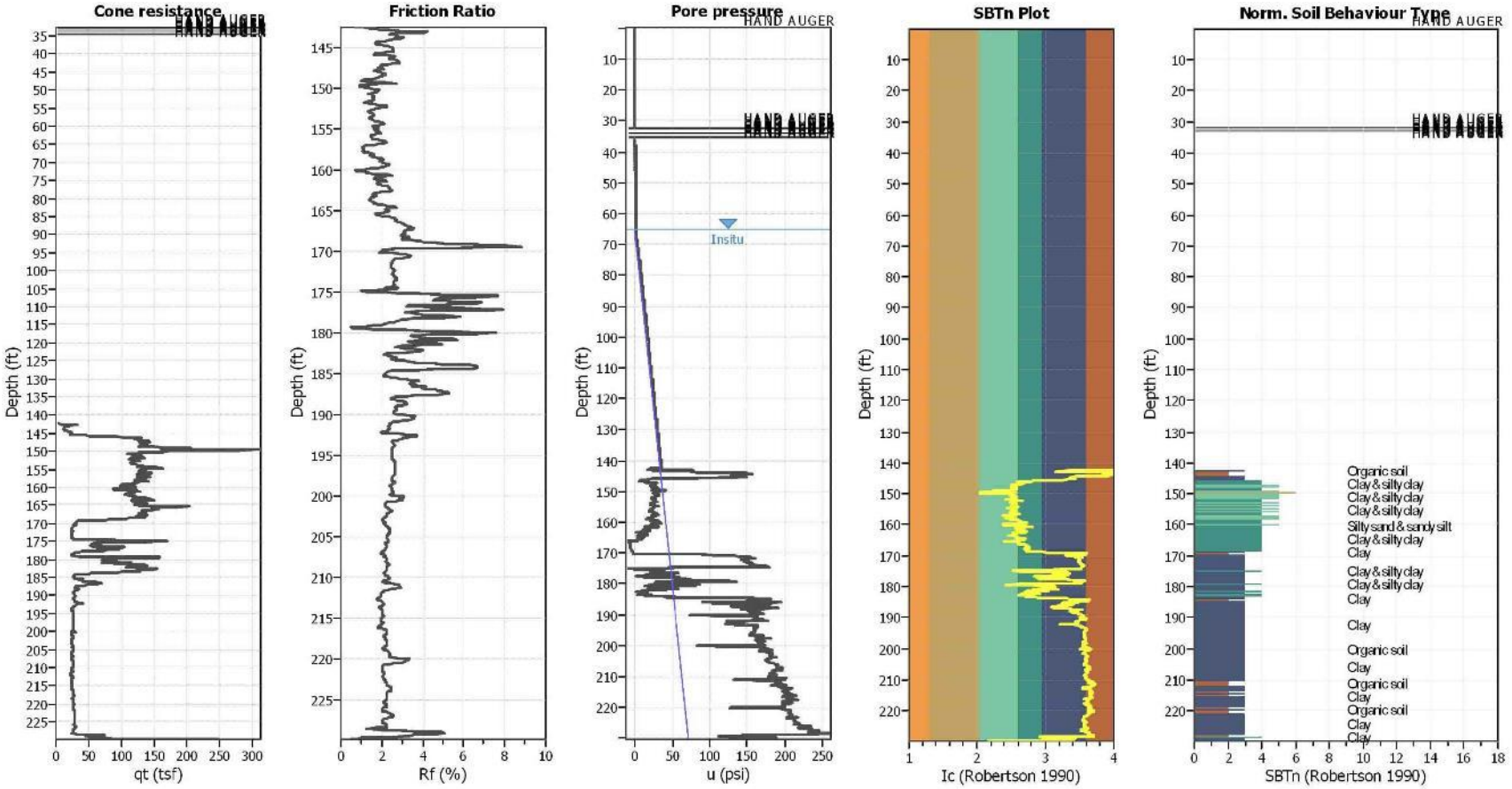

Figure 5.22: Variation of corrected tip resistance, friction ratio, pore pressure, and SBT index values with depth for Abner Fork impoundment location B (toe) obtained from CLiq (Version 1.7).

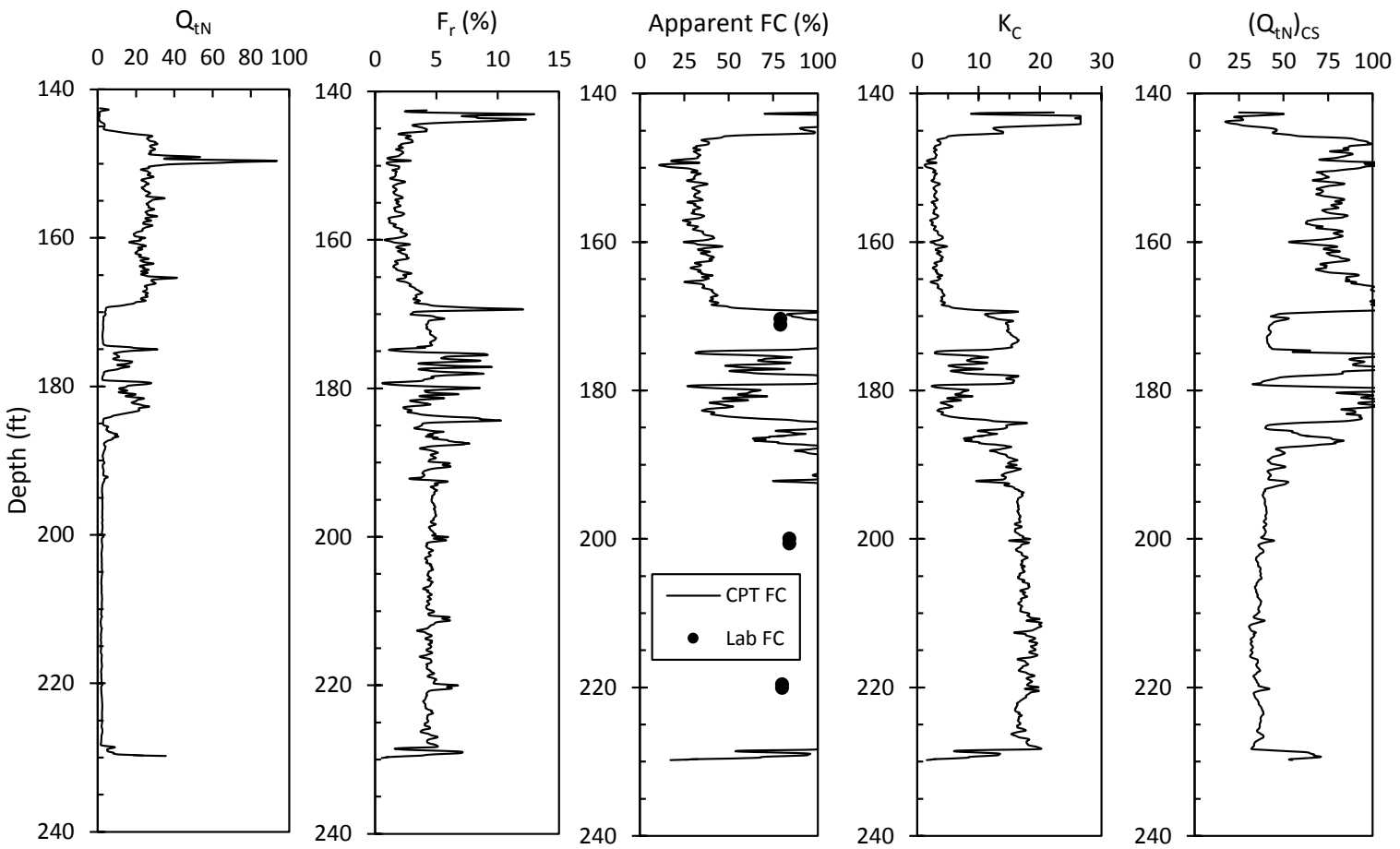

Figure 5.23: Variation of normalized cone tip resistance, normalized sleeve friction, apparent fines content, Kc, and the equivalent clean sand normalized cone tip resistance $(Q_{tN})_{CS}$ with depth for the Abner Fork impoundment at location B (toe).

5.2.3 Standard Penetration Tests Results

Standard Penetration Testing was performed at 20-ft intervals (6-m) at both the Big Branch and Abner Fork impoundments. The results of these tests consisting of the corrected SPT blow counts, $(N_1)_{60}$, are presented in this section. The SPT blow counts were corrected following the recommended method discussed in Section 5.2 and by applying the overburden correction factor C_N, the energy ratio C_E, the borehole diameter factor C_B, the rod length C_R, and the sampler factor C_S. Equation 5.1 was utilized which was discussed in detail in Section 5.2. In Figure 5.24 and Figure 5.25, the corrected SPT blow counts at the locations D (crest) and A (toe) at Big Branch are illustrated. The fine grained coal mine tailings are generally soft soils and therefore exhibit low resistance in the Standard Penetration Tests. In fact, in some zones the fine grained tailings did not have any resistance and the SPT tool could sink in solely by its weight and no blow counts were required to drive the tool in. Therefore, in those zones the SPT blow counts are reported to be zero.

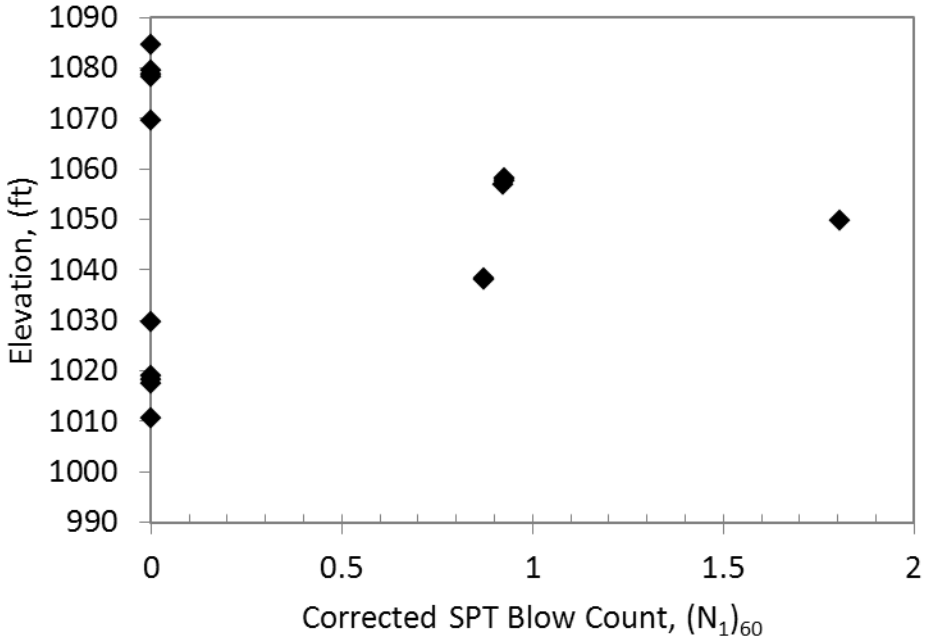

Figure 5.24: Corrected Standard Penetration Test (SPT) blow counts at Big Branch Location D (crest).

The SPT blow counts at Big Branch Location A appear to increase at the bottom of the CPT log as shown in Figure 5.25. In this dataset, the SPT blow count at the bottom of the log is measured on the original bottom of the holler. In this dataset, it appears that the SPT blow counts in the tailings increase with depth. This may be attributed to the effect of the in-situ confining stress. As the depth increases, the thickness and consequently the weight of the tailings layer causing the confining stress are increased as well. Therefore, the material exhibits higher resistance to penetration due to the effect of higher confinement.

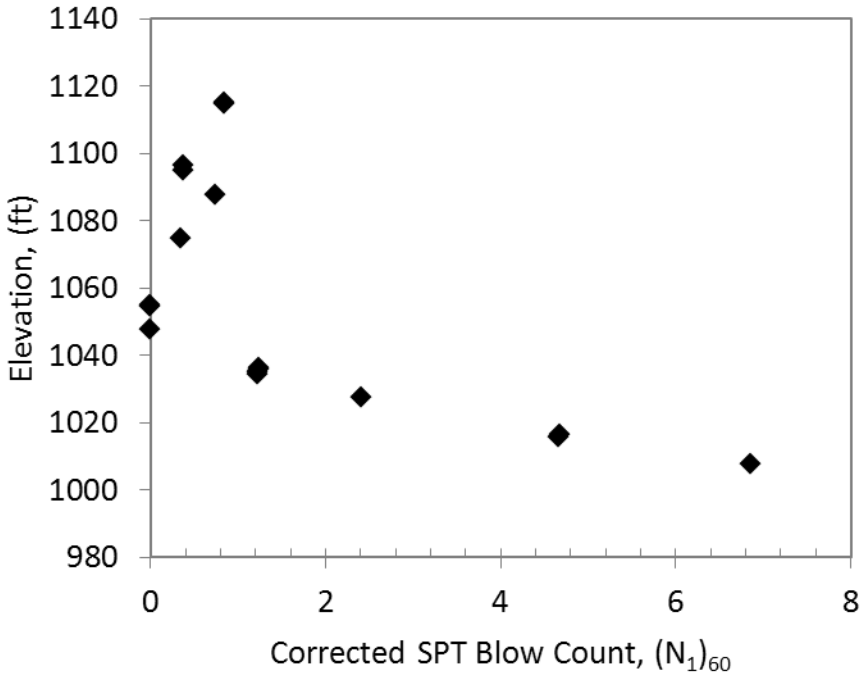

Figure 5.25: Corrected Standard Penetration Test (SPT) blow counts at Big Branch Location A (toe).

The results of SPT tests at the Abner Fork impoundment are presented in Figure 5.26 and Figure 5.27. The SPT blow counts are generally higher compared to the Big Branch SPT blow counts although the data are scattered. The Abner Fork dam is a taller structure which has been operating since the early 1980's while the Big Branch impoundment is a smaller structure and has not been in use for most of the past 20 years. Therefore, due to higher consolidation stresses, differences in age, and the fabric of the material, the SPT blow counts appear to be site specific and are slightly different from one site to the other. It should be noted that the SPT testing was not proceeded to the original ground surface that the impoundment was founded upon. Although an increase in blow count with depth is observed in the results of the SPT values at Abner Fork Location A (crest) as depicted in Figure 5.26, the results are not conclusive due to the lack of data

from the bottom layers. Therefore, unlike the results from the Big Branch location A illustrated in Figure 5.25, the increase in the SPT value with depth is not observed in the Abner Fork data.

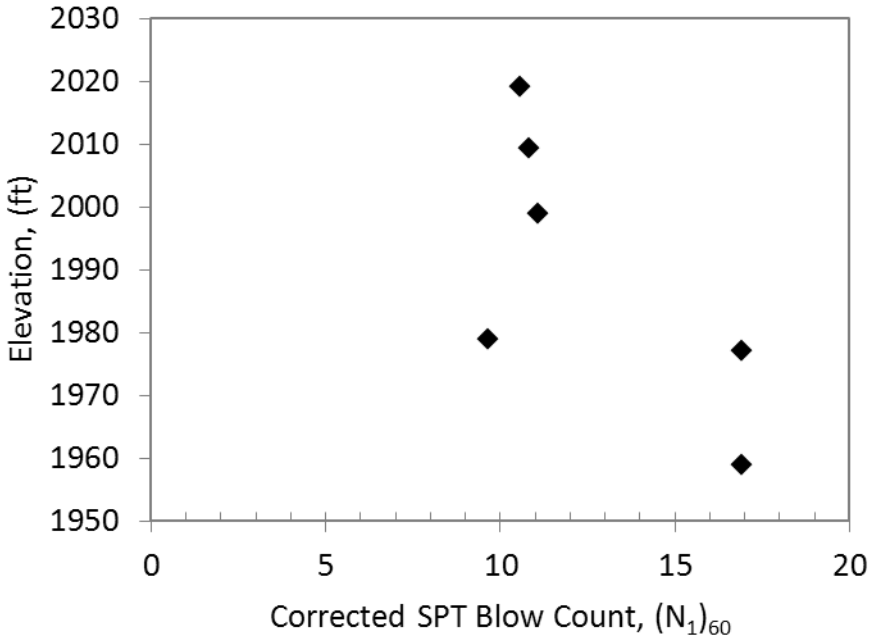

Figure 5.26: Corrected Standard Penetration Test (SPT) blow counts at Abner Fork location A (crest).

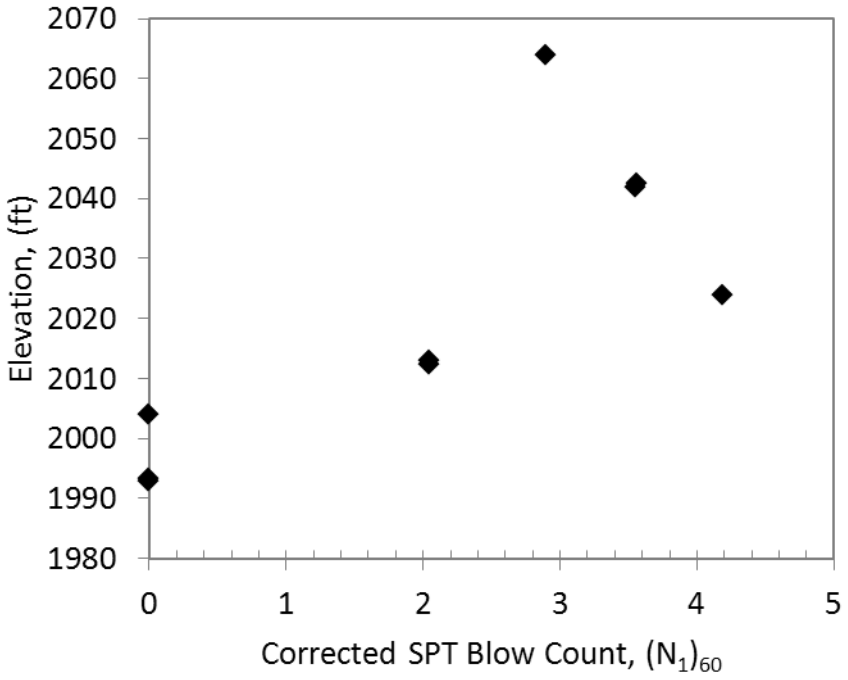

Figure 5.27: Corrected Standard Penetration Test (SPT) blow counts at Abner Fork location B (toe).

5.2.4 Field Vane Shear Tests

While performing the vane shear test, typically two strength values are recorded which include the peak field vane shear resistance, S_{pf}, and the residual field vane shear resistance, S_{rf}. The peak value is the maximum value that the torque gauge obtains during turning the vane. After that point the test is continued by turning the vane until the gauge reaches a constant value regardless of the increasing strain imparted by turning the vanes. This value is referred to the remolded or the residual vane shear strength of the material and is denoted by S_{rf}. In Figure 5.28, variation of vane shear resistance with depth at the Big Branch impoundment is presented. The empty diamonds represent the peak shear resistance and the filled diamonds represent the remolded shear resistance.

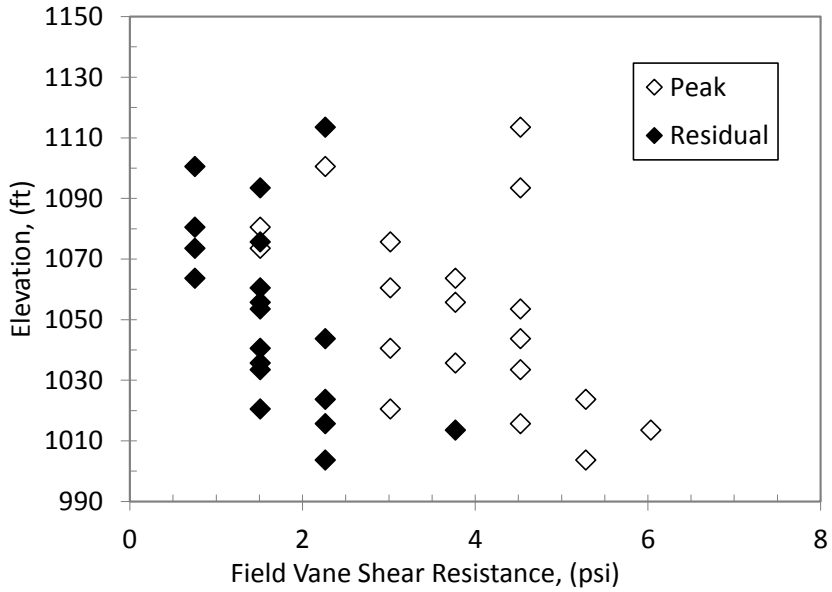

Figure 5.28: Variation of field vane shear resistance with depth at the Big Branch impoundment.

It appears that both of peak and residual shear resistance values increase with depth. This could be due to the increase in the confining stress and higher consolidation stresses resulting in higher shear resistances at deeper depths. In Figure 5.29, variation of vane shear resistance with depth at the Abner Fork impoundment is presented. The empty diamonds represent the peak shear resistance and the filled diamonds represent the remolded shear resistance. The shear strength values at Abner Fork increase with depth similar to the Big Branch values. However, it is noted that the Abner Fork samples exhibit higher shear resistance compared to the Big Branch samples. The peak strength values range from 34 psi to 68 psi (234.4 to 468.8 kPa) for the Abner Fork samples and from 1.5 psi to 6.0 psi (10.3 to 41.4 kPa) at Big Branch. Also, the range for the residual strength values range from 12 psi to 44 psi (82.7 to 303.4 kPa) for Abner Fork and from 0.75 psi to 4.0 psi (5.2 to 27.6 kPa) for Big Branch.

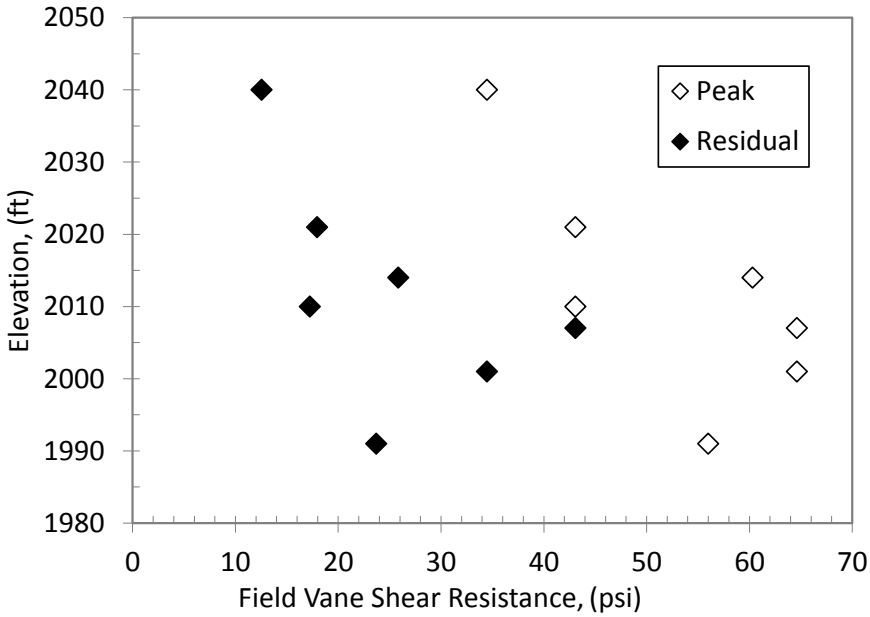

Figure 5.29: Variation of field vane shear resistance with depth at the Abner Fork impoundment.

5.2.5 Shear Wave Velocity Measurements

The shear wave velocities of coal mine tailings were recorded by three different methods which include sCPTu (seismic CPT), SASW, and downhole seismic method. These tests were only performed at the Abner Fork impoundment. None of these methods could provide the shear wave velocity at the Big Branch impoundment. The procedures to perform these tests were discussed in Chapter 2. The SASW and the sCPTu methods were utilized in the summer of 2006 at the Abner Fork impoundment and the downhole seismic methods was used in the summer of 2007. During the one year time difference between these tests, the height of the Abner Fork impoundment was increased by 17 ft (5.2 m) due to upward expansion of the dike.

Due to the influence of the overburden pressure on the density and void ratio of the soil material, various studies recommend to correct the results of shear wave velocity

measurements for the overburden pressure (Youd et al., 2001; Andrus and Stokoe, 2000; Sykora, 1987; Kayen et al., 1992; Robertson et al. 1992; Hardin and Drnevich, 1972). This correction which is similar to the correction factor (Equation 5.2) utilized in SPT and CPT overburden correction factors, is

$$V_s' = V_s(P_a/\sigma_{v0}')^{0.25}, \quad (5.10)$$

where, V_s' is the overburden-corrected shear wave velocity, V_s is the in-situ measured shear wave velocity, P_a is the atmospheric pressure approximated by 100kPa (1 tsf), and σ_{v0}' is the effective vertical stress in the same units as P_a. The overburden-corrected shear wave velocity measurements at Abner Fork recorded in the summer of 2006 using the SASW and sCPTu methods were presented in Figure 5.4 and Figure 5.5. These results are presented in Figure 5.30 in addition to the downhole seismic results recorded in the summer of 2007.

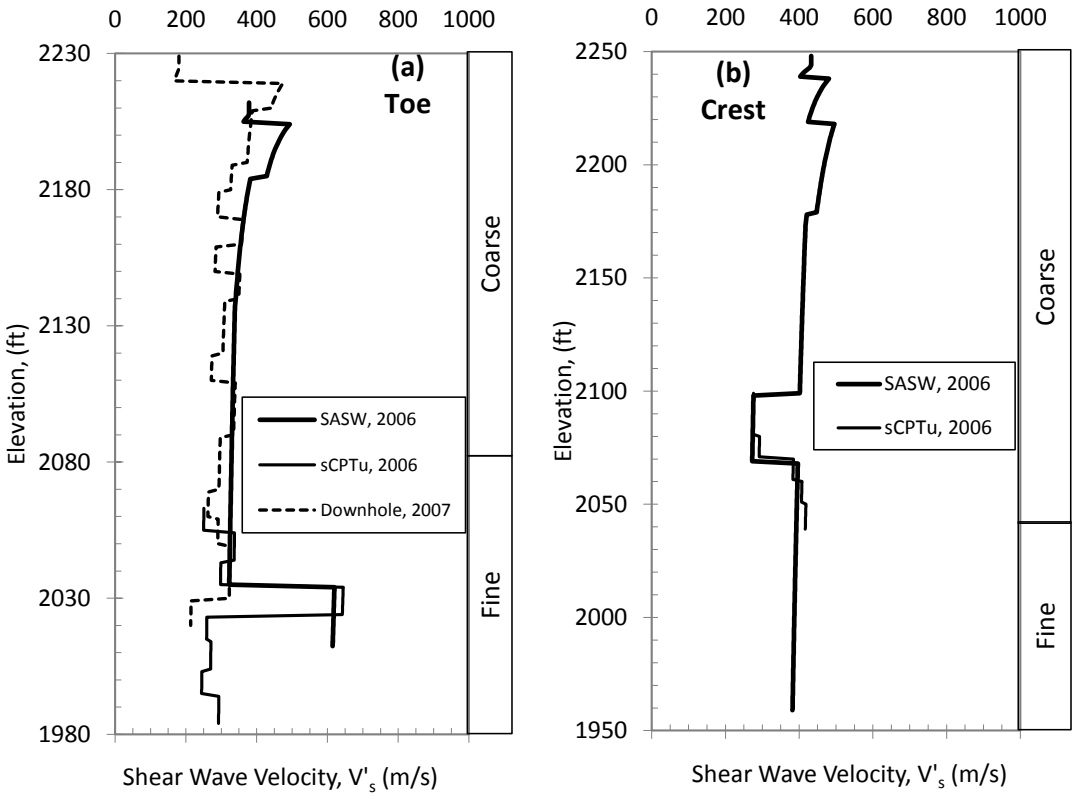

Figure 5.30: Overburden corrected shear wave velocities at the Abner Fork impoundment: (a) Toe Location, (b) Crest Location.

As illustrated in Figure 5.30, the sCPTu method was utilized at depths below 150 ft (45.7 m). Also, it is observed that generally all of the methods predict similar shear wave velocity profiles, although the values measured by the downhole seismic method used in 2007 at the toe location are slightly lower than the other methods. At approximately 200 ft (60.9 m) of depth, the SASW and sCPTu methods measured higher values of shear wave velocities which could be due to mixed zones of coarse and fine coal mine tailings. However, this increase was not captured by the downhole seismic method. Robertson et al. (1986) compared the values of shear wave velocity measured by the sCPTu method with crosshole seismic method measurements at various sites. In their study, a reasonable

agreement was observed between these two methods for fine grained soils encountered at the Imperial Valley, California and Drammen, Norway.

5.2.6 Basic Geotechnical Parameters

As it was discussed in Section 5.2, “undisturbed” fine grained coal mine tailings samples were obtained at 20-ft intervals (6.1-m) , using a piston sampler. These samples were transported to the geotechnical laboratory at the University of Kentucky and were used to perform various geotechnical tests. During each laboratory test, some of the geotechnical properties of samples such as the void ratio, e, moist unit weight,γ_{wet}, liquid limit, LL, and plasticity index, PI, were measured. In this section, variations of such parameters with depth for each of the field testing locations are presented. It should be noted that since these values were determined from the undisturbed piston samples, the number of data points is different than the number of in-situ field testing at each location. For example, at Abner Fork Location A, only one undisturbed sample was successfully used in laboratory testing and therefore, a variation of geotechnical properties with depth could not be presented. In Table 5.5, the laboratory measured geotechnical properties of the undisturbed fine-grained coal mine tailings samples obtained from the Big Branch impoundment at location D (crest) are presented. These values, including void ratio, e, moist unit weight, γ_{wet} , and Atterberg limits, and their variation with depth, are illustrated in Figure 5.31.

Table 5.5: Laboratory measured geotechnical properties of Big Branch samples at Location D (crest).

sample name	Depth ft	Elevation Ft	γ_{wet} pcf	e	LL %	PI %
TBBLDPST1S1	84.3	1079.4	96.9	0.64	39	9
TBBLDPST1S2	84.9	1078.7	102	0.55	39	9
TBBLDPST1S3	85.6	1078.1	97.1	0.58	39	9
TBBLDPST2S2	105.5	1058.2	95.3	0.97	37	10
TBBLDPST2S3	106.1	1057.6	105.5	0.97	37	10
TBBLDPST2S4	106.7	1057.0	107.4	0.89	37	10
TBBLDPST3S2	125.3	1038.4	102.6	0.72	38	11
TBBLDPST3S3	125.7	1038.0	97.9	0.81	38	11
TBBLDPST4S1	144.8	1018.9	87.4	0.72	38	5
TBBLDPST4S2	145.5	1018.2	92.9	0.72	38	5
TBBLDPST4S3	146.2	1017.5	89.9	0.78	38	5

Definitions:
Depth: depth of the location relative to the surface
Elevation: Elevation of the test location relative to the bench mark
γ_{wet}: Moist unit weight
e: Void ratio
LL: Liquid limit
PI: Plasticity Index

As seen in Figure 5.31, void ratio in this location varied from 0.64 to 0.97. Although a sharp variation in the first 30 ft (9.1 m) of depth is noticed, it appears that the rest of the samples had relatively similar void ratios. The density of the material seems to be decreasing with depth which could be attributed to heterogeneity of the material and also disturbance of the sample during various stages of sampling or laboratory testing. The liquid limit and plasticity index seem to be in a medium range. The liquid limit varied from 37 - 41% and the plasticity index ranged from 5-11%.

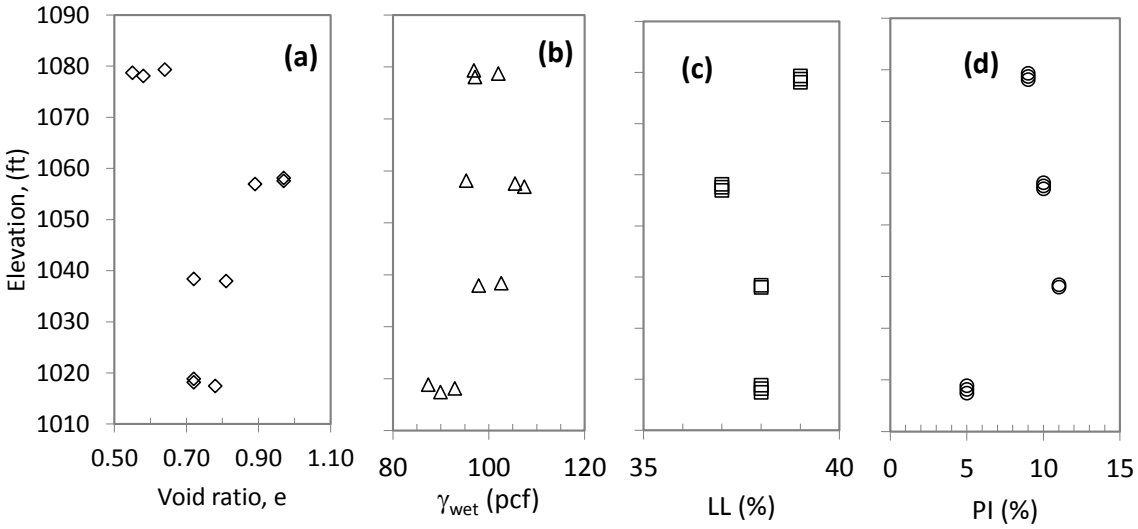

Figure 5.31: Variation of some of the geotechnical parameters at Big Branch Location D (crest) with depth: (a) Void ratio, e, (b) Moist density, γ_{wet}, (c) Liquid Limit, LL, (d) Plasticity Index, PI.

In Table 5.6, the variation of void ratio, e, moist unit weight, γ_{wet}, liquid limit, LL, and plasticity index, PI with depth at Big Branch impoundment Location A (toe) are presented. These values are graphically presented in Figure 5.32. Similar to the crest location at Big Branch, the moist unit weight does not follow a meaningful trend with depth, which may be attributed to heterogeneity of the material. In general, void ratio, liquid limit, and plasticity index increased with depth at this location. The void ratio varied between approximately 0.50-1.23, which is a relatively wide range. It is noticed that in this location, (Location A, toe), the range of the liquid limit and plasticity index values are slightly wider compared to the samples obtained at Location D (crest). The lower limits of liquid limit and plasticity index were lower than the crest location samples and in fact at the top of the surface non-plastic samples (PI = 0%) were obtained. The maximum values of these two indices are slightly higher than the samples obtained at Big Branch crest

samples. However, generally the samples obtained from both locations at Big Branch had low to moderate plasticity.

Table 5.6: Laboratory measured geotechnical properties of Big Branch samples at location A (toe). See Table 5.5 for definitions.

sample name	Depth ft	Elevation ft	γ_{wet} pcf	e	LL %	PI %
TBBLAPST11S3	36.5	1115.0	85.4	0.62	30	0
TBBLAPST11S4	36.9	1114.6	85.9	0.63	30	0
TBBLAPST12S1	55.3	1096.2	91	0.62	33	8
TBBLAPST12S2	56.5	1095.0	94.2	0.55	33	8
TBBLAPST13S4	76.7	1074.8	103.3	0.62	36	12
TBBLAPST14S3	96.5	1055.0	105	0.97	38	14
TBBLAPST14S4	97.0	1054.5	100.4	1.07	38	14
TBBLAPST15S1	115.2	1036.3	100.5	0.56	39	10
TBBLAPST15S2	115.8	1035.7	98.1	0.62	39	10
TBBLAPST15S3	116.4	1035.1	97.5	0.62	39	10
TBBLAPST15S4	117.1	1034.4	94.9	0.61	39	10
TBBLAPST16S1	135.3	1016.3	92.8	0.96	43	7
TBBLAPST16S2	136.0	1015.5	83.6	1.23	43	7

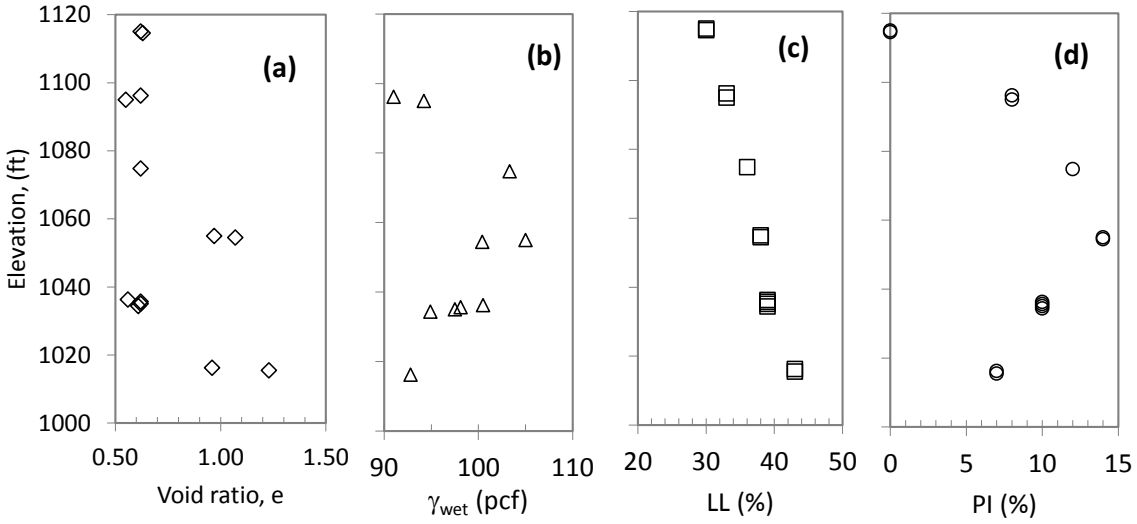

Figure 5.32: Variation of some of the geotechnical parameters at Big Branch Location A (Toe) with depth: (a) Void ratio, e, (b) Moist density, γ_{wet}, (c) Liquid Limit, LL, (d) Plasticity Index, PI.

In Figure 5.33 and Table 5.7, the variation of void ratio, e, moist unit weight, γ_{wet}, liquid limit, LL, and plasticity, PI with depth at the Abner Fork impoundment are presented. It should be noted that the samples reported in this table include the samples from both of the testing locations at the crest and toe. Some of the samples obtained at the crest location at Abner Fork, were heavily disturbed during handling and therefore, only one undisturbed sample was used in the cyclic triaxial testing. Hence, the measured values at this location of the Abner Fork tailings dam are limited to one sample. In Figure 5.33, the variations of these properties at the toe location at Abner Fork are presented. It is noticed that all of the parameters generally have increased with depth. Also it is noted that the range of all of these parameters is much smaller compared to the Big Branch samples. The void ratio varied from 0.51-0.64, which indicates that all through the fine refuse layer, the coal mine tailings material is consistently denser. Also, the relatively high values of moist unit weight varied from 96-100 pcf (15.0-15.7 kN/m^3), which illustrates the small difference in the density of the samples at Abner Fork Location B (toe).

Table 5.7: Laboratory measured geotechnical properties of Abner Fork samples, (locations: Toe and crest). See Table 5.5 for definitions.

sample name	Depth ft	Elevation ft	γ_{wet} pcf	e	LL %	PI %
TAFLBPST1S1	170.4	2042.6	96.4	0.53	39	10
TAFLBPST1S2	171.2	2041.8	96.6	0.52	39	10
TAFLBPST2S1	200	2013	99.7	0.51	43	16
TAFLBPST2S2	200.6	2012.4	99.6	0.51	43	16
TAFLBPST3S1	219.6	1993.4	100.4	0.61	42	16
TAFLBPST3S2	220.1	1992.9	98.3	0.64	42	16
TAFLAPST1S1	239.6	2009.4	97.8	0.52	38	14

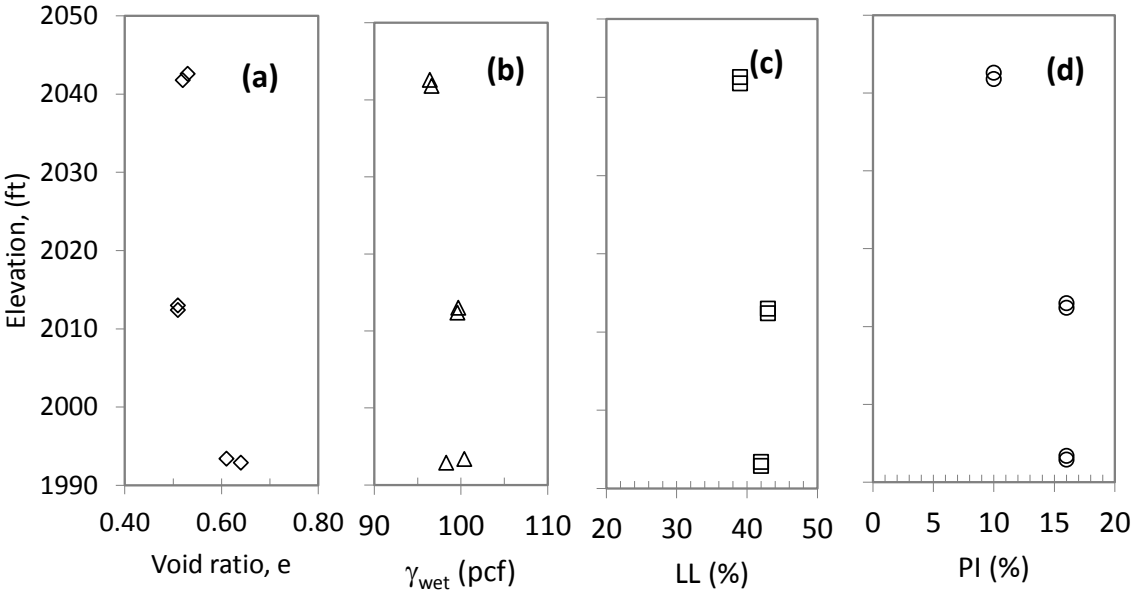

Figure 5.33: Variation of some of the geotechnical parameters at Abner Fork Location B (toe) with depth: (a) Void ratio, e, (b) Moist density, γ_{wet}, (c) Liquid Limit, LL, (d) Plasticity Index, PI Abner Fork.

According to Figure 5.33, the liquid limit values varied only from 39-43% and the plasticity indices ranged from 10-16%, which indicates the medium- to high-plasticity behavior of these samples obtained at Location B (toe) from the Abner Fork impoundment.

In Figure 5.34 to Figure 5.36, the values of corrected Standard Penetration Test, $(N_1)_{60}$, and corrected Cone Penetration Test, q_c', corresponding to the locations of undisturbed samples are illustrated. It should be noted that the SPT tests and vane shear tests were performed at the same borehole that the piston sampling was performed. Therefore, the depths at which the SPT tests or field vane shear tests were performed were chosen to be different than the sample depths to avoid sample disturbance. As a result, the values from these tests do not necessarily represent the properties of the piston samples. To correlate the results of SPT and vane shear tests to the piston sample

locations, the average value between the tests performed at a higher and lower depth relative to the sample location was obtained and assigned to the location of the piston samples.

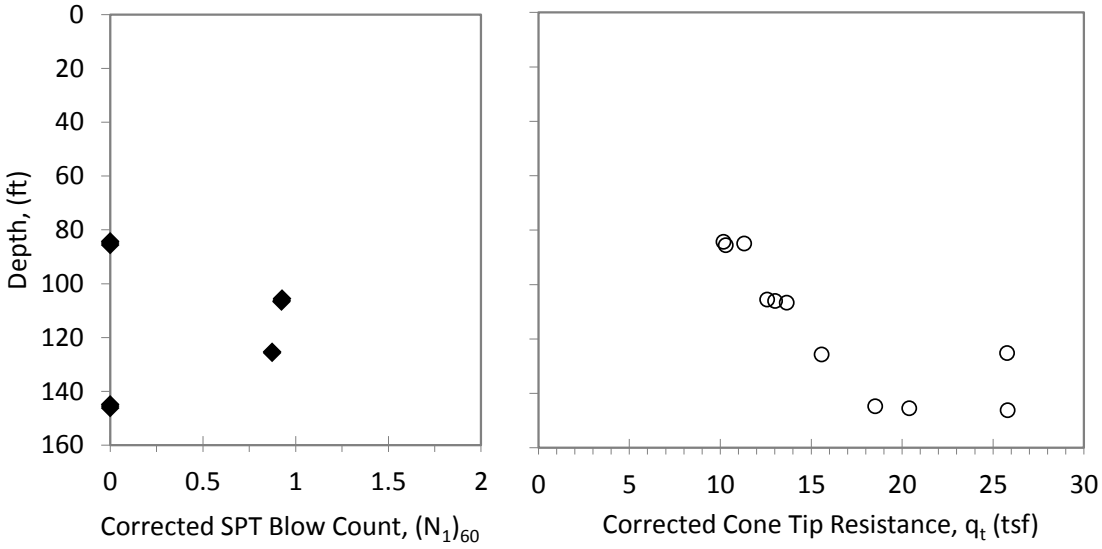

Figure 5.34: Corrected SPT blow counts and pore water pressure corrected CPT tip resistance values at the depths corresponding to "undisturbed" samples locations recorded at the Big Branch impoundment Location D (crest).

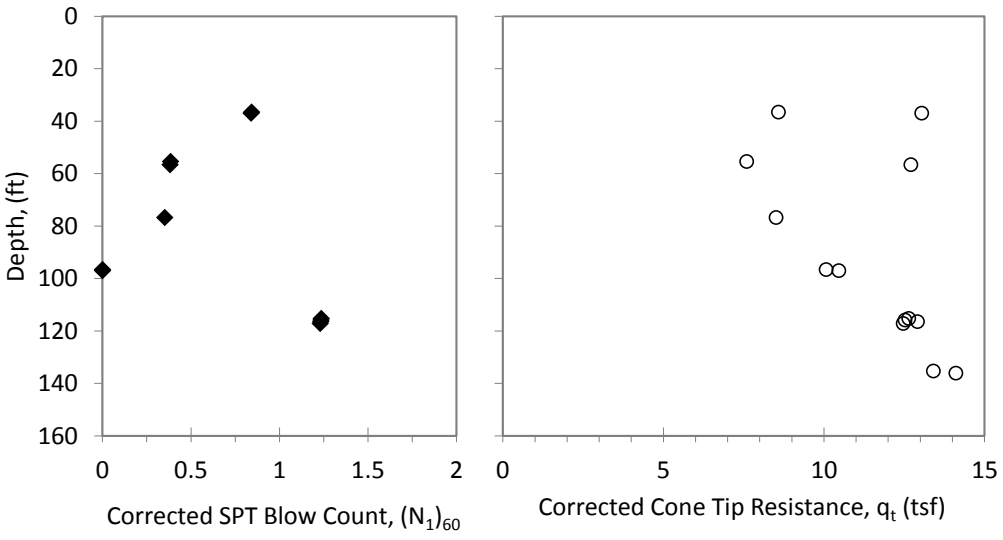

Figure 5.35: Corrected SPT blow counts and pore water pressure corrected CPT tip resistance values at the depths corresponding to "undisturbed" samples locations at the Big Branch impoundment Location A (toe).

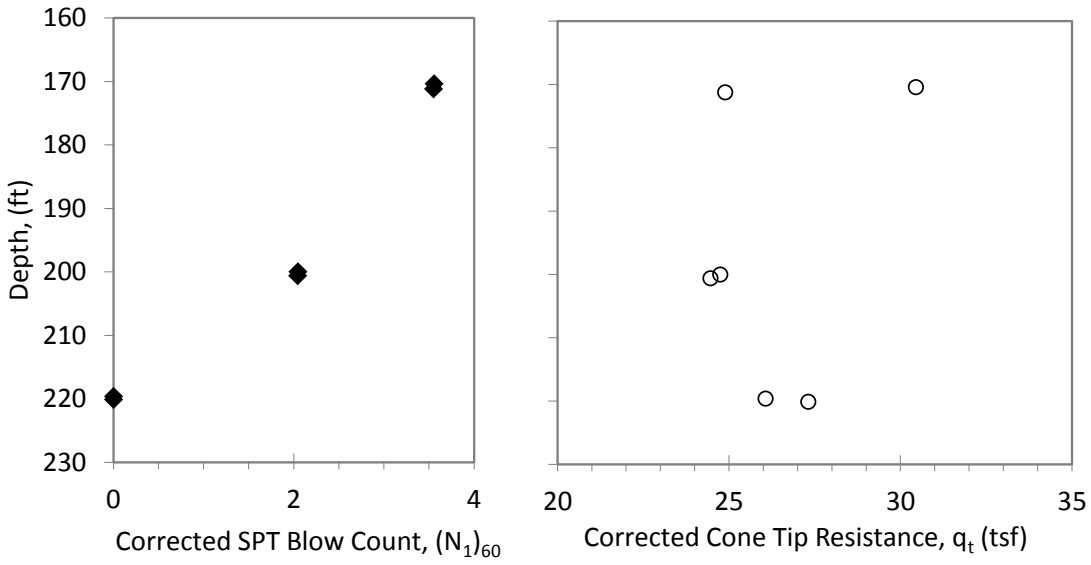

Figure 5.36: Corrected SPT blow counts and pore water pressure corrected CPT tip resistance values at the corresponding depths to "undisturbed" samples locations recorded at the Abner Fork impoundment Location B (toe).

5.3 Correlation of Results

In this section, the results of various geotechnical tests performed in the field or at the laboratory are correlated. In Section 5.3.1, only the correlations between the in-situ geotechnical parameters are presented, while in Section 5.3.2, the relationship between the in-situ parameters and the laboratory values are discussed. The summary of the entire in-situ and laboratory measured geotechnical properties of coal mine tailings obtained from Big Branch and Abner Fork impoundments is presented in Table 5.8.

5.3.1 Correlation of In-Situ Parameters

In this section the correlations between some of the selected in-situ strength parameters of the coal mine tailings material are presented. The utilized methods to record these parameters in the laboratory or in the field or calculate them based on the

other geotechnical parameters of the coal mine tailings samples are discussed in Chapters 2 to 5.

Table 5.8: Summary of the entire in-situ and laboratory geotechnical properties of coal mine tailings specimens.

sample name	depth (ft)	LL %	PI %	e	CSR	N_{ru}	τ_p psi	τ_r psi	$(N_1)_{60}$ (blows/ft)	$(N_1)_{60CS}$ (blows/ft)	q_t (psf)	Q_{tN}	Q_{tNCS}	f_s psf	S_{pf} (psf)	S_{rf} (psf)
TBBLAPST11S3	36.5	30	0	0.62	0.15	92	5.2		1	6	8.6	6.0	56.4	420	652	326
TBBLDPST4S1	144.8	38	5	0.72	0.29	12	13.6		0	5	18.5	2.3	38.9	920	652	326
TBBLDPST4S2	145.5	38	5	0.72	0.21	155	5.4		0	5	20.4	2.8	36.5	640	652	326
TBBLDPST4S3	146.2	38	5	0.78	0.25	47	6.7		0	5	25.8	3.8	47.3	1260	652	326
TBBLAPST16S1	135.3	43	7	0.96	0.43	2	10.3		5	11	13.4	1.3	27.7	460	869	543
TBBLAPST16S2	136.0	43	7	1.23	0.34	3	7.0		5	11	14.1	1.5	29.7	520	869	543
TBBLAPST12S1	55.3	33	8	0.62	0.20	79	7.7		0	5	7.6	2.6	46.8	600	652	217
TBBLDPST1S2	84.9	39	9	0.55	0.26	70	8.1		0	5	11.3	2.6	37.8	460	434	217
TBBLDPST1S3	85.6	39	9	0.58	0.32	6	7.9	2.9	0	5	10.3	2.0	33.5	360	434	217
TBBLDPST2S2	105.5	37	10	0.97	0.36	4	5.5		1	6	12.6	2.0	34.8	520	543	217
TBBLDPST2S3	106.1	37	10	0.97	0.27	20	12.0		1	6	13.0	2.2	43.3	1080	543	217
TBBLDPST2S4	106.7	37	10	0.89	0.20	140	20.9		1	6	13.6	2.9	47.1	1080	543	217
TBBLAPST15S1	115.2	39	10	0.56	0.24	55	4.5		1	6	12.6	1.7	31.4	460	652	217
TBBLAPST15S2	115.8	39	10	0.62	0.34	6	21.0		1	6	12.5	1.6	31.3	500	652	217
TBBLAPST15S3	116.4	39	10	0.62	0.28	24	14.2		1	6	12.9	1.7	31.7	480	652	217
TAFLBPST1S2	171.2	39	10	0.52	0.41	7	45.6	14.1	4	9	24.9	2.9	42.7	1240	4963	1809
TBBLDPST3S2	125.4	38	11	0.72	0.17	109	39.6		1	6	16.9	2.6	44.2	1200	597	272
TBBLAPST13S4	76.7	36	12	0.62	0.28	11	4.1		0	5	8.5	1.7	37.0	580	217	109
TBBLAPST14S3	96.5	38	14	0.97	0.29	11	8.6	2.1	0	5	10.1	1.5	33.7	580	652	217
TBBLAPST14S4	97.0	38	14	1.07	0.26	20	7.8		0	5	10.5	1.6	32.6	480	652	217
TAFLAPST1S1	239.6	38	14	0.52	0.37	21			10	0					9306	6204
TAFLBPST3S1	219.6	42	16	0.61	0.36	124	48.5		0	5	26.1	2.0	35.9	1240	8065	3412
TAFLBPST3S2	220.1	42	16	0.64	0.40	37	51.0	15.9	0	5	27.3	2.2	40.6	1800	8065	3412
TBBLDPST1S1	84.3	39	9	0.64	0.20		14.6		0	5	10.2	2.0	34.9	400	434	217
TAFLBPST2S1	200	43	16	0.51	0.40		37.6	11.7	2	7	24.8	2.2	38.7	1400	6204	2482
TAFLBPST2S2	200.6	43	16	0.51	0.32		30.6	7.1	2	7	24.5	2.1	37.7	1260	6204	2482

Definitions:

Depth: depth of the location relative to the surface
LL: Liquid Limit
PI: Plasticity Index
e: Void ratio
CSR: Cyclic Stress Ratio
N_{ru}: Number of cycles to obtain peak pore pressure ratio (r_u=1.0)
τ_p: Peak laboratory measured vane shear
τ_r: Residual laboratory measured vane shear
$(N_1)_{60}$: Overburden corrected SPT blow counts (blows/ft)
$(N_1)_{60CS}$: Fines content corrected $(N_1)_{60}$
q_t: pore water pressure corrected CPT Test tip resistance
Q_{tN}: Normalized and pore water pressure corrected CPT Test tip resistance
Q_{tNCS}: Clean sand corrected normalized CPT tip resistance
Fs: CPT Sleeve friction
S_{pf}: Peak field vane shear resistance
S_{rf}: Residual field vane shear resistance

In Figure 5.37, a schematic illustration of the mechanical state of the soil mass zones near a CPT cone is presented. Point E is relatively far from the cone but is still slightly loaded and therefore, in the elastic range. Points D represents the zone that is considerably loaded by the cone and could be considered “at yield”. Point C is significantly loaded and has experienced considerable strains and therefore is at failure. According to Robertson (2012), the mechanical state of Points C and D could represent the peak shear strength of the soil and therefore the pore pressure corrected tip resistance, q_t , should illustrate a correlation with the values of peak shear strength obtained from other field tests such as vane shear tests.

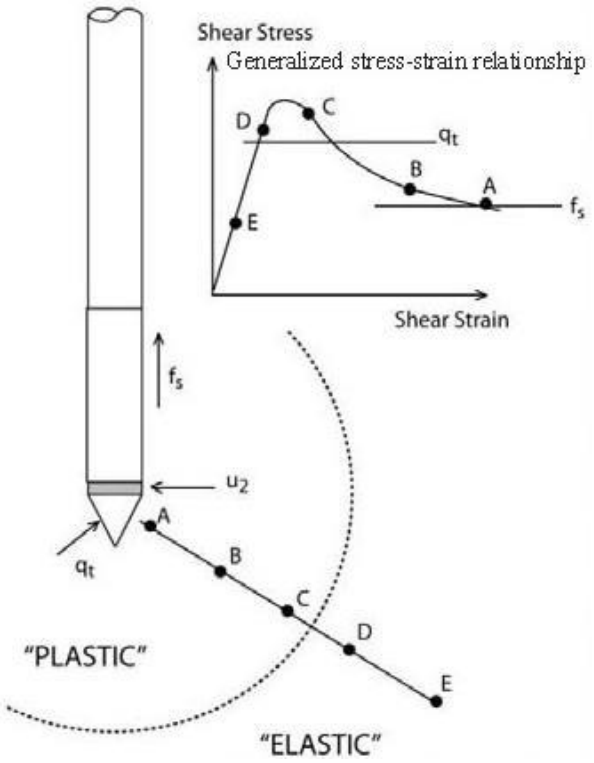

Figure 5.37: Mechanical state of the zones near the tip and the sleeve of a CPT cone, (Robertson, 2012).

Points B and A are fairly close to the cone and have experienced very large strains. Robertson (2012), suggest that the mechanical state of Point A could represent the remolded shear strength of the soil and therefore a correlation could be found between the sleeve friction, f_s, and the remolded shear strength values obtained from field tests such as field vane shear tests. It should be noted that the stress-strain curve illustrated in Figure 5.37 is for the soils that experience softening behavior. If the soil behavior is an elastic-perfectly plastic behavior, the mechanical state of Points D to A would be the same and all of the zones would be at failure. Therefore, either peak or remolded shear strengths obtained from field tests could be correlated to the CPT tip resistance or the sleeve friction.

In Figure 5.38, the correlations between the peak field vane shear resistance, S_{pf}, and the corresponding pore pressure corrected cone tip resistance, q_t, at the same depth are illustrated. The results consist of the two testing locations at Big Branch and the toe location at Abner Fork. The CPT test at the crest location at Abner Fork was not continued to the depth at which the vane shear tests were performed and consequently, at this location no correlation could be made.

According to Boulanger and Idriss (2004), soils with Plasticity Index (PI) smaller than 7% are the transitional soils that could exhibit sand-like mechanical behavior. The vane shear is a method to measure the undrained shear strength and if the material exhibits sand-like behavior, drainage during shearing is expected. At the depths which field vane shear tests were performed, Plasticity index testing was not performed.

Therefore, the PI was estimated based on the PI of the samples at higher or lower depths. It should be noted that as was discussed in previous chapters, the mine tailings impoundments are comprised of many thin layers and are heterogeneous. Therefore, the PI of one layer could not necessarily be assigned to a nearby layer.

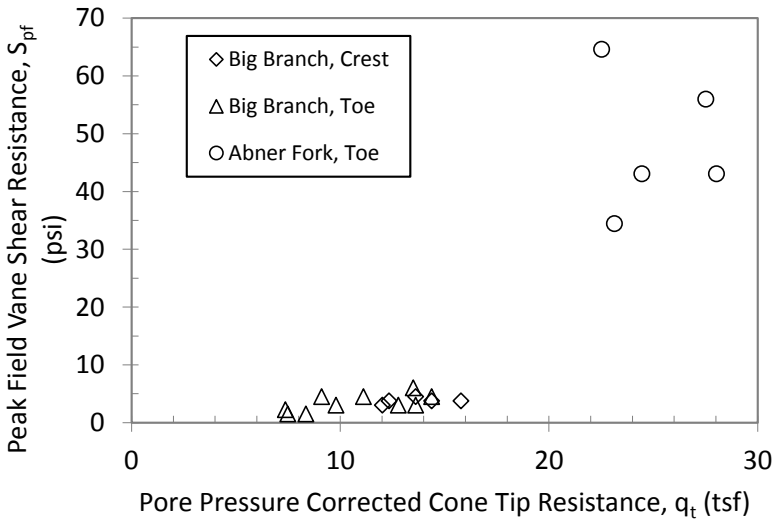

Figure 5.38: Correlations between the peak field vane shear resistance, S_{pf}, and the corrected cone tip resistance, q_t, at Big Branch and Abner Fork impoundments.

The correlations illustrated in Figure 5.38 appear to be divided into two groups. The data points from Abner Fork seems to follow a different trend compared to Big Branch data points and the results could be site specific. The difference in the range of normalized SBT index values between the two impoundments that was discussed in Section 5.2.1 agrees with this assumption. However, if all of data points are considered together and the gap in between them is ignored, it appears that the data points with higher corrected tip resistance q_t had higher peak field vane shear strength. It is assumed that if the datasets are separated based on the impoundment that they are obtained from, a trend

could be identified. Therefore, the results are separated based on the impoundment and presented in Figure 5.39.

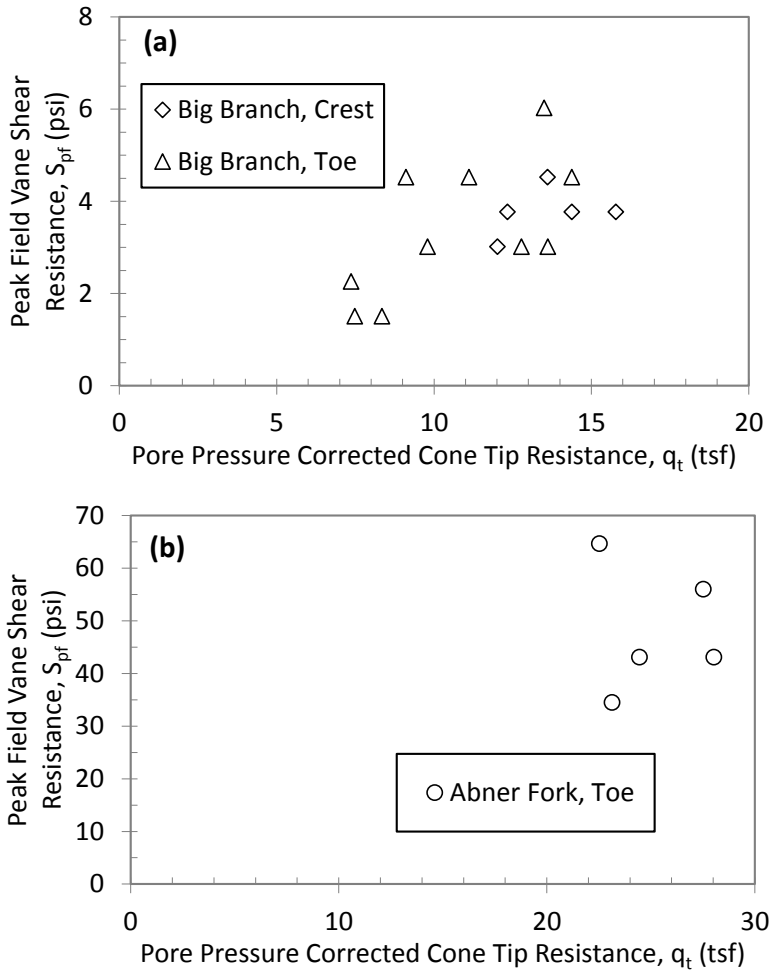

Figure 5.39: Correlations between the peak field vane shear resistance, S_{pf}, and the corrected cone tip resistance, q_c', at (a) Big Branch and (b) Abner Fork impoundments.

By inspecting Figure 5.39a, the Big Branch field results appear to follow a trend, although scatter in the data is observed. The results suggest that at the Big Branch impoundment, at lower values of CPT tip resistance, the peak field vane shear resistance was low as well. By a twofold increase in the CPT tip resistance value from 7.0 tsf to 14 tsf

(670.3 to 1340.6 kPa), the peak vane shear resistance increased threefold from 1.5 psi to 4.5 psi (10.3 to 31.0 kPa).

In Figure 5.39b, the correlation between the peak field vane shear resistance, S_{pf}, and the corrected cone tip resistance, q_t, at Abner Fork is illustrated. It is observed that the correlation does not exhibit a clear trend, although this could be attributed to the small number of data points. It is believed that if the CPT tip resistance values were spread over a wider range of values, a trend could be observed and the vane shear resistance of the material could exhibit a correlation with CPT tip resistance. Nonetheless, for the coal mine tailings with the available data no clear conclusion can be made.

In Figure 5.40, the correlations between the residual field vane shear resistance, S_{rf}, and the corrected cone tip resistance, q_t, at both of the tailings dams are illustrated. The results appear to follow the same trend as what was observed in Figure 5.39, although the residual values are smaller than the peak values. The combined dataset of both impoundments illustrated in Figure 5.40a exhibit a pattern of increasing peak field vane shear strength with increasing tip resistance. However, by separating the results based on the site that they were obtained from, this trend was not observed in the individual data sets presented in Figure 5.40b and Figure 5.40c. The residual field vane shear resistance values recorded at Big Branch (Figure 5.40b) appear to have the same value for the majority of data points. It should be noted that the quality of testing and the experience of the operators in the field could influence the results as well. Due to lack of

sufficient data points from a wide range of cone penetration resistance values for the Abner Fork data points, a clear trend cannot be identified as observed in Figure 5.40c.

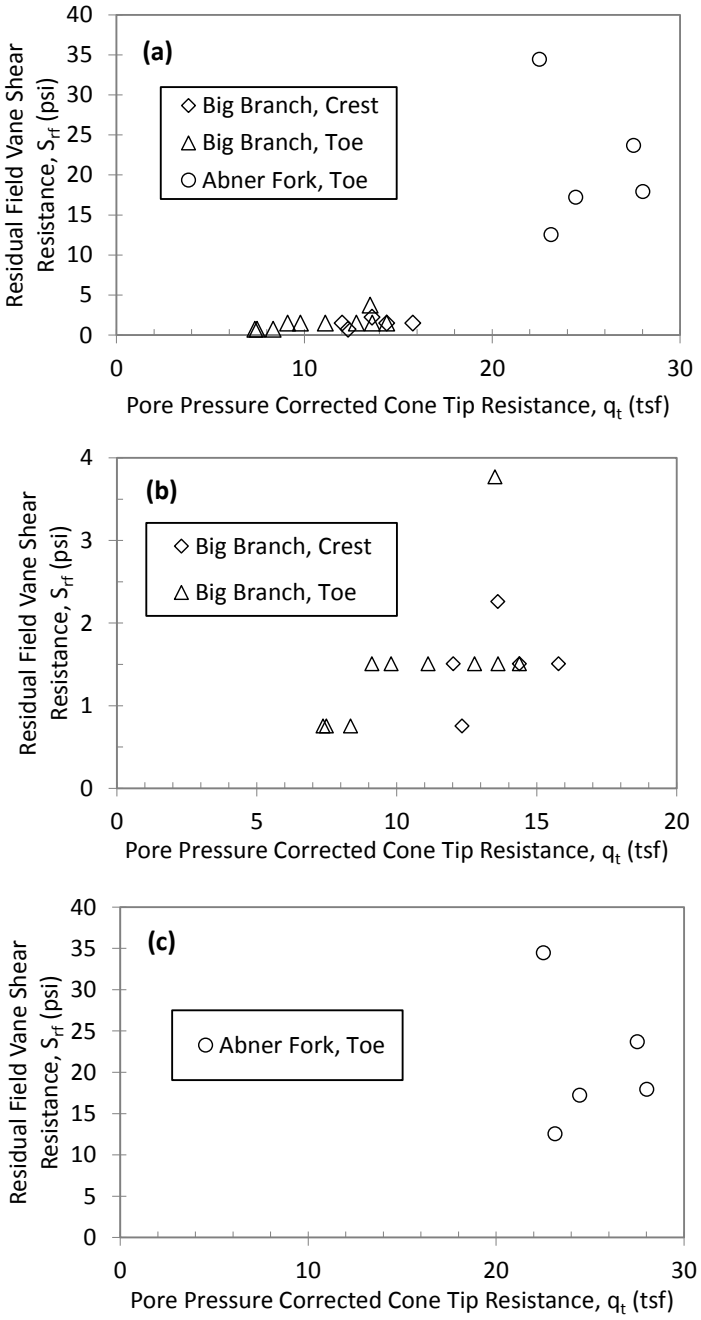

Figure 5.40: Correlations between the residual field vane shear resistance, S_{rf}, and the corrected cone tip resistance, q_t, at (a) both impoundments, (b) Big Branch and (c) Abner Fork.

Robertson (2009) suggested that for normally consolidated soils, the peak undrained shear strength can be estimated by the following equation:

$$\left(S_{pf}/\sigma'_{v0}\right) = Q_{tN}/N_{kt} \tag{5.11}$$

where N_{kt} is a cone factor that varies from about 10 to 20, with an average of 14. The plot of undrained shear strength ratio, $\left(S_{pf}/\sigma'_{v0}\right)$, versus normalized CPT tip resistance, Q_{tN}, was prepared to compare the values of the parameter N_{kt} from a linear best fit to the data set which is illustrated in Figure 5.41.

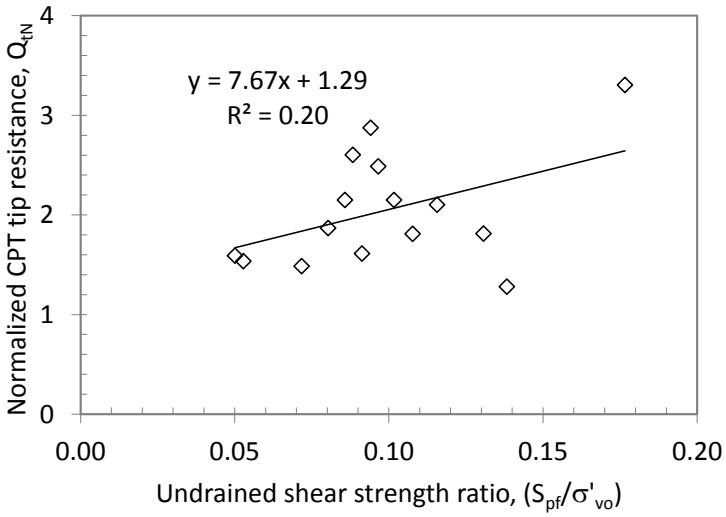

Figure 5.41: Correlation between the normalized CPT tip resistance, Q_{tN}, and the undrained shear strength ratio, $\left(S_{pf}/\sigma'_{v0}\right)$ for coal mine tailings at Big Branch and Abner Fork impoundments.

As can be seen in Figure 5.41 the linear regression to the data set illustrated a poor fit to the data set with a coefficient of determination value, R^2, of 0.19. Lunne et al. (1997) and Senneset et al. (1982) reported that undrained shear strength values obtained by correlations with tip resistance using the N_{kt} parameter are particularly questionable for

soils generating small pore pressures, especially corresponding to $B_q < 0.4$. They also state that such conditions may be representative of materials coarser than clayey silts. B_q is the normalized pore pressure parameter defined by

$$B_q = \Delta u / q_n \tag{5.12}$$

where Δu is the excess pore pressure and q_n is the net cone resistance. For the coal mine tailings samples which their field vane shear resistance were used, the corresponding values of B_q were examined and it appears that of the 20 data points utilized in such correlations, 20% of the data points had B_q values smaller than 0.4, 55% had B_q values smaller than 0.5, and 85% had B_q values smaller than 0.6. Therefore, either due to human errors involved in field testing during field vane shear testing or the drainage properties of low plasticity mine tailings, a clear trend was not observed between the CPT tip resistance and the field vane shear strength.

In Figure 5.42 and Figure 5.43, the correlations between the CPT sleeve friction and the peak and residual field vane shear strength are presented. The observed trend is similar to what was observed for the CPT tip resistance. If both impoundments are considered together, it appears that higher vane shear strength values are observed by increasing sleeve friction values. However, this trend does not cover the whole range of data set and a gap between the data sets from two impoundments is observed. If the data set is divided based on the impoundments that they are obtained from, the correlation for Abner Fork does not show a clear trend.

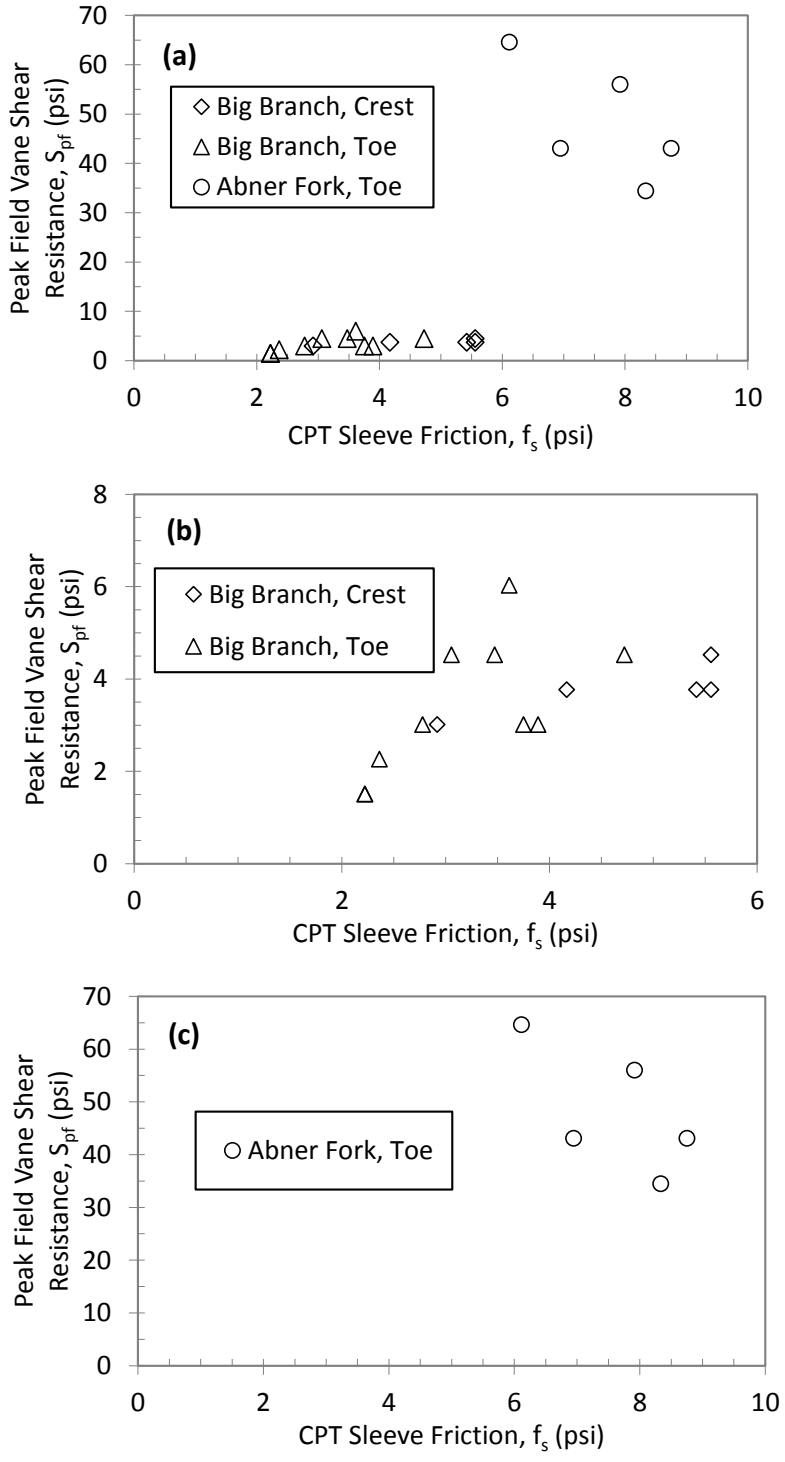

Figure 5.42: Correlations between the peak field vane shear resistance, S_{rf}, and the CPT sleeve friction, f_s, at (a) both impoundments, (b) Big Branch and (c) Abner Fork.

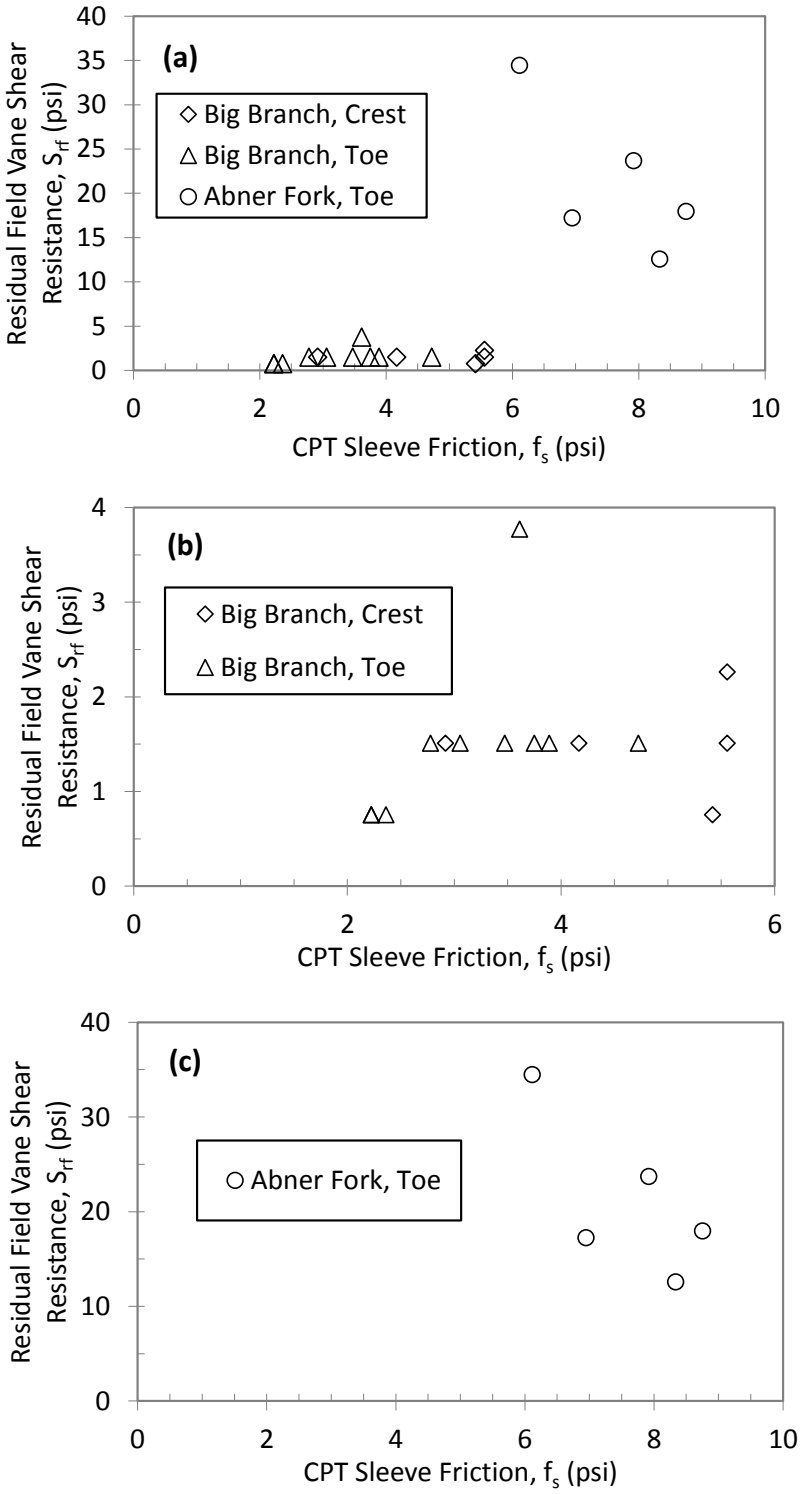

Figure 5.43: Correlations between the residual field vane shear resistance, S_{rf}, and the sleeve friction, f_s, at (a) both impoundments, (b) Big Branch and (c) Abner Fork.

By inspecting Figure 5.42b, the Big Branch field results appear to follow a trend, although scatter in the data is observed. The results suggest that at the Big Branch impoundment, at lower values of CPT sleeve friction, the peak field vane shear resistance was low as well. By a 1.5-fold increase in the CPT sleeve friction value from 2.0 to 3.0 psi (13.8 to 20.7 kPa), the peak vane shear resistance was increased threefold from 1.5 to 4.5 psi (10.3 to 31.0 kPa). The residual field vane shear resistance recorded at Big Branch (Figure 5.43b) appears to have the same value for the majority of data points. As was discussed for Figure 5.40, it should be noted that the quality of testing could have been influenced by the experience of the operators in the field.

Robertson (2009), and Lunne et al. (1997) suggested that for normally consolidated soils, the remolded undrained shear strength of fine grained soils are often similar to the CPT sleeve friction. Based on the studies performed at Scoggins Dam, Farrar et al. (2008) found good agreement between the sleeve friction measurements and the remolded undrained shear strength. Lunne et al. (1997) cautioned that in very sensitive soft clays, the small remolded strength can result in very low sleeve friction values with an inherent loss of accuracy. Based on the assumption that the sleeve friction, f_s, measures the remolded undrained shear strength of the soil (i.e. $f_s = S_{rf}$), the remolded undrained shear strength ratio is given by:

$$S_{rf}/\sigma'_{v0} = f_s/\sigma'_{v0} = F_r Q_{tN}/100. \quad (5.13)$$

By combining this equation and equation 5.11, soil sensitivity can be defined as:

$$S_t = S_{pf}/S_{rf} = 100/(N_{kt}F_r), \quad (5.14)$$

where S_t is the soil sensitivity, S_{pf} is the peak field vane shear strength, S_{rf} is the remolded (residual) field vane shear strength, and N_{kt} is a cone factor that varies from about 10 to 20, with an average of 14. The plot of soil sensitivity for the coal mine tailings, $\left(S_{pf}/S_{rf}\right)$, versus the inverse of normalized CPT sleeve friction, F_r, was prepared to compare the values of the parameter N_{kt} from a linear best fit to the data set which is illustrated in Figure 5.44.

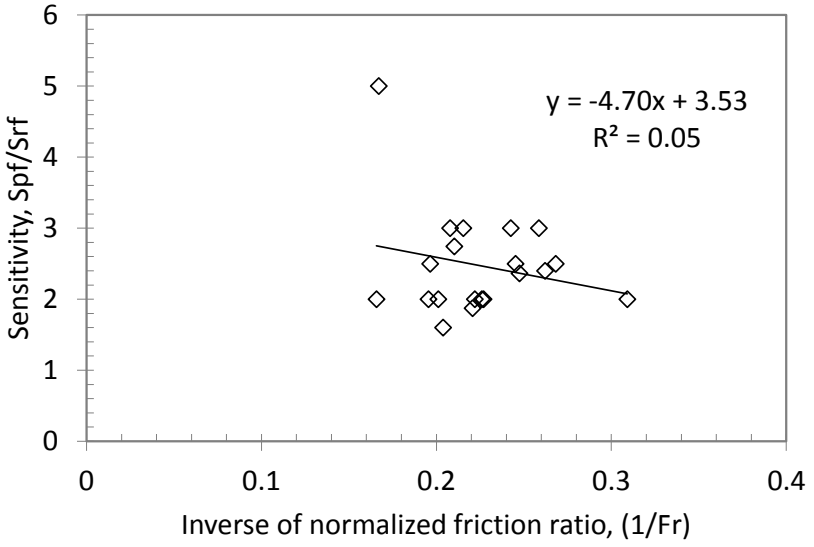

Figure 5.44: Soil sensitivity versus the inverse of normalized friction ratio.

As can be seen in Figure 5.44 the linear regression illustrated a poor fit to the data set with a coefficient of determination value, R^2, of 0.05. As was discussed for Figure 5.41, either the vane shear data were recorded with low precision or the material at corresponding depths are silty soils. If the soil is capable of drainage during vane shear testing, the results have low accuracy.

Both of the corrected Standard Penetration Test (SPT) blow counts $(N_1)_{60}$ and the pore pressure corrected CPT tip resistance q_t are frequently utilized to measure the in situ strength of the soil. In Figure 5.45, the correlation between the corrected Standard Penetration Test (SPT) blow counts $(N_1)_{60}$ and the pore pressure corrected CPT tip resistance q_t is presented. The data points do not show a clear trend and therefore no conclusion can be made. However it should be noted that the observed range for the SPT blow counts in this study is very small compared to the range of SPT values for fine grained soils. Therefore, it is believed that on a wider range of SPT blow counts some correlations could be observed.

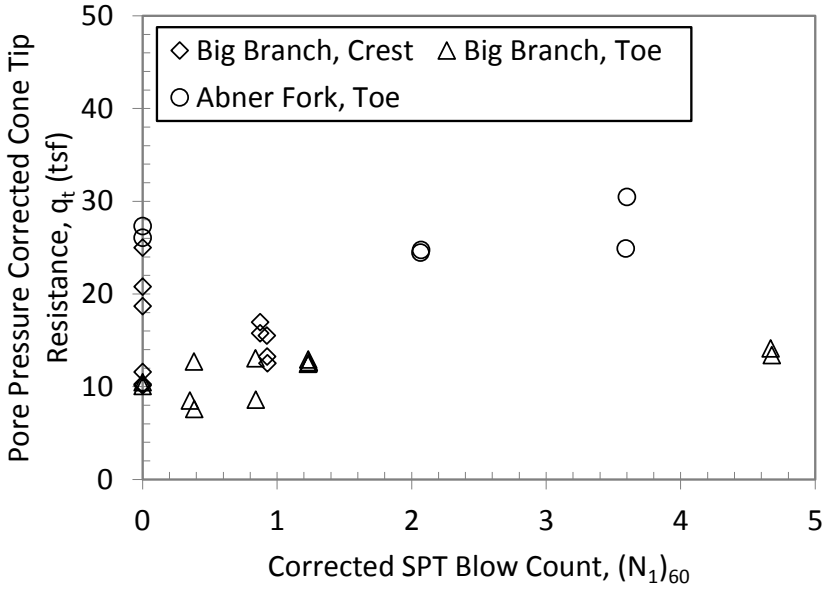

Figure 5.45: Correlation between the pore pressure corrected CPT tip resistance, q_t, and corrected SPT blow count, $(N_1)_{60}$.

In Figure 5.46, the correlation between the corrected Standard Penetration Test (SPT) blow counts $(N_1)_{60}$ and the normalized CPT tip resistance Q_{tN} is presented.

Utilizing the normalized values for the cone tip resistance does not seem to improve the correlation and no clear trend is observed in this plot.

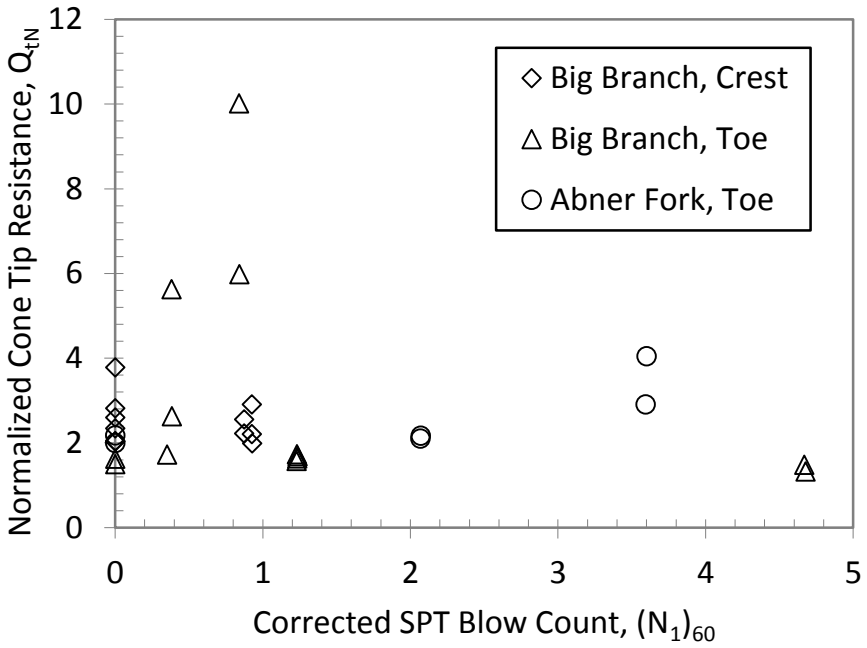

Figure 5.46: Correlation between the normalized CPT tip resistance, Q_{tN}, and corrected SPT blow count, $(N_1)_{60}$.

In Figure 5.47, the correlation between the clean sand corrected Standard Penetration Test (SPT) blow counts $(N_1)_{60CS}$ and the clean sand normalized CPT tip resistance Q_{tNCS} is presented. Generally, it appears that by an increase in the $(N_1)_{60CS}$ values the Q_{tNCS} also decreases, although a large amount of scatter exists. Therefore, based on the limited data points and the short range of the field strength parameters, no conclusion can be made.

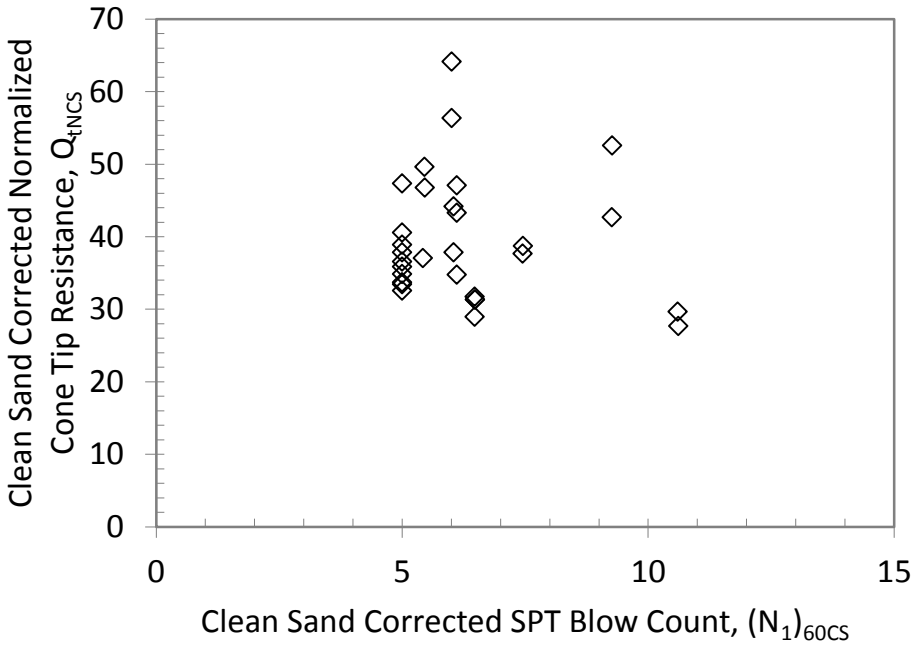

Figure 5.47: Correlation between the clean sand corrected normalized CPT tip resistance, Q_{tNCS}, and clean sand corrected SPT blow count, $(N_1)_{60CS}$.

5.3.2 Correlations between In-Situ and Laboratory Parameters

In this section, the correlations between the in-situ geotechnical parameters and the laboratory measured properties of the coal mine tailings samples are presented. The in-situ parameters include the Standard Penetration Test blow count, $(N_1)_{60}$, pore pressure corrected Cone Penetration Test tip resistance, q_t, and the peak and residual field vane shear strength. The geotechnical parameters measured in the laboratory include the liquid limit, LL, Plasticity Index, PI, Cyclic Stress Ratio (CSR), and the peak and residual laboratory vane shear strength. The main objective of this study was to indicate an in-situ method that will correlate well with the liquefaction susceptibility of the coal mine tailings material. Therefore, in this section, various in-situ geotechnical parameters

are examined to identify any relation between them and the possibility of “liquefaction” or “cyclic mobility” in these samples.

One of the most common geotechnical field tests to investigate the liquefaction susceptibility of soils is the Standard Penetration Test. The relation between the corrected SPT blow counts, $(N_1)_{60}$, and the cyclic stress ratio, CSR, applied during the cyclic triaxial tests to the undisturbed samples is illustrated in Figure 5.48.

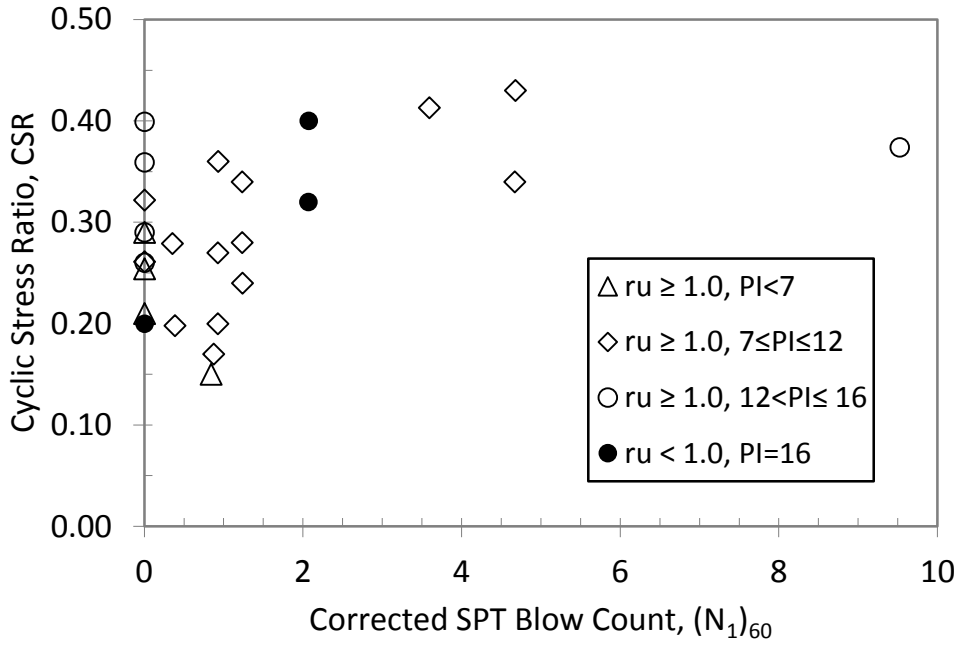

Figure 5.48: Correlation between the Standard Penetration Number, $(N_1)_{60}$, and the Cyclic Stress Ratio, CSR applied to samples from Big Branch and Abner Fork impoundments.

In this figure, the empty data points represent the specimens that achieved the peak pore pressure ratio, $(r_u = 1.0)$, during the cyclic triaxial test and the pore water pressure became equal to the confining pressure. The filled data points indicate the samples that never achieved the peak pore pressure ratio even by applying numerous cycles of deviator stress (Up to 500 cycles), during the cyclic traixial test. In this figure, the

data points are differentiated based on their corresponding plasticity index which through the laboratory results analysis appeared to have the highest influence on the behavior of the coal mine tailings samples. It should be noted that the recorded SPT blow counts for the coal mine tailings material is in a narrow range compared to the observed range in the typical soil samples. In fact all of the corrected SPT values except one are equal or smaller than 5. However, considering the short range of SPT blow counts and the limited number of data points, the data appear to be conclusive. The data suggests that the required deviator stress to achieve the peak pore pressure ratio, $(r_u = 1.0)$, increases with increasing SPT blow counts. Even by excluding the single data point with the highest SPT value, this conclusion still holds valid.

By classifying the data points based on their plasticity index, PI, another conclusion can be drawn. It appears that the samples with the lowest PI values, from 0% to 7% and depicted by empty triangles, required the lowest CSR values to achieve the peak pore water pressure ratio, $(r_u = 1.0)$. Although the scatter of the data is observed, it can be concluded that the higher the PI of the specimen was, a higher CSR was required to induce the peak pore pressure ratio. As it is illustrated in Figure 5.48, the samples with the highest PI values, from 12% to 16% and depicted with empty circles, are located in the higher CSR range. The samples with the medium range of PI, from 7% to 12% and depicted by empty diamonds, are located roughly between the samples with the highest and the lowest Plasticity indices. Also, it is noticed that the few samples that did not achieve the peak pore pressure ratio, depicted by the filled circle, had the highest PI value (PI=16%) but did not have the highest SPT blow counts.

As it was mentioned earlier, due to lack of sufficient undisturbed samples the number of valid data points was small. The limited number of available samples became even smaller due to the high level of disturbance imparted to the samples during preparation. Also, the cyclic triaxial test results obtained from some of the specimens were not valid due to the complexity involved with the operation of equipment in applying the correct uniform cyclic deviator stress. Nonetheless, the correlation between the laboratory cyclic stress ratio, CSR, and the corrected SPT blow counts, $(\mathrm{N}_1)_{60}$, appears to indicate a trend.

The correlation between the CSR and $(\mathrm{N}_1)_{60}$ can be compared to the correlations provided in different studies such as Youd et al. (2001). However, in that study the utilized cyclic stress ratios are based on case studies of liquefaction occurrence in the field. In contrast to laboratory cyclic simple shear and cyclic triaxial tests, earthquakes produce shear stresses in different directions. As mentioned by Kramer (1995) and Pyke et al. (1975), pore pressures are increased more rapidly in multidirectional shaking than unidirectional shaking. Seed et al. (1975) suggested that the CSR required to produce initial liquefaction in the field was about 10% less than that required in unidirectional cyclic simple shear tests. Therefore, the relation between the field CSR and the laboratory CSR applied in a cyclic simple shear test or a cyclic triaxial test is as follows:

$$(CSR)_{field} = 0.9(CSR)_{SS} = 0.9C_{tx}(CSR)_{tx} \quad (5.15)$$

where $(CSR)_{SS}$ is the cyclic stress ratio applied in a cyclic simple shear test, $(CSR)_{tx}$ is the cyclic stress ratio applied in a cyclic triaxial test, and C_{tx}, is the correction factor to

correlate the CSR of these two tests. As discussed in Chapter 3, the cyclic simple shear and cyclic triaxial tests impose quite different loading, and their cyclic stress ratios are not equivalent. Finn et al. (1971), Seed and Peacock (1971), and Castro (1975) suggested different relations for C_{tx} depending on the past stress history of the specimen. These relations are function of the coefficient of earth pressure at rest, K_0 , and mainly based on studies performed on sandy samples. In this study, considering the deposition mechanism of the tailings material and lack of evidence of erosion of the material and the consequent unloading, it is safe to assume that the coal tailings samples were normally consolidated. Based on the plasticity index of silty and clayey soils, Massarsch (1979) suggested an equation for the K_0 value of soils:

$$K_0 = 0.44 + 0.42(PI/100) \tag{5.16}$$

Considering the average values of plasticity index of 9% and 14% for the Big Branch and Abner Fork impoundment samples respectively, it seems that an average value of K_0 equal to 0.5 is appropriate. Using the equations proposed by Finn et al. (1971) and Castro (1975), shown in equations 5.17 and 5.18, the C_{tx} for the coal tailings samples is approximately 0.75.

$$C_{tx} = (1 + K_0)/2 \tag{5.17}$$

$$C_{tx} = 2(1 + 2K_0)/3\sqrt{3} \tag{5.18}$$

The calculated value of C_{tx} equal to 0.75 is used in equation 5.15 and it seems that the laboratory applied CSR values in this study should be multiplied by 0.67 to be

comparable to the field CSR values. The correlation between the equivalent field CSR of coal tailings samples and $(N_1)_{60}$ is compared to the commonly used method from Youd et al. (2001) in Figure 5.49.

Figure 5.49 is plotted on the SPT clean-sand base curve which was provided in a comprehensive and collaborative workshop performed for the National Center for Earthquake Engineering Research (NCEER) by Youd et al. (2001). This plot which was modified at that workshop from Seed et al. (1985) study, is a graph of CSR and the corresponding $(N_1)_{60}$ data from sites where liquefaction effects were or were not observed following past earthquakes with magnitudes of approximately 7.5. The curves shown on this plot are developed for granular soils with the fines content of 5% or less, 15%, and 35%. The CRR curves in this plot are valid only for magnitude 7.5 earthquakes and for other magnitudes, scaling factors are addressed in the same study.

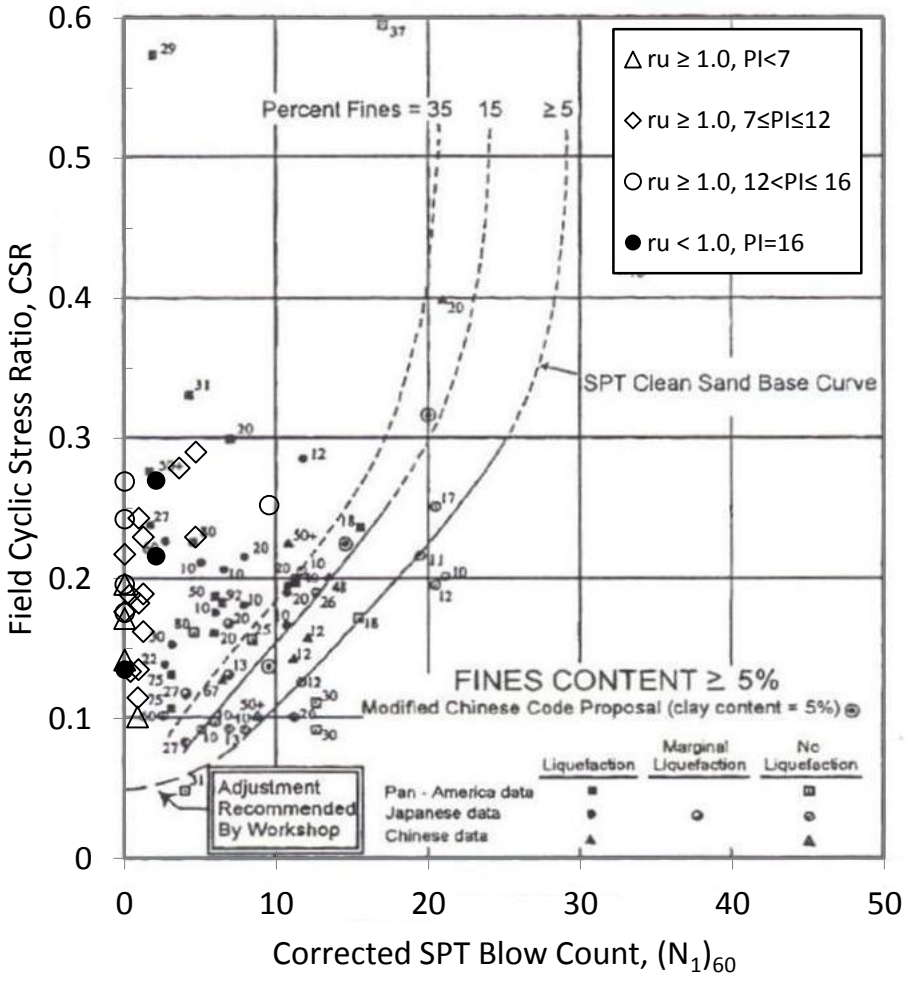

Figure 5.49: Comparison between the correlation of CSR and SPT blow counts in coal mine tailings and soils (after Youd et al., 2001).

As shown in Figure 5.49, the data points for the coal mine tailings are located to the left of the SPT curves which indicates that based on this plot, these samples could be considered liquefiable. Although, it should be considered the CSR values from this study are field equivalent of laboratory measured CSR parameters based on experimental studies and do not necessarily represent a case history liquefaction incident. Also, it should be noted that the fines content of the coal mine tailings are much higher than 35% (greater than 70%) and therefore in the studies performed by Seed et al. (1985) these

samples would have been considered too clayey to liquefy. As was discussed in Chapter 1, case histories indicate that in fact some coal mine tailings impoundments around the world have experienced liquefaction during strong earthquakes. Therefore, if a curve for samples with higher fines content was to be defined, it would have been located further towards the left side of the plot. It is observed that due to the low values of SPT blow counts, the majority of these data points are located far from the SPT curves shown on the plots. This indicates that if an earthquake capable of producing equivalent shear stresses of laboratory applied CSR values, has a duration equivalent to the number of uniform cycles applied in the laboratory (Kramer, 1996; Seed et al., 1975), it is possible that it will induce peak pore pressure ratios $(r_u = 1.0)$ in the coal mine tailings material.

Another widely used geotechnical field method to assess the in-situ strength of the soils is the Cone Penetration test, CPT, and the parameter that is reported is the normalized corrected cone tip resistance, Q_{tN}. At the beginning of the introduction of this method to the geotechnical community in the United States, this method was not as popular as the SPT method. However it has gained more attention and has become a popular method of in-situ strength testing. As was discussed in Section 5.2, the CPT tip resistance could be utilized in the pore pressure corrected form, q_t, in the normalized pore pressure corrected form, Q_{tN}, or in the clean sand normalized pore pressure corrected form, Q_{tNCS}.

In Figure 5.50, the correlation between the laboratory cyclic stress ratio, CSR, and the pore pressure corrected cone penetration tip resistance, q_t, measured in the field is

presented. The empty data points depict the samples that experienced the peak pore pressure ratio during the cyclic triaxial test in the lab and the filled data points are the samples that did not reach that state despite many cycles of applied deviator stress (up to 500 cycles).

The results illustrated in Figure 5.50, suggest that the samples with higher tip resistance required higher CSR values to obtain a pore pressure ratio of 1.0, although scatter is observed. By a 3.6-fold increase in the CPT tip resistance from 7.6 tsf to 27.3 tsf (727.8 kPa to 2614.2 kPa) the CSR doubled from 0.2 to 0.4.

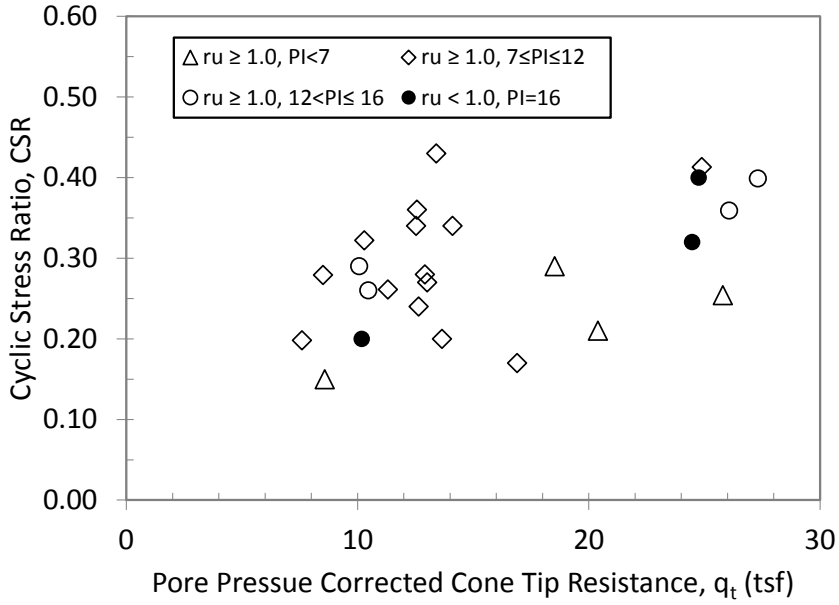

Figure 5.50: Correlation between the pore pressure corrected CPT Resistance, q_t, and the Cyclic Stress Ratio, CSR applied to samples from Big Branch and Abner Fork impoundments.

By categorizing the data points based on the Plasticity Index, PI, an additional trend is identified. The samples with the low PI values, (PI < 7%, depicted by empty triangles), required the lowest CSR values to obtain a pore pressure ratio of 1.0, but did

not necessarily exhibited the lowest CPT values. Although, the samples with the PI values greater than 7% required higher CSR values, a distinct difference based on PI values could not be identified. For example, the samples with PI values ranging from 12% to 16% (depicted with empty diamonds), required equal or lower CSR values compared to the samples with the PI ranging from 7% to 12% (depicted with the empty circles). Similar to the observed results from the SPT blow count correlation with the CSR, the samples that did not achieve the peak pore pressure ratio, depicted by filled circles, did not have the highest cone tip resistance although they had the highest PI values.

In Figure 5.51, the correlation between the laboratory cyclic stress ratio, CSR, and the normalized cone penetration tip resistance, Q_{tN}, measured in the field is presented. The empty data points depict the samples that experienced a pore pressure ratio of 1.0 during the cyclic triaxial test in the lab and the filled data points are the samples that did not reach that state despite numerous cycles of applied deviator stress (up to 500 cycles). The results illustrated in this figure, suggest that the samples with higher normalized tip resistance required lower CSR values to obtain a pore pressure ratio of 1.0, which appears to be counter-intuitive. This could be attributed to the normalization of the tip resistance values. Although scatter is observed, it appears that by a 4.6-fold increase in the normalized CPT tip resistance from 1.3 to 6.0, the CSR was decreased from 0.43 to 0.15 (2.8 times).

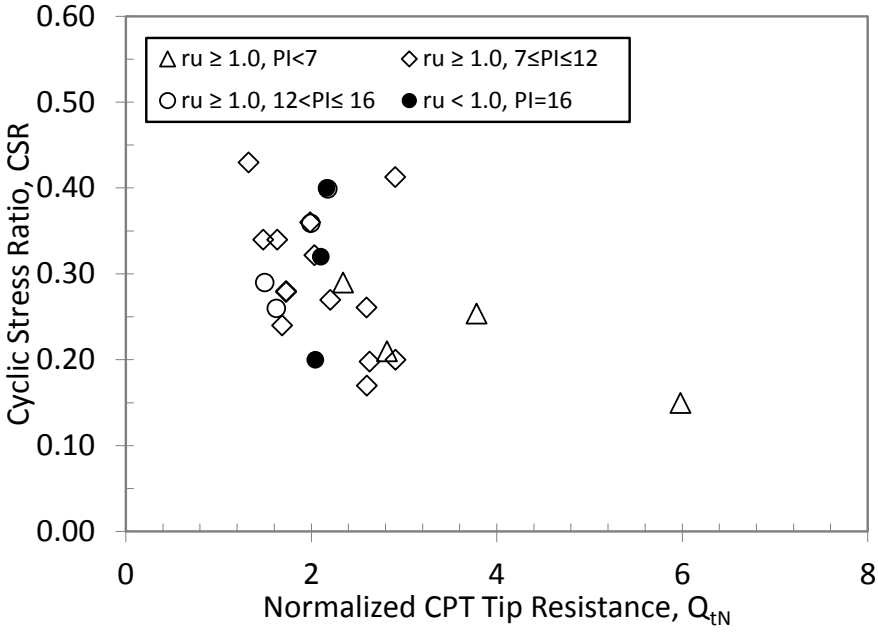

Figure 5.51: Correlation between the normalized CPT, Q_{tN}, and the Cyclic Stress Ratio, CSR applied to samples from Big Branch and Abner Fork impoundments.

Studies by different researchers were performed to identify the correlation between the CSR values and the normalized CPT tip resistance, Q_{tN}. Robertson (2009b) re-evaluated the correlation suggested by Moss et al. (2006) based on 182 case histories of liquefaction in soils. Moss et al. (2006) compiled a comprehensive database based on CPT records from the study performed by Moss (2003). In this database, of the 182 case histories, 30 cases were labeled as "class C," which included results recorded by "non-standard or mechanical" cones or without sleeve friction data. The results based on no friction sleeve data are less reliable especially for methods such as Moss et al. (2006), Robertson and Wride (1998), or Juang et al. (2003) that make use of such parameters. Also, Robertson and Campanella (1983) showed that mechanical cone friction sleeve values can be significantly different from standard electric cone values in the same soil.

Robertson (2009b) presented the updated database for earthquakes with magnitude equal to 7.5 by not including the “Class C” data which is shown in Figure 5.52.

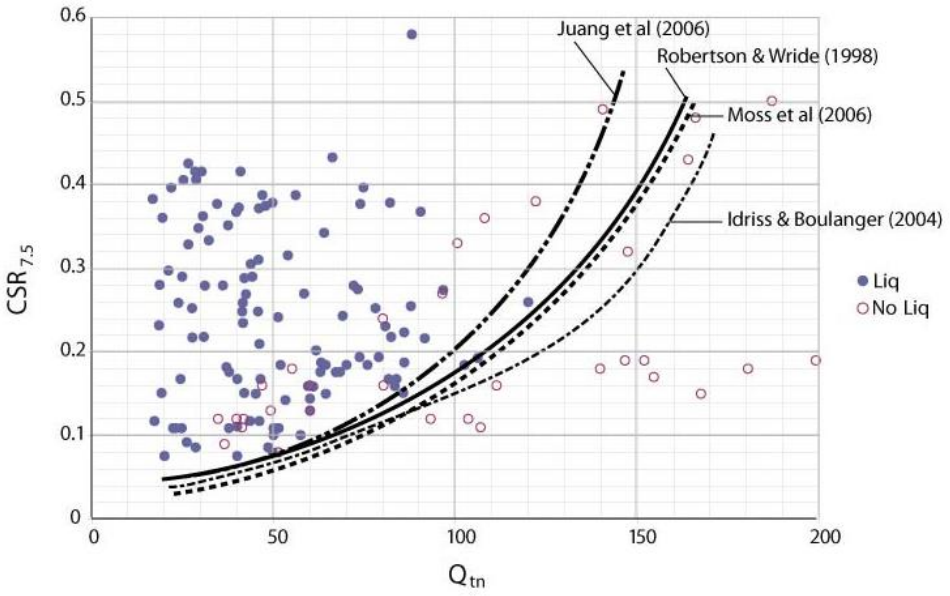

Figure 5.52: Correlation of CSR and normalized CPT tip resistance in soils based on case histories with moment magnitude equal to 7.5 (after Robertson, 2009b).

The correlations presented in Figure 5.52, are only applied for “clean sands”. For soils that are not “clean sands”, the traditional approach which was evoloved from the SPT-based approach has been to adjust the in-situ penetration results to an ”equivalent clean sand” value. It appears that the easiest parameter to quantify changes in grain characteristics was the percent of fines content (Robertson, 2009b).

Robertson (2009b) indicates that the fines content alone does not adequately capture the change in soil behavior. It is common to collect the full SPT sample into a container for grain size analysis. Robertson (2009b) suggested the “average” fines content resulting from this approach is misleading and therefore, the SPT sample may not always

reflect the variation in grain characteristics in heterogeneous soils. Based on this evaluation, that study did not recommend the use of the Idriss and Boulanger (2008) CPT-based method. The Idriss and Boulanger (2008) CPT-based approach uses only fines content from samples to make adjustments to cone resistance.

The normalized CPT tip resistance, Q_{tN}, was corrected for fines content based on the Soil Behavior Type index, I_c, following the methodology proposed by Robertson (2009b), and the clean sand equivalent normalized tip resistance, Q_{tNCS} was calculated. In Figure 5.53, Q_{tNCS} values are correlated to the CSR values recorded in the laboratory. The trend appears to be similar to what was observed between Q_{tN} and CSR values presented in Figure 5.51.

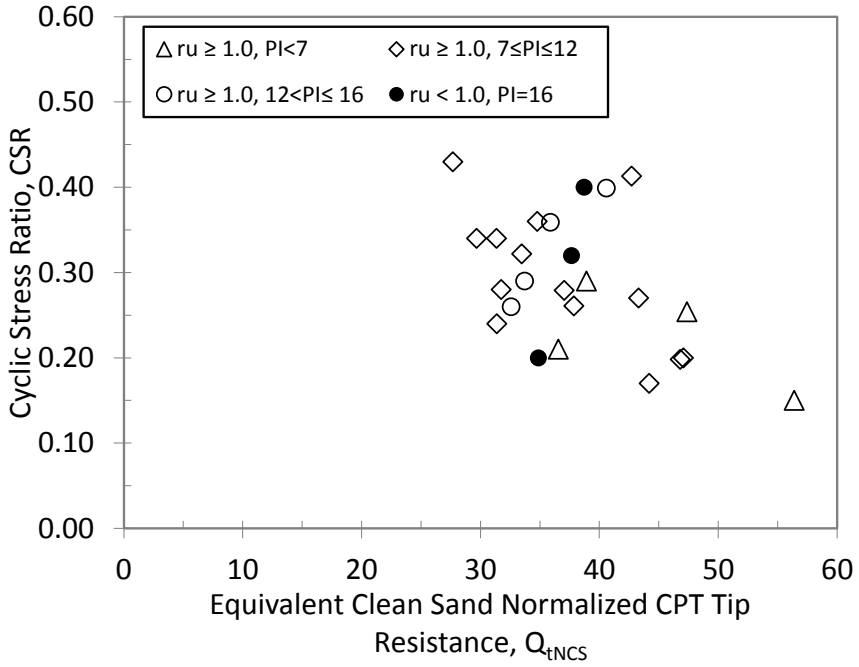

Figure 5.53: Correlation between the clean sand equivalent normalized CPT tip resistance, Q_{tNCS}, and the Cyclic Stress Ratio, CSR applied to samples from the Big Branch and Abner Fork impoundments.

The correlations illustrated in Figure 5.53, were plotted on the correlations between Q_{tNCS} and CSR based on the updated case history database provided by Robertson (2009b). This correlation is presented in Figure 5.54. It should be noted that in this figure, the discussion provided for Figure 5.49 regarding the field equivalent of laboratory applied CSR values was followed as well. Therefore, the laboratory applied CSR values were multiplied by 0.67 before being plotted in Figure 5.54.

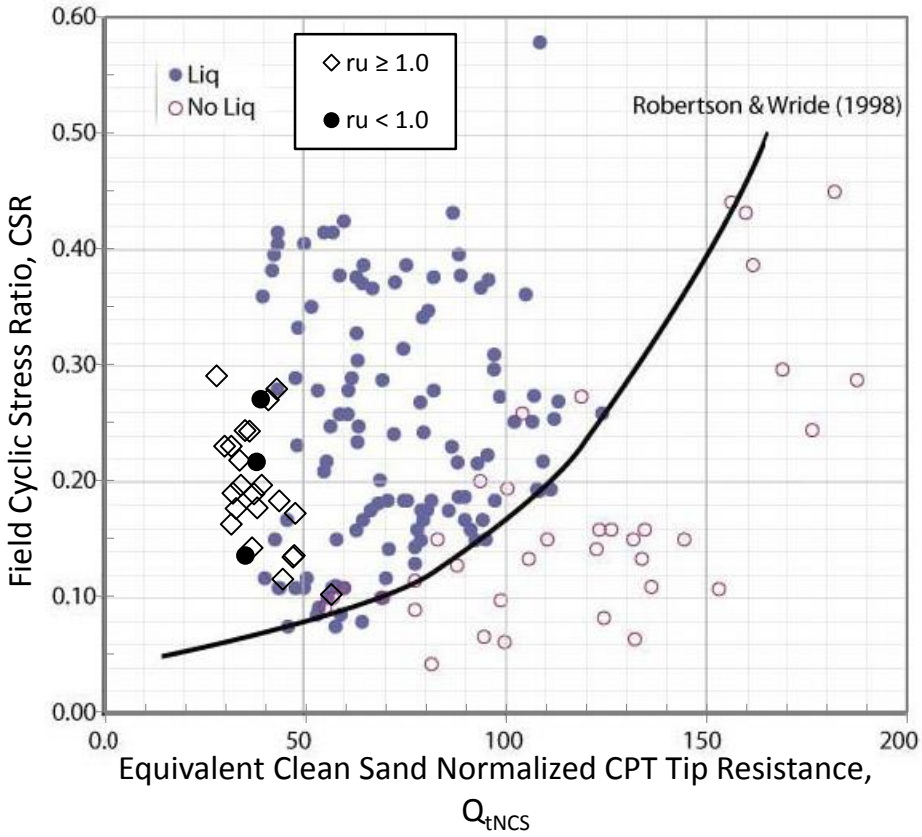

Figure 5.54: Comparison between the correlation of CSR and clean sand equivalent normalized CPT tip resistance, Q_{tNCS}, in coal mine tailings and soils (after Robertson, 2009b).

The correlation presented in Figure 5.54, shows that the data points representing the coal mine tailings, are located to the left side of the suggested curve by Robertson

and Wride (1998). This indicates that if an earthquake capable of producing equivalent shear stresses of laboratory applied CSR values, has a duration equivalent to the corresponding number of uniform cycles applied in the laboratory (Kramer, 1996; Seed et al., 1975), it is possible that it will induce peak pore pressure ratios $(r_u = 1.0)$ in the coal mine tailings material. The coal mine tailings exhibited relatively lower values of Q_{tNCS} ranging between 27.7 and 56.4. For samples that did not liquefy, the peak pore pressures are also located on the left side of the suggested curve. It is emphasized that the CSR values representing the coal mine tailings samples are equivalent of the laboratory applied loads in cyclic triaxial tests, while the CSR values shown for the case histories are from actual earthquake events.

Considering the significant margin of error involved with the SPT testing in the field and the less reliable results for fine grained soils in this method, it is believed that the CPT testing is a more reliable field testing technique for tailings material. This conclusion is strengthened by the comparison between the SPT blow counts and the CPT tip resistance which indicates that even for the tailings material with SPT blow count of zero, the CPT testing could record the low resistance of the material. Also, it should be considered that additional data including the excess pore pressure and the sleeve friction are provided during CPT testing.

As discussed in Section 4.5, after performing cyclic triaxial testing on some of the samples, a laboratory vane shear test was performed. The maximum shear strength exhibited by the samples during the laboratory vane shear test is correlated to the cyclic

stress ratio values and the results are presented in Figure 5.55. In this figure, similar to the other plots discussed in this section, the samples that achieved the peak pore pressure ratio, $(r_u = 1.0)$, are depicted with empty data points and the samples that did not are marked with filled data points. The data suggest that generally the higher the peak vane shear resistance of the sample was, the greater the required CSR value was, although it is acknowledged that the data is scattered. Also, by categorizing the samples based on the Plasticity Index value, PI, further trends are identified. The samples with the lowest PI values, (PI from 0% to 7% and depicted by empty triangles), required the lowest CSR values. A clear distinction between the samples with the PI from 7% to 12%, depicted with empty diamonds, and the samples with the PI from 12% to 16%, depicted with empty circles, cannot be detected. However, these samples generally required higher CSR values and exhibited higher peak laboratory vane shear resistance compared to the samples with PI less than 7%. The two samples that did not achieve the peak pore pressure ratio, exhibited a high laboratory vane shear resistance although this strength was not the highest.

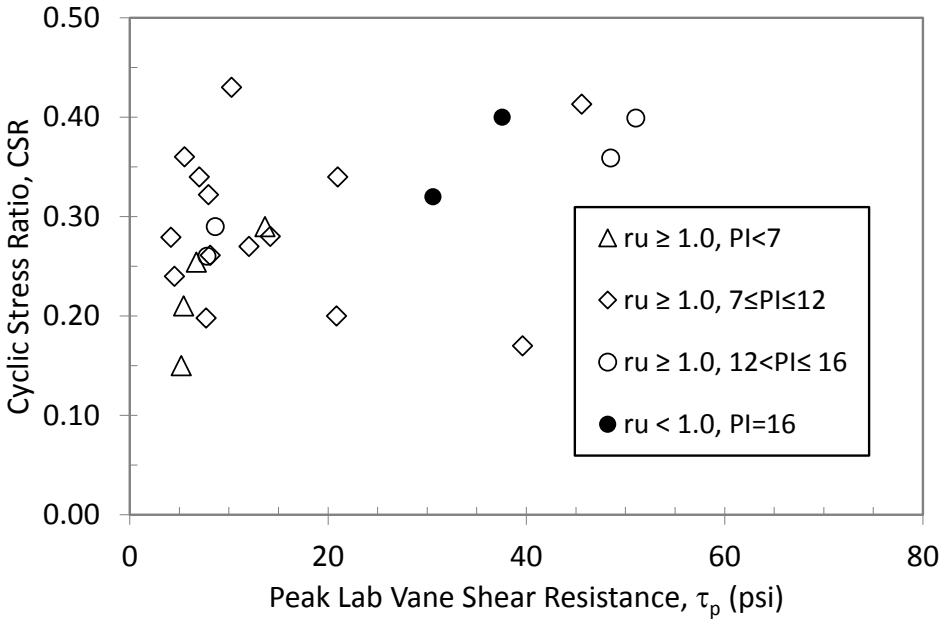

Figure 5.55: Correlation between the peak laboratory vane shear resistance, τ_p, and the Cyclic Stress Ratio, CSR, applied to samples from Big Branch and Abner Fork impoundments.

In Figure 5.56, the relationship between the cyclic stress ratio and the plasticity index of the coal mine tailings samples is presented. Although the data are relatively scattered, the trend of the data points suggests that to obtain the peak pore pressure ratio, samples with higher plasticity index values required higher cyclic stress ratios. Also, it is noticed that the samples that never achieved the peak pore pressure ratio had the highest value of plasticity index equal to 16% (despite the numerous cycles of deviator stress (up to 500 cycles)).

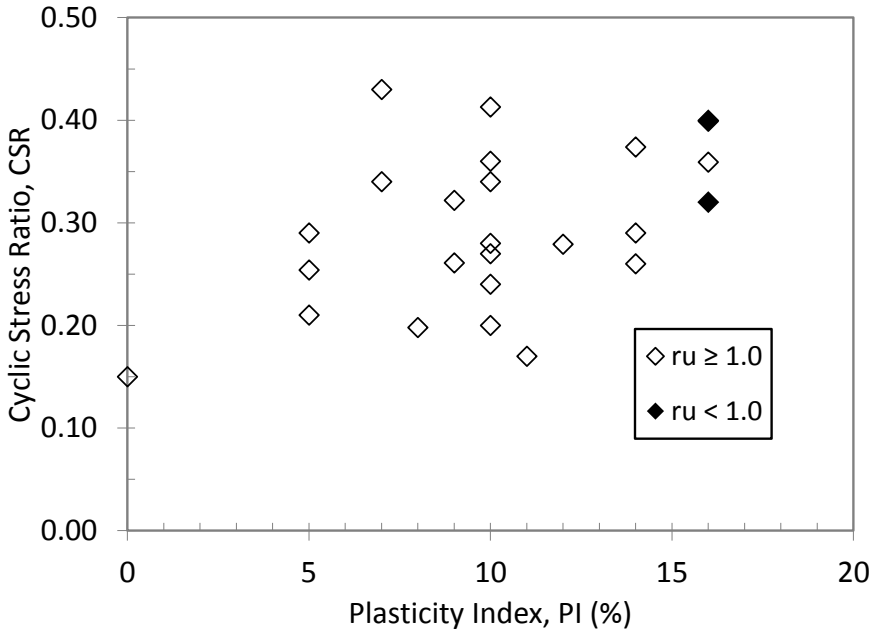

Figure 5.56: Correlation between the plasticity index, PI, and the Cyclic Stress Ratio, CSR, applied to the samples from Big Branch and Abner Fork impoundments.

In Figure 5.57, the relationship between the liquid limit of the coal mine tailings samples and the applied cyclic deviator stress, CSR required to obtain a pore pressure ratio of 1.0, during the cyclic triaxial testing is illustrated. The observed trend is very similar to the observed trend illustrated in Figure 5.56. To induce the peak pore pressure ratio, the higher the liquid limit of the sample was, the greater the CSR needed to be. Also, the samples that did not achieve that state had the highest liquid limit values equal to 43%.

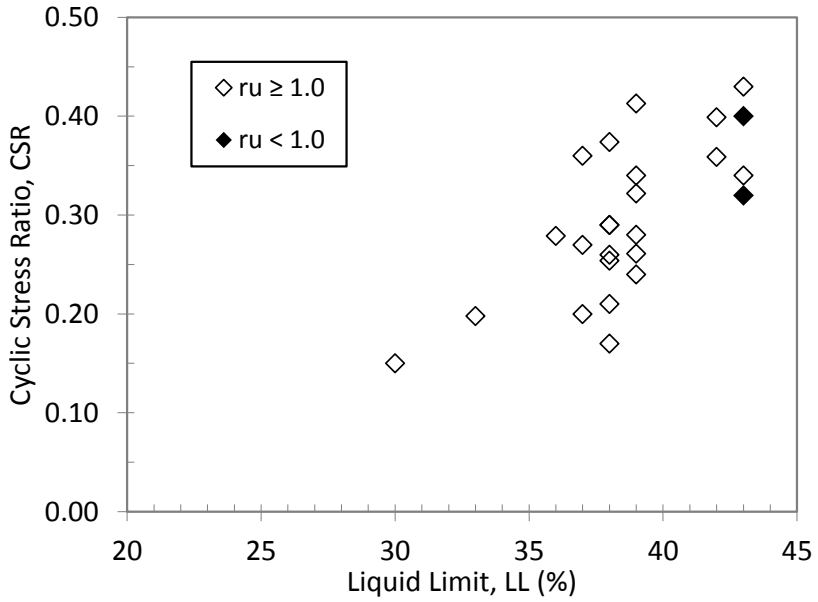

Figure 5.57: Correlation between the liquid limit, LL, and the Cyclic Stress Ratio, CSR, applied to the samples from Big Branch and Abner Fork impoundments.

In Figure 5.58, the relationship between the results of the field vane shear strength of the coal mine tailings and the applied CSR is illustrated. In this series of field tests, two strength values of peak and residual were recorded which are presented in part (a) and (b) of the figure respectively. In this figure, the samples are categorized based on the plasticity index values and also the condition of the pore pressure ratio. In this correlation, the results of the samples with plasticity index values greater than 7% are considered. The samples with lower PI values have relatively higher permeability constants and the condition of the vane shear tests is not undrained.

The data in both part (a) and (b) suggest that the samples with the mid-range plasticity index, from 7% to 12% and depicted by empty diamonds, did not show a distinct different behavior than the samples with PI greater than 12%. In fact, some of the samples with the highest PI values had some of the lowest vane shear strength values. The samples

that did not achieve the peak pore pressure ratio, depicted with filled circles, had the highest PI value, PI=16%, but did not exhibit the highest field vane shear strength. It appears that the data are divided into two clusters and it is not well distributed. Therefore, it can be concluded that the field vane shear test did not illustrate a clear relationship with the laboratory CSR. As expected, the recorded values for the residual strength of the coal mine tailings samples are smaller than the peak strength values, although the trends are similar.

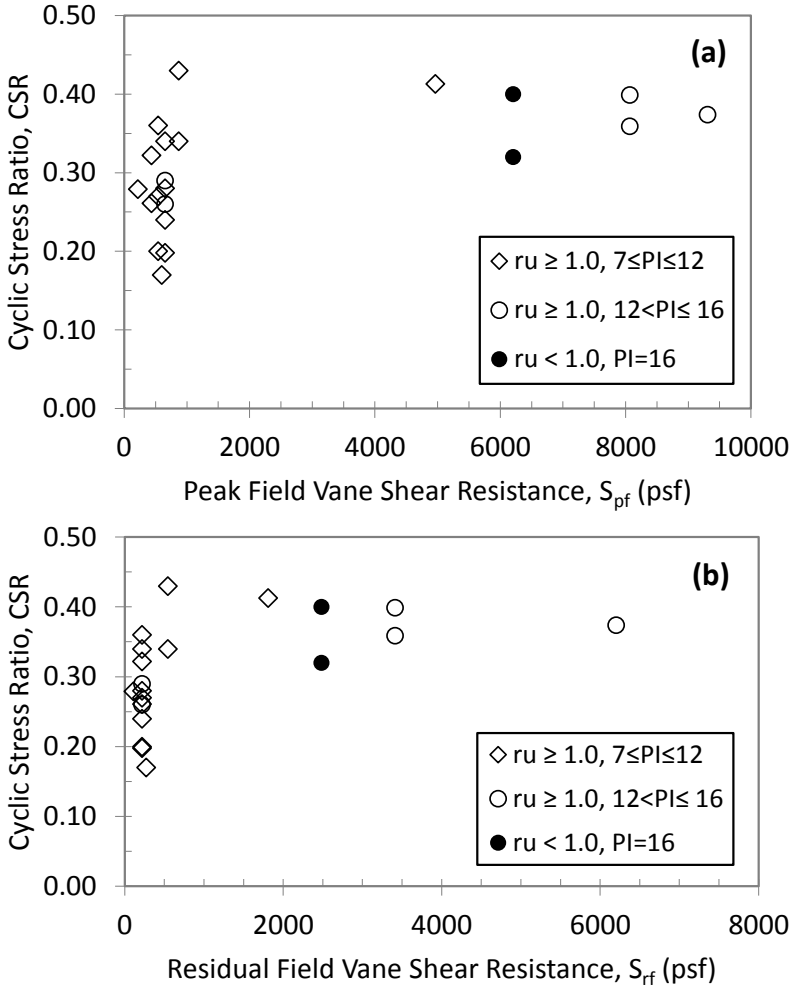

Figure 5.58: Correlation between the cyclic stress ratio, CSR, and the field vane shear test: (a) Peak shear strength, (b) Residual shear strength.

The data presented in Figure 5.59 illustrate the relationship between the peak field vane shear resistance and the applied laboratory cyclic stress ratio by dividing the data set based on the tailings impoundments that the samples were obtained from. In Figure 5.59a, the results from the Big Branch samples and in Figure 5.59b the results of the Abner Fork samples are presented. It appears that a trend between the CSR value and the peak field vane shear strength of the tailings samples could not be identified for any of the individual impoundments. However, as evident for some of the samples, the same value of peak field shear strength is recorded. Considering the nature of the coal mine tailings and the properties of soil materials, this does not appear to be very common. It is believed that the field data points are recorded with equipment or human errors. Also, it should be mentioned that the number of data points are limited and with more data points, the conclusion could be more reliable.

By comparing the results of the two impoundments it is understood that the Big Branch samples with generally lower PI values exhibited lower peak vane shear resistance, while the Abner Fork samples with higher PI values required higher CSR values to reach the peak pore pressure ratio state and had higher peak vane shear strength. Therefore, it can be concluded that the field vane shear results for the coal mine tailings samples in this study were site specific and could not be categorized solely on the PI values.

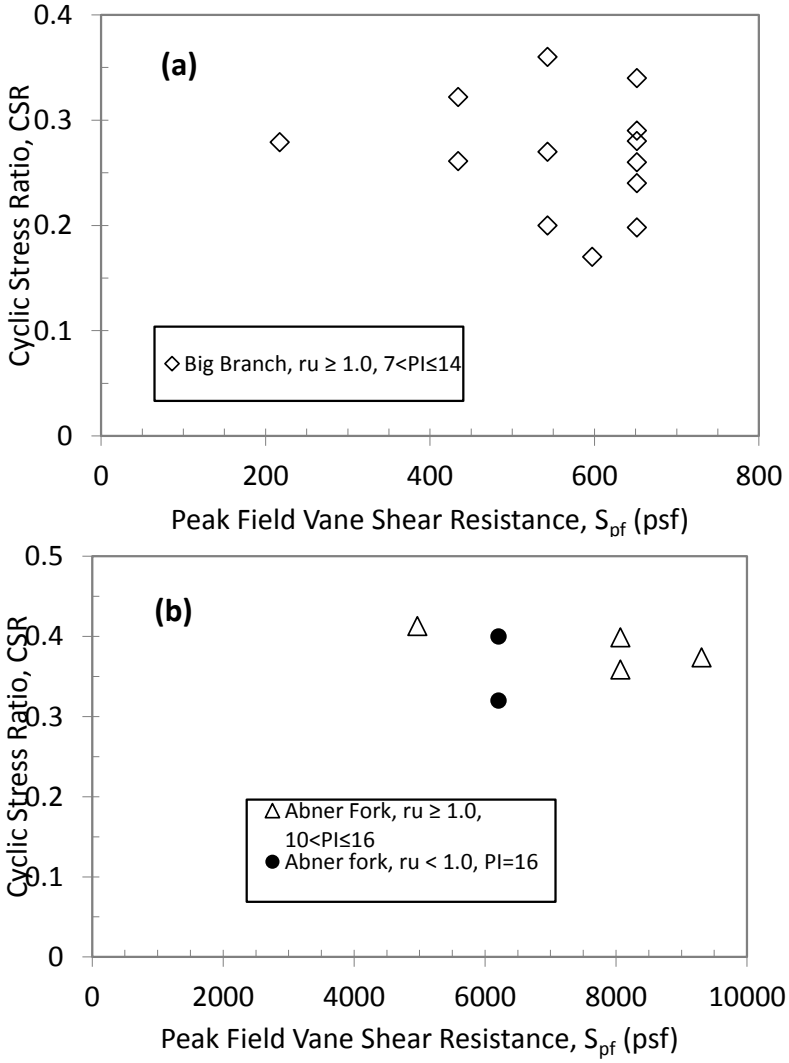

Figure 5.59: Correlation between the cyclic stress ratio, CSR, and the peak field vane shear test: (a) Big Branch, (b) Abner Fork.

In Figure 5.60, the results of the residual field vane shear test are correlated to the laboratory cyclic stress ratios applied to the coal mine tailings. The samples from the Big Branch and Abner Fork are depicted in part (a) and part (b) of the figure respectively. Similar to the correlations presented in Figure 5.59, no clear trend could be identified for any of the impoundments. The samples from Big Branch with generally lower PI values demonstrated lower residual field vane shear strength and required lower CSR values to reach the peak pore pressure ratio state. However, the Abner Fork samples with higher

PI values required higher CSR levels to achieve the peak pore pressure ratio and exhibited higher residual field vane shear strength compared to the Big Branch specimens. Therefore, due to the results of the correlations depicted in this figure and also the results of Figure 5.58 it can be concluded that these correlations are site specific and the parameter PI alone cannot capture the differences in the field vane shear strength of the material. As expected, the residual field vane shear strength of the coal mine tailings were smaller than the peak values.

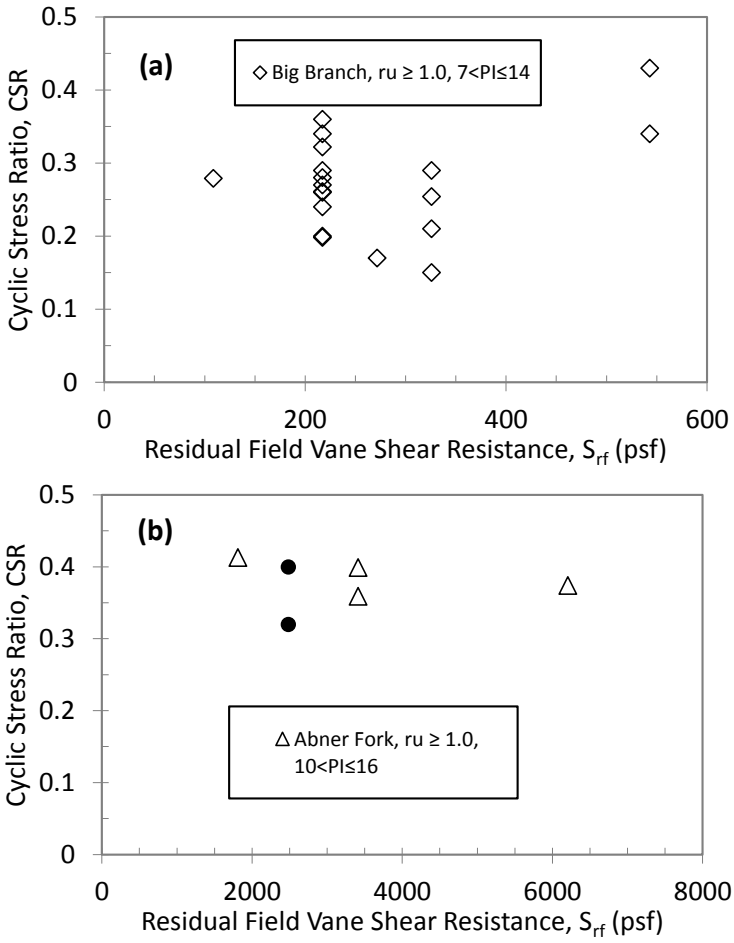

Figure 5.60: Correlation between the cyclic stress ratio, CSR, and the residual field vane shear test: (a) Big Branch, (b) Abner Fork.

As was discussed in Section 5.3.1, Lunne et al. (1997), Farrar et al. (2008), and Robertson (2009) have shown that the sleeve friction values are often similar to the remolded undrained shear strength of fine-grained soils. The residual shear strength of the samples was not recorded for all of the samples in this study and the number of data points is limited. The residual laboratory vane shear resistance values are correlated to the corresponding CPT sleeve friction values in Figure 5.61. The correlation appears to show a clear linear relationship between these two parameters. However, this correlation is based on only four data points and therefore cannot be strongly relied on.

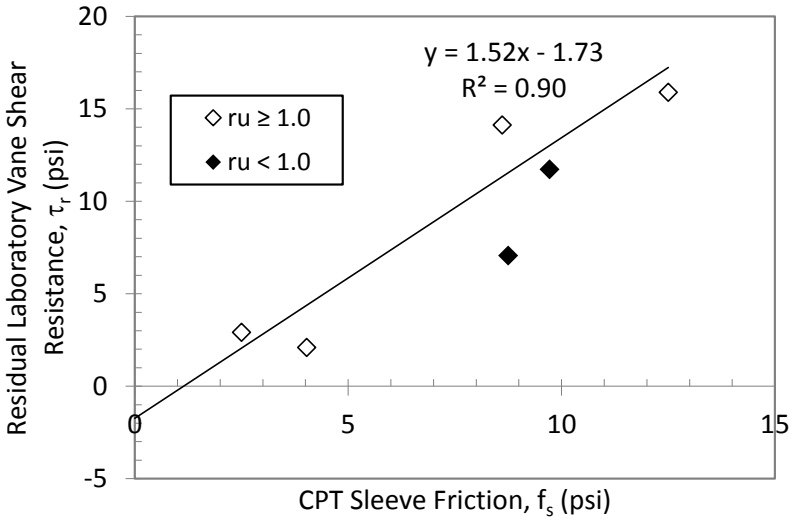

Figure 5.61: Correlation between the residual laboratory vane shear strength and the CPT sleeve friction for samples with PI > 7.0%.

In Figure 5.62, the peak laboratory vane shear strength is correlated to the CPT sleeve friction resistance. The data suggest that the samples with higher sleeve friction values exhibited higher peak laboratory vane shear strength. The coefficient of determination, R^2 was equal to 0.77 which appears to be moderately high.

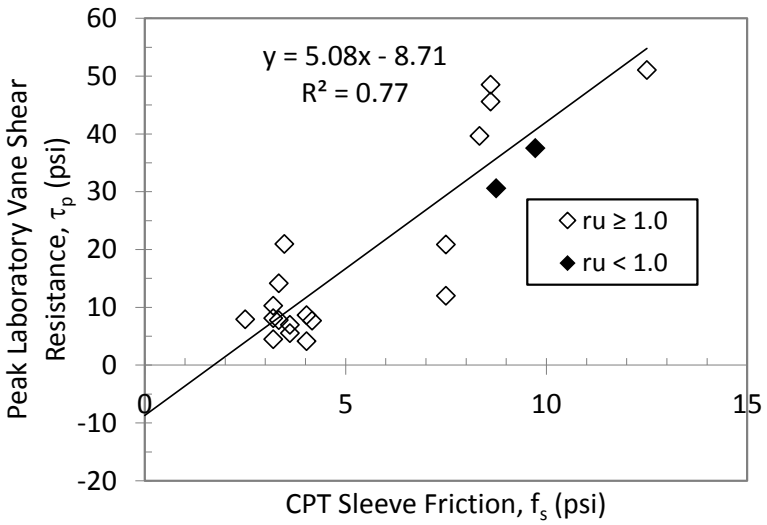

Figure 5.62: Correlation between the peak laboratory vane shear strength and the CPT sleeve friction for samples with PI > 7.0%.

Andrus and Stokoe (2000) studied the correlation between in-situ shear wave velocity and the cyclic stress ratio (CSR) or cyclic stress resistance (CRR) of various soils. This study utilized the data from Andrus et al. (1999) which studied 26 earthquakes and the accompanying test data. By combining the 139 test data and the 26 earthquakes, a total of 225 case histories were obtained, with 149 from the United States, 36 from Taiwan, 34 from Japan, and 6 from China. The occurrence of liquefaction was based on the appearance of surface evidence, such as sand boils, ground cracks and fissures, and ground settlements. At five sites the assessment of liquefaction or non-liquefaction was supported by pore water pressure measurements. For some cases, liquefaction occurrence was assigned based on the strong ground motion. In these cases, liquefaction was identified by observation of a sudden drop in the strong ground motion and small ground motion afterwards (Idriss, 1990; de Alba et al., 1994). Of the 225 case histories, 99 were liquefaction case histories and 126 were non-liquefaction case histories. Based

on the criteria used to evaluate liquefaction in these cases and as it discussed by them, Andrus and Stokoe (2000) studied the occurrence of liquefaction in coarse grained soils such as sands and gravels. Therefore, comparing the results of this study to those case histories would not produce a meaningful conclusion. Nonetheless, this comparison is shown in Figure 5.63. It is indicated that the CSR values representing the coal mine tailings samples are the field equivalent of laboratory applied CSR values as discussed for Figure 5.49.

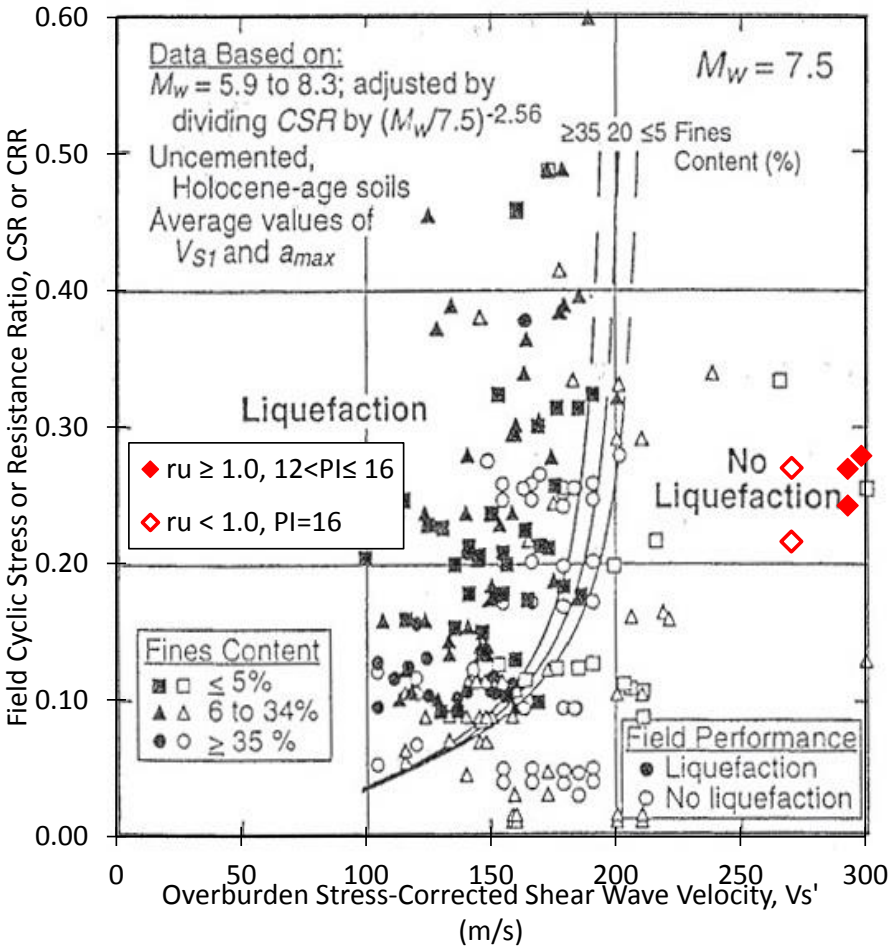

Figure 5.63: Comparison of the correlation of CSR to the corrected shear wave velocity from Abner Fork impoundment to Andrus and Stokoe (2000) results.

As illustrated in Figure 5.63, the Abner Fork samples including the samples that obtained or did not obtain the peak pore pressure ratio are considered non-liquefiable according to the proposed correlation by Andrus and Stokoe (2000). However, it should be noted that the focus of their study has been on the classic liquefaction mainly observed in sandy soils and silty sands. As shown in that figure, they considered silty sands with fine contents greater than 35%. However, the samples evaluated in this study were coal mine tailings classified as silts with fine contents above 70% which generally during liquefaction do not exhibit the same liquefaction behavior as sands and mainly experience cyclic softening.

It is reiterated that the Abner Fork samples exhibited higher plasticity indices compared to Big Branch samples. The Big Branch samples required lower cyclic stress ratios and obtained the peak pore pressure ratio with lower number of cycles. Due to lack of sufficient data, a clear conclusion on the correlation of shear wave velocity and the CSR could not be made. The values of in-situ shear wave velocities and the CSR applied in the lab on the Abner Fork samples are presented in Table 5.9.

Table 5.9: In-situ measured shear wave velocities and the CSR applied in the laboratory for the Abner Fork samples.

sample name	CSR	CPT V_s' (m/s)	SASW V_s' (m/s)	downhole V_s' (m/s)	r_u
TAFLBPST1S1		299	323	325	
TAFLBPST1S2	0.41	298	323	324	≥ 1.0
TAFLBPST3S1	0.36	293			≥ 1.0
TAFLBPST3S2	0.40	293			≥ 1.0
TAFLAPST1S1	0.37		388		≥ 1.0
TAFLBPST2S1	0.40	271	615		< 1.0
TAFLBPST2S2	0.32	270	615		< 1.0

Definitions:
CSR: Cyclic Stress Ratio applied in the laboratory
$V_{s'}$: corrected shear wave velocity measured by sCPTu, SASW, or downhole method
r_u: peak pore pressure ratio

5.4 Summary and Conclusions

In this chapter, the results of in-situ tests performed at the Big Branch and Abner Fork impoundments were presented. The procedures utilized to correct the results for various field conditions and soil types were discussed as well. Also, the in situ results were correlated to identify any relations between different field parameters of coal mine tailings. The main objective of this study was to identify any correlations between the in-situ parameters and the laboratory measured dynamic properties of the coal mine tailings. These correlations were studied and discussed in detail in this chapter.

By performing cone penetration tests (CPT) at these two sites, it was observed that the coal mine tailings materials encountered at these two locations exhibited mechanical behaviors similar to fine grained soils. The variation of tip resistance, sleeve friction, pore pressure, and the soil behavior type index indicated that this material behaved as silty and clayey soils. The comparison between the laboratory measured fines

content and the apparent fines content estimated by the soil behavior type index indicates a reasonable agreement between these two methods.

The SPT values appear to be generally higher for the Abner Fork impoundment, especially for the crest location. At this location due to geometry of the impoundment, the fine grained material is in a closer distance to the coarse grained mine tailings. Therefore, not only the material can be drained faster compared to the toe location, but the likelihood of mixing with coarse grained material is higher as well. Also, the Abner Fork impoundment is an older and taller structure compared to Big Branch. Therefore, due to higher consolidation stresses the material is possibly stiffer and the SPT blow counts are higher.

It was observed that the peak and residual field vane shear strength values increase with increasing depth. This is believed to be due to higher confining stresses and higher consolidation stresses.

The shear wave velocity was measured at the studied impoundments by three methods which include: seismic CPT, SASW, and downhole seismic. The results from these methods were in reasonable agreement.

Basic geotechnical parameters such as the void ratio, unit weight, liquid limit, and plasticity index were measured at various depths for the Big Branch and Abner Fork impoundment. No clear trend was observed with depth for these parameters. The

plasticity index (PI) varied from 0% to 16% for the coal mine tailings samples. The Big Branch samples generally exhibited lower PI values relative to the Abner Fork samples.

The pore pressure corrected CPT tip resistance did not exhibit a clear correlation with the field peak or residual shear strength. Also, the CPT sleeve friction did not correlate well with the field peak or residual shear strength.

The CPT tip resistance and the SPT blow counts for the coal mine tailings did not exhibit a distinct correlation with each other. Normalized values of the tip resistance did not improve the relation with the SPT blow count. However, it was noted that the range of the SPT blow counts was very small and it is believed that by having a wider range of blow counts a trend could possibly be identified.

The SPT blow counts were correlated to the Cyclic Stress Ratio (CSR) applied in the laboratory. Although scatter is observed, it appears that generally, samples with higher SPT blow counts required higher CSR values to obtain a pore pressure ratio of 1.0. This correlation was plotted over the widely used correlations provided by Youd et al. (2001) and the data points from this study appear to be in agreement with those correlations. However, it should be noted that the correlations published by Youd et al. (2001) are based on case histories and the data points from this study are from laboratory tests.

The pore pressure corrected CPT tip resistance from the two studied impoundments were correlated to CSR values. The results suggest that the samples with higher tip resistance required higher CSR values to obtain a pore pressure ratio of 1.0

although scatter is observed. It was also noticed that the samples with Plasticity Indices from 0% to 7% required the lowest CSR values to obtain the peak pore pressure ratio.

Considering the significant margin of error involved with the SPT testing in the field and the less reliable results for fine grained soils in this method, it is believed that the CPT testing is a more reliable field testing technique for tailings material. This conclusion is strengthened by the comparison between the SPT blow counts and the CPT tip resistance which indicates that even for the tailings material with SPT blow count of zero, the CPT testing could record the low resistance of the material. Also, it should be considered that additional data including the excess pore pressure and the sleeve friction are provided during CPT testing.

The normalized tip resistance values were also correlated to the CSR values. The normalized tip resistance values appear to have a reverse relation with the CSR values. Samples with higher normalized tip resistance required lower CSR values.

The clean sand equivalent of normalized tip resistance of coal mine tailings were plotted on the correlations provided by Robertson (2009b). The results appear to be in agreement with the observed results in the studied case histories by Robertson (2009b).

Post-liquefaction laboratory peak vane shear strength was correlated to the CSR values. Generally, the samples with higher peak laboratory vane shear strength required higher CSR values to obtain a pore pressure ratio of 1.0. The plasticity index, liquid limit

and the field vane shear strength values did not illustrate a clear trend with the CSR values.

It appears that the peak and residual laboratory vane shear strength values exhibit a clear trend with the CPT sleeve friction values. Although additional data points are required to make this statement stronger, it is in agreement with the observations by Lunne et al. (1997) and Robertson (2009b).

The shear wave velocity values recorded at the corresponding depths of the undisturbed samples that were tested for the dynamic properties of the tailings material were compared to the correlations provided by Andrus and Stokoe (2000). The comparisons appear to produce mixed results. All of the samples that did or did not achieve the peak pore pressure ratio during the laboratory testing, were classified as non-liquefiable by their correlations. It was noted that Andrus and Stoke (2000) mainly studied sands and silty sands. Therefore, comparing the results of this study could not produce meaningful results unless appropriate corrections are applied.

Chapter 6

Summary and Conclusion

6.1 Summary

This research was driven by the observation of liquefaction in mine tailings material around the world, the existence of numerous coal mine tailings in the Appalachia region, and the close proximity of these impoundments to various active seismic zones. To study the dynamic behavior of coal mine tailings, the experimental phase of the research was divided into two main steps: in-situ testing and laboratory testing. For testing and sampling, two representative coal mine tailings in Kentucky, Big Branch and Abner Fork, were selected.

State-of-practice in situ testing techniques were utilized to provide commonly used geotechnical properties of the material. In situ boring with the implementation of Standard Penetration Test (SPT), Cone Penetration Tests (CPT), and vane shear tests were carried out at the crest and near the pond of these two impoundments. The shear wave velocity of the material was measured during the CPT tests, by utilizing the Spectral Analysis of Surface Waves (SASW), and by the downhole seismic method. Undisturbed samples were obtained by fixed piston sampling at these locations and the Shelby tube samples were transported to the geotechnical laboratory of University of Kentucky for laboratory testing.

The laboratory program on the undisturbed samples included cyclic triaxial tests, post-cyclic triaxial tests, and vane shear tests. Other geotechnical properties of the samples such as the moisture content, specific gravity, plasticity index, and void ratio were also measured following the recommended ASTM standards. Finally, the correlations between various in situ geotechnical parameters of the samples, and the correlations between the geotechnical properties of the samples measured in the laboratory and the field were studied. Based on the results of these studies, the following observations were made:

- The Abner Fork samples with higher confining stresses (52 psi average or 358.5 kPa) relative to Big Branch samples (25 psi average or 172.4 kPa), required significantly higher cyclic stress ratios to achieve the peak pore pressure ratio $r_u = 1.0$. Due to the limited number of specimens, the influence of confining pressure could not be quantified for the samples of each individual tailings dam.

- The comparison of the cyclic strength curves (correlation between the cyclic stress ratio and the number of cycles to obtain peak pore pressure ratio $r_u = 1.0$) between the coal mine tailings and other tailings materials provided by Wijewickreme et al. (2005) indicates that the Big Branch samples behaved similar to the Quartz slimes from Ishihara et al. (1980) study and the general behavior was in agreement with the rest of the tailings material types. It appears that the Abner Fork samples exhibited higher cyclic strength compared to the other tailings material. However, these

samples were kept for an extended time in the Shelby tubes and the results could be affected.

- The influence of overconsolidation ratio was not studied in depth due to limited number of undisturbed samples from each impoundment. However, the samples from one Shelby tube were tested at an overconsolidation ratio of 1.3. These lightly overconsolidated specimens did not exhibit a significant different behavior than the other samples and the results were in the same range.

- The influence of plasticity of the coal tailings samples was investigated. The average plasticity index for Big Branch samples was 9 ranging from 0 to 14, while the Abner Fork specimens had an average PI of 14 ranging from 10 to 16. By comparing the samples obtained from the same impoundment it was observed that samples with higher PI values could require higher or lower number of cycles to achieve the peak pore pressure ratio $r_u = 1.0$, and therefore no clear trend was suggested. Also by studying this influence in conjunction with the influence of void ratio, the trend was not clear. However, by grouping the results of each impoundment together, a clear trend was observed. Abner Fork specimens with higher plasticity indices and lower void ratios exhibited higher cyclic strength when compared to Big Branch samples. The increase in the CSR value with the increase in PI value is in agreement with the results of the study by Ishihara et al. (1981) on a broad range of tailings samples throughout Japan. Although they did not observe a close correlation between the void ratio and the cyclic strength of the material.

- Following the ideas presented by Boulanger and Idriss (2004), it was observed that the coal tailings samples exhibited sand-like, clay-like and transitional type cyclic behavior. Almost all of the samples dilated when reaching the state of peak pore pressure ratio and developed “banana loops” in their stress-strain curves.

- Unconsolidated Undrained compression triaxial (UU) tests were performed on the samples after the cyclic traixial test. All of the samples exhibited highly overconsolidated behavior which is in agreement with the laboratory loading history of them. The coal tailings samples are usually normally consolidated due to the method construction. They have been constantly loaded and the overburden stress has never been removed. However, if the construction of the dam and filling of the pond is stopped, the top layer could be desiccated due to extended exposure to elements and therefore becomes overconsolidated. In the lab, the samples were tested in the cyclic triaxial chamber as normally consolidated samples. After achieving the peak pore pressure ratio, the effective confining stress essentially becomes zero. Since the post-cyclic triaxial tests are performed as unconsolidated undrained tests, the samples behave as highly overconsolidated samples. The pore pressure was increased slightly at smaller strains and was decreased significantly at higher strains which indicates the dilation of the samples. The samples from the same tube could behave slightly different due to the difference in the stratigraphy of the material.

- The post-cyclic undrained shear strength of the samples at different levels of strain measured by post-cyclic triaxial testing was studied in correlation with their PI value.

It appears that samples with higher PI values exhibited higher undrained shear strength, although some scatter was observed in the results.

- Modulus reduction curves and damping ratio curves were provided for the coal tailings samples. It appears that the Abner Fork samples with lower void ratios, higher plasticity indices, and higher in-situ vertical effective pressures had higher modulus and lower damping ratio values. The effect of structure and aging was not measured quantitatively, however based on practical experience with the samples during handling in the lab, the Abner Fork samples appeared to be more rigid and resilient to deformation. The normalized shear modulus curves and the damping ratio curves were compared with the curves presented by Vucetic and Dobry (1991). The modulus reduction curves of coal tailings samples follows those of higher plasticity soils and the values decrease at a faster rate at higher strains compared to fine grained soils. The shape of the damping ratio curves follows the trend of fine grained soil curves, although the values fall in the range of highly plastic soils.

- The liquefaction susceptibility of coal mine tailings material was investigated by using the available liquefaction criteria such as Chinese criteria, Andrews and Martin (2000), Seed et al. (2003), and Bray et al. (2004). The performance of Chinese criteria as shown by other researchers, was not satisfactory. Of the 28 samples that were found to be susceptible to $r_u = 1.0$ in this study and experienced considerable deformation, none of them met all three conditions of the Chinese Criteria and hence would be considered “non-liquefiable”. None of the samples met the criteria presented by

Andrews and Martin (2000) either. By using Bray et al. (2004) criteria, 54% of the samples were considered susceptible to liquefaction or further tests were recommended. By using the Seed et al. (2003) criteria all of the samples were considered susceptible or further testing was recommended. Therefore, the Seed et al. (2003) method was the most effective procedure in determining the liquefaction susceptibility of coal mine tailings.

- The cyclic behavior of the coal mine tailings was studied by using the ideas presented by Boulanger and Idriss (2004) and were categorized into sand-like, clay-like, and transition type material. This classification was shown to be effective in distinguishing the determining cyclic behavior type of coal mine tailings and the potential for liquefaction.

- By performing cone penetration tests (CPT) at these two sites, it was observed that the coal mine tailings materials encountered at these two locations exhibited mechanical behaviors similar to fine grained soils. The variation of tip resistance, sleeve friction pore pressure, and the soil behavior type index indicated that this material behaved as silty and clayey soils. The comparison between the laboratory measured fines content and the apparent fines content estimated by the soil behavior type index indicates a reasonable agreement between these two methods.

- The SPT values appear to be generally higher for the Abner Fork impoundment, especially for the crest location. At this location due to geometry of the impoundment, the fine grained material is in a closer distance to the coarse grained mine tailings.

Therefore, not only the material can be drained faster compared to the toe location, but the likelihood of mixing with coarse grained material is higher as well. Also, the Abner Fork impoundment is an older and taller structure compared to Big Branch. Therefore, due to higher consolidation stresses the material is possibly stiffer and the SPT blow counts are higher.

- Considering the significant margin of error involved with the SPT testing in the field and the less reliable results for fine grained soils in this method, it is believed that the CPT testing is a more reliable field testing technique for tailings material. This conclusion is strengthened by the comparison between the SPT blow counts and the CPT tip resistance which indicates that even for the tailings material with SPT blow count of zero, the CPT testing could record the low resistance of the material. Also, it should be considered that additional data including the excess pore pressure and the sleeve friction are provided during CPT testing.

- It was observed that the peak and residual field vane shear strength values increase with increasing depth. This is believed to be due to higher confining stresses and higher consolidation stresses.

- The shear wave velocity was measured at the studied impoundments by three methods which include: seismic CPT, SASW, and downhole seismic. The results from these methods were in reasonable agreement.

- Basic geotechnical parameters such as the void ratio, unit weight, liquid limit, and plasticity index were measured at various depths for the Big Branch and Abner Fork impoundment. No clear trend was observed with depth for these parameters. The plasticity index (PI) varied from 0% to 16% for the coal mine tailings samples. The Big Branch samples generally exhibited lower PI values relative to the Abner Fork samples.

- The pore pressure corrected CPT tip resistance did not exhibit a clear correlation with the field peak or residual shear strength. Also, the CPT sleeve friction did not correlate well with the field peak or residual shear strength.

- The CPT tip resistance and the SPT blow counts for the coal mine tailings did not exhibit a distinct correlation with each other. Normalized values of the tip resistance did not improve the relation with the SPT blow count. However, it was noted that the range of the SPT blow counts was very small and it is believed that by having a wider range of blow counts a trend could possibly be identified.

- The SPT blow counts were correlated to the Cyclic Stress Ratio (CSR) applied in the laboratory. Although scatter is observed, it appears that generally samples with higher SPT blow counts required higher CSR values to obtain a pore pressure ratio of 1.0. This correlation was plotted over the widely used correlations provided by Youd et al. (2001) and the data points from this study appear to be in agreement with those correlations. However, it should be noted that the correlations published by Youd et

al. (2001) are based on case histories and the data points from this study are from laboratory tests.

- The pore pressure corrected CPT tip resistance from the two studied impoundments were correlated to CSR values. The results suggest that the samples with higher tip resistance required higher CSR values to obtain a pore pressure ratio of 1.0 although scatter is observed. It was also noticed that the samples with Plasticity Indices from 0% to 7% required the lowest CSR values to obtain the peak pore pressure ratio.

- The normalized tip resistance values were also correlated to the CSR values. The normalized tip resistance values appear to have a reverse relation with the CSR values. Samples with higher normalized tip resistance required lower CSR values.

- The clean sand equivalent of normalized tip resistance of coal mine tailings were plotted on the correlations provided by Robertson (2009b). The results appear to be in agreement with the observed results in the studied case histories by Robertson (2009b).

- Post-liquefaction laboratory peak vane shear strength was correlated to the CSR values. Generally, the samples with higher peak laboratory vane shear strength required higher CSR values to obtain a pore pressure ratio of 1.0. The plasticity index, liquid limit and the field vane shear strength values did not illustrate a clear trend with the CSR values.

- It appears that the peak and residual laboratory vane shear strength values exhibit a clear trend with the CPT sleeve friction values. Although additional data points are required to make this statement stronger, it is in agreement with the observations by Lunne et al. (1997) and Robertson (2009b).

- The shear wave velocity values recorded at the corresponding depths of the undisturbed samples that were tested for the dynamic properties of the tailings material were compared to the correlations provided by Andrus and Stokoe (2000). The comparisons appear to produce mixed results. All of the samples that did or did not achieve the peak pore pressure ratio during the laboratory testing, were classified as non-liquefiable by their correlations. It was noted that Andrus and Stoke (2000) mainly studied sands and silty sands. Therefore, comparing the results of this study could not produce meaningful results unless appropriate corrections are applied.

6.2 Recommendations for Future Research

This study, performed on the dynamic behavior of coal mine tailings, was extensive since it included in situ work, laboratory work, and some analysis. Due to budget and time limitations, some topics were either beyond the scope of this work or were too extensive to be included in this study. Thus, for future work the following could be considered:

- By performing a broader in situ testing program and obtaining a larger number of undisturbed sampling, a broader range of in situ or laboratory geotechnical properties of the coal mine tailings material can be studied. In this study, due to lack of sufficient

number of specimens, static triaxial tests were not performed on the undisturbed samples. The undrained shear strength of samples can be utilized in determining the mechanical behavior of the samples.

- The cyclic behavior of the material can be studied by performing a series of cyclic direct simple shear tests. The loading mechanism in this system is more comparable to the in situ conditions and the results will be more reliable. In addition, the results of this study can be compared to the results of the cyclic direct simple shear tests. Also, the complexities involved with the specific cyclic triaxial system utilized in this study, resulted in losing some of the limited undisturbed samples. For future work, using a more user friendly equipment will produce more meaningful results.

- The storage time between sampling and performing the laboratory tests on the undisturbed samples should be minimized. In this study, the sampling phase was performed by other researchers at least 3 years before the laboratory testing phase. In the future studies, it is highly recommended that the laboratory testing program be carried out immediately after sampling to minimize the exposure of the samples to elements.

- The field and laboratory vane shear tests can be performed with higher accuracy to produce more meaningful data. In this study, some of the field vane shear measurement appeared to be non-representing of the highly variable conditions of the tailings material.

- By incorporating the results of this study into the assessment of the post-earthquake stability of the studied impoundments, the safety of the impoundments can be reevaluated. Also, this work can potentially initiate a broad stability evaluation program for the existing coal mine tailings impoundments.

- Due to the similarities between the geotechnical properties of coal mine tailings and Fly Ash, the results of this study can be considered in assessing the stability of Fly Ash impoundments.

Appendix A

Laboratory Test Results

A.1 Cyclic Triaxial Tests

In this section, a summary of the results of cyclic triaxial testing on each of the samples utilized in this study are presented.

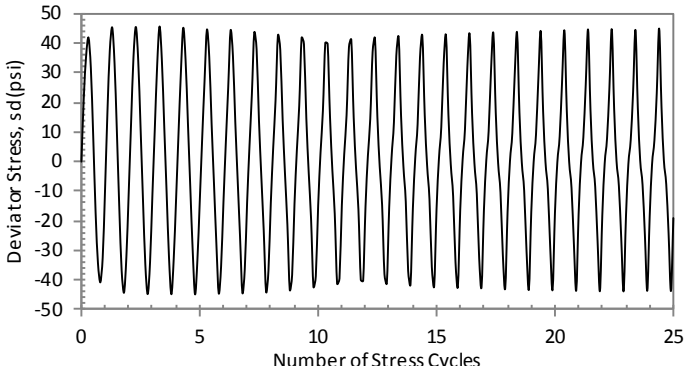

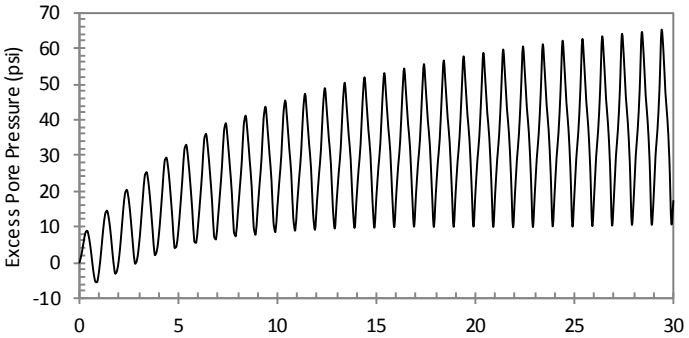

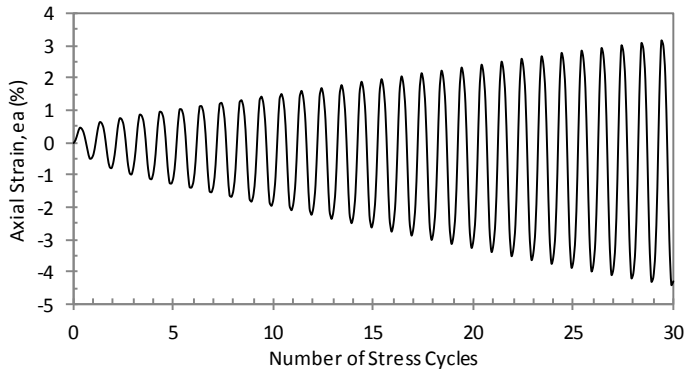

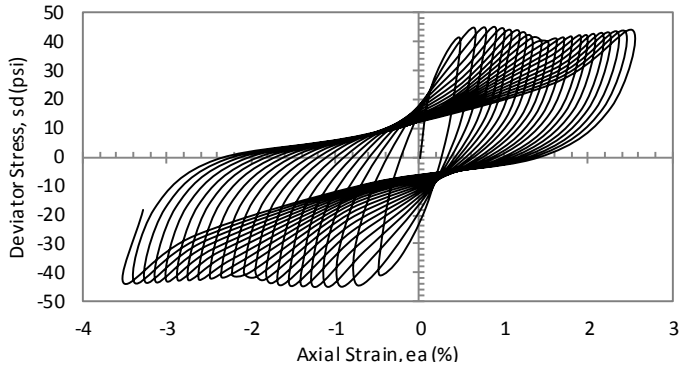

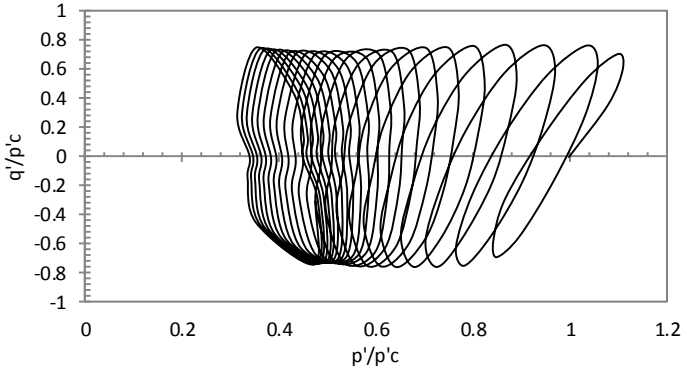

CYCLIC TRIAXIAL TEST DATA

Specimen Name:	TAFLAPST1S1	f (Hz):	1
Test Date:	Dec-1-2011	B-Value (%):	100
Diameter (cm):	7.26	G_s:	2.02
Height (cm):	16.70	σ_d (kPa):	606.3
Wet Mass (gr):	1080	CSR:	0.37
W_n (%):	17.4	N_L:	21
σ'_c(kPa):	405.8	Depth (ft):	239-241
e_0:	0.52	Sampling Date:	Aug-08-2006
γ_{wet} (kN/m^3):	15.3		

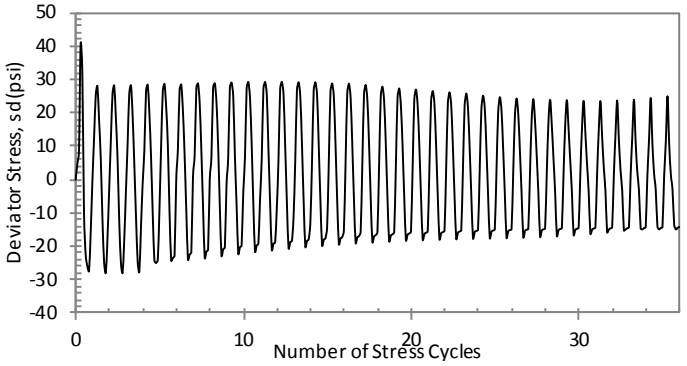

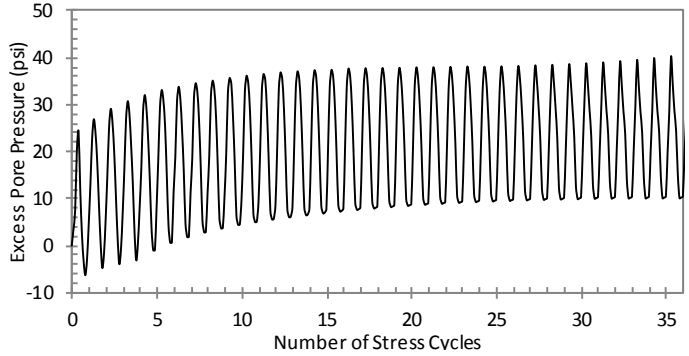

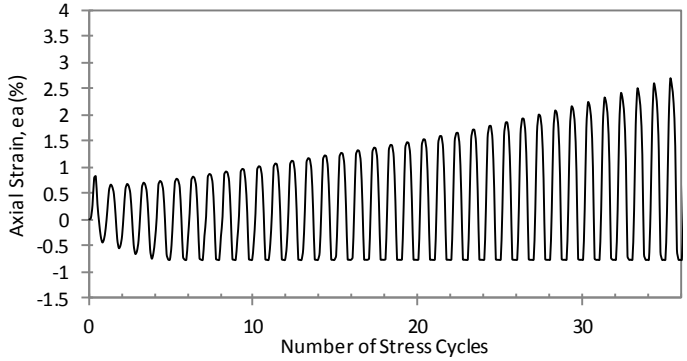

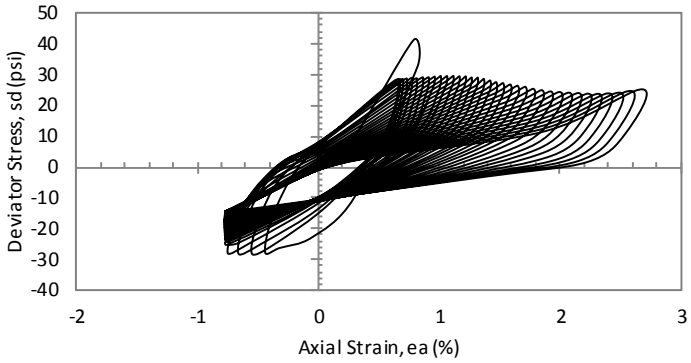

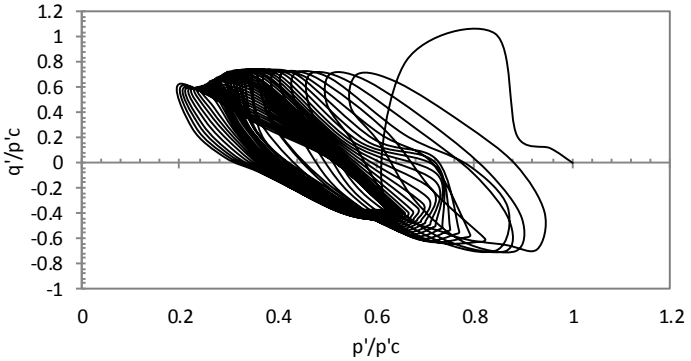

CYCLIC TRIAXIAL TEST DATA

Specimen Name:	TAFLBPST1S1	f (Hz):	1
Test Date:	Oct-2-2011	B-Value (%):	99.0
Diameter (cm):	7.28	G_s:	1.91
Height (cm):	17.30	σ_d (kPa):	305.9
Wet Mass (gr):	1113.2	CSR:	0.28
W_n (%):	23.5	N_L:	35
σ'_c(kPa):	274.2	Depth (ft):	169-171.5
e_0:	0.53	Sampling Date:	Aug-15-2006
γ_{wet} (kN/m^3):	15.1		

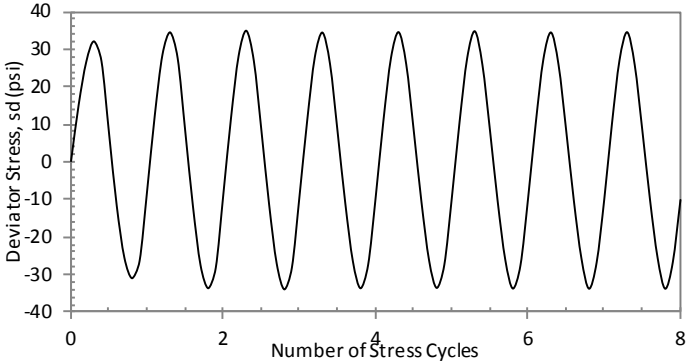

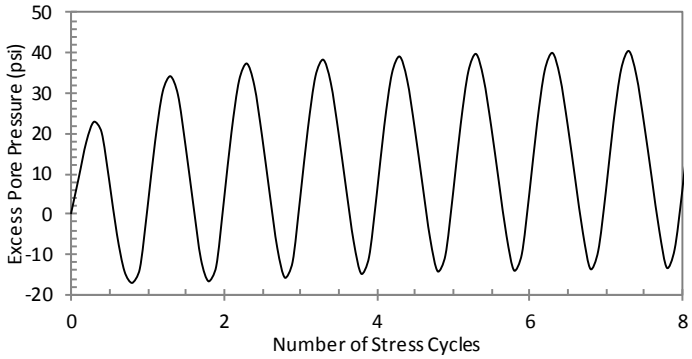

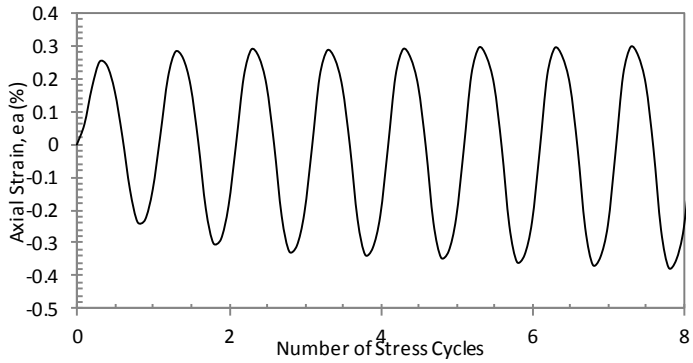

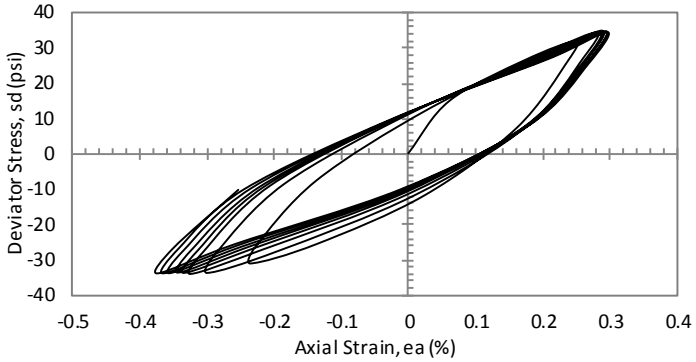

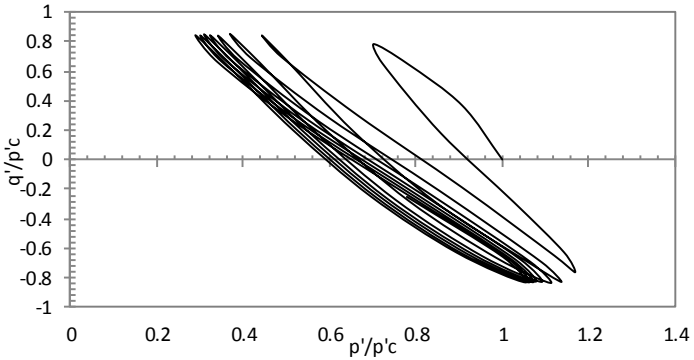

CYCLIC TRIAXIAL TEST DATA

Specimen Name:	TAFLBPST1S2	f (Hz):	1
Test Date:	Oct-11-2011	B-Value (%):	100
Diameter (cm):	7.32	G_s:	1.91
Height (cm):	16.80	σ_d (kPa):	463.0
Wet Mass (gr):	1091.5	CSR:	0.42
W_n (%):	22.7	N_L:	7
σ'_c(kPa):	278.6	Depth (ft):	169-171.5
e_0:	0.52	Sampling Date:	Aug-15-2006
γ_{wet} (kN/m^3):	15.3		

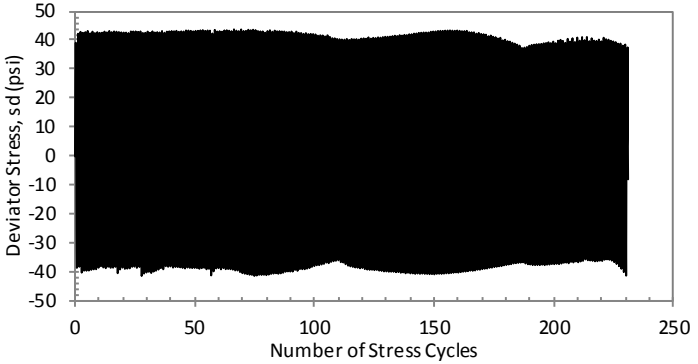

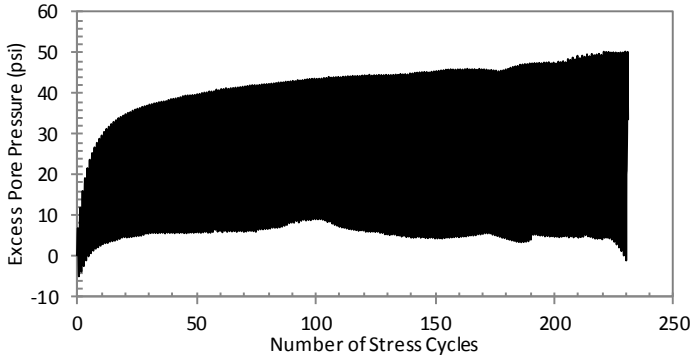

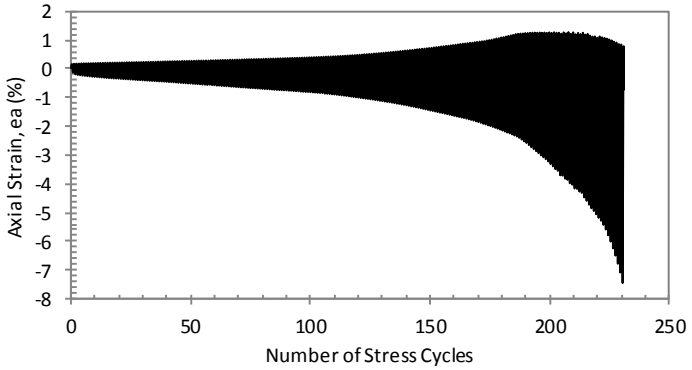

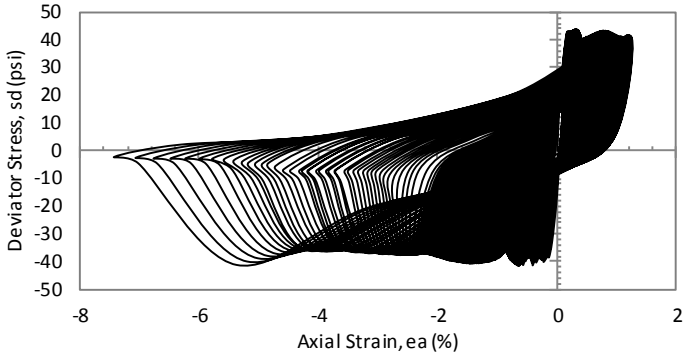

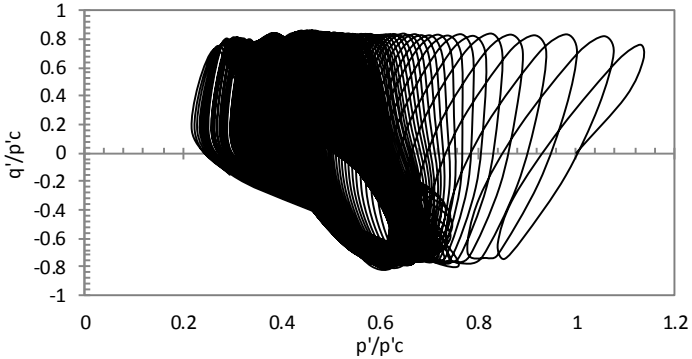

CYCLIC TRIAXIAL TEST DATA

Specimen Name:	TAFLBPST2S1	f (Hz):	1
Test Date:	Oct-20-2011	B-Value (%):	96.1
Diameter (cm):	7.32	G_s:	1.90
Height (cm):	16.10	σ_d (kPa):	562.2
Wet Mass (gr):	1080.1	CSR:	0.39
W_n (%):	26.3	N_L:	
σ'_c(kPa):	356.9	Depth (ft):	199-201.5
e_0:	0.51	Sampling Date:	Aug-15-2006
γ_{wet} (kN/m^3):	15.6		

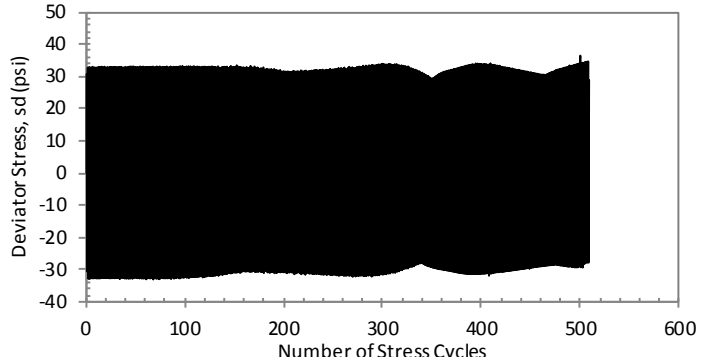

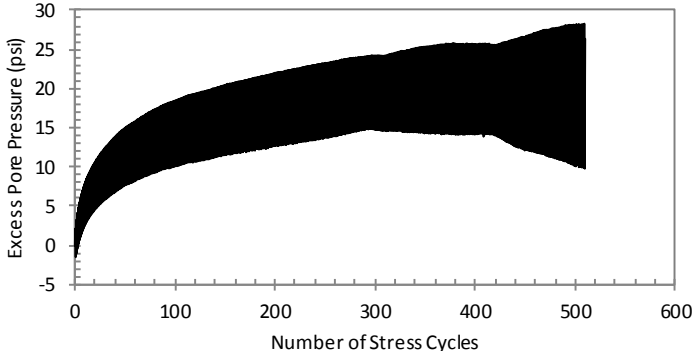

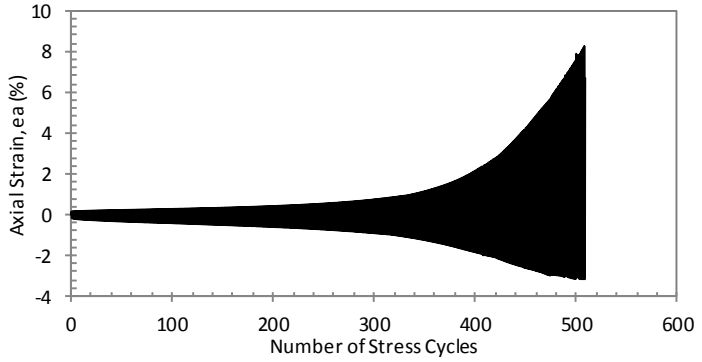

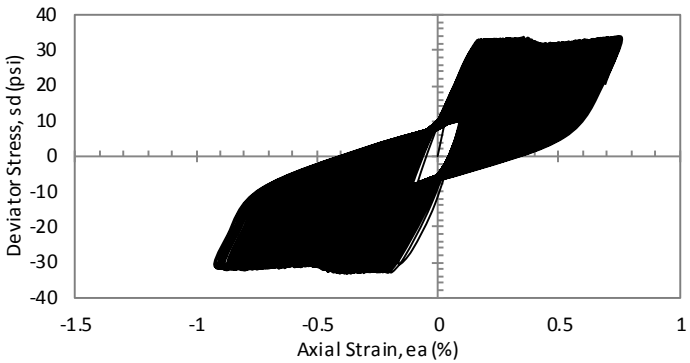

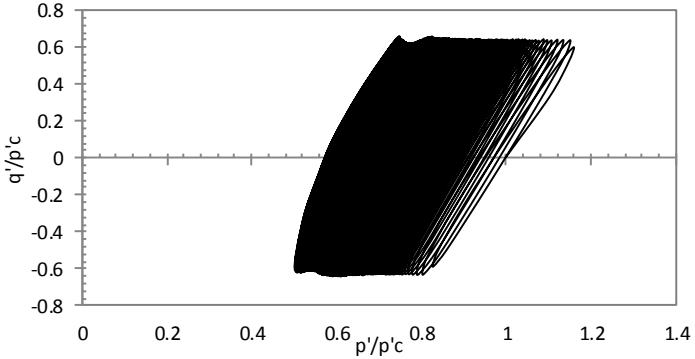

CYCLIC TRIAXIAL TEST DATA

Specimen Name:	TAFLBPST2S2	f (Hz):	1
Test Date:	Oct-26-2011	B-Value (%):	99.1
Diameter (cm):	7.31	G_s:	1.90
Height (cm):	16.80	σ_d (kPa):	454.7
Wet Mass (gr):	1122	CSR:	0.32
W_n (%):	26.5	N_L:	
σ'_c(kPa):	359.0	Depth (ft):	199-201.5
e_0:	0.51	Sampling Date:	Aug-15-2006
γ_{wet} (kN/m^3):	15.6		

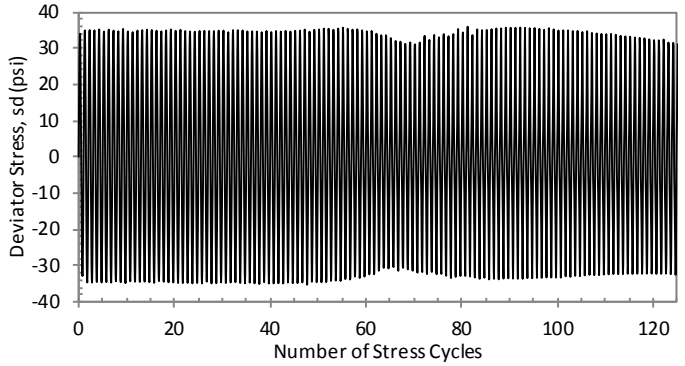

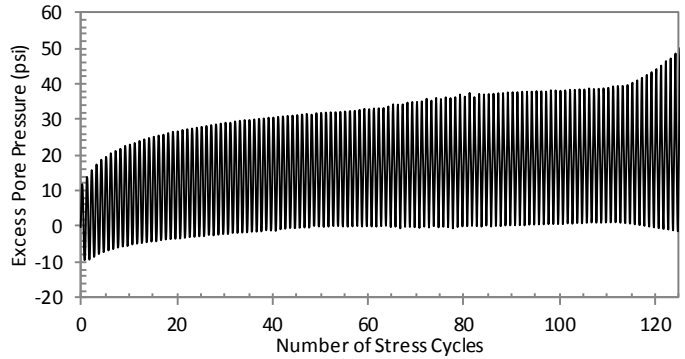

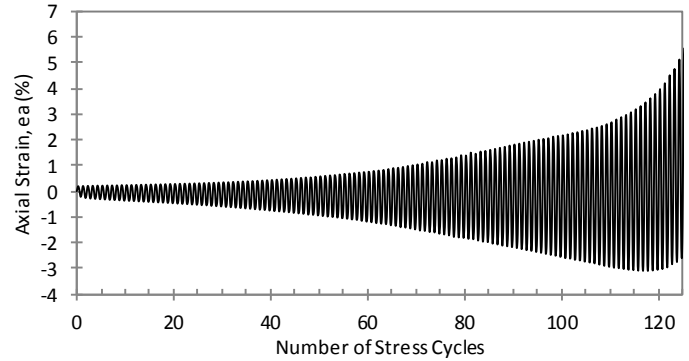

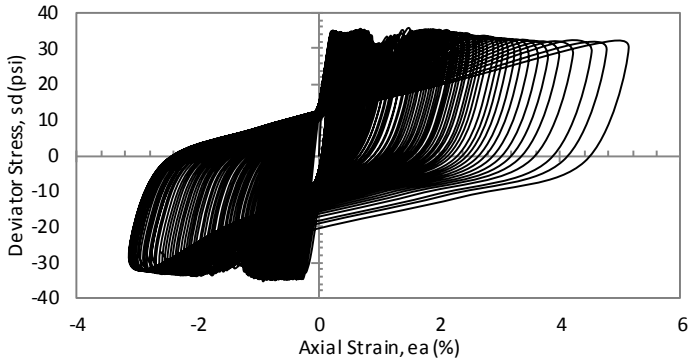

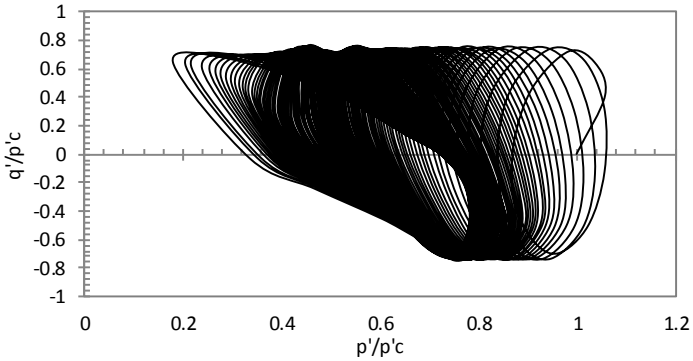

CYCLIC TRIAXIAL TEST DATA

Specimen Name:	TAFLBPST3S1	f (Hz):	1
Test Date:	Nov-21-2011	B-Value (%):	97.8
Diameter (cm):	7.27	G_s:	2.06
Height (cm):	15.65	σ_d (kPa):	474.0
Wet Mass (gr):	1042.5	CSR:	0.36
W_n (%):	25.6	N_L:	124
σ'_c(kPa):	329.3	Depth (ft):	219-220.5
e_0:	0.61	Sampling Date:	Aug-15-2006
γ_{wet} (kN/m^3):	15.7		

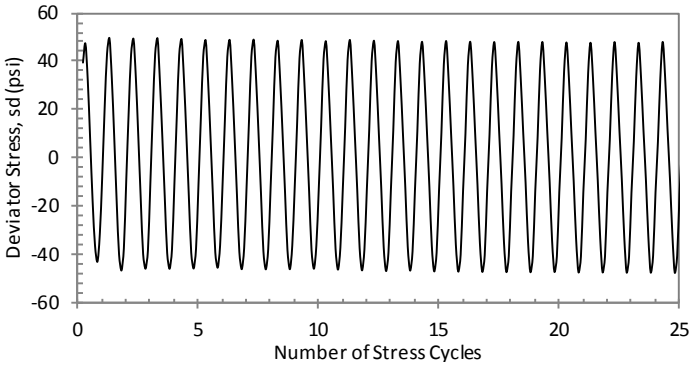

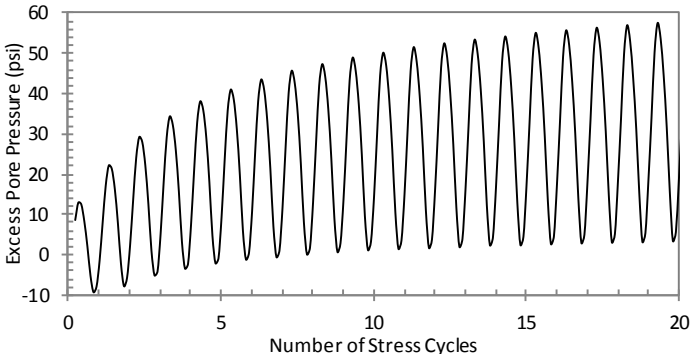

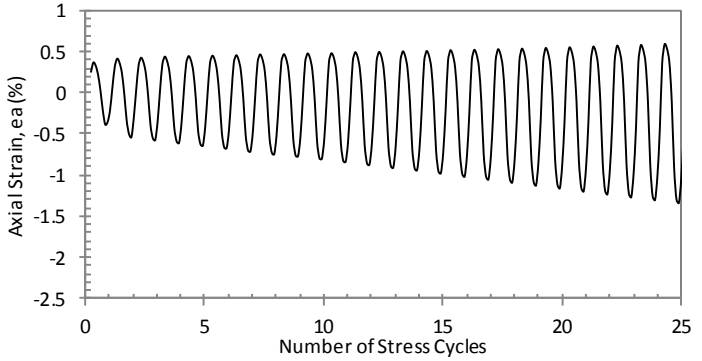

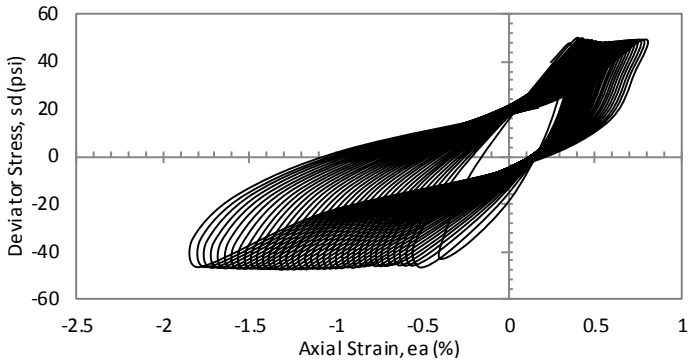

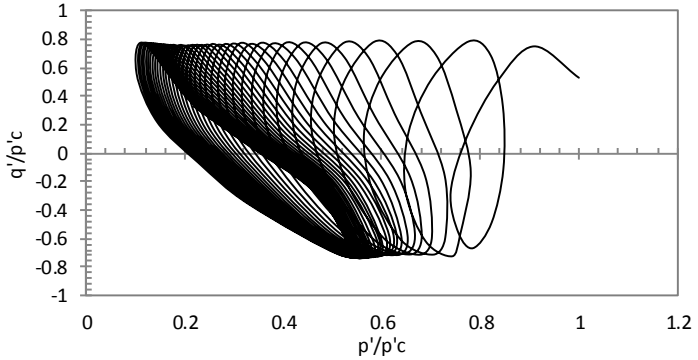

CYCLIC TRIAXIAL TEST DATA

Specimen Name:	TAFLBPST3S2	f (Hz):	1
Test Date:	Nov-30-2011	B-Value (%):	100
Diameter (cm):	7.28	G_s:	2.06
Height (cm):	16.20	σ_d (kPa):	606.3
Wet Mass (gr):	1059.44	CSR:	0.40
W_n (%):	25.1	N_L:	37
σ'_c(kPa):	379.6	Depth (ft):	219-220.5
e_0:	0.64	Sampling Date:	Aug-15-2006
γ_{wet} (kN/m^3):	15.4		

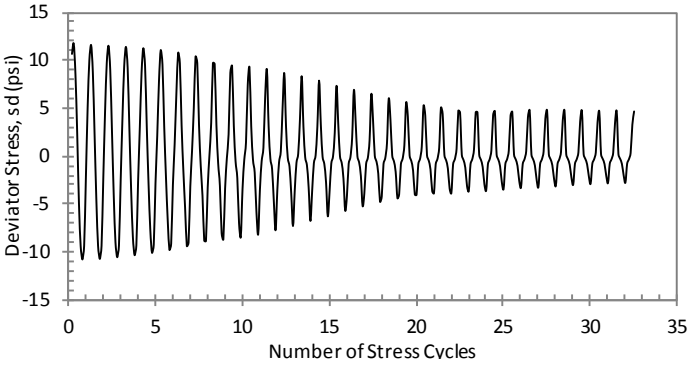

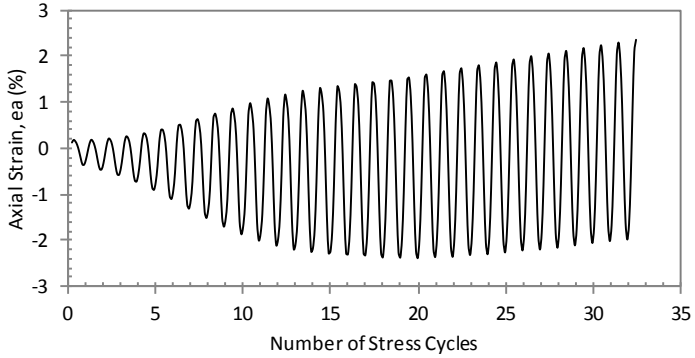

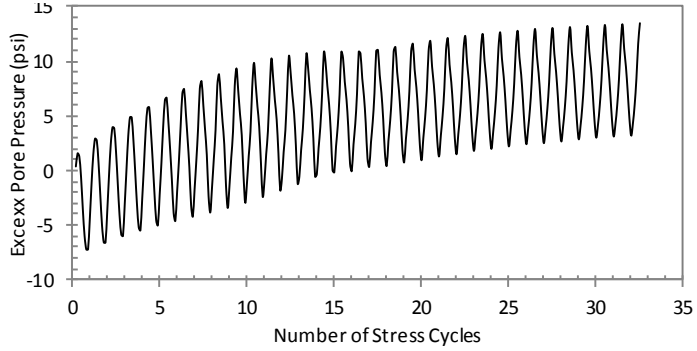

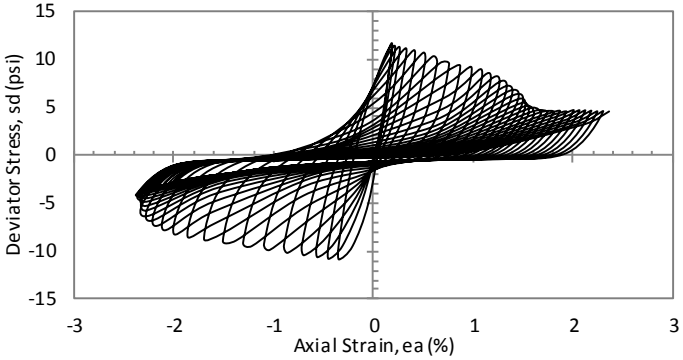

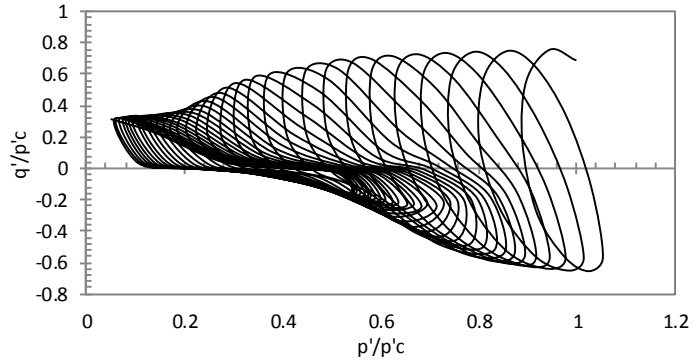

CYCLIC TRIAXIAL TEST DATA

Specimen Name:	TBBLAPST11S3	f (Hz):	1
Test Date:	Mar-17-2011	B-Value (%):	97.8
Diameter (cm):	7.33	G_s:	1.69
Height (cm):	16.90	σ_d (kPa):	107.5
Wet Mass (gr):	966	CSR:	0.30
W_n (%):	29.6	N_L:	26
σ'_c(kPa):	89.6	Depth (ft):	34.5-37
e_0:	0.62	Sampling Date:	Aug-14-2007
γ_{wet} (kN/m^3):	13.3		

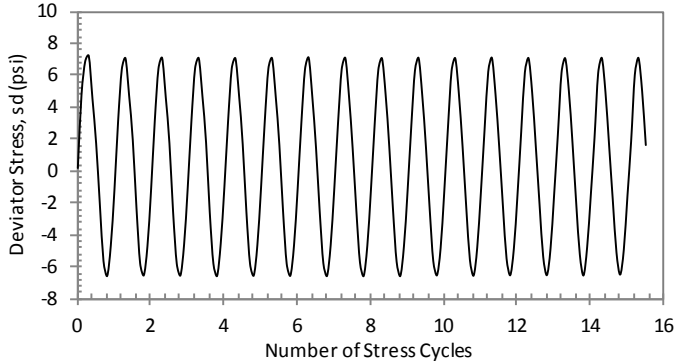

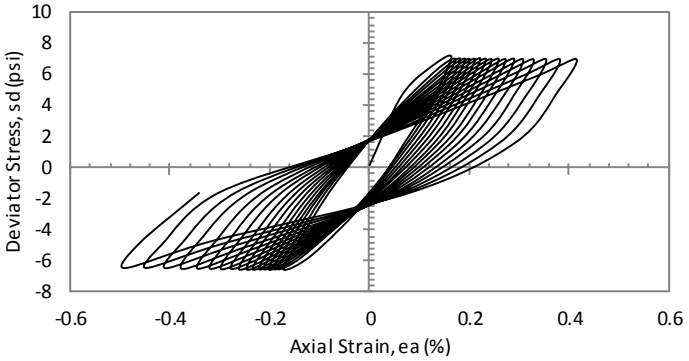

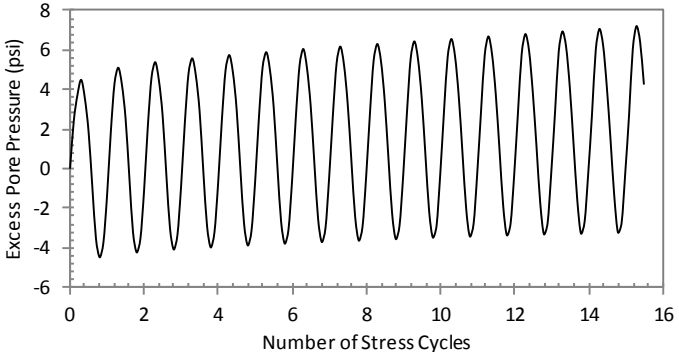

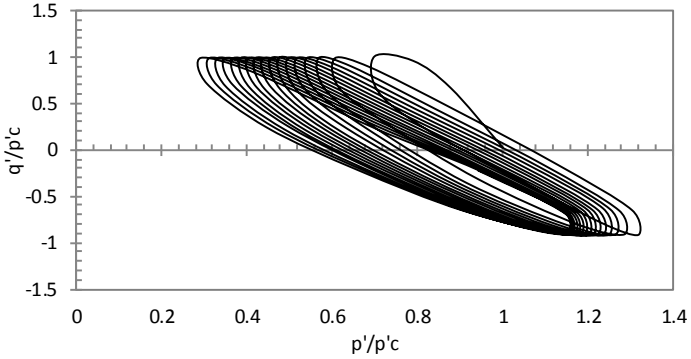

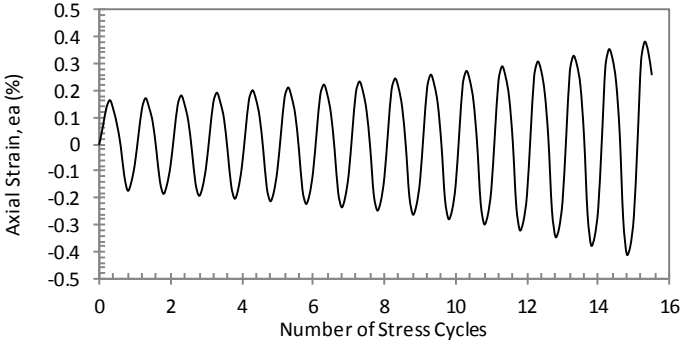

CYCLIC TRIAXIAL TEST DATA

Specimen Name:	TBBLAPST11S4	f (Hz):	1
Test Date:	Mar-21-2011	B-Value (%):	100.0
Diameter (cm):	7.14	G_s:	1.69
Height (cm):	16.50	σ_d (kPa):	93.7
Wet Mass (gr):	947.33	CSR:	0.47
W_n (%):	37.7	N_L:	15
σ'_c(kPa):	48.9	Depth (ft):	34.5-37
e_0:	0.63	Sampling Date:	Aug-14-2007
γ_{wet} (kN/m^3):	14.1		

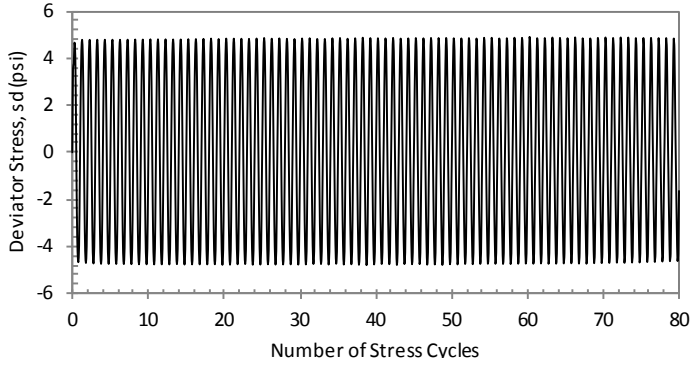

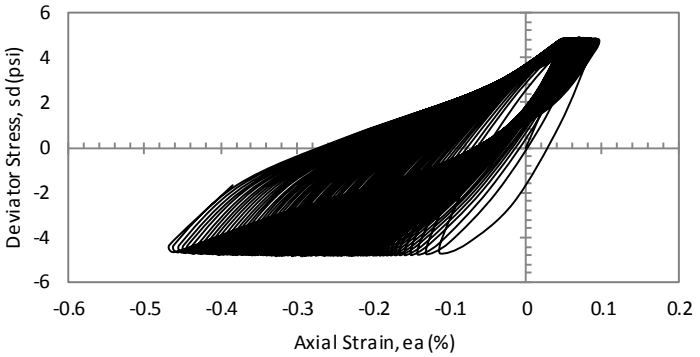

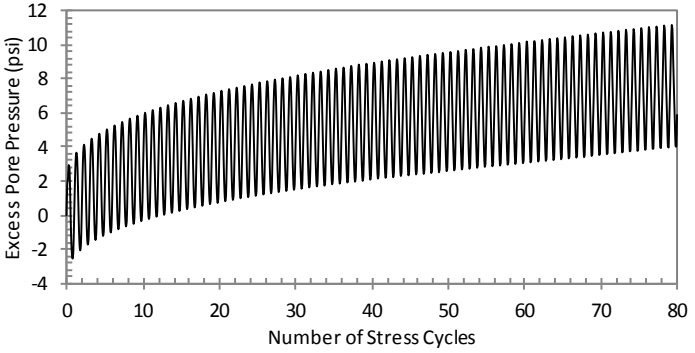

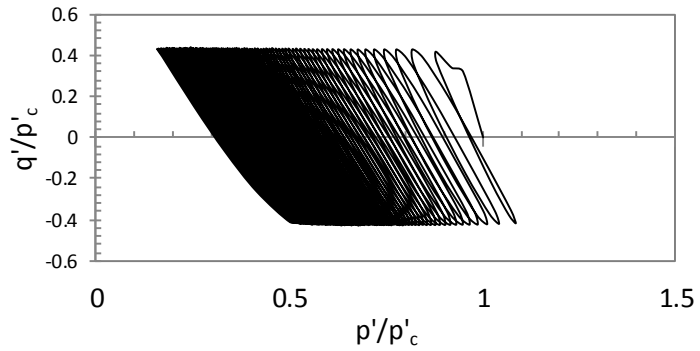

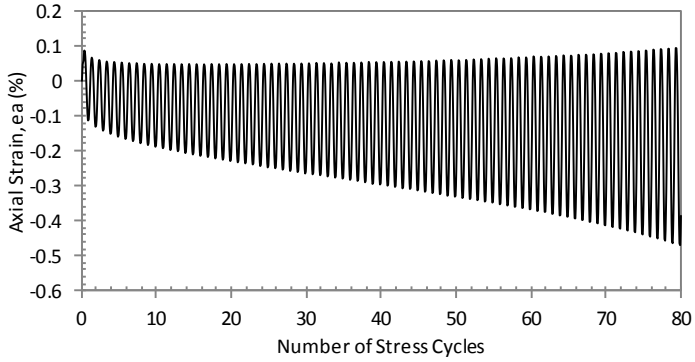

CYCLIC TRIAXIAL TEST DATA

Specimen Name:	TBBLAPST12S1	f (Hz):	1
Test Date:	Aug-27-2011	B-Value (%):	100.0
Diameter (cm):	7.32	G_s:	1.76
Height (cm):	16.70	σ_d (kPa):	60.6
Wet Mass (gr):	1023.27	CSR:	0.20
W_n (%):	33.6	N_L:	79
σ'_c(kPa):	76.5	Depth (ft):	54.5-57
e_0:	0.62	Sampling Date:	Aug-14-2007
γ_{wet} (kN/m^3):	14.3		

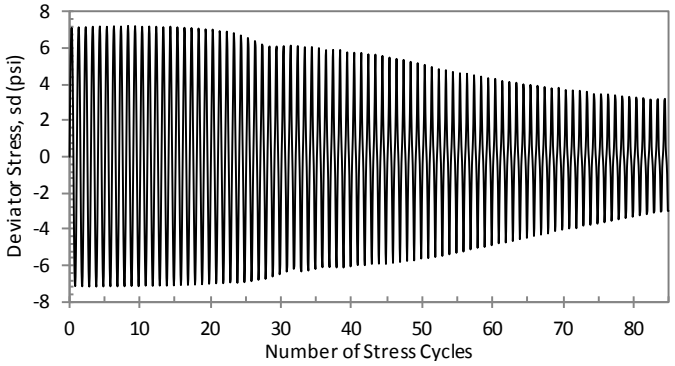

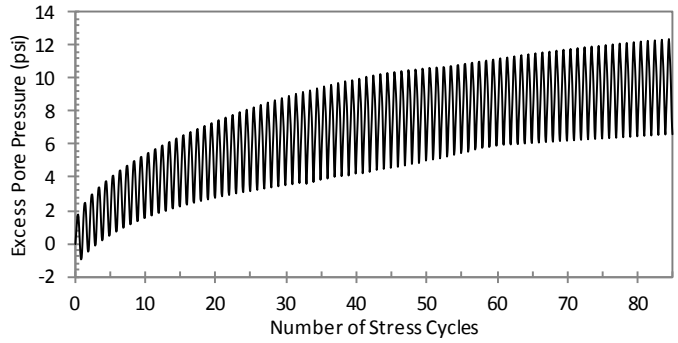

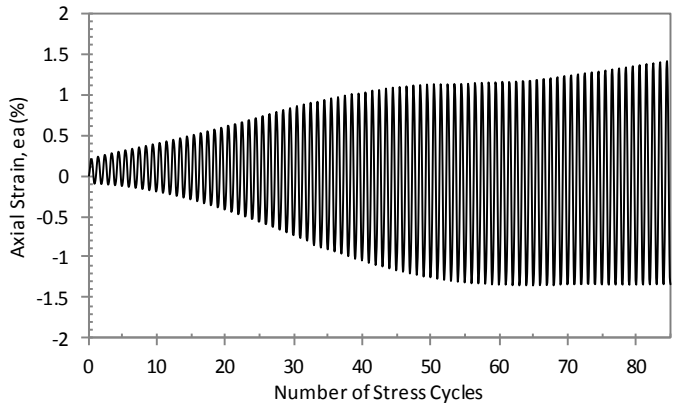

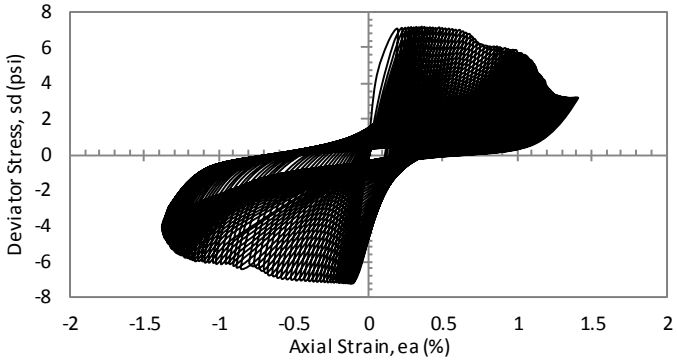

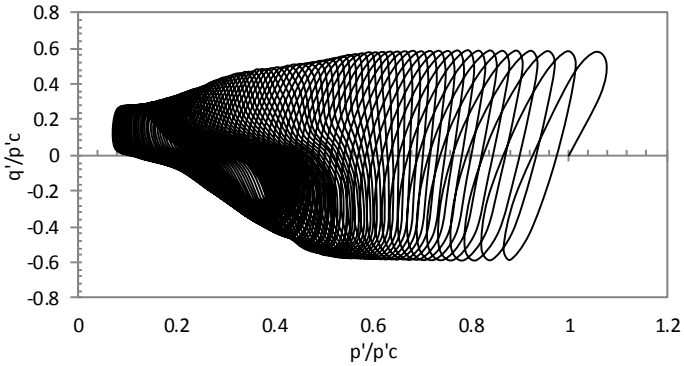

CYCLIC TRIAXIAL TEST DATA

Specimen Name:	TBBLAPST12S2	f (Hz):	1
Test Date:	Sep-03-2011	B-Value (%):	96.4
Diameter (cm):	7.21	G_s:	1.76
Height (cm):	16.80	σ_d (kPa):	90.9
Wet Mass (gr):	1032.78	CSR:	0.27
W_n (%):	32.4	N_L:	84
σ'_c(kPa):	84.7	Depth (ft):	54.5-57
e_0:	0.55	Sampling Date:	Aug-14-2007
γ_{wet} (kN/m^3):	14.3		

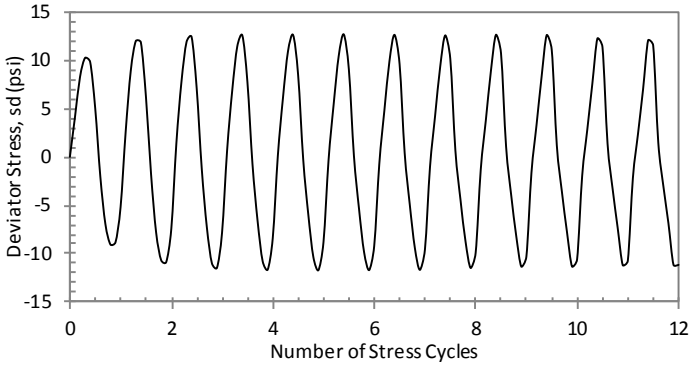

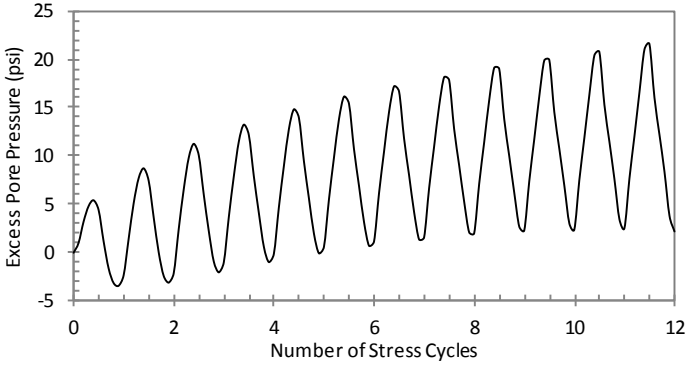

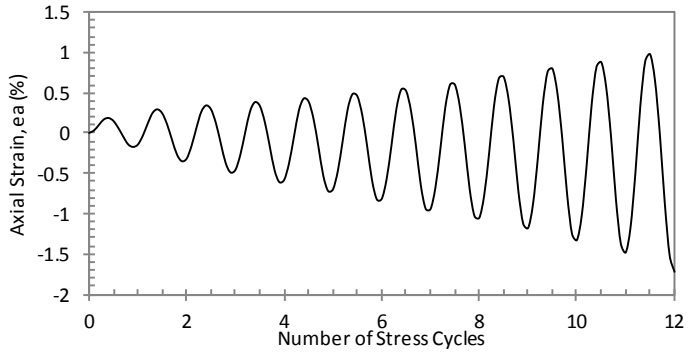

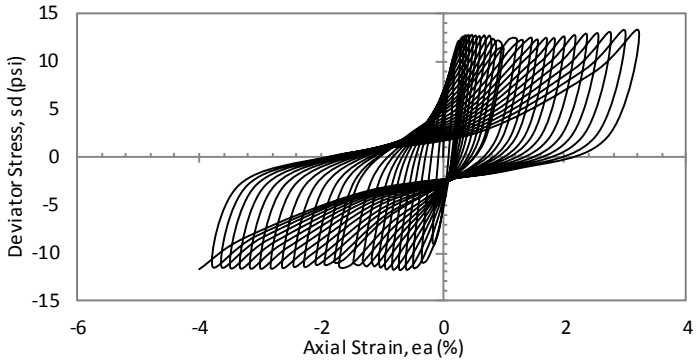

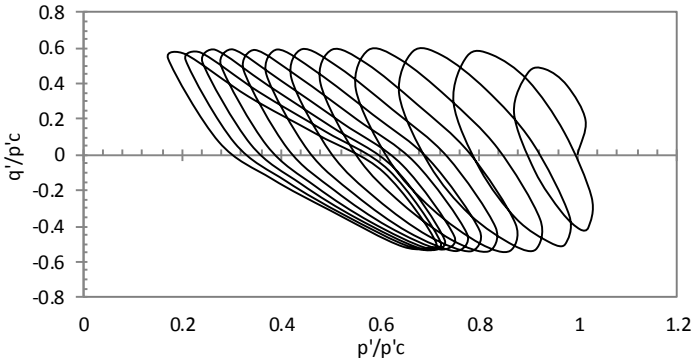

CYCLIC TRIAXIAL TEST DATA

Specimen Name:	TBBLAPST13S4	f (Hz):	1
Test Date:	Jul-05-2011	B-Value (%):	99.0
Diameter (cm):	7.08	G_s:	2.08
Height (cm):	16.80	σ_d (kPa):	165.4
Wet Mass (gr):	1082.43	CSR:	0.28
W_n (%):	28.6	N_L:	11
σ'_c(kPa):	148.1	Depth (ft):	74.5-77
e_0:	0.62	Sampling Date:	Aug-14-2007
γ_{wet} (kN/m^3):	16.2		

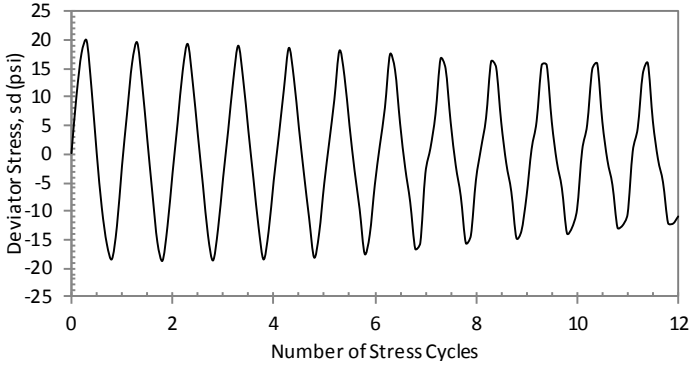

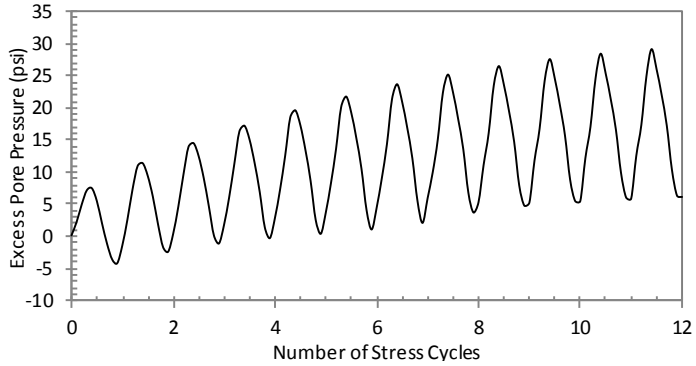

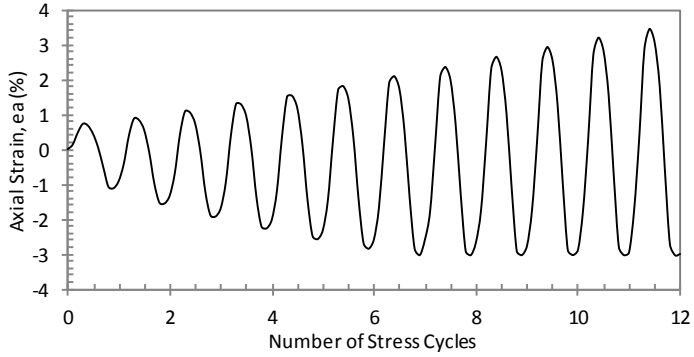

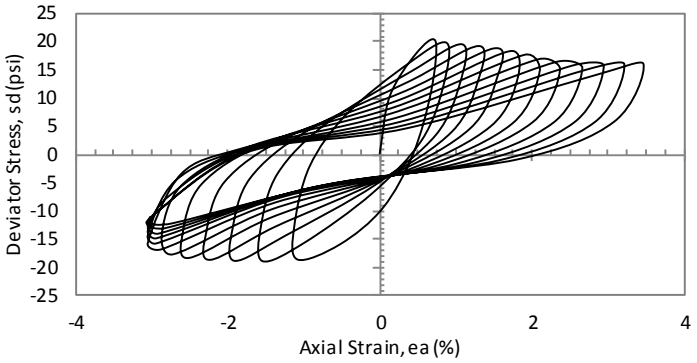

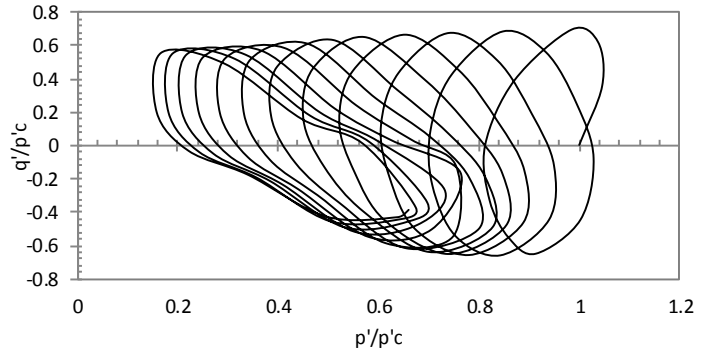

CYCLIC TRIAXIAL TEST DATA

Specimen Name:	TBBLAPST14S3	f (Hz):	1
Test Date:	Apr-18-2011	B-Value (%):	100.0
Diameter (cm):	7.30	G_s:	2.47
Height (cm):	17.40	σ_d (kPa):	223.2
Wet Mass (gr):	1223.06	CSR:	0.29
W_n (%):	34.0	N_L:	11
σ'_c(kPa):	195.7	Depth (ft):	94.5-97
e_0:	0.97	Sampling Date:	Aug-14-2007
γ_{wet} (kN/m^3):	16.5		

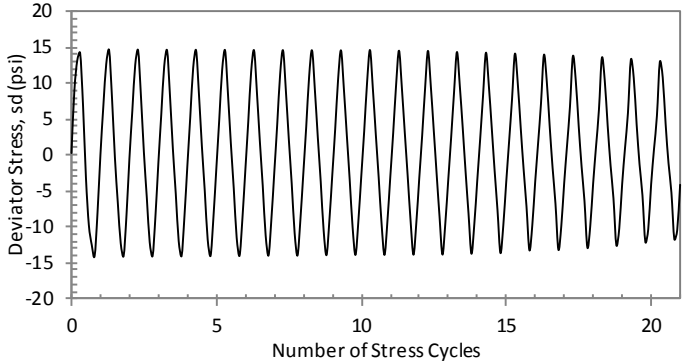

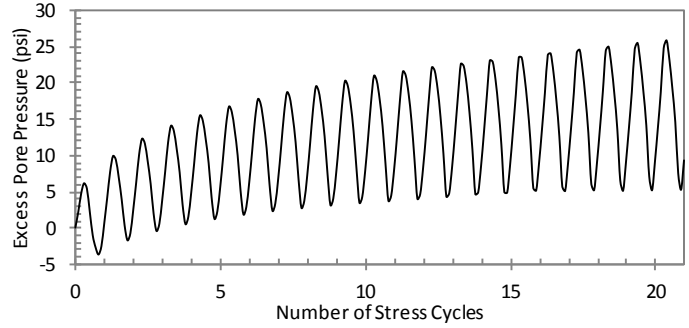

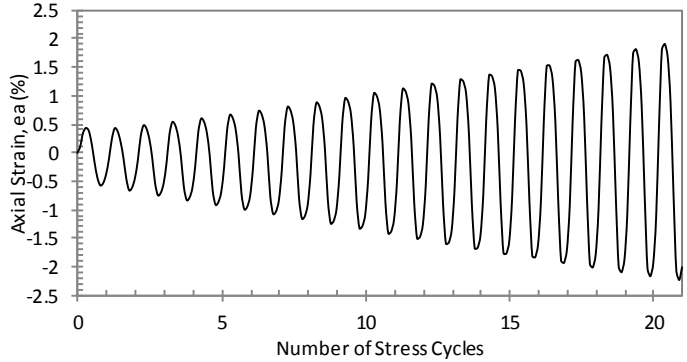

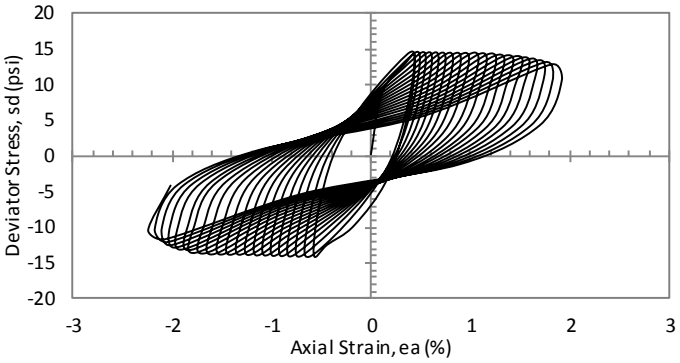

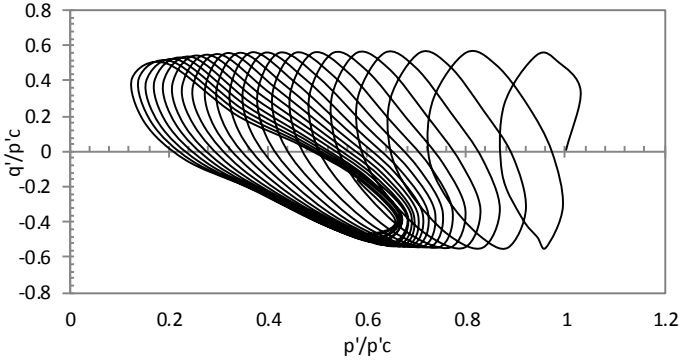

CYCLIC TRIAXIAL TEST DATA

Specimen Name:	TBBLAPST14S4	f (Hz):	1
Test Date:	Apr-21-2011	B-Value (%):	100.0
Diameter (cm):	7.45	G_s:	2.47
Height (cm):	17.10	σ_d (kPa):	187.4
Wet Mass (gr):	1196.1	CSR:	0.26
W_n (%):	34.8	N_L:	20
σ'_c(kPa):	177.1	Depth (ft):	94.5-97
e_0:	1.07	Sampling Date:	Aug-14-2007
γ_{wet} (kN/m^3):	15.7		

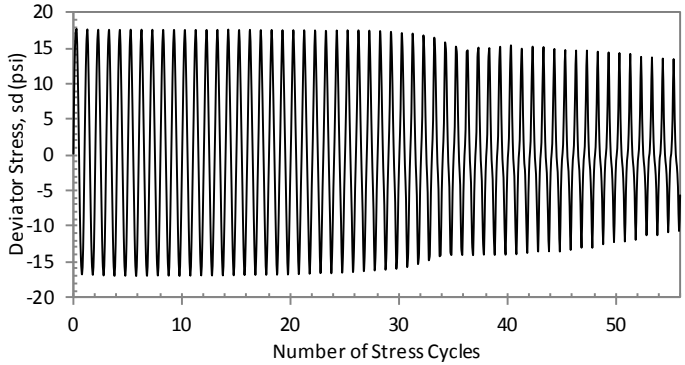

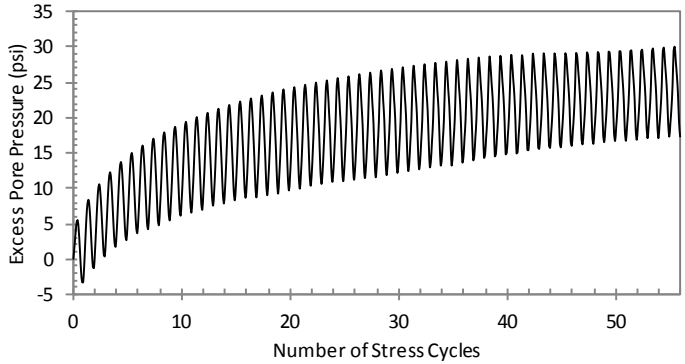

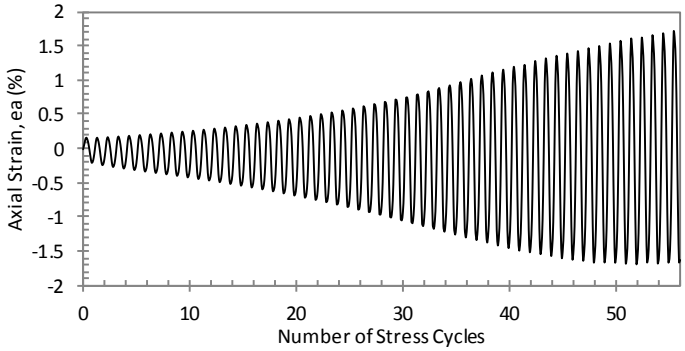

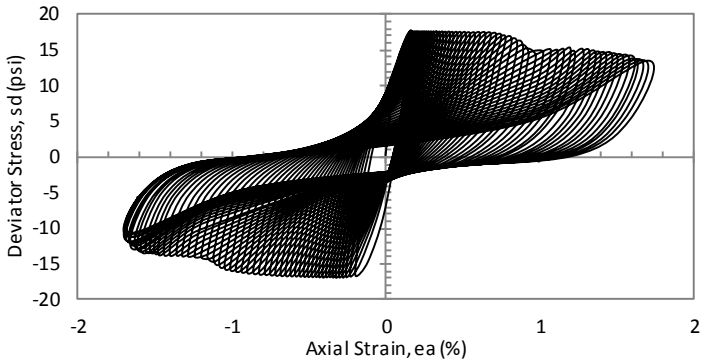

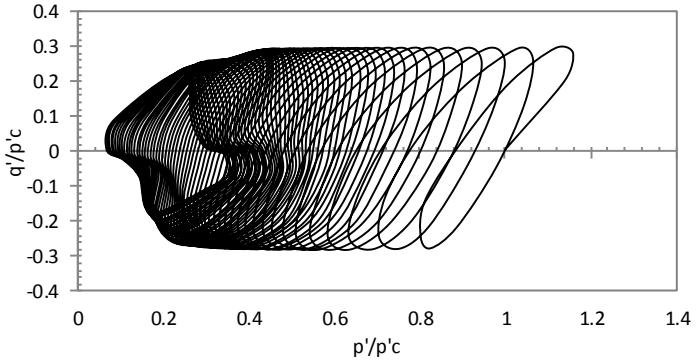

CYCLIC TRIAXIAL TEST DATA

Specimen Name:	TBBLAPST15S1	f (Hz):	1
Test Date:	Feb-28-2011	B-Value (%):	97.7
Diameter (cm):	7.35	G_s:	1.92
Height (cm):	17.40	σ_d (kPa):	199.8
Wet Mass (gr):	1185.8	CSR:	0.24
W_n (%):	30.1	N_L:	55
σ'_c(kPa):	206.0	Depth (ft):	114.5-117
e_0:	0.56	Sampling Date:	Aug-14-2007
γ_{wet} (kN/m^3):	15.8		

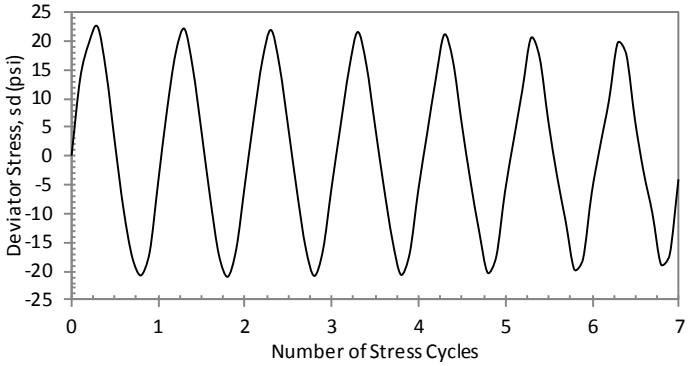

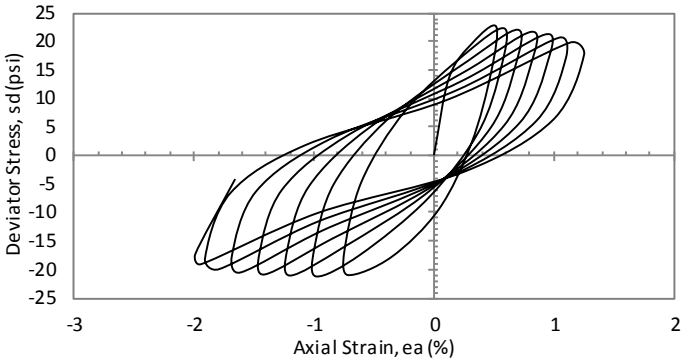

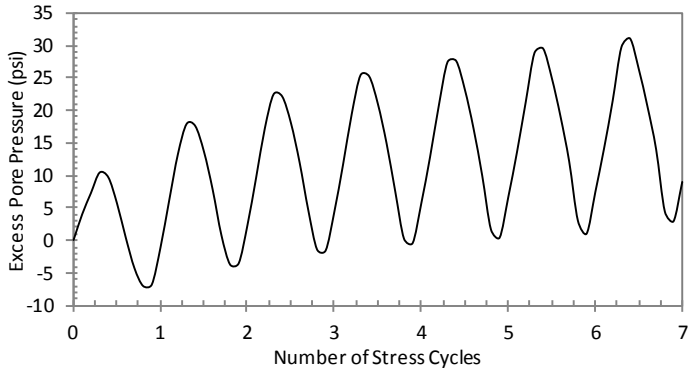

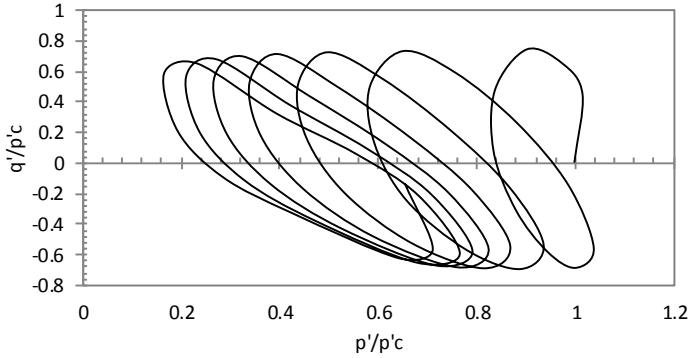

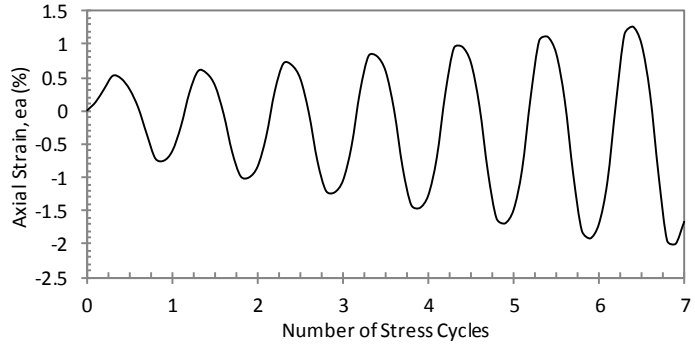

CYCLIC TRIAXIAL TEST DATA

Specimen Name:	TBBLAPST15S2	f (Hz):	1
Test Date:	Mar-06-2011	B-Value (%):	98.7
Diameter (cm):	7.25	G_s:	1.92
Height (cm):	17.50	σ_d (kPa):	286.6
Wet Mass (gr):	1133.35	CSR:	0.34
W_n (%):	32.3	N_L:	6
σ'_c(kPa):	208.1	Depth (ft):	114.5-117
e_0:	0.62	Sampling Date:	Aug-14-2007
γ_{wet} (kN/m^3):	15.4		

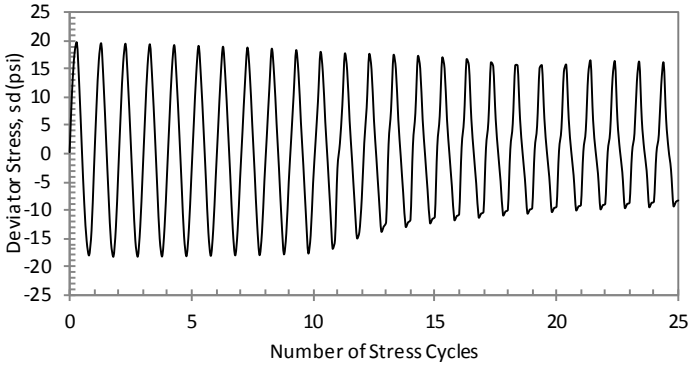

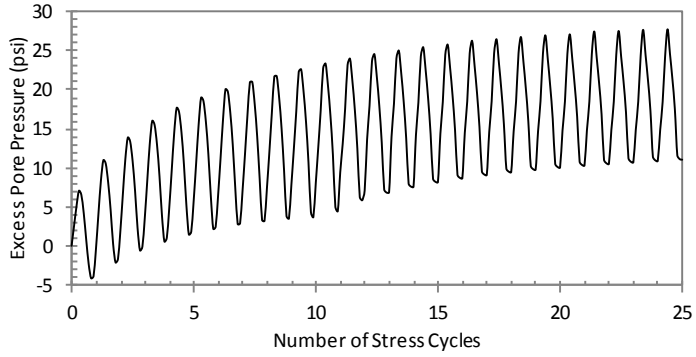

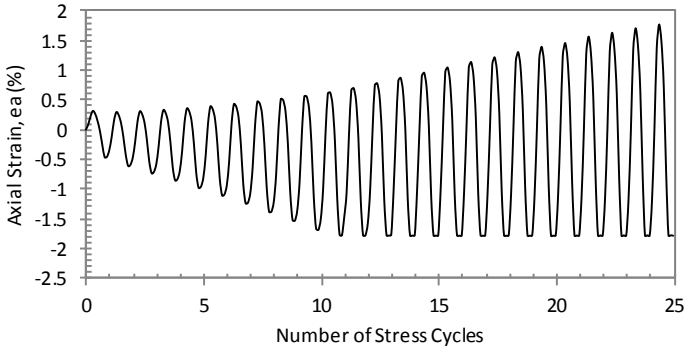

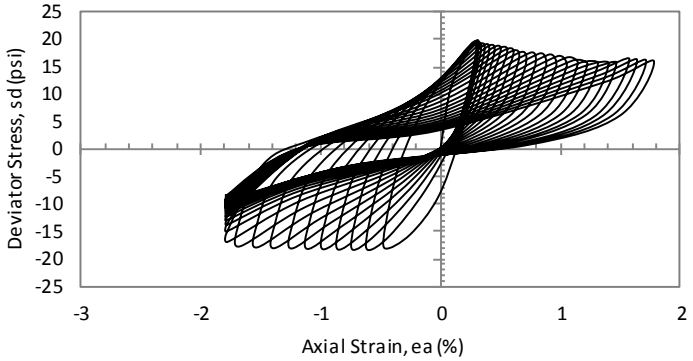

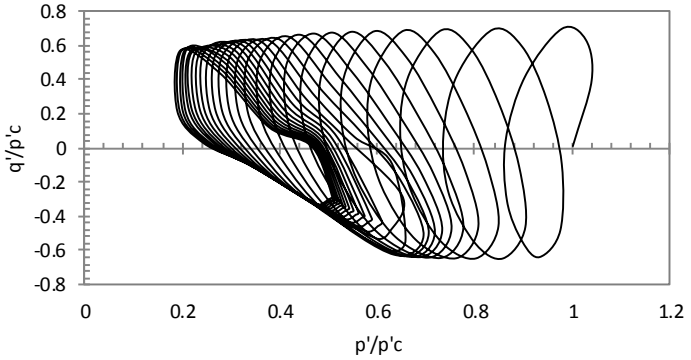

CYCLIC TRIAXIAL TEST DATA

Specimen Name:	TBBLAPST15S3	f (Hz):	1
Test Date:	Mar-10-2011	B-Value (%):	96.0
Diameter (cm):	7.20	G_s:	1.92
Height (cm):	17.30	σ_d (kPa):	215.0
Wet Mass (gr):	1098.17	CSR:	0.28
W_n (%):	31.7	N_L:	24
σ'_c(kPa):	192.9	Depth (ft):	114.5-117
e_0:	0.62	Sampling Date:	Aug-14-2007
γ_{wet} (kN/m^3):	15.3		

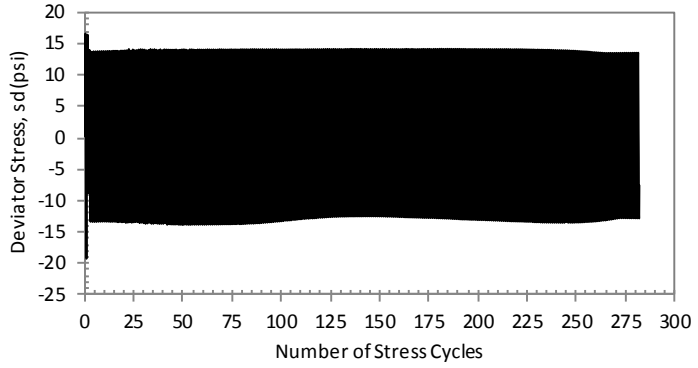

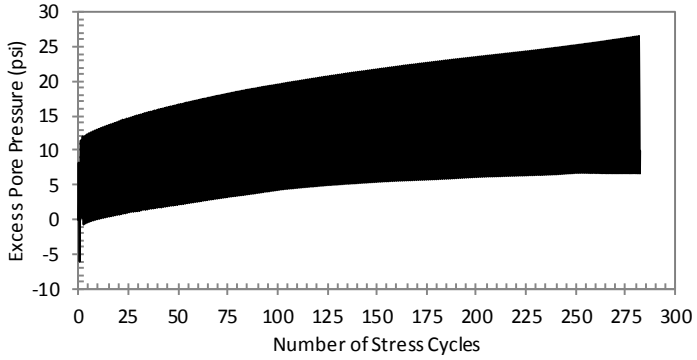

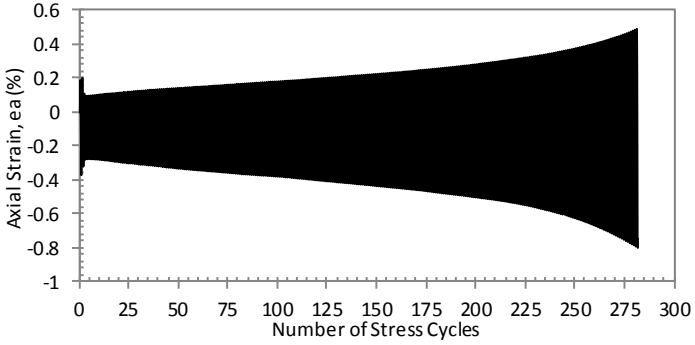

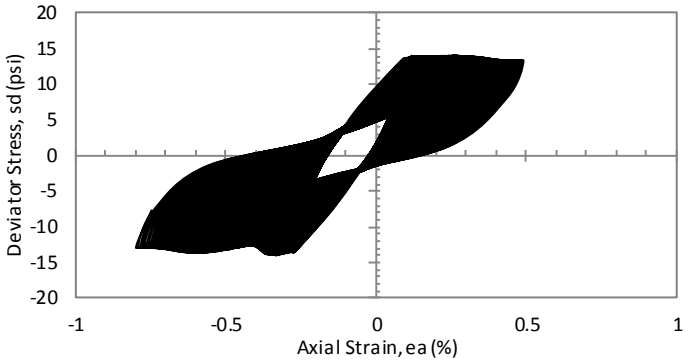

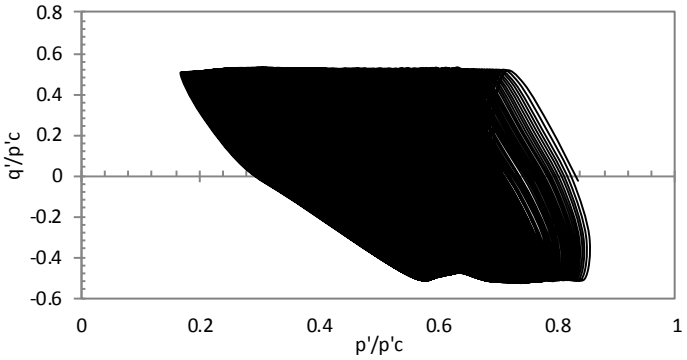

CYCLIC TRIAXIAL TEST DATA

Specimen Name:	TBBLAPST15S4	f (Hz):	1
Test Date:	Mar-15-2011	B-Value (%):	96.6
Diameter (cm):	7.30	G_s:	1.92
Height (cm):	17.20	σ_d (kPa):	181.9
Wet Mass (gr):	1092	CSR:	0.25
W_n (%):	26.8	N_L:	281
σ'_c(kPa):	182.6	Depth (ft):	114.5-117
e_0:	0.61	Sampling Date:	Aug-14-2007
γ_{wet} (kN/m^3):	14.9		

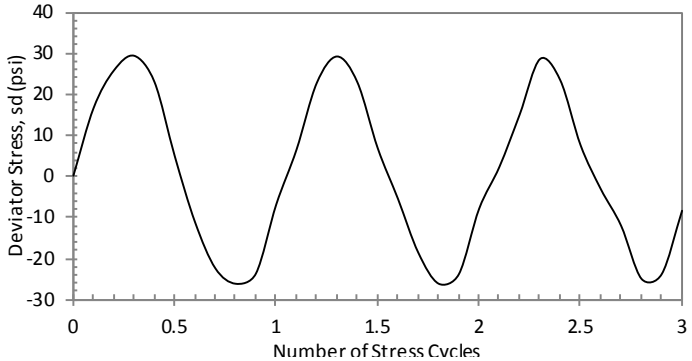

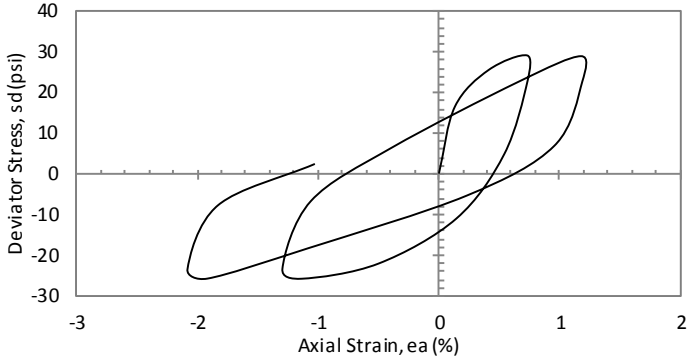

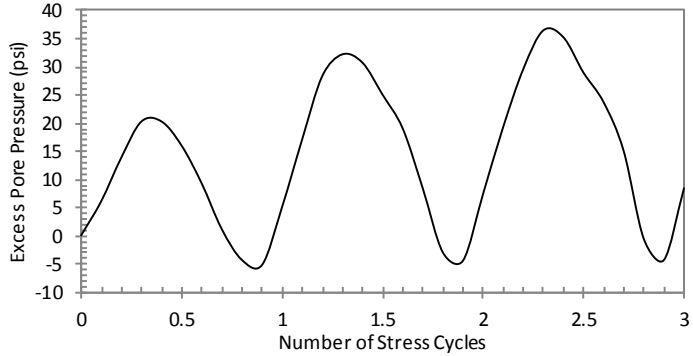

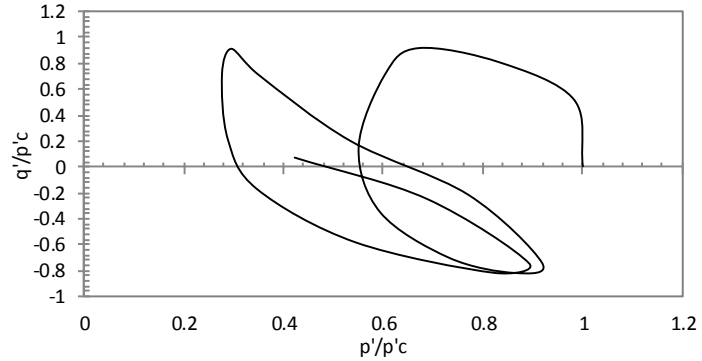

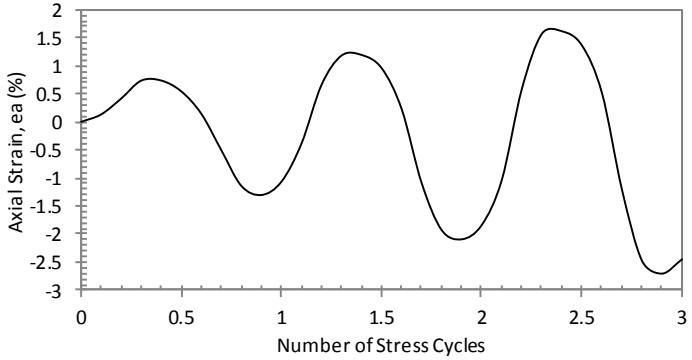

CYCLIC TRIAXIAL TEST DATA

Specimen Name:	TBBLAPST16S1	f (Hz):	1
Test Date:	Feb-11-2011	B-Value (%):	98.8
Diameter (cm):	7.00	G_s:	2.16
Height (cm):	17.00	σ_d (kPa):	379.0
Wet Mass (gr):	970.2	CSR:	0.43
W_n (%):	34.4	N_L:	2
σ'_c(kPa):	219.1	Depth (ft):	134.5-137
e_0:	0.96	Sampling Date:	Aug-14-2007
γ_{wet} (kN/m^3):	14.5		

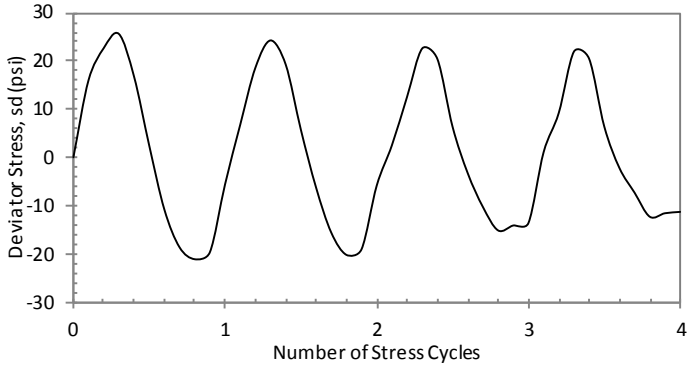

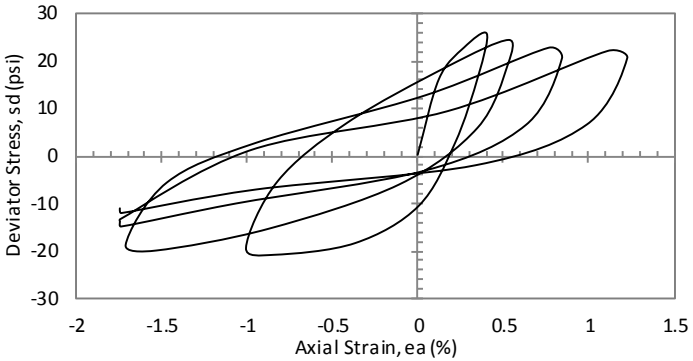

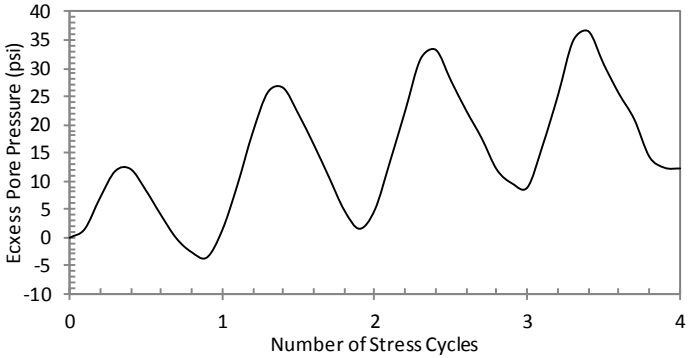

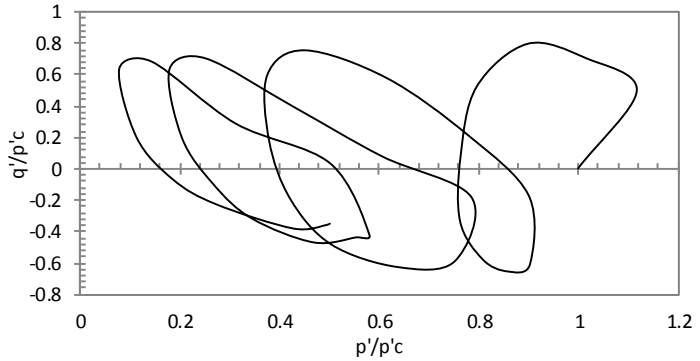

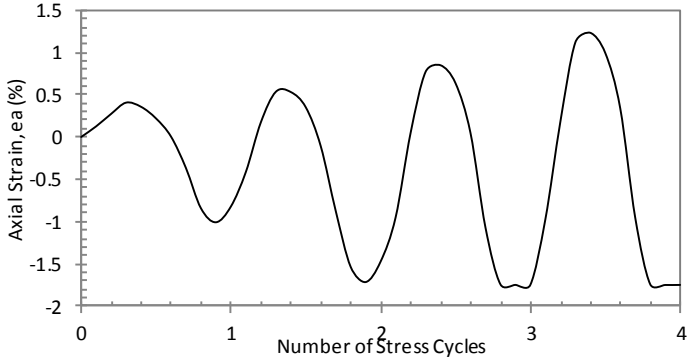

CYCLIC TRIAXIAL TEST DATA

Specimen Name:	TBBLAPST16S2	f (Hz):	1
Test Date:	Feb-14-2011	B-Value (%):	96.2
Diameter (cm):	7.27	G_s:	2.16
Height (cm):	17.30	σ_d (kPa):	303.2
Wet Mass (gr):	961.2	CSR:	0.34
W_n (%):	37.7	N_L:	3
σ'_c(kPa):	220.5	Depth (ft):	134.5-137
e_0:	1.23	Sampling Date:	Aug-14-2007
γ_{wet} (kN/m^3):	13.1		

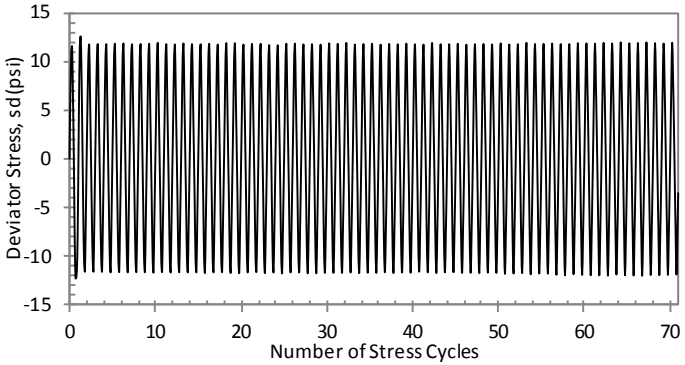

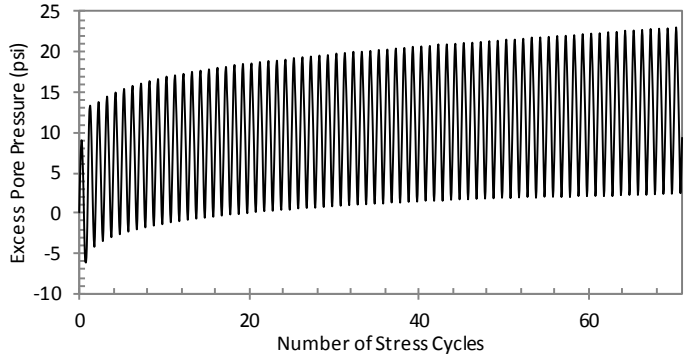

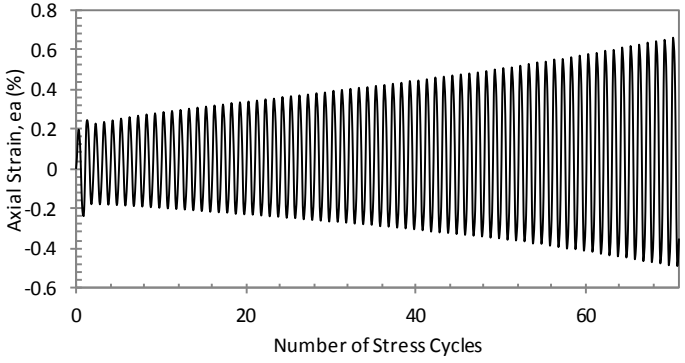

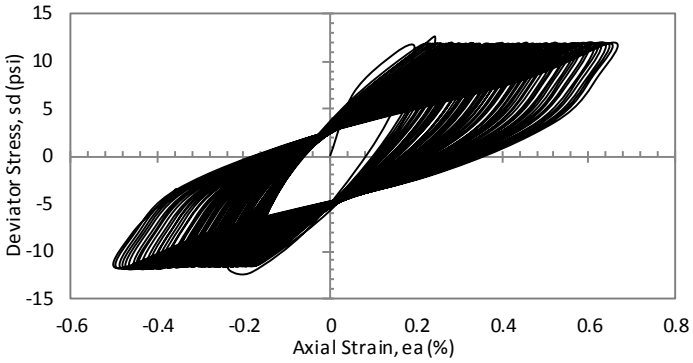

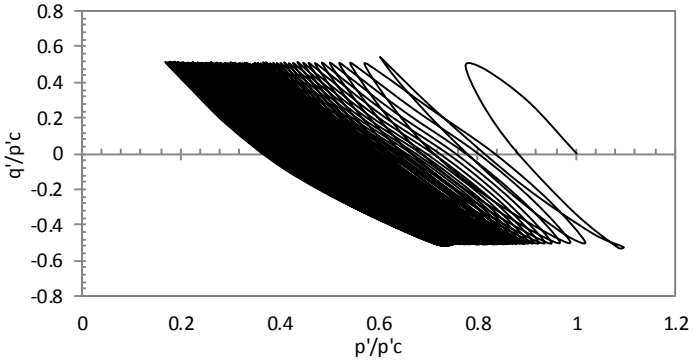

CYCLIC TRIAXIAL TEST DATA

Specimen Name:	TBBLDPST1S2	f (Hz):	1
Test Date:	Sep-16-2011	B-Value (%):	100.0
Diameter (cm):	7.26	G_s:	1.95
Height (cm):	17.10	σ_d (kPa):	165.4
Wet Mass (gr):	1154.9	CSR:	0.26
W_n (%):	29.9	N_L:	70
σ'_c(kPa):	158.5	Depth (ft):	84-86.5
e_0:	0.55	Sampling Date:	Aug-08-2007
γ_{wet} (kN/m^3):	16.0		

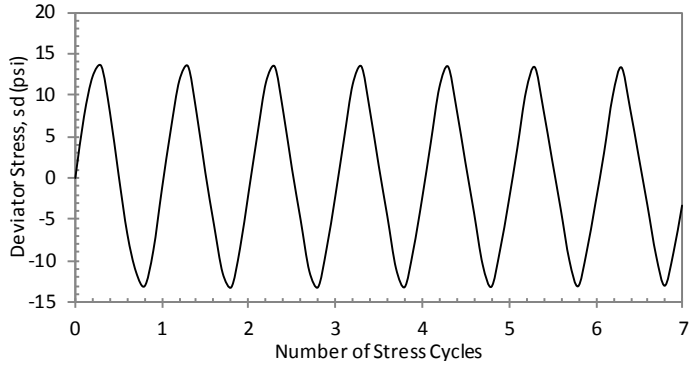

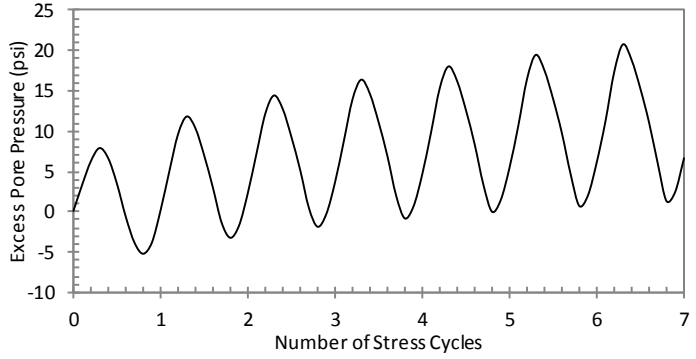

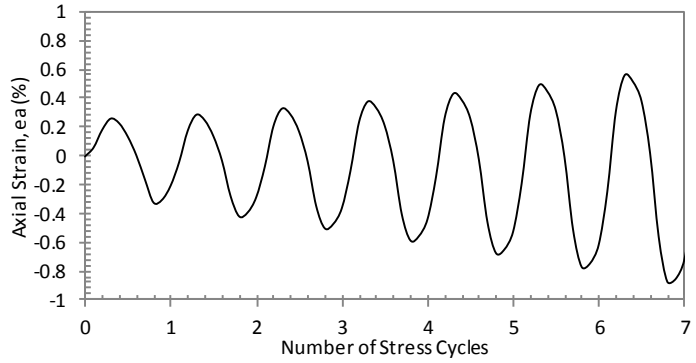

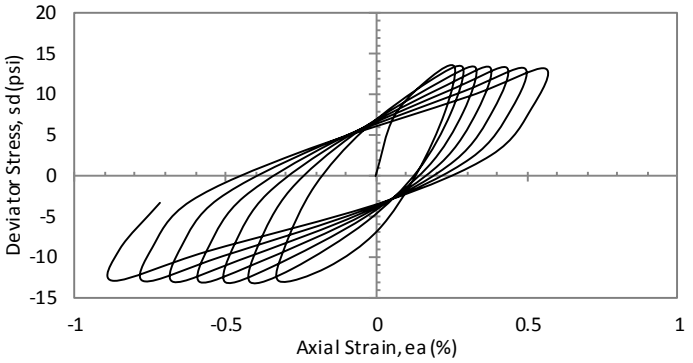

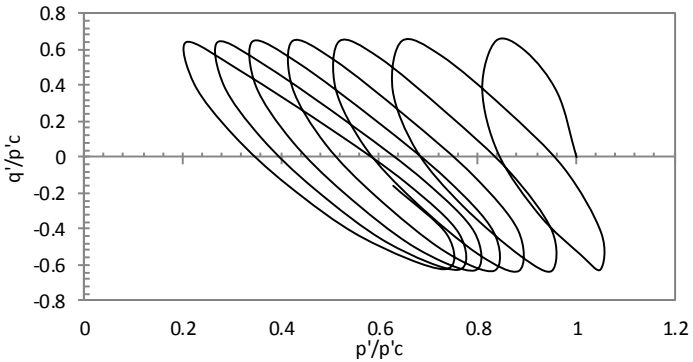

CYCLIC TRIAXIAL TEST DATA

Specimen Name:	TBBLDPST1S3	f (Hz):	1
Test Date:	Sep-24-2011	B-Value (%):	100.0
Diameter (cm):	7.36	G_s:	1.95
Height (cm):	17.35	σ_d (kPa):	181.9
Wet Mass (gr):	1147.2	CSR:	0.32
W_n (%):	25.7	N_L:	6
σ'_c(kPa):	141.9	Depth (ft):	84-86.5
e_0:	0.58	Sampling Date:	Aug-08-2007
γ_{wet} (kN/m^3):	15.2		

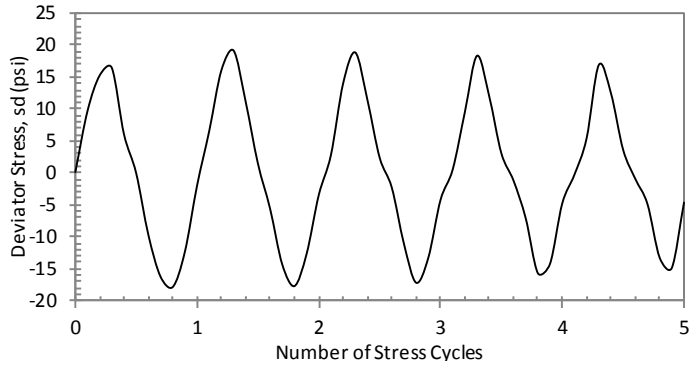

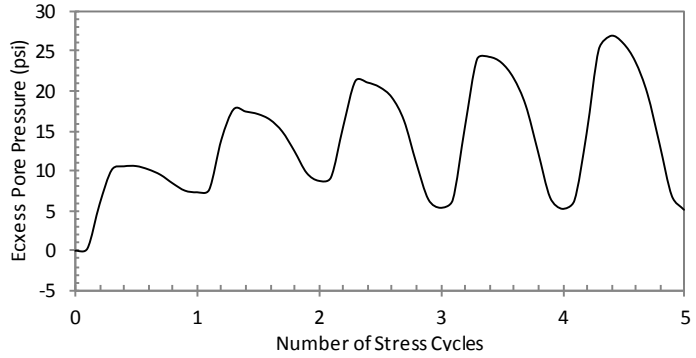

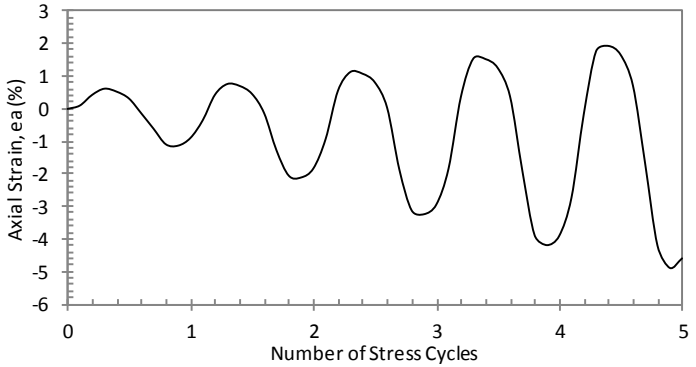

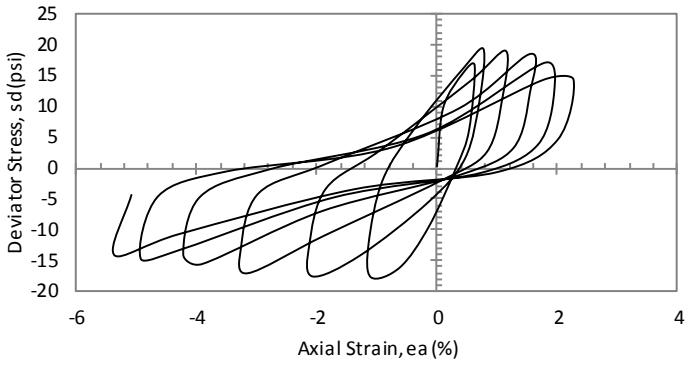

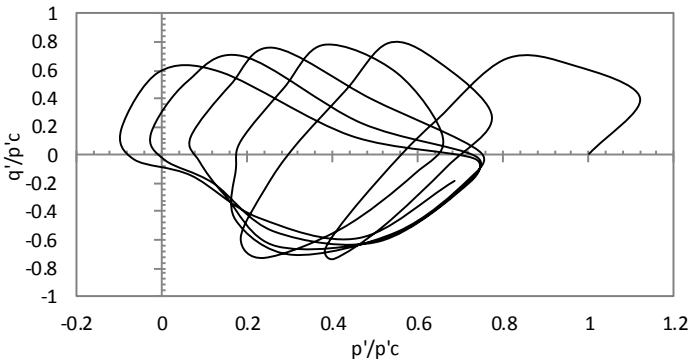

CYCLIC TRIAXIAL TEST DATA

Specimen Name:	TBBLDPST2S2	f (Hz):	1
Test Date:	May-02-2011	B-Value (%):	101.2
Diameter (cm):	7.24	G_s:	2.50
Height (cm):	16.40	σ_d (kPa):	237.0
Wet Mass (gr):	1028.1	CSR:	0.36
W_n (%):	19.8	N_L:	4
σ'_c(kPa):	166.7	Depth (ft):	104-106.5
e_0:	0.97	Sampling Date:	Aug-08-2007
γ_{wet} (kN/m^3):	14.9		

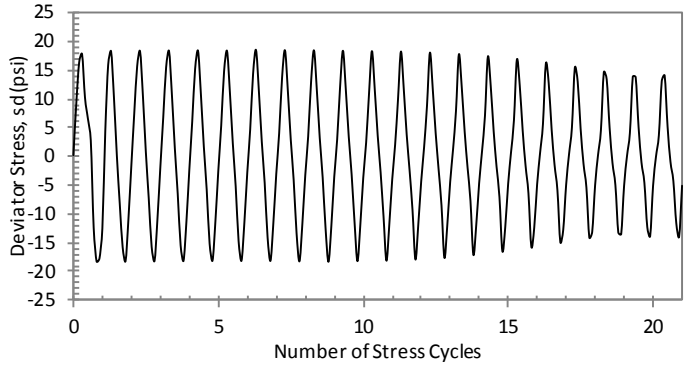

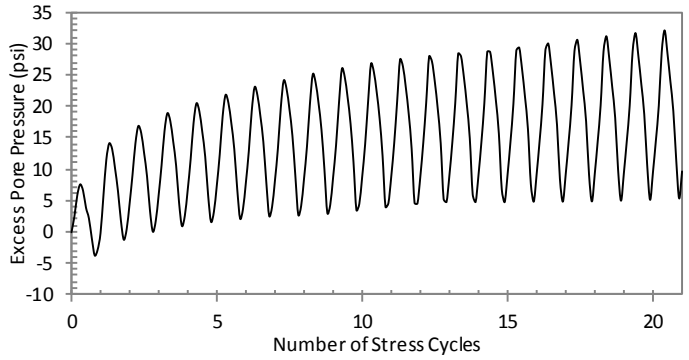

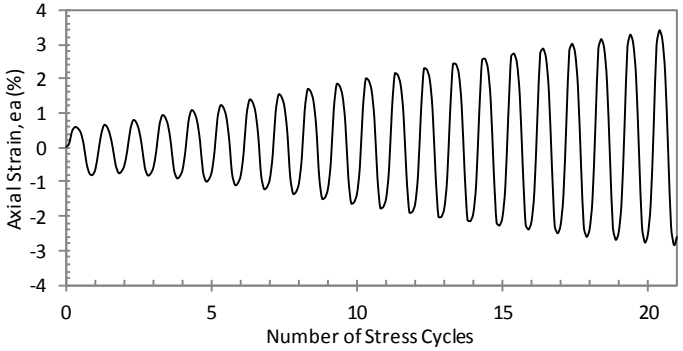

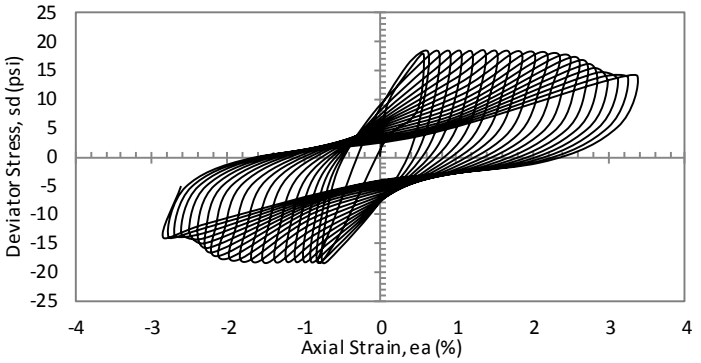

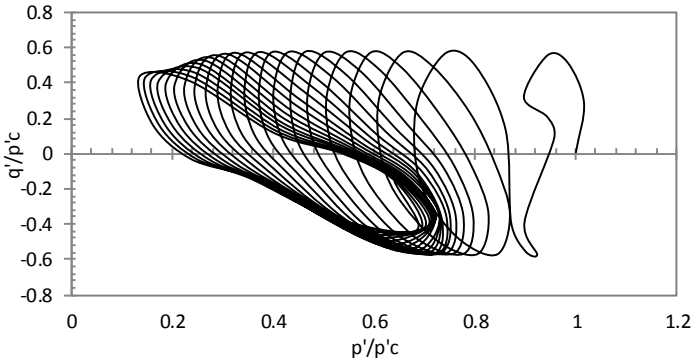

CYCLIC TRIAXIAL TEST DATA

Specimen Name:	TBBLDPST2S3	f (Hz):	1
Test Date:	May-05-2011	B-Value (%):	100.0
Diameter (cm):	7.29	G_s:	2.50
Height (cm):	17.20	σ_d (kPa):	234.3
Wet Mass (gr):	1210.3	CSR:	0.27
W_n (%):	33.0	N_L:	20
σ'_c(kPa):	219.8	Depth (ft):	104-106.5
e_0:	0.97	Sampling Date:	Aug-08-2007
γ_{wet} (kN/m^3):	16.5		

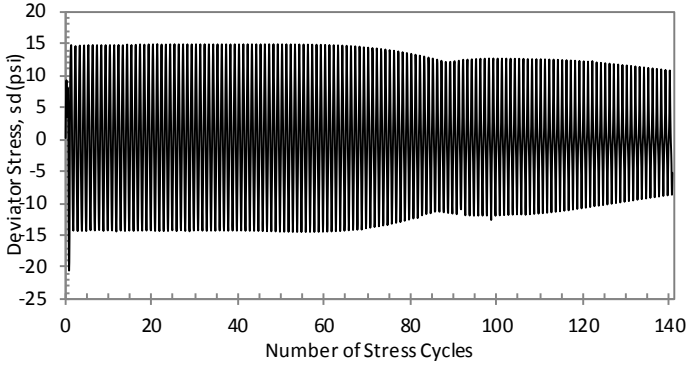

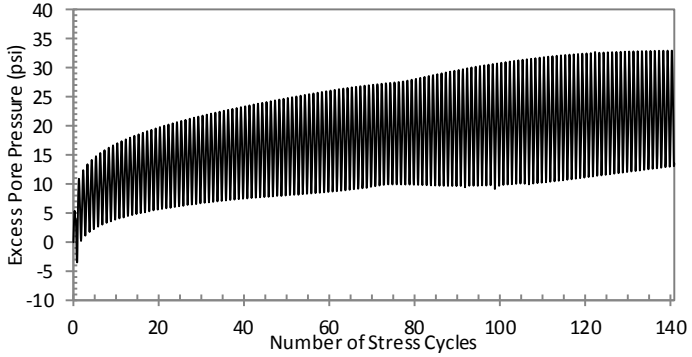

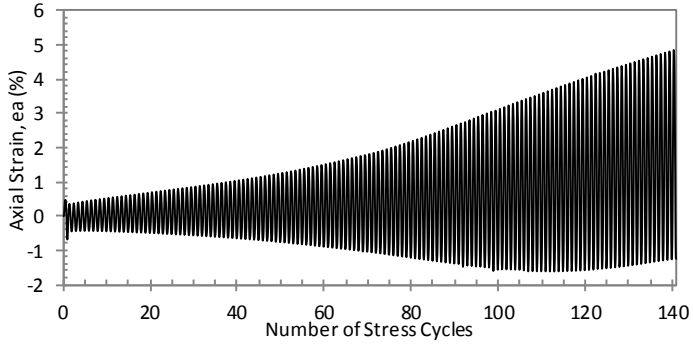

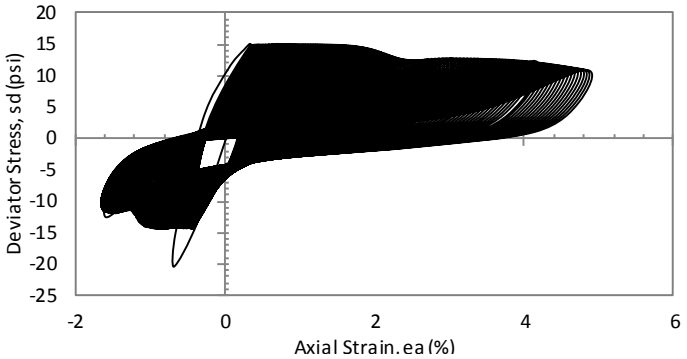

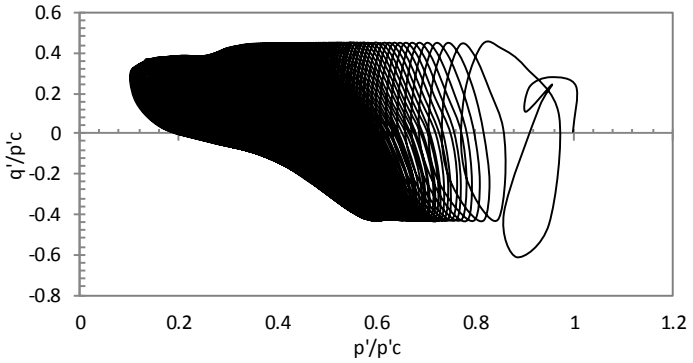

CYCLIC TRIAXIAL TEST DATA

Specimen Name:	TBBLDPST2S4	f (Hz):	1
Test Date:	May-12-2011	B-Value (%):	98.8
Diameter (cm):	7.17	G_s:	2.50
Height (cm):	17.40	σ_d (kPa):	179.1
Wet Mass (gr):	1207.0	CSR:	0.20
W_n (%):	30.1	N_L:	140
σ'_c(kPa):	230.1	Depth (ft):	104-106.5
e_0:	0.89	Sampling Date:	Aug-08-2007
γ_{wet} (kN/m^3):	16.8		

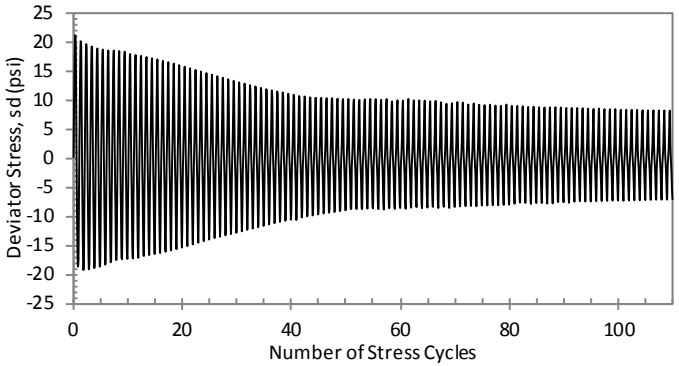

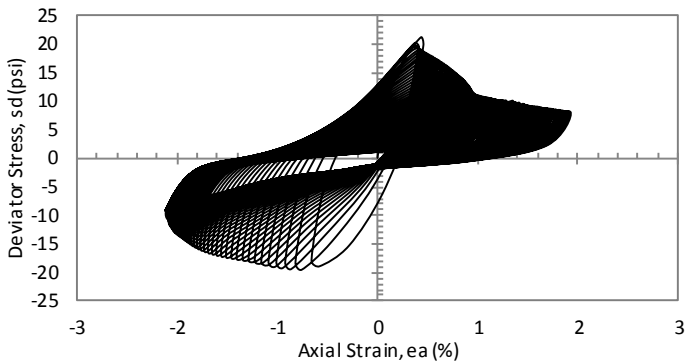

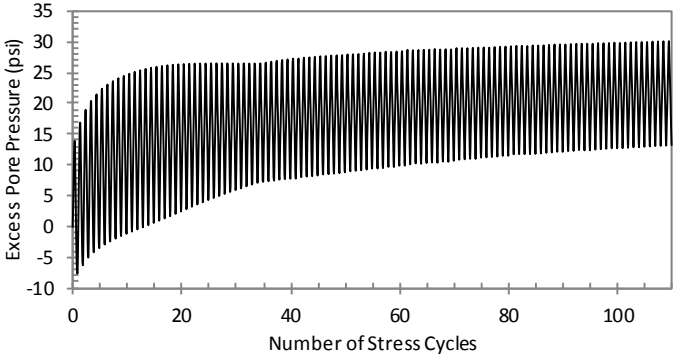

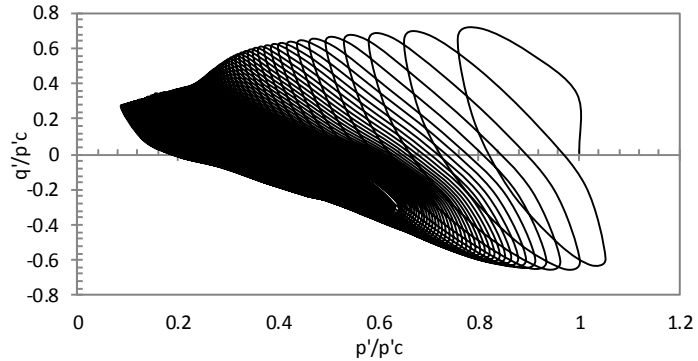

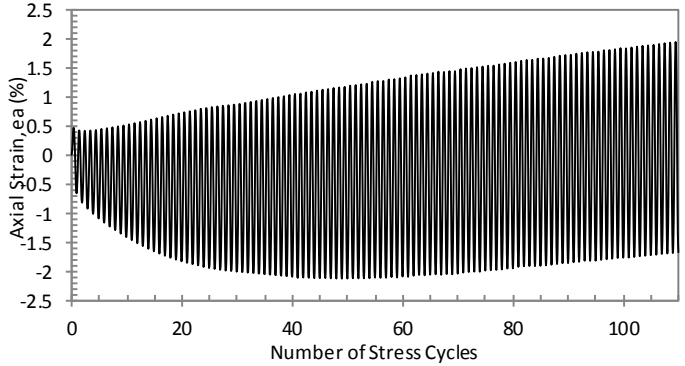

CYCLIC TRIAXIAL TEST DATA

Specimen Name:	TBBLDPST3S2	f (Hz):	1
Test Date:	Jan-05-2011	B-Value (%):	100.0
Diameter (cm):	7.36	G_s:	2.09
Height (cm):	16.50	σ_d (kPa):	137.8
Wet Mass (gr):	1151.3	CSR:	0.17
W_n (%):	35.3	N_L:	109
σ'_c(kPa):	206.7	Depth (ft):	124-126.5
e_0:	0.72	Sampling Date:	Aug-08-2007
γ_{wet} (kN/m^3):	16.1		

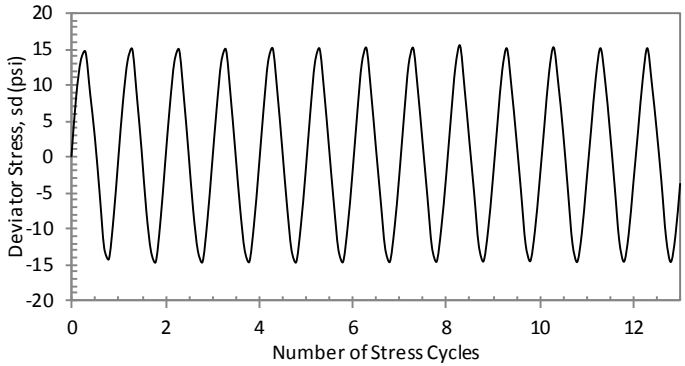

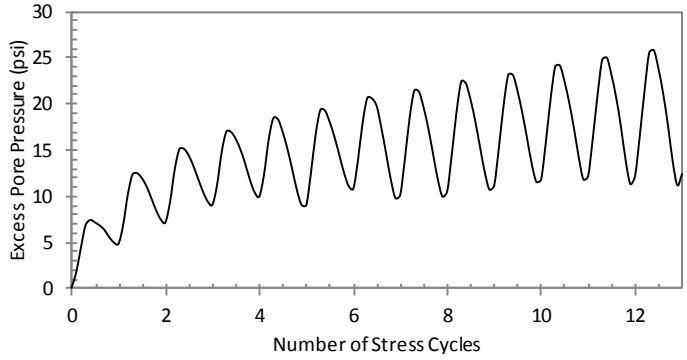

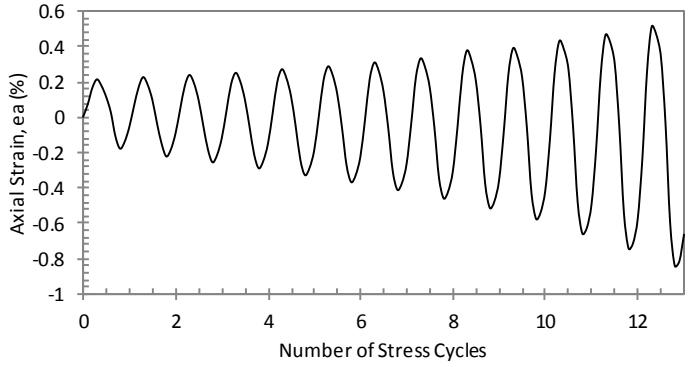

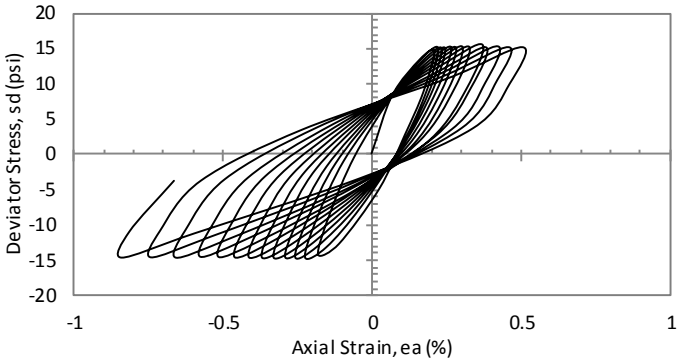

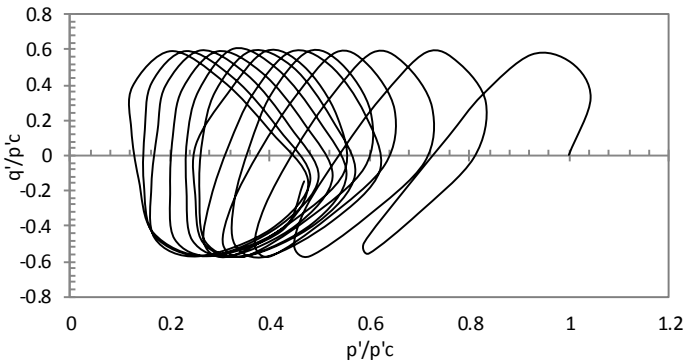

CYCLIC TRIAXIAL TEST DATA

Specimen Name:	TBBLDPST4S1	f (Hz):	1
Test Date:	Jul-09-2011	B-Value (%):	97.9
Diameter (cm):	7.23	G_s:	1.89
Height (cm):	17.40	σ_d (kPa):	206.7
Wet Mass (gr):	995.6	CSR:	0.29
W_n (%):	26.9	N_L:	12
σ'_c(kPa):	177.1	Depth (ft):	144-146.5
e_0:	0.72	Sampling Date:	Aug-08-2007
γ_{wet} (kN/m^3):	13.7		

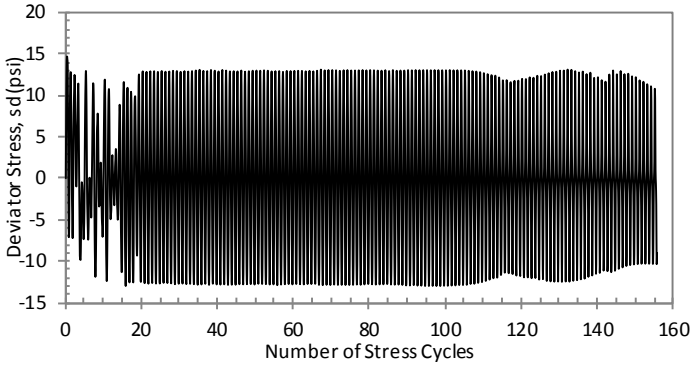

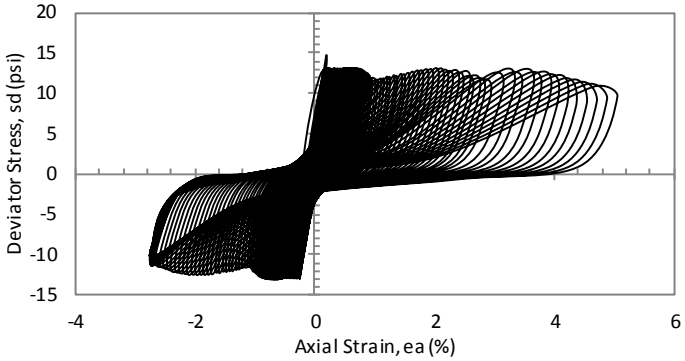

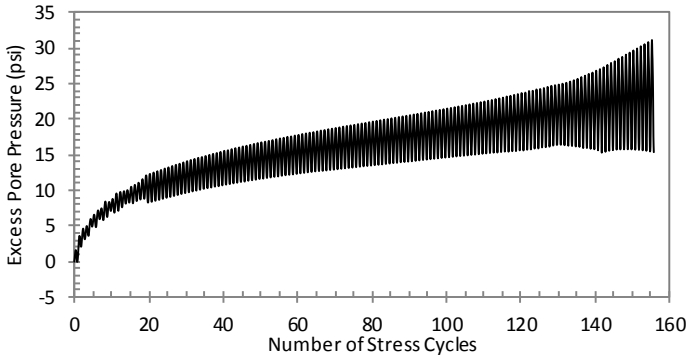

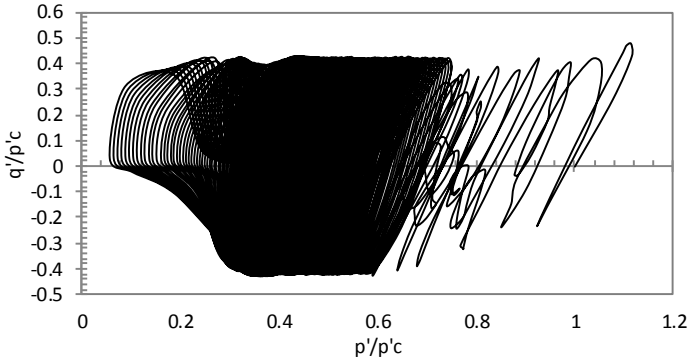

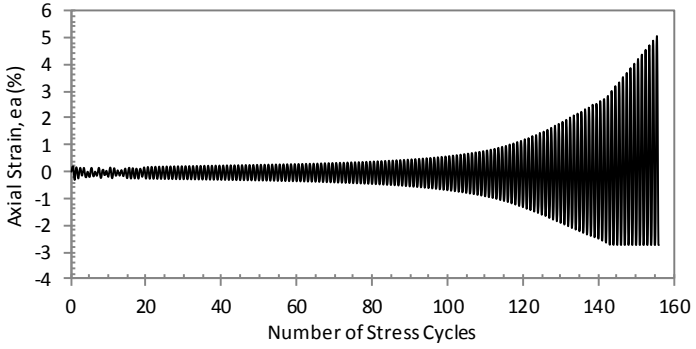

CYCLIC TRIAXIAL TEST DATA

Specimen Name:	TBBLDPST4S2	f (Hz):	1
Test Date:	Jul-24-2011	B-Value (%):	97.8
Diameter (cm):	7.28	G_s:	1.89
Height (cm):	17.20	σ_d (kPa):	179.1
Wet Mass (gr):	1063.3	CSR:	0.21
W_n (%):	35.3	N_L:	155
σ'_c(kPa):	212.2	Depth (ft):	144-146.5
e_0:	0.72	Sampling Date:	Aug-08-2007
γ_{wet} (kN/m^3):	14.6		

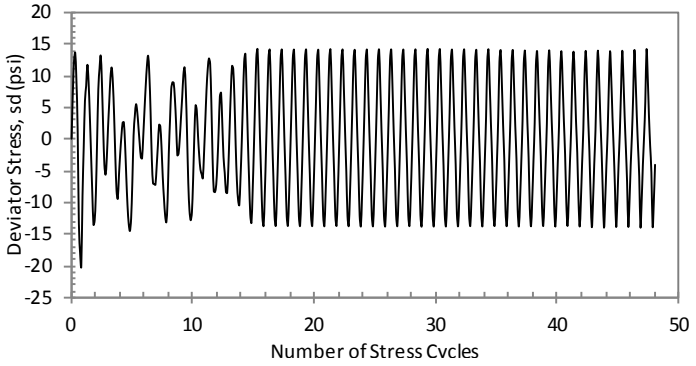

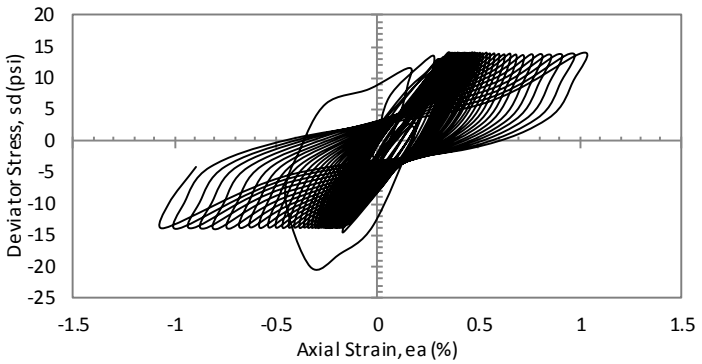

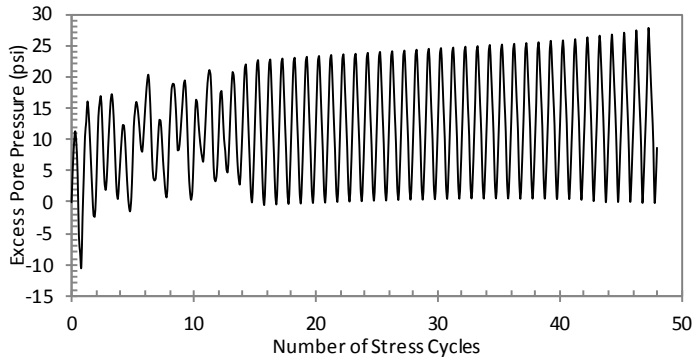

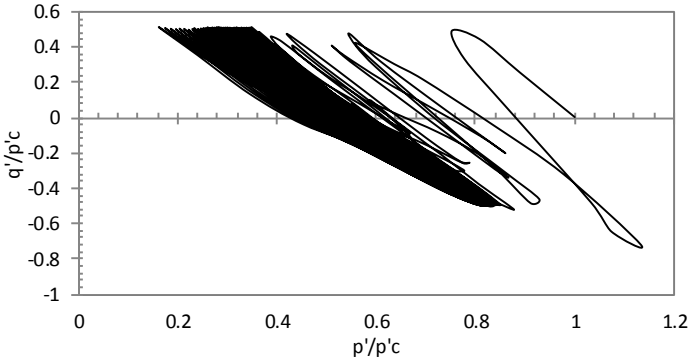

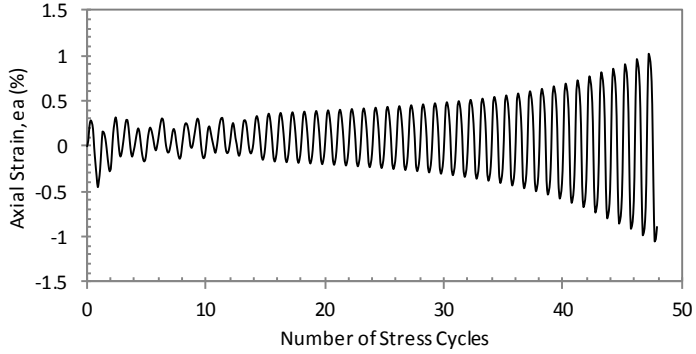

CYCLIC TRIAXIAL TEST DATA

Specimen Name:	TBBLDPST4S3	f (Hz):	1
Test Date:	Aug-13-2011	B-Value (%):	97.8
Diameter (cm):	7.27	G_s:	1.89
Height (cm):	17.11	σ_d (kPa):	192.9
Wet Mass (gr):	1020.8	CSR:	0.25
W_n (%):	35.1	N_L:	47
σ'_c(kPa):	190.2	Depth (ft):	144-146.5
e_0:	0.78	Sampling Date:	Aug-08-2007
γ_{wet} (kN/m^3):	14.1		

Appendix A.2

A.2 Post-cyclic Static Triaxial Tests

In this section, a summary of the results of static compression triaxial testing on each of the samples following the cyclic triaxial tests are presented.

POST CYCLIC UNDRAINED STATIC TRIAXIAL TEST
TAFLAPST1S1

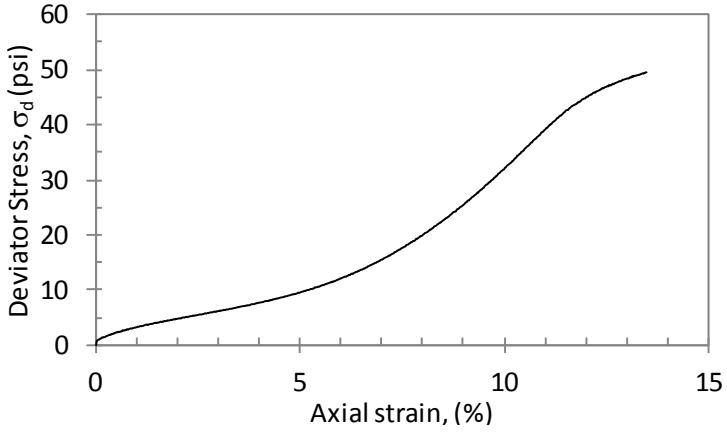

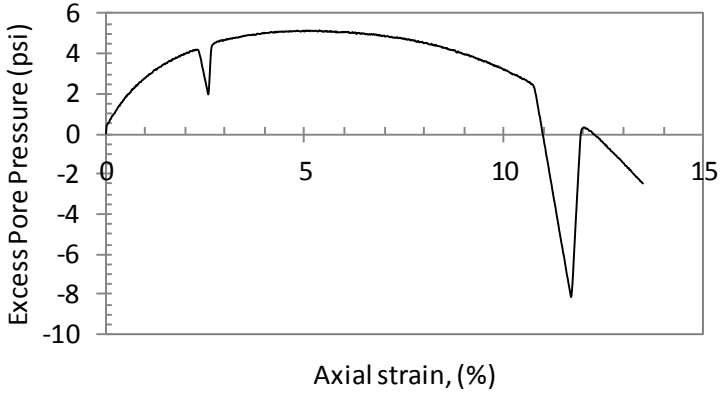

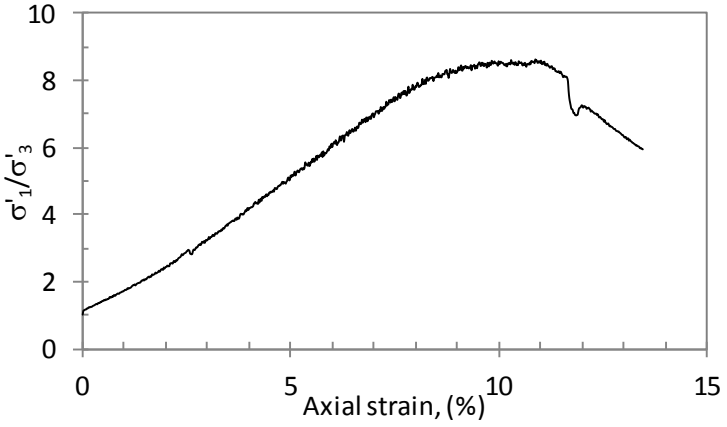

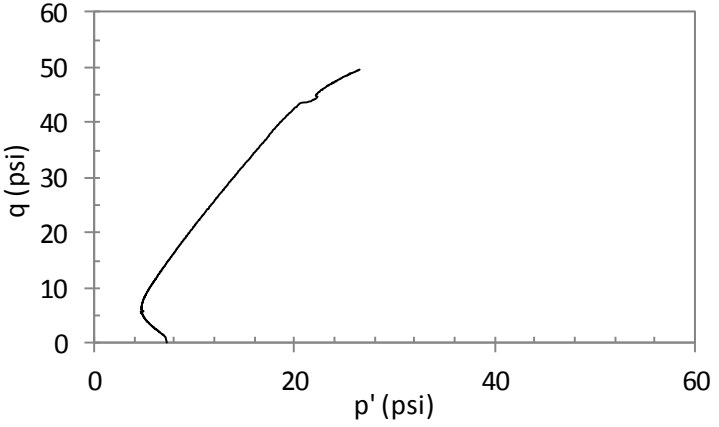

POST CYCLIC UNDRAINED STATIC TRIAXIAL TEST

TAFLBPST1S1

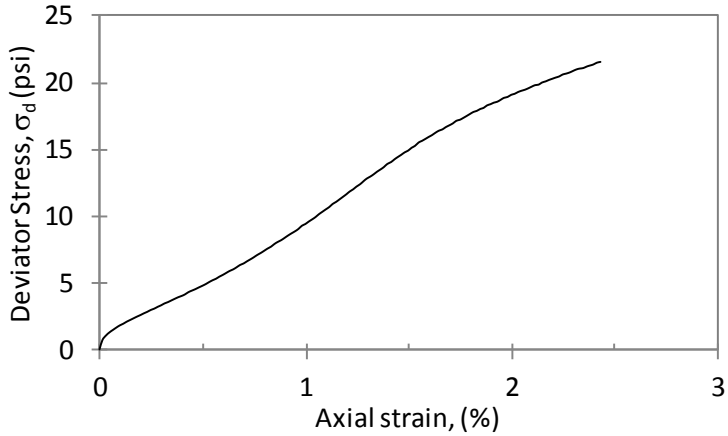

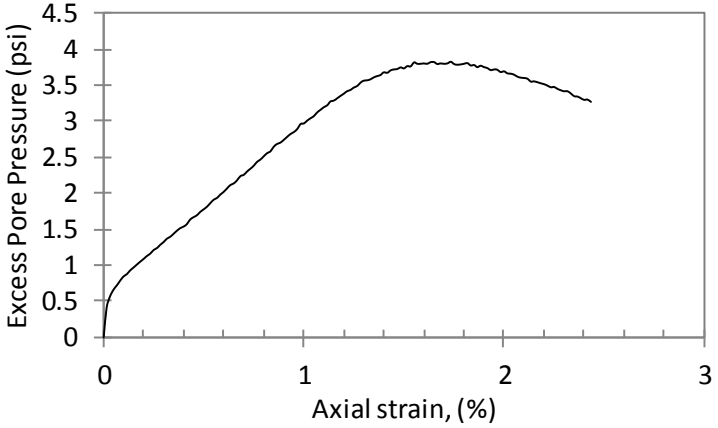

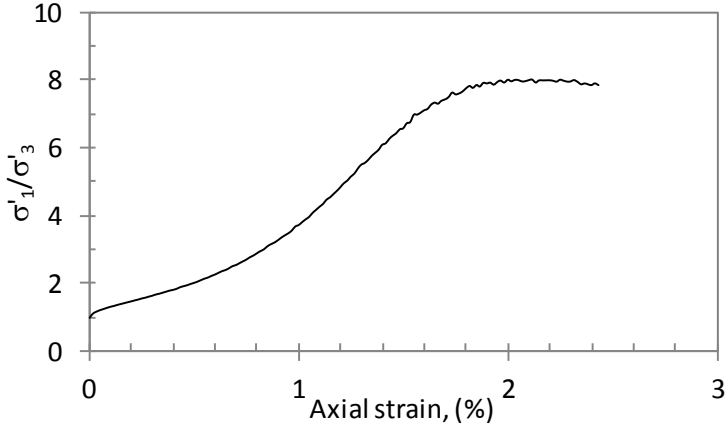

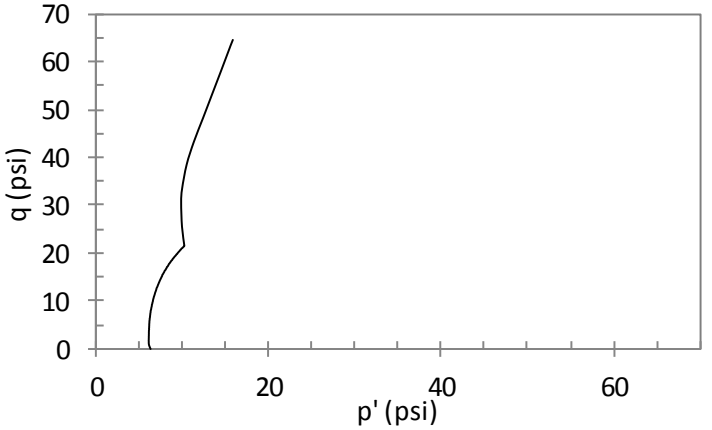

POST CYCLIC UNDRAINED STATIC TRIAXIAL TEST
TAFLBPST1S2

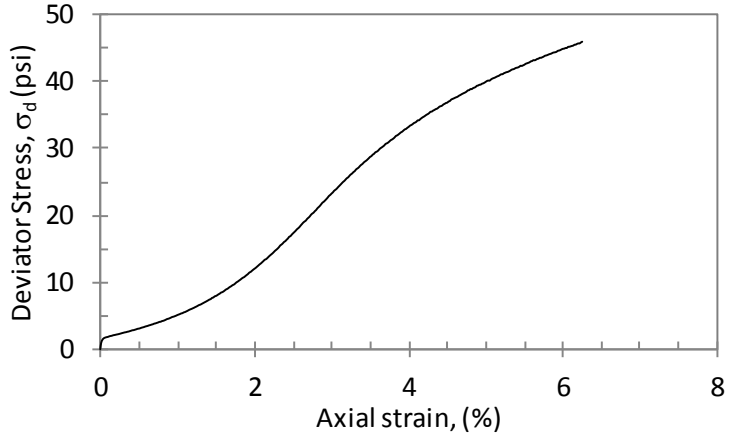

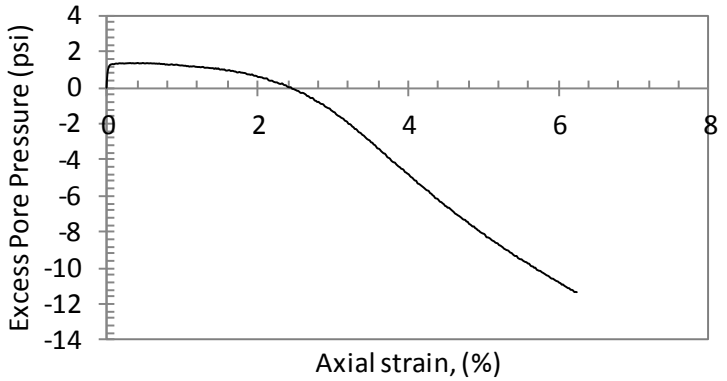

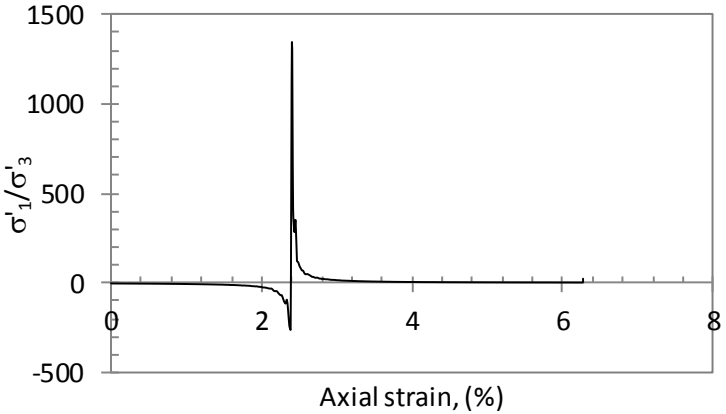

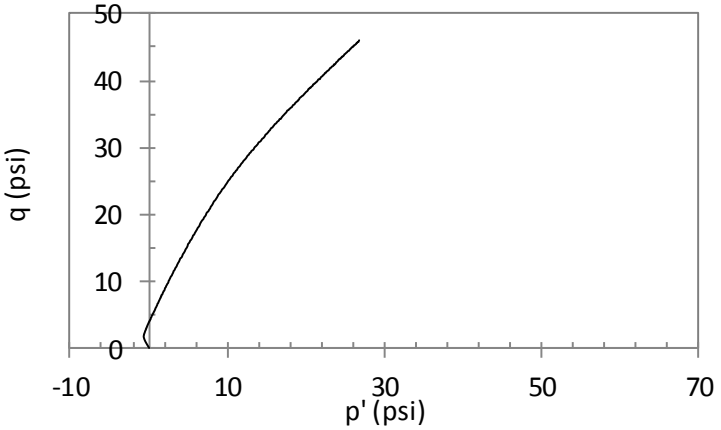

POST CYCLIC UNDRAINED STATIC TRIAXIAL TEST
TAFLBPST2S1

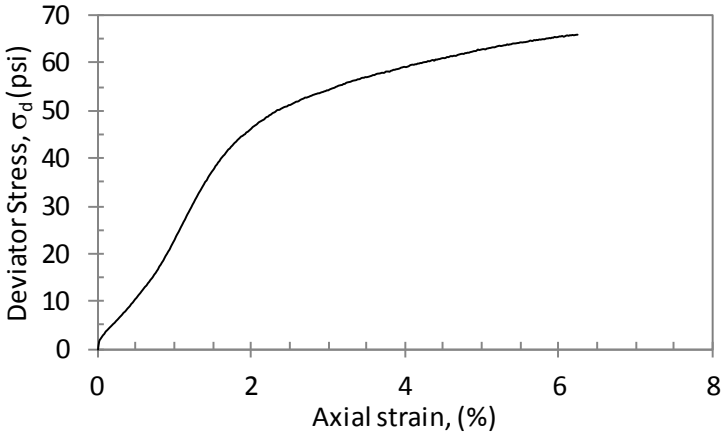

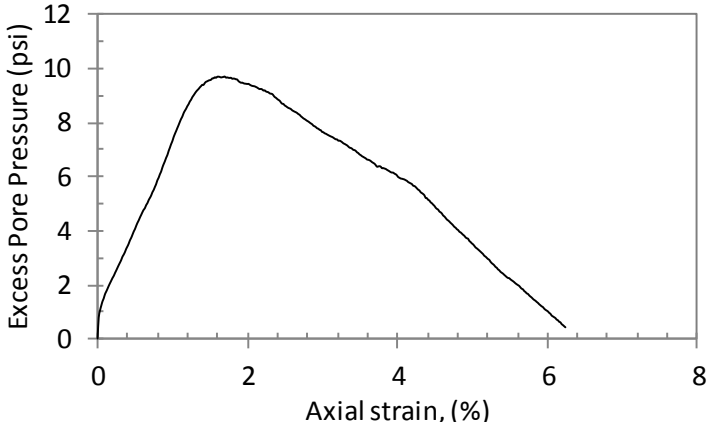

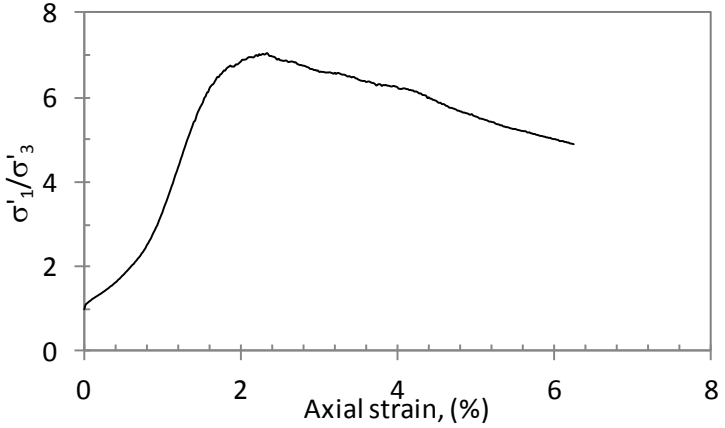

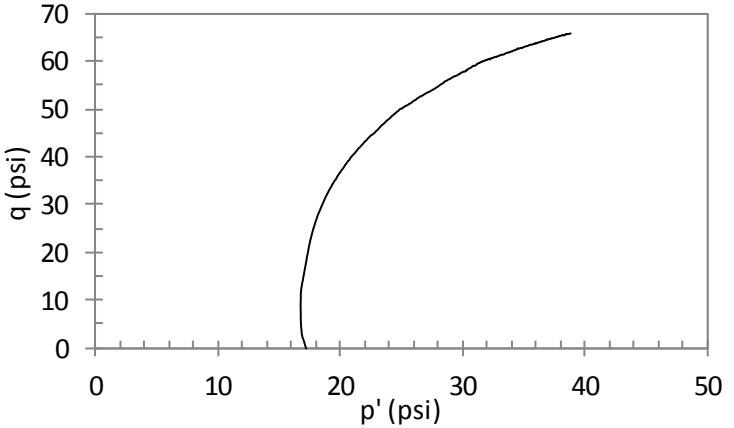

POST CYCLIC UNDRAINED STATIC TRIAXIAL TEST
TAFLBPST2S2

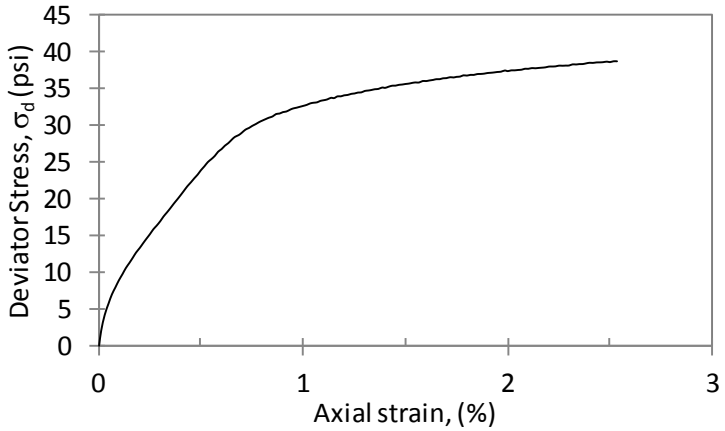

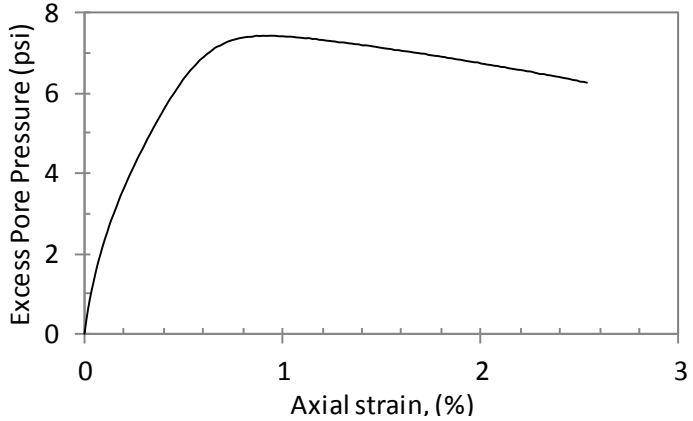

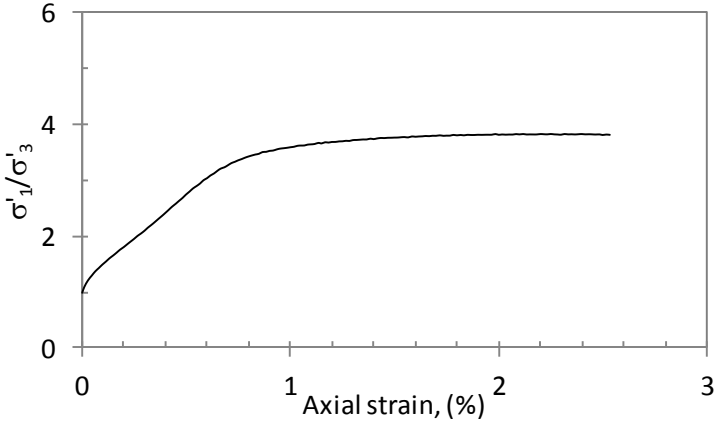

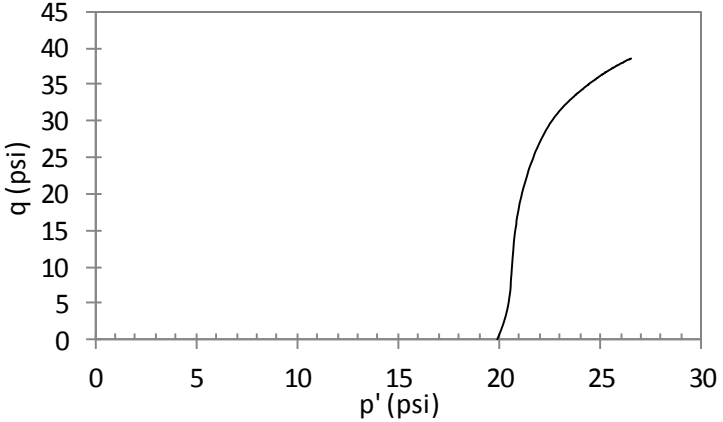

POST CYCLIC UNDRAINED STATIC TRIAXIAL TEST

TAFLBPST3S2

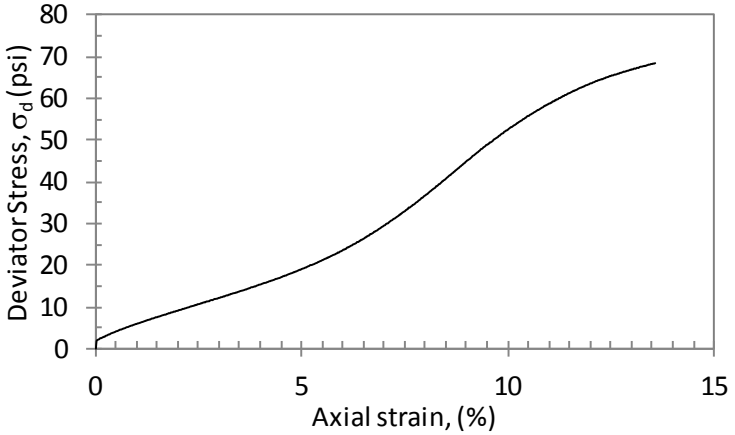

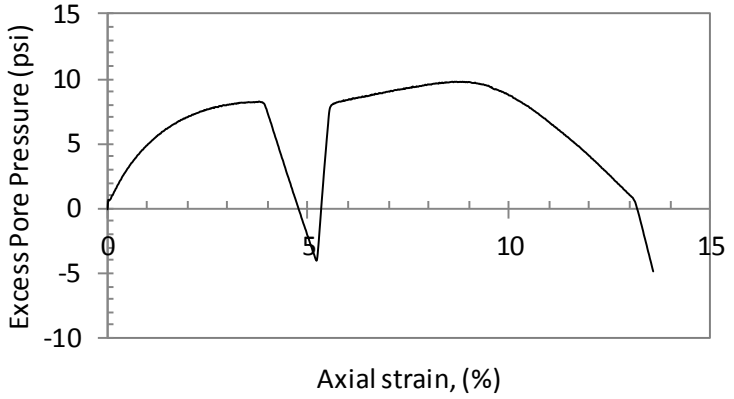

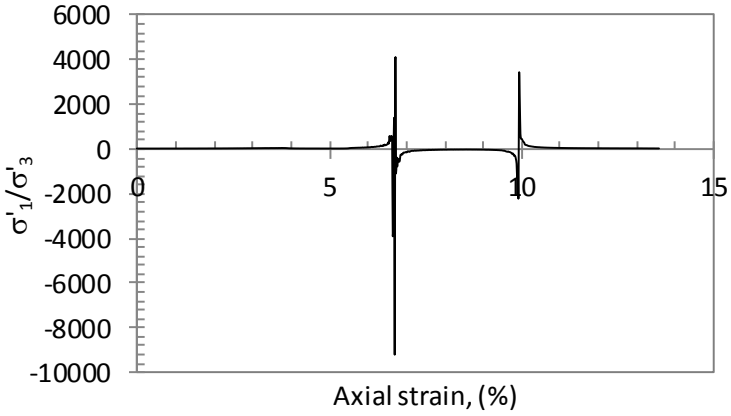

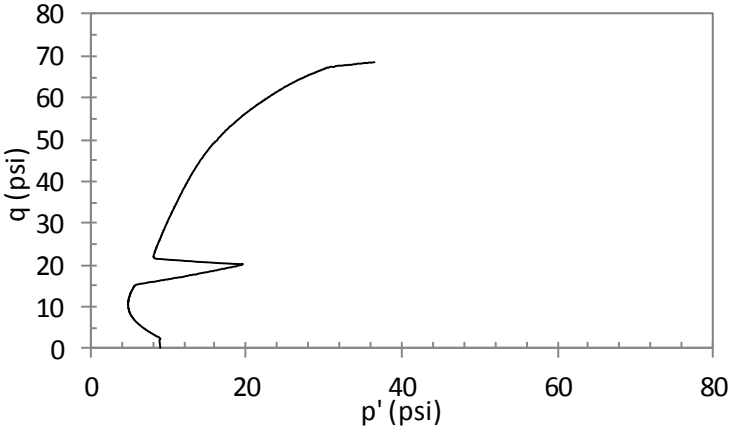

POST CYCLIC UNDRAINED STATIC TRIAXIAL TEST

TBBLAPST11S3

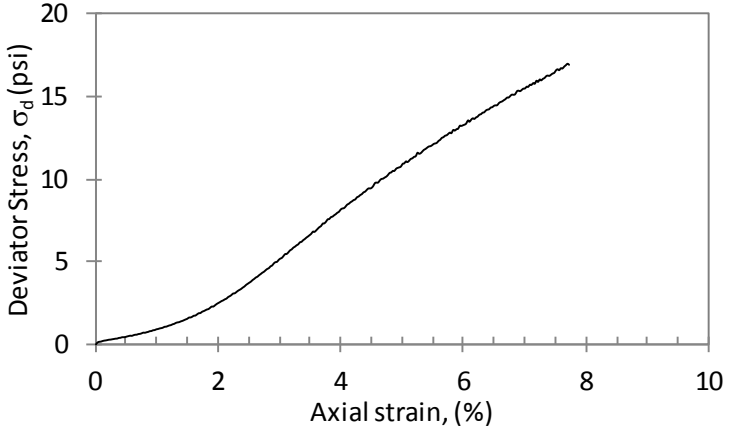

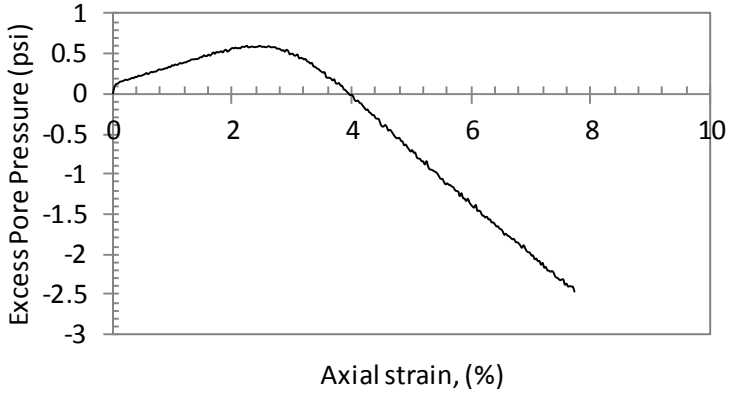

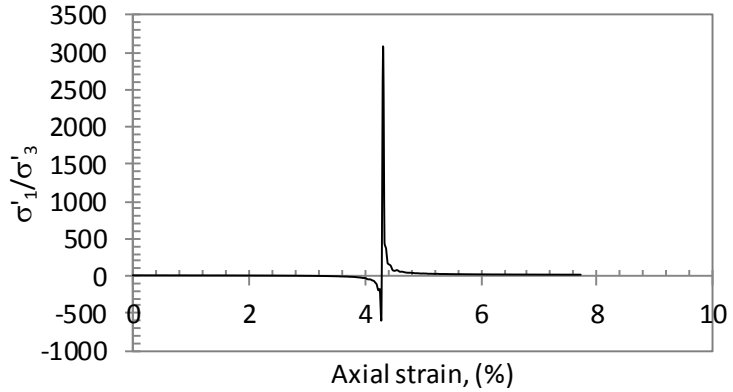

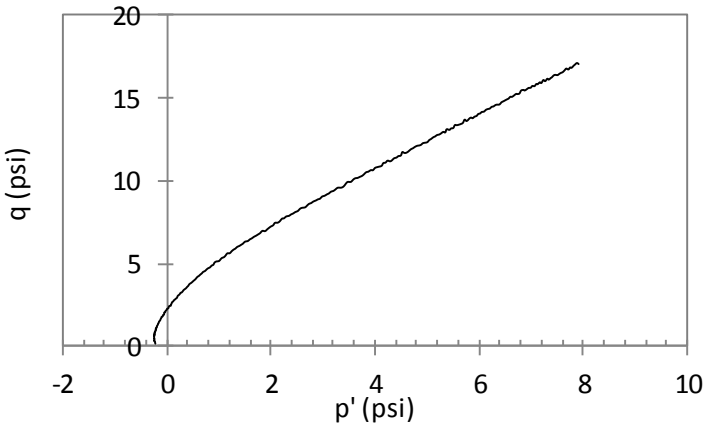

POST CYCLIC UNDRAINED STATIC TRIAXIAL TEST

TBBLAPST11S4

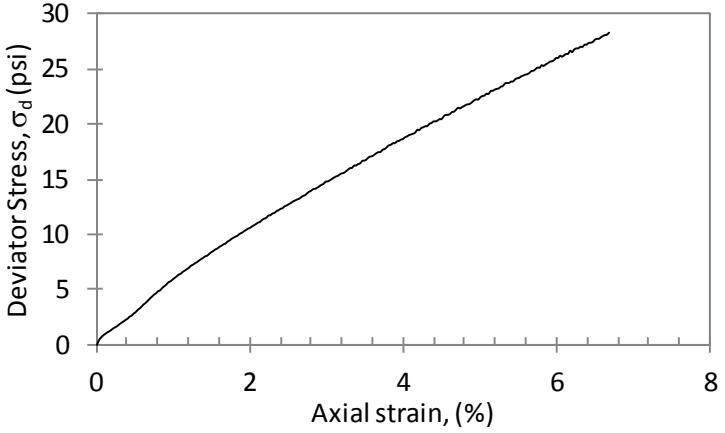

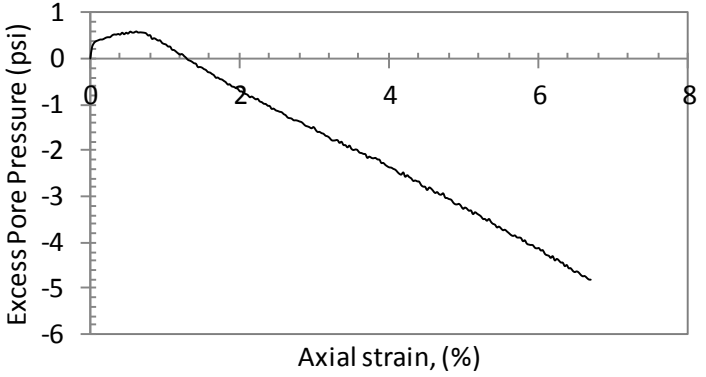

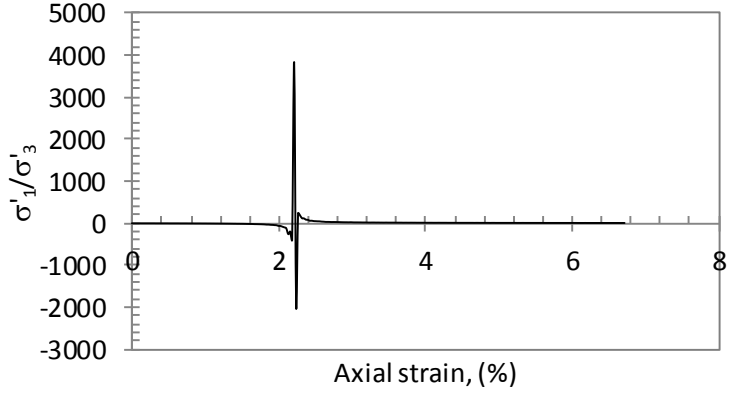

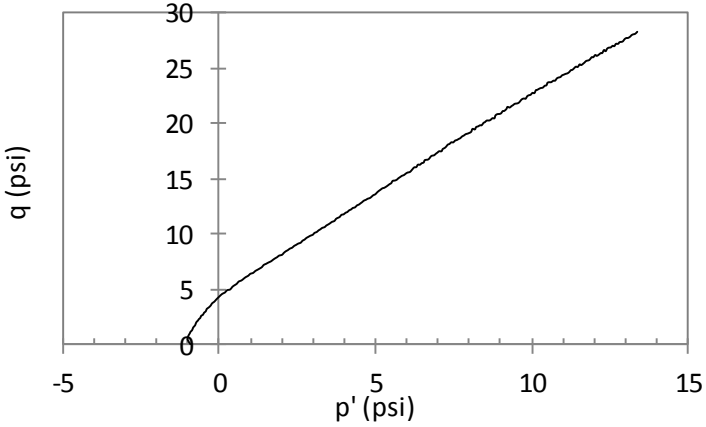

POST CYCLIC UNDRAINED STATIC TRIAXIAL TEST
TBBLAPST12S1

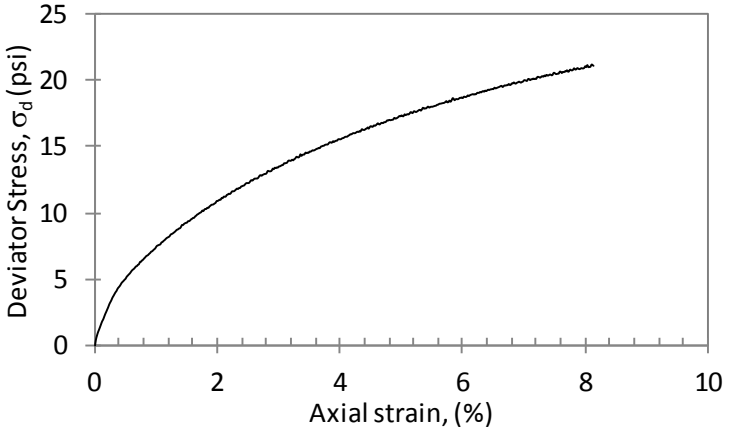

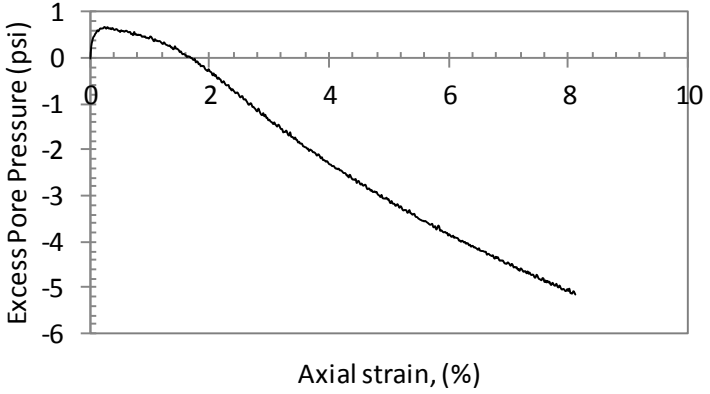

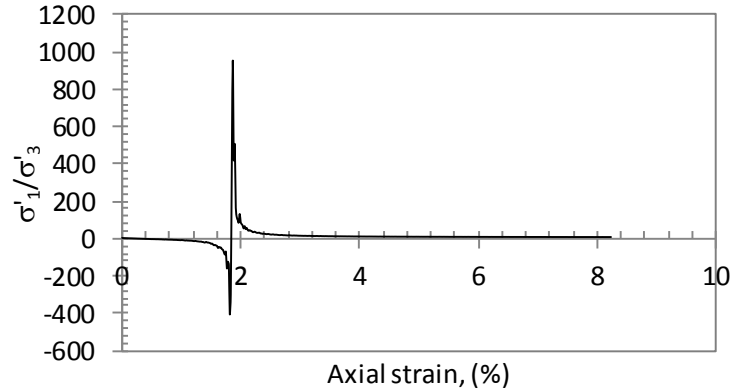

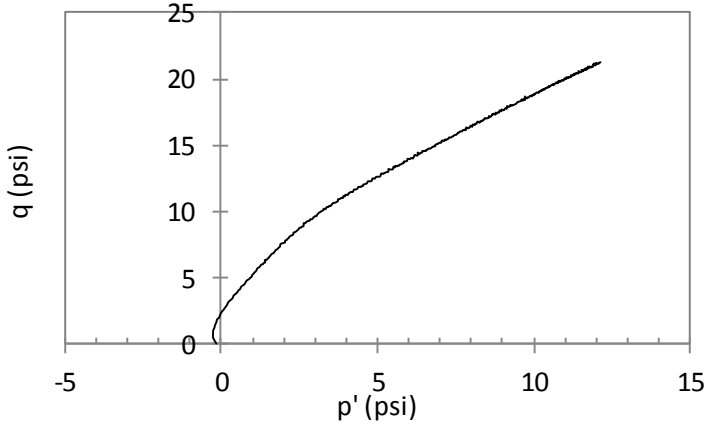

POST CYCLIC UNDRAINED STATIC TRIAXIAL TEST
TBBLAPST12S2

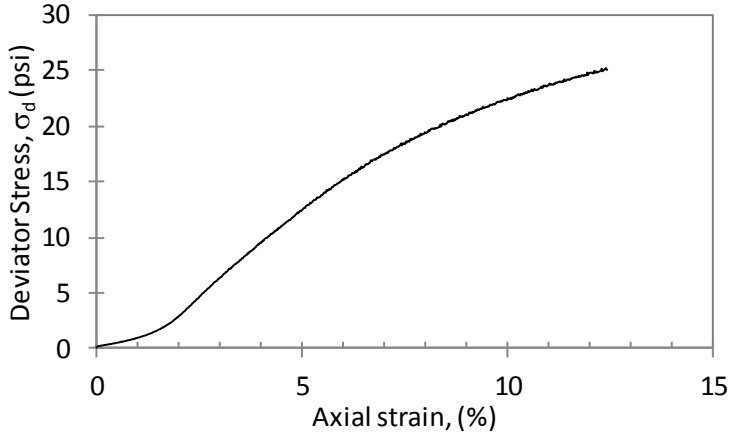

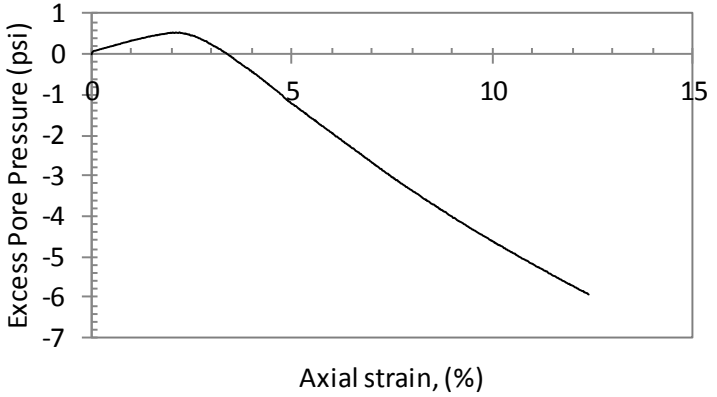

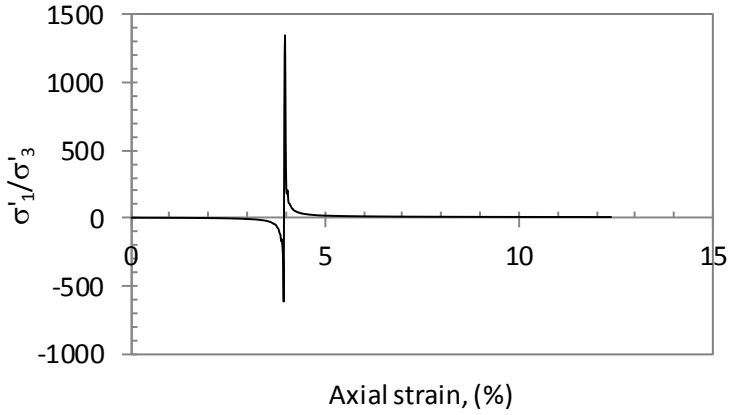

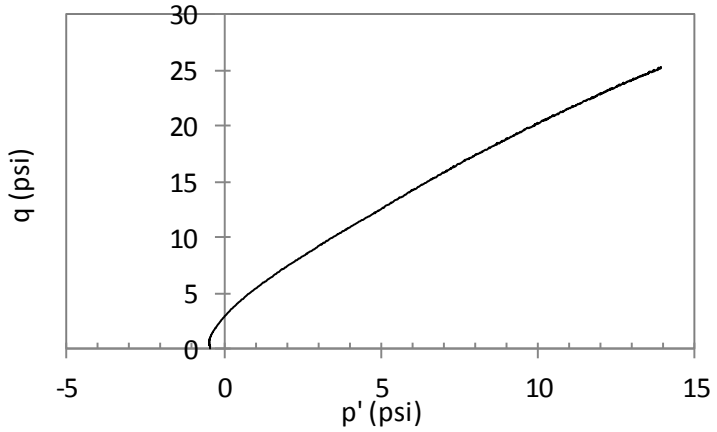

POST CYCLIC UNDRAINED STATIC TRIAXIAL TEST

TBBLAPST14S3

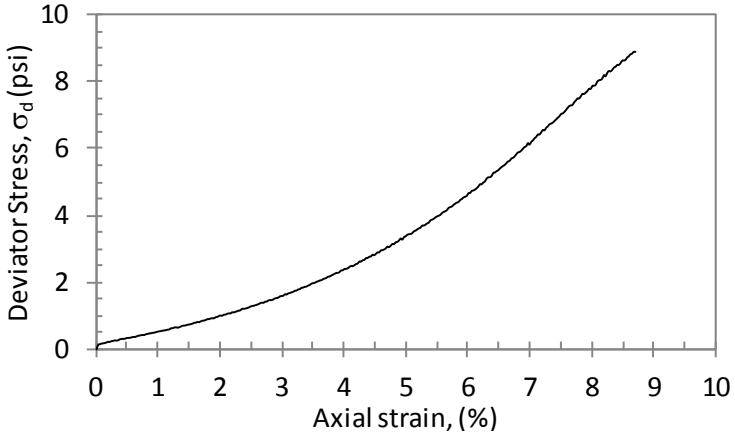

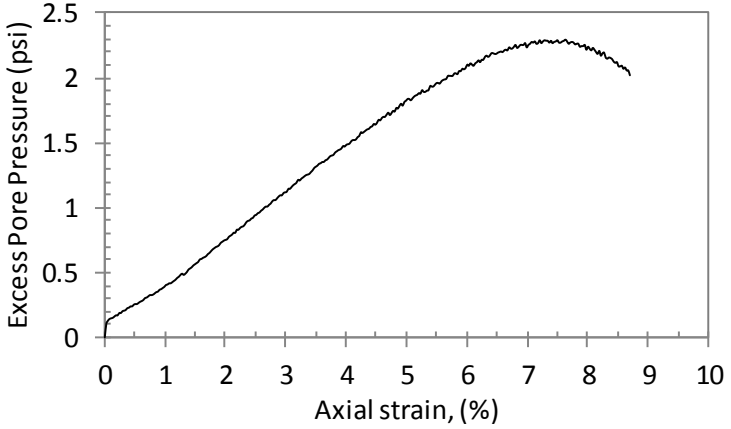

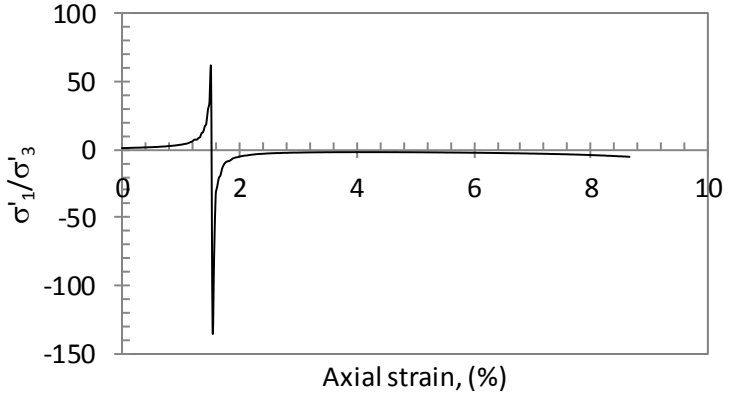

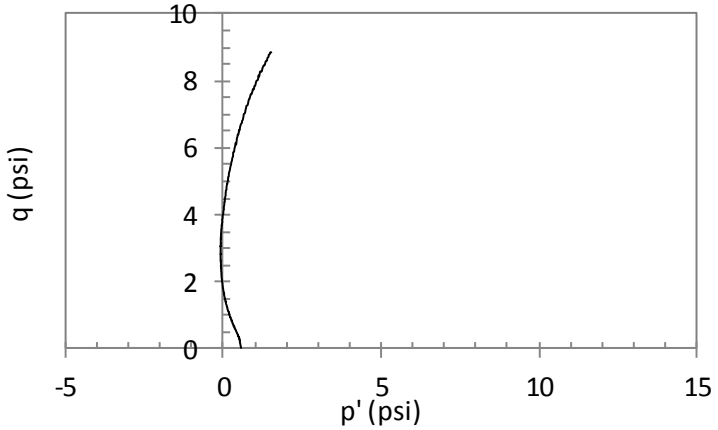

POST CYCLIC UNDRAINED STATIC TRIAXIAL TEST

TBBLAPST14S4

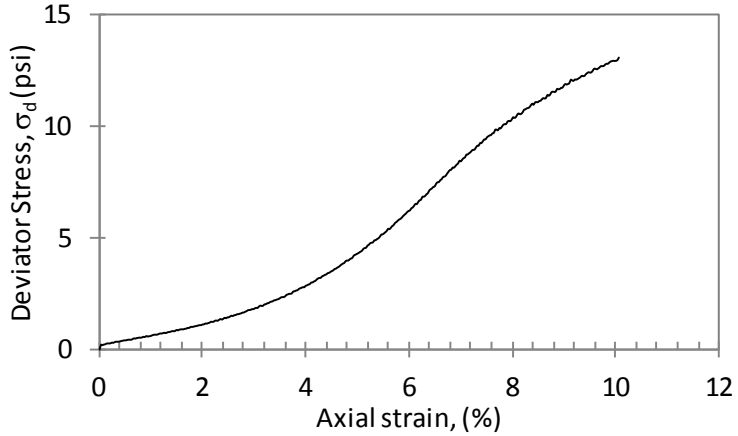

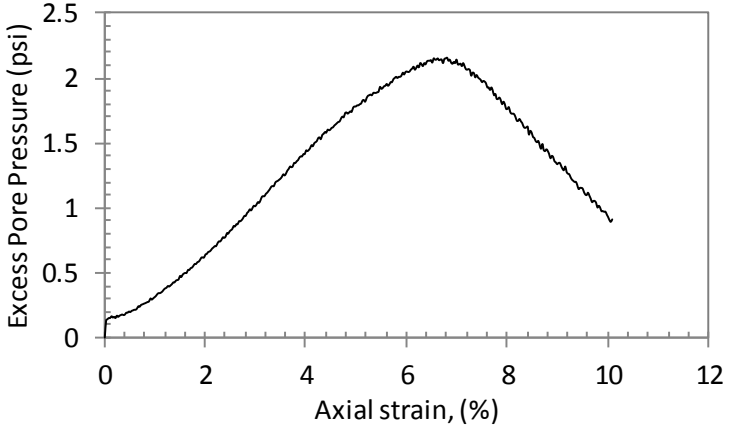

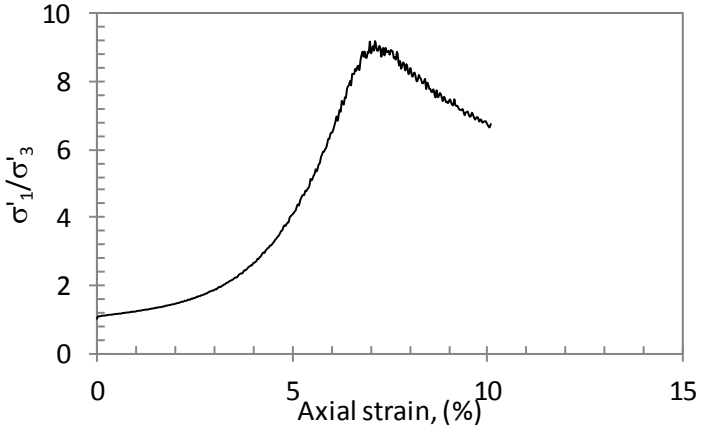

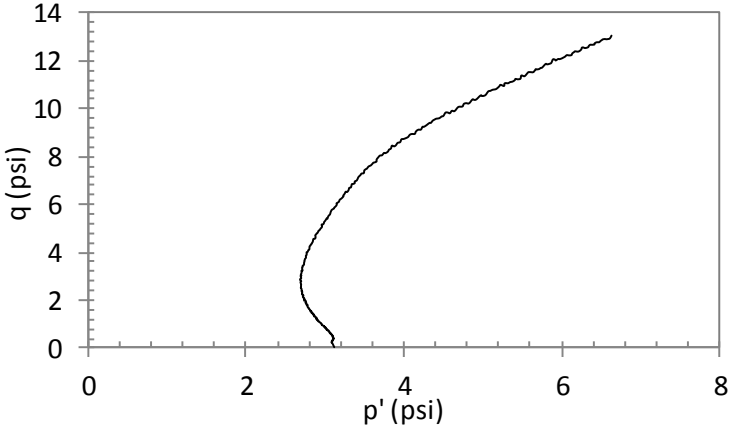

POST CYCLIC UNDRAINED STATIC TRIAXIAL TEST

TBBLAPST15S1

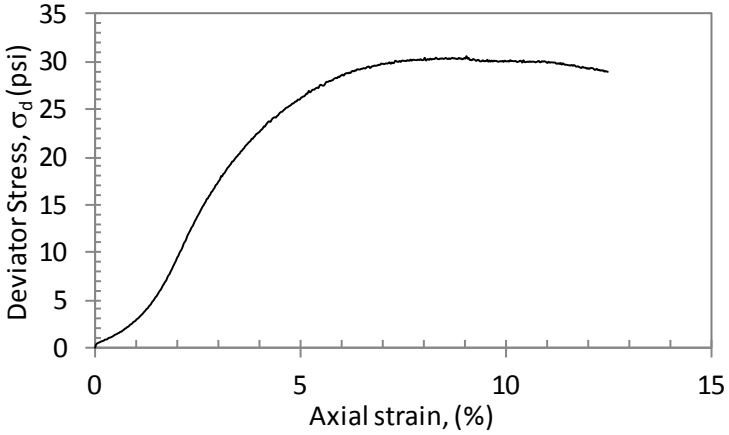

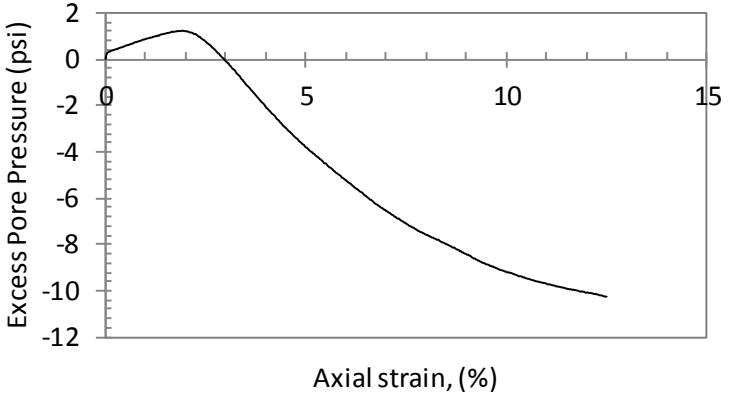

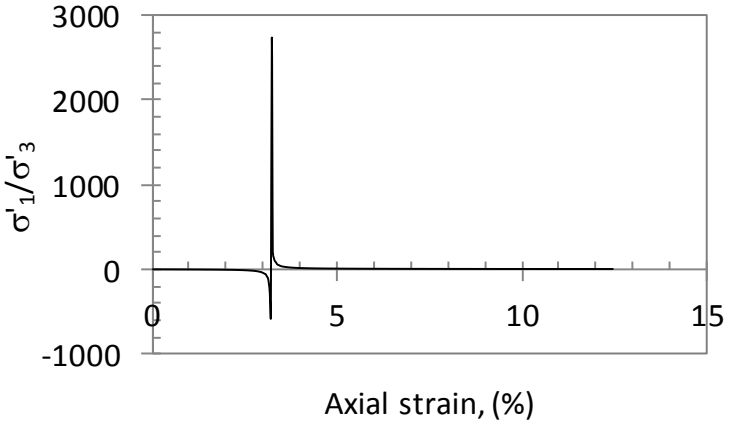

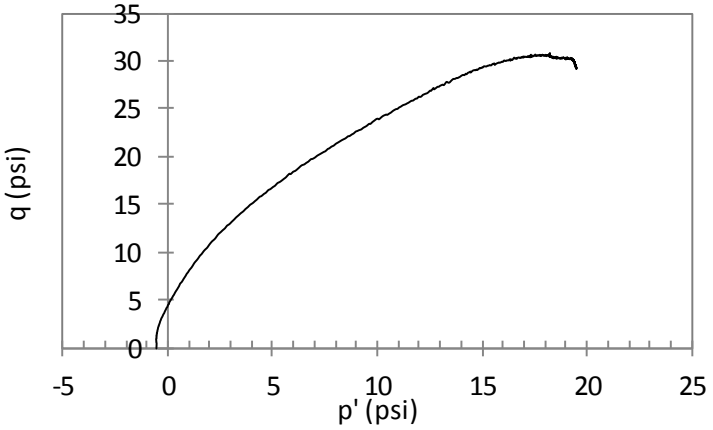

POST CYCLIC UNDRAINED STATIC TRIAXIAL TEST

TBBLAPST15S2

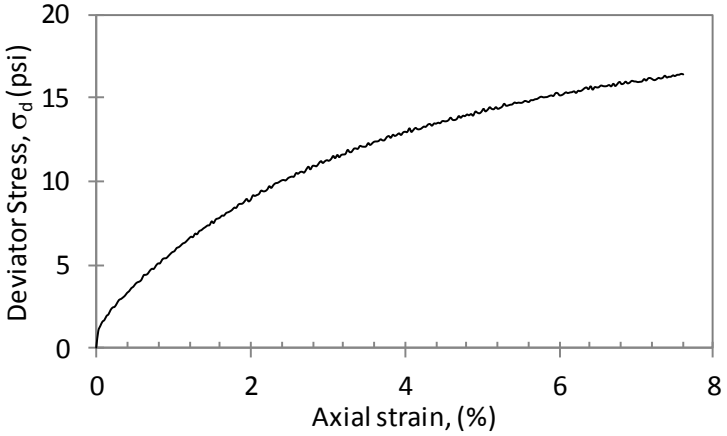

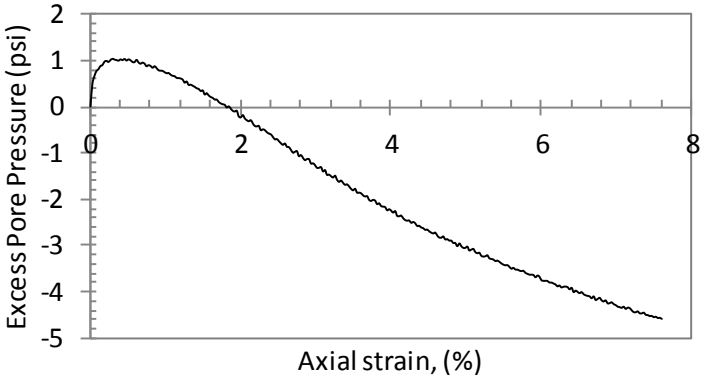

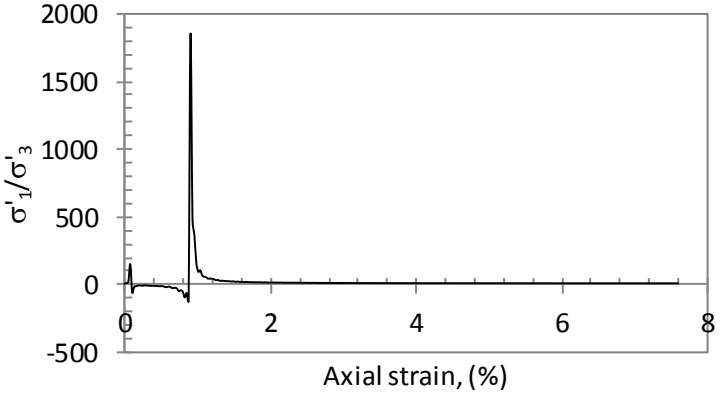

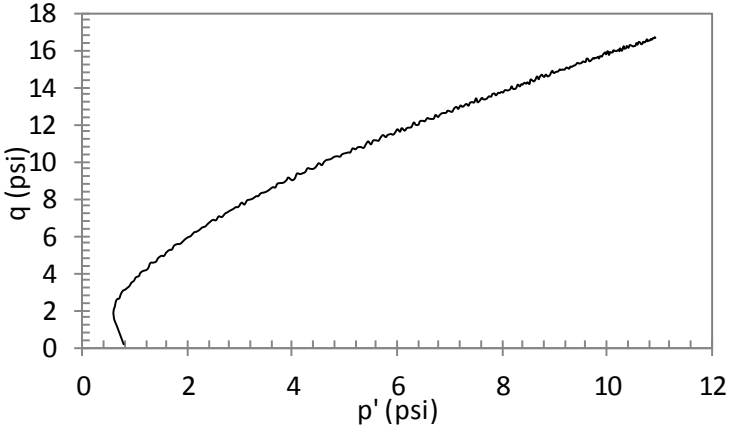

POST CYCLIC UNDRAINED STATIC TRIAXIAL TEST

TBBLAPST15S3

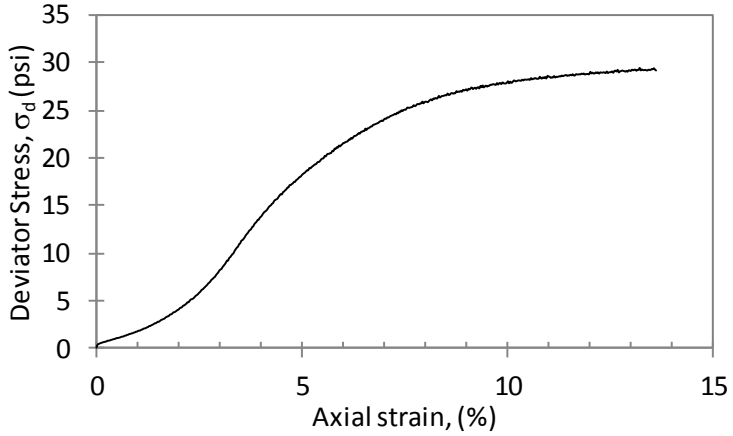

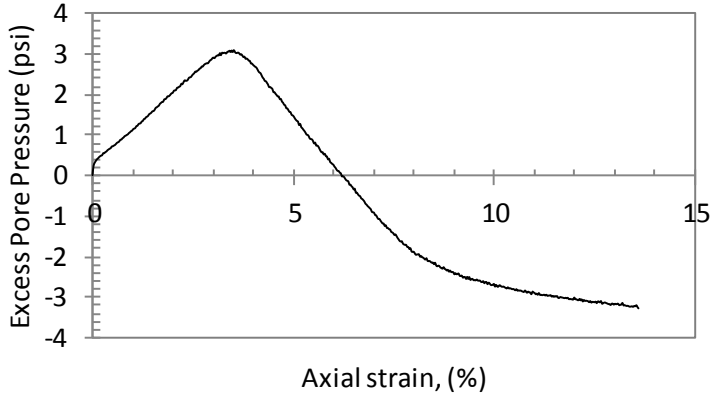

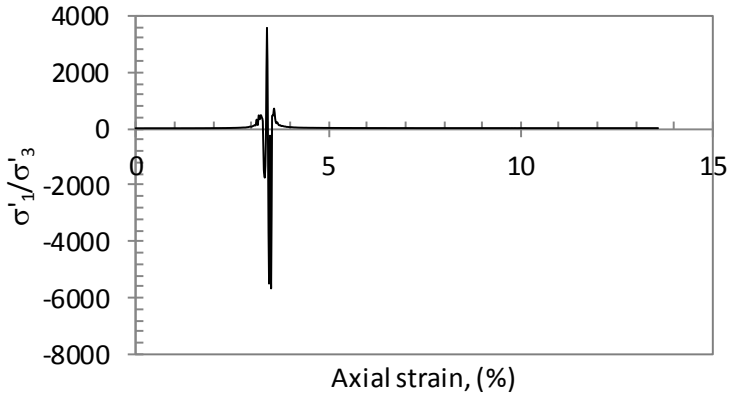

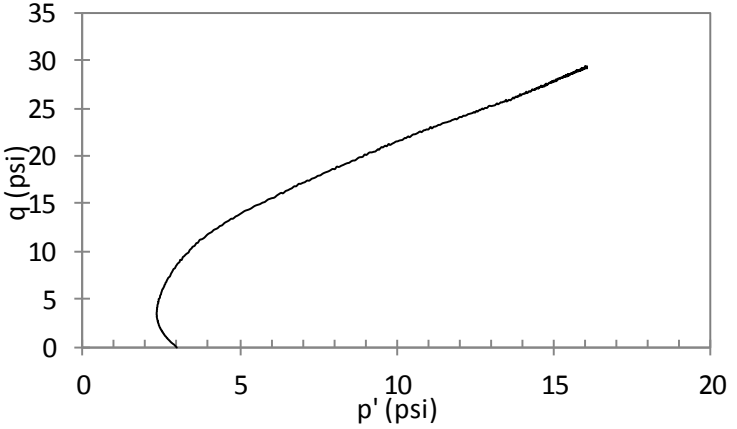

POST CYCLIC UNDRAINED STATIC TRIAXIAL TEST
TBBLAPST15S4

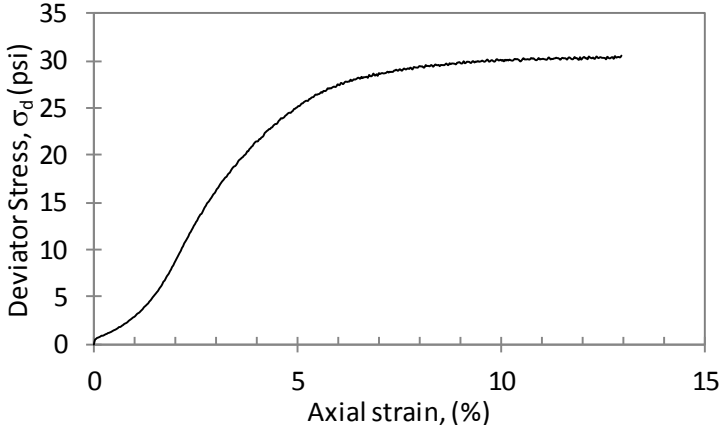

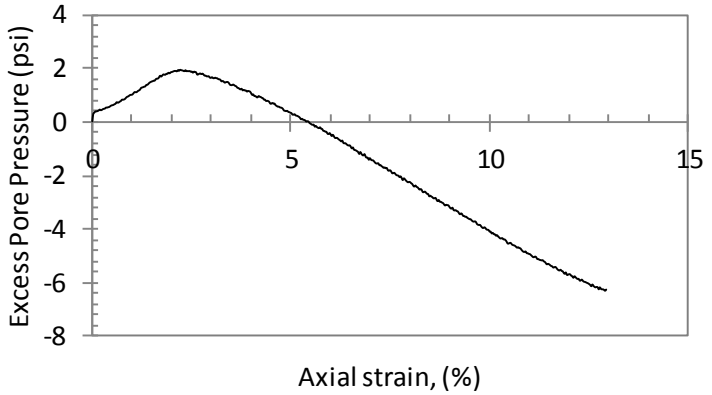

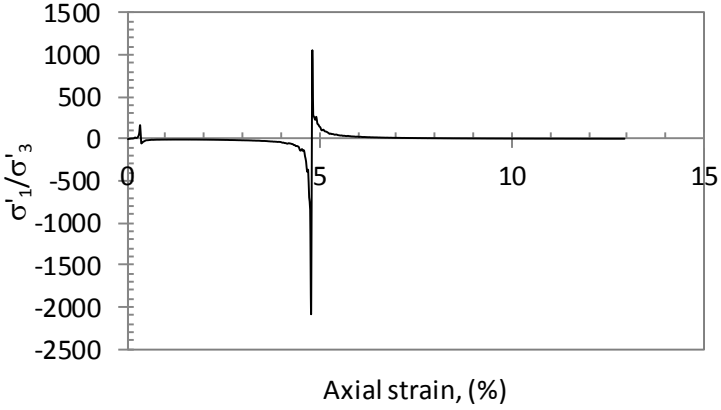

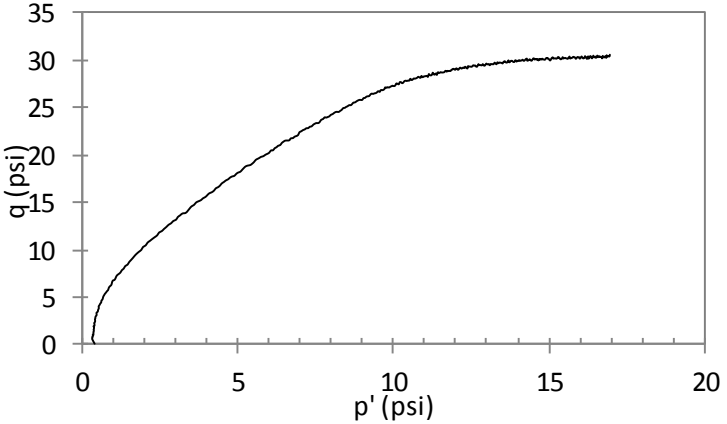

POST CYCLIC UNDRAINED STATIC TRIAXIAL TEST
TBBLAPST16S2

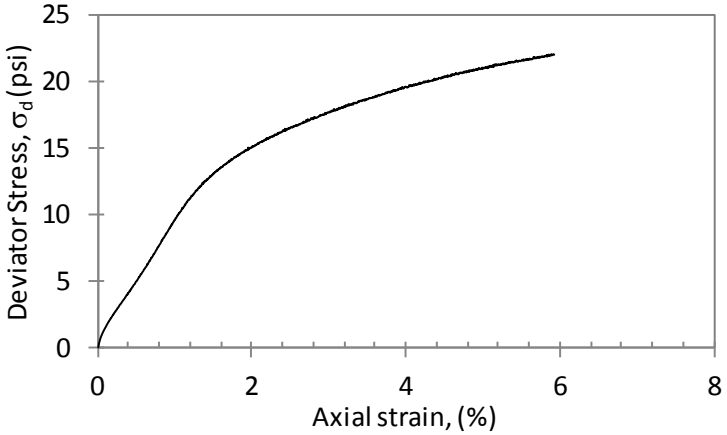

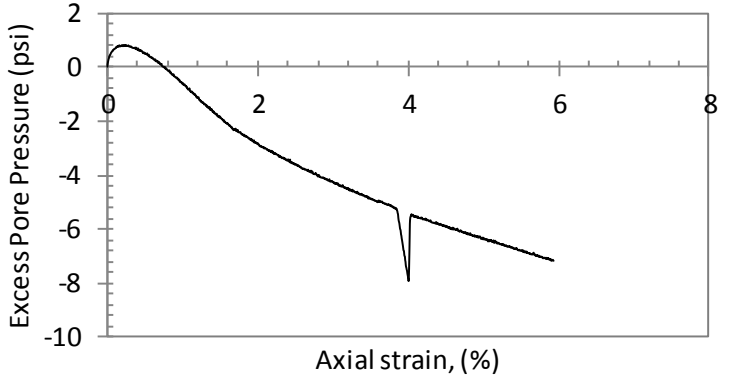

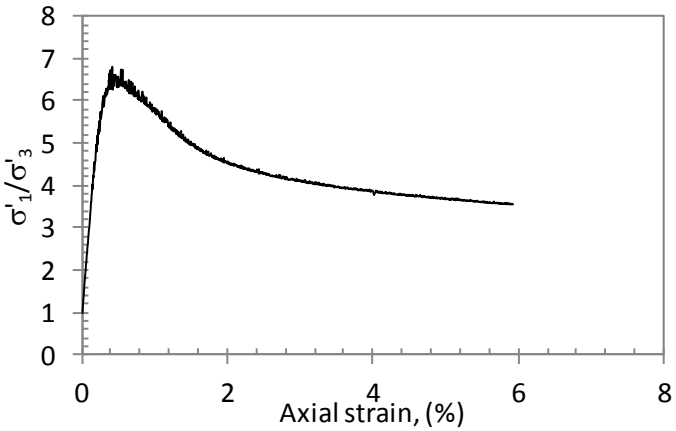

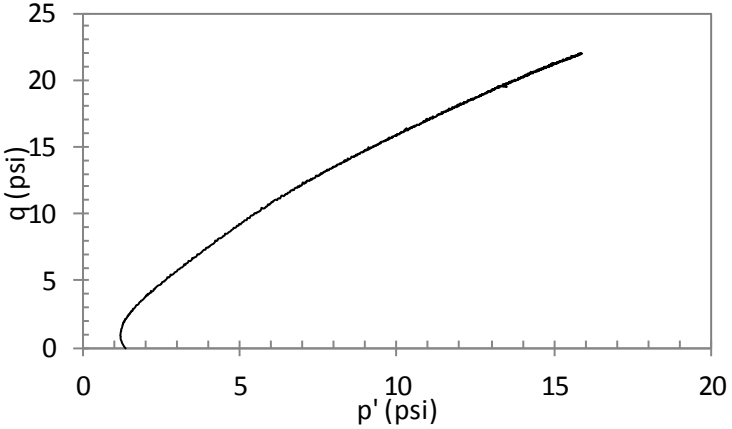

POST CYCLIC UNDRAINED STATIC TRIAXIAL TEST

TBBLDPST1S1

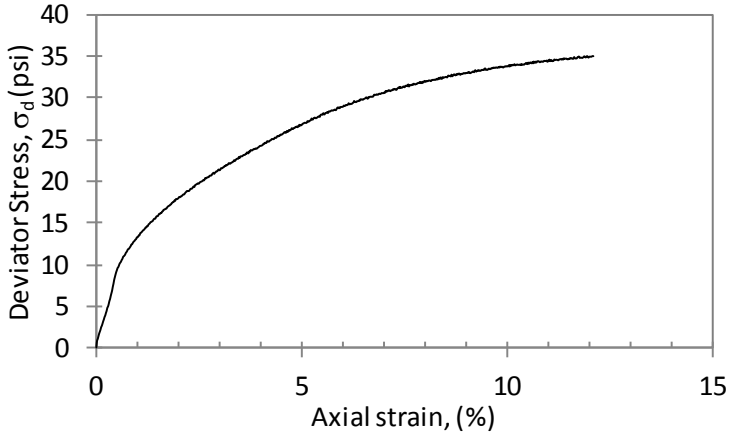

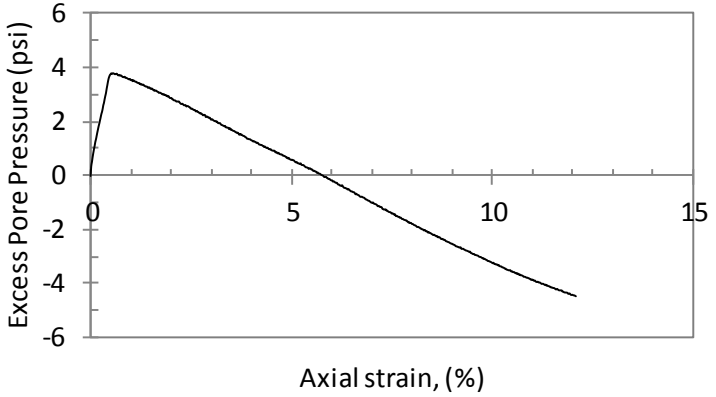

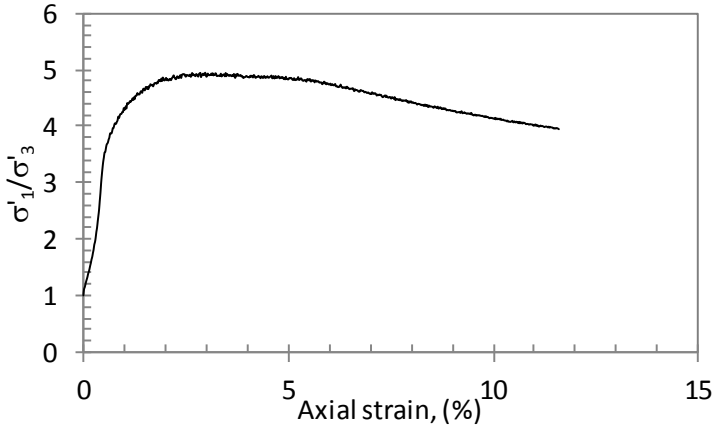

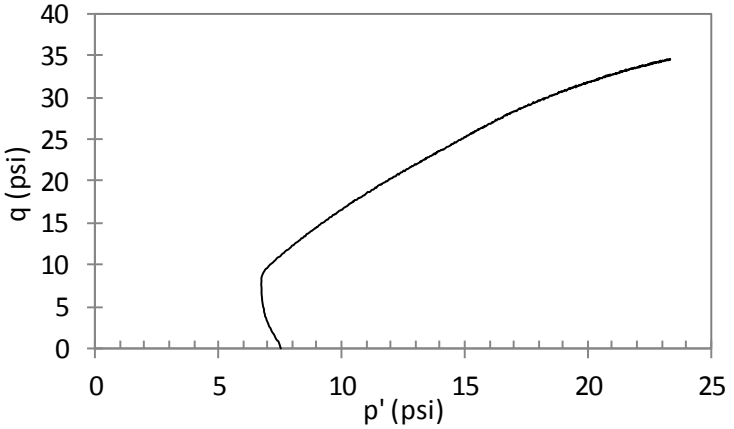

POST CYCLIC UNDRAINED STATIC TRIAXIAL TEST

TBBLDPST1S2

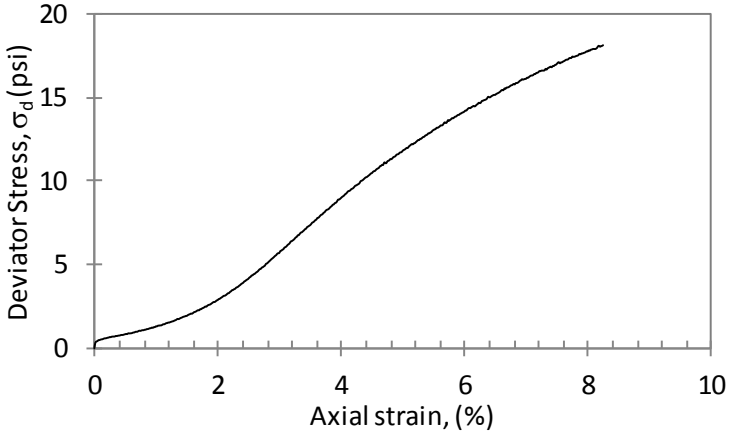

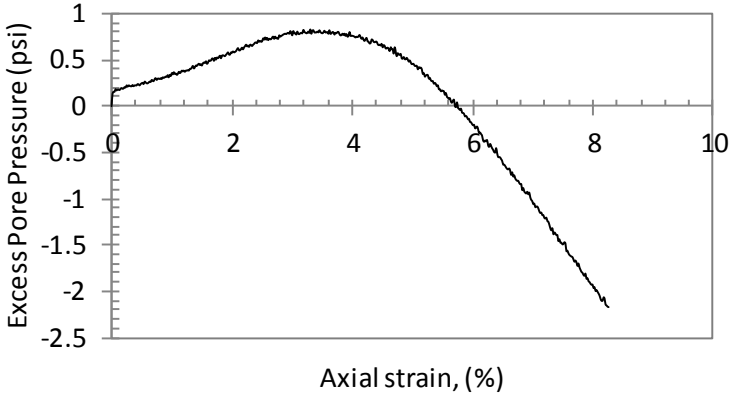

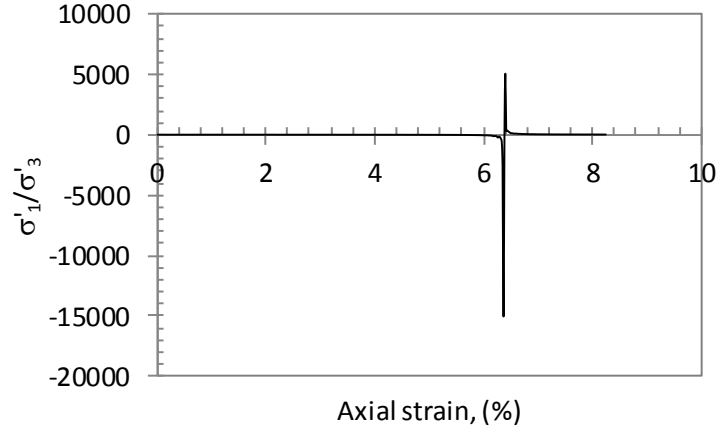

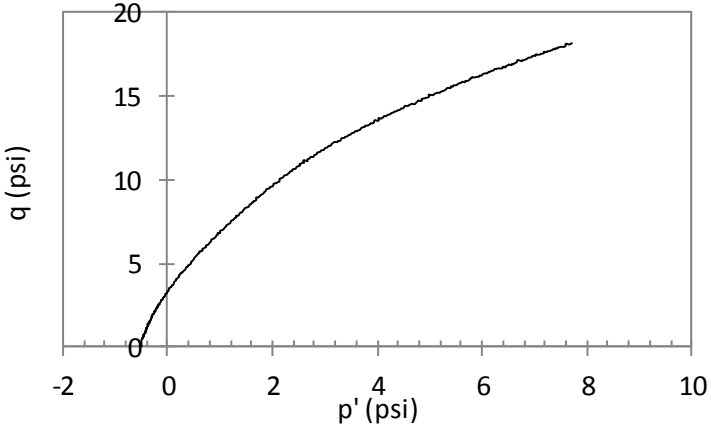

POST CYCLIC UNDRAINED STATIC TRIAXIAL TEST

TBBLDPST1S3

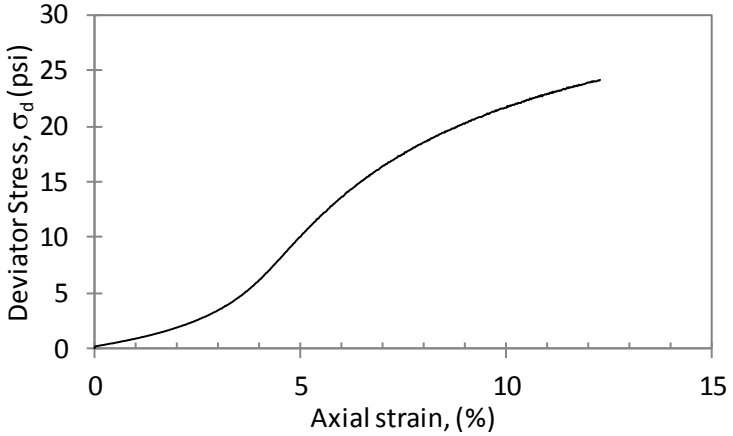

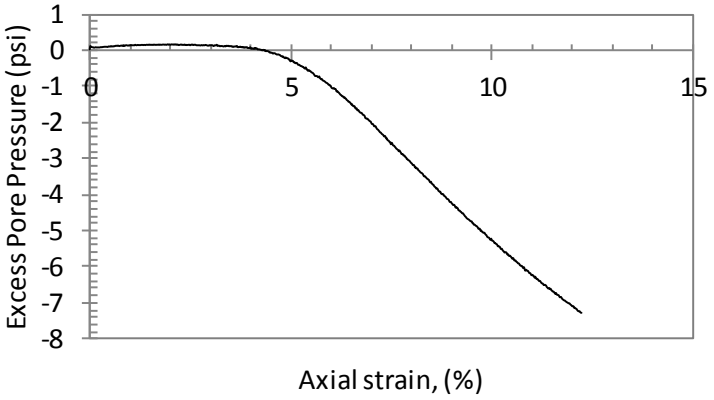

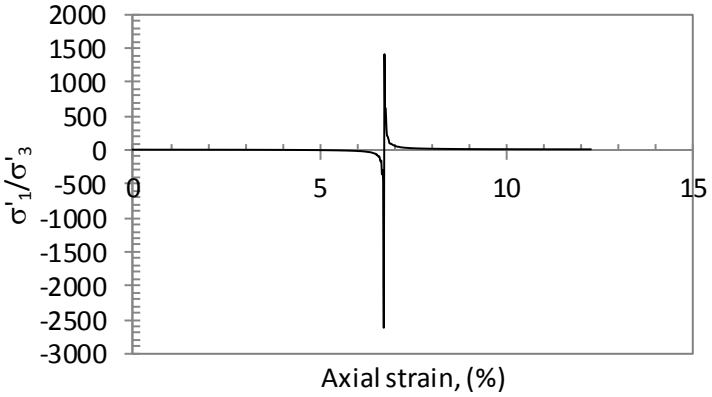

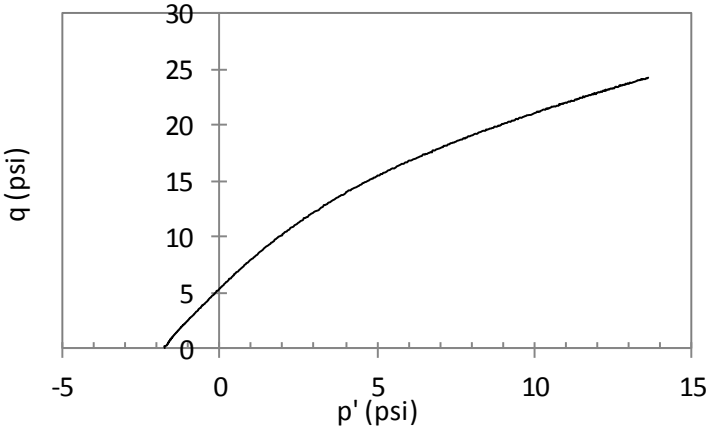

POST CYCLIC UNDRAINED STATIC TRIAXIAL TEST

TBBLDPST2S2

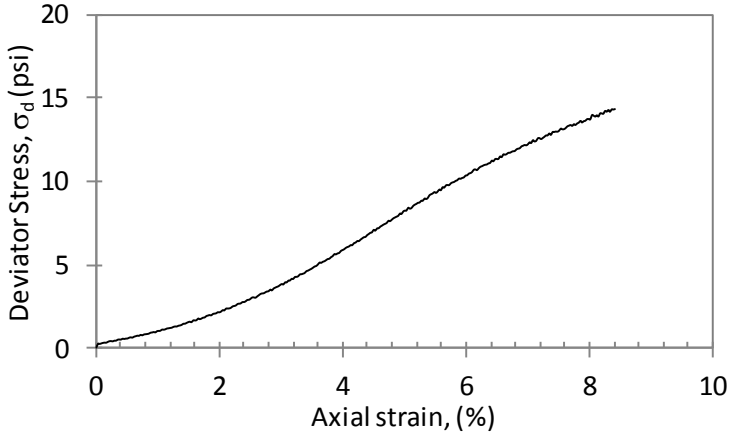

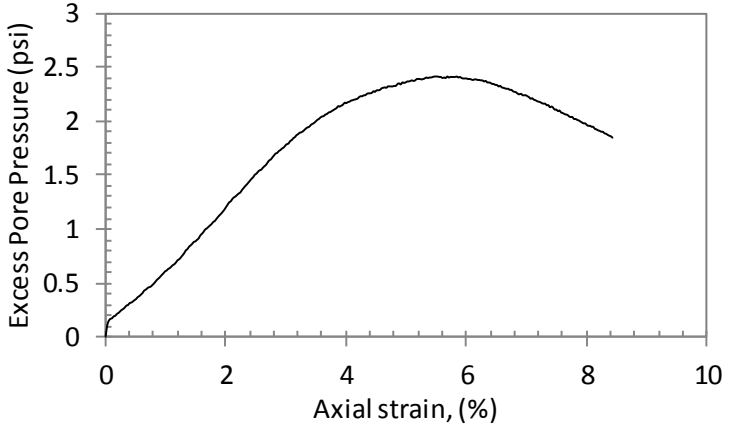

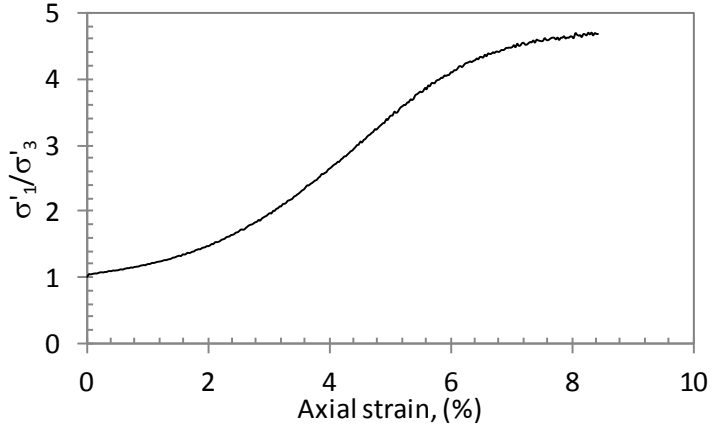

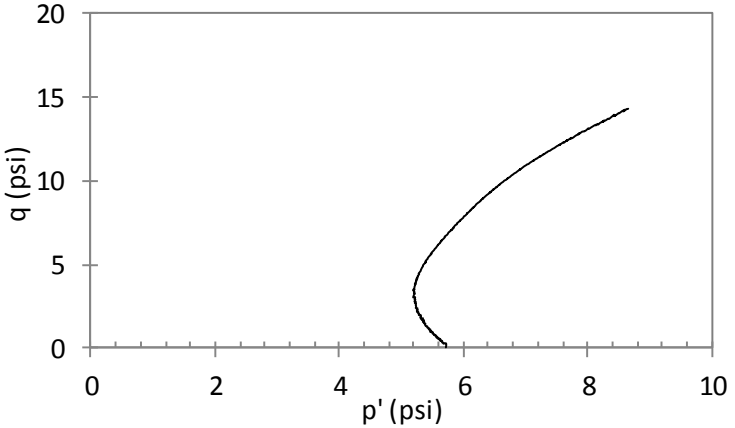

POST CYCLIC UNDRAINED STATIC TRIAXIAL TEST

TBBLDPST2S3

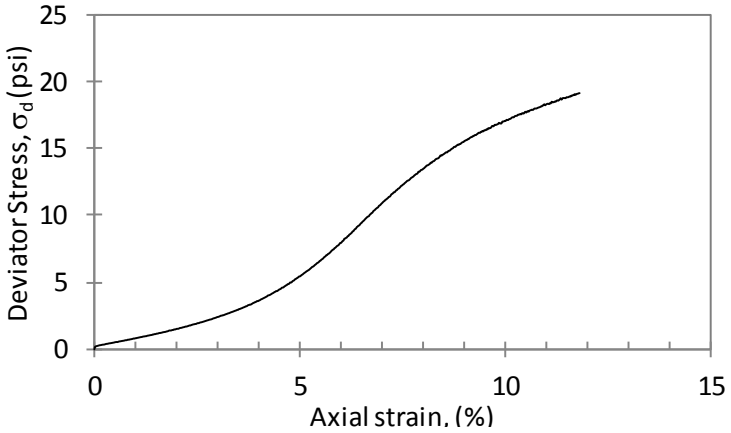

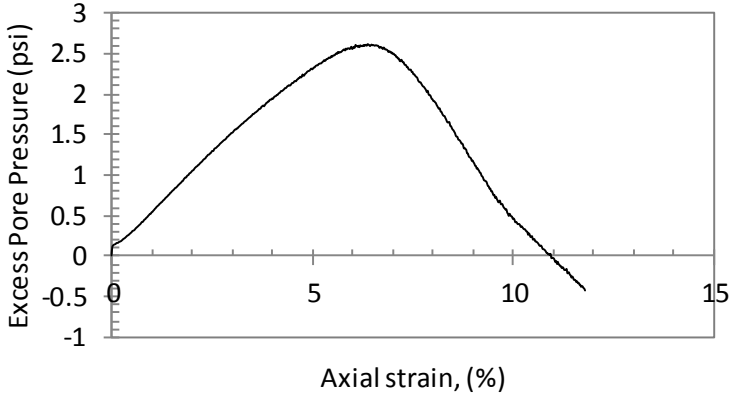

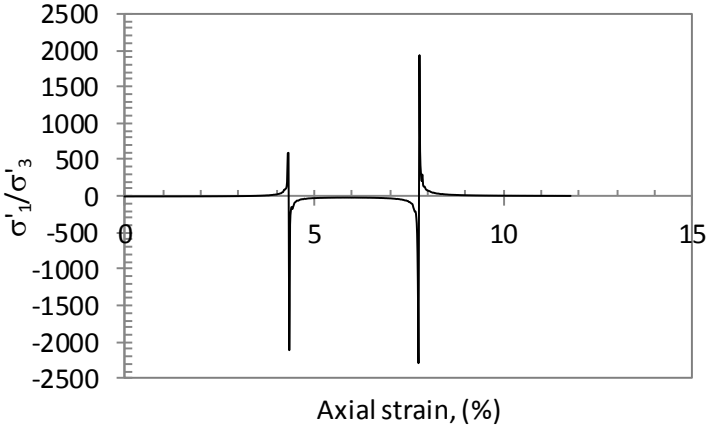

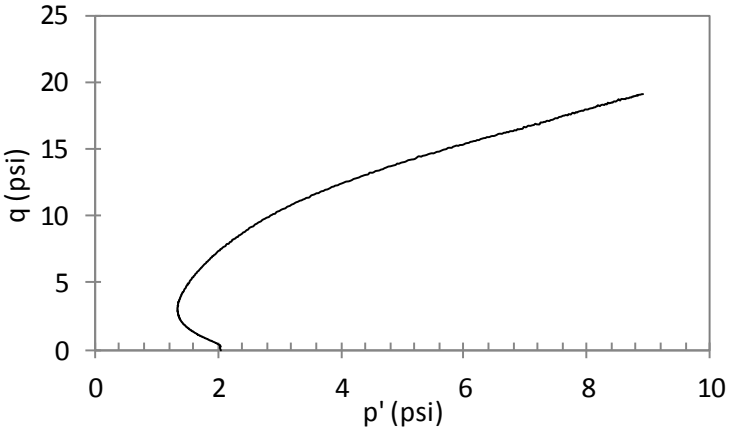

POST CYCLIC UNDRAINED STATIC TRIAXIAL TEST

TBBLDPST2S4

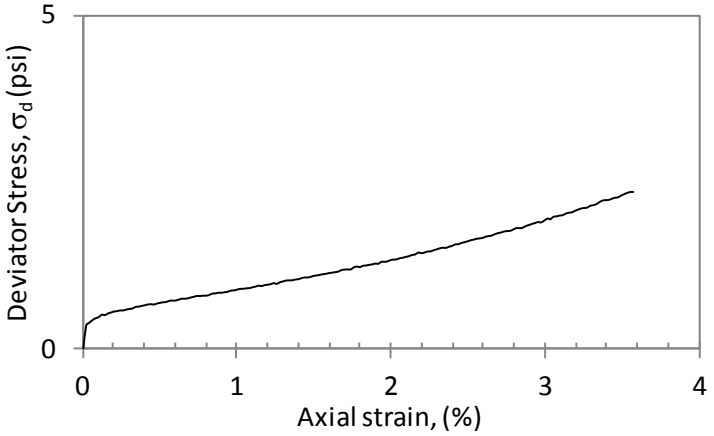

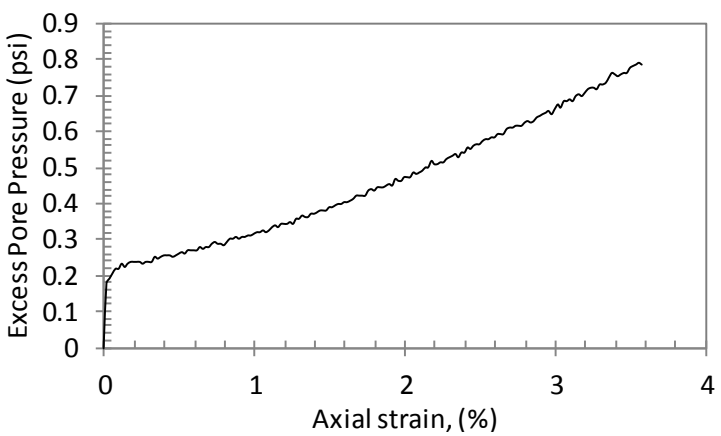

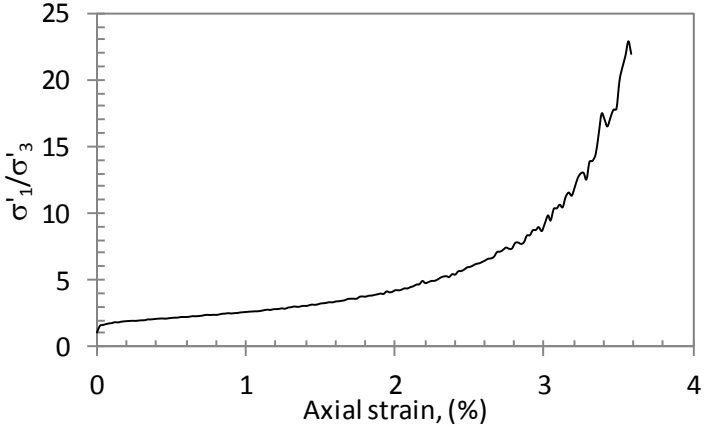

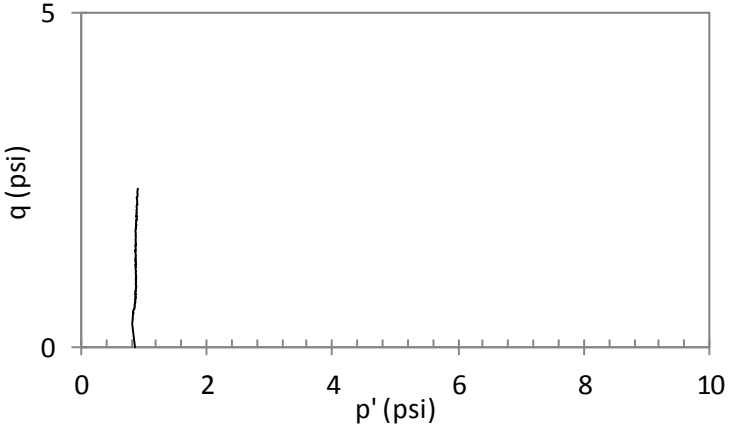

POST CYCLIC UNDRAINED STATIC TRIAXIAL TEST
TBBLDPST4S1

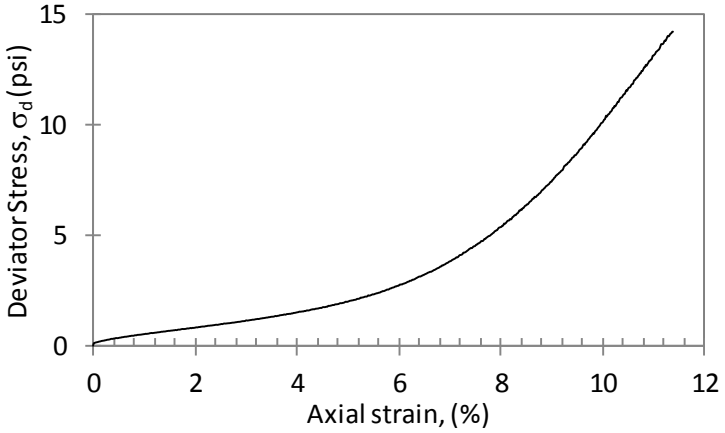

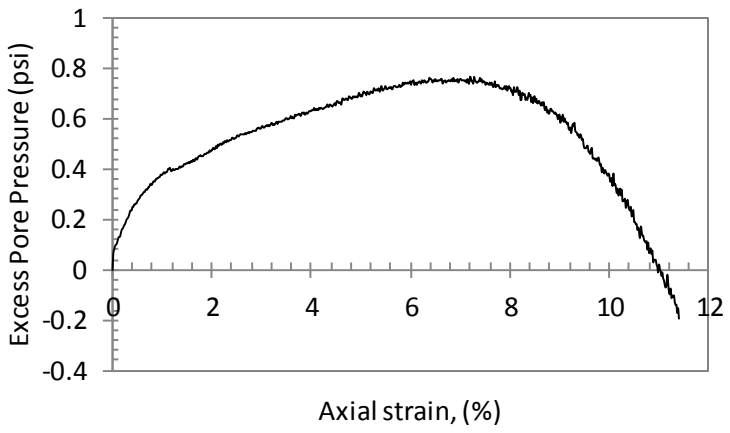

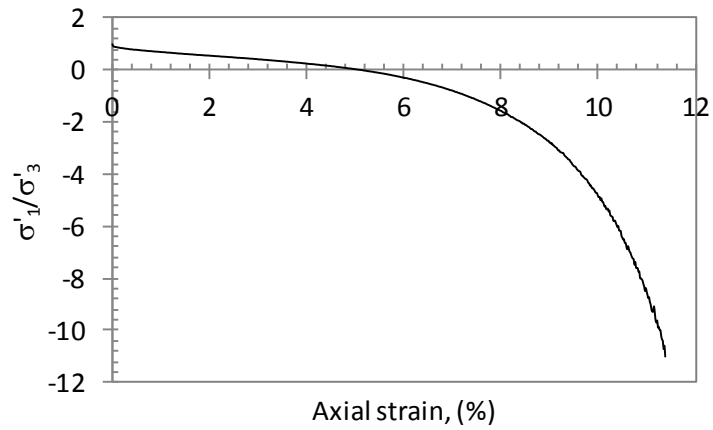

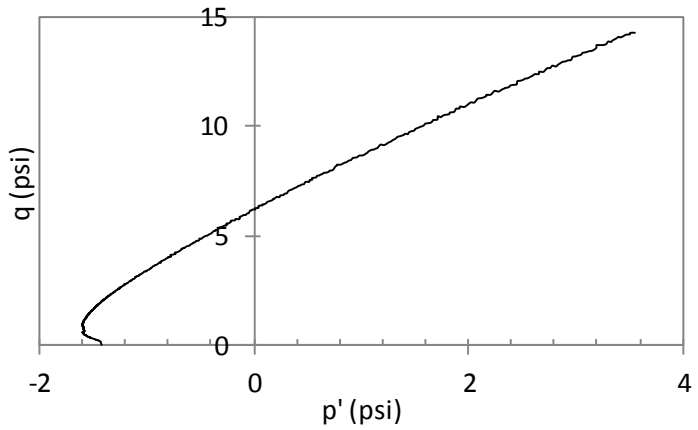

POST CYCLIC UNDRAINED STATIC TRIAXIAL TEST

TBBLDPST4S2

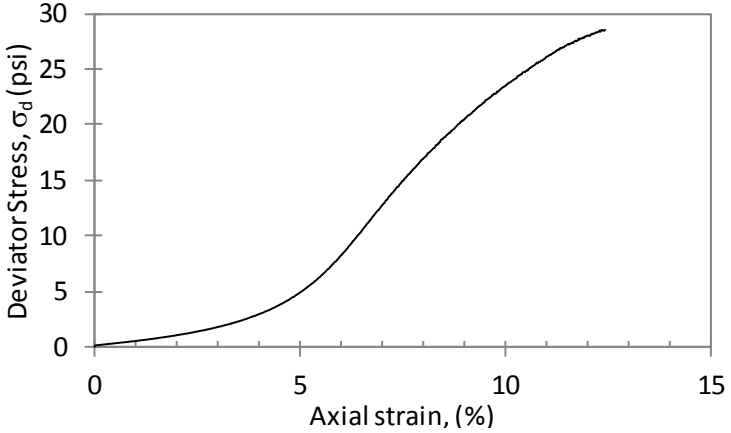

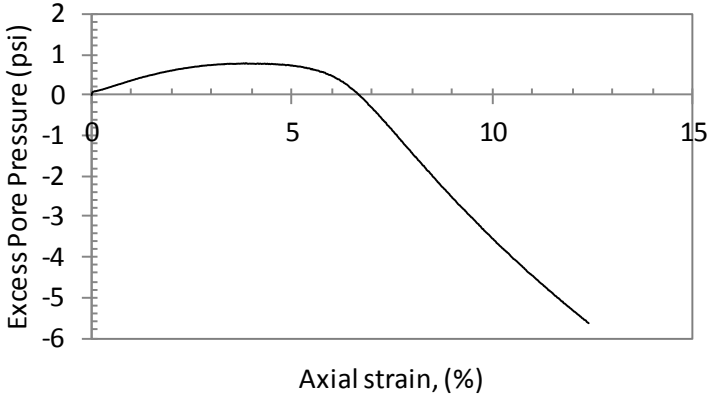

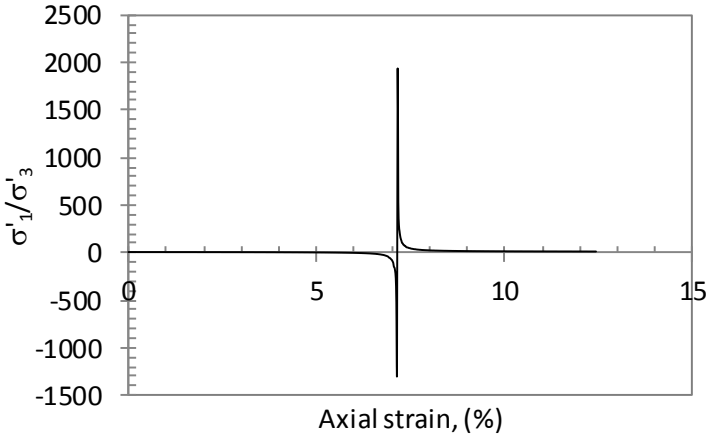

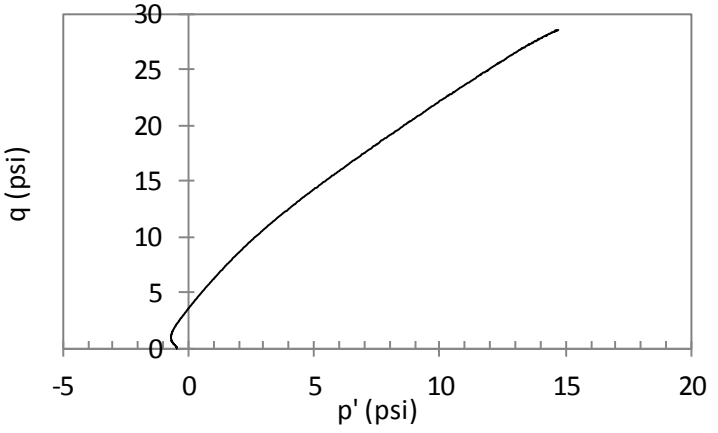

Appendix B

Cyclic Triaxial Testing Procedure

B.1 Cyclic Triaxial Testing System

In this section, the procedures and tools used to perform the cyclic triaxial experiments are explained. The utilized system in this research consisted of a cyclic triaxial chamber, a pressure board, a hydraulic pressure generator (gear box), an air compressor, a SCON-1500 controller computer, a personal computer, and a controlling software. In Figure B.1, four of these components are illustrated.

Figure B.1: pressure board, hydraulic pressure generator, personal computer, and the controlling computer.

In the subsequent sections, the components of this system are introduced and the applied procedure to perform cyclic triaxial experiments is presented.

B.2 Required Tools and Materials

The required tools and materials to perform a cyclic triaxial test are as follows. A small spatula, water content containers, scale, ruler, caliper capable of measuring at least 3-in, pipe cutter, measuring tape, 9/16-in wrench, ¾-in wrench, 2.8-in diameter neoprene membrane, four 2.8 in O-rings, two filter papers, membrane stretcher mold, level, small hacksaw, small wire saw. A number of the applied tools are shown in Figure B.2.

Figure B.2: Some of the employed tools.

B.3 Cyclic Triaxial Testing Steps

Performing a cyclic triaxial test includes the following steps which are discussed in the subsequent sections:

B.3.1 Filling the water storage tank and de-airing the water

B.3.2 Water content measurement

B.3.3 Retrieving the sample from the Shelby tube

B.3.4 Patching the surface of the sample

Trimming the end surfaces of the sample

B.3.6 Measuring the mass and dimensions of the sample

B.3.7 Covering the sample with the membrane

B.3.8 Applying vacuum

B.3.9 Sensor initialization

B.3.10 Sealing off the chamber

B.3.11 Applying the seating load

B.3.12 Filling the chamber

B.3.13 Applying the cell pressure

Flooding the sample

B.3.15 Saturating the sample

B.3.16 Measuring the B-value

B.3.17 Consolidating the sample

B.3.18 Cyclic triaxial loading of the sample

B.3.1 Filling the water storage tank and de-airing the water

This stage was not a recurring stage and once it was performed it would provide de-aired water for many experiments. To avoid the accumulation of tap water residue in the valves and connections, distilled water was used which was provided by the environmental laboratory. One end of a long ¼ in tube was submerged in the water container and the other end was connected to the back of the pressure board cabinet. The valve beside the connection was turned to the open position. With the air compressor attached to the board, vacuum switch #2 was flipped up which is shown in Figure 3.

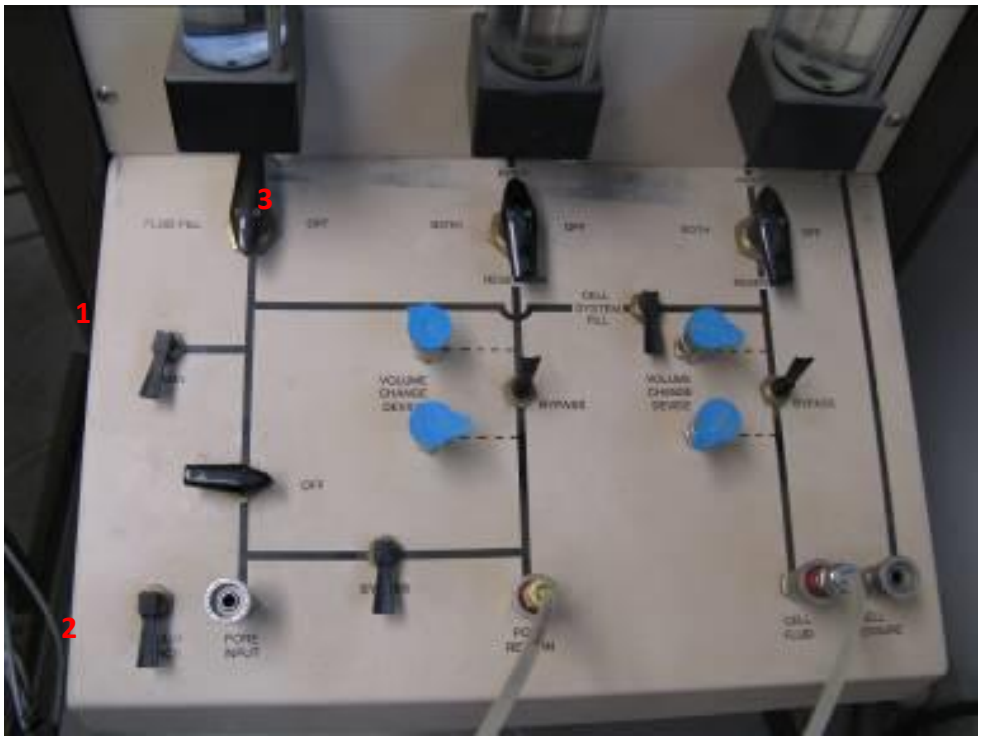

Figure B.3: Pressure board valves and connections.

By turning the valve #3 to the “Fluid fill” position, the water started flowing from the container to the tank inside the pressure board cabinet. The water level in the tank was observed through the first burette from left which is shown in Figure B.4. The filling process could be stopped at any desired water level by either flipping down switch #2 or turning valve #3 to point to the black line on the board. Thereafter, the valve on the back of the pressure board cabinet was turned to the off position.

Figure B.4: Pressure board containing the burettes, regulators, and the valves.

To de-air the water in the tank, the vacuum switch was flipped up to activate the vacuum valve. Valve #3 was turned to the position pointing to the black line on the board. Soon after, the vacuum started pulling the air bubbles out of the water. This process was continued for a few hours since the water was newly placed in the tank. A reliable clue to identify that little air was left in the water was that no visible air bubbles were present in the left burette at the end of this process.

B.3.2 Water content measurement

For measuring the water content of each sample, the method described in ASTM D2216-98 was followed. For each specimen, water content samples from the top and bottom of the sample were obtained. The mathematical average of these two values was

reported and applied as the water content value of the sample. After breaking the seal of the Shelby tube, the actual length of the recovered specimen was measured. Based on this length and the quality of the recovered sample, the number of potential specimens in reasonable testing condition was estimated which usually ranged between two to three samples. In rare cases, some tubes produced one or four samples as well. By considering the movement range of the shearing rod in the triaxial cell, the length of the testing specimen was measured and marked. As shown in Figure B.5, by using a pipe cutter the specimen was cut from the rest of the tube and the tube was sealed again to maintain the moisture.

Figure B.5: Cutting the tube to retrieve specimens.

B.3.3 Retrieving the sample from the Shelby tube

The samples provided for this research were 2.8-in in diameter and obtained by fixed piston sampling method in summer 2006 and summer 2007. By the beginning of the cyclic triaxial testing phase of this research in fall 2010, the tubes were untouched for approximately three to four years. Due to the prolonged waiting time, it was safe to imagine that the tubes could be rusted from inside. Also, the samples were attained from different depths and therefore had different densities. By retrieving a few trial samples, a methodology based on the age and the density of the samples was established. In this methodology, the retrieving method differentiated between soft or younger samples and dense or older samples. To achieve the best method for retrieving the specimen with the least disturbance, a number of methods were experienced.

The retrieving methods included cutting the Shelby tube with a hack saw, detaching the sample from the inner surface of the tube with a wire saw, detaching the sample from the inner surface of the tube by using a small spatula, cutting the Shelby tube with an electric saw, pushing the sample out with a hydraulic jack, and drilling holes along the length of the sample on the perimeter to facilitate separating the specimen surface from the inner surface of the tube. Each of these procedures had their own cons and pros which resulted in eliminating some and leaving a few to be chosen based on the condition of the sample.

Cutting the tube with a hack saw was very time consuming considering that one cut was not enough to release the sample due to the rusty inner surface of the tube

sticking to the sample. A wire saw was used in order to detach the sample from the tube and break the rust bond which could be carried out in two ways. One technique was to drill a hole along the length of the sample on the perimeter while it was in the tube and then thread a wire into the hole and attach it to the saw. This method required a lot of manual force and was almost impossible to be performed. The other technique was to cut the tube along the length, slide the wire inside the tube and use the wire saw to detach the sample which was not successful due to the same issues with the first technique. Therefore, both of these techniques were eliminated. Detaching the sample from the tube with a spatula required a lot of manual force and often resulted in an uneven shape of the sample. Due to the difficulty of this technique and the relatively high level of disturbance this method was eliminated as well.

Cutting the tubes with an electric saw would create a lot of vibration in the sample. This vibration could be easily handled by dry and stiff specimens while it could cause catastrophic deformations for soft and wet samples. Soft samples could practically liquefy in the Shelby tube due to the vibrations from the machine very quickly. Therefore, this method was not suitable for shallow to medium depth specimens. However, this method was chosen as the least disturbing retrieving method for stiff and dry samples. To break the rust bond between the sample and the tube, the tube was cut into eight longitudinal sections. An illustration of the result is shown in Figure B.6. Due to the rigidity of the stiffer samples none of them were disturbed or disintegrated using this method. This method required wearing protective work gear as illustrated in Figure B.7.

Pushing the samples out of the tube with a hydraulic jack can be used if performed at a slow rate. However this method was not very successful in retrieving stiff specimens due to high levels of rusting and existence of a strong bond between the tube and the sample. For stiff samples, this method commonly resulted in bent samples or detaching and tearing large pieces of the tailing material. Although, the same issue existed for softer and wetter samples, but it was considerably less destructive.

Figure B.6: Cutting the tube with an electric saw.

Figure B.7: Wearing protective gear during using the electric saw.

Samples from shallow depths have gone under a much lower effective pressure and essentially have higher water contents, greater void ratio and lower densities. Therefore, during pushing a wet sample out of the tube, negative pressures can be developed easier and the level of disturbance is higher than of a stiff sample. To alleviate this issue, prior to pushing the sample a series of holes were drilled along the length of the sample. Creating these opening on the perimeter of the sample would create air passages to cancel or reduce the negative pressure on the perimeter of the specimen. After retrieving the sample, these holes could be patched with excess tailing material from the same sample in an effort to limit the disturbance to the minimum level. Consequently, it is believed that drilling the holes and pushing the samples would be the least disturbing technique for retrieving soft samples. An illustration of the said technique is shown in Figure B.8 and Figure B.9.

Figure B.8: Drilled holes to relieve negative pressure during sample extruding.

Figure B.9: The hydraulic jack for extruding the specimen.

During the steps required to prepare the sample and prior to applying the confining stress, care should be taken to limit the disturbance and damage to the sample.

A useful practice to prevent any breakage and splitting in the sample was to carry the

sample by holding it on the palm of the hand and not carry it hanging. Soil material can barely resist extension loading and holding the sample from the top would apply such stresses resulting in splitting the sample.

B.3.4 Patching the surface of the sample

The samples were retrieved by one of the two techniques described in the previous section. In the case of dry and stiff samples, due to cutting the tube into eight sections with a power saw, eight grooves were carved on the surface of the sample. In the case of wet and soft samples drilling the holes on the length of the samples and pushing them out of the tube by a hydraulic jack would create a non-smooth surface. Sometimes some pieces of the tailings material could be separated from the surface of the sample which was due to rusting, non-homogeneity of the samples, or human error. Thus, the level of disturbance was assessed to either proceed with patching the rough surface of the sample or exclude the specimen from testing. If the decision was made to fix the surface gaps and holes, to keep the disturbance at a minimum level, the tailing materials that were detached from the samples were used to fill in the gaps and holes using a spatula.

In the case of the wet and soft samples, a procedure was considered to generate an insight into the level of the disturbance during the extraction of the sample. Due to the applied stresses, it is reasonable to include the void ratio as one of the sample properties which is subjected to variation in this phase. Therefore, after cutting the tube to the desired length, the diameter and the mass of the specimen were measured to calculate

the in-tube void ratio of the sample. After the sample extraction the void ratio value was compared to the post-extraction value and could be a useful piece of information in evaluating the disturbance. Although most of the specimens did not experience large variations in the void ratio, it is not known whether the structure of the sample was altered or not.

Application of this comparison was not practical for the dry and stiff samples due to the fact that the tube was cut into pieces to extract the sample. Since the mass of the empty tube was not available, measuring the mass of the sample in the tube was not possible and therefore the calculation of the void ratio in the tube could not be accomplished.

B.3.5 Trimming the end surfaces of the sample

According to ASTM 5311-92, the top and bottom ends of the samples should be flat to inhibit stress concentration during shearing. To trim the top and bottom surfaces, a cutting guide was used. The sample was placed on the countertop standing upright and the cutting mold was put together around the sample carefully. Then by sliding the sample to the edge of the countertop the required support was given by holding the bottom of the sample. The mold was laid on the side and depending on the rigidity of the sample, the ends were trimmed by using a small hacksaw or a wire saw as shown in Figure B.10.

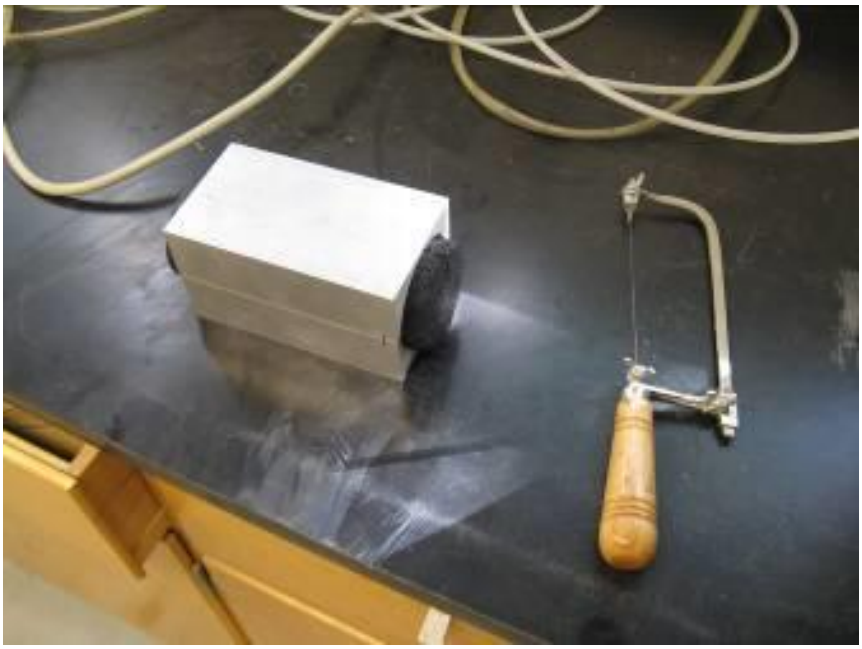

Figure B.10: Trimming the ends of the sample.

Although, this procedure might seem to be relatively insignificant, but overlooking it would not only create stress concentrations on the ends of the sample but also would cause issues specific to this system. In this system, as explained in Section B.3.7, the top platen is consisted of two halves. The bottom half is secured on top of the sample and the top half is hanging from the loading rod placed on the top part of the chamber (Figure B.11).

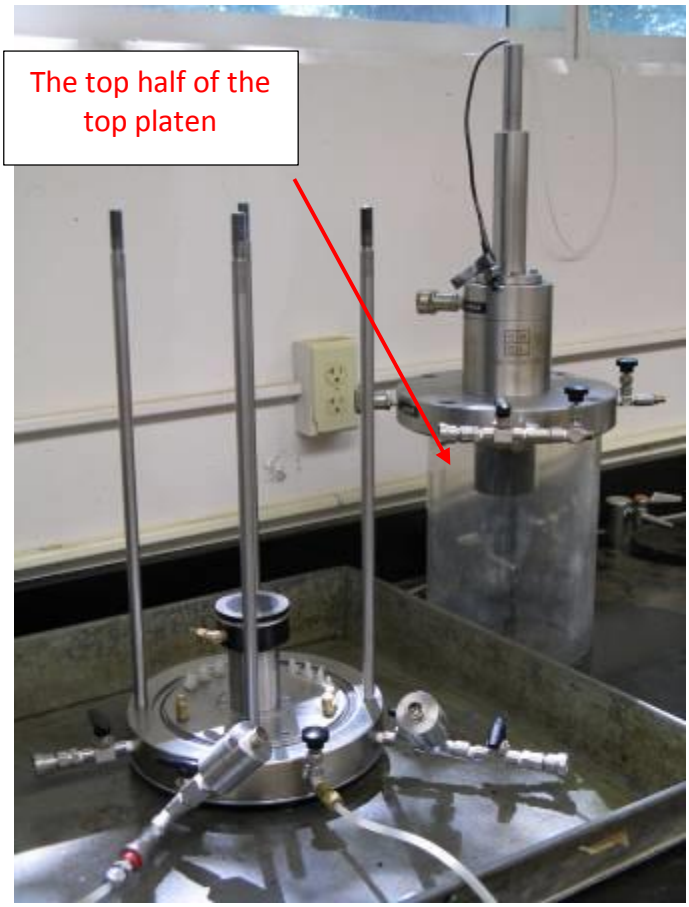

Figure B.11: The top half of the top platen is secured to the loading rod.

After assembling the chamber, the top half should be lowered through the interface software to fit on top of the bottom half. Considering the lack of access to the sample by hand at this stage, it is crucial to mount the specimen perfectly vertical. Otherwise, the top half would apply unnecessary stresses on the sample and in the case of severely tilted samples it may never fit.

B.3.6 Measuring the mass and dimensions of the sample

The mass, diameter, and length of the sample should be measured before placing the sample in the membrane and mounting it on the pedestal. All of this information is used to calculate the density, void ratio, stress and strain level, and other parameters

used in the calculation and interpretation of the results. Measurement of the mass was performed by using an Ohaus countertop Explorer Pro scale, model EP4102C, with 0.001 g precision. To diminish drying of the sample due to exposure to the air, it was decided to measure the diameter of the sample after putting the membrane on it. The diameter was measured at the top, middle, and bottom of the sample and in three directions at each level following the ASTM 5311-92 recommendation. The diameter of the sample was obtained by averaging these nine measurements and subtracting twice of the membrane thickness from that average. The caliper used to measure the diameter of the sample was a Mitutoyo 500-196-20 with 0.001-in precision. The length of the sample was measured using a metal ruler with 0.5 cm precision before putting the membrane on the specimen.

B.3.7 Covering the sample with the membrane

After recording the measurements on the sample, the sample needed to be covered with the membrane. In this system the load cell is installed inside the chamber and sits below the sample. To compensate for the chamber pressure, a hole is positioned on the body of the load cell. Presence of this hole obliterates the option to use water for pressurizing the chamber due to electrical issues. On the other hand, due to the high pressures that were supposed to be applied, it was highly unsafe to pressurize the chamber with air considering the chance of presence of invisible cracks on the Plexiglas chamber. Therefore, the chamber was filled with oil and consequently neoprene membranes were used to prevent breakage that could happen by using latex membranes.

The bottom platen which holds the porous stone was placed on top of the load cell and was secured by tightening the provided screw with a small Allen wrench. The 1/8-in tube connecting this platen to the bottom valve was attached to the connection using a combination wrench. In this research, the dry method as explained in ASTM 5311-92 was used to saturate the sample. Therefore, the bottom platen was not soaked. A filter paper was placed on the porous stone before putting the sample on the platen. To cover the sample with the membrane a membrane stretcher was used. By preference, the membrane was sealed with four O-rings at the top and bottom of the sample instead of two. To seal the bottom of the membrane, two of the O-rings were placed at the lower end of the stretcher. The membrane was stretched by applying vacuum to the mold as shown in Figure B.12. The procedure explained in this section can be performed in advance in order to shorten the exposure of the sample to air.

Figure B.12: Stretching the membrane by applying vacuum.

After slowly lowering the mold on the sample, the bottom of the membrane was rolled down to cover the groove on the bottom platen. Then, the two O-rings were rolled down and one was carefully placed snugly on the groove to ensure a tight seal. The second O-ring was used for extra protection against oil or water leakage. Following that, the top of the membrane was rolled up and the mold was raised slowly. At this stage, the vacuum on the mold could be cut off. The second filter paper was placed on top of the specimen afterwards.

As explained in Section B.3.5, the top platen consisted of two halves which were held together by applying vacuum into the space between them. An O-ring seals this space to maintain the vacuum throughout the experiment. The two top membrane O-rings were placed on the lower half of the top platen which holds the top porous stone too. To facilitate the placement of the top platen, the membrane was rolled down to cover just to the top of the sample. With the porous stone facing the top of the specimen the platen was placed on top of the filter paper. The procedure explained for sealing the bottom of the sample was repeated for the top. The 1/8 in tube connected to the top platen was wrapped around the sample to facilitate lowering Plexiglas chamber and was attached to the proper connection as shown in Figure B.13.

Figure B.13: Connecting the tubes and applying vacuum.

B.3.8 Applying vacuum

The undisturbed samples retrieved from Shelby tubes can slump and deform if a confining pressure is not applied on them. This is even more plausible for soft and wet samples. Therefore, the process of cutting the tubes and preparing the samples should be carried out as quickly as possible. After the membrane is placed on the sample and the top and bottom hoses are attached to the proper connection, a vacuum pressure was applied on the sample to inhibit slumping of the sample.

Applying the vacuum would confine the sample in the same manner the effective stress would do. The depth that the sample is obtained from would determine the in-situ

effective stress that the sample has experienced before. In order to limit the disturbance of the sample and to maintain it as a normally consolidated specimen, the applied vacuum should not exceed the in-situ effective stress. After applying the vacuum, a level can be used to ensure the flatness of the ends of the sample. The sample setup appeared similar to the sample presented in Figure B.13. The vacuum was applied at the top and bottom of the sample.

B.3.9 Sensor initialization

After checking the ends for levelness, the top platen O-ring could be placed on the bottom half. A thin layer of vacuum grease was applied on the O-ring for a better sealing quality. The load cell reading should be zeroed at this stage. All the cables connecting the sensors to the computer including the load cell, pore pressure transducers, cell pressure transducer, and LVDT sensor were attached to the proper port. The computer and the SCON-1500 system were switched on and initialized and the interface software (known as CATS) was loaded. By clicking on the “sensors” push button a table was displayed. The table contained the names and the current reading of all sensors attached to the system. By clicking on the load cell value, another window was displayed which included a push button to zero the load cell. The push button was pushed and the reading for the load cell was changed to zero lbs. The accuracy of the load cell was checked by a moderate precision method. A few scale weights were placed on top of the top platen bottom half and the load cell reading was read off of the monitor display.

It was reasonable to zero out the pressure transducers readings before starting to pressurize the chamber. To avoid losing the vacuum on the sample, two valves were installed on each connection to the top and bottom of the sample. The valves closer to the specimen were closed and a quick connector was inserted. The connector was open to the air and therefore the reading should have been zero psi. If the reading was not zero, the same procedure explained above for the load cell would be applied to zero out the pore pressure and cell pressure transducer readings. To avoid contaminating the pore water with the chamber oil, two separate quick connectors were used.

B.3.10 Sealing off the chamber

At this stage, the Plexiglas chamber was placed and the top of the cell was attached to the rest of the assembly. The proper O-ring was cleaned, covered with vacuum grease and positioned in the groove carved on the bottom of the triaxial cell. The bottom contact surface of the Plexiglas chamber was cleaned and covered with vacuum grease as well. Then it was lowered to fit correctly in the bottom groove. Afterwards, the top surface of the chamber was cleaned and covered with vacuum grease.

Placing the top part of the triaxial cell was a delicate task. The top part contains the hydraulic actuator portion of the loading system which eliminates the need to a load frame, making the top portion a hefty piece. Also, the top part holds the O-ring to seal the top of the Plexiglas chamber. Therefore, lowering it to have the chamber fit in the groove should be done slowly to avoid pinching the O-ring. To hover and maneuver the top portion, a 500 lbs crane was used.

After placing the top portion, a visual inspection was performed to check if the top O-ring was fitting in the groove correctly or not. Afterwards, the washers and nut caps were put on the screws and tightened to seal the chamber. Air pressure was used to detect any leaks in the chamber due to misplacement of the O-rings. Using the air pressure provided through the pressure board, the chamber was pressurized to 10 psi and then the experiment coordinator would listen to detect any air leaks. If no leaks were found, the chamber would be de-pressurized.

Before applying the seating load on the sample, a brief inspection was carried out to check for any leaks on the membrane or the connections. The vacuum pressure on the sample was recorded and then the valves connecting the sample to the vacuum source were shut off. The vacuum pressure on the sample was observed to detect any quick declining trend. A relatively quick decrease in the vacuum pressure suggests a leak on the membrane, a misplaced sample O-ring, or a leaky connection on the tubes. The vacuum pressure on the sample would eventually decline depending on the time length of the application of the vacuum. Most likely, if the vacuum has been applied for a short period of time, the center part of the sample was not affected by it yet. Hence, by shutting off the vacuum the pressures in the sample would start to balance and might appear as a leak. Therefore, care should be taken not to confuse a balance in the internal sample pressure with a leak.

B.3.11 Applying the seating load

After ensuring that the chamber and the specimen were properly sealed, the seating load could be applied on the sample. During the steps for pressurizing the chamber, sample saturation and consolidation, the sample could experience a broad range of stresses. To avoid a stress disturbance on the sample, a seating load is applied and maintained on the sample throughout the experiment. The seating load was chosen to be zero lbs, and in this system this process was carried out automatically. The system responds to the variation of stresses including compression and extension stresses using the load cell reading and will maintain the requested seating load constantly.

At this stage, the two halves of the top platen were connected. To achieve that, the hydraulic hoses were attached to the top portion of the triaxial chamber. The hoses were marked to identify the upper and lower hose distinctively. If they were mistaken, the machine would apply the load in the opposite direction of the requested load. The hydraulic pump was switched on to provide a constant 700 psi pressure in the hydraulic hoses. Using the CATS software, the loading rod position controller window was opened. The LVDT sensor was selected as the controlling sensor. The LVDT range was 1000 mills and the starting point for the platen was -500 mills. Movement of the LVDT to the bottom indicates a compressive direction. Therefore, the LVDT reading would increase by lowering the platen. By clicking on the position director, the top platen was lowered slowly while observing the gap between the two halves.

When the two halves became very close, the load cell reading was used to determine if any contact had occurred between them or not. The process was continued slowly at the rate of one mill on every click. At the contact point between the halves, the load cell began reading about 0.1 lbs. At this point, the top platen halves were inspected visually for a level contact. If it was found that the sample was tilted and connecting the top pieces would apply too much of stress concentration on the sample, the process would have been stopped and the triaxial cell would have been dis-assembled to correct the issue. If a level contact between the pieces was achieved, the top part was lowered more to sit on the bottom section. The load cell reading was observed constantly to ensure not to exceed 4 psi deviator stress on the sample. If the top part was positioned correctly on the bottom half, the O-ring would fit snugly and seal the space between them. At this point, vacuum pressure could be applied in this space to complete the process.

The vacuum should be applied slowly to avoid a stress shock to the sample. The machine should be allowed to respond to the stress variations until application of vacuum would cause no more change in the response. To automate the machine response, the controlling parameter in the loading rod position control window was selected to be the deviator stress. The requested deviator stress was selected to be zero psi throughout the experiment. Then the vacuum pressure was fully applied at the top platen. The machine responded to the deviator stress variation, corrected the deviator stress and maintained it at zero psi. From this point on, the machine responded to any variations in the deviator stress caused by cell pressure or pore pressure changes.

B.3.12 Filling the chamber

Once the chamber was sealed and the seating load was applied, the chamber was ready to be filled with oil. The reason for filling the chamber with oil is explained in Section B.3.7. The oil used in this research was DOT25 Shell which was recommended by the triaxial machine manufacturer. The vacuum source was connected to the top of the chamber and the chamber valves were submerged into the oil bucket. By opening the top of the chamber to the vacuum source and the bottom chamber valves to the oil source, the oil started filling the chamber slowly as illustrated in Figure B.14. The maximum vacuum pressure applied on the chamber in this experiment was -11.0 psi which was large enough to overcome the gravity and the viscosity forces in the tubes.

Figure B.14: Filling the chamber with oil.

It should be noted that using high magnitude vacuum would cause the oil to start boiling which in return reduces the delivery rate due to the formation of bubbles in the tubes. It is important to note that the vacuum magnitude should not exceed the vacuum pressure in the sample at any time. At this stage, the sample was still under vacuum pressure to inhibit slumping of the sample. If the vacuum in the chamber would have surpassed the sample vacuum, the membrane would start to inflate and detach from the sample. Also, if the chamber vacuum would have exceeded the vacuum pressure in the top platen, the two halves would separate from each other. Therefore, during filling of the chamber the pressure readings from the cell and pore transducers were constantly monitored and controlled for the abovementioned issue.

To avoid stress disturbance, it was always considered that the applied vacuum pressure on the sample would not exceed the in-situ effective stress. Considering the depth of the specimens and the location of the experiment, applying -13.0 psi vacuum on the sample and -11.0 psi on the chamber was sufficient to not vaporize the oil and not disturb the specimen stress history. However, for soft samples from shallow depth, lower values were used depending on the in-situ effective stress. Using the available configuration, this step took about 30 to 45 minutes.

B.3.13 Applying the cell pressure

Since the chamber was going to be pressurized with oil, care was taken not to let the oil infiltrate the pressure board. The pressure board applies the pressure by applying air pressure on the column of water in the cell pressure burette. On triaxial cells that can

be filled with water, the burette is directly connected to the chamber and can pressurize the chamber. However, in this system, an intermediate cell was used to provide a contact surface between the oil and water. The cell as shown in Figure B.15, provided a large space for this contact area to accommodate the volume changes without allowing the oil seep into the board. Since oil and water do not blend, no membrane was needed to transfer the pressure from the water to the oil.

Figure B.15: The chamber filled with oil and the intermediate cell to transfer pressure from water to oil.

After filling the chamber with oil, all the valves on the chamber were shut off. The tube connected to the cell pressure transducer was pulled from the oil bucket, cleaned and connected to the oil-water contact chamber. Keeping the chamber valve shut, a minimum cell pressure was adjusted on the pressure board which in this experiment 4.0 psi pressure was used. The chamber valve was opened, the cell was pressurized, and the load cell started reading a small compression load. The machine responded to that change

and maintained the zero psi seating pressure on the sample by moving the LVDT. At this point, if the other valves on the chamber were left open, the oil would have started to spill through that valve and the cell would have not been pressurized.

B.3.14 Flooding the sample

In this research, the sample was saturated following the dry method suggested by ASTM D5311-92. To facilitate pushing the air bubbles out of the sample, the saturation was performed from the bottom to the top. At this stage, the sample was still under vacuum although the purpose was not to avoid the sample deformations anymore, considering that the applied cell pressure would resolve that issue. The purpose of keeping the vacuum on the sample was simply to avoid letting air into the sample. It would be possible to saturate the sample faster and at lower pore pressures if the air content of the sample is reduced. The valve on bottom of the specimen was shut closed and the vacuum tube was disconnected from the bottom.

While the vacuum on top of the sample was maintained, a ¼ -in tube with quick connectors at both ends was used to flood the sample from the bottom. Before attaching the tube to the bottom of the sample, the tube was completely filled with de-aired water. The tube was connected to the bottom port on the sample. Before starting the flooding process, a number of parameters were recorded to be observed during the saturation and consolidation phases as suggested by ASTM D5311-92. These parameters included the LVDT reading, the pore and cell pressure, and the burette reading to monitor the volume

of water flowing in or out of the sample. All of this information was used to calculate the volume changes in the sample which lead to obtaining updated sample dimensions.

The pore pressure to be applied was adjusted by the regulator on the pore pressure water column. With the pore pressure valve shut, the LVDT and the burette reading were recorded. To make it visually traceable, the burette was only allowed to be pressurized through the annulus. Therefore, the inner tube level could not be changed and made it easy to compare the initial and the final levels. It should be noted that in this procedure, the term “inner tube” is used instead of burette to avoid confusing it with the burette that refers to the cylindrical assembly of the tube and the annulus. The pore pressure valve was opened and the water started flowing into the sample from the bottom. The change in the pore pressure will apply some pressure on the sample. Therefore, the system will respond to this change and maintains the seating load at zero psi by moving the LVDT.

The back pressure for flooding the sample was set at 3 psi to be lower than the cell pressure set at 4.5 psi. The vacuum on top of the sample in this process was supplied by the building vacuum system which is averaging around -8.0 psi. During the flooding phase, the effective stresses at the top and bottom of the sample were different. In the presented example, the effective stress on top and bottom of the sample were 12.5 psi and 1.5 psi respectively. However, this difference could be obliterated by applying the consolidation pressure. This explains why the vacuum was not applied on top of the soft samples with in-situ effective stresses less than 12.5 psi.

To determine correctly which specimen could be exposed to vacuum for a long period of time, the in-situ effective stress of the sample should have been calculated. At this stage of the experiment, all of the input parameters except the void ratio were available. The void ratio could be calculated using weight-volume relationships. Therefore, the water content of the sample needed to be identified. It would take a few hours for the water content samples to be dried in the oven. Consequently, the experiment conductor estimated the water content to proceed with the flooding stage. In a few hours after starting the flooding, the water content could be measured and precise calculations could be made to confirm the possibility of application of vacuum. By experience it was confirmed that for all of the specimens except the ones retrieved from depths lower than 30 ft., the vacuum could be applied.

By employing the abovementioned configuration, water would start flooding the sample from the bottom to the top and filling the void space in the sample. An approximate observation to stop flooding and start the saturation phase was the discontinuation of air bubbles exuding from the top of the sample. A typical flooding phase would usually range between one to two days, depending on the permeability of the sample and the application of the vacuum on top.

B.3.15 Saturating the sample

Before starting the saturation phase, the vacuum would be cut off from the top with the valve in the shut position, and the burette and LVDT readings were recorded. To saturate the sample a small chamber was used to transfer the pressure to the specimen.

The chamber was consisted of two small chambers which were in contact through a rubber membrane. The chamber which is normally used to deal with contaminated liquids is shown in Figure B.15. During the saturation phase, the water would flow into the sample; however it is pushed out of the sample during the consolidation phase. If a tube was used to pressurize the sample, during the consolidation phase pore water contaminated with dissolved or floating substances from the sample could be transferred to the pressure board. The contamination which included the Shelby tube rust or other chemicals washed out of the specimen could be left in the pressure board connections and cause accelerated oxidization or clogging of the tubes.

A T-connection was used to branch one of the small chambers to the top and bottom of the sample. The pressure set to flood the specimen was applied to the saturating chamber. By opening the valves on top and bottom of the sample to the saturating chamber, both ends of the sample were exposed to approximately 1.5 psi effective stress. Since the top was under approximately 12.5 psi effective pressure in the previous phase, the top valve was opened to avoid a stress shock. The water flows into the top to balance the pressure difference. The sample was left in this condition for a short period of time, and the machine constantly corrected the LVDT position to maintain the zero psi seating pressure.

Before starting the saturation process, the in-situ effective stress needed to be determined. At this stage of the experiment, the water content and void ratio of the specimen were precisely measured, and therefore the in-situ effective stress of the

specimen was known. The reason to know the effective stress of the sample at the saturation phase was the limited level of available air pressure.

The provided air compressor was capable of providing air at 150 psi pressure. However, by using the supplied air, the pressure would be dropped and the compressor would not be started until the pressure was lowered to 110 psi. Therefore, the maximum reliable air pressure was determined to be 110 psi which could be used to apply the cell pressure. By subtracting the in-situ effective stress of the sample from the maximum reliable air pressure, the maximum saturation pressure could be determined. For example, if the in-situ effective stress of a sample was calculated to be 30 psi, the maximum cell pressure and the maximum pore pressure in the consolidation phase could be set at 110 psi and 80 psi respectively. During the saturation phase, there was no advantage in exceeding 80 psi pore pressure for the said sample, since it had to be lowered in the consolidation phase.

When the LVDT reading stopped changing and the in-situ effective stress of the sample was identified, the saturation could be started. At this stage, the cell pressure was 1.5 psi greater than the pore pressure which was sufficient for confining the specimen. The pore pressure and cell pressure increase were applied in 5 psi increments in order to let the machine respond to the variation in the seating load which in return would inhibit the stress shock. By reaching the desired pore pressure level, the cell pressure would still be 1.5 psi greater than the pore pressure. The specimen could be left at this condition for

a day to let all the remaining air bubbles be dissolved into water and provide a saturated sample.

B.3.16 Measuring the B-value

At any desired time after starting the saturation, the saturation level could be obtained by measuring the Skempton's parameter B which a B value of 1.00 is taken to demonstrate complete saturation. For all of the specimens a B value of 0.98 was achieved which is the recommended value by ASTM D5311 for fine grained samples. Although the limitations on the air pressure did not allow high pore pressures, but for most of the specimens achieving a B value of 1.0 was possible. The procedure for checking the B value was followed as recommended by ASTM D5311.

To measure the B value, the top and bottom valves on the specimen were shut to stop pressurizing by the pressure board, while the transducers could still measure the pore pressure. The pore pressure was allowed to be balanced and the small pressure variation due to closing of the valves would be dissipated. The pore pressure and cell pressure values were recorded and the cell pressure was increased by 10 psi. The pore pressure would increase and the machine would try to maintain the seating pressure of zero psi by adjusting the LVDT position. The pore pressure value was observed and after a while it would be observed that the pore pressure had reached a constant value. By using the equation B= the Skempton's parameter B would be calculated. If the B value was still under 0.98, the saturation phase would be continued. This would be done by reducing the cell pressure to the previous value and exposing the specimen to the

backpressure for a longer time by opening the pore pressure valves. However, the back pressure could be increased if it still had not reached the maximum available back pressure as was explained in Section B.3.15.

B.3.17 Consolidating the sample

After achieving a B value of at least 0.98, the consolidation phase could be started. The burette reading and the LVDT value were recorded before starting this phase. At this stage, the pore pressure was set at a value that resulted in full saturation of the sample, and the cell pressure was set to approximately 1.5 psi higher than that value. To normally consolidate the sample, the cell pressure needed be increased to a level to provide an effective stress equivalent to the in-situ effective stress of the sample. Therefore, the pore pressure was maintained constant while the cell pressure was increased to the desired value. It was observed that the water was pushed out of the sample and started filling the pore pressure burette. Again, the machine responded to the stress variations and maintained the seating load by adjusting the LVDT position.

This process would take a few hours to be completed depending on the permeability of the sample and the applied effective pressure. Although the samples had a fine gradation, the consolidation process did not take a long time to be accomplished. This indicated that the specimens relatively had higher permeability compared to typical fine grained soils. Therefore, the idea of liquefaction of these samples seemed more plausible.

The LVDT position and the burette reading were observed over the consolidation period to identify a final constant value. If theses readings would reach a constant value it was an indicator of the completion of the consolidation phase. Before making any final decision on termination of the consolidation phase, the recorded values of LVDT over time were exported from the machine. This data was used to plot a sample deformation versus log scale of time to identify the completion of the consolidation phase and calculating the parameter Cv (compression index) for each specimen.

Upon completion of the consolidation phase, the final values of LVDT and the pore pressure burette reading were recorded. These parameters along with the same parameters recorded for the saturation phase, were used to update the dimensions of the sample. The procedure to calculate the final dimensions of the specimen is explained in ASTM D5311. The samples would approximately become 0.02-in to 0.06-in (0.5 mm - 1.5 mm) shorter at the end of consolidation compared to the initial height of the sample measured before putting the membrane around them.

B.3.18 Cyclic triaxial loading of the sample

By identifying the completion of primary consolidation of the specimen, the loading phase could be started. To have all the necessary data recorded during the cyclic triaxial loading a specimen file was created. Considering the number of specimens to be tested, the information folder was divided into two subfolders denoting the location of the mine tailings the samples were provided from. These subfolders included Abner Fork, and Big Branch. In each of these subfolders, two subfolders identifying the crest samples

or the toe samples were created. The format for the name of the file was chosen to be concise and at the same time provide the most information about the sample. For example, a specimen from the Big Branch mine tailings, obtained at the toe (location A), in piston 11, and from the top of the piston (Sample 1) would be stored by the following format:

Mine Tailings\Big Branch\Loc A\TBBLAPST11S1

In the sample file, parameters such as the sample mass, dimensions, specific gravity, and membrane thickness were stored. Thereafter, the amplitude of the cyclic waves to be applied was. Based on the experience of the experiment conductor, the magnitude of the load was chosen to result in the cyclic stress ratios (CSR) greater than 0.25. The CSR parameters greater than 0.25 would normally result in the liquefaction of the specimens with the number of cycles depending on the load amplitude, density, void ratio, level of saturation, and age of the specimen.

Either the frequency or the period of the cyclic load should be adjusted on the tab provided in the loading window. The suggested range by ASTM D5311 for the frequency of cyclic liquefaction experiments is 0.5 Hz -2 Hz. In this research a frequency of 1 Hz equivalent to a period of 1 sec was applied.

References

Andersen, K. H., Kleven, A., and Heien, D. (1988). “Cyclic soil data for design of gravity structures.” *Journal of Geotechnical Engineering*. 114(5), 517-539.

Andrews, D. C. A. and Martin, G. R. (2000). “Criteria for liquefaction of silty soils.” *Proceedings of the 12th World Conference on Earthquake Engineering*, New Zealand, Paper No. 0312

Andrus, D. R., and Stokoe, K. H., II, (1997). “Liquefaction Resistance Based on Shear Wave Velocity,” *Proceedings, NCEER Workshop on Evaluation of Liquefaction Resistance of Soils*, T.Y. Youd and I.M. Idriss, Eds., Buffalo, NY.

Andrus, R. D., Stokoe, K. H., II, and Chung, R. M. (1999). “Draft Guidelines for Evaluating Liquefaction Resistance Using Shear Wave Velocity Measurements and Simplified Procedures.” *NISTIR 6277*, National Institute of Standard and Technology, Gaithersburg, MD.

Andrus, D. R., and Stokoe, K. H., II (2000). “Liquefaction Resistance of Soils from Shear-Wave Velocity,” *ASCE, Journal of Geotechnical and Geoenvironmental Engineering*, 126(11), 1015-1025.

Arthur, J. R. F., Dunstan, T., Rodriguez del, C. J. I., and Chua, K. S. (1980). “Principal stress rotation: a missing parameter.” *Journal of the Geotechnical Engineering Division, ASCE*, 106(GT4): 419–433.

ASTM D422 - 63(2007) Standard Test Method for Particle-Size Analysis of Soils. American Society for Testing and Materials, Annual Book of ASTM Standards. Vol. 04.08.

ASTM D854 - 10 Standard Test Methods for Specific Gravity of Soil Solids by Water Pycnometer. American Society for Testing and Materials, Annual Book of ASTM Standards. Vol. 04.08.

ASTM D1586 - 99 Standard test method for penetration test and split-barrel sampling of soils. American Society for Testing and Materials, Annual Book of ASTM Standards. Vol. 04.08.

ASTM D1587 - 00 Standard practice for thin-walled tube sampling of soils for geotechnical purposes. American Society for Testing and Materials, Annual Book of ASTM Standards. Vol. 04.08.

ASTM D2216 - 10 Standard Test Methods for Laboratory Determination of Water (Moisture) Content of Soil and Rock by Mass. American Society for Testing and Materials, Annual Book of ASTM Standards. Vol. 04.08.

ASTM D2573 - 08 Standard Test Method for Field Vane Shear Test in Cohesive Soil. American Society for Testing and Materials, Annual Book of ASTM Standards. Vol. 04.08.

ASTM D2850 - 03a (2007) Standard Test Method for Unconsolidated-Undrained Triaxial Compression Test on Cohesive Soils. American Society for Testing and Materials, Annual Book of ASTM Standards. Vol. 04.08.

ASTM D3441 - 05 Standard Test Method for Mechanical Cone Penetration Tests of Soil. American Society for Testing and Materials, Annual Book of ASTM Standards. Vol. 04.08.

ASTM D3999 - 11 Standard Test Methods for the Determination of the Modulus and Damping Properties of Soils Using the Cyclic Triaxial Apparatus. American Society for Testing and Materials, Annual Book of ASTM Standards. Vol. 04.08.

ASTM D4318 - 10 Standard Test Methods for Liquid Limit, Plastic Limit, and Plasticity Index of Soils. American Society for Testing and Materials, Annual Book of ASTM Standards. Vol. 04.08.

ASTM D5311 - 11 Standard Test Method for Load Controlled Cyclic Triaxial Strength of Soil. American Society for Testing and Materials, Annual Book of ASTM Standards. Vol. 04.08.

ASTM D6066 - 11 Standard Practice for Determining the Normalized Penetration Resistance of Sands for Evaluation of Liquefaction Potential. American Society for Testing and Materials, Annual Book of ASTM Standards. Vol. 04.08.

ASTM D7400 - 08 Standard Test Methods for Downhole Seismic Testing. American Society for Testing and Materials, Annual Book of ASTM Standards. Vol. 04.08.

Atkinson, J. H., Allman, M. A., and Boese, R. J. (1992). “Influence of laboratory sample preparation procedures on the strength and stiffness of intact Bothkennar soil recovered using the Laval sampler.” *Geotechnique*, 42(2), 349-354.

Atukorala, U. D., Wijewickreme, D., and McCammon, N. R. (2000). Some observations related to liquefaction susceptibility of silty soils. In Proceedings of the 12th World Conference on Earthquake Engineering, Auckland, New Zealand, 30 January – 4 February

2000. New Zealand Society for Earthquake Engineering, Upper Hutt, New Zealand. Paper 1324.

Averitt, P. (1975). *Coal resources of the United States*, January 1, 1974: U.S. Geological Survey, Bulletin 1412, 131 p.

Baligh, M. M. (1985). “Strain path method.” *Journal of Geotechnical Engineering*. 111(9), 1108-1136.

Baligh, M. M., Azzouz, A. S., and Chin, C. (1987). “Disturbances due to "ideal" tube sampling.” *Journal of Geotechnical Engineering*. 113(7), 739-757.

Bollinger, G. A., Davison, F. C., Sibol, M. S., and Birch J. B. (1989). “Magnitude recurrence relations for the southeastern United States and its subdivisions,” Journal of Geophysical Research, 94, 2857-2873.

Boulanger, R. W., Meyers, M. W., Mejia, L. H., and Idriss I. M. (1998). “Behavior of a fine-grained soil during the Loma Prieta earthquake.” *Canadian Geotechnical Journal*, 35, 146-158.

Boulanger, R. W., and Idriss, I. M. (2004). *Evaluating the potential for liquefaction or cyclic failure of silts and clays.* Rep. No. UCD/CGM-04/01, Center for Geotechnical Modeling, Dept. of Civil and Environmental Engineering, Univ. of California, Davis, Calif.

Boulanger, R. W. and Idriss, I. M. (2004b). "State normalization of penetration resistances and the effect of overburden stress on liquefaction resistance." Proc., 11th Int. Conf. on Soil Dynamics and Earthquake Engineering, and 3rd Int. Conf. on Earthquake Geotechnical Engineering, D. Doolin et al., eds., Stallion Press, Vol. 2, 484-491.

Boulanger, R. and Idriss, I. (2006). ”Liquefaction Susceptibility Criteria for Silts and Clays.” *Journal of Geotechnical and Geoenvironmental Engineering*, 132(11), 1413–1426.

Brady, L. L. (1979). *Kansas Coal Resources and Production*, Kansas Geological Survey, Guidebook 4.

Bray, J. D., Sancio, R. B., Riemer, M. F., and Durgunoglu, T. (2004). “Liquefaction susceptibility of fine-grained soils.” Proc., 11th Int. Conf. on Soil Dynamics and Earthquake Engineering and 3rd Int. Conf. on Earthquake Geotechnical Engineering, D. Doolin et al., eds., Stallion Press, Singapore, 655–662.

Byrne, P. M. and M. Seid-Karbasi (2003). "Seismic Stability of Impoundments." *17th Annual Symposium*, Vancouver Geotechnical Society.

Campanella, R. G. and Lim, B. S. (1981). "Liquefaction characteristics of undisturbed soils." *Proceedings of the International Conference on Recent Advances in Geotechnical Earthquake Engineering and Soil Dynamics*. Vol. 1, pp. 227-230.

Campanella, R. G., Robertson, P. K., Gillespie, D. (1983). "Cone penetration testing in deltaic soils." *Canadian Geotechnical Journal*, 20(1), 23-35.

Casagrande, A., (1976), "Liquefaction and Cyclic Mobility of Sands: a Critical Review", Harvard Soil Mechanics Series 88, Harvard University, Cambridge, Massachusetts.

Castro, G. (1975). "Liquefaction and cyclic mobility of saturated sands." *Journal of the Geotechnical Engineering Division, Proceedings of the ASCE*, 101(6), 551- 569.

Castro, G. (2003). "Evaluation of Seismic Stability of Tailings Dams," Proceedings, 12th Pan American Conference on Soil Mechanics and Geotechnical Engineering and 39th U.S. Rock Mechanics Symposium, Cambridge, MA, pp. 2229-2234.

Castro, G. and Poulos, S. J. (1977). "Factors affecting liquefaction and cyclic mobility." *Journal of the Geotechnical Engineering Division, Proceedings of the ASCE*, 103(6), 501-516.

Castro, G., and Troncoso, J. H. (1989). "Effects of 1985 Chilean Earthquake on Three Tailings Dams," *Proceedings of the Fifth Chilean conference on Seismology and Earthquake Engineering*, August 7-11, 1989, Santiago, Chile.

Clayton, C. R. I., Matthews, M. C. and Simons, N. E., (1995). *Site Investigations*. Blackwell Science, Oxford, 2nd Edition, ISBN 0-632-02908-0.

CLiq (Version 1.7) [Computer Software], GeoLogismiki, Retrieved January 2013, Available from http://www.geologismiki.gr.

Coffman, J. L., and Von Hake, C. A. (1970). *Earthquake History of the United States* Publication 41-1. United States Department of Commerce / United States Department of the Interior. p. 25.

CUSEC, (2002). *The Elected Officials Guide to Earthquakes in the Central United States*. Central United States Earthquake Consortium Publication No. CUSEC PA-EOG-2002.

Davies, M. P. and Martin, T. E. (2000). “Upstream Constructed Tailings Dams — A Review of the Basics.” *Proceedings, Tailings and Mine Waste 2000*. A. A. Balkema Publishers, Rotterdam, p. 3-15.

de Alba, P., Benoit, J., Pass, D. G., Carter, J. J., Youd, T. L., and Shakal, A. F. (1994). “Deep instrumentation array at Treasure Island Naval Station.” *U. S. Geological Survey Professional Paper*, 1551-A, 155-168.

Dobry, R., and Alavarez, L. (1967). “Seismic Failures of Chilean Tailings Dams,” *Journal of the Soil Mechanics and Foundations Division, Proceedings of the ASCE*, 93(SM6), 237-260.

Dobry, R., Yokel, F. Y., and Ladd, R. S. (1981). “Liquefaction potential of overconsolidated sands in areas with moderate seismicity.” *Proceedings of Earthquakes and Earthquake Engineering: the Eastern United States*, pp. 643-664.

Donaghe, R. T., and Gilbert, P. A. (1983). “Cyclic rotation of principal planes to investigate liquefaction of sands,” *US Waterways Experiment Station*, Vicksburg, Miss., Miscellaneous Paper GL-83-24.

El Hosri, M. S., Biarez, J., and Hicher, P. Y. (1984). “Liquefaction Characteristics of Silty Clay”, *8th World Conf. on Earthquake Engineering*, Prentice-Hall Eaglewood Cliffs, N.J., 3. 277-284.

Ellison, R. D. and Cho, Y. Y. (1976). “Liquefaction Considerations for Fine Coal Refuse,” *Ohio River Valley Soils Seminar*, Lexington, KY.

Farrar, J. A., Torres, R., and Crutchfield, L. G. (2008). *Cone penetrometer testing, Scoggins Dam, Tualatin Project, Oregon*. Engineering Geology Group Bureau of Reclamation, Technical Services Center, Denver, Colo. Report No. 86–68320.

Finn, W. D. L., Pickering, D. J., and Bransby, P. L. (1971). “Sand liquefaction in triaxial and simple shear tests,” *Journal of the Soil Mechanics and Foundations Division, ASCE*, 97(4), 639-659.

Finn, W. D. L., Vaid, Y. P., and Bhatia, S. K. (1978). “Constant volume simple shear testing,” *In Proceedings of the 2nd International Conference on Microzonation for Safer Construction*, Research and Application, San Francisco, California, 26 November - 1 December 1978. Vol. 2, 839–851.

Finn, W. D. L., Ledbetter, R. H., and Wu, G. (1994). “Liquefaction in silty soils: design and analysis.” *In Ground failures under seismic conditions*. Edited by S. Prakash and P.

Dakoulas. American Society of Civil Engineers, Geotechnical Special Publication 44, pp. 51–76.

Frankel, A. D., Applegate, D., Tuttle, M. P., and Williams, R. A. (2009). *Earthquake hazard in the New Madrid Seismic Zone remains a concern*. U.S. Geological Survey Fact Sheet 2009–3071, 2 p.

Google Maps, (2013a, March 03). "Abner Fork impoundment aerial photo." Google, Retrieved from http://maps.google.com.

Google Maps, (2013b, March 03). "Big Branch impoundment aerial photo." Google, Retrieved from http://maps.google.com.

Guo, T., and Prakash, S. (1999). "Liquefaction of Silts and Silt-Clay Mixtures." *Journal of Geotechnical and Geoenvironmental Engineering*, 132(6), 716-735.

Haile, J. P. (1997). "Discussion on the failure of the Omai tailings dam." *Geotechnical News*, 15, p. 44-49.

Hardin, B. O. & Drnevich, V. P. (1972). "Shear modulus and damping in soils: Design equations and curves." *Journal of Soil Mechanics and Foundations Division, ASCE*. 98(7): 667-692.

Heisey, J. S., Stokoe II, K. H., and Meyer, A. H. (1982). *Moduli of pavement systems from Spectral Analysis of Surface Waves.* Transportation Research Record 853, Transportation Research Board Washington, D.C.

Hight, D. W., Boese, R., Butcher, A. P., Clayton, R. I., and Smith, P. R. (1992). "Disturbance of the Bothkennar clay prior to laboratory testing." *Geotechnique*, 42(2), 199-217.

Hight, D. W., and Georgiannou, V. N. (1995). "Effects of sampling on the undrained behaviour of clayey sands." *Geotechnique*, 45(2), 237-247.

Holtz, R. D., Kovacs, W. D. (1981). *An Introduction to Geotechnical Engineering*, 1st edition, Englewood Cliffs, NJ: Prentice Hall.

Holtz, R. D., Kovacs, W. D., and Sheahan, T. C. (2011). *An Introduction to Geotechnical Engineering*, 2nd Edition, Upper Saddle River, NJ: Pearson Prentice-Hall, 853 pp.

Hvorslev. M. J. (1949). *Subsurface Exploration and Sampling of Soils for Civil Engineering Purposes*. Waterways Experiment Station, Vicksburg, Mississippi.

Hough, S. E. (2009). *Cataloging the 1811-1812 New Madrid*, Central U.S., Earthquake Sequence, Seismological Research Letters, 80(6), 1045-1053.

Hynes, M. E. and Olsen, R. S. (1999). "Influence of confining stress on liquefaction resistance." *Physics and Mechanics of Soil Liquefaction*, Lade and Yamamuro (editors), pp. 145-151.

Idriss I. (1990). "Response of soft soil sites during earthquakes." *H. B. Seed Memorial Symposium*, Vol.2, Bi Tech: 273-289.

Idriss, I. W., and Boulanger, R. W. (2006). "Semiempirical procedures for evaluating liquefaction potential during earthquakes." *Soil Dynamics and Earthquake Engineering*, 26(2), 115-130.

Idriss, I. M., and Boulanger, R. W. (2007). "SPT- and CPT-based relationships for residual shear strength of liquefied soils." *Proc., 4th Int. Conf. on Earthquake Geotechnical Engineering*, K. D. Pitilakis, ed., Springer, New York, 1–22.

Idriss, I. M., and Boulanger, R. W. (2008). *Soil Liquefaction during Earthquakes.* MNO-12, Earthquake Engineering Research Institute, Oakland, CA.

Ishihara, K., Sokekawa, M., and Tanaka, Y. (1978). "Effects of overconsolidation on liquefaction characteristics of sands containing silts." *Dynamic Geotechnical Testing, ASTM Special Technical Publication 654, ASTM*, pp. 246-264.

Ishihara, K, Tatsuoka, F., and Yasuda, S. (1975). "Undrained deformation and liquefaction of sand under cyclic stresses." *Soils and Foundations*, 15, 29-44.

Ishihara, K. and Takatsu, H. (1979). "Effects of overconsolidation and K_0 conditions on the liquefaction characteristics of sands." *Soils and Foundations*. 19(4), 59-68.

Ishihara, K., Troncoso, J., Kawase, Y., and Takahashi, Y. (1980). "Cyclic strength characteristics of tailings materials." *Soils and Foundations*. 20(4), 127-142.

Ishihara, K., Yasuda, S., and Yokota, K. (1981). "Cyclic Strength of Undisturbed Mine Tailings", *Proceedings of the International Conference on Recent Advances in Geotechnical Earthquake Engineering and Soil Dynamics*, St. Louis, Missouri, University of Missouri - Rolla, Vol. 1, pp. 53-58.

Ishihara, K. (1993a). “Post-Earthquake Failure of a Tailings Dam Due to Liquefaction of the Pond Deposit.” *Proceedings of the Third International Conference on Case Histories in Geotechnical Engineering*, July 1-4, 1993, Saint Louis, Missouri, pp. 1129-1143.

Ishihara, K. (1993b). “Liquefaction and flow failure during earthquakes.” *Geotechnique*, 43(3), 351–451.

Ishihara, K. (1996). *Soil Behaviour in Earthquake Geotechnics*. Oxford University Press, Oxford.

Jamiolkowski, M., Ladd, C. C., Germaine, J. T., and Lanellotta, R. (1985). “New Developments in Field and Laboratory Testing of Soils: Theme Lecture No. 2.” *Proceedings of the 11th International Conference of Soil Mechanics and Foundation Engineering*, San Francisco, Vol. 1, pp. 57-155.

Jeyapalan, J., Duncan, J., and Seed, H. (1983). ”Analyses of Flow Failures of Mine Tailings Dams.” *Journal Geotechnical Engineering*, 109(2), 150–171.

Jeyapalan, J., Duncan, J., and Seed, H. (1983). ”Investigation of Flow Failures of Tailings Dams.” *Journal Geotechnical Engineering*, 109(2), 172–189.

Johnston, A. C., and Schweig, E. S. (1996). *The enigma of the New Madrid earthquakes of 1811-1812*. Annual Review of Earth and Planetary Sciences, 24, 339-384.

Juang, C. H., Yuan, H., Lee, D. H., and Lin, P. S. (2003). “Simplified Cone Penetration Test-based Method for Evaluating Liquefaction Resistance of Soils.” *Journal of Geotechnical and Geoenvironmental Engineering, ASCE*, Vol. 129(1) 66-80.

Kalinski, M. E. (2011). *Lightweight inflatable borehole receiver unit for seismic testing.* United States patent No. 7,954,595.

Kalinski, M. E. (2012). “A Small, Lightweight Borehole Receiver for Crosshole and Downhole Seismic Testing,” *Geotechnical Testing Journal*, 35(2), 363-366.

Kalinski, M. E. and Phillips, J. L. (2008). “Development of methods to predict the dynamic behavior of fine coal refuse: Preliminary results from two sites in Appalachia.” In Zeng, X.; Manzari, M. T.; and Hitunen, D. R. (Editors), *Proceedings of the Conference of Geotechnical Earthquake Engineering and Soil Dynamics IV: GSP-181*, pp. 1–10, American Society of Civil Engineers, Reston, VA, 10 p.

Kayen, R.E., Mitchell, J.K., Lodge, A., Seed, R.B., Nishio, S., and Coutinho, R. (1992). "Evaluation of SPT-, CPT-, and shear wave-based methods for liquefaction potential assessment using Loma Prieta data." *Proc. of the Fourth Japan - U.S. Workshop on Earthquake Resistant Design of Lifeline Facilities and Countermeasures for Soil Liquefaction*, in M. Hamada and T.D. O'Rourke, eds., NCEER Res Tech. Rep. (1) 177-204.

Kramer, S. L., (1996). *Geotechnical Earthquake Engineering*, 1st edition. Prentice Hall. Upper Saddle River, New Jersey, 653 pp.

Ladd, C. C. and Lambe, T. W. (1963). "The strength of "undisturbed" clay determined from undrained tests." *Preliminary copy of a paper for the ASTM-NRC Symposium on Laboratory Testing of Soils*, Ottawa, Canada. 30 pages.

Ladd, C. C. and DeGroot, D. J. (2003). "Recommended practice for soft ground site characterization." *The Arthur Casagrande Lecture, Proceedings of the 12th Panamerican Conference on Soil Mechanics and Geotechnical Engineering*, Boston, MA, 3-57.

Landva, A., (1964). "Equipment for cutting and mounting undisturbed specimens of clay in testing devices." *Norwegian Geotechnical Institute Publication*, No. 56.

La Rochelle, P., Sarrailh, J., Tavenas, F., Roy, M., and Leroueil, S. (1981). "Causes of sampling disturbance and design of a new sampler for sensitive soils." *Canadian Geotechnical Journal*, 18,52–66.

Lee, K. L. and Focht, J. A. Jr. (1975). "Liquefaction potential at Ekofisk Tank in North Sea." *Journal of the Geotechnical Engineering Division, Proceedings of the ASCE*. 101(1), 1-18.

Lee, K. L. and Focht, J. A. Jr. (1976). "Strength of clay subjected to cyclic loading." *Marine Geotechnology*. 1(3), 165-185.

Lee, K. L. and Roth, W. (1977). "Seismic stability analysis of Hawkins hydraulic fill dam." *Journal of the Geotechnical Engineering Division, Proceedings of the ASCE*. 103(6), 627-644.

Lee, K. L., Seed, H. B., Idriss, I. M. and Makdisi, F. I. (1975). "Properties of soil in the San Fernando hydraulic fill dams." *Journal of the Soil Mechanics and Foundations Division, Proceedings of the ASCE*, 101(8), 801-821.

Lee, K. L. and Seed, H. B. (1967). "Cyclic stress conditions causing liquefaction of sand." *Journal of the Soil Mechanics and Foundations Division, Proceedings of the ASCE*, 93(1), pp. 47-70.

Lunne, T., Robertson, P. K., and Powell, J. J. M. (1997). *Cone penetration testing in geotechnical practice*. Blackie Academic, EF Spon/Routledge, New York.

Marcuson, W.F. III (Chairman) Committee on Soil Dynamics of the Geotechnical Engineering Division (1978) Definition of terms related to liquefaction. *Journal of the Geotechnical Engineering Division, Proceedings of the ASCE*, Vol. 104, No. 9, pp. 1197-1200.

Marcuson, W. F., Ballard, R. F., and Ledbetter, R. H. (1979). "Liquefaction Failure of Tailings Dams Resulting from the Near Izu Oshima Earthquake, 14 and 15 January 1978," *Proceedings of the Sixth Pan-American Conference on Soil Mechanics and Foundation Engineering*, Lima, Peru, pp. 69-80.

Marcuson, W. F., Hynes, M. E., and Franklin, A. G. (1990). "Evaluation and use of residual strength in seismic safety analysis of embankments". *Earthquake Spectra, EERI*, 6(3): 529–572.

McKee, B. E., Robinson, K. E., and Urlich, C. M. (1979). "Upstream design for extension of an abandoned tailings pond." *In Tailings Disposal Today: Proceedings of the 2nd International Tailings Symposium*, Denver, Colo., May 1978. Edited by G.O. Argall. Miller Freeman Publications, San Francisco, Calif. Vol. 2, pp. 210–233.

Moriwaki, Y., Akky, M. R., Ebeling, R., Idriss, I. M., and Ladd, R. S. (1982). "Cyclic strength and properties of tailing slimes." *Proceedings of Specialty Conference on Dynamic Stability of Tailings Dams, ASCE*.

Moss, R. (2003). "CPT-based Probabilistic Assessment of Seismic Soil liquefaction initiation." Ph.D. Dissertation, University of California, Berkeley.

Moss, R. E. S., Seed, R. B., and Olsen, R. S. (2006). "Normalizing the CPT for overburden stress." *Journal of Geotechnical and Geoenvironmental Engineering*, 132(3): 378-387.

MSHA, (2001). "Report of Investigation: Surface Impoundment Facility Underground Coal Mine, Non-injury Impoundment Failure/Mine Inundation Accident, October 11, 2000, Big Branch Refuse Impoundment, Martin County Coal Corporation, Inez, Martin County, Kentucky." United States Department of Labor - Mine Safety and Health Administration.

Munson, P. J., Obermeier, S. F., Munson, C. A., and Hajic, E. R. (1997). *Liquefaction evidence for Holocene and latest Pleistocene seismicity in the southern halves of Indiana and Illinois: a preliminary overview.* Seismological Research Letters, 68(4).

Nagase, H., Yasuda, S., Tsujino, S. Shinji, R., and Yanagihata, T. (1996). "Liquefaction Strength characteristics of overconsolidated sand samples." *Proceedings of the Eleventh World Conference on Earthquake Engineering*, Oxford, England. Paper 1089.

Nazarian, S., Stokoe II, K. H., and Hudson, W. R. (1983). *Use of spectral analysis of surface waves method for determination of moduli and thicknesses of pavement systems.* Transportation Research Record 930, Washington D.C., p. 38-45.

Noorany, I., and Seed, H. B. (1965). "In situ strength characteristics of soft clays." *Journal of Soil Mechanics and Foundation Division, ASCE*, 91(SM2), 49-80.

NRC, (1985). *Liquefaction of soils during earthquakes*. US National Research Council Report CETS-EE-001, National Academic Press, Washington, D.C.

NSF, (2003). Proceedings of the International Workshop on Seismic Stability of Tailings Dams, http://ecivwww.cwru.edu/civil/xxz16/Tailings%20Dam/.

Nuttli, O. W., and Herrmann, R. B. (1978). *State-of-the-art for assessing earthquake hazards in the United States*. Report 12, credible earthquakes for the central United States. U.S. Army Corps of Engineers Miscellaneous Paper S-73-1, 99p.

Nuttli, O. W. (1981). *On the problem of maximum magnitude of earthquakes.* USGS Open Report, 13p.

Nuttli, O. W., Bollinger, G. A., and Griffiths, D. W. (1979). "On the relation between Modified Mercalli intensity and body-wave magnitude." *Seismological Society of America Bulletin*, 69, 893-909.

Obermeier, S. F., Munson, P. J., Munson, C. A., Martin, J. R., Frankel, A. D., Youd, T. L., and Pond, E. C. (1992). "Liquefaction evidence for strong Holocene earthquake(s) in the Wabash valley of Indiana-Illinois." *Seismological Research Letters*, 63(3).

Obermeier, S. F., Martin, J. R., Frankel, A. D., Youd, T. L., Munson, P. J., Munson, C. A., and Pond, E. C. (1993). "Liquefaction Evidence for One or More Strong Holocene Earthquakes in the Wabash Valley of Southern Indiana and Illinois, with a Preliminary Estimate of Magnitude." United States Geological Survey Professional Paper 1536, 27 pp. 1993.

Omarov, M. (2010). "Liquefaction potential and post-liquefaction settlement of saturated clean sands and effect of geofiber reinforcement." M.S, Thesis, University of Alaska Fairbanks, 209 pp.

Peters, G., and Verdugo, R. (2003). “Seismic design considerations of tailings dams.” *In Soil Rock America 2003: Proceedings of the 12th Panamerican Conference on Soil Mechanics and Geotechnical Engineering*, Massachusetts Institute of Technology, Cambridge, Mass., 22–26 June 2003. Edited by P. J. Culligan, H. N. Einstein, and A. J. Whittle. Verlag Gluckauf, Essen, Germany. Vol. 2, pp. 2241–2246. [In Spanish.]

Petersen, M. D., Frankel, A. D., Harmsen, S. C., Mueller, C. S., Haller, K. M., Wheeler, R. L., Wesson, R. L., Zeng, Y., Boyd, O. S., Perkins, D. M., Luco, N., Field, E. H., Wills, C. J., Rukstales, K. S. (2008). “Documentation for the 2008 Update of the United States National Seismic Hazard Maps,” *U.S. Geological Survey*, Open File Report 2008-1128.

Polito, C. P., and Martin, J. R. (2001). “Effect of non-plastic fines on the liquefaction resistance of sands.” *Journal of Geotechnical and Geoenvironmental Engineering, ASCE*, 127(5): 408–415.

Pond, E. C. and Martin, J. R. (1997). “Estimated magnitudes and accelerations associated with prehistoric earthquakes in the Wabash Valley region of the central United States.” *Seismological Research Letters*, 68(4), 611-623.

Powell, C. A., Bollinger, G. A., Chapman, M. C., Sibol, M. S., Johnston, A. C., and Wheeler, R. L. (1994). “A seismotectonic model for the 300-kilometer-long eastern Tennessee seismic zone.” *Science* 264, 686-688.

Poulos, S., Castro, G., and France, J. (1985). ”Liquefaction Evaluation Procedure.” *Journal of Geotechnical Engineering, ASCE*, 111(6), 772–792.

Poulos, S. J., Robinsky, E. I., and Keller, T. O. (1985). “Liquefaction resistance of thickened tailings.” *Journal of Geotechnical Engineering, ASCE*, 111(12): 1380–1394.

Prakash, S., and Puri, V. K. (2006). *Liquefaction of fine grained soils*. Earthquake Engineering Research Institute.

Pyke, R. (1979). “Discussion of definition of terms related to liquefaction.” *Journal of the Geotechnical Engineering Division, Proceedings of the ASCE*, 105(10), 1260.

Pyke, R., Seed H. B. and Chan C. K. (1975). “Settlements of sands under multi-directional loading,” *Journal of the Geotechnical Engineering Division, ASCE*, 101(GT4), 379-39.

Robertson, P.K. (1994). “Suggested Terminology for Liquefaction.” *47th Canadian Geotechnical Conference*, September 21-23, 1994, Halifax, Nova Scotia, 10 pages.

Robertson, P. K., and Campanella, R. G. (1983). “Interpretation of cone penetration tests. Part I: Sand.” *Canadian Geotechnical Journal*, 20(4): 718-733.

Robertson, P. K., and Campanella, R. G. (1983). “Interpretation of cone penetration tests. Part II: Clay.” *Canadian Geotechnical Journal*, 20(4): 718-733.

Robertson, P., Campanella, R., Gillespie, D., and Rice, A. (1986). ”Seismic CPT to Measure in Situ Shear Wave Velocity.” *Journal of Geotechnical Engineering*, 112(8), 791–803.

Robertson, P. K., and Wride, C. E. (1998). “Evaluating cyclic liquefaction potential using the CPT.” *Canadian Geotechnical Journal*, 35(3), 442–459.

Robertson, P.K. (1990). “Soil classification using the cone penetration test.” *Canadian Geotechnical Journal*, 27(1): 151-158.

Robertson, P.K. (2009). “Interpretation of cone penetration tests – a unified approach.” *Canadian Geotechnical Journal*, 46:1337-1355.

Robertson, P.K. (2009). “Performance based earthquake design using the CPT.” *Proceedings, IS-Tokyo 2009*, June 2009, Tokyo, Japan, pp. 3-20.

Robertson, P. K. (2010). “Estimating in situ state parameter in sandy soils from the CPT.” Proc., *2nd Int. Symp. of the Cone Penetration Test, CPT ‘10*, Omnipress Publishers, Madison, Wis.

Robertson, P.K. (2010). “Evaluation of Flow Liquefaction and Liquefied strength using the Cone Penetration Test.” *ASCE Journal of Geotechnical and Geoenvironmental Engineering*, 136(6): 842 – 853.

Robertson, P.K. (2012). “Evaluating flow (static) liquefaction using the CPT: an update.” Under Review.

Robertson, P.K. (2013). Personal communication.

Romero, S. (1995). “The behavior of silt as clay content is increased.” M.S. Thesis, University of California, Davis, 108 pp.

Roscoe, K. H. (1970). “10th Rankine Lecture: the influence of strains in soil mechanics,” *Géotechnique*, 20(2): 129–170.

Sancio, R. B. (2003). “Ground failure and building performance in Adapazari, Turkey.” Ph.D. Dissertation, University of California, Berkeley, 747p.

SCON 1500 (Version 1.0) [Computer Software], GCTS Testing Systems, Provided June 2009, Available from http://www.gcts.com/.

Seed, H. B. (1979). “Soil liquefaction and cyclic mobility evaluation for level ground during earthquakes.” *Journal of the Soil Mechanics and Foundations Division, Proceedings of the ASCE*, 105(2), 201-255.

Seed, H. B. (1983). “Earthquake Resistant Design of Earth Dams.” *Proceedings of the Symposium on Seismic Design of Earth dams and Caverns*, Philadelphia, Pennsylvania, ASCE, N.Y.

Seed, H. B. (1987). “Design problems in soil liquefaction.” *Journal of Geotechnical Engineering*. 113(8), 827-845.

Seed, R. B. and Harder, L. F. Jr. (1991). “SPT-based analysis of cyclic pore pressure generation and undrained residual strength.” *Proceedings of the H. B. Seed Memorial Symposium*, BiTech Publishers Ltd., Vol. 2, pp. 351-376.

Seed, H. B. and Idriss, l. M. (1971). “Simplified procedure for evaluating soil liquefaction potential.” *Journal of the Soil Mechanics and Foundations Division, Proceedings of the ASCE*. 97(9), 1249-1272.

Seed, H. B. and Lee, K. L. (1966). “Liquefaction of saturated sand during cyclic loading.” *Journal of the Soil Mechanics and Foundations Division, Proceedings of the ASCE*, 92(6), 105-134.

Seed, H. B. and Peacock, W. H. (1971). “Test procedures for measuring soil liquefaction characteristics.” *Journal of the Soil Mechanics and Foundations Division, Proceedings of the ASCE*, 97(8), 1099-1119.

Seed, H. B., Lee, K. L., Idriss, I. M. (1969). “Analysis of Sheffield dam failure.” *Journal of the Soil Mechanics and Foundations Division, Proceedings of the ASCE*. 95(6), 1453-1490.

Seed, H. B., Mori, K., and Chan, C. K. (1975). "Influence of seismic history on the liquefaction characteristics of sands," *Report EERC 75-25*, *Earthquake Engineering Research Center*, University of California, Berkeley.

Seed, H. B., Idriss, I. M., Makdisi, F., and Banerjee, N. (1975). “Representation of irregular stress-time history by equivalent uniform stress series in liquefaction analyses,” *Report No. EERC 75-29, Earthquake Engineering Research Center*, University of California, Berkeley.

Seed, H. B., Tokimatsu, K., Harder, L., and Chung, R. (1985). ”Influence of SPT Procedures in Soil Liquefaction Resistance Evaluations.” *Journal of Geotechnical Engineering*, 111(12), 1425–1445.

Seed, R. B.; Moss, R. E. S.; Kammerer, A. M.; Wu, J.; Pestana, J. M.; Riemer, M. F.; Sancio, R. B.; Bray, J. D.; Kayen, R. E.; Faris, A.; and Çetin, K. Ö., (2003). “Recent advances in soil liquefaction engineering: a unified and consistent framework,” *Earthquake Engineering Research Center*, University of California, Berkeley, 71 pages (400/E177/2003-06).

Senneset, K., Janbu, N. & Svano, G. (1982). “Strength and deformation parameters from cone penetration tests.” *Proc. 2nd European Symposium on Penetration Testing*, Amsterdam, 2: 863-870.

Silver, M. L., Chan, C. K., Ladd, R. S., Lee, K. L., Tiedmann, D. A., Townsend, F. C., Valera, J. E. and Wilson, J. H. (1976). “Cyclic triaxial strength of standard test sand.” *Journal of the Geotechnical Engineering Division*, 102(GT5), 511-523.

Skempton, A. W. (1986). “Standard penetration test procedures and the effects in sands of overburden pressure, relative density, particle size, aging and overconsolidation.” *Geotechnique*, 36(3), 425-447.

Skempton, A. W., and Sowa, V. A. (1963). “The behaviour of saturated clays during sampling and testing.” *Geotechnique*, 13(4), 269-290.

Sowers, G. F. (1979). *Introductory Soil Mechanics and Foundations*, 4th edition. Macmillan, 621, New York.

Stamatopoulos, C., Stamatopoulos, A., and Kotzias, P. (1995). “Effect of prestress on the liquefaction potential of silty sands.” *Soil Dynamics and Earthquake Engineering VII*, Computational Mechanics Publications, pp. 181-188.

Stark, T. D. and Mesri, G. (1992). “Undrained shear strength of liquefied sands for stability analysis.” *Journal of Geotechnical Engineering*. 118(11), 1727-1747.

Stark, T. and Olson, S. (1995). ”Liquefaction Resistance Using CPT and Field Case Histories.” *Journal of Geotechnical Engineering*, 121(12), 856–869.

Stokoe II, K. H., Wright, S. G., Bay, J. A., and Roesset, J. M. (1994). “Characterization of geotechnical sites by SASW method,” *Geophysical characterization of sites.* ISSMFE Technical Committee #10, edited by R. D. Woods, Oxford Publishers, New Delhi.

Stover, C. W. and Coffman, J. L. (1993). “Seismicity of the United States.” *Geological Survey Professional Paper 1527*.

Street, R. (1980). “An instrumental $m_{b,Lg}$ magnitude estimate of the 1897 Giles County, Virginia earthquake.” *Earthquake Notes*, 50, 21-24.

Street, R. (1982). “Ground motion values obtained for the 27 July 1980 Sharpsburg, Kentucky, earthquake.” *Bulletin of the Seismological Society of America*, 72(4), 1295-1307.

Street, R. and Woolery, R. (2000). “Seismic Study of Dewey Dam, Floyd County, Kentucky.” *Fuller Mossbarger Scott and May Report Prepared for U.S. Army Corps of Engineers*, Huntington District, Huntington, West Virginia. 0.1.1.LX1999164. 28 p.

Sykora D. W. (1987). “Creation of a data base of seismic shear wave velocities for correlation analyses.” *Misc. Paper GL-87-26. U.S. Army Corps of Engineers WES*, Vicksburg, MS.

Tarr, A. C., and Wheeler, R. L. (2006). “Earthquakes in Virginia and vicinity 1774 - 2004: U.S. Geological Survey Open-File Report 2006–1017.

USGS, (2013, March 03). “MMI Hazard for a M7.7 earthquake located northwest of Memphis, on a fault coincident with the southwest linear zone of modern seismicity.” United Satates Geological Survey, Retrieved from http://earthquake.usgs.gov/regional/ceus/products/regional.php

USGS, (2002). “Earthquake Hazard in the Heart of the Homeland.” United States Geological Survey Fact Sheet 131-02.

Vaid, Y. P., and Finn, W. D. L. (1979). “Static shear and liquefaction potential.” *Journal of the Geotechnical Engineering Division, ASCE*, 105(GT10): 1233–1246.

Vaid, Y. P., Negussey, D., and Zergoun, M., (1987), “A Stress and Strain-Controlled Monotonic and Cyclic Loading System”, Advanced Triaxial Testing of Soil and Rock, ASTM STP 977, Robert T. Donaghe, Ronald C. Chaney, and Marshall L. Silver, Eds., American Society for Testing and Materials, Philadelphia, pp. 119-131.

Vessely, D. A., Riemer, M., and Arango, I. (1996). “Liquefaction susceptibility of soft alluvial silts in the Willamette valley.” *Oregon Geology*, 58(6), 142-145.

Vick, S. G. (1997). “Failure of the Omai tailings dam: Closure.” *Geotechnical News*, 15, p. 49-55.

Vick, S. G. (1983). *Planning, design and analysis of tailings dams*. Wiley Series on Geotechnical Engineering. John Wiley & Sons Inc., New York.

Vidich, D., Beckwith, G. H., and Keaton, J. R. (1998). “Liquefaction assessment of mine tailings dams.” *Geotechnical Site Characterization*, P. Robertson and P. Mayne, Eds., Balkema, pp. 543-548.

Vucetic, M. and Dobry, R. (1991). ”Effect of Soil Plasticity on Cyclic Response.” *Journal of Geotechnical Engineering*, 117(1), 89–107.

Wang W. (1979). “Some findings in soil liquefaction.” *Water Conservancy and Hydroelectric Power Scientific Research Institute*, Beijing, China.

Wijewickreme, D., 2007, “Constant Volume Shear Response of Natural Low-plastic Silt”, *Paper for Special Lecture, In Proc. 1st Sri Lankan International Conference on Geotechnical Engineering*, August 2007, Colombo, Sri Lanka.

Wijewickreme, D., and Sanin, M. V. (2004). “Cyclic shear loading response of Fraser River Delta silt.” *In Proceedings of the 13th World Conference on Earthquake Engineering*, Vancouver, B.C., 1–6 August 2004. Canadian Association for Earthquake Engineering, c/o Department of Civil Engineering, University of Ottawa, Ottawa, Ont. Paper No. 499.

Wijewickreme, D., and Vaid, Y. P. (1993). “Behaviour of loose sand under simultaneous increase in stress ratio and principal stress rotation.” *Canadian Geotechnical Journal*, 30(6): 953–964.

Wijewickreme, D., Sanin, M. V., and Greenaway, G. R. (2005). “Cyclic shear response of fine-grained mine tailings.” *Canadian Geotechnical Journal*, 42(5): 1408-1421.

Wu, J., Kammerer, A. M., Riemer, M. F., Seed, R. B., and Pestana, J. M. (2004). “Laboratory study of liquefaction triggering criteria.” *In Proceedings of the 13th World Conference on Earthquake Engineering*, Vancouver, B.C., 1–6 August 2004. Canadian Association for Earthquake Engineering, c/o Department of Civil Engineering, University of Ottawa, Ottawa, Ont. Paper No. 2580.

Zeng, X., Wu, J., and Rohlf, R. (1998). “Seismic stability of coal-waste tailings dams,” *Geotechnical Earthquake Engineering and Soil Dynamics III*. pp. 951–961.

Youd, T. L., Idriss, I. M., Andrus, R. D., Arango, I., Castro, G., Christian, J. T., Dobry, R., Finn, W. D. L., Harder, L. F., Jr., Hynes, M. E., Ishihara, K., Koester, J. P., Liao, S. S. C., Marcuson, W. F., III, Martin, G. R., Mitchell, J. K., Moriwaki, Y., Power, M. S., Robertson, P. K., Seed, R. B., and Stokoe, K. H., II. (2001). "Liquefaction resistance of soils: summary report from the 1996 NCEER and 1998 NCEER/NSF workshops on evaluation of liquefaction resistance of soils." *Journal of Geotechnical and Geoenvironmental Engineering, ASCE*, 127(10): 817–833.

Zergoun, M. and Vaid, Y. P. (1994). "Effective stress response of clay to undrained cyclic loading." *Canadian Geotechnical Journal*. 31, 714-727.

Zhang, G., Robertson, P. K., Brachman, R. W. I. (2002). "Estimating liquefaction-induced ground settlements from CPT for level ground." *Canadian Geotechnical Journal*, 39(5): 1168-1180.

Zhou, Y. and Chen, Y. (2007). "Laboratory Investigation on Assessing Liquefaction Resistance of Sandy Soils by Shear Wave Velocity." *Journal of Geotechnical and Geoenvironmental Engineering, ASCE*, 133(8), 959–972.

Vita

Author's Name: Ali Salehian

Birthplace: Shiraz, Iran

Education

Master of Science in Civil Engineering – Geotechnical Engineering
University of Kentucky
December 18, 2009

Master of Science in Civil Engineering – Geotechnical Engineering
Shiraz University
September, 2006

Bachelor of Science in Civil Engineering
Shiraz University
February, 2003

Research/ Teaching Experience

University of Kentucky
Lexington, KY
August, 2007-April, 2012
Research Assistant/ Ph.D. Candidate

University of Kentucky
Lexington, KY
January, 2008 - April, 2012
Teaching Assistant

Shiraz University
Shiraz, Iran
September, 2003 – September, 2006
Teaching Assistant

Shiraz University
Shiraz, Iran
December, 2004 – March, 2005
Research Assistant

Professional Positions

ENGEO Incorporated
San Francisco, CA
July, 2012 – Present
Staff Engineer

S&ME Incorporated
Lexington, KY
May, 2011 – August, 2011
Geotechnical Laboratory Assistant

Asmari Consulting Engineers
Shiraz, Iran
October, 2004 – January, 2006
Geotechnical Staff Engineer

Beton Arshe Co.
Shiraz, Iran
April, 2003 – October, 2003
Staff Engineer

Papers, Posters

Published

Bryson, S. L. and Salehian, A., (2011). "Performance of Constitutive Models in Predicting the Behavior of Remolded Clay", Acta Geotechnica, (6): 143-154.

Jahanandish, M. and Salehian, A., (2007). "Application of the Method of Characteristics in Determining the Ultimate Dynamic Bearing Capacity of Rock Masses", 3rd Iranian Rock Mechanics Conference, Nov 2007, Tehran.

Salehian, A. and Kalinski, M., (2012). "Predicting the Dynamic Behavior of Coal Mine Tailings Using State-of-Practice Geotechnical Field Methods", 2012 ASCE Geo-Congress - State of the Art and Practice in Geotechnical Engineering, Poster session, March 2012, Oakland, CA.

Salehian, A. and Kalinski, M., (2012). "Predicting the Dynamic Behavior of Coal Mine Tailings Using State-of-Practice Geotechnical Field Methods", 2012 EERI Annual Meeting & National Earthquake Conference, Poster session, April 2012, Memphis, TN.

Submitted

Jeffrey S. Dingrando, Michael E. Kalinski, Ali Salehian, Benjamin B. Zand, (2013). "Cyclic Triaxial Testing of Water-Pluviated Fly Ash Specimens." WOCA Conference, April, 2012, Lexington, KY.

Salehian, A. and Bryson, S. L., “Sensitivity Analysis of Input Parameters for Several Constitutive Models”, Acta Geotechnica, 2011, Under Review.

Certificates, Honors, Awards

Awarded Lyman T. Johnson fellowship, University of Kentucky, 2010-2012
Awarded Kentucky Opportunities fellowship, University of Kentucky, 2008
Ranked in top 1% in national universities entrance exam for B.Sc., Iran, 1998
Ranked in top 5% in national universities entrance exam for M.Sc., Iran, 2003
Ranked high (3.9/4.0) in teaching evaluations for the Soil Mechanics lab at the University of Kentucky

Certificates, Society Memberships

EIT, Passed the FE exam, spring 2011
Member of the American Society of Civil Engineers (ASCE), 2010
Member of the Chi-Epsilon honor society, University of Kentucky, 2010